



NONLINEAR GEOMETRIC & MATERIAL BEHAVIOR OF COMPOSITE SHELLS WITH LARGE STRAINS

Scott A. Schimmels, Capt, USAF
Structures Division
Wright Laboratory
Wright Patterson AFB, OH

August 1995

Final Report for Period April 1993 to July 1995

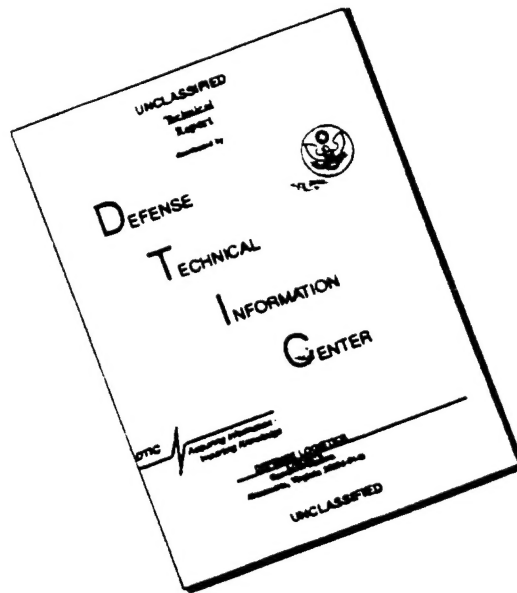
APPROVED FOR PUBLIC RELEASE; DISTRIBUTION UNLIMITED

19960401 017

FLIGHT DYNAMICS DIRECTORATE
WRIGHT LABORATORY
AIR FORCE MATERIEL COMMAND
WRIGHT-PATTERSON AFB, OHIO 45433-7562

DTIC QUALITY INSPECTED 1

DISCLAIMER NOTICE




THIS DOCUMENT IS BEST
QUALITY AVAILABLE. THE COPY
FURNISHED TO DTIC CONTAINED
A SIGNIFICANT NUMBER OF
PAGES WHICH DO NOT
REPRODUCE LEGIBLY.

NOTICE

When Government drawings, specifications, or other data are used for any purpose other than in connection with a definitely Government-related procurement, the United States Government incurs no responsibility or any obligation whatsoever. The fact that the government may have formulated or in any way supplied the said drawings, specifications, or other data, is not to be regarded by implication, or otherwise in any manner construed, as licensing the holder, or any other person or corporation; or as conveying any rights or permission to manufacture, use, or sell any patented invention that may in any way be related thereto.

This report is releasable to the National Technical Information Service (NTIS). At NTIS, it will be available to the general public, including foreign nations.

This technical report has been reviewed and is approved for publication.


NELSON D. WOLF
TECHNICAL MANAGER
DESIGN METHODS DEVELOPMENT
SECTION


GEORGE R. HOLDERBY
BRANCH CHIEF
DESIGN DEVELOPMENT BRANCH

If your address has changed, if you wish to be removed from our mailing list, or if the addressee is no longer employed by your organization please notify _____, WPAFB, OH 45433-_____ to help us maintain a current mailing list.

Copies of this report should not be returned unless return is required by security considerations, contractual obligations, or notice on a specific document.

REPORT DOCUMENTATION PAGE			Form Approved OMB No. 0704-0188	
Public reporting burden for this collection of information is estimated to average 1 hour per response, including the time for reviewing instructions, searching existing data sources, gathering and maintaining the data needed, and completing and reviewing the collection of information. Send comments regarding this burden estimate or any other aspect of this collection of information, including suggestions for reducing this burden, to Washington Headquarters Services, Directorate for Information Operations and Reports, 1215 Jefferson Davis Highway, Suite 1204, Arlington, VA 22202-4302, and to the Office of Management and Budget, Paperwork Reduction Project (0704-0188), Washington, DC 20503.				
1. AGENCY USE ONLY (Leave blank)	2. REPORT DATE AUG 1995	3. REPORT TYPE AND DATES COVERED FINAL Apr 93 - Aug 95		
4. TITLE AND SUBTITLE NONLINEAR GEOMETRIC AND MATERIAL BEHAVIOR OF COMPOSITE SHELLS WITH LARGE STRAINS		5. FUNDING NUMBERS		
6. AUTHOR(S) CAPT SCOTT A. SCHIMMELS				
7. PERFORMING ORGANIZATION NAME(S) AND ADDRESS(ES) FLIGHT DYNAMICS DIRECTORATE WRIGHT LABORATORY AIR FORCE MATERIAL COMMAND WRIGHT-PATTERSON AFB OH 45433-7562		8. PERFORMING ORGANIZATION REPORT NUMBER WL-TR-96-3012		
9. SPONSORING/MONITORING AGENCY NAME(S) AND ADDRESS(ES)		10. SPONSORING/MONITORING AGENCY REPORT NUMBER		
11. SUPPLEMENTARY NOTES				
12a. DISTRIBUTION/AVAILABILITY STATEMENT APPROVED FOR PUBLIC RELEASE. DISTRIBUTION UNLIMITED		12b. DISTRIBUTION CODE		
13. ABSTRACT (Maximum 200 words) A two-dimensional, geometrically and materially nonlinear shell theory applicable to arbitrary geometries described by orthogonal curvilinear coordinates and encompassing large displacements, moderate rotations for large strain situations has been developed. Additionally, the theory includes Jacobian transformation matrices, based upon displacement parameters, for the Cauchy - 2nd Piola-Kirchhoff stress-state and the Cauchy (Almansi) - Green strain-state transformations, and a layered material approach is included for the elastoplastic analysis to allow for variation of plasticity through-the-thickness. Doubly curved 20, 28, and 36 degree-of-freedom finite elements are defined based on specialization of the theory to spherical coordinates. The computer program includes algorithms for linear and nonlinear problems. Post-collapse nonlinear solutions are found through a displacement-control incrementation scheme. This provides solutions to classical von Karman flat plate and Donnell spherical shell equations, intermediate von Karman flat plate and Donnell spherical shell equations, and large displacement and moderate rotational formulations. For deep shells exhibiting large rotations and displacements over 15-20% of the shell's surface, the Lagrangian constitutive relations (including the Jacobian transformation matrices for the stress- and strain-states) should be included to accurately reflect the variation of the material coordinate system with respect to the structural axis system. For those plates and shells exhibiting large strains, along with large rotations and displacements over 15-18% of the outer surface, plasticity should be included in the model.				
14. SUBJECT TERMS COMPOSITES, SHELLS, FINITE ELEMENTS, NONLINEAR ANALYSIS, PLASTICITY, LARGE STRAINS, TOTAL LAGRANGIAN, TRANSVERSE SHEAR, LAGRANGIAN-CAUCHY TRANSFORMATIONS			15. NUMBER OF PAGES 480	
			16. PRICE CODE	
17. SECURITY CLASSIFICATION OF REPORT UNCLASSIFIED	18. SECURITY CLASSIFICATION OF THIS PAGE UNCLASSIFIED	19. SECURITY CLASSIFICATION OF ABSTRACT UNCLASSIFIED	20. LIMITATION OF ABSTRACT U	

FORWARD

This technical report was prepared by Capt. Scott A. Schimmels, Design and Development Branch, Structures Division of the Flight Dynamics Directorate. This effort is in support of Capt. Schimmels pursuing his Doctorate in Aeronautical Engineering at the Air Force Institute of Technology with sponsorship by the Air Force Offices of Scientific Research (AFOSR) and the Design and Development Branch. The results presented in this report were obtained using a nonlinear geometric finite element code that included large strain theory developed by Captain Schimmels.

This technical report covers work accomplished from April 1993 to July 1995.

This report was reviewed and approved.

Acknowledgements

Dr Anthony Palazotto, my committee chairman, guided me through this research and through my entire course of study from the beginning of my Master's program to the conclusion of this effort. His patient advice, questions, and leadership helped me to define and appropriately pursue this research effort to its end. Thank you Dr Palazotto for your help and patience, and for your confidence in me. Dr Peter Torvik and Dr John Jones Jr. served as members of my committee. I wish to thank them both for their guidance and suggestions regarding this research and in the preparation of my dissertation. Dr Mark Oxley joined my committee in the final months of my research after Dr Jones retired. I wish to thank him for his willingness to step in at the end of my effort. He helped clarify how the theory was presented and ensured it was correct.

I wish to thank Dr Spencer Wu, AFOSR, for sponsoring this work. I also wish to thank Mr Nelson Wolf, WL/FIBA, for sponsoring me in the PhD Scholar program. Without his sponsorship, I was not able to enter the PhD program directly after finishing my Master's thesis. He provided a position for me here at Wright Lab and graciously gave me time to finish writing this dissertation while working in the branch. Thank you Nelson.

This work would not have been possible without the strength, wisdom, perseverance, patience, and love the Lord Jesus Christ has given to me. He also blessed me with a loving wife, Jeanne, to whom I'm forever grateful and indebted to. She nurtured and cared for our daughter, Jennifer Marlayne, almost single-handedly for the last four years. In addition, our son, Ethan Christian, was born in the midst of this effort. She has also been a tremendous source of encouragement and support to me in the pursuit of this degree. My sincere thanks, deepest apologies, and all the love in my heart is extended to my wife, daughter, and son. They have given me love and support while receiving so little of the love, time, and attention they richly deserve.

Scott A. Schimmels

TABLE OF CONTENTS

	Page
Acknowledgements	iii
Table of Contents	iv
List of Figures	x
List of Tables	xxii
List of Symbols	xxv
Abstract	xxxi
1. Introduction	1-1
2. Literature Review	2-1
2.1. Nonlinear Material Behavior	2-2
2.2. Curved Shell Finite Element Models	2-5
2.2.1. First-Order Transverse Shear Deformation Theories (FTSD)	2-6
2.2.2. Higher-Order Transverse Shear Deformation Theories (HTSD)	2-7
2.3 Literature Assessment	2-7
3. Theoretical Background	3-1
3.1 Surface Geometric Considerations	3-1
3.2 Strain Tensor Definition	3-7
3.3 Composite Material Analysis	3-14
3.4 Transverse Shear Deformation	3-18
3.4.1. First-Order Transverse Shear Deformation Theories (FTSD)	3-19

	Page
3.4.2. <i>Higher-Order Transverse Shear Deformation Theories (HTSD)</i>	3-22
3.5 Mathematical Theory of Plasticity	3-25
3.5.1. <i>The Yield Criteria</i>	3-25
3.5.2. <i>Work or Strain Hardening</i>	3-29
3.5.3. <i>Elasto-Plastic Stress-Strain Relations</i>	3-33
3.5.4. <i>Uniaxial Yield Test on a Strain-Hardening Material</i>	3-34
3.5.5. <i>Matrix Formulation</i>	3-36
3.5 Anisotropic Elastic-Plastic Theory	3-38
4. Theory Development	4-1
4.1 Spherical Geometric Behavior	4-2
4.2 Nonlinear Material Behavior	4-4
4.2.1. <i>Layered Isotropic Material</i>	4-5
4.2.2. <i>Layered Composite Material</i>	4-9
4.2.3. <i>Large Strain Formulation</i>	4-9
4.3 Element Independent Stiffness Formulation	4-31
4.3.1. <i>Elastic Material Formulation</i>	4-31
4.3.2. <i>Large Strain Formulation</i>	4-40
4.3.3. <i>Elastic-Plastic Formulation</i>	4-41
4.4 Symbolic Generation of the Elemental Codes	4-45
4.5 Finite Element Solution	4-47

	Page
4.5.1. Elastic Finite Element Solution	4-47
4.5.2. Large Strain Finite Element Solution	4-48
4.5.3. Elastic-Plastic Finite Element Solution	4-48
4.6 The 36 Degree-of-Freedom Finite Element	4-50
4.7 The 28 Degree-of-Freedom Finite Element	4-61
4.7.1 SIXX & S2XX Codes	4-61
4.7.2 S0XX Code	4-63
4.8 The 20 Degree-of-Freedom Finite Element	4-65
4.9 The Incremental, Displacement-Control, Elastic-Plastic Algorithm	4-66
4.9.1. The Load-Control, Newton-Raphson Algorithm	4-66
4.9.2. The Displacement-Control, Newton-Raphson Algorithm	4-70
4.9.3. The Incremental, Displacement-Control, Elasto-Plastic, Newton-Raphson Algorithm	4-72
5. Discussion of Elastic Shell Analysis	5-1
5.1 Flat, Quasi-Isotropic Panel with Uniform Transverse Pressure Load	5-2
5.2 Simply Supported, Isotropic, Deep Arches	5-5
5.3 Hinged-Free, Isotropic, Cylindrical Shell Panel, 0.635-cm Thick, with Transverse Point Load	5-11
5.4 Clamped-Free, Quasi-Isotropic, Cylindrical Shell Panel, with Transverse Point Load	5-20
5.5 Clamped-Free, Quasi-Isotropic, Cylindrical Shell Panel, with Axial Compression Load	5-32

	Page
<i>5.6 Hinged-Hinged, Isotropic, Spherical Shell Cap, with Transverse Point Load</i>	5-38
<i>5.7 Hinged-Hinged Quasi-Isotropic Spherical Shell Cap, with Transverse Point Load</i>	5-43
6. Discussion of Elastic-Plastic Shell Analysis	6-1
<i>6.1 Point Loaded, Simply Supported, Perfectly Plastic Isotropic Plate</i>	6-3
<i>6.2 Deep, Hinged, Perfectly Plastic Isotropic Cylindrical Arch with Transverse Point Load</i>	6-8
<i>6.3 Pinched, Perfectly Plastic Isotropic Cylinder with Rigid Membranes, and Two Transverse Point Loads</i>	6-15
<i>6.4 Hinged, Perfectly Plastic Isotropic Spherical Cap with Apex Load</i>	6-22
<i>6.5 Axially Loaded Graphite Polyetherether Ketone (Gr/PEEK) Tensile Coupon</i>	6-28
<i>6.6 Clamped-Free Quasi-Isotropic Cylindrical Shell Panel, with Transverse Point Load</i>	6-35
<i>6.7 Clamped-Free Quasi-Isotropic Cylindrical Shell Pane Under Axial Loading (Buckling)</i>	6-43
<i>6.8 Hinged Quasi-Isotropic Spherical Shell Cap with Transverse Point Load</i>	6-55
7. Results and Conclusions	7-1
<i>7.1 Theory</i>	7-1
<i>7.2 Elastic Shell Analysis</i>	7-13
<i>7.3 Elastic-Plastic Shell Analysis</i>	7-18
<i>7.4 Conclusions</i>	7-22

	Page
8. Bibliography	8-1
Appendix A. Arbitrary Shell Strain-Displacement Relations	A-1
<i>A.1 Midsurface Strain Components for the Arbitrary Shell</i>	<i>A-1</i>
<i>A.2 Midsurface Strain Components for the Arbitrary Shell with a General Quartic Displacement Field Assumption</i>	<i>A-2</i>
<i>A.3 Approximation of 60 Shell Factor Functions with Second Order Taylor's Series Expansions</i>	<i>A-18</i>
Appendix B. Strain-Displacement Relations for General Spherical Shell Code	B-1
Appendix C. Strain-Displacement Relations for S0XX Elemental Codes	C-1
Appendix D. Strain-Displacement Relations for S1XX Elemental Codes	D-1
Appendix E. Strain-Displacement Relations for S2XX Elemental Codes	E-1
Appendix F. MACSYMA Routine for Elemental Code Generation	F-1
<i>F.1 SPHSTRN.MAC Input Deck</i>	<i>F-1</i>
<i>F.2 SPHINIT.MAC Input Deck</i>	<i>F-11</i>
<i>F.3 SPHK.MAC Input Deck</i>	<i>F-15</i>
<i>F.4 SPHN1.MAC Input Deck</i>	<i>F-19</i>
<i>F.5 SPHN2.B1 Input Deck</i>	<i>F-31</i>
<i>F.6 SPHN2.B2 Input Deck</i>	<i>F-39</i>
<i>F.7 SPHN2.B3 Input Deck</i>	<i>F-41</i>
<i>F.8 SPHN2S.MAC Input Deck</i>	<i>F-43</i>

	Page
<i>F.9 PLASTRN.MAC Input Deck</i>	<i>F-49</i>
<i>F.10 PLASINIT.MAC Input Deck</i>	<i>F-59</i>
Appendix G. The Elasto-Plastic Algorithm	<i>G-1</i>
Vita	<i>VITA-1</i>

LIST OF FIGURES

Figure	Page
3.1 Base Vectors and Coordinate Curves [229]	3-3
3.2 Body Before and After Deformation [192, 229]	3-8
3.3 Material Axes for a Transversely Isotropic Lamina [11:20]	3-16
3.4 Shear Deformation of a Thin Elastic Body [167:234]	3-19
3.5 Deformation of Normals for FTSD and HTSD Theories	3-21
3.6 Parabolic and Cubic Transverse Shear Distributions for a Curved Shell	3-23
3.7 Geometrical Representation of the Tresca and von Mises Yield Surfaces in Principal Stress Space	3-27
3.8 Two-dimensional Representations of the Tresca and von Mises yield Criteria. (a) π Plane Representation. (b) Conventional Engineering Representation.	3-28
3.9 Mathematical Models for Representation of Strain	3-30
3.10 Geometrical Representation of the Normality Rule of Associated Plasticity	3-32
3.11 Elasto-plastic Strain Hardening Behavior for the Uniaxial Case.	3-35
4.1 Spherical Shell Domain for Derivation of the HTSD Theory	4-3
4.2 Yielding of Layered Section [144]	4-5
4.3 Definition of 2nd Piola-Kirchhoff Stress Tensor [229]	4-16

Figure	Page
4.4 Definition of Cauchy Stress Tensor [229]	4-18
4.5 36 DOF Spherical Shell Finite Element - For S1XX & S2XX Codes	4-52
4.6 Rotational DOF Definitions for the 36 DOF Spherical Shell Element	4-54
4.7 7 x 7 and 5 x 5 Gauss Quadrature Elements	4-58
4.8 Integration of Gauss Points Through the Element's Layers	4-61
4.9 28 DOF Spherical Shell Finite Element - For S1XX & S2XX Codes	4-62
4.10 28 DOF Spherical Shell Element - For S0XX Code	4-64
4.11 20 DOF Spherical Shell Element - For S0XX Code	4-66
4.12 Load-Control Solution Algorithm	4-68
4.13 Second Increment of Load-Control Solution Algorithm	4-69
4.14 Displacement Control Solution Algorithm	4-71
5.1 1.6-Inch Thick, Hinged Plate with Uniform Pressure Load	5-4
5.2 Comparisons of Flat Plate Displacement Results for Variations of Geometric Nonlinearity	5-5
5.3 Hinged Transverse Point-Loaded Isotropic Cylindrical Arch	5-7
5.4 Deep Arch Crown Displacement vs Load - C10X Theory	5-8
5.5 Deep Arch Crown Displacement vs Load - C100 & C20X Theory	5-9

Figure	Page
5.6 Two-Dimensional View of Deformation of Hinged Isotropic Deep Circular Arch at Four Specified Increments of Transverse Displacement - C201 Theory	5-10
5.7 Meridian Values of ψ_2 for 8 Increment, 4-Inches each, of Transverse Displacement of Hinged Isotropic Deep Circular Arch - C201 Theory	5-11
5.8 0.25-Inch Hinged-Free Transversely Point-Loaded Isotropic Cylindrical Shell	5-12
5.9 Equilibrium Curves for Transverse Point Loaded 0.635-cm Hinged-Free Isotropic Cylindrical Shell--CDON, C101, & C201 Theories	5-14
5.10 Meridian Values of ψ_2 for 10 Increment, 0.1-Inch each, of Transverse Displacement of 0.25-Inch Hinged-Free Isotropic Cylindrical Shell - C201 Theory	5-15
5.11 0.635-cm Hinged Free, Transversely Point-Loaded, Quasi-Isotropic, Cylindrical Shell	5-16
5.12 Equilibrium Curves for Transverse Point Loaded 0.635-cm Hinged-Free Isotropic Cylindrical Shell - C10X & C20X Theories	5-19
5.13 Meridian Values of ψ_2 for 10 Increments, 0.1-Inch each, of Transverse Displacement of 0.25-Inch Quasi-Isotropic Hinged-Free Cylindrical Shell - C201 Theory	5-19
5.14 Clamped-Free Composite Shell with Transverse Point Load	5-21
5.15 Two-Dimensional (2D) Profiles of Clamped-Free Laminated Composite Cylindrical Shells at Various Prescribed Transverse Displacements	5-23
5.16 Three-Dimensional Views of 0.102-cm Clamped-Free Quasi-Isotropic Cylindrical Shell at Specified Transverse Displacements - C201 Theory	5-25

Figure	Page
5.17 Three-Dimensional Views of 0.102-cm Clamped-Free Quasi-Isotropic Cylindrical Shell at Specified Transverse Displacements - C201 Theory	5-26
5.18 Equilibrium Path Comparisons for Transverse Center Point Loaded 0.102-cm Clamped-Free Quasi-Isotropic ([0/-45/45/90] _s) Cylindrical Shell - CDON, C200 & C201 Theories	5-27
5.19 Meridian Values of ψ_2 for 10 Increments, 0.1875-Inch each, of Transverse Displacement of 0.04-Inch Hinged-Free Quasi-Isotropic ([0/-45/45/90] _s) Cylindrical Shell - C201 Theory	5-27
5.20 Equilibrium Path Comparisons for Transverse Center Point Loaded 0.04-Inch Clamped-Free Quasi-Isotropic ([0 ₂ /90 ₂] _s) Cylindrical Shell - C201 Theory	5-28
5.21 Meridian Values of ψ_2 for 10 Increments, 0.1875-Inch each, of Transverse Displacement of 0.04-Inch Hinged-Free Quasi-Isotropic ([0 ₂ /90 ₂] _s) Cylindrical Shell - C201 Theory	5-28
5.22 Equilibrium Path Comparisons for Transverse Center Point Loaded 0.04-Inch Clamped-Free Quasi-Isotropic ([0 ₈]) Cylindrical Shell - C201 Theory	5-29
5.23 Meridian Values of ψ_2 for 10 Increments, 0.1875-Inch each, of Transverse Displacement of 0.04-Inch Hinged-Free Quasi-Isotropic ([0 ₈]) Cylindrical Shell - C201 Theory	5-29
5.24 Equilibrium Path Comparisons for Transverse Center Point Loaded 0.04-Inch Clamped-Free Quasi-Isotropic ([90 ₈]) Cylindrical Shell - C201 Theory	5-30
5.25 Meridian Values of ψ_2 for 10 Increments, 0.1875-Inch each, of Transverse Displacement of 0.04-Inch Hinged-Free Quasi-Isotropic ([90 ₈]) Cylindrical Shell - C201 Theory	5-30

Figure	Page
5.26 Quasi-Isotropic 30.48-cm Radius Cylindrical Composite Shell with Centered 4-Inch Cutout and Free Edges Loaded in Axial Compression	5-34
5.27 Total Equilibrium Load vs Axial Displacement for a Quasi-Isotropic Cylindrical Shell Panel with a Centered 10.16-cm Cutout.	5-36
5.28 Total Equilibrium Load vs Axial Displacement for a Quasi-Isotropic Cylindrical Shell Panel without Cutout	5-36
5.29 Quasi-Isotropic Cylindrical Shell Under Axial Load, Clamped-Free, with 10.16-cm Centered Cutout, ($u = 0.0279$ cm)	5-37
5.30 Quasi-Isotropic Cylindrical Shell Under Axial Load, Clamped-Free, with 10.16-cm Centered Cutout, ($u = 0.0305$ cm)	5-37
5.31 Hinged Apex-Loaded Isotropic Spherical Cap	5-39
5.32 Equilibrium Curves for Transverse Point Loaded 0.04-cm Hinged Isotropic Spherical Shell Cap - Ref [6] & SXX1 Theories	5-41
5.33 Two-Dimensional (2D) Profiles of Hinged Isotropic Spherical Shell Cap at Various Prescribed Transverse Displacements	5-42
5.34 Meridian Values of ψ_2 for 10 Increments, 0.0476-cm each, of Transverse Displacement of Hinged Isotropic Spherical Shell Cap - C201 Theory	5-43
5.35 Equilibrium Curves for Transverse Point Loaded Hinged Quasi-Isotropic [08] Spherical Shell Cap - C200 & C201 Theories	5-46
5.36 Meridian Values of ψ_2 for 10 Increments, 0.0476-cm each, of Transverse Displacement of Hinged Quasi-Isotropic [0 ₈] Spherical Shell Cap - C201 Theory	5-47

Figure	Page
5.37 Equilibrium Curves for Transverse Point Loaded Hinged Quasi-Isotropic $[0_2/90_2]_s$ Spherical Shell Cap - C200 & C201 Theories	5-48
5.38 Meridian Values of ψ_2 for 10 Increments, 0.01875-Inch each, of Transverse Displacement of Hinged Quasi-Isotropic $[0_2/90_2]_s$ Spherical Shell Cap - C201 Theory	5-48
5.39 Equilibrium Curves for Transverse Point Loaded Hinged Quasi-Isotropic $[0/-45/45/90]_s$ Spherical Shell Cap - C200 & C201 Theories	5-49
5.40 Meridian Values of ψ_2 for 10 Increments, 0.01875-Inch each, of Transverse Displacement of Hinged Quasi-Isotropic $[0/-45/45/90]_s$ Spherical Shell Cap - C201 Theory	5-50
6.1 Simply Supported Isotropic Plate with Transverse Point Load with no Work Hardening	6-5
6.2 Load-Displacement Curves for Simply Supported Isotropic Plate with no Work Hardening. Owen & Hinton [130:370-371] & PX11 Theories	6-5
6.3 Evolution of Plastic Zone in Simply Supported Isotropic Plate with no Work Hardening $w^* = 5.0$	6-6
6.4 Evolution of Plastic Zone in Simply Supported Isotropic Plate with no Work Hardening $w^* = 10.0$	6-6
6.5 Evolution of Plastic Zone in Simply Supported Isotropic Plate with no Work Hardening $w^* = 15.0$	6-7
6.6 Evolution of Plastic Zone in Simply Supported Isotropic Plate with no Work Hardening $w^* = 20.0$	6-7
6.7 Hinged, Point-Loaded, Perfectly Plastic, Isotropic Cylindrical Arch	6-9

Figure	Page
6.8 Deep Arch Crown Displacement vs Load - C100 & C2XX Theories	6-10
6.9 Evolution of Plastic Zones for Perfectly Plastic Isotropic Cylindrical Arch: $w = 20.32$ cm	6-12
6.10 Evolution of Plastic Zones for Perfectly Plastic Isotropic Cylindrical Arch: $w = 30.48$ cm	6-12
6.11 Evolution of Plastic Zones for Perfectly Plastic Isotropic Cylindrical Arch: $w = 40.64$ cm	6-13
6.12 Evolution of Plastic Zones for Perfectly Plastic Isotropic Cylindrical Arch: $w = 50.80$ cm	6-13
6.13 Evolution of Plastic Zones for Perfectly Plastic Isotropic Cylindrical Arch: $w = 60.96$ cm	6-14
6.14 Pinched, Perfectly Plastic, Isotropic Cylinder Bounded with Rigid Membranes under Transverse Point Loads	6-16
6.15 Predicted Equilibrium Load for Prescribed Transverse Displacement for Pinched, Perfectly Plastic, Isotropic Cylinder with Rigid Membrane	6-18
6.16 Evolution of Plastic Zone for Convex Surface in Pinched, Perfectly Plastic, Isotropic Cylinder: $w = 50.0$	6-18
6.17 Evolution of Plastic Zone for Convex Surface in Pinched, Perfectly Plastic, Isotropic Cylinder: $w = 100.0$	6-19
6.18 Evolution of Plastic Zone for Convex Surface in Pinched, Perfectly Plastic, Isotropic Cylinder: $w = 150.0$	6-19

Figure	Page
6.19 Evolution of Plastic Zone for Convex Surface in Pinched, Perfectly Plastic, Isotropic Cylinder: $w = 200.0$	6-20
6.20 Evolution of Plastic Zone for Convex Surface in Pinched, Perfectly Plastic, Isotropic Cylinder: $w = 250.0$	6-20
6.21 Evolution of Plastic Zone for Middle Surface in Pinched, Perfectly Plastic, Isotropic Cylinder: $w = 150.0$	6-21
6.22 Evolution of Plastic Zone for Middle Surface in Pinched, Perfectly Plastic, Isotropic Cylinder: $w = 250.0$	6-21
6.23 Hinged Apex-Loaded Isotropic Elastic Perfectly-Plastic Spherical Cap	6-23
6.24 Load-Displacement Equilibrium Curves for Hinged Isotropic Elastic-Perfectly Plastic Spherical Shell Cap	6-25
6.25 Evolution of Plastic Zones for Concave Surface of Hinged Isotropic Elastic-Perfectly Plastic Spherical Shell Cap: $w = 0.0478$ cm	6-25
6.26 Evolution of Plastic Zones for Concave Surface of Hinged Isotropic Elastic-Perfectly Plastic Spherical Shell Cap: $w = 0.429$ cm	6-26
6.27 Evolution of Plastic Zones for Concave Surface of Hinged Isotropic Elastic-Perfectly Plastic Spherical Shell Cap: $w = 0.523$ cm	6-26
6.28 Evolution of Plastic Zones for Middle Surface of Hinged Isotropic Elastic-Perfectly Plastic Spherical Shell Cap: $w = 0.0478$ cm	6-27
6.29 Evolution of Plastic Zones for Middle Surface of Hinged Isotropic Elastic-Perfectly Plastic Spherical Shell Cap: $w = 0.429$ cm	6-27

Figure	Page
6.30 $\pm 45^\circ$ Axially Loaded Gr/PEEK Tensile Coupon	6-29
6.31 Experimental $\sigma_{11} - \varepsilon_{11}$ Curve for Gr/PEEK [71]	6-29
6.32 Experimental $\sigma_{22} - \varepsilon_{22}$ Curve for Gr/PEEK [71]	6-30
6.33 Experimental $\sigma_{12} - \varepsilon_{12}$ Curve for Gr/PEEK [71]	6-30
6.34 Predicted Equilibrium Load for Prescribed Axial Displacement for Gr/PEEK Tensile Coupon - Experimental [71], PX11 Theories	6-32
6.35 Evolution of Plastic Zones in Gr/PEEK Tensile Coupon: $u = 0.254$ cm	6-33
6.36 Evolution of Plastic Zones in Gr/PEEK Tensile Coupon: $u = 2.54$ cm	6-33
6.37 Evolution of Plastic Zones in Gr/PEEK Tensile Coupon: $u = 4.57$ cm	6-34
6.38 Clamped-Free Graphite Epoxy Shell with Transverse Point Load	6-36
6.39 Experimental $\sigma_{11} - \varepsilon_{11}$ Curve for Graphite Epoxy	6-38
6.40 Experimental $\sigma_{22} - \varepsilon_{22}$ Curve for Graphite Epoxy	6-38
6.41 Experimental $\sigma_{12} - \varepsilon_{12}$ Curve for Graphite Epoxy	6-39
6.42 Equilibrium Path Comparisons for Transverse Point Loaded, 0.102 cm, Clamped-Free, Quasi-Isotropic, Cylindrical Shell - CDON, C200, C201 & C211 Theories	6-39
6.43 Evolution of Plastic Zones in $[0/-45/45/90]_s$, Clamped-Free, Cylindrical Shell with a Transverse Load, $w = 1.43$ cm	6-41

Figure	Page
6.44 Evolution of Plastic Zones in $[0/-45/45/90]_s$, Clamped-Free, Cylindrical Shell with a Transverse Load, $w = 2.858$ cm	6-42
6.45 Evolution of Plastic Zones in $[0/-45/45/90]_s$, Clamped-Free, Cylindrical Shell with a Transverse Load, $w = 5.715$ cm	6-42
6.46 Graphite-Epoxy 30.48 cm Radius Cylindrical Shell with Centered 10.16 cm Cutout and Free Edges Loaded in Axial Compression	6-46
6.47 24×24 Element Meshes for Axially Loaded, Composite, Cylindrical Shell	6-48
6.48 Predicted Compressive Load for Prescribed Axial Displacement for Composite Cylindrical Shell Panel $[0/-45/45/90]_s$ without Cutout	6-49
6.49 Evolution of Plastic Zones for Clamped-Free, Composite Cylindrical Shell Panel $[0/-45/45/90]_s$ without Cutout. $w = 0.00508$ cm	6-49
6.50 Evolution of Plastic Zones for Clamped-Free, Composite Cylindrical Shell Panel $[0/-45/45/90]_s$ without Cutout. $w = 0.0254$ cm	6-50
6.51 Evolution of Plastic Zones for Clamped-Free, Composite Cylindrical Shell Panel $[0/-45/45/90]_s$ without Cutout. $w = 0.04572$ cm	6-50
6.52 Predicted Compressive Load for Prescribed Axial Displacement for Composite Cylindrical Shell Panel $[0/-45/45/90]_s$ with 10.16 cm Cutout	6-52
6.53 Evolution of Plastic Zones for Clamped-Free, Composite Cylindrical Shell Panel $[0/-45/45/90]_s$ with a Cutout. $w = 0.00254$ cm	6-52
6.54 Evolution of Plastic Zones for Clamped-Free, Composite Cylindrical Shell Panel $[0/-45/45/90]_s$ with a Cutout. $w = 0.0381$ cm	6-53

Figure	Page
6.55 Evolution of Plastic Zones for Clamped-Free, Composite Cylindrical Shell Panel [0/-45/45/90] _s with a Cutout. $w = 0.0508$ cm	6-53
6.56 Hinged Apex-Loaded Graphite-Epoxy Spherical Shell Cap	6-56
6.57 Refined Mesh Used for Quasi-Isotropic, Hinged, Spherical Shell Cap Models	6-57
6.58 Equilibrium Curves for Transverse Point Loaded Quasi-Isotropic [0/-45/45/90] _s Spherical Shell Cap - C200, C201, & C211 Theories	6-59
6.59 Evolution of Plastic Zones for Hinged [0/-45/45/90] _s Composite Spherical Shell Panel. $w = 0.1905$ cm	6-59
6.60 Evolution of Plastic Zones for Hinged [0/-45/45/90] _s Composite Spherical Shell Panel. $w = 0.286$ cm	6-59
6.61 Evolution of Plastic Zones for Hinged [0/-45/45/90] _s Composite Spherical Shell Panel. $w = 0.505$ cm	6-60
6.62 Equilibrium Curves for Transverse Point Loaded Quasi-Isotropic [0 _g] Spherical Shell Cap - C200, C201, & C211 Theories	6-62
6.63 Evolution of Plastic Zones for Hinged [0 _g] Composite Spherical Shell Panel. $w = 0.1905$ cm	6-62
6.64 Evolution of Plastic Zones for Hinged [0 _g] Composite Spherical Shell Panel. $w = 0.286$ cm	6-63
6.65 Evolution of Plastic Zones for Hinged [0 _g] Composite Spherical Shell Panel. $w = 0.505$ cm	6-63
G.1 Master Flow Chart of Elasto-Plastic Algorithm	G-2

Figure	Page
G.2 Flow Chart of the STIFF Subroutine for the Elasto-Plastic Algorithm, Part 1	G-3
G.3 Flow Chart of the STIFF Subroutine for the Elasto-Plastic Algorithm, Part 2	G-4

LIST OF TABLES

Table	Page
4.1 Definitions of Elemental Codes for Variations of Theory	4-46
5.1 Definitions of Elemental Codes for Variations of Elastic Theory	5-2
5.2 Comparison of Flat Plate Displacement (cm) Results for Various Geometric Nonlinear Theories	5-4
5.3 Equilibrium Point Load (10^3 N) Predicted for Prescribed Transverse Displacement of Isotropic Cylindrical Arch ($w = 10.16 - 40.64$ cm)	5-7
5.4 Equilibrium Point Load (10^3 N) Predicted for Prescribed Transverse Displacement of Isotropic Cylindrical Arch ($w = 50.8 - 71.12$ cm)	5-8
5.5 Predicted Load (N) for Prescribed Center Transverse Displacement (cm) of 0.635-cm Hinged-Free Isotropic Cylindrical Shell Panel ($w = 0.254 - 1.27$ cm)	5-13
5.6 Predicted Load (N) for Prescribed Center Transverse Displacement (cm) of 0.635-cm Hinged-Free Isotropic Cylindrical Shell Panel ($w = 1.524 - 2.54$ cm)	5-13
5.7 Convergence Study for Quasi-Isotropic Shell Panel	5-17
5.8 Transverse Center Point Load (10^3 N) Predicted for Prescribed Transverse Displacement of a 0.635-cm Hinged-Free Quasi-Isotropic Cylindrical Shell Panel	5-18
5.9 Transverse Center Point Load (N) Predicted for Prescribed Transverse Displacement (cm) of a 0.102-cm, Clamped-Free Quasi-Isotropic Cylindrical Shell Panel, $[0/-45/45/90]_s$	5-24

Table	Page
5.10 Axial Displacement vs Transverse Displacement and Load for a 30.48-cm Radius, 30.48-cm 30.48-cm, Quasi-Isotropic Cylindrical Shell Panel with Centered 10.16-cm Cutout under Axial Compression Load - C101 and C201 Theories	5-35
5.11 Axial Displacement vs Transverse Displacement and Load for a 30.48-cm Radius 30.48-cm 30.48-cm Quasi-Isotropic Cylindrical Shell Panel under Axial Compression Load - C101 and C201 Theories	5-35
5.12 Predicted Load (N) for Prescribed Center Transverse Displacement (cm) of 0.04-cm, Hinged, Isotropic, Spherical Shell Cap	5-42
5.13 Predicted Load for Prescribed Transverse Displacement of Hinged Quasi-Isotropic $[0_8]$ Spherical Shell Cap	5-46
5.14 Predicted Load for Prescribed Transverse Displacement of Hinged Quasi-Isotropic $[0_2/90_2]_s$ Spherical Shell Cap	5-47
5.15 Predicted Load for Prescribed Transverse Displacement of Hinged Quasi-Isotropic $[0/-45/45/90]_2$ Spherical Shell Cap	5-49
6.1 Definitions of Elemental Codes for Variations of Plastic Theory	6-2
6.2 Predicted Load for Prescribed Transverse Displacement of Simply Supported, Elastic Perfectly-Plastic, Isotropic Plate	6-4
6.3 Equilibrium Point Load (10^3 N) for Prescribed Transverse Displacement (cm) of Perfectly Plastic, Isotropic, Cylindrical Arch	6-10
6.4 Predicted Equilibrium Load (10^3 Units) for Prescribed Transverse Displacement of Pinched, Perfectly- Plastic, Isotropic Cylinder	6-17

Table	Page
6.5 Predicted Equilibrium Load (N) for Prescribed Transverse Displacement (cm) of Hinged, Elastic Perfectly-Plastic, Isotropic Spherical Shell Cap	6-24
6.6 Predicted Equilibrium Load (10^3 N) for Prescribed Axial Displacement (cm) of a 2.134-cm Clamped-Free Quasi-Isotropic Gr/PEEK Tensile Coupon	6-31
6.7 Predicted Transverse Equilibrium Load (N) for Prescribed Transverse Displacement (cm) of 0.102-cm, Clamped-Free, Quasi-Isotropic, Cyindrical Shell Panel, [0/-45/45/90] _s	6-40
6.8 Predicted Total Compression Load (10^3 N) for Prescribed Axial Displacement (cm) of Clamped-Free, 30.48-cm \times 30.48-cm, Quasi-Isotropic Cylindrical Shell Panel - Experimental and C2XX Theories	6-48
6.9 Predicted Total Compression Load (10^3 N) for Prescribed Axial Displacement (cm) of Clamped-Free, 30.48-cm \times 30.48-cm, Quasi-Isotropic Cylindrical Shell Panel with a Centered 10.16-cm Cutout - Experimental and C2XX Theories	6-51
6.10 Predicted Equilibrium Load (10^3 N) for Prescribed Transverse Displacement (cm) of Hinged, Quasi-Isotropic [0/-45/45/90] ₂ Spherical Shell Cap	6-58
6.11 Predicted Equilibrium Load (10^3 N) for Prescribed Transverse Displacement (cm) of Hinged, Quasi-Isotropic [0 ₈] Spherical Shell Cap	6-61

LIST OF SYMBOLS

a	one half of the finite element planform in the s_1 direction
a_{ij}	anisotropic interaction parameters
A_α	Lame' parameters
$A_{ij} - T_{ij}$	higher-order elasticity arrays of Eqn (4.87)
\vec{a}_α	covariant basis vectors
$a_{\alpha\beta}$	elements of the covariant surface metric tensor
b	one half of the finite element planform in the s_2 direction
$b_{\alpha\beta}$	elements of the curvature tensor
C_{ij}	elasticity constants
$C_{ij}^{(p+r)}$	higher-order elasticity arrays of Eqs (4.104)-(4.111)
$C_{ij}^{*(p+r)}$	higher-order elasticity or elastic-plastic arrays, including material transformation, of Eqs (4.112)-(4.114)
$C_{ij}^{ep(p+r)}$	higher-order elastic-plastic arrays of Eqs (4.125)-(4.128)
\vec{dr}	incremental position vector
ds	length of infinitesimal line segment
ds^*	deformed length of infinitesimal line segment
dA_n	two-dimensional domain of an individual element n
dy	incremental shell curvilinear coordinates

dy^*	deformed incremental shell curvilinear coordinates
$\{d(\xi,\eta)\}$	a column array of continuum displacement parameters
$[\hat{D}(\xi,\eta)]$	an array of nodal interpolation functions in natural coordinates
$[\hat{D}(s_1,s_2)]$	an array of nodal interpolation functions in shell coordinates
E	isotropic elastic modulus
E_i	orthotropic elasticity moduli
\vec{e}_α	orthonormal basis vectors
$\vec{e}_{\alpha,\beta}$	derivatives of the orthonormal basis vectors
e_{ij}	elements of Cauchy strain tensor
$\{F^k\}$	components of prescribed forces
\vec{g}_i	orthogonal basis vectors
\vec{g}_i^*	deformed orthogonal basis vectors
G_{ij}	shear moduli
g_{ij}	elements of the metric tensor
g_{ij}^*	elements of the deformed metric tensor
h	shell thickness
h_i	scale factors
$[H_k]$	an array of Hermitian shape functions
$[H_i^p]$	a symmetric array of the constant coefficients of terms in ϵ_i (Eq 4.118)

	containing the product of two displacement parameters
$I(\xi, \eta)$	Gaussian quadrature integral evaluated at Gauss integration points (ξ, η)
$[J]^{-1}$	inverse of Jacobian matrix
k	curvature constant, $= -4/(3h^2)$
k_i	Ramberg-Osgood coefficients for nonlinear $\sigma - \epsilon$ curve
$[K]$	an array of constant stiffness coefficients
$[\hat{K}]$	an element independent array dependent upon $\{L_i^P\}$
l_i	direction cosines
$\{L_i^P\}$	a column array of the constant coefficients of terms in ϵ_i (Eq 4.118) containing only one displacement parameter
n_i	Ramberg-Osgood exponent for nonlinear $\sigma - \epsilon$ curve
\vec{n}	unit normal vector
$[N_K]$	an array of linear Lagrangian interpolation functions
$[N_1]$	an array of nonlinear coefficients with each term dependent on one of the displacement parameters ($[N_1]$ is linear in terms of displacement)
$[\hat{N}_1]$	an element independent array dependent upon $\{d\}$, $\{L_i^P\}$, and $[H_i^P]$
$[N_2]$	an array of nonlinear coefficients with each term dependent on the product of two displacement parameters ($[N_2]$ is quadratic in terms of displacement)
$[\hat{N}_2]$	an element independent array dependent upon $\{d\}$ and $[H_i^P]$
O	origin

$\{P^k\}$	components of body forces
Q_{ij}	reduced stiffness
\bar{Q}_{ij}	transformed reduced stiffnesses
$\{q\}$	a column array of nodal displacement parameters
$\{\Delta q\}$	a column array of incremental nodal displacement parameters
$[Q_k]$	an array of quadratic Lagrangian interpolation functions
R_α	surface radii of curvature
\vec{r}	position vector to undeformed coordinates
\vec{r}^*	position vector to deformed coordinates
$\{R\}$	a column array of nodal loads
S	shell mid-surface
\vec{t}	unit tangent vector
U	internal potential energy
U_1	internal potential energy for in-plane terms
U_1	internal potential energy for shear terms
u	displacement in 1-direction
\vec{U}	displacement vector
$\vec{V}(\theta_\alpha)$	vector field on the middle surface of the shell

$\overrightarrow{V}_{,\alpha}$	derivatives of vector field
v	displacement in 2-direction
w	displacement in 3-direction
$W_i W_j$	weighting factors
y_i	shell curvilinear coordinates
z	distance in the normal direction from shell mid-surface
α, β, λ	terms in Eq (3.73) to determine various kinematic theories
Δ	denominator term in elasticity array
ϵ_{ij}	elements of physical strain tensor
$\bar{\epsilon}$	effective strain
$\bar{\epsilon}^p$	effective plastic strain
ξ, η	natural coordinates of the finite element
ξ_i	coordinates in the deformed coordinate system
$\xi_{i,j}$	Jacobian transformation matrix from 2nd Piola-Kirchhoff stress to Cauchy stress
$\gamma_\alpha, \phi_\alpha, \theta_\alpha$	degrees of freedom in kinematic
Π_p	potential energy
$\delta \Pi_p$	first variation of potential energy
Γ	inverse of the Jacobian matrix
γ_{ij}	elements of Green's strain tensor

ν	isotropic Poisson's ratio
ν_{ij}	orthotropic Poisson's ratio
ϕ	ply orientation angle
γ_α	rotational degree of freedom, bending of normal
σ_{ij}	elements of 2nd Piola-Kirchhoff stress tensor
σ^E_{ij}	elements of Cauchy stress tensor
σ_{ijY}	orthotropic yield stresses
θ_α	lines of constant curvature, coordinate curves
χ_i	coordinates in the undeformed coordinate system
$\chi_{i,j}$	Jacobian transformation matrix from Green's strain to Cauchy (Almansi)strain
∇	user specified convergence tolerance

ABSTRACT

A two-dimensional, geometrically and materially nonlinear shell theory applicable to arbitrary geometries described by orthogonal curvilinear coordinates and encompassing large displacements, moderate rotations for large strain situations has been developed. Additionally, the theory includes Jacobian transformation matrices, based on displacement parameters, for the Cauchy-2nd Piola-Kirchhoff stress-state and the Cauchy(Almansi)-Green strain-state transformations. A layered material approach is included for the elasto-plastic analysis to allow for variation of plasticity through-the-thickness. Doubly curved 20, 28, and 36 degree-of-freedom finite elements are defined based on specialization of the theory to spherical coordinates. The computer program includes algorithms for linear and nonlinear problems. Post-collapse nonlinear solutions are found through a displacement-control incrementation scheme. This provides solutions to classical von Karman flat plate and Donnell spherical shell equations, intermediate nonlinear von Karman flat plate and Donnell spherical shell equations, and large displacement and moderate rotational formulations.

For deep shells that exhibited large rotations ($\psi_i > 15^\circ$) and displacements ($u, w > 5h$, h = shell thickness) over 15-20% of the shell's surface, the Lagrangian constitutive relations (including the Jacobian transformation matrices for the stress- and strain-states) should be included to accurately reflect the variation of the material coordinate system with respect to the structural axis system. This variation usually occurs as a decrease in the shell's stiffness, thereby reducing the buckling or snapping load by 10-25% in magnitude with little or no increase in displacement. Convergence tolerances remained the same as for the general, nonlinear, Cauchy elastic solutions. The displacement increments, and therefore the number of iterations, were chosen to be 1/10th - 1/15th the total displacement desired for the particular problem.

For those plates and shells that exhibited large strains ($\epsilon_i > 2.25\%$) along with large rotations ($\psi_i > 15^\circ$) and displacements ($u, w > 5h$, h = shell thickness) over 15-18% of the outer surface, the elasto-plastic constitutive relations need to be included to accurately reflect the reduction in shell stiffness due to the presence of plasticity occurring along the outer surface(s). For composite materials, an additional indicator is the ratio of $(\sigma_{12Y}/\sigma_{11Y})$ yield stresses which indicate the influence of the material's shear stiffness. Both Gr/PEEK and Gr/Ep exhibit significant depen-

dence upon the shear stiffness and are significantly influenced (severe reduction of shell stiffness) by the presence of small amounts of plasticity. Peak buckling or snapping loads were reduced by 18-45% and corresponding displacements increased by 12-27% (compared to the elastic solutions) when the elasto-plastic material model was included in the analysis. To maintain similar convergence tolerances with the elastic solutions, increments of displacement were reduced by one-half to one-fourth of the elastic solutions, with the number of iterations to achieve convergence for each increment rising by at least an order of magnitude. Thus, the CPU times for the elasto-plastic solutions, compared to the elastic solution, for a particular shell problem increase by 200-500% depending upon the material properties, number of elements, and the boundary conditions applied.

The software and user's manual is maintained by the Aeronautics & Astronautics Department of the Engineering School (AFIT/ENY). The point of contact is Dr Anthony Palazotto.

NONLINEAR GEOMETRIC & MATERIAL BEHAVIOR OF COMPOSITE SHELLS WITH LARGE STRAINS

1. Introduction

Recent interest in composite shell analysis has been generated by the use of fiber-reinforced composite materials for aerospace applications. A second factor in the proliferation of composite shell research is the use of modern digital computers. With computers, solutions can now be found for problems which before were impossible to solve analytically. In particular, problems involving geometric and material nonlinearities can be solved by numerical methods.

In 1987, Noor and Atluri [134] indicated several compelling reasons for vigorously developing computational structural mechanics (see also Noor and Burton [135, 137] and Noor [138]). First, there are unsolved practical problems awaiting numerical solution. These include impact response, dynamics of flexible structures, thermoviscoplastic response of propulsion systems, and future flight vehicle design. Also, fundamental mechanics concepts such as finite strain inelastic material behavior are currently being explored. Secondly, computational structural mechanics is needed to reduce the dependence on testing which is often expensive in terms of manpower and material. Noor and Atluri also indicate the development of efficient finite elements for modelling curved shell structures as an area of continuing research activity. Wempner states in a 1989 review article [231], "Clearly, the theory and approximation of inelastic shells pose intellectual and practical challenges for current investigators and engineers." Recent research on shell structures at the Air Force Institute of Technology is actively supported by the US Air Force Office of Scientific Research [41, 42, 48, 49, 51, 81, 82, 154 - 161, 197, 198, 207, 208, 217, 220, 223, 224]. This research on geometrically nonlinear behavior of cylindrical laminated composite shells is restricted to elastic material response. The extension to include finite-strain nonlinear material response as a result of large deformations with moderate rotations and curvatures is feasible.

Composite shell structures are used in many US Air Force and defense-related systems because of the inherently high strength-to-weight ratios of composite shell. Historically, thin isotropic shells have been analyzed for many years according to the linear elastic theory formulated by A.E.H. Love [114] in the late 1800's. Love's theory assumes normals to the shell's mid-surface remain straight and normal during deformation. This assumption, like the Kirchhoff assumption for flat plates, implies transverse shear strain and stress are zero throughout the shell. Also, since the shell is assumed to be very thin compared to its other characteristic lengths, many terms in the equations are approximated (e.g., terms with radius in the denominator are assumed negligible). More recently, Donnell [55], Mushtari, and Vlasov [227] independently derived comparable theories for thin elastic shells that included nonlinear terms (functions of transverse displacement) for the in-plane strains. These theories, however, still ignored transverse shear and most terms with the radius in the denominator.

In general, shell theories that ignore transverse shear effects will predict stiffer behavior than experimental data show. Inclusion of transverse shear effects reduces this stiff behavior. Like Love's theory, the newer Donnell, Mushtari, and Vlasov theories invoked the Kirchhoff hypothesis. Thus, they also ignored transverse shear strain and stress. For thick shells, however, the transverse shear terms can not be ignored in all cases. Likewise, transverse shear terms become more significant with the introduction of anisotropic composite materials. This is primarily due to the small transverse shear modulus of fiber-reinforced composite materials.

During the last two decades, many composite shell problems with transverse shear-effects included have been solved using numerical solution techniques. Some investigators have solved these problems using fully three-dimensional models. These models, however, generally require excessive computational times. They may also exhibit singularities and other mathematical problems when used to analyze thin shells. These singularities occur due to the term $h/2$ becoming very small as $h \rightarrow 0$ for a thin shell. Depending upon the precision of the computer, and the complexity of the equations governing normal stress (σ_3) and normal strain (ϵ_3), as $h \rightarrow 0$ quantities with $(h/2)$ in the denominator begin to approach infinity. Other investigators have solved these problems using shell theories, which require less computational effort, with either first-order or higher-order transverse shear deformation.

The "order" of transverse shear deformation theories refers to the highest order polynomial, in

terms of the thickness coordinate, used to describe the assumed displacement field. This does not, in general, imply that higher-order shear theories have more independent degrees of freedom. The first-order transverse shear deformation (FTSD) theories use shear correction factors and reduced integration. These artifices compensate for the theoretically incorrect distribution of transverse shear strain. The higher-order transverse shear deformation (HTSD) theories allow normals to the shell's mid-surface to rotate from normal and also to warp. This assumption results in a transverse shear strain distribution that is parabolic through the thickness of a flat plate. Most previous theories for geometrically nonlinear shell problems with HTSD theory have retained some nonlinear strain-displacement terms for the in-plane strain components. Most, however, have also ignored nonlinear strain-displacement terms and the effect of higher-order thickness expansions for transverse shear components.

Numerical analysis of laminated composite shells, including geometric and material nonlinearities is relatively a recent occurrence (see [10, 28, 40, 46, 48, 62, 67, 69, 102, 118, 145 - 147, 160, 164, 189, 0207]), again due to the advent of increasingly powerful high-speed computer work stations. The composite laminates are treated as an equivalent single layer [32] or as a degenerated 3-D continuum [34, 37, 48, 154, 207]. The geometric nonlinearity used in single-layer theories is analogous to the von Karman relations for plates or the Donnell relations for shells, whereas the full nonlinearity is used in the degenerated 3-D theories. The material nonlinearity has been approached from either *micromechanics* or *macromechanics* points of view. In the micromechanics approach, the matrix is considered as an elastic-plastic material while the fibers are considered to be brittle-elastic. There are a multitude of papers published regarding various theories and methods, most notably Aboudi [1, 2] and Dvorak [58]. However, since the global structural response of the shell is a primary interest of this research, a micromechanical model is not appropriate. In a macromechanical approach for composites, some attempt is made in determining the in-plane interaction of the fiber orientation and the material coordinate system and the analysis is usually carried on an individual ply basis. Failure and yielding are allowed to occur independently on each ply. Several methods have been published in this area. Hahn and Tsai [73, 74] modelled nonlinear shear response of a composite by introducing a complementary elastic energy density function which produced fair results.

The anisotropic plasticity theory of Hill [78 - 80] has led many subsequent researchers to

develop constitutive models. Hill originally proposed his theory to model weakly orthotropic behavior typically found in cold rolled metals. Several author's have suggested extensions to Hill's theory. Hu [85] and Jensen, et al [93] proposed work hardening rules. Dubey and Hiller [60] developed a more general yield criterion which was an associated flow rule based upon invariant principles. Shih and Lee [203] formulated a simple extension which allows distortion of the yield surface and variations of the anisotropic yield parameters during deformation. Durocher and Palazotto [61], formulated a finite difference technique to analyze the buckling equations of anisotropic plates. They developed a series of Ramberg-Osgood directionally oriented stress-strain equations to characterize the nonlinear portion of the stress-strain curves for a particular material of interest. By incorporating the Ramberg-Osgood parameters into Hill's anisotropic plasticity theory, they were able to characterize either perfectly plastic or work-hardening materials quite easily. Chandrashekhara and Reddy [32, 176] developed a 2-D shell element that included the transverse shear stresses and the modified von Mises yield function with the in-plane interaction term. Most of the methods published incorporated an updated Lagrangian approach with either a FTSD or HTSD theory while ignoring most of the in-plane nonlinear strain-displacement terms. None of the published literature allowed for a large strain formulation which implies the Eulerian coordinate system and the Lagrangian coordinate system are no longer coincident from an experimental material point-of-view.

For this research, the full nonlinear strain-displacement relations for the in-plane strain components with linear strain-displacement relations for the transverse strain components of a spherical shell were developed. These relations were then incorporated into a proven finite element formulation to investigate the accuracy of various geometries for curvature and displacements and the effect of a HTSD theory with a nonlinear material analysis for large strains.

A review of related research in the areas of composite shells, transverse shear deformation, and nonlinear material analysis is included in Chapter 2. Some theoretical concepts are presented in Chapter 3. These concepts, common in most published literature addressing the subject of this dissertation, were not independently developed by this author. They are included in the dissertation to assure a common understanding of the theoretical background of this research. The theoretical discussion necessary to develop the new finite element formulation, by the author, is presented in Chapter 4. Since the strain equations for this theory are very lengthy, abridged equa-

tions are used in Chapter 4. The unabridged equations of strain components are listed in the appendices. Typical composite shell problems of interest to the USAF and some classical isotropic shell problems were investigated to determine the effect of spherical geometry and nonlinear material properties with a HTSD theory. A significant tool used in the development of this theory was a computerized symbolic manipulation code called MACSYMA [119]. Use of a symbolic code, like MACSYMA, allows the formulation of the nonlinear HTSD theory for cylindrical and spherical composite shells. The use of one "symbolic input program" to generate the variations of theory provides reliability and confidence that the FORTRAN codes were correctly generated. Part of the symbolic input program is included as an appendix since it played such an important role in this research effort.

2. Literature Review

Studying large deformation nonlinear material behavior of composite shells provides unique data not currently published in the technical literature. Literally hundreds of papers were published in the last several years on related topics. One of the most recent review articles by Noor and Burton [135] reviews 400 published works on computational models for multi-layered composite shells. Thin composite shells are becoming important in structures due to their high strength and stiffness efficiency. However, these thin shells are susceptible to buckling which is inherently a nonlinear phenomenon. The nonlinearities are attributed to the occurrence of large rotations, and the coupling of curvatures and large membrane forces. In addition, as the shell's thickness is increased or laminated composite material is introduced, the effects of parabolic transverse shear distribution is more important. Classical shell theories based on the Kirchhoff-Love hypothesis neglect the transverse shear distribution. Hence, the shell element is excessively stiff as the thickness is increased. Typical linear and simple nonlinear shell models often drastically overestimate buckling loads. Conversely, these models underestimate transverse displacements and stresses. Most advanced composites have a low ratio of transverse shear modulus to in-plane modulus. Thus, transverse shear deformation plays an important role in reducing effective flexural stiffness of laminated plates and shells made of composites.

Knight, Starnes, and Williams [97] investigated the postbuckling response and failure characteristics of graphite-epoxy cylindrical panels loaded in axial compression. They used the STAGSC-1 computer code [4] to determine postbuckling response of the cylindrical shells and panels and compared results with experimental data. They determined that a severe reduction in load occurs at buckling and that failure begins near regions containing severe local bending gradients. Knight et al. pointed out that many previous studies of the postbuckling behavior of composite cylindrical panels were extensions of classical methods. These often ignored the effects of large rotations. They determined that even low values of normalized applied load can cause high local bending gradients. Local failures occurred in regions of large radial displacements and severe bending gradients which cause large surface strains [97:132]. They were able to predict responses that correlated well with experimental data up to buckling. They blame the influence of local failures for deteriorating the correlation after buckling. They note STAGSC-1 assumes the

composite material system remains linearly elastic throughout the analysis. This assumption is inaccurate since many composites suffer severe reduction in local stiffness as a result of local failures. Furthermore, the local failures which occurred near regions of large changes in curvature cannot be analytically modelled by STAGSC-1 [97:147]. Using both Tsai-Wu and a maximum strain failure criteria, they were able to predict the load level and location of the local failures, but not the dominant failure mode. This study points out the need to address nonlinear material response occurring with the large rotations for this class of problems and materials.

Palazotto and others also used the STAGSC-1 computer code [156, 197, 198]. They compared analytical predictions of buckling response to experimental work on graphite-epoxy cylindrical panels. Their work included the effects of rectangular unreinforced cutouts. They also recorded large radial displacements, large curvatures over small regions, and severe curvature gradients for loads as low as ten percent of the critical buckling load. As before, the assumption of linearly elastic material response is used for the STAGSC-1 code. Under small loads, no permanent damage occurred, and thus some investigators argue the linearly elastic material assumption is adequate. These studies and the one by Knight suggest these severe local bendings warrant the use of a better model. A model capable of accurately predicting both geometric and material nonlinear response should be more suitable.

Yang and Liaw [236] studied the effects of plasticity on the dynamic buckling response of isotropic shells. Their model used a thin-shell Kirchhoff-Love theory with a von Mises yield criterion and the Prandtl-Reuss flow law. They determined a 50 percent reduction in the static buckling load occurred for perfect spherical caps when plasticity is included in the analysis [236:482]. Larger rotations and curvatures may occur as a result of composite anisotropy for these problems. This implies the effect of an inelastic model for composite shells may be more significant than for isotropic shells.

2.1 Nonlinear Material Behavior

A finite element model for the nonlinear analysis of composite shells must approximate the physical phenomena occurring in an extremely complex nonlinear problem. Some of the com-

plexities, e.g. the coupling of membrane and bending effects due to the curvature of the shell and the effect of transverse shear distribution, were previously considered. Other complexities, e.g. the effect of nonlinear material response and the effects of constituent behavior under large strain, are considered in this research. Many studies were performed after making various assumptions to simplify these complexities. For composite shells, some studies use a first-order transverse shear theory with bi-linear elastic-plastic material behavior [6, 10, 13, 16, 17, 20, 31, 36, 57, 58, 67, 88, 89, 90, 101, 102, 111, 118, 145, 146, 149, 150, 151, 215, 218, 230]. Several studies used a layered approach to yield parabolic distribution of transverse shear strains through-the-thickness. Some investigators used a higher-order transverse shear theory or more sophisticated nonlinear material behavior models, but only for specific shells or isotropic materials (see [21, 22, 23, 28, 46, 48 - 51, 53, 56, 62, 71, 81, 82, 99, 162, 163, 174 - 182, 187, 188, 206] or [96, 103 - 106, 158, 164, 174, 176, 194, 195] for details).

This research will formulate material response model for a degenerated shell element with higher-order transverse shear deformation with large strains. The first-order shear and bi-linear formulations used in [81, 82, 102, 145] may not adequately account for the effect of transverse shear distribution. Furthermore, their formulations allow for small rotations only. The study by Knight et al. accounts for some rotational effects, but does not adequately account for large local curvature and transverse shear deformation effects.

The response of the structure to loading is critically dependent upon accurate constitutive modelling of material behavior. Simple material models such as linear isotropic and linear kinematic hardening, may be inadequate for some engineering applications. Problems involving large nonlinear material deformation and failure may require rate-dependent plasticity models [54, 112, 147, 172, 191]. These models are developed by using phenomenological models of small or finite strain, plastic material behavior or by micromechanical models of material behavior [1, 2, 65, 100, 113, 115, 116].

Extensive work is devoted to micromechanical models for predicting the behavior and failure characteristics of materials. In the context of developing a shell theory, the use of a micromechanical model is not appropriate. Our intent is to reduce the computational effort by modelling the shell as a quasi two-dimensional structure.

Many investigators used a form of the von Mises yield criteria to determine the onset of non-

linear material behavior for ductile materials. This theory is effectively modified for use with composite materials [67, 102, 145, 236]. Other yield criteria for possible comparisons are the Tsai-Wu, Tsai-Hill, Hahn-Tsai, and Sandhu failure criteria to establish the onset of plasticity. These are not yield criteria, i.e. they do not predict elastic-plastic behavior. They are simply criteria that predict the initial failure of a fiber-matrix lamina. As such, they are not particularly useful for an elastic-plastic, laminated composite shell analysis. The first two criteria are considered linear criteria, i.e. only accurate up to the point where the stress-strain relationship is still linear. This is not a useful assumption for many polymeric matrix composite materials having a nonlinear stress-strain relation in shear. The Hahn-Tsai and Sandhu criteria are nonlinear, but assume all transverse stresses are zero. Chen compared ultimate load predictions for angle-ply laminate using Hahn-Tsai (nonlinear) and Tsai-Hill (linear) yield criteria [40]. For fiber orientation angles of 0 degrees or 75-90 degrees, the two theories predict ultimate tensile load to within 1/2 of a percent. However, for angles of 15-60 degrees, the linear analysis predicts a 10-20 percent greater ultimate tensile load than the nonlinear analysis. This implies the linear analysis is unconservative for laminates with 15-60 degree lamination angles.

Another method of analyzing composite materials is the use of the independent failure criteria. This method assumes the failure modes of delamination, fiber breakage, and matrix cracking are independent, but each has an effect upon the element's stiffness matrix. This method was used by several investigators to analyze progressive failure of composites. Ochoa and Engblom [142] used a fiber failure, matrix failure, and delamination as their failure criteria. Their matrix failure criteria is based upon those of Hashin [75]. Hwang and Sun [91] used failure criteria based upon the Tsai-Wu theory and Hashin's theory [91]. Their work also included fiber failure, matrix failure, and two forms of delamination failure. Fiber or matrix failure effects are modelled by setting the appropriate entries in the element stiffness matrix to zero. Reference [142] uses a two-dimensional shell model and if delamination occurs, the analysis is stopped. Reference [91] uses a full three-dimensional model. If delamination occurs, a new finite element configuration is modelled at the free surface at the new ply interface. Singularity crack tip elements are used at the delamination front [91:44]. Ochoa and Engblom [142], however, predict composite response beyond first-ply failure.

This disparity in approach reveals the debate over how to predict progressive failure of com-

posites, an important analytical tool in structural design. A research program developing a theory for collapse of a composite is an area of high interest. The use of composites in the aerospace and transportation industries, where traditionally metals are used, requires a different outlook about residual strength. With metallic structures, adequate analytical tools exist to predict material yielding under service loads, load transfer through damaged structure, and residual strength. With composites however, these analytical tools are not available nor convenient. Thus, the most common failure criteria predict only that a failure of some type occurred in a particular finite element. This information is not enough to determine residual strength of the structure. Composites have shown considerable residual strength after first ply failure (see [33, 40, 97, 121, 130, 142, 143] for example or [155, 157, 190, 196, 211, 212, 213, 215]). The designer may choose a conservative approach and design based upon first ply failure. For advanced high performance aerospace vehicles however, the added weight and cost of the conservative approach may be prohibitive. Thus, the designer should be able to predict progressive failure of the advanced composite structure.

A paradox arises, however, when considering shells with nonlinear material behavior. The large radial displacements and curvatures occurring over a small region, as shown by Knight et al. [97], cause severe gradients in stresses through-the-thickness. Shell theories try to exploit the thinness of the shell. Normal stresses are assumed negligible, and various assumptions are made about the deformation of line elements normal to the shell's mid-surface. These assumptions are made to reduce the three-dimensional problem down to a two-dimensional problem. For a thin shell, various studies have shown the two-dimensional shell can accurately predict the load-displacement response [48, 107, 109]. The two-dimensional theory is acceptable for shell thickness less than $1/5^{th}$ the radius of curvature [48, 207]. Since this research is directed at the load-displacement response of a composite shell with nonlinear material behavior, the two-dimensional shell theory is adequate for this study.

2.2 Curve Shell Finite Element Models

Many research efforts have been conducted in developing reliable and efficient elements for modelling complicated structures. Of particular interest is the development of curved shell elements. According to Noor et al. [134, 135, 137], this area continues to be an active research area.

Many authors advocate the use of thin two-dimensional shell elements and "grow" the parameters in the thickness direction. They increase the number of layers to achieve accurate through-the-thickness stress results. This process is expensive since the number of layers could be excessively high. Other authors use two-dimensional models with higher order approximations or even full three-dimensional models [48, 136, 154, 160, 207, 213]. Noor and Burton indicate the use of both three-dimensional and quasi three-dimensional models for laminated anisotropic plates is expensive. Thus, these methods are not economical for practical composites plates [136]. Most two-dimensional theories are, however, adequate for predicting the gross response characteristics of medium-thick laminated plates and shells.

There are basically two methods of formulating a finite element shell model. The traditional method is a single-field formulation where displacement is the field. A more recent approach is the mixed field formulation. Various schemes for constructing two-dimensional shear-deformation theories for multi-layered shells are available. One approach, an extension of the Kirchhoff hypothesis, results in first-order shear deformation theories.

2.2.1 First-Order Transverse Shear Deformation (FSDT) Theories: These theories assume line elements originally perpendicular to the shell's mid-surface remain straight during deformation, but can rotate from the normal. Thus, through-the-thickness shearstrains are constant. This assumption is closer to reality than the classical Kirchhoff-Love theory, but not exact. The classical theory assumes line elements normal to the undeformed shell mid-surface always remain inextensible, straight, and normal to the deformed mid-surface. Hence, classical theory predicts zero through-the-thickness shear stresses. This assumption was shown to be inaccurate for laminated composite shells. The accepted distribution of the shear stress is some form of a parabolic function. Hence, the FSDT must include a shear correction factor to assure the strain energy associated with the shear deformation is accurate. For isotropic materials, the shear correction factor is a constant $k = 5/6$. For anisotropic materials or for laminated composite materials, these factors are typically not equal to $5/6$. The shear correction factor is a function of geometry, material, and loading conditions. For composites, some investigators assume $k = 5/6$ rather than determine a better approximation. The use of $k = 5/6$ is justified by considering the relationship between the predominant roles of flexural and extensional deformations versus the lesser role of transverse shear in a thin shell. If one wants to accurately determine the through-the-thickness shear distribu-

tion, then other studies [136] have shown that for anisotropic materials or laminated composite materials, the correct shear correction factor in the FSDT is critical.

2.2.2 *Higher-Order Transverse Shear Deformation (HTSD) Theories:* These theories overcome the difficulties of shear correction factors by assuming the line element normal to the shell mid-surface can warp [48 - 51, 107, 160, 175, 176, 179, 198, 208, 223, 224] This assumption allows shear strain to vary through the shell's thickness as a function of the thickness coordinate of the shell. The HSDT still assumes the stress normal to the shell's mid-surface is negligible. These models provide a more accurate estimate of the shell response than the classical theory or FSDT [48, 160, 176, 208, 209].

The FSDT and HSDT are based on the assumption of the normal stress being negligible. Because of this assumption, neither of these theories accurately predict all stresses in the shell. This is because the equilibrium and compatibility equations are not exactly satisfied at all points within the shell. Hence, some investigators use three-dimensional approximations for shell problems [224, 231]. Others use a two-dimensional shell theory to predict gross global responses. Once these are determined, local stresses are computed by numerically integrating the three-dimensional equations of equilibrium [38, 39, 63, 64, 132, 133, 136, 142, 143, 152] These global/local methods efficiently predict accurate stress distributions without resorting to the computational effort required for the full three-dimensional finite element of the shell [64].

2.3 Literature Assessment

No study was published using the proposed theory to predict the load-displacement behavior of composite shells with nonlinear material behavior undergoing moderate deformations and rotations with large strains. The work by Engblom [63, 64] is restricted to thin and moderately thick inelastic shells undergoing small deformations and rotations. As shown by earlier references [97, 156], the collapse analysis and failure of laminated composite shells is preceded by large deformations, rotations, and changes in curvatures. Any analysis of progressive failure assuming linear strain is suspect.

The previous research conducted by Dennis [48, 159] will be extended by this research to include a spherical shell element, the transformation of the constitutive relations from the Cauchy

stress-strain (Eulerian coordinates) to the second Piola stress-Green strain (Lagrangian coordinates), and an incremental model of inelastic isotropic or orthotropic material behavior. The results of this research on inelastic composite shells undergoing snap-through and axial post-buckling deformation will be unique.

3. Theoretical Background

The primary goal of this research was to consider the ability of a nonlinear material with a higher-order transverse shear deformation (HTSD) theory to model deformation of a composite shell undergoing large displacements, rotations, strains, and changes in curvature. In particular, spherical geometry, transformation of the Cauchy stress-strain relations to the 2nd Piola stress-Green strain relations, and elastic-plastic, through-the-thickness material behavior were considered in this research. Many HTSD models have been developed in recent years [48, 180]. These theories are suitable for linear and nonlinear problem solving by a number of numerical solution methods. This chapter of the dissertation includes some theoretical background material. The background material is necessary to assure a common understanding of the concepts underlying the nonlinear HTSD theory. A presentation of the nonlinear HTSD theory developed for this research is included in Chapter 4.

3.1 Surface Geometric Considerations

Components of particular physical quantities, such as displacement, stress, and strain, however, are more generally defined for arbitrary curvilinear coordinate systems as being either covariant or contravariant. These quantities are identified in the text as being covariant or contravariant when the tensorial nature of the quantity is generally accepted in the literature. Conventional tensor notation requires that contravariant quantities be identified by superscripts and covariant quantities be identified by subscripts. This practice is generally followed throughout this dissertation. For convenience, however, coordinates are always identified with subscripts. The basic assumptions of a two-dimensional shell theory are tied to the concepts of a reference surface, the midsurface of the shell, and a local curvilinear coordinate system associated with this surface. When this curvilinear coordinate system is based on lines of principal curvature, which by definition are orthogonal, then the coordinate system is also orthogonal. In an orthogonal coordinate system, the components of the metric tensor form a diagonal matrix. Thus, contravariant and covariant components of tensors are identical. For this research, the author has decided to restrict the theoretical development to orthogonal coordinate systems based upon lines of constant

curvature. This is one of the most common coordinate systems used for analysis of shells [126, 139].

The development of nonlinear strain displacement relations generally begins with the mathematical description of the midsurface geometry. If one considers a surface in a three-dimensional space, then the positions of points on its surface can be defined by

$$\vec{r} = \vec{r}(\theta_1, \theta_2) \quad , \quad (3.1)$$

where \vec{r} is the position vector from the origin O to points on the surface [126, 192]. The parameters (θ_1, θ_2) are defined in a closed and bounded region S in the (θ_1, θ_2) plane. Next, assume the unit normal vector to the surface exists and is $\vec{a}_3(\theta_1, \theta_2)$ and the thickness of the shell is $h = h(\theta_1, \theta_2)$, where $h > 0$. The position vector of a point within the shell can be written in terms of \vec{r} and \vec{a}_3 . This position vector, $\vec{p}(\theta_1, \theta_2, h)$, is given by

$$\vec{p}(\theta_1, \theta_2, z) = \vec{r}(\theta_1, \theta_2) + z\vec{a}_3(\theta_1, \theta_2) \quad , \quad (3.2)$$

where $(\theta_1, \theta_2) \in S$ and $|z| = (1/2)h(\theta_1, \theta_2)$. The (θ_1, θ_2) -plane defined by the S is called the middle surface. The curves defined by the map of $\theta_1 = \text{constant}$ and $\theta_2 = \text{constant}$ are called coordinate curves. These curves define a curvilinear coordinate system with covariant base vectors \vec{a}_1 and \vec{a}_2 given by

$$\vec{a}_1 = \frac{\partial}{\partial \theta_1} \vec{r}, \quad \vec{a}_2 = \frac{\partial}{\partial \theta_2} \vec{r} \quad (3.3)$$

or

$$\vec{a}_\alpha = \frac{\partial}{\partial \theta_\alpha} \vec{r} \quad \alpha = 1, 2, \quad (3.4)$$

An infinitesimal vector connecting two points on the surface with coordinates (θ_1, θ_2) and $(\theta_1 + d\theta_1, \theta_2 + d\theta_2)$ is given by

$$d\vec{r} = \frac{\partial \vec{r}}{\partial \theta_1} d\theta_1 + \frac{\partial \vec{r}}{\partial \theta_2} d\theta_2 = \sum_{\alpha=1}^2 \vec{a}_\alpha d\theta_\alpha \equiv \vec{a}_\alpha d\theta_\alpha, \quad (3.5)$$

where the repeated subscripts imply summation as shown in Eq (3.5). The length of this vector is denoted by ds and is given by

$$(ds)^2 = d\vec{r} \cdot d\vec{r} = (a_\alpha \cdot a_\beta) d\theta_\alpha d\theta_\beta. \quad (3.6)$$

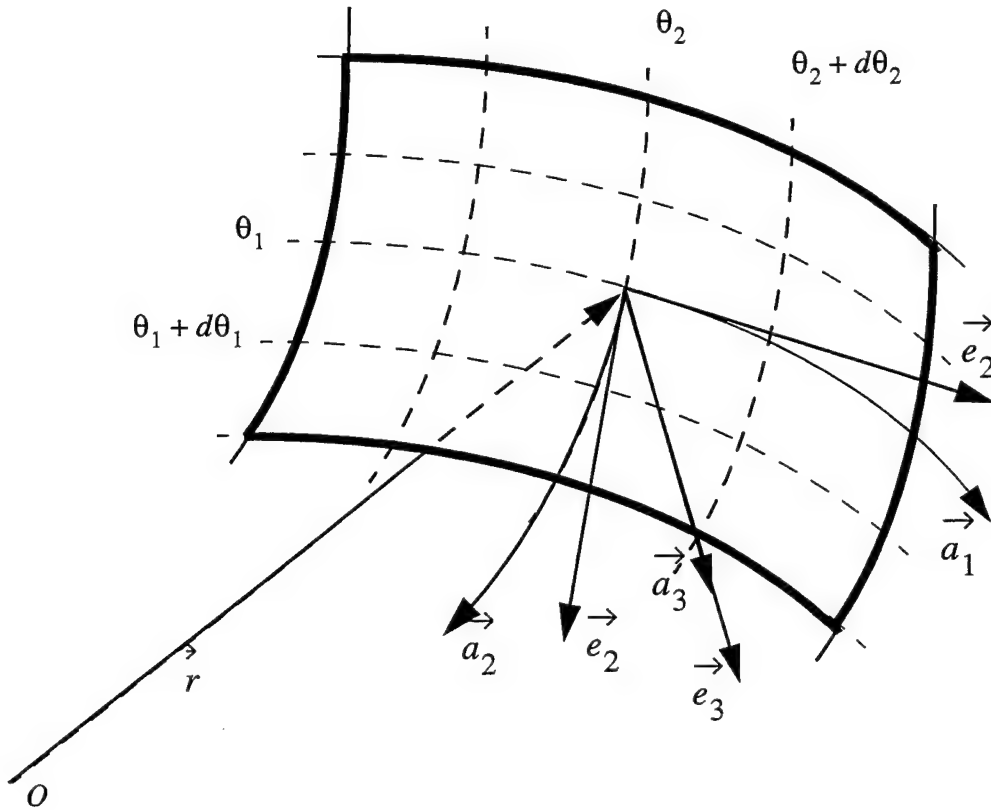


Figure 3.1 Base Vectors and Coordinate Curves [229]

Defining the covariant surface metric tensor as

$$a_{\alpha\beta} = \vec{a}_\alpha \cdot \vec{a}_\beta = a_{\beta\alpha}, \quad (3.7)$$

allows one to write $(ds)^2$ in terms of the covariant surface metric tensor as

$$(ds)^2 = a_{\alpha\beta} d\theta_\alpha d\theta_\beta. \quad (3.8)$$

Equation (3.8) is called the first fundamental form of the surface.

Next, consider a point on the middle surface with coordinates θ_α and a unit vector \vec{t} in the tangent plane at this point. The normal curvature associated with the direction determined by \vec{t} is given by

$$\frac{1}{R} ds = -d\vec{a}_3 \cdot \vec{t}, \quad (3.9)$$

or

$$\frac{1}{R} = -\frac{d\vec{a}}{ds} \cdot \vec{t}. \quad (3.10)$$

If one substitutes Eq (3.5) and (3.6) into Eq (3.10), then one finds

$$\vec{t} = \frac{d\vec{r}}{ds} = \vec{a}_1 \frac{d\theta_1}{ds} + \vec{a}_2 \frac{d\theta_2}{ds} \quad (3.11)$$

and

$$\frac{d\vec{a}}{ds} = \vec{a}_{3,1} \frac{d\theta_1}{ds} + \vec{a}_{3,2} \frac{d\theta_2}{ds}, \quad (3.12)$$

where a comma in the subscripts implies differentiation with respect to the coordinate following the comma. Substituting Eqs (3.11), (3.12), and (3.8) into Eq (3.10) gives

$$\frac{1}{R} = -\frac{\sum_{\alpha, \beta=1}^2 \vec{a}_{3,\alpha} \cdot \vec{a}_\beta d\theta_\alpha d\theta_\beta}{\sum_{\alpha, \beta=1} a_{\alpha\beta} d\theta_\alpha d\theta_\beta} \quad (3.13)$$

The quantity $b_{\alpha\beta}$ can be defined, such that

$$b_{\alpha\beta} = -\vec{a}_{3,\alpha} \cdot \vec{a}_\beta = \vec{a}_\beta \cdot \vec{a}_{3,\alpha} = \vec{a}_3 \cdot \vec{a}_{\alpha,\beta} = b_{\beta\alpha} \quad (3.14)$$

The curvature can now be defined as

$$\frac{1}{R} = \frac{\sum_{\alpha, \beta=1}^2 b_{\alpha\beta} d\theta_\alpha d\theta_\beta}{\sum_{\alpha, \beta=1}^2 a_{\alpha\beta} d\theta_\alpha d\theta_\beta} \quad (3.15)$$

where $b_{\alpha\beta} d\theta_\alpha d\theta_\beta$ is called the second fundamental form of the surface. Thus, the normal curvature is given by the ratio between the first and second fundamental forms.

If one defines the coordinate curves of Figure 3.1 to be lines of principal curvature of the shell, then the θ_1 and θ_2 curves are mutually orthogonal families of curves [126, 139]. In this coordinate system, the lengths A_α of the basis vectors \vec{a}_α are given by

$$A_\alpha = |\vec{a}_\alpha| = \sqrt{\vec{a}_\alpha \cdot \vec{a}_\alpha} \quad (3.16)$$

where the A_α are called the Lamé parameters of the surface.

Next, define mutually orthogonal unit vectors \vec{e}_1 , \vec{e}_2 , and \vec{e}_3 in the directions of the base vectors \vec{a}_1 , \vec{a}_2 , and the normal vector \vec{a}_3 , respectively. These unit vectors are given by

$$\vec{e}_\alpha = \frac{\vec{a}_\alpha}{A_\alpha} \quad (3.17)$$

where $\alpha = 1, 2$.

The derivatives of the orthonormal unit vectors are given by [126:8]

$$\begin{aligned}
 \vec{e}_{1,1} &= -\frac{A_{1,2}}{A_2} \vec{e}_2 + \frac{A_1}{R_1} \vec{e}_3 & \vec{e}_{1,2} &= \frac{A_{2,1}}{A_1} \vec{e}_2 \\
 \vec{e}_{2,1} &= \frac{A_{1,2}}{A_2} \vec{e}_1 & \vec{e}_{2,2} &= -\frac{A_{2,1}}{A_1} \vec{e}_2 + \frac{A_2}{R_2} \vec{e}_3 \\
 \vec{e}_{3,1} &= \frac{A_1}{R_1} \vec{e}_1 & \vec{e}_{3,2} &= \frac{A_2}{R_2} \vec{e}_2
 \end{aligned} \tag{3.18}$$

where R_1 and R_2 are radii of curvature for the $\theta_1 = \text{constant}$ and $\theta_2 = \text{constant}$ curves respectively.

If one now considers a vector field $\vec{v}(\theta_1, \theta_2)$ on the middle surface of the shell, then one can resolve this field in the directions of the orthonormal base vectors \vec{e}_1 , \vec{e}_2 , and \vec{e}_3 as follows

$$\vec{v}(\theta_1, \theta_2) = v_1 \vec{e}_1 + v_2 \vec{e}_2 + v_3 \vec{e}_3 \tag{3.19}$$

Differentiating Eq (3.19) with respect to θ_1 and θ_2 gives

$$\vec{v}_{,\alpha} = v_{i,\alpha} \vec{e}_i + v_i \vec{e}_{i,\alpha} \tag{3.20}$$

where repeated indices imply summation and Italicized letter subscripts have the values 1,2,3 and Greek letter subscripts have values 1,2. If one substitutes Eq (3.18) for the derivatives of the base vectors into Eq (3.20), then the derivatives of the vector $\vec{v}(\theta_\alpha, \theta_\beta)$ are given as follows

$$\begin{aligned}
 \vec{v}_{,1} &= \left(v_{1,1} + \frac{A_{1,2}}{A_2} v_2 - \frac{A_1}{R_1} v_3 \right) \vec{e}_1 + \left(v_{2,1} - \frac{A_{1,2}}{A_2} v_1 \right) \vec{e}_2 + \left(v_{3,1} + \frac{A_1}{R_1} v_1 \right) \vec{e}_3 \\
 \vec{v}_{,2} &= \left(v_{1,2} - \frac{A_{2,1}}{A_1} v_2 \right) \vec{e}_1 + \left(v_{2,2} + \frac{A_{2,1}}{A_1} v_1 - \frac{A_2}{R_2} v_3 \right) \vec{e}_2 + \left(v_{3,2} + \frac{A_2}{R_2} v_2 \right) \vec{e}_3
 \end{aligned} \tag{3.21}$$

One can show that certain relationships between A_1 , A_2 , R_1 , and R_2 must be specified. These relationships are given by Codazzi's equations

$$\left(\frac{A_1}{R_1} \right)_{,2} = \frac{A_{1,2}}{R_2} \quad \left(\frac{A_2}{R_2} \right)_{,1} = \frac{A_{2,1}}{R_1} \tag{3.22}$$

and Gauss's equation

$$\left(\frac{A_{1,2}}{R_1} \right)_{,1} + \left(\frac{A_{1,2}}{R_2} \right)_{,2} = \frac{A_1 A_2}{R_1 R_2} \quad (3.23)$$

3.2 Strain Tensor Definition

In Figure 3.3, consider the displacement of a body in a three-dimensional space from its original undeformed state to a new deformed state denoted by a superscript star. The coordinates y_1 , y_2 , and y_3 are chosen to form an orthogonal curvilinear coordinate system. This system is not the same coordinate system as the two-dimensional (θ_1, θ_2) system of the shell midsurface. In the (y_1, y_2, y_3) system, the original length $(ds)^2$ of the line M to N is given by

$$(ds)^2 = g_{ij} dy_i dy_j \quad (3.24)$$

where g_{ij} is the metric tensor associated with the undeformed curvilinear coordinate system (y_1, y_2, y_3) . The components of g_{ij} are given by the scalar product $\vec{g}_i \cdot \vec{g}_j$.

In the deformed system of coordinates, the distance (ds^*) from point M^* to N^* is given by

$$(ds^*)^2 = g_{ij}^* dy_i^* dy_j^* \quad (3.25)$$

If we use a Lagrangian description of deformation, we attempt to express all variables in terms of conditions prior to deformation [192]. From Figure 3.2, the displacement \vec{u} of point M and the derivatives of \vec{u} are given by

$$\vec{u} = \vec{r}^* - \vec{r} \quad (3.26)$$

$$\frac{\partial \vec{u}}{\partial y_i} = \frac{\partial \vec{r}^*}{\partial y_i} - \frac{\partial \vec{r}}{\partial y_i} = \vec{g}_i^* - \vec{g}_i \quad (3.27)$$

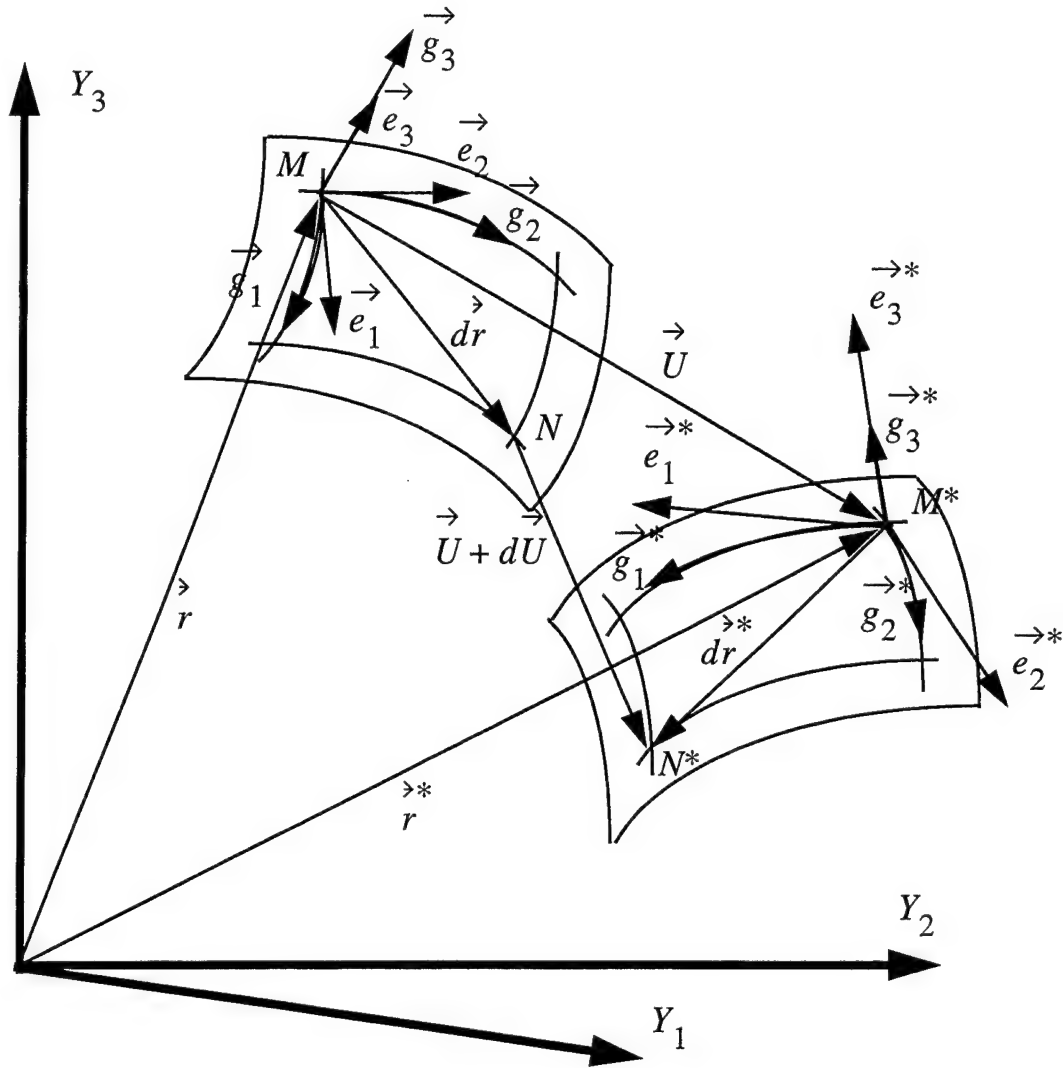


Figure 3.2 Body Before and After Deformation [192, 229]

Combining Eqs (3.24) and (3.25), yields the strain tensor γ_{ij} defined as

$$2\gamma_{ij} = (g_{ij}^* - g_{ij}) \quad (3.28)$$

Substituting Eq (3.27) into Eq (3.28), gives the strain tensor γ_{ij} as

$$2\gamma_{ij} = \vec{g}_i \cdot \frac{\partial \vec{u}}{\partial y_j} + \vec{g}_j \cdot \frac{\partial \vec{u}}{\partial y_i} + \frac{\partial \vec{u}}{\partial y_i} \cdot \frac{\partial \vec{u}}{\partial y_j} \quad (3.29)$$

The orthogonal base vectors $\{\vec{g}_1, \vec{g}_2, \vec{g}_3\}$ are related to a new set of orthonormal base vectors

$\{\vec{e}_1, \vec{e}_2, \vec{e}_3\}$ by the following relationship

$$\vec{e}_i = \frac{\vec{g}_i}{|\vec{g}_i|} = \frac{\vec{g}_i}{\sqrt{\vec{g}_i \cdot \vec{g}_i}} = \frac{\vec{g}_i}{h_i} \quad (3.30)$$

where the h_i are called scale factors [192:118]. The displacement vector \vec{u} can be written in terms of \vec{e}_1, \vec{e}_2 , and \vec{e}_3 at point M as follows

$$\vec{u} = u_1 \vec{e}_1 + u_2 \vec{e}_2 + u_3 \vec{e}_3 \quad (3.31)$$

Substituting Eq (3.31) into Eq (3.29) produces

$$2\gamma_{ij} = \vec{g}_i \cdot \frac{\partial (u_k e_k)}{\partial y_j} + \vec{g}_j \cdot \frac{\partial (u_l e_l)}{\partial y_i} + \frac{\partial (u_m e_m)}{\partial y_i} \cdot \frac{\partial (u_n e_n)}{\partial y_j} \quad (3.32)$$

Next expanding the implied summations on k, l, m , and n over their values of 1, 2, and 3, to get the result

$$\begin{aligned} 2\gamma_{ij} = & \vec{g}_i \cdot \frac{\partial (u_k e_k)}{\partial y_j} (u_1 \vec{e}_1 + u_2 \vec{e}_2 + u_3 \vec{e}_3) \\ & + \vec{g}_j \cdot \frac{\partial (u_l e_l)}{\partial y_i} (u_1 \vec{e}_1 + u_2 \vec{e}_2 + u_3 \vec{e}_3) \\ & + \frac{\partial (u_m e_m)}{\partial y_i} (u_1 \vec{e}_1 + u_2 \vec{e}_2 + u_3 \vec{e}_3) \cdot \frac{\partial (u_n e_n)}{\partial y_j} (u_1 \vec{e}_1 + u_2 \vec{e}_2 + u_3 \vec{e}_3) \end{aligned} \quad (3.33)$$

Using the relationships of Eqs (3.17) and (3.18), the strain components γ_{ij} , for shells, can be written in terms of the displacement components and Lamé parameters [192:136-137] as follows

$$\begin{aligned} \gamma_{11} = & h_1 \frac{\partial u_1}{\partial y_1} + \frac{h_1 u_2}{h_2} \frac{\partial h_1}{\partial y_2} + \frac{h_1 u_3}{h_3} \frac{\partial h_1}{\partial y_3} \\ & + \frac{1}{2} \left(\frac{\partial u_1}{\partial y_1} + \frac{u_2}{h_2} \frac{\partial h_1}{\partial y_2} + \frac{u_3}{h_3} \frac{\partial h_1}{\partial y_3} \right)^2 \\ & + \frac{1}{2} \left(\frac{\partial u_2}{\partial y_1} - \frac{u_1}{h_2} \frac{\partial h_1}{\partial y_2} \right)^2 + \frac{1}{2} \left(\frac{\partial u_3}{\partial y_1} - \frac{u_1}{h_3} \frac{\partial h_1}{\partial y_3} \right)^2 \end{aligned} \quad (3.34)$$

$$\gamma_{22} = h_2 \frac{\partial u_2}{\partial y_2} + \frac{h_2 u_1}{h_1} \frac{\partial h_2}{\partial y_1} + \frac{h_2 u_3}{h_3} \frac{\partial h_2}{\partial y_3} \quad (3.35)$$

$$+ \frac{1}{2} \left(\frac{\partial u_2}{\partial y_2} + \frac{u_1}{h_1} \frac{\partial h_2}{\partial y_1} + \frac{u_3}{h_3} \frac{\partial h_2}{\partial y_3} \right)^2$$

$$+ \frac{1}{2} \left(\frac{\partial u_1}{\partial y_2} - \frac{u_2}{h_1} \frac{\partial h_2}{\partial y_1} \right)^2 + \frac{1}{2} \left(\frac{\partial u_3}{\partial y_2} - \frac{u_2}{h_3} \frac{\partial h_2}{\partial y_3} \right)^2$$

$$\gamma_{11} = h_3 \frac{\partial u_3}{\partial y_3} + \frac{h_3 u_1}{h_1} \frac{\partial h_3}{\partial y_1} + \frac{h_3 u_2}{h_2} \frac{\partial h_3}{\partial y_2} \quad (3.36)$$

$$+ \frac{1}{2} \left(\frac{\partial u_3}{\partial y_3} + \frac{u_1}{h_1} \frac{\partial h_3}{\partial y_1} + \frac{u_2}{h_2} \frac{\partial h_3}{\partial y_2} \right)^2$$

$$+ \frac{1}{2} \left(\frac{\partial u_1}{\partial y_3} - \frac{u_3}{h_1} \frac{\partial h_3}{\partial y_1} \right)^2 + \frac{1}{2} \left(\frac{\partial u_2}{\partial y_3} - \frac{u_3}{h_2} \frac{\partial h_3}{\partial y_2} \right)^2$$

$$\gamma_{23} = \frac{1}{2} \left(h_2 \frac{\partial u_2}{\partial y_3} + h_3 \frac{\partial u_3}{\partial y_2} - u_2 \frac{\partial h_2}{\partial y_3} - u_3 \frac{\partial h_3}{\partial y_2} \right) \quad (3.37)$$

$$+ \frac{1}{2} \left(\frac{\partial u_2}{\partial y_3} - \frac{u_3}{h_2} \frac{\partial h_3}{\partial y_2} \right) \left(\frac{\partial u_2}{\partial y_2} + \frac{u_1}{h_1} \frac{\partial h_2}{\partial y_1} + \frac{u_3}{h_3} \frac{\partial h_2}{\partial y_3} \right)$$

$$+ \frac{1}{2} \left(\frac{\partial u_3}{\partial y_2} - \frac{u_2}{h_3} \frac{\partial h_2}{\partial y_3} \right) \left(\frac{\partial u_3}{\partial y_3} + \frac{u_1}{h_1} \frac{\partial h_3}{\partial y_1} + \frac{u_2}{h_2} \frac{\partial h_3}{\partial y_2} \right)$$

$$+ \frac{1}{2} \left(\frac{\partial u_1}{\partial y_2} - \frac{u_2}{h_1} \frac{\partial h_2}{\partial y_1} \right) \left(\frac{\partial u_1}{\partial y_3} - \frac{u_3}{h_1} \frac{\partial h_3}{\partial y_1} \right)$$

$$\gamma_{13} = \frac{1}{2} \left(h_1 \frac{\partial u_1}{\partial y_3} + h_3 \frac{\partial u_3}{\partial y_1} - u_1 \frac{\partial h_1}{\partial y_3} - u_3 \frac{\partial h_3}{\partial y_1} \right) \quad (3.38)$$

$$+ \frac{1}{2} \left(\frac{\partial u_1}{\partial y_3} - \frac{u_3}{h_1} \frac{\partial h_3}{\partial y_1} \right) \left(\frac{\partial u_1}{\partial y_1} + \frac{u_2}{h_2} \frac{\partial h_1}{\partial y_2} + \frac{u_3}{h_3} \frac{\partial h_1}{\partial y_3} \right)$$

$$+ \frac{1}{2} \left(\frac{\partial u_3}{\partial y_1} - \frac{u_1}{h_3} \frac{\partial h_1}{\partial y_3} \right) \left(\frac{\partial u_3}{\partial y_3} + \frac{u_1}{h_1} \frac{\partial h_3}{\partial y_1} + \frac{u_2}{h_2} \frac{\partial h_3}{\partial y_2} \right)$$

$$+ \frac{1}{2} \left(\frac{\partial u_2}{\partial y_1} - \frac{u_1}{h_2} \frac{\partial h_1}{\partial y_2} \right) \left(\frac{\partial u_2}{\partial y_3} - \frac{u_3}{h_2} \frac{\partial h_3}{\partial y_2} \right)$$

$$\gamma_{12} = \frac{1}{2} \left(h_1 \frac{\partial u_1}{\partial y_2} + h_2 \frac{\partial u_2}{\partial y_1} - u_1 \frac{\partial h_1}{\partial y_2} - u_2 \frac{\partial h_2}{\partial y_1} \right) \quad (3.39)$$

$$\begin{aligned} & + \frac{1}{2} \left(\frac{\partial u_1}{\partial y_2} - \frac{u_2}{h_1} \frac{\partial h_2}{\partial y_1} \right) \left(\frac{\partial u_1}{\partial y_1} + \frac{u_2}{h_2} \frac{\partial h_1}{\partial y_2} + \frac{u_3}{h_3} \frac{\partial h_1}{\partial y_3} \right) \\ & + \frac{1}{2} \left(\frac{\partial u_2}{\partial y_1} - \frac{u_1}{h_2} \frac{\partial h_1}{\partial y_2} \right) \left(\frac{\partial u_2}{\partial y_2} + \frac{u_1}{h_1} \frac{\partial h_2}{\partial y_1} + \frac{u_3}{h_3} \frac{\partial h_2}{\partial y_3} \right) \\ & + \frac{1}{2} \left(\frac{\partial u_3}{\partial y_1} - \frac{u_1}{h_3} \frac{\partial h_1}{\partial y_3} \right) \left(\frac{\partial u_3}{\partial y_2} - \frac{u_2}{h_3} \frac{\partial h_2}{\partial y_3} \right) \end{aligned} \quad (3.40)$$

For a shell discussed earlier, the Lamé parameters A_α , $\alpha = 1, 2$, describe the *two-dimensional* relationship between the orthogonal surface base vectors \vec{a}_α and their orthonormal counterparts \vec{e}_α (refer to Eq (3.17)). For the strains of Eqs (3.34) - (3.39), the scale factors h_i , $i = 1, 2$, describe the *three-dimensional* relationship between the orthogonal base vectors \vec{g}_i of the three-dimensional orthogonal curvilinear coordinate system y_i and their orthonormal counterparts \vec{e}_i (refer to Eq (3.30)). For a two-dimensional orthogonal curvilinear coordinate system, the scale factors of Eqs (3.34) - (3.39) become [192]

$$h_1 = A_1 \left(1 - \frac{y_3}{R_3} \right) \quad h_2 = A_2 \left(1 - \frac{y_3}{R_3} \right) \quad h_3 = 1 \quad , \quad (3.41)$$

where recalling Eqs (3.4) and (3.16), we have

$$A_1 = \left(\frac{\partial \vec{r}}{\partial \theta_1} \cdot \frac{\partial \vec{r}}{\partial \theta_1} \right)^{1/2} \quad A_2 = \left(\frac{\partial \vec{r}}{\partial \theta_2} \cdot \frac{\partial \vec{r}}{\partial \theta_2} \right)^{1/2} \quad . \quad (3.42)$$

Thus, for the convenient case of a cylindrical shell with radius R_2 and local coordinates $\theta_1 = x$, $\theta_2 = s$, z described in orthogonal space with global coordinates $y_1 = x$, $y_2 = s$, $y_3 = z$, the position vector $\vec{r}(y_1, y_2, y_3)$ would be given by

$$\vec{r} = xe_1 + se_2 + ze_3, \quad (3.43)$$

and the Lamé parameters reduce to $A_1 = A_2 = 1$. For the same shell described in terms of an angle, say ϕ , the circumferential coordinate s would be given by $ds = R_2 d\phi$. In this case, $d\vec{r}(y_1, y_2, y_3)$ is given by

$$d\vec{r} = dx\vec{e}_1 + R_2 d\phi\vec{e}_2 + dz\vec{e}_3, \quad (3.44)$$

and the Lamé parameters would be $A_1 = 1$ and $A_2 = 1$. For the case of a spherical shell with radius R_2 and local coordinates $\theta_1 = s_1$, $\theta_2 = s_2$, z described in an orthogonal space with global coordinates $y_1 = s_1$, $y_2 = s_2$, $y_3 = z$, the position vector $\vec{r}(y_1, y_2, y_3)$ would be given by

$$\vec{r} = s_1\vec{e}_1 + s_2\vec{e}_2 + z\vec{e}_3, \quad (3.45)$$

and the Lamé parameters reduce to $A_1 = A_2 = 1$. For the same shell described in terms of angles, say ϕ_1 and ϕ_2 , the circumferential coordinate s_α , $\alpha = 1, 2$ would be given by $ds_\alpha = R d\phi_\alpha$. In this case, $d\vec{r}(y_1, y_2, y_3)$ is given by

$$d\vec{r} = R d\phi_1\vec{e}_1 + R d\phi_2\vec{e}_2 + dz\vec{e}_3, \quad (3.46)$$

and the Lamé parameters would be $A_1 = A_2 = R$.

At this point, it is important to realize the strain components of Eqs (3.34) - (3.39) are related to the orthogonal basis vectors \vec{a}_1 , \vec{a}_2 , and \vec{a}_3 , which change in magnitude and direction. This strain tensor is called the Green-Lagrange strain tensor [229]. These tensorial strain components must be converted to physical components in order to complete the analysis. For the infinitesimal linear problem, the linear parts of this strain tensor can be related to the physical strain of the line from point M to N [192:129]. The change in length of the line segment from M to N , shown in Figure 3.3, is given by

$$\epsilon_{MN} = \frac{1}{2} \left(\frac{(ds^*)^2 - (ds)^2}{(ds)^2} \right). \quad (3.47)$$

This equation can be written in terms of the curvilinear coordinates y_1 , y_2 , and y_3 as follows

$$\epsilon_{MN} = \gamma_{ij} \frac{dy_i}{ds} \frac{dy_j}{ds} \quad (3.48)$$

The derivatives appearing in Eq (3.47) can be written in terms of the direction cosines l_1, l_2 , and l_3 of the line from M to N relative to the orthonormal base vectors \vec{e}_1, \vec{e}_2 , and \vec{e}_3 . These direction cosines are given by

$$l_1 = h_1 \frac{dy_1}{ds}, l_2 = h_2 \frac{dy_2}{ds}, l_3 = h_3 \frac{dy_3}{ds} \quad (3.49)$$

If one substitutes Eq (3.48) into Eq (3.47) and expand the summations, then

$$\begin{aligned} \epsilon_{MN} = & \gamma_{11} \left(\frac{l_1}{h_1} \right)^2 + \gamma_{22} \left(\frac{l_2}{h_2} \right)^2 + \gamma_{33} \left(\frac{l_3}{h_3} \right)^2 \\ & + 2\gamma_{12} \left(\frac{l_1 l_2}{h_1 h_2} \right) + 2\gamma_{13} \left(\frac{l_1 l_3}{h_1 h_3} \right) + 2\gamma_{23} \left(\frac{l_2 l_3}{h_2 h_3} \right) \end{aligned} \quad (3.50)$$

This equation can be written in terms of physical strain components ϵ_{IJ} as follows

$$\begin{aligned} \epsilon_{MN} = & \epsilon_{11} l_1^2 + \epsilon_{22} l_2^2 + \epsilon_{33} l_3^2 \\ & + 2\epsilon_{12} l_1 l_2 + 2\epsilon_{13} l_1 l_3 + 2\epsilon_{23} l_2 l_3 \end{aligned} \quad (3.51)$$

where

$$\begin{aligned} \epsilon_{11} = \frac{\gamma_{11}}{h_1^2} \quad \epsilon_{22} = \frac{\gamma_{22}}{h_2^2} \quad \epsilon_{33} = \frac{\gamma_{33}}{h_3^2} \\ \epsilon_{12} = \frac{\gamma_{12}}{h_1 h_2} \quad \epsilon_{13} = \frac{\gamma_{13}}{h_1 h_3} \quad \epsilon_{23} = \frac{\gamma_{23}}{h_2 h_3} \end{aligned} \quad (3.52)$$

are the physical components of strain for the case of a finite displacement \vec{U} defined by Eq (3.31) [126, 192].

3.3 Composite Material Analysis

In the previous sections of this dissertation, the concept of strain for a shell in an orthogonal curvilinear coordinate system were presented. Next, the subject of constitutive relations are discussed. One can consider the material of a composite laminate from amicroscopic viewpoint or from a macroscopic viewpoint [11, 31, 94, 232]. For this research, the macro-mechanical behavior of the laminate is assumed sufficient provided stresses are small enough to assure no material failure occurs. Thus, the material of each lamina is treated as a homogeneous anisotropic material. More specifically, we shall assume the material is transversely isotropic (i.e. one plane of material property symmetry [31:35]). First, however, consider an *orthotropic* material system. This means the material has properties that are different in three mutually orthogonal directions with three mutually perpendicular planes of material symmetry. The Cauchy stress-strain constitutive relations for an *orthotropic* material are written in matrix form as follows [94:35]

$$\begin{pmatrix} \sigma_{11} \\ \sigma_{22} \\ \sigma_{33} \\ \tau_{23} \\ \tau_{13} \\ \tau_{12} \end{pmatrix} = \begin{bmatrix} C_{11} & C_{12} & C_{13} & 0 & 0 & 0 \\ C_{12} & C_{22} & C_{23} & 0 & 0 & 0 \\ C_{13} & C_{23} & C_{33} & 0 & 0 & 0 \\ 0 & 0 & 0 & C_{44} & 0 & 0 \\ 0 & 0 & 0 & 0 & C_{55} & 0 \\ 0 & 0 & 0 & 0 & 0 & C_{66} \end{bmatrix} \begin{pmatrix} \epsilon_{11} \\ \epsilon_{22} \\ \epsilon_{33} \\ 2\epsilon_{23} \\ 2\epsilon_{13} \\ 2\epsilon_{12} \end{pmatrix}, \quad (3.53)$$

where, for *orthotropic* materials, the non-zero C_{ij} 's are given by

$$\begin{aligned}
C_{11} &= (1 - \nu_{23}\nu_{32}) E_1 / \Delta \\
C_{22} &= (1 - \nu_{13}\nu_{31}) E_2 / \Delta \\
C_{33} &= (1 - \nu_{12}\nu_{21}) E_3 / \Delta \\
C_{12} &= (\nu_{21} - \nu_{31}\nu_{23}) E_1 / \Delta = (\nu_{12} - \nu_{13}\nu_{32}) E_2 / \Delta \\
C_{13} &= (\nu_{31} - \nu_{21}\nu_{32}) E_1 / \Delta = (\nu_{13} - \nu_{12}\nu_{23}) E_3 / \Delta \\
C_{23} &= (\nu_{32} - \nu_{12}\nu_{31}) E_2 / \Delta = (\nu_{23} - \nu_{21}\nu_{13}) E_3 / \Delta \\
C_{44} &= G_{23}, C_{55} = G_{13}, C_{66} = G_{12}
\end{aligned} \tag{3.54}$$

and

$$\Delta = 1 - \nu_{12}\nu_{21} - \nu_{23}\nu_{32} - \nu_{31}\nu_{13} - 2\nu_{21}\nu_{32}\nu_{13} \tag{3.55}$$

The terms of Eqs (3.53) and (3.54) are not all independent. The relationship between these terms are given by

$$\frac{\nu_{ij}}{E_i} = \frac{\nu_{ji}}{E_j} \quad i, j = 1, 2, 3 \tag{3.56}$$

As a further simplification, if the material properties are the same in the 2-direction as in the 3-direction, shown in Figure 3.3, then the material is *transversely isotropic* [94:35]. For this type of material there is no distinction between properties in the 2- and 3-directions. Thus, $E_2 = E_3$, $\nu_{21} = \nu_{31}$, $\nu_{12} = \nu_{13}$, and $\nu_{23} = \nu_{32}$. With this assumption, Eqs (3.53) and (3.54) become

$$\begin{aligned}
C_{11} &= \left(1 - \nu_{23}^2\right) E_1 / \Delta, C_{22} = C_{33} = (1 - \nu_{12}\nu_{21}) E_2 / \Delta \\
C_{12} &= C_{13} = \nu_{21} (1 + \nu_{23}) E_1 / \Delta, C_{23} = (\nu_{23} - \nu_{12}\nu_{21}) E_2 / \Delta \\
C_{44} &= G_{23} = G_{13}, C_{55} = G_{13}, C_{66} = G_{12}
\end{aligned} \tag{3.57}$$

where, for *transversely isotropic* materials, Δ is given by

$$\Delta = 1 - 2\nu_{12}\nu_{21} - \nu_{23}^2 - 2\nu_{12}\nu_{21}\nu_{23} \tag{3.58}$$

and the relationships of Eq (3.55) apply.

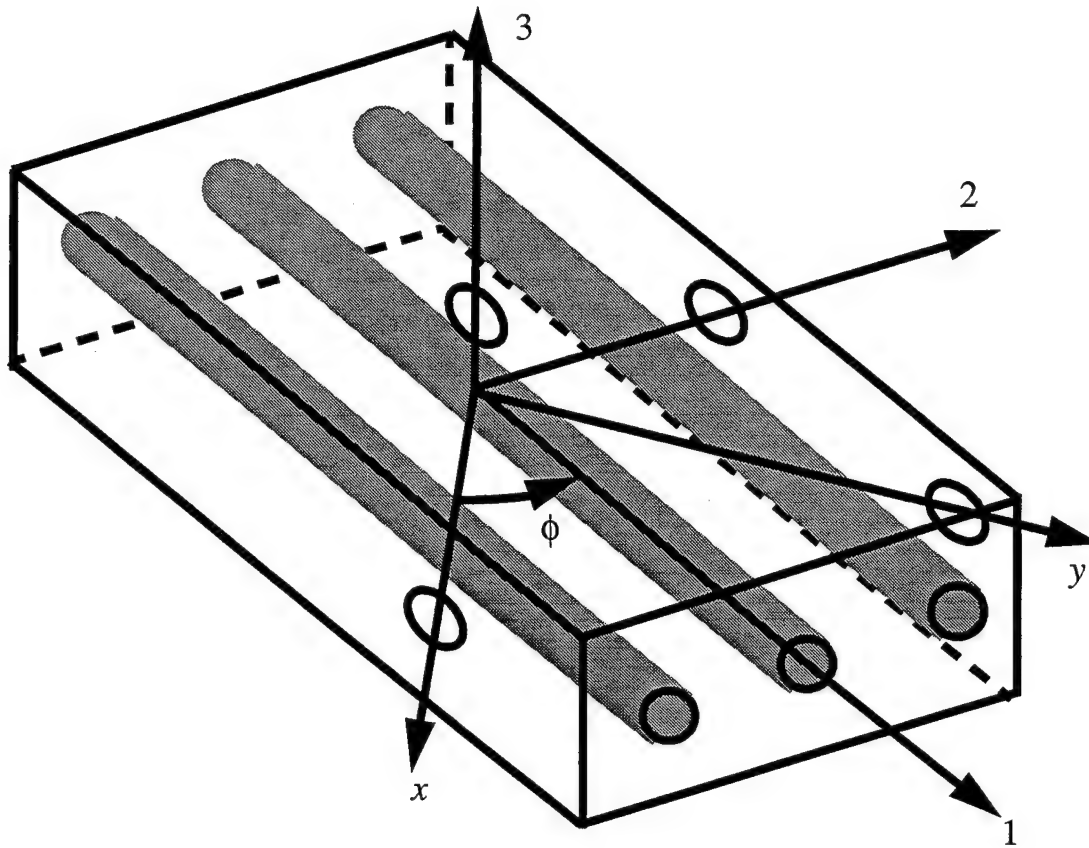


Figure 3.3 Material Axes for a Transversely Isotropic Lamina [11:20]

For a thin flat structural member, such as a plate, a state of plane stress is often assumed [44] where $\sigma_{13} = \sigma_{23} = \sigma_{33} = 0$. In this research, however, the effects of linear transverse shear deformation are considered. Thus, σ_{13} and σ_{23} are not assumed to be zero. The direct normal stress, σ_{33} , however, is still assumed to be zero. This assumption is necessary to reduce the three-dimensional problem to a two-dimensional problem. If $\sigma_{33} = 0$ is substituted into Eq (3.52), the direct transverse normal strain becomes

$$\epsilon_{33} = -\frac{C_{13}}{C_{33}}\epsilon_{11} - \frac{C_{23}}{C_{33}}\epsilon_{22} \quad (3.59)$$

Thus, rewriting Eq (3.52) using Eq (3.58) to eliminate ϵ_{33} , yields

$$\begin{pmatrix} \sigma_{11} \\ \sigma_{22} \\ \tau_{23} \\ \tau_{13} \\ \tau_{12} \end{pmatrix} = \begin{bmatrix} Q_{11} & Q_{12} & 0 & 0 & 0 \\ Q_{12} & Q_{22} & 0 & 0 & 0 \\ 0 & 0 & Q_{44} & 0 & 0 \\ 0 & 0 & 0 & Q_{44} & 0 \\ 0 & 0 & 0 & 0 & Q_{55} \end{bmatrix} \begin{pmatrix} \epsilon_{11} \\ \epsilon_{22} \\ 2\epsilon_{23} \\ 2\epsilon_{13} \\ 2\epsilon_{12} \end{pmatrix}, \quad (3.60)$$

where

$$\begin{aligned} Q_{11} &= C_{11} - C_{13}^2/C_{33} = E_1/(1 - \nu_{12}\nu_{21}) \\ Q_{22} &= C_{22} - C_{23}^2/C_{33} = E_2/(1 - \nu_{12}\nu_{21}) \\ Q_{12} &= C_{12} - C_{13}C_{23}/C_{33} = \nu_{21}E_2/(1 - \nu_{12}\nu_{21}) \\ Q_{44} &= G_{13}, \quad Q_{55} = G_{12} \end{aligned} \quad (3.61)$$

To form a structural component, the lamina are assumed to be perfectly bonded together with their fibers oriented at a particular angle with respect to the structure's reference axis. The stiffness contribution of each lamina in the laminate can be determined. These stiffnesses must first be transformed to a common reference system of axes. If one assumes the k th lamina's fibers are all in the same direction (say, the 1-direction of Figure 3.3), and this direction is at an angle ϕ from the reference axis (say, the x axis) then the constitutive relations in the reference system are given by

$$\begin{pmatrix} \sigma_x \\ \sigma_y \\ \tau_{yz} \\ \tau_{xz} \\ \tau_{xy} \end{pmatrix}_k = \begin{bmatrix} \bar{Q}_{11} & \bar{Q}_{12} & 0 & 0 & \bar{Q}_{16} \\ \bar{Q}_{12} & \bar{Q}_{22} & 0 & 0 & \bar{Q}_{26} \\ 0 & 0 & \bar{Q}_{44} & \bar{Q}_{45} & 0 \\ 0 & 0 & \bar{Q}_{45} & \bar{Q}_{55} & 0 \\ \bar{Q}_{16} & \bar{Q}_{26} & 0 & 0 & \bar{Q}_{66} \end{bmatrix}_k \begin{pmatrix} \epsilon_x \\ \epsilon_y \\ 2\epsilon_{yz} \\ 2\epsilon_{xz} \\ 2\epsilon_{xy} \end{pmatrix}_k, \quad (3.62)$$

where

$$\begin{aligned}
 \bar{Q}_{11} &= Q_{11} \cos^4 \phi + 2(Q_{12} + 2Q_{66}) \cos^2 \phi \sin^2 \phi + Q_{22} \sin^4 \phi \\
 \bar{Q}_{22} &= Q_{11} \sin^4 \phi + 2(Q_{12} + 2Q_{66}) \cos^2 \phi \sin^2 \phi + Q_{22} \sin^4 \phi \\
 \bar{Q}_{12} &= (Q_{11} + Q_{22} - 4Q_{66}) \cos^2 \phi \sin^2 \phi + Q_{12} (\cos^4 \phi + \sin^4 \phi) \\
 \bar{Q}_{16} &= (Q_{11} - Q_{12} - 2Q_{66}) \cos^3 \phi \sin \phi + (Q_{12} - Q_{22} + 2Q_{66}) \cos \phi \sin^3 \phi \\
 \bar{Q}_{26} &= (Q_{11} - Q_{12} - 2Q_{66}) \cos \phi \sin^3 \phi + (Q_{12} - Q_{22} + 2Q_{66}) \cos^3 \phi \sin \phi \\
 \bar{Q}_{44} &= Q_{44} \cos^2 \phi + Q_{55} \sin^2 \phi \\
 \bar{Q}_{45} &= (Q_{44} - Q_{55}) \cos \phi \sin \phi \\
 \bar{Q}_{55} &= Q_{44} \sin^2 \phi + Q_{55} \cos^2 \phi
 \end{aligned} \tag{3.63}$$

In Eqs (3.61) and (3.62), each lamina has a specific orientation of fibers. Thus, each lamina can have different values of Q_{ij} given by Eq (3.62). These constitutive relations are valid for small strains where the material behaves as a linear elastic solid. Equation (3.58) relates the direct normal strain ϵ_{33} to changes in the direct in-plane strains ϵ_{11} and ϵ_{22} for $\sigma_{33} = 0$. The assumption that Eq (3.58) is valid for an arbitrary laminated composite shell is important for composite shell analysis. Without this assumption, the stress state is fully three-dimensional and the reduced computational effort of the two-dimensional model is lost. With the assumption, however, the two-dimensional model will never accurately predict the stress distribution within the shell, since σ_{23} generally will not be zero in the real structure. Research in the 1960's and 1970's, by many investigators, has validated the acceptability of this assumption for certain problems.

3.4 Transverse Shear Deformation

When a thin body undergoes a small (infinitesimal) deformation, material points on a line normal to the middle surface of the body will move relative to each other, as shown in Figure 3.4. This movement results in rotation and warping of the normal. The angle between the geometric normal to the midsurface and the warped normal is maximum at the midsurface and zero at the upper and lower surface. For a linear elastic material under-

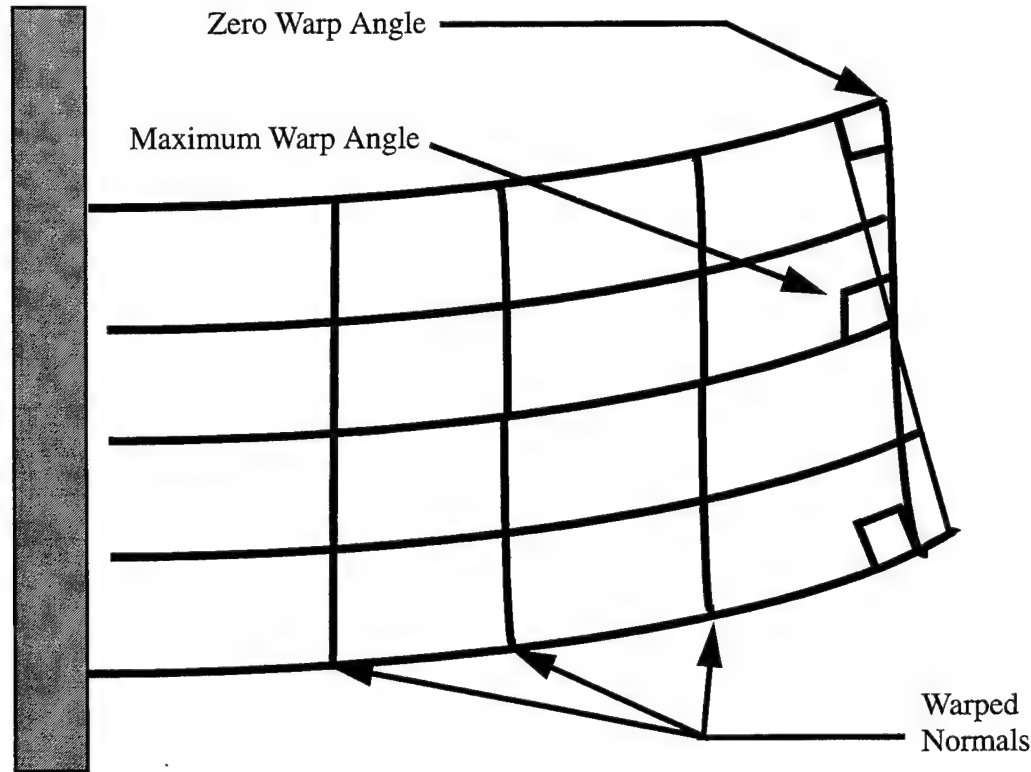


Figure 3.4 Shear Deformation of a Thin Elastic Body [167:234]

going infinitesimal displacement (i.e., linear strain displacement relation hold), this angle of deviation is equal to the transverse shear strain. The distribution of transverse shear strain for the infinitesimal linear case is parabolic through the thickness of a flat plate. Under the classical Kirchhoff assumption, one assumes the normal (or cross-section of a beam) remains normal, straight, and inextensible. This assumption results in zero transverse shear strain. For a thin shell, where $h/R \ll 1$, the Kirchhoff assumption allows accurate predictions of transverse deflection versus load for small displacements. For thick shells, where $h^2/R^2 \ll 1$, or when anisotropic material properties are assumed, transverse shear effects become more apparent. Thick shell and composite shells generally will show greater transverse deflection for a given load when the effect of transverse shear is included in the theoretical model.

3.4.1 First-Order Transverse Shear Deformation (FTSD) Theories. There are several ways to include transverse shear deformation. Transverse shear effects can be included using a first-order

transverse shear deformation (FTSD) theory. In this case, material lines originally normal to the midsurface are allowed to deviate from the normal to the shell midsurface as shown in Figure 3.5. These lines remain straight and inextensible. Since the angle of deviation is constant, the displacement field varies linearly. The constant angle also implies transverse shear strain is constant, and thus, is not zero at the upper and lower surfaces of the shell. This inconsistent distribution results in an overly stiff model of the structure. This stiffening effect, called shear locking, becomes more pronounced as the shell thickness approaches zero. First-order transverse shear theories can be used, provided some artificial corrections are made. The excessive strain energy resulting from the constant shear strain assumption is usually reduced by multiplying the transverse strains by a constant factor of 5/6 for isotropic materials. Although 5/6 is often used for composite materials, there is no generally accepted method of determining shear correction factors for anisotropic materials. The predicted response of the FTSD model is sensitive to the values of shear correction factors. Hence, some have suggested that theories of composite shells should not depend upon any numerical factors [18:698].

The derivation of transverse shear deformation theories is, generally, based on writing the displacement vector \vec{u} , of Eq (3.31), as a function of the thickness coordinate of the shell. According to Reddy [176], this approach was pioneered in 1890 by A. B. Bassett. According to literature cited by Dennis [48], Bassett expanded the displacement components u_i in an infinite power series as shown below

$$u_i(y_1, y_2, y_3) = u_i(y_1, y_2, 0) + y_3 \left. \frac{\partial u_i}{\partial y_3} \right|_{y_3=0} + y_3^2 \left. \frac{\partial^2 u_i}{\partial y_3^2} \right|_{y_3=0} + \dots \quad (3.64)$$

This displacement field, when substituted into Eqs (3.38) and (3.39), will give nonzero transverse shear strains γ_{13} and γ_{23} . Also, the u_3 component is a function of the thickness coordinate y_3 . This will result in a nonzero σ_{33} .

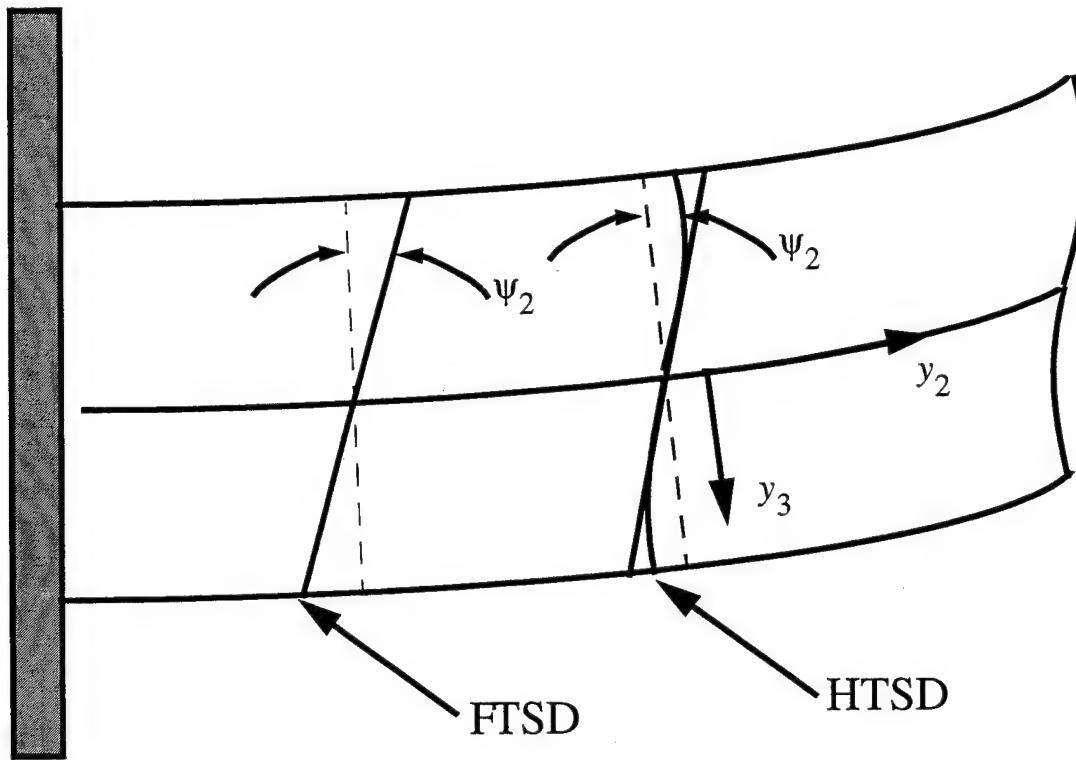


Figure 3.5 Deformation of Normals for FTSD and HTSD Theories

Hildebrand, Reissner, and Thomas [77] examined the importance of the terms leading to the transverse strains for orthotropic shells. They truncated the expressions of Eq (3.63) for u_1 and u_2 at the second order terms. They also assumed, for the case of $\sigma_{33} \approx 0$ with ϵ_{33} given by Eq (3.58), that u_3 could be determined by integrating Eq (3.58) through the thickness of the shell. Their investigations showed that the resulting linear and quadratic y_3 terms present in u_3 could be neglected. Thus, the displacement field of Hildebrand et al. has a u_3 displacement function that does not vary through the thickness of the shell. Theories based upon the assumptions of Hildebrand et al. [77] are called first-order shear deformation theories. These types of theories were extensively studied by Reissner and Mindlin in the 1940's and 1950's [124, 186] for plates, and hence, are often called Reissner-Mindlin theories. For a shell, the FTSD theory is given by the following displacement field:

$$\begin{aligned}
 u_1 &= u(1 - y_3/R_1) + \psi_1 y_3 \\
 u_2 &= v(1 - y_3/R_2) + \psi_2 y_3 \\
 u_3 &= w
 \end{aligned}
 \tag{3.65}$$

where the five degrees of freedom (dof), u , v , w , ψ_1 , and ψ_2 , are functions of the in-plane curvilinear coordinates y_1 and y_2 .

3.4.2 Higher-Order Transverse Shear Deformation (HTSD) Theories. Higher-order transverse shear deformation (HTSD) theories generally eliminate the need for shear correction factors. The HTSD theory allows the normal to rotate and warp as shown in Figure 3.5. Some HTSD theories also allow the normal to change length. The HTSD theory for a flat plate produces a parabolic distribution of shear strain as shown in Figure 3.6. This distribution matches the exact distribution of shear strain for the linear infinitesimal case. The results for curved shells, however, are different because of the curvature of the shell. Due

to curvature of the shell, the transverse shear strain is distorted as shown in Figure 3.6 by the heavier line labeled cubic transverse shear. Since the small-strain transverse shear distribution for a shell is a cubic function of the thickness coordinate, the displacement field should be at least quartic in the thickness coordinate. For a shell, the curvature generally creates coupling between in-plane extension and bending activity. To include this effect, one needs to include quartic terms in the displacement field or include nonlinear strain displacement terms. Assuming a general quartic displacement field, as given in Eq (3.65), the derivation of a quasi-nonlinear HTSD theory for a shell follows

$$\begin{aligned}
 u_1(y_1, y_2, y_3) &= u\left(1 - y_3/R_1\right) + \Psi_1 y_3 + \phi_1 y_3^2 + \gamma_1 y_3^3 + \theta_1 y_3^4 \\
 u_2(y_1, y_2, y_3) &= v\left(1 - y_3/R_1\right) + \Psi_2 y_3 + \phi_2 y_3^2 + \gamma_2 y_3^3 + \theta_2 y_3^4 \\
 u_3(y_1, y_2) &= w
 \end{aligned}
 \tag{3.66}$$

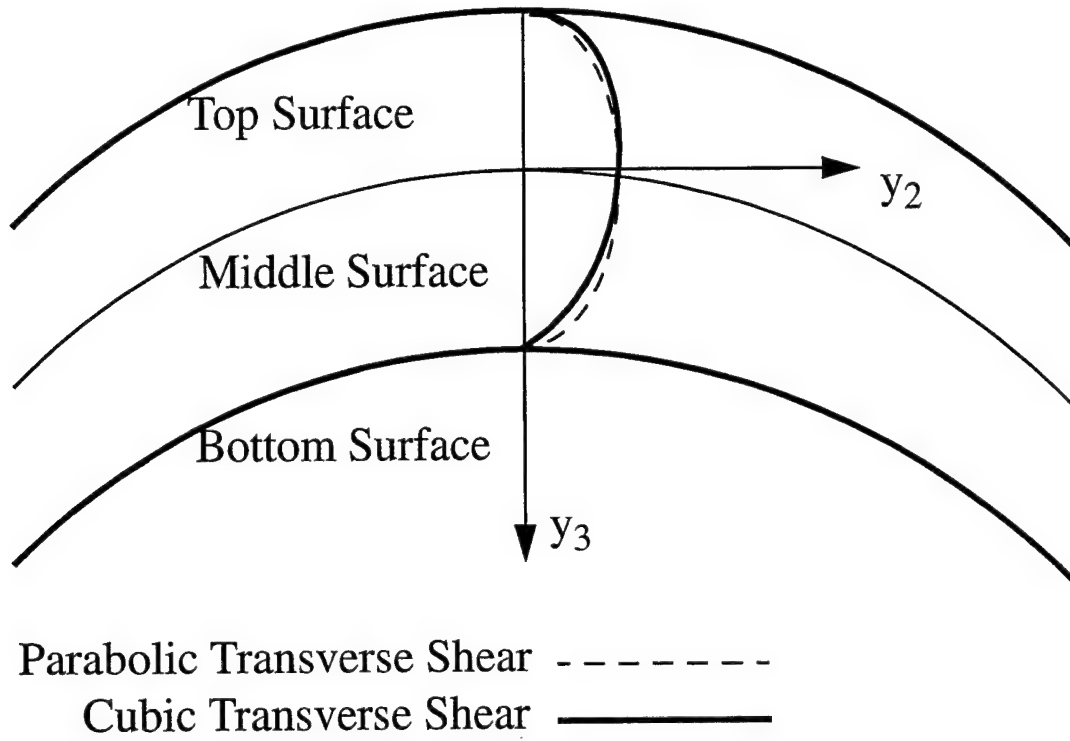


Figure 3.6 Parabolic and Cubic Transverse Shear Distributions for a Curved Shell

where $u = u(y_1, y_2)$, $v = v(y_1, y_2)$, $w = w(y_1, y_2)$, $\Psi_\alpha = \Psi_\alpha(y_1, y_2)$, $\phi_\alpha = \phi_\alpha(y_1, y_2)$, $\gamma_\alpha = \gamma_\alpha(y_1, y_2)$, and $\theta_\alpha = \theta_\alpha(y_1, y_2)$ are degrees of freedom defined only at the midsurface of the shell. These degrees of freedom are functions of the in-plane coordinates y_1 and y_2 and will vary from point to point on the shell's midsurface. For the shell with $h_1 = (1 - y_3/R_1)$, $h_2 = (1 - y_3/R_2)$, and $h_3 = 1$, along with the displacement field of Eq (3.65), the linear transverse shear strains (given by the first line of Eqs (3.38) and (3.39)) are as follows

$$\gamma_{13} = \frac{1}{(1 - y_3/R_1)} \left[\frac{\partial u_3}{\partial y_1} + (1 - y_3/R_1) \frac{\partial u_1}{\partial y_3} - u_1 \frac{\partial (1 - y_3/R_1)}{\partial y_3} \right] \quad (3.67)$$

$$\gamma_{23} = \frac{1}{(1 - y_3/R_2)} \left[\frac{\partial u_3}{\partial y_2} + (1 - y_3/R_2) \frac{\partial u_2}{\partial y_3} - u_2 \frac{\partial (1 - y_3/R_2)}{\partial y_3} \right] \quad (3.68)$$

Substituting Eq (3.65) into Eq (3.67) yields

$$\gamma_{23} = \frac{1}{(1 - y_3/R_2)} \left[\frac{\partial w}{\partial y_2} + \Psi_2 - 2\phi_2 y_3 + \left(\frac{\phi_2}{R_2} - 3\gamma_2 \right) y_3^2 + \left(\frac{2\gamma_2}{R_2} - 4\theta_2 \right) y_3^3 + \frac{3\theta_2}{R_2} y_3^4 \right] \quad (3.69)$$

For this equation to be zero at $y_3 = \pm h/2$ and yield a parabolic distribution of γ_{23} , the coefficients of odd powers of y_3 must cancel each other or be equal to zero. If one assumes $\phi_2 = 0$ and $\theta_2 = \gamma_2/R_2$ these coefficients vanish and γ_{23} is given by

$$\gamma_{23} = \frac{1}{(1 - y_3/R_2)} \left[\frac{\partial w}{\partial y_2} + \Psi_2 - 3\gamma_2 y_3 + \frac{3\gamma_2}{2R_2} y_3^4 \right] \quad (3.70)$$

Evaluating Eq (3.69) at $y_2 = h/2$ and solving for γ_2 gives

$$-\frac{3h^2}{4} \left(1 - \frac{h^2}{8R_2} \right) \gamma_2 = \left(\frac{\partial w}{\partial y_2} + \Psi_2 \right) \quad (3.71)$$

For a shell with radius R_2 no smaller than five times the thickness h , the term h^2/R_2^2 in Eq (3.70) is less than or equal to 1/400. If one ignores this term, then γ_2 is given by

$$\gamma_2 = -\frac{4}{3h^2} \left(\frac{\partial w}{\partial y_2} + \Psi_2 \right) \quad (3.72)$$

Similarly, γ_1 can be found. If one substitutes Eq (3.71) and $\phi_2 = \theta_2 = 0$ and similar relations for ϕ_1, γ_1 , and θ_1 into Eq (3.65), the final form of the displacement field of a third-order quasi-nonlinear transverse shear deformation theory is obtained

$$\begin{aligned} u_1(y_1, y_2, y_3) &= u \left(1 - \frac{y_3}{R_1} \right) + \Psi_1 y_3 - \frac{4}{3h^2} \left(\frac{\partial w}{\partial y_1} + \Psi_1 \right) y_3^3 \\ u_2(y_1, y_2, y_3) &= v \left(1 - \frac{y_3}{R_2} \right) + \Psi_2 y_3 - \frac{4}{3h^2} \left(\frac{\partial w}{\partial y_2} + \Psi_2 \right) y_3^3 \\ u_3(y_1, y_2) &= w \end{aligned} \quad (3.73)$$

This third-order displacement field has two additional degrees of freedom not present in the

first-order theory. These two degrees of freedom are the differentials of transverse displacement w . The third-order theory allows the slopes of the elastic curve, $w_{,i}$, to be different from the bending angles, ψ_i . These differences are directly related to the transverse shear strains of the structure.

3.5 The Mathematical Theory of Plasticity

The object of this section is to provide a theoretical description of the relationship between stress and strain for a material which exhibits an elasto-plastic response. In essence, plastic behavior is characterized by an irreversible straining which is not time dependent and which can only be sustained once a certain level of stress has been reached. In this section the basic assumptions and associated theoretical expressions for a general continuum are shown. For a more complete development see [79, 83, 168]. In order to formulate a theory which models elasto-plastic material deformation, three requirements must be met:

- An explicit relationship between stress and strain must be formulated to describe material behavior under elastic conditions, i.e., before the onset of plastic deformation.
- A yield criterion indicating the stress level at which plastic flow commences must be postulated.
- A relationship between stress and strain must be developed for post-yield behavior, i.e., when the deformation is made up of both elastic and plastic components.

Before the onset of plastic yielding, the relationship between stress and strain is given by the standard linear expression. Note: Einstein's summation convention is employed.

$$\sigma_{ij} = D_{ijkl} \epsilon_{kl} \quad (3.74)$$

where σ_{ij} and ϵ_{kl} are the stress and strain components respectively and D_{ijkl} is the tensor of elastic constants which for an isotropic material has the explicit form

$$D_{ijkl} = \lambda \delta_{ij} \delta_{kl} + \mu \delta_{ik} \delta_{jl} + \mu \delta_{il} \delta_{jk} \quad (3.75)$$

where λ and μ are the Lamé constants and δ_{ij} is the Kronecker delta function defined by

$$\delta_{ij} = \begin{cases} 1 & \text{if } i = j \\ 0 & \text{if } i \neq j \end{cases} \quad (3.76)$$

3.5.1 The Yield Criteria: The yield criteria determines the stress level at which plastic deformation commences.

mation begins and can be written in the general form

$$f(\sigma_{ij}) = k(\kappa) , \quad (3.77)$$

where f is some function and k a material parameter to be determined experimentally. The term k may be a function of a hardening parameter κ discussed later in Section 3.5.2. On physical grounds, any yield criteria should be independent of the orientation of the coordinate system employed and therefore it should be a function of the three stress invariants only

$$\begin{aligned} J_1 &= \sigma_{ii} \\ J_2 &= \frac{1}{2} \sigma_{ij} \sigma_{ij} \\ J_3 &= \frac{1}{3} \sigma_{ij} \sigma_{jk} \sigma_{ki} \end{aligned} \quad (3.78)$$

Experimentally observations, notably by Bridgeman [27], indicate that plastic deformation of metals is essentially independent of hydrostatic pressure. Consequently, the yield function can only be of the form

$$f(J'_2, J'_3) = k(\kappa) , \quad (3.79)$$

where J'_2 and J'_3 are the second and third invariants of the deviatoric stresses,

$$\sigma'_{ij} = \sigma_{ij} - \frac{1}{3} \delta_{ij} \sigma_{kk} \quad (3.80)$$

Most of the various yield criteria that have been suggested for metals are now only of historic interest, since they conflict with experimental predictions. The two simplest which do not have this fault are the Tresca and the von Mises criteria.

The Tresca Yield Criteria (1864)

This states that yielding begins when the maximum shear stress reaches a certain value. If the principal stresses are s_1, s_2, s_3 where $\sigma_1 \geq \sigma_2 \geq \sigma_3 > 0$ then yielding begins when

$$\sigma_1 - \sigma_3 = Y(\kappa) , \quad (3.81)$$

where Y is a material parameter to be experimentally determined and which may be a function of the hardening parameter κ . By considering all other possible maximum shearing stress values

(e.g. $s_2 - s_1$ if $\sigma_2 \geq \sigma_3 \geq \sigma_1$) it can be shown that this yield criteria may be represented in the $s_1 s_2 s_3$ stress space by the surface of an infinitely long regular hexagonal cylinder as shown in Figure 3.7. The axis of the cylinder coincides with the *space diagonal*, defined by points $s_1 = s_2 = s_3$, and since each normal section of the cylinder is identical (due to the assumption that hydrostatic stress does not influence yielding), the *yield surface* is represented geometrically by projecting it onto the so-called π -plane, $\sigma_1 + \sigma_2 + \sigma_3 = 0$ as shown in Figure 3.8 (a). When the yield function f depends on J_2' and J_3' alone it can be written in the form $f(\sigma_1 - \sigma_2, \sigma_2 - \sigma_3, \sigma_3 - \sigma_1)$ and a two-dimensional plot of the surface $f = k$ is then possible as shown in Figure 3.8(b). It can be shown generally [79, 168] that yield surfaces must be convex and that they must contain the stress origin.

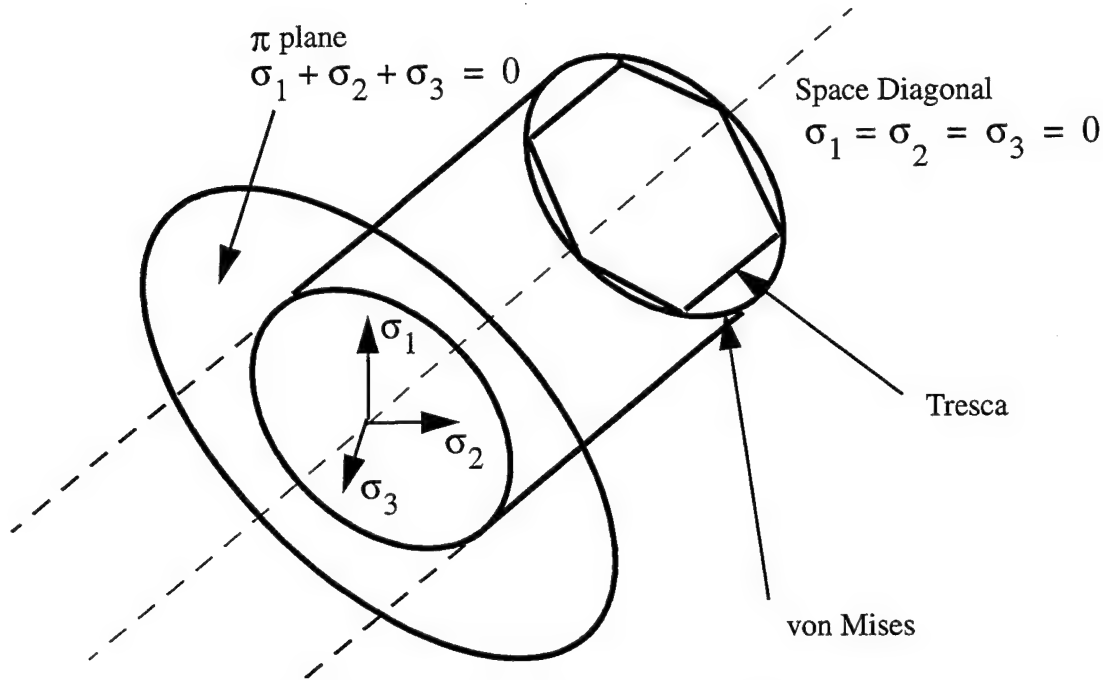


Figure 3.7 Geometrical Representation of the Tresca and von Mises Yield Surfaces in Principal Stress Space

The von Mises Yield Criteria (1913)

Von Mises suggested that yielding occurs when J_2' reaches a critical value, or

$$\left(J_2'\right)^{1/2} = k(\kappa) \quad , \quad (3.82)$$

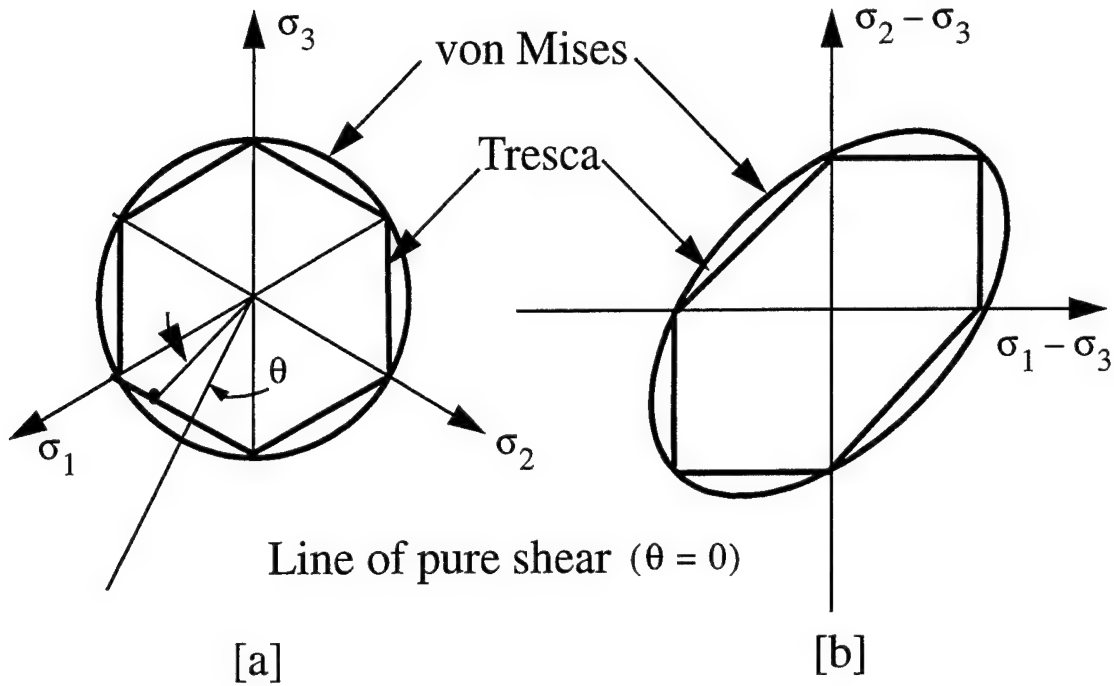


Figure 3.8 Two-dimensional Representations of the Tresca and von Mises yield Criteria.
(a) π -Plane Representation. (b) Conventional Engineering Representation.

in which k is a material parameter to be determined. The second deviatoric stress invariant, J_2' is explicitly written as

$$\begin{aligned} J_2' &= \frac{1}{2} \sigma_{ij}' \sigma_{ij}' = \frac{1}{6} [(\sigma_1 - \sigma_2)^2 + (\sigma_2 - \sigma_3)^2 + (\sigma_3 - \sigma_1)^2] \\ &= \frac{1}{2} [\sigma_x'^2 + \sigma_y'^2 + \sigma_z'^2] + \sigma_{xy}'^2 + \sigma_{yz}'^2 + \sigma_{xz}'^2 \end{aligned} \quad (3.83)$$

The yield criteria in Eq (3.81) is in alternate form

$$\bar{\sigma} = \sqrt{3} (J_2')^{1/2} = \sqrt{3} k \quad , \quad (3.84)$$

where

$$\bar{\sigma} = \sqrt{\frac{3}{2}} (\sigma_{ij}' \sigma_{ij}')^{1/2} \quad , \quad (3.85)$$

and $\bar{\sigma}$ is termed the *effective stress*. Some physical insight into the definition of $\bar{\sigma}$ is shown in Section 3.5.2 where the case of uniaxial yielding is considered. There are two physical interpretations of the von Mises yield condition. Nadai (1937) introduced the parameter *octahedral shear stress* τ_{oct} , which is the shear stress on the planes of a regular octahedron, the apices of which coincide with the principal axes of stress. The value of τ_{oct} is related to J_2' by

$$\tau_{oct} = \sqrt{2J_2'/3} \quad (3.86)$$

Thus, yielding can be interpreted to begin when τ_{oct} reaches a critical value. Hencky (1924) pointed out that the von Mises law implies that yielding when the (recoverable) elastic energy of distortion reaches a critical value.

Figure 3.7 shows the geometrical interpretation of the von Mises yield surface to be a circular cylinder whose projection onto the π -plane is a circle of radius $\sqrt{2}k$ as shown in Figure 3.8(a). The two dimensional plot of the von Mises yield surface is the ellipse shown in Figure 3.8(b). A physical meaning of the constant k can be obtained by considering the yielding of materials under simple stress states. The case of pure shear ($\sigma_1 = -\sigma_2$, $\sigma_3 = 0$) requires on use of Eqs (3.81) & (3.83) that k must equal the yield shear stress. Alternatively the case of uniaxial tension ($\sigma_2 = \sigma_3 = 0$) requires that $\sqrt{3}k$ is the uniaxial yield stress.

The Tresca yield locus is a hexagon with distances of $\sqrt{(2/3)}Y$ from origin to apex on the π -plane whereas the von Mises yield surface is a circle of radius $\sqrt{2}k$. By suitably choosing the constant Y , the criteria can be made to agree with each other, and with experiment, for a single state of stress. This may be selected arbitrarily; it is conventional to make the circle pass through the apices of the hexagon by taking the constant $Y = \sqrt{3}k$, the yield stress in simple tension. The criteria then differ most for a state of pure shear, where the von Mises criterion gives a yield stress $2/\sqrt{3} \approx 1.5$ times that given by the Tresca criterion. For most metals, von Mises' law fits the experimental data more closely than Tresca's, but Tresca's criteria is simpler to use in theoretical applications.

3.5.2 Work or Strain Hardening: After initial yielding, the stress level at which further plastic

deformation occurs may be dependent on the current degree of plastic straining. Such a phenomenon is termed work hardening or strain hardening. Thus, the yield surface will vary at each stage of the plastic deformation, with the subsequent yield surfaces being dependent on the plastic strains in some way. Some alternative models which describe strain hardening in a material are shown in Figure 3.9. A perfectly plastic material is shown in Figure 3.9(a) where the yield stress level does not depend in any way on the degree of plasticity. If the subsequent yield surfaces are a uniform expansion of the original yield curve, without translation, as shown in Figure 3.9(b), the strain-hardening model is said to be *isotropic*. Alternatively, if the subsequent yield surfaces preserve their shape and orientation but translate in the stress space as a rigid body as shown in Figure 3.9(c), *kinematic* hardening is said to take place. Such a hardening model demonstrates the experimentally observed Bauschinger effect on cyclic loading.

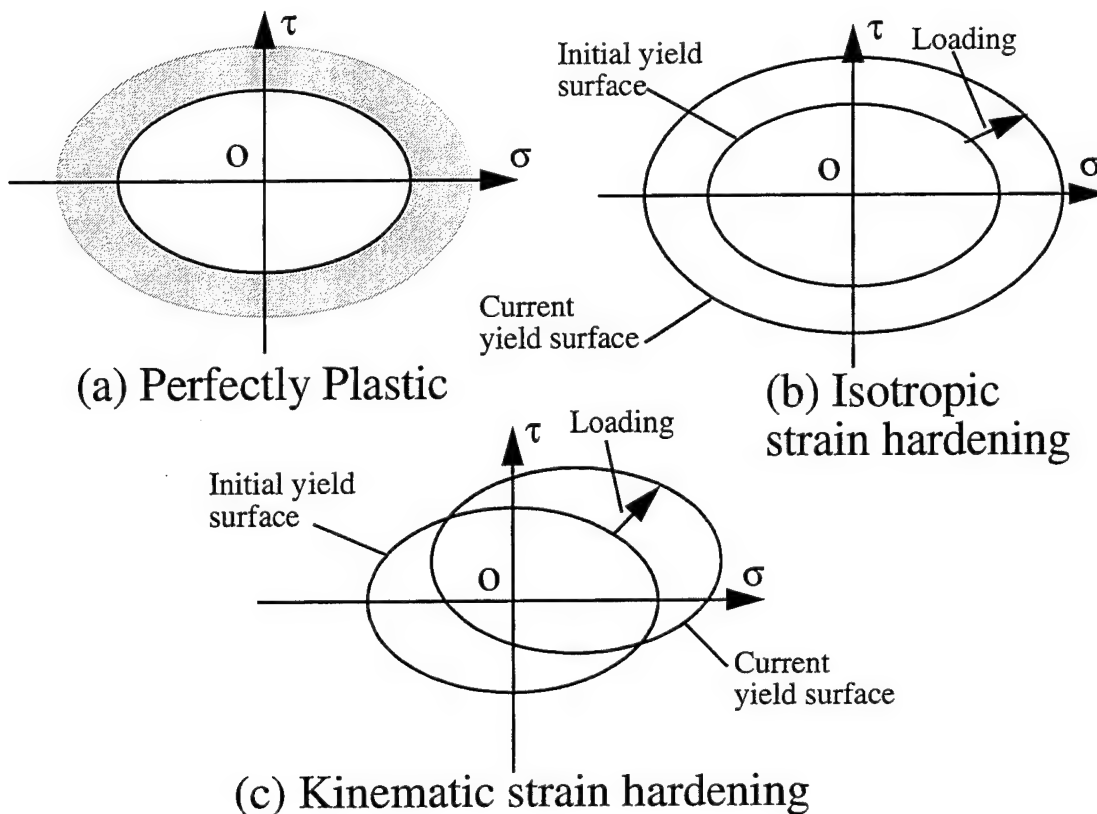


Figure 3.9 Mathematical Models for Representation of Strain

For some materials, notably soils, the yield surface may not strain harden but *strainsoften*

instead, so that the yield stress level at a point decreases with increasing plastic deformation. Therefore, for an isotropic model, the original yield curve contracts progressively without translation. Consequently yielding implies local failure and the yield surface becomes a *failure criteria*.

The progressive development of the yield surface can be defined by relating the yield stress k to the plastic deformation by means of the hardening parameter κ . This can be done in two ways. First, the amount of *work hardening* is defined as a function of the total plastic work, W_p only. Then,

$$\kappa = W_p \quad , \quad (3.87)$$

where

$$W_p = \int \sigma_{ij} \left(d\epsilon_{ij}^p \right) \quad , \quad (3.88)$$

in which $(d\epsilon_{ij}^p)$ are the plastic components of strain occurring during a strain increment. Alternatively, κ can be related to a measure of the total plastic deformation termed the *effective plastic strain* which is defined incrementally as

$$d\bar{\epsilon}^p = \sqrt{\frac{2}{3}} \left(\left(d\epsilon_{ij}^p \right) \left(d\epsilon_{ij}^p \right) \right)^{1/2} \quad . \quad (3.89)$$

A physical insight of this definition is provided in Section 3.5.2 where uniaxial yielding is considered. For situations where the assumption that yielding is independent of any hydrostatic stress is valid, $d\epsilon_{ii}^p = 0$ and hence $d\epsilon_{ij}^p = d\epsilon_{ij}^p$. Consequently Eq (3.88) becomes

$$d\bar{\epsilon}^p = \sqrt{\frac{2}{3}} \left(\left(d\epsilon_{ij}^p \right) \left(d\epsilon_{ij}^p \right) \right)^{1/2} \quad . \quad (3.90)$$

Then the hardening parameter, κ , is assumed to be defined as

$$\kappa = \bar{\epsilon}^p \quad , \quad (3.91)$$

where $\bar{\epsilon}^p$ is the result of integrating $d\bar{\epsilon}^p$ over the strain path. This behavior is termed *strain hardening*. Only an isotropic hardening model is discussed.

Stress states for which $f = k$ represent plastic states, while elastic behavior is characterized by $f < k$. At a plastic state, $f = k$, the incremental change in the yield function due to an incremental stress change is

$$df = \frac{\partial f}{\partial \sigma_{ij}} d\sigma_{ij} \quad (3.92)$$

Then if:

$df < 0$ elastic unloading occurs (elastic behavior) and the stress point returns inside the yielding surface

$df = 0$ neutral loading (plastic behavior for a perfectly plastic material) and the stress point remains on the yield surface

$df > 0$ plastic loading (plastic behavior for a strain hardening material) and the stress point remains on the expanding yield surface.

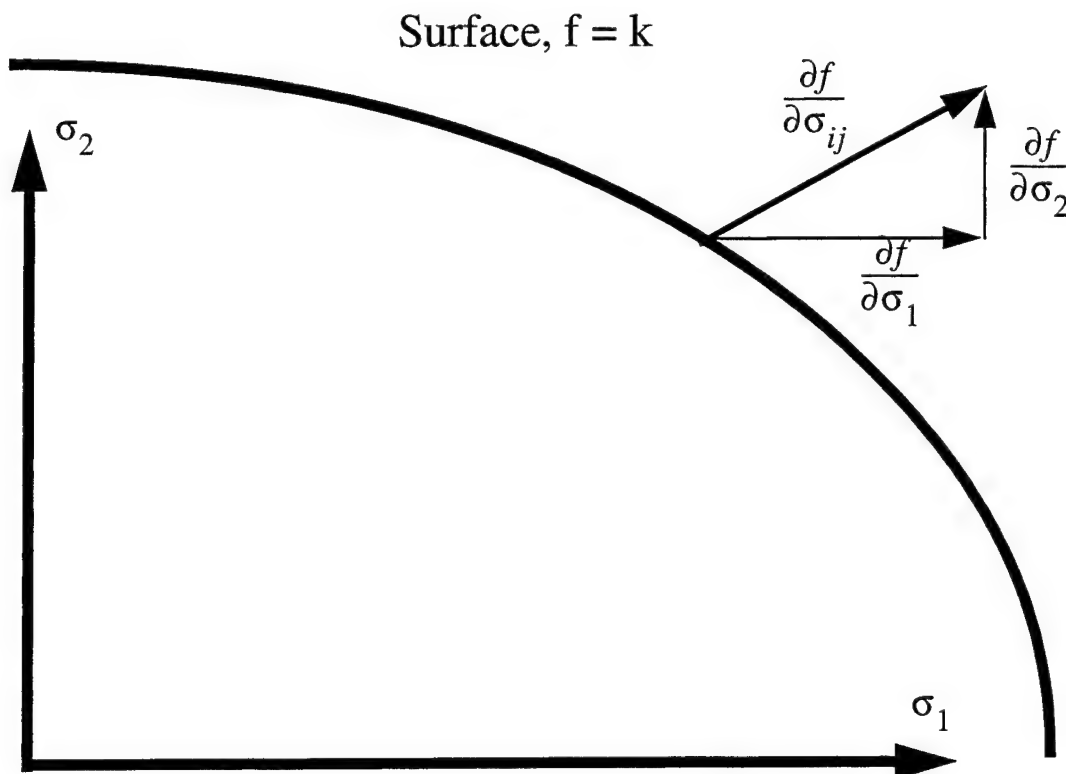


Figure 3.10 Geometrical Representation of the Normality Rule of Associated Plasticity.

It can also be shown [79, 83, 168] that, for a stable material the initial and all subsequent yield surfaces must be convex.

3.5.3 Elasto-plastic Stress-Strain Relation: After initial yielding, the material behavior will be partly elastic and partly plastic. During any increment of stress, the changes of strain are assumed to be devisable into elastic and plastic components, so that

$$d\epsilon_{ij} = d\epsilon_{ij}^e + d\epsilon_{ij}^p \quad (3.93)$$

The elastic strain increment is related to the stress increment by Eq (3.73). One can decompose the stress terms into deviatoric and hydrostatic components

$$d\epsilon_{ij}^e = \frac{d\sigma'_{ij}}{2\mu} + \frac{(1-2\nu)}{E} \delta_{ij} d\sigma_{kk} \quad (3.94)$$

where E and ν are respectively the elastic modulus and Poisson's ratio of the material.

In order to derive the relationship between the plastic strain component and the stress increment, a further assumption on the material behavior must be made. In particular, it will be assumed that the plastic strain increment is proportional to the stress gradient of a quantity termed the *plastic potential* Q , so that

$$d\epsilon_{ij} = d\lambda \frac{\partial Q}{\partial \sigma_{ij}} \quad (3.95)$$

where $d\lambda$ is a proportionality constant termed the *plastic multiplier*. A theoretical basis for this assumption is developed in Ref [79]. Eq (3.94) is termed the *flow rule* since it governs the plastic flow after yielding. The potential Q must be a function of J_2' and J_3' but as yet it cannot be determined in its most general form. However, the relation $f = Q$ has a special significance in the mathematical theory of plasticity, since for this case certain variational principles and uniqueness theorems can be formulated. The identity $f \equiv Q$ is a valid one since it was postulated that both are functions of J_2' and J_3' and such an assumption gives rise to an *associated* theory of plasticity. In this case, Eq (3.94) becomes

$$d\epsilon_{ij}^p = d\lambda \frac{\partial f}{\partial \sigma_{ij}} \quad (3.96)$$

and is termed the *normality condition* since $\partial f / \partial \sigma_{ij}$ is a vector directed normal to the yield surface at the stress point under consideration as shown in Figure 3.10. It is seen that the components

of the plastic strain increment are required to combine vectorially in n -dimensional space to give a vector which is normal to the yield surface. For the particular case of $f = J_2'$

$$\frac{\partial f}{\partial \sigma_{ij}} = \frac{\partial J_2'}{\partial \sigma_{ij}} = \sigma'_{ij} \quad (3.97)$$

Then Eq (3.95) becomes

$$d\epsilon_{ij}^p = d\lambda \sigma'_{ij} \quad (3.98)$$

which are known as the *Prandtl-Reuss equations* [79] and have been extensively employed in theoretical work. Experimental observations indicate that the normality condition is an acceptable assumption for metals. Thus, using Eqs (3.92), (3.93), and (3.94), the complete incremental relationship between stress and strain for elasto-plastic deformation becomes

$$d\epsilon_{ij} = \frac{d\sigma'_{ij}}{2\mu} + \frac{(1-2\nu)}{E} \delta_{ij} d\sigma_{kk} + d\lambda \sigma'_{ij} \quad (3.99)$$

3.5.4 Uniaxial Yield Test on a Strain-hardening Material: Consider the uniaxial testing of an elasto-plastic material which produces the stress-strain curve shown in Figure 3.11. The behavior is initially elastic characterized by an elastic modulus E until yielding commences at the uniaxial yield stress σ_Y . Then the material response is elasto-plastic with the local tangent to the curve continually varying and is termed *the elasto-plastic tangent modulus*, E_T . The hardening law $k = k(\kappa)$ could just as easily be expressed in terms of

the effective stress, overline sigma (since it is proportional to J_2') to give, for the strain hardening hypothesis

$$\bar{\sigma} = H'(\bar{\epsilon}^p) \quad (3.100)$$

and differentiating yields

$$\frac{d\bar{\sigma}}{d\bar{\epsilon}^p} = H'(\bar{\epsilon}^p) \quad (3.101)$$

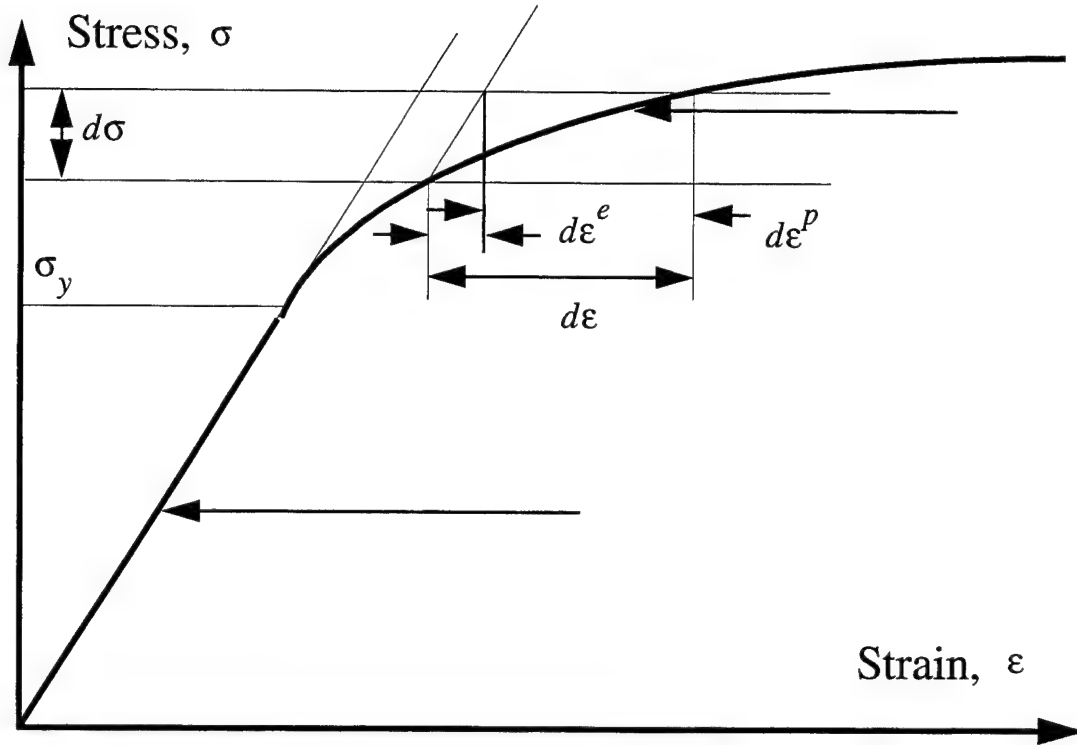


Figure 3.11 Elasto-plastic Strain Hardening Behavior for the Uniaxial Case.

For the uniaxial case under consideration $\sigma_1 = \sigma$, $\sigma_1 = \sigma_2 = 0$ and then from Eq (3.84)

$$\tilde{\sigma} = \sqrt{\frac{3}{2}} \left(\sigma'_{ij} \sigma'_{ij} \right)^{1/2} = \sigma \quad (3.102)$$

If the plastic strain increment in the direction of loading is $d\epsilon^p$, then $d\epsilon_1^p = d\epsilon^p$ and since plastic straining is assumed to be incompressible, Poisson's ration is effectively 0.5 and $d\epsilon_2^p = d\epsilon_3^p = -(1/2) d\epsilon^p$. Then from Eq (3.89), the effective plastic strain becomes

$$d\bar{\epsilon}^p = \sqrt{\frac{2}{3}} \left(\epsilon_{ij}^{p'} \epsilon_{ij}^{p'} \right)^{1/2} = d\epsilon^p \quad (3.103)$$

Eqs (3.101) & (3.102) explain the apparent arbitrary constants employed in the definition of $\bar{\sigma}$ and $\bar{\epsilon}^p$, since these terms are required to become the actual stress and strain for uniaxial yielding. By using Eqs (3.101) and (3.102), Eq (3.100) becomes

$$H'(\bar{\epsilon}^p) = \frac{d\sigma}{d\epsilon^p} = \frac{d\sigma}{d\epsilon - d\epsilon^e} = \frac{1}{(d\epsilon/d\sigma - d\epsilon^p/d\sigma)} = \frac{E_T}{1 - E_T/E} \quad (3.104)$$

Thus, the hardening function H' can be determined experimentally from a simple uniaxial yield test.

3.5.5 Matrix Formulation: The theoretical expressions developed previously are now converted into matrix form [235, 238]. The yield function, first defined in Eq (3.76), can be rewritten as

$$f(\sigma) = k(\kappa) \quad (3.105)$$

where σ is the stress vector and κ is the hardening parameter which governs the expansion of the yield surface. In particular, from Eqs (3.86) and (3.87), $d\kappa = \sigma^T d\epsilon^p$ for the work hardening hypothesis and from Eq (3.90), $d\kappa = d\epsilon^p$ for the strain hardening hypothesis. If Eq (3.104) is rearranged, the result is

$$F(\sigma, \kappa) = f(\sigma) - k(\kappa) = 0 \quad (3.106)$$

If Eq (3.105) is differentiated, one obtains

$$dF = \frac{\partial F}{\partial \sigma} d\sigma + \frac{\partial F}{\partial \kappa} d\kappa = 0 \quad (3.107)$$

or

$$\{a\}^T d\sigma - A d\lambda = 0 \quad (3.108)$$

with the definitions

$$\{a\}^T = \frac{\partial F}{\partial \sigma} = \left[\frac{\partial F}{\partial \sigma_x}, \frac{\partial F}{\partial \sigma_y}, \frac{\partial F}{\partial \sigma_z}, \frac{\partial F}{\partial \tau_{yz}}, \frac{\partial F}{\partial \tau_{xz}}, \frac{\partial F}{\partial \tau_{xy}} \right] \quad (3.109)$$

and

$$A = -\frac{1}{d\lambda} \frac{\partial F}{\partial \kappa} d\kappa \quad (3.110)$$

The vector $\{a\}$ is termed the *flow vector*. Eq (3.98) is rewritten as

$$d\epsilon = [D]^{-1} d\sigma + d\lambda \frac{\partial F}{\partial \sigma} \quad (3.111)$$

where $[D]$ is the usual matrix of elastic constants. Premultiplying both sides of Eq (3.110) with $\{d_D\}^T = \{a\}^T [D]$ and eliminating $\{a\}^T d\sigma$ by the use of Eq (3.107), we obtain the plastic multiplier $d\lambda$ to be

$$d\lambda = \frac{1}{[A + \{a\}^T [D] \{a\}]} \{a\}^T \{d_D\} d\epsilon \quad . \quad (3.112)$$

Or substituting Eq (3.111) into Eq (3.110), we obtain the complete elasto-plastic incremental stress-strain relation to be

$$\{d\sigma\} = [D_{ep}] \{d\epsilon\} \quad , \quad (3.113)$$

with

$$[D_{ep}] = [D] - \frac{\{d_D\} \{d_D\}^T}{A + \{d_D\} \{a\}} \quad , \quad \{d_D\} = [D] \{a\} \quad . \quad (3.114)$$

The remaining discussion centers on determining the explicit form of the scalar term, A . The work hardening hypothesis is more general from a thermodynamic viewpoint [25] than the strain hardening hypothesis and is employed in this discussion. Thus,

$$d\kappa = \{\sigma\}^T \{d\epsilon^p\} \quad . \quad (3.115)$$

Eq (3.105) is rewritten in the form

$$F(\sigma, \kappa) = f(\sigma) - \sigma_Y(\kappa) = 0 \quad , \quad (3.116)$$

since the uniaxial stress, $\sigma_Y = \sqrt{3} \kappa$. Thus, from Eq (3.109)

$$A = -\frac{1}{d\lambda} \frac{\partial F}{\partial \kappa} d\kappa = \frac{1}{d\lambda} \frac{d\sigma_Y}{d\kappa} d\kappa \quad . \quad (3.117)$$

Note that the full differential may be employed in the last term since σ_Y is a function of κ only.

Employing the normality condition in Eq (3.114) to express $d\epsilon^p$, we have

$$d\kappa = \{\sigma\}^T \{d\epsilon^p\} = \{\sigma\}^T d\lambda \{a\} = d\lambda \{a\}^T \{\sigma\} \quad . \quad (3.118)$$

Or, for the uniaxial case $\sigma = \bar{\sigma} = \sigma_Y$ and $d\epsilon^p = d\bar{\epsilon}^p$ where $\bar{\sigma}$ and $\bar{\epsilon}^p$ are respectively the effective stress and plastic strain, Eq (3.117) becomes

$$d\kappa = \{\sigma_Y\} \{d\bar{\epsilon}^p\} = d\lambda \{a\}^T \{\sigma\} \quad . \quad (3.119)$$

Also, from Eq (3.100) we have

$$H' = \frac{d\bar{\sigma}}{d\bar{\epsilon}^p} = \frac{d\sigma_Y}{d\bar{\epsilon}^p} \quad . \quad (3.120)$$

Using Euler's theorem [144:228] applicable to all homogeneous functions of order one, we can write from Eq (3.115)

$$\left(\frac{\partial F}{\partial \sigma}\right)(\sigma) = \sigma_Y \quad . \quad (3.121)$$

Or, from Eq (3.108)

$$\{a\}^T \{\sigma\} = \sigma_Y \quad . \quad (3.122)$$

If Eqs (3.119) and (3.121) are substituted into Eqs (3.114) & (3.116), one obtains

$$\begin{aligned} d\lambda &= d\bar{\epsilon}^p \\ A &= H' \end{aligned} \quad . \quad (3.123)$$

Thus, A is obtained to be the local slope of the uniaxial stress/plastic strain curve and can be determined experimentally from Eq (3.103).

3.6 Anisotropic Elastic-Plastic Theory

The formulation of the stress-strain relations for anisotropic material proceeds in a similar manner to the isotropic case (see Ref [61] for complete development). The plastic potential function (effective stress) is defined as [61]:

$$F(\sigma_{ij}) = \bar{\sigma}^{-2} = \alpha_{12}(\sigma_{11} - \sigma_{22})^2 + \alpha_{23}(\sigma_{22} - \sigma_{33})^2 + \alpha_{31}(\sigma_{33} - \sigma_{11})^2 + 3\alpha_{44}\sigma_{23}^2 + 3\alpha_{55}\sigma_{13}^2 + 3\alpha_{66}\sigma_{12}^2 \quad (3.124)$$

where α_{ij} 's are parameters whose values are characteristic of the present state of anisotropy. It should be noted that no linear terms are included in the definition of the effective stress. This is tantamount to assuming the material exhibits no Baushinger effect and the subsequent yield loci will be concentric with the initial yield surface. The subscripts 1,2,3 indicate that the stress tensor is referred to the principal material axes. Hill [79] has shown, from plastic work considerations, that the plastic strain increment is found from the equation

$$d\epsilon_{ij}^p = \frac{\partial F(\sigma_{ij})}{\partial \sigma_{ij}} d\lambda \quad (3.125)$$

in much the same manner as the isotropic case. Carrying out the differentiation and rewriting the result, the following set of equations are obtained

$$d\epsilon_{11}^p = (\alpha_{11}\sigma_{11} - \alpha_{12}\sigma_{22} - \alpha_{31}\sigma_{33}) d\lambda \quad (3.126a)$$

$$d\epsilon_{22}^p = (\alpha_{22}\sigma_{22} - \alpha_{23}\sigma_{33} - \alpha_{12}\sigma_{11}) d\lambda \quad (3.126b)$$

$$d\epsilon_{33}^p = (\alpha_{33}\sigma_{33} - \alpha_{31}\sigma_{11} - \alpha_{23}\sigma_{22}) d\lambda \quad (3.126c)$$

$$d\epsilon_{23}^p = \frac{3}{2}\alpha_{44}\sigma_{23}d\lambda \quad (3.126d)$$

$$d\epsilon_{13}^p = \frac{3}{2}\alpha_{55}\sigma_{13}d\lambda \quad (3.126e)$$

$$d\epsilon_{12}^p = \frac{3}{2}\alpha_{66}\sigma_{12}d\lambda \quad (3.126f)$$

The conditions of incompressibility, or constant volume, in plastic deformation are applied,

$$d\epsilon_{11}^p = d\epsilon_{22}^p = d\epsilon_{33}^p = 0 \quad (3.126)$$

and the relations between the α_{ij} parameters are developed. To satisfy the condition of constant volume in plastic deformation, the α_{ij} 's must satisfy the following equations

$$\begin{aligned}\alpha_{11} &= \alpha_{12} + \alpha_{31} \\ \alpha_{22} &= \alpha_{23} + \alpha_{12} \\ \alpha_{33} &= \alpha_{31} + \alpha_{23}\end{aligned}\tag{3.127}$$

Experimental investigations of Hill's theory of anisotropic plasticity have been conducted by several investigators [68, 95, 122]. A very thorough experimental investigation of Zircaloy-2, which is highly anisotropic, was undertaken by Mehan [122]. The results of this investigation are listed in Lubahn and Felgar [117]. From the results of Mehan's work it can be seen that the anisotropic parameters are not quite constant but the variation is relatively small. If the anisotropic parameters are assumed to be constants, they may be evaluated from Eq (3.128). Let the value of the effective stress at which the material deforms plastically equal to K . The anisotropic parameters may be evaluated by letting all stress components equal zero except one. Thus,

$$\alpha_{11} = \alpha_{12} + \alpha_{31} = \left(\frac{K}{Y_{11}} \right)^2, \tag{3.129a}$$

$$\alpha_{22} = \alpha_{23} + \alpha_{12} = \left(\frac{K}{Y_{22}} \right)^2, \tag{3.129b}$$

$$\alpha_{33} = \alpha_{31} + \alpha_{23} = \left(\frac{K}{Y_{33}} \right)^2, \tag{3.129c}$$

$$\alpha_{44} = \frac{1}{3} \left(\frac{K}{Y_{23}} \right)^2, \tag{3.129d}$$

$$\alpha_{55} = \frac{1}{3} \left(\frac{K}{Y_{13}} \right)^2, \tag{3.129e}$$

$$\alpha_{66} = \frac{1}{3} \left(\frac{K}{Y_{12}} \right)^2. \tag{3.129f}$$

The Y_{ij} values are the yield stresses in each of the given directions indicated by the subscripts.

To completely define the plastic stress-strain increment relations, $d\lambda$, the scalar factor of proportionality, must be evaluated. The relation defining $d\lambda$ may be found by investigating the increment of plastic work expressions. For a plastically deformed body, the increment of plastic work

per unit volume is:

$$d\bar{W}^p = \sigma_{ij} d\epsilon_{ij}^p \quad (3.128)$$

By substituting for the strain increments from Eqs (3.126a) - (3.126f), Eq (3.130), in expanded form, becomes:

$$\begin{aligned} d\bar{W}^p = & \sigma_{11} (\alpha_{11} \sigma_{11} - \alpha_{12} \sigma_{22} - \alpha_{31} \sigma_{33}) d\lambda \\ & + \sigma_{22} (\alpha_{22} \sigma_{22} - \alpha_{23} \sigma_{33} - \alpha_{12} \sigma_{11}) d\lambda \\ & + \sigma_{33} (\alpha_{33} \sigma_{33} - \alpha_{31} \sigma_{11} - \alpha_{23} \sigma_{22}) d\lambda \\ & + 2\sigma_{23} ((3/2) \alpha_{44} \sigma_{23}) d\lambda + 2\sigma_{13} ((3/2) \alpha_{55} \sigma_{13}) d\lambda \\ & + 2\sigma_{12} ((3/2) \alpha_{66} \sigma_{12}) d\lambda \end{aligned} \quad (3.129)$$

Equation (3.131) can be simplified, reducing to

$$d\bar{W}^p = \bar{\sigma}^2 d\lambda \quad (3.130)$$

The increment of effective plastic strain is defined by the equation

$$\begin{aligned} (d\bar{\epsilon}^p)^2 = & \frac{1}{G^2} \left[\alpha_{12} (\alpha_{23} d\epsilon_{11}^p - \alpha_{31} d\epsilon_{22}^p)^2 \right. \\ & + \alpha_{23} (\alpha_{31} d\epsilon_{22}^p - \alpha_{12} d\epsilon_{33}^p)^2 \\ & + \alpha_{31} (\alpha_{12} d\epsilon_{33}^p - \alpha_{23} d\epsilon_{11}^p)^2 \left. \right] \\ & + \frac{4}{3} \left[\frac{(d\epsilon_{23}^p)^2}{\alpha_{44}} + \frac{(d\epsilon_{13}^p)^2}{\alpha_{55}} + \frac{(d\epsilon_{12}^p)^2}{\alpha_{66}} \right] \end{aligned} \quad (3.131)$$

where $G = \alpha_{12}\alpha_{23} + \alpha_{23}\alpha_{31} + \alpha_{31}\alpha_{12}$. Hu [85] has shown that:

$$d\lambda = \frac{d\bar{\epsilon}^{-p}}{\bar{\sigma}} \quad (3.132)$$

Substituting for $d\lambda$ in Eq (3.134) into Eq (3.132) leads to the differential work expression

$$d\bar{W}^p = \bar{\sigma} d\bar{\epsilon} \quad (3.133)$$

Hill has shown that if there is a functional relationship existing between the plastic work and the effective stress, there also exists a functional relation between the effective stress and the effective strain. The $d\lambda$ constant is next submitted into Eqs (3.126a) - (3.126f) giving the following incremental plastic strain equations

$$d\epsilon_{11}^p = (\alpha_{11}\sigma_{11} - \alpha_{12}\sigma_{22} - \alpha_{31}\sigma_{33}) \frac{d\bar{\epsilon}^{-p}}{d\bar{\sigma}} \quad (3.136a)$$

$$d\epsilon_{22}^p = (\alpha_{22}\sigma_{22} - \alpha_{23}\sigma_{33} - \alpha_{12}\sigma_{11}) \frac{d\bar{\epsilon}^{-p}}{d\bar{\sigma}} \quad (3.136b)$$

$$d\epsilon_{33}^p = (\alpha_{33}\sigma_{33} - \alpha_{31}\sigma_{11} - \alpha_{23}\sigma_{22}) \frac{d\bar{\epsilon}^{-p}}{d\bar{\sigma}} \quad (3.136c)$$

$$d\epsilon_{23}^p = \frac{3}{2}\alpha_{44}\sigma_{23} \frac{d\bar{\epsilon}^{-p}}{d\bar{\sigma}} \quad (3.136d)$$

$$d\epsilon_{13}^p = \frac{3}{2}\alpha_{55}\sigma_{13} \frac{d\bar{\epsilon}^{-p}}{d\bar{\sigma}} \quad (3.136e)$$

$$d\epsilon_{12}^p = \frac{3}{2}\alpha_{66}\sigma_{12} \frac{d\bar{\epsilon}^{-p}}{d\bar{\sigma}} \quad (3.136f)$$

The increment of plastic strain is based on the previous value of stress rather than the incremented value of stress. Eqs (3.123), (3.128), (3.133), (3.139) & (3.136a) - (3.136f) form a set of fundamental equations for determining the stress-strain distribution in an anisotropic body.

To complete the anisotropic plasticity equations, the relation between effective stress and

strain must be established. For isotropic material, this relation is found from a uniaxial tensile stress-strain curve described by a Ramberg-Osgood type of algebraic equation [61]. The relationship between effective stress and effective strain for anisotropic material is much more complicated since a series of uniaxial tension tests would generally yield widely differing results depending on the orientation of the material axes with respect to the loading axis. Hu [85] assumes that $\bar{\sigma}$ and $\bar{\epsilon}$ vary in the same manner as σ_{11} and ϵ_{11} . That is, if

$$\epsilon_{11}^p = k \sigma_{11}^n \quad , \quad (3.134)$$

then

$$\bar{\epsilon} = k \bar{\sigma}^{-n} \quad . \quad (3.135)$$

This would be true if all uniaxial tests yielded the same result. Since the material is anisotropic, by the very definition of anisotropy, different results should be expected from a series of uniaxial tests in different directions. The results of Mehan's investigation of Zircaloy-2 verify that Hu's assumption, that $\bar{\sigma}$ and $\bar{\epsilon}$ are directly related to σ_{11} and ϵ_{11} , is, in general, a poor one.

Since we are dealing with an anisotropic material the stress-strain curve in every direction will be different. Therefore, some form of average effective stress-strain curve must be formulated. This average effective stress-strain curve might be described by a Ramberg-Osgood type equation and should be based on the stress-strain curves of the material in uniaxial tension as well as shear. If a uniaxial test in the σ_{11} direction yields $\bar{\epsilon} = g_1(\bar{\sigma})$, with similar algebraic forms in the other 5 tests. We may define an effective stress-strain relation by averaging the uniaxial stress-strain relations in a form similar to Eq (3.123) [61]. An equation of this nature fulfills the two requirements that the effective strain is a function of the effective stress and that the effective stress-strain equation changes as the stress ratios vary. The effective stress-strain relation may be defined as

$$\begin{aligned} \bar{\varepsilon} = g(\bar{\sigma}) = & \alpha_{11}g_1\left(\frac{\sigma_{11}}{\bar{\sigma}}\right)^2 + \alpha_{22}g_2\left(\frac{\sigma_{22}}{\bar{\sigma}}\right)^2 + \alpha_{33}g_3\left(\frac{\sigma_{33}}{\bar{\sigma}}\right)^2 \\ & - 2\alpha_{12}g_{12}\frac{\sigma_{11}\sigma_{22}}{\bar{\sigma}^2} - 2\alpha_{23}g_{23}\frac{\sigma_{22}\sigma_{33}}{\bar{\sigma}^2} - 2\alpha_{31}g_{13}\frac{\sigma_{11}\sigma_{33}}{\bar{\sigma}^2} \\ & + 3\alpha_{44}g_4\left(\frac{\sigma_{23}}{\bar{\sigma}}\right)^2 + 3\alpha_{55}g_5\left(\frac{\sigma_{13}}{\bar{\sigma}}\right)^2 + 3\alpha_{66}g_6\left(\frac{\sigma_{12}}{\bar{\sigma}}\right)^2 \end{aligned} \quad (3.136)$$

In the above equation, g_{ij} are chosen weighted average of g_i and g_j . The g_i is the nonlinear portion of the $\sigma - \varepsilon$ curve, shown in . The simplest way of averaging is to take g_{ij} equal to g_i or g_j depending on which α_{ii} is taken as unity. With the addition of Eq (3.133), (3.139), a complete theory of anisotropy plasticity, which is applicable to engineering problems, is formulated.

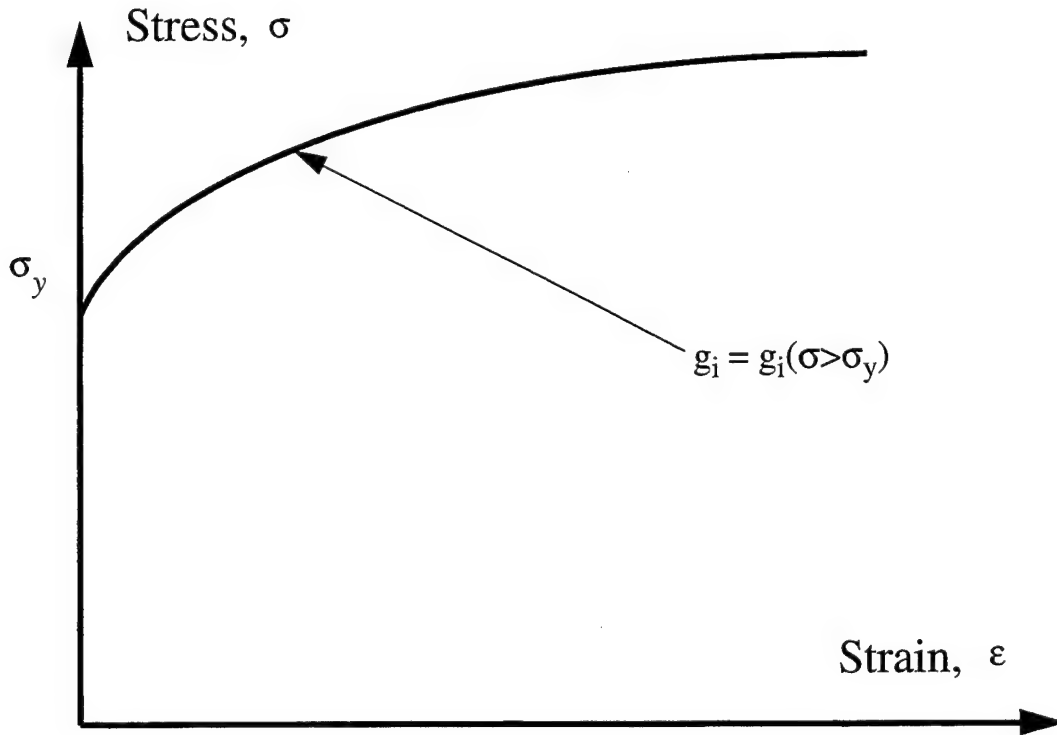


Figure 3.12 Nonlinear $\sigma - \varepsilon$ Curve Demonstrating Relationship of $\sigma > \sigma_Y$ to g_i

In the formulation of the equations to be used, it is assumed that: the state of stress is a plane

state, $g_{ij} = g_i$, $K = Y_{11}$, and $\alpha_{11} = 1$. The general form of the Ramberg-Osgood equation for a uniaxial stress state is taken as

$$\varepsilon = \frac{\sigma}{E} + k\sigma^n \quad , \quad (3.137)$$

where

$E \equiv$ modulus of elasticity

$k \equiv$ strength coefficient

$n \equiv$ strain hardening coefficient.

If this type of equation is used to describe the stress-strain relations in the σ_{11} , σ_{22} , and σ_{12} directions, the following set of equations is obtained considering only the plastic portion of the strain

$$\begin{aligned} \bar{\varepsilon}^{-p} &= k_1 \bar{\sigma}^{-n} = g_1 \\ \bar{\varepsilon}^{-p} &= k_2 \bar{\sigma}^{-n} = g_2 \\ \bar{\varepsilon}^{-p} &= k_3 \bar{\sigma}^{-n} = g_3 \end{aligned} \quad (3.138)$$

Therefore, the average effective stress-strain relation for plane stress becomes

$$\begin{aligned} \bar{\varepsilon} = g(\bar{\sigma}) &= \alpha_{11} g_1 \left(\frac{\sigma_{11}}{\bar{\sigma}} \right)^2 + \alpha_{22} g_2 \left(\frac{\sigma_{22}}{\bar{\sigma}} \right)^2 \\ &- 2\alpha_{12} g_1 \frac{\sigma_{11}\sigma_{22}}{\bar{\sigma}^2} + 3\alpha_{66} g_3 \left(\frac{\sigma_{12}}{\bar{\sigma}} \right)^2 \end{aligned} \quad (3.139)$$

It has been tacitly implied by the use of the same exponent in Eq (3.141) that the three stress-strain curves have somewhat the same general shape. This is by no means a necessary assumption, but it does simplify the formulation of the equations somewhat. If the basic shape of the three stress-strain curves were completely different, then the equations should be assumed to be of

the form

$$\begin{aligned}\varepsilon^{-p} &= k_1 \sigma^{-n_1} = g_1 \\ \varepsilon^{-p} &= k_2 \sigma^{-n_2} = g_2 \\ \varepsilon^{-p} &= k_3 \sigma^{-n_3} = g_3\end{aligned}\tag{3.140}$$

4. Theoretical Development

The third-order cubic-nonlinear transverse shear deformation theory for elastic shells is suitable for many problems of practical interest. However, there are four areas of analysis that require further examination. Specific problems of interest are those that consider spherical geometry, rotations and curvature within the element become very large, nonlinear material behavior in the element, and when strains within the element becoming large. The first problem of interest is the area of spherical shell geometry. As mentioned previously in Chapters 1 & 2, the area of cylindrical shell analysis has been thoroughly studied in the area of geometrical nonlinearity for both isotropic and composite materials. The area of spherical shell analysis is being studied but still offers many opportunities for investigation. According to Dennis [48] and Librescu [107, 108], the assumptions of a third-order displacement field of the cubic-nonlinear HTSD theory are accurate for problems where the in-plane strains and stresses are larger than transverse quantities. These judgements are based upon Koiter's work [98] and the ratio of h/R . Dennis [48, 49, 51] evaluated problems with various ratios of h/R , and concluded the cubic-nonlinear HTSD was acceptable provided the criteria of $h/R < 1/5$ was met. Smith [208], in developing higher-order thickness expansions, determined that a more appropriate criteria for the cubic-nonlinear HTSD theory is $h^2/R^2 \ll 1$. Thus, the cubic-nonlinear HTSD theory is applicable for spherical geometries.

A second area of interest is in nonlinear material analysis. The area of nonlinear material analysis for cylindrical shells is being studied but still requires further analysis, particularly in the area of composite materials. However, little research has been accomplished in the area of spherical shells, due mainly to the complexity of the strain-displacement relations with the added curvature terms. The last area of interest is when strains become large enough such that the Cauchy stress-strain (Eulerian) and the second Piola stress-Green strain (Lagrangian) coordinate systems are no longer coincident. This has been addressed from a theoretical aspect [229] but has not been approached from a numerical aspect.

Some problems investigated using the cubic-nonlinear HTSD theory, however, would seem to have exhibited large stresses and strains despite small values of h/R . For example, a graphite-epoxy (AS4-350) cylindrical shell panel with clamped lateral edges and transverse point load was

analyzed by Tsai and Palazotto [223, 224]. This shell had a 12-inch radius and was 0.04-inches thick, therefore, h/R was equal to $1/300$. Transverse displacements for this problem exceeded 65 times the panel thickness (2.5-inch displacement). A deep circular arch problem Dennis investigated had transverse displacements of over 30 times the thickness [48:257-265]. The effects of material nonlinearity and a large strain analysis were not determined during these studies

4.1 Spherical Geometric Behavior

From Eq (3.72), a third-order displacement field for the spherical shell shown in Figure 4.1, which includes the higher-order transverse shear deformation (HTSD) theory, is represented by

$$\begin{aligned} u_1(y_1, y_2, y_3) &= u(1 - Dy_3) + \psi_1 y_3 + k(w_{,1} + \psi_1) y_3^3 \\ u_2(y_1, y_2, y_3) &= v(1 - Cy_3) + \psi_2 y_3 + k(w_{,2} + \psi_2) y_3^3 \\ u_3(y_1, y_2) &= w \end{aligned} \quad (4.1)$$

where the seven degrees of freedom u , v , w , $w_{,1}$, $w_{,2}$, ψ_1 , and ψ_2 are functions of the midsurface coordinates (y_1, y_2) only. The ψ_i are rotations of the normals, and we define $D = 1/R_1$, $C = 1/R_2$, and $k = -4/(3h^2)$. These kinematic equations give exactly zero linear transverse shear strains at the upper and lower surface of a flat plate where $y = \pm h/2$. However, Smith [207] showed that for a curved shell, the linear transverse shear strains are only "approximately" zero at the upper and lower surfaces. As long as the shell meets the criteria of $h/R < 5$, the error is minimized. If the shell no longer meets this criteria, the error becomes too large, and the extensions by Smith [207:Chap 4, pp 3-9, Appendix D] must be included to enforce the exact zero boundary conditions at the upper and lower surfaces. For a curved shell, Eq (4.1) yields approximately zero linear transverse shear terms for $y = \pm h/2$ [48, 207, 208]. The additional term (D) in Eq (4.1) is required to account for curvature in the s_1 -direction yielding spherical geometry. The strain-displacement relations for the quasi-nonlinear HTSD theory are given by

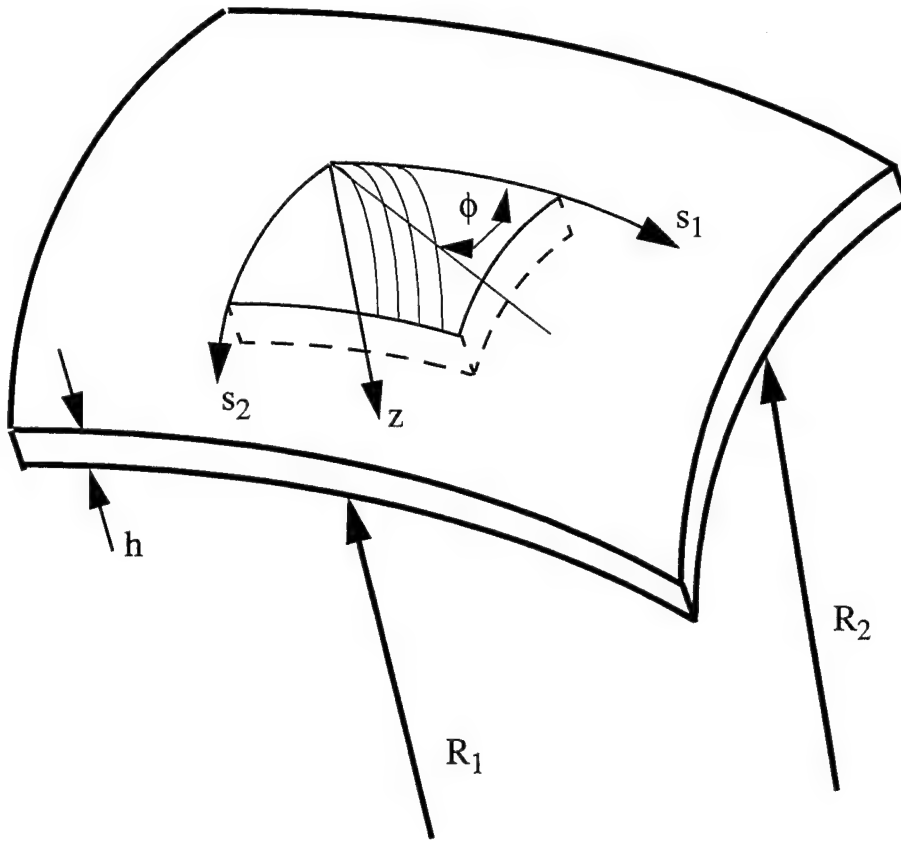


Figure 4.1 Spherical Shell Domain for Derivation of the HTSD Theory

$$\begin{aligned} \epsilon_1 = & \frac{u_{1,1}}{h_1} + \frac{u_2 h_{1,2}}{h_1 h_2} + \frac{u_3 h_{1,3}}{h_1 h_3} + \frac{1}{2h_1^2} \left(u_{1,1} + \frac{u_2 h_{1,2}}{h_2} + \frac{u_3 h_{1,3}}{h_3} \right)^2, \\ & + \frac{1}{2h_1^2} \left(u_{2,1} - \frac{u_1 h_{1,2}}{h_2} \right)^2 + \frac{1}{2h_1^2} \left(u_{3,1} - \frac{u_1 h_{1,3}}{h_3} \right)^2 \end{aligned} \quad (4.2a)$$

$$\begin{aligned} \epsilon_2 = & \frac{u_{2,2}}{h_2} + \frac{u_1 h_{2,1}}{h_1 h_2} + \frac{u_3 h_{2,3}}{h_2 h_3} + \frac{1}{2h_2^2} \left(u_{2,2} + \frac{u_1 h_{2,1}}{h_1} + \frac{u_3 h_{2,3}}{h_3} \right)^2, \\ & + \frac{1}{2h_2^2} \left(u_{1,2} - \frac{u_2 h_{2,1}}{h_1} \right)^2 + \frac{1}{2h_2^2} \left(u_{3,2} - \frac{u_2 h_{2,3}}{h_3} \right)^2 \end{aligned} \quad (4.2b)$$

$$\varepsilon_4 = \frac{1}{2} \left(\frac{u_{2,3}}{h_3} + \frac{u_{3,2}}{h_2} - \frac{u_3 h_{3,2}}{h_2 h_3} - \frac{u_2 h_{2,3}}{h_2 h_3} \right) \quad , \quad (4.2c)$$

$$\varepsilon_5 = \frac{1}{2} \left(\frac{u_{1,3}}{h_3} + \frac{u_{3,1}}{h_1} - \frac{u_3 h_{3,1}}{h_1 h_3} - \frac{u_1 h_{1,3}}{h_1 h_3} \right) \quad , \quad (4.2d)$$

$$\begin{aligned} \varepsilon_6 = & \frac{1}{2} \left(\frac{u_{1,3}}{h_3} + \frac{u_{3,1}}{h_1} - \frac{u_3 h_{3,1}}{h_1 h_3} - \frac{u_1 h_{1,3}}{h_1 h_3} \right) \quad (4.2e) \\ & + \frac{1}{2h_1 h_2} \left(u_{1,2} - \frac{u_2 h_{2,1}}{h_1} \right) \left(u_{1,1} + \frac{u_2 h_{1,2}}{h_2} + \frac{u_3 h_{1,3}}{h_3} \right) \\ & + \frac{1}{2h_1 h_2} \left(u_{2,1} - \frac{u_1 h_{1,2}}{h_2} \right) \left(u_{2,2} + \frac{u_1 h_{2,1}}{h_1} + \frac{u_3 h_{2,3}}{h_3} \right) \\ & + \frac{1}{2h_1 h_2} \left(u_{3,1} - \frac{u_1 h_{1,3}}{h_3} \right) \left(u_{3,2} - \frac{u_1 h_{2,3}}{h_3} \right) \end{aligned}$$

The complete strain-displacement relations are given in Appendix E. The comparison of the results based upon the kinematics of Eq (4.1) with published results, and the results of problems not yet published, is a significant part of this research.

4.2 Nonlinear Material Behavior

It is well established that unique relations do not exist between stress and strain in the plastic region (when strains are large). The strain depends not only on the final state of stress, but also the loading history. Therefore, the standard stress-strain relations in the theory of elasticity must be replaced by relations between increments of stress and strain using incremental theories of plasticity. These theories are often called incremental strain theory or flow theory of plasticity.

In this section, of nonlinear material behavior is discussed in three parts. Initially, layered isotropic materials are discussed for nonlinear elastic and elastic-plastic considerations. The approach considered incorporates a layered method to effectively consider bending. Secondly, nonlinear elastic and elastic-plastic relations are discussed from a layer method for laminated composite materials. Finally, a large strain formulation is discussed. This requires transforming the constitutive relations from Eulerian coordinates to Lagrangian coordinates for both the stress-

state and strain-state relations.

4.2.1 Layered Isotropic Material: In Chapter 9 of Owen and Hinton [144], Mindlin plate bending relations are formulated to include transverse shear strain using multiple layers. This layered approach is used to capture the spread of plasticity over the depth of the plate or shell. Thus, the shell is divided into a number of layers, each of which may become plastic separately. As the number of layers is increased, the model provides a more realistic representation of the gradual spread of plasticity over the shell cross-section. References [144 - 147] suggest a total of eight layers are needed.

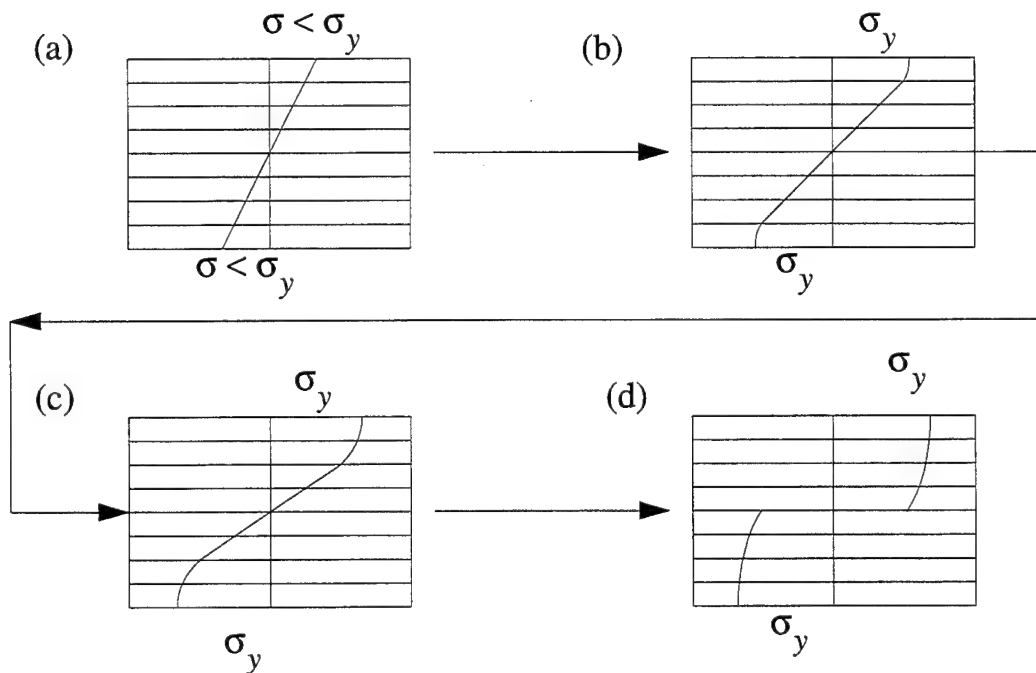


Figure 4.2 Yielding of Layered Section [144]

It is assumed that as the stress in the middle of the outer layers reaches the yield value, then the outer layers become plastic, while the rest of the layers remain elastic, as shown in Figures 4.2(a) and 4.2(b). Then, as more stress is applied, more layers become plastic, until the whole cross-section eventually becomes plastic (Figures 4.2(b)-4.2(d)). This layered approach is easily incorporated into an elastic-plastic laminated composite material analysis. Since the analysis of elastic-plastic laminated composites is a primary thrust of the author's work, this method is

extremely important in attempting to quantify the nonlinear material behavior of composites.

For elastic isotropic materials, the stress-strain relations are given by

$$\{d\sigma\} = [D']^k \{d\epsilon^e\} , \quad (4.3)$$

where $d\epsilon^e$ is the elastic strain component, and k denotes each layer. The constitutive matrix is given by

$$[D']^k = \frac{E}{(1-\nu^2)} \begin{bmatrix} 1 & \nu & 0 & 0 & 0 \\ 0 & 1 & 0 & 0 & 0 \\ 0 & 0 & \frac{(1-\nu)}{2} & 0 & 0 \\ 0 & 0 & 0 & \frac{(1-\nu)}{2} & 0 \\ 0 & 0 & 0 & 0 & \frac{(1-\nu)}{2} \end{bmatrix}^k = \begin{bmatrix} D'_f & 0 \\ 0 & D'_s \end{bmatrix}^k , \quad (4.4)$$

or with more typical notation

$$[D']^k = [Q_{ij}]^k = \begin{bmatrix} Q_{11} & Q_{12} & 0 & 0 & 0 \\ Q_{12} & Q_{11} & 0 & 0 & 0 \\ 0 & 0 & Q_{66} & 0 & 0 \\ 0 & 0 & 0 & Q_{66} & 0 \\ 0 & 0 & 0 & 0 & Q_{66} \end{bmatrix}^k , \quad (4.5)$$

where

$$Q_{11} = \frac{E}{(1-\nu^2)}$$

$$Q_{12} = \frac{\nu E}{(1-\nu^2)}$$

$$Q_{66} = \frac{E}{2(1-\nu)} = G$$

This implies

$$\begin{bmatrix} D'_f \end{bmatrix}^k = \begin{bmatrix} Q_{11} & Q_{12} & 0 \\ Q_{12} & Q_{11} & 0 \\ 0 & 0 & Q_{66} \end{bmatrix}^k, \begin{bmatrix} D'_s \end{bmatrix}^k = \begin{bmatrix} Q_{66} & 0 \\ 0 & Q_{66} \end{bmatrix}^k \quad (4.6)$$

For the layered isotropic material, we can assume a yield function F is a function of the stresses associated with flexure σ_f but not the transverse shear stresses, σ_s . This assumption is based on the thinness of the shell, which implies that transverse shear strains remain linear. This, in turn, implies that transverse shear stresses never develop magnitudes that require a plasticity analysis in the transverse directions. The assumption is consistent with the author's desire to develop a shell oriented analysis and not a three-dimensional plasticity approach. The yield function F is also a function of the hardening parameter, H' .

When yielding occurs at some point, it is assumed, unless loading occurs, the stresses always remain on the yield surface such that

$$F(\sigma_f, H') = 0 \quad (4.7)$$

Then the incremental elastic-plastic stress-strain relationship is written as

$$\{d\sigma\}^k = \begin{bmatrix} D'_{ep} \end{bmatrix}^k \{d\epsilon\} \quad (4.8)$$

Here $d\epsilon = d\epsilon^e + d\epsilon^p$ is the sum of the elastic and plastic strain components. The constitutive relations take the form of the *Prandtl-Reuss flow equations* (see Section 3.5.4) and are shown below

$$\begin{bmatrix} D'_{ep} \end{bmatrix}^k = \begin{bmatrix} (D'_{ep})_f & 0 \\ 0 & D'_s \end{bmatrix}^k, \quad (4.9)$$

where

$$\begin{bmatrix} (D'_{ep})_f \end{bmatrix}^k = \begin{bmatrix} D'_f \end{bmatrix}^k - \frac{\{d_D\} \{d_D\}^T}{A + \{d_D\} \{a\}^T}, \quad (4.10a)$$

$$\{d_D\} = [D'_f]^k \{a\} \quad , \quad (4.10b)$$

$$\{a\}^T = \left[\frac{\partial F}{\partial \sigma_{11}}, \frac{\partial F}{\partial \sigma_{22}}, \frac{\partial F}{\partial \sigma_{12}} \right] \quad , \quad (4.10c)$$

$$A = -\frac{1}{\lambda} \frac{\partial F}{\partial H} dH \quad . \quad (4.10d)$$

The plastic potential function for a material following the von Mises yield criteria is given by

$$\begin{aligned} F(\sigma) &= \bar{\sigma}^2 = 3(J_2) = \frac{3}{2} \sigma'_{ij} \sigma'_{ij} \\ &= \frac{3}{2} [\sigma'^2_{11} + \sigma'^2_{22} + \sigma'^2_{33}] + 3(\sigma'^2_{23} + \sigma'^2_{13} + \sigma'^2_{12}) \end{aligned} \quad (4.11)$$

To incorporate the strain-hardening effect, it is necessary to determine the scalar A , the strain hardening parameter. Owen & Hinton [144] show that

$$A = H' = \frac{d\sigma_Y}{d\varepsilon} = \frac{d\bar{\sigma}}{d\varepsilon} \quad . \quad (4.12)$$

Thus, by experimentally determining the material's effective stress versus effective plastic strain relationship, it is possible to numerically quantify the strain hardening parameter A . A straightforward method of characterizing the nonlinear stress-strain curves is assuming the material takes the general form of the Ramberg-Osgood equation [61] for a uniaxial stress state. The Ramberg-Osgood equation, for a strain-dependent formulation, is given by

$$\varepsilon_m = \frac{\sigma_{m-1}}{E} + k \sigma_{m-1}^n \quad , \quad (4.13)$$

where E is the modulus of elasticity, k is the strength coefficient, n is the strain hardening characteristic, and m is the current strain interval. This implies that the plastic strain is determined by the stress state at the previous step shown by Eq (4.14)

$$\varepsilon_m^p = k \sigma_{m-1}^n \quad , \quad (4.14)$$

or

$$\bar{\epsilon}_m^{-p} = k \bar{\sigma}_{m-1}^{-n} \quad (4.15)$$

By differentiation, we write

$$d\bar{\epsilon}_m^{-p} = kn \bar{\sigma}_{m-1}^{-n-1} d\bar{\sigma}_{m-1} \quad (4.16)$$

Thus, in terms of the Ramberg-Osgood relations, the strain hardening parameter $A = H'$ is defined to be

$$H' = \frac{d\bar{\sigma}_{m-1}}{d\bar{\epsilon}_m^{-p}} = \frac{1}{kn \bar{\sigma}_{m-1}^{-n-1}} \quad (4.17)$$

4.2.2 Layered Composite Material: The layered approach for through-the-thickness plasticity is again incorporated into developing the laminated composite elastic-plastic constitutive relations. In general, the elastic laminated composite constitutive relations are determined by integrating through-the-thickness, per lamina (see reference [61] for details). Thus, incorporating the layered plasticity analysis is a relatively simple and straight forward procedure. Again, an incremental approach is included to approximate the nonlinear material effects of the laminate. In the first increment, the material is assumed to be completely elastic. Thus,

$$\{d\sigma\}^k = \left[\bar{Q}_{ij}^e \right]^k \{d\epsilon\} \quad (4.18)$$

where

$$\left[\bar{Q}_{ij}^e \right]^k = \begin{bmatrix} \bar{Q}_{11} & \bar{Q}_{12} & \bar{Q}_{16} & 0 & 0 \\ \bar{Q}_{12} & \bar{Q}_{22} & \bar{Q}_{26} & 0 & 0 \\ \bar{Q}_{16} & \bar{Q}_{26} & \bar{Q}_{66} & 0 & 0 \\ 0 & 0 & 0 & \bar{Q}_{44} & \bar{Q}_{45} \\ 0 & 0 & 0 & \bar{Q}_{45} & \bar{Q}_{55} \end{bmatrix}^k = \begin{bmatrix} \left(\bar{Q}_{ij}^e \right)_f & 0 \\ 0 & \left(\bar{Q}_{ij}^e \right)_s \end{bmatrix}^k \quad (4.19)$$

are the material stiffnesses of the k^{th} laminate in the material axis system for the in-plane and transverse shear portions (f and s respectively). These material stiffnesses are defined in Eq (3.62).

After the first increment, yielding is determined for each layer. If a layer has yielded, the stress-strain relation for the plastic range is given by

$$\{d\sigma\}^k = [\bar{Q}_{ij}^p]^k \{d\epsilon\} = \begin{bmatrix} \left(\bar{Q}_{ij}^p\right)_f & 0 \\ 0 & \left(\bar{Q}_{ij}^e\right)_s \end{bmatrix}^k \{d\epsilon\} \quad , \quad (4.20)$$

where

$$\left[\left(\bar{Q}_{ij}^p\right)_f\right]^k = \left[\left(\bar{Q}_{ij}^e\right)_f\right]^k - \frac{\{d_D\} \{d_D\}^T}{A - \{d_D\} \{a\}^T} \quad , \quad (4.21a)$$

$$\{d_D\} = \left[\left(\bar{Q}_{ij}^e\right)_f\right]^k \{a\} \quad , \quad (4.21b)$$

$$\{a\}^T = \left[\frac{\partial F}{\partial \sigma_{11}}, \frac{\partial F}{\partial \sigma_{22}}, \frac{\partial F}{\partial \sigma_{12}} \right] \quad , \quad (4.21c)$$

$$A = -\frac{1}{\lambda} \frac{\partial F}{\partial H} dH \quad . \quad (4.21d)$$

The plastic potential function, based on the modified Huber-Mises law for anisotropic composites [67, 85, 86, 102, 144 - 146] is given by

$$\begin{aligned} F(\sigma) = \bar{\sigma}^2 = & a_{12} (\sigma_{11} - \sigma_{22})^2 + a_{23} (\sigma_{22} - \sigma_{33})^2 \\ & + a_{31} (\sigma_{33} - \sigma_{11})^2 + 3a_{44} \sigma_{23}^2 + 3a_{55} \sigma_{13}^2 + 3a_{66} \sigma_{12}^2 = 0 \end{aligned} \quad (4.22)$$

In this equation, $\bar{\sigma}$ is called the effective stress, and the a_{ij} are *anisotropic interaction* parameters determined experimentally. For the layered approach, each layer would have its own plastic potential function. With the assumption of negligible transverse normal stress for shell theory, the plastic potential function defined in Eq (4.22) reduces to

$$F(\sigma) = \bar{\sigma}^2 = a_{12}(\sigma_{11} - \sigma_{22})^2 + a_{23}\sigma_{22}^2 + a_{31}\sigma_{11}^2 + 3a_{44}\sigma_{23}^2 + 3a_{55}\sigma_{13}^2 + 3a_{66}\sigma_{12}^2 = 0 \quad (4.23)$$

To satisfy the condition of constant volume in plastic deformation [61], the a_{ij} parameters must satisfy the following equations

$$\begin{aligned} a_{11} &= a_{12} + a_{31} \\ a_{22} &= a_{23} + a_{12} \\ a_{33} &= a_{31} + a_{23} \end{aligned} \quad (4.24)$$

Experimental investigations of Hill's theory of anisotropic plasticity have been conducted by several investigators [68, 95, 122]. A very thorough experimental investigation of Zircaloy-2, which is highly anisotropic, was undertaken by Mehan [122]. The result of this investigation are listed in Lubahn and Felgar [117]. From the results of Mehan's work it can be seen that the anisotropic interaction parameters are not quite constant but the variation is relatively small. If the anisotropic interaction parameters are assumed to be constants, they may be evaluated from Eq (4.24). Let the value of the effective stress at which the material deforms plasticity equal to K . The anisotropic parameters may be evaluated by letting all the stress components equal zero except one. Thus,

$$a_{11} = a_{12} + a_{31} = \left(\frac{K}{Y_{11}}\right)^2, \quad (4.25a)$$

$$a_{22} = a_{23} + a_{12} = \left(\frac{K}{Y_{22}}\right)^2, \quad (4.25b)$$

$$a_{33} = a_{31} + a_{23} = \left(\frac{K}{Y_{33}}\right)^2, \quad (4.25c)$$

$$a_{44} = \frac{1}{3}\left(\frac{K}{Y_{23}}\right)^2, \quad (4.25d)$$

$$a_{55} = \frac{1}{3}\left(\frac{K}{Y_{13}}\right)^2, \quad (4.25e)$$

$$a_{66} = \frac{1}{3} \left(\frac{K}{Y_{12}} \right)^2 \quad (4.25f)$$

The Y_{ij} values are the yield stresses in each of the given directions indicated by the subscripts. Since transversely isotropic materials are being analyzed (implying $Y_{22} = Y_{33}$, $Y_{12} = Y_{13}$, $Y_{23} = (0.8)Y_{12}$), and allowing $K = Y_{11}$, Eqs (4.25a) - (4.25f) become

$$a_{11} = a_{12} + a_{31} = \left(\frac{Y_{11}}{Y_{11}} \right)^2 = 1 \quad (4.26a)$$

$$a_{22} = a_{23} + a_{12} = \left(\frac{Y_{11}}{Y_{22}} \right)^2 \quad (4.26b)$$

$$a_{33} = a_{31} + a_{23} = \left(\frac{Y_{11}}{Y_{33}} \right)^2 = \left(\frac{Y_{11}}{Y_{22}} \right)^2 \quad (4.26c)$$

$$a_{44} = \frac{1}{3} \left(\frac{Y_{11}}{Y_{23}} \right)^2 = \frac{1}{3} \left(\frac{Y_{11}}{(0.8)Y_{12}} \right)^2 = \frac{1}{3(0.64)} \left(\frac{Y_{11}}{Y_{12}} \right)^2 \quad (4.26d)$$

$$a_{55} = \frac{1}{3} \left(\frac{Y_{11}}{Y_{13}} \right)^2 = \frac{1}{3} \left(\frac{Y_{11}}{Y_{12}} \right)^2 \quad (4.26e)$$

$$a_{66} = \frac{1}{3} \left(\frac{Y_{11}}{Y_{12}} \right)^2 \quad (4.26f)$$

The effective strain for anisotropic materials is defined as

$$\begin{aligned} \bar{\epsilon}^p = & a_{11}g_1 \left(\frac{\sigma_{11}}{\sigma} \right)^2 + a_{22}g_2 \left(\frac{\sigma_{22}}{\sigma} \right)^2 + a_{33}g_3 \left(\frac{\sigma_{33}}{\sigma} \right)^2 \\ & -2a_{12}g_{12} \frac{\sigma_{11}\sigma_{22}}{\sigma} -2a_{23}g_{23} \frac{\sigma_{22}\sigma_{33}}{\sigma} -2a_{31}g_{31} \frac{\sigma_{11}\sigma_{33}}{\sigma} \\ & +3a_{44}g_4 \left(\frac{\sigma_{23}}{\sigma} \right)^2 +3a_{55}g_5 \left(\frac{\sigma_{13}}{\sigma} \right)^2 +3a_{66}g_6 \left(\frac{\sigma_{12}}{\sigma} \right)^2 \end{aligned} \quad (4.27)$$

In the equation above, g_{ij} are a chosen weighted average of g_i and g_j . The g_{ij} represent the nonlinear portion of the $\sigma - \epsilon$ curve and is demonstrated in Figure 3.12. The simplest way of

averaging is to take g_{ij} equal to g_i or g_j depending on which a_{ii} is taken as unity. Since the assumption is that $K = Y_{II}$ and $a_{II} = 1$, then $g_{ij} = g_i$. From Eq (4.15), we define the following set of equations

$$\begin{aligned}\bar{\varepsilon}^{-p} &= k_1 \bar{\sigma}^{-n} = g_1 \\ \bar{\varepsilon}^{-p} &= k_2 \bar{\sigma}^{-n} = g_2 \\ \bar{\varepsilon}^{-p} &= k_3 \bar{\sigma}^{-n} = g_3\end{aligned}\quad (4.28)$$

Therefore, incorporating the shell assumption of $\sigma_{33} \approx 0$, and including the definitions of Eq (4.28), Eq (4.27) becomes

$$\begin{aligned}\bar{\varepsilon}^{-p} &= a_{11}g_1 \left(\frac{\sigma_{11}}{\bar{\sigma}} \right)^2 + a_{22}g_2 \left(\frac{\sigma_{22}}{\bar{\sigma}} \right)^2 - 2a_{12}g_{12} \frac{\sigma_{11}\sigma_{22}}{\bar{\sigma}^2} \\ &+ 3a_{44}g_4 \left(\frac{\sigma_{23}}{\bar{\sigma}} \right)^2 + 3a_{55}g_5 \left(\frac{\sigma_{13}}{\bar{\sigma}} \right)^2 + 3a_{66}g_6 \left(\frac{\sigma_{12}}{\bar{\sigma}} \right)^2\end{aligned}\quad (4.29)$$

or

$$\begin{aligned}\bar{\varepsilon}^{-p} &= a_{11}k_1\sigma_{11}^2\bar{\sigma}^{-(n-2)} + a_{22}k_2\sigma_{22}^2\bar{\sigma}^{-(n-2)} \\ &- 2a_{12}k_1\sigma_{11}\sigma_{22}\bar{\sigma}^{-(n-2)} + 3a_{44}k_3\sigma_{23}^2\bar{\sigma}^{-(n-2)} \\ &+ 3a_{55}k_3\sigma_{13}^2\bar{\sigma}^{-(n-2)} + 3a_{66}k_3\sigma_{12}^2\bar{\sigma}^{-(n-2)}\end{aligned}\quad (4.30a)$$

$$\begin{aligned}\bar{\varepsilon}^{-p} &= \left[k_1 \left(a_{11}\sigma_{11}^2 - 2a_{12}\sigma_{11}\sigma_{22} \right) + k_2 a_{22}\sigma_{22}^2 \right. \\ &\left. + 3k_3 \left(a_{44}\sigma_{23}^2 + a_{55}\sigma_{13}^2 + a_{66}\sigma_{12}^2 \right) \right] \bar{\sigma}^{-(n-2)}\end{aligned}\quad (4.30b)$$

It has been tacitly implied by the use of the same exponent in Eq (4.28) that the three stress-

strain curves have somewhat the same general shape. This is by no means a necessary assumption, but it does simplify the formulation of the equations somewhat. If the basic shape of the three stress-strain curves were completely different, or if individual curve fits were used for each stress-strain curve, then the equations are of the form

$$\begin{aligned}\bar{\epsilon}^{-p} &= k_1 \bar{\sigma}^{-n_1} = g_1 \\ \bar{\epsilon}^{-p} &= k_2 \bar{\sigma}^{-n_2} = g_2 \\ \bar{\epsilon}^{-p} &= k_3 \bar{\sigma}^{-n_3} = g_3\end{aligned}\quad (4.31)$$

Then Eqs (4.30a) & (4.30b) would take the form

$$\begin{aligned}\bar{\epsilon}^{-p} &= a_{11} k_1 \bar{\sigma}_{11}^2 \bar{\sigma}^{-(n_1-2)} + a_{22} k_2 \bar{\sigma}_{22}^2 \bar{\sigma}^{-(n_2-2)} \\ &\quad - 2a_{12} k_1 \bar{\sigma}_{11} \bar{\sigma}_{22} \bar{\sigma}^{-(n_1-2)} + 3a_{44} k_3 \bar{\sigma}_{23}^2 \bar{\sigma}^{-(n_3-2)} \\ &\quad + 3a_{55} k_3 \bar{\sigma}_{13}^2 \bar{\sigma}^{-(n_3-2)} + 3a_{66} k_3 \bar{\sigma}_{12}^2 \bar{\sigma}^{-(n_3-2)} \\ &= k_1 \left(a_{11} \bar{\sigma}_{11}^2 - 2a_{12} \bar{\sigma}_{11} \bar{\sigma}_{22} \right) \bar{\sigma}^{-(n_1-2)} + k_2 a_{22} \bar{\sigma}_{22}^2 \bar{\sigma}^{-(n_2-2)} \\ &\quad + 3k_3 \left(a_{44} \bar{\sigma}_{23}^2 + a_{55} + a_{44} \bar{\sigma}_{12}^2 \right) \bar{\sigma}^{-(n_3-2)}\end{aligned}\quad (4.32)$$

Referring back to Eq (4.30b), then by differentiation we have

$$\begin{aligned}d\bar{\epsilon}^{-p} &= (n-2) \left[k_1 \left(a_{11} \bar{\sigma}_{11}^2 - 2a_{12} \bar{\sigma}_{11} \bar{\sigma}_{22} \right) + k_2 a_{22} \bar{\sigma}_{22}^2 \right. \\ &\quad \left. + 3k_3 \left(a_{44} \bar{\sigma}_{23}^2 + a_{55} + a_{44} \bar{\sigma}_{12}^2 \right) \right] \bar{\sigma}^{-(n-3)} d\bar{\sigma}\end{aligned}\quad (4.33)$$

Thus, in terms of the Ramberg-Osgood parameters, the strain-hardening parameter H' , for anisotropic materials, is defined to be

$$\begin{aligned}H' &= d\bar{\sigma} / (d\bar{\epsilon}^{-p}) = 1 / \left((n-2) \left[k_1 \left(a_{11} \bar{\sigma}_{11}^2 - 2a_{12} \bar{\sigma}_{11} \bar{\sigma}_{22} \right) \right. \right. \\ &\quad \left. \left. + k_2 a_{22} \bar{\sigma}_{22}^2 + 3k_3 \left(a_{44} \bar{\sigma}_{23}^2 + a_{55} + a_{44} \bar{\sigma}_{12}^2 \right) \right] \bar{\sigma}^{-(n-3)} \right)\end{aligned}\quad (4.34)$$

For the more general form, where n is no longer constant for all $\bar{\sigma} - \bar{\epsilon}$ curves, Eq (4.33) becomes

$$\begin{aligned}
 d\bar{\epsilon}^{-p} = & (n_1 - 2) k_1 \left(a_{11} \sigma_{11}^2 - 2a_{12} \sigma_{11} \sigma_{22} \right) \bar{\sigma}^{-(n_1 - 3)} \\
 & + (n_2 - 2) k_2 a_{22} \sigma_{22}^2 \bar{\sigma}^{-(n_2 - 3)} \\
 & + (n_3 - 2) k_3 \left(a_{44} \sigma_{23}^2 + a_{55} \sigma_{13}^2 + a_{66} \sigma_{12}^2 \right) \bar{\sigma}^{-(n_3 - 3)}
 \end{aligned} \quad (4.35)$$

and Eq (4.34) becomes

$$\begin{aligned}
 H = d\bar{\sigma}/d\bar{\epsilon}^{-p} = & 1 / \left[(n_1 - 2) k_1 \left(a_{11} \sigma_{11}^2 - 2a_{12} \sigma_{11} \sigma_{22} \right) \bar{\sigma}^{-(n_1 - 3)} \right. \\
 & + (n_2 - 2) k_2 a_{22} \sigma_{22}^2 \bar{\sigma}^{-(n_2 - 3)} \\
 & \left. + (n_3 - 2) k_3 \left(a_{44} \sigma_{23}^2 + a_{55} \sigma_{13}^2 + a_{66} \sigma_{12}^2 \right) \bar{\sigma}^{-(n_3 - 3)} \right]
 \end{aligned} \quad (4.36)$$

4.2.3 Large Strain Formulation: According to Washizu [229] and Dvorak [58], when strains are no longer assumed to be small, the rotation of the material axis system relative to the undeformed structural axis system becomes substantial and therefore must be accounted for. Due to the large rotations and strains, the material properties are no longer constant when considered in a total Lagrangian coordinate system (x_i). If one defines a local Eulerian coordinate system (X_i) at a point $P^{(0)}$ before deformation, one can formulate the transformation law between the Green's strain tensor and the Eulerian (Cauchy) strain tensor. Let the strain tensor defined with respect to the local Eulerian coordinates be denoted by $e_{\lambda\mu}$. Then the Cauchy strain components defined with respect to the general Green strain components are given by [229]

$$e_{ij} = \chi_{i,k} \chi_{j,l} \epsilon_{kl} = \frac{\partial x_i}{\partial X_k} \frac{\partial x_j}{\partial X_l} \epsilon_{kl} \quad (4.37)$$

Note the Cauchy strain components is a by-product of deformation occurring by arriving at a deformed orthogonal axis system. The Green strain components is the state of deformation coming from an orthogonal coordinate system to a deformed non-orthogonal set of axes.

In the above expression, the $\chi_{i,j} = (\partial x_i)/(\partial X_j)$ terms are elements of the transformation between the Cauchy (Eulerian) coordinate system (X) and the 2nd Piola stress-Green strain

(Lagrangian) coordinate system (x).

There is a similar transformation between the 2nd Piola-Kirchhoff (Lagrangian) stress tensor, σ_{ij} , and the Cauchy (Euler) stress tensor, σ_{ij}^E . The 2nd Piola-Kirchhoff stress tensor is defined with respect to the undeformed (Lagrangian) coordinates, after deformation has occurred, as shown in Figure 4.3. The Cauchy stress tensor is defined with respect to the local (Eulerian) coordinates as shown in Figure 4.4. The transformation between the Kirchhoff stress tensor and the Cauchy stress tensor is given by

$$\sigma_{ij}^E = \frac{1}{D} \xi_{i,k} \xi_{j,l} = \frac{1}{D} \frac{\partial X_i}{\partial x_k} \frac{\partial X_j}{\partial x_l} \sigma_{kl} \quad , \quad (4.38)$$

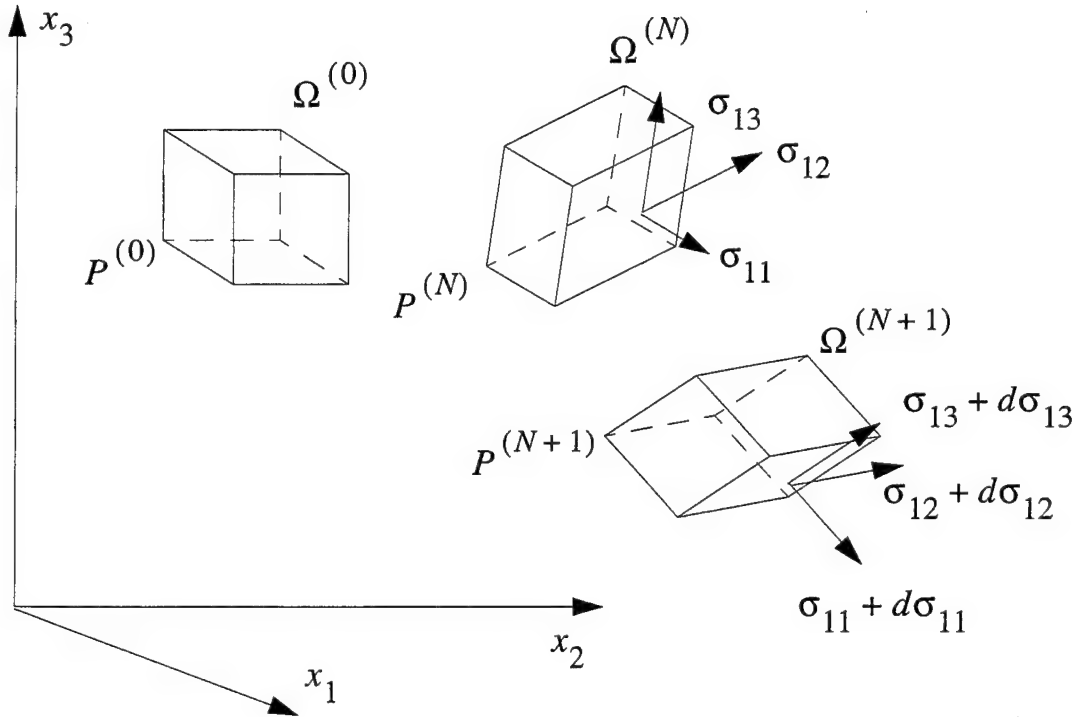


Figure 4.3 Definition of 2nd Piola-Kirchhoff Stress Tensor [229]

where ξ_i is the coordinate in the deformed state and

$$\xi_{i,j} = \frac{\partial X_i}{\partial x_j} = X_{i,j} = \delta_{ij} + u_{i,j} = \delta_{ij} + \frac{\partial u_i}{\partial x_j} \quad , \quad (4.39)$$

with

$$D = \det[\xi_{i,j}] = \xi_{1,1}\xi_{2,2}\xi_{3,3} + \xi_{1,2}\xi_{2,3}\xi_{3,1} + \xi_{1,3}\xi_{2,1}\xi_{3,2} - \xi_{1,1}\xi_{2,3}\xi_{3,2} - \xi_{1,3}\xi_{2,2}\xi_{3,1} - \xi_{1,2}\xi_{2,1}\xi_{3,3} \quad (4.40)$$

We define in Eulerian coordinates the stress-strain relations to be

$$(\sigma^E) = [a] (\epsilon) \quad , \quad (4.41)$$

where $[a]$ is the Eulerian constitutive matrix. We can denote the transformation of the stress-state from 2nd Piola-Kirchhoff stress to Cauchy stress by

$$(\sigma^E) = \frac{1}{D} [T_1] (\sigma) \quad , \quad (4.42)$$

and the transformation of the strain-state from the Green to the Cauchy strain directions by

$$(e) = \frac{1}{D^2} [T_2] (\epsilon) \quad . \quad (4.43)$$

Substituting Eqs (4.29) and (4.30a) into Eq (4.41) yields

$$\frac{1}{D} [T_1] (\sigma) = \frac{1}{D^2} [a] [T_2] (\epsilon) \quad , \quad (4.44)$$

or rewriting yields

$$(\sigma) = \frac{1}{D} [T_1]^{-1} [a] [T_2] (\epsilon) = [D] (\epsilon) \quad , \quad (4.45)$$

where $[D]$ is the Lagrangian constitutive matrix. To generate the constitutive matrix, it is necessary to find D , $[T_1]$ and $[T_2]$.

To accomplish this we begin by noting

$$\xi_{i,j} = \delta_{ij} + u_{i,j} \quad , \quad (4.46)$$

and

$$\xi_{i,k} \chi_{k,j} = \frac{\partial X_i}{\partial x_k} \frac{\partial x_k}{\partial X_j} = \delta_{ij} \quad , (i,j=1-3) \quad (4.47)$$

which implies

$$\chi_{k,j} = [\xi_{i,k}]^{-1} \quad , \quad (4.48)$$

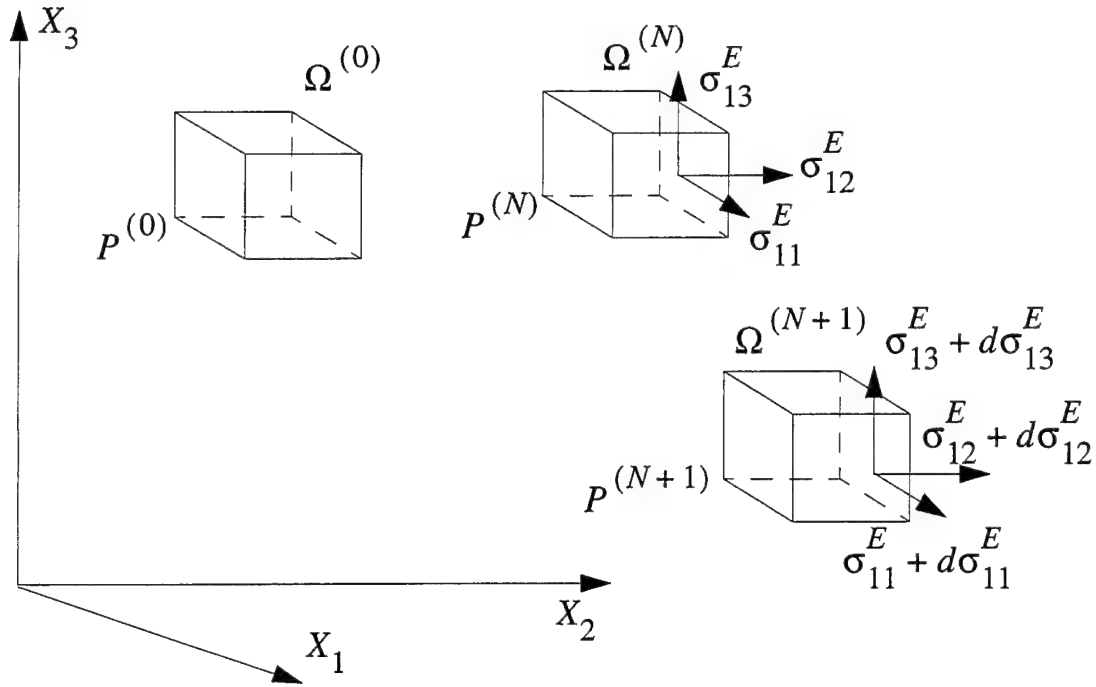


Figure 4.4 Definition of Cauchy Stress Tensor [229]

or

$$\chi_{1,1} = (\xi_{2,2}\xi_{3,3} - \xi_{2,3}\xi_{3,2})/D \quad , \quad (4.49a)$$

$$\chi_{1,2} = -(\xi_{1,2}\xi_{3,3} - \xi_{1,3}\xi_{3,2})/D \quad , \quad (4.49b)$$

$$\chi_{1,3} = (\xi_{1,2}\xi_{2,3} - \xi_{1,3}\xi_{2,2})/D \quad , \quad (4.49c)$$

$$\chi_{2,1} = -(\xi_{2,1}\xi_{3,3} - \xi_{2,3}\xi_{3,1})/D \quad , \quad (4.49d)$$

$$\chi_{2,2} = (\xi_{1,1}\xi_{3,3} - \xi_{1,3}\xi_{3,1})/D \quad , \quad (4.49e)$$

$$\chi_{2,3} = -(\xi_{1,1}\xi_{2,3} - \xi_{1,3}\xi_{2,1})/D \quad , \quad (4.49f)$$

$$\chi_{3,1} = (\xi_{2,1}\xi_{3,2} - \xi_{2,2}\xi_{3,1})/D \quad , \quad (4.49g)$$

$$\chi_{3,2} = -(\xi_{1,1}\xi_{3,2} - \xi_{1,2}\xi_{3,1})/D \quad , \quad (4.49h)$$

$$\chi_{3,3} = (\xi_{1,1}\xi_{2,2} - \xi_{1,2}\xi_{2,1})/D \quad . \quad (4.49i)$$

Using the transformation law between σ_{ij}^E and σ_{ij} , a stress-state transformation is determined to be

$$\begin{aligned} \sigma_{11}^E = \frac{1}{D} & (\xi_{1,1}\xi_{1,1}\sigma_{11} + \xi_{1,1}\xi_{1,2}\sigma_{12} + \xi_{1,1}\xi_{1,3}\sigma_{13} \\ & + \xi_{1,2}\xi_{1,1}\sigma_{21} + \xi_{1,2}\xi_{1,2}\sigma_{22} + \xi_{1,2}\xi_{1,3}\sigma_{23} + \xi_{1,3}\xi_{1,1}\sigma_{31} \\ & + \xi_{1,3}\xi_{1,2}\sigma_{32} + \xi_{1,3}\xi_{1,3}\sigma_{33}) \end{aligned} \quad , \quad (4.50a)$$

$$\begin{aligned} \sigma_{22}^E = \frac{1}{D} & (\xi_{2,1}\xi_{2,1}\sigma_{11} + \xi_{2,1}\xi_{2,2}\sigma_{12} + \xi_{2,1}\xi_{2,3}\sigma_{13} \\ & + \xi_{2,2}\xi_{2,1}\sigma_{21} + \xi_{2,2}\xi_{2,2}\sigma_{22} + \xi_{2,2}\xi_{2,3}\sigma_{23} + \xi_{2,3}\xi_{2,1}\sigma_{31} \\ & + \xi_{2,3}\xi_{2,2}\sigma_{32} + \xi_{2,3}\xi_{2,3}\sigma_{33}) \end{aligned} \quad , \quad (4.50b)$$

$$\begin{aligned} \sigma_{33}^E = \frac{1}{D} & (\xi_{3,1}\xi_{3,1}\sigma_{11} + \xi_{3,1}\xi_{3,2}\sigma_{12} + \xi_{3,1}\xi_{3,3}\sigma_{13} \\ & + \xi_{3,2}\xi_{3,1}\sigma_{21} + \xi_{3,2}\xi_{3,2}\sigma_{22} + \xi_{3,2}\xi_{3,3}\sigma_{23} + \xi_{3,3}\xi_{3,1}\sigma_{31} \\ & + \xi_{3,3}\xi_{3,2}\sigma_{32} + \xi_{3,3}\xi_{3,3}\sigma_{33}) \end{aligned} \quad , \quad (4.50c)$$

$$\begin{aligned} \sigma_{23}^E = \frac{1}{D} & (\xi_{2,1}\xi_{3,1}\sigma_{11} + \xi_{2,1}\xi_{3,2}\sigma_{12} + \xi_{2,1}\xi_{3,3}\sigma_{13} \\ & + \xi_{2,2}\xi_{3,1}\sigma_{21} + \xi_{2,2}\xi_{3,2}\sigma_{22} + \xi_{2,2}\xi_{3,3}\sigma_{23} + \xi_{2,3}\xi_{3,1}\sigma_{31} \\ & + \xi_{2,3}\xi_{3,2}\sigma_{32} + \xi_{2,3}\xi_{3,3}\sigma_{33}) \end{aligned} \quad , \quad (4.50d)$$

$$\begin{aligned} \sigma_{13}^E = \frac{1}{D} & (\xi_{1,1}\xi_{3,1}\sigma_{11} + \xi_{1,1}\xi_{3,2}\sigma_{12} + \xi_{1,1}\xi_{3,3}\sigma_{13} \\ & + \xi_{1,2}\xi_{3,1}\sigma_{21} + \xi_{1,2}\xi_{3,2}\sigma_{22} + \xi_{1,2}\xi_{3,3}\sigma_{23} + \xi_{1,3}\xi_{3,1}\sigma_{31} \\ & + \xi_{1,3}\xi_{3,2}\sigma_{32} + \xi_{1,3}\xi_{3,3}\sigma_{33}) \end{aligned} \quad , \quad (4.50e)$$

$$\begin{aligned} \sigma_{12}^E = \frac{1}{D} & (\xi_{1,1}\xi_{2,1}\sigma_{11} + \xi_{1,1}\xi_{2,2}\sigma_{12} + \xi_{1,1}\xi_{2,3}\sigma_{13} \\ & + \xi_{1,2}\xi_{2,1}\sigma_{21} + \xi_{1,2}\xi_{2,2}\sigma_{22} + \xi_{1,2}\xi_{2,3}\sigma_{23} + \xi_{1,3}\xi_{2,1}\sigma_{31} \\ & + \xi_{1,3}\xi_{2,2}\sigma_{32} + \xi_{1,3}\xi_{2,3}\sigma_{33}) \end{aligned} \quad , \quad (4.50f)$$

Since the 2nd Piola-Kirchhoff tensor, σ_{ij} , is symmetric, we write

$$\begin{aligned} \sigma_{11}^E = \frac{1}{D} & (\xi_{1,1}\xi_{1,1}\sigma_{11} + \xi_{1,2}\xi_{1,2}\sigma_{22} + \xi_{1,3}\xi_{1,3}\sigma_{33} \\ & + 2\xi_{1,2}\xi_{1,3}\sigma_{23} + 2\xi_{1,1}\xi_{1,3}\sigma_{13} + 2\xi_{1,1}\xi_{1,2}\sigma_{12}) \end{aligned} \quad , \quad (4.51a)$$

$$\begin{aligned} \sigma_{22}^E = \frac{1}{D} & (\xi_{2,1}\xi_{2,1}\sigma_{11} + \xi_{2,2}\xi_{2,2}\sigma_{22} + \xi_{2,3}\xi_{2,3}\sigma_{33} \\ & + 2\xi_{2,2}\xi_{2,3}\sigma_{23} + 2\xi_{2,1}\xi_{2,3}\sigma_{13} + 2\xi_{2,1}\xi_{2,2}\sigma_{12}) \end{aligned} \quad , \quad (4.51b)$$

$$\begin{aligned} \sigma_{33}^E = \frac{1}{D} & (\xi_{3,1}\xi_{3,1}\sigma_{11} + \xi_{3,2}\xi_{3,2}\sigma_{22} + \xi_{3,3}\xi_{3,3}\sigma_{33} \\ & + 2\xi_{3,2}\xi_{3,3}\sigma_{23} + 2\xi_{3,1}\xi_{3,3}\sigma_{13} + 2\xi_{3,1}\xi_{3,2}\sigma_{12}) \end{aligned} \quad , \quad (4.51c)$$

$$\begin{aligned} \sigma_{23}^E = \frac{1}{D} & (\xi_{2,1}\xi_{3,1}\sigma_{11} + \xi_{2,2}\xi_{3,2}\sigma_{22} + \xi_{2,3}\xi_{3,3}\sigma_{33} \\ & + (\xi_{2,2}\xi_{3,3} + \xi_{2,3}\xi_{3,2})\sigma_{23} + (\xi_{2,1}\xi_{3,3} + \xi_{2,3}\xi_{3,1})\sigma_{13} \\ & + (\xi_{2,1}\xi_{3,2} + \xi_{2,2}\xi_{3,1})\sigma_{12}) \end{aligned} \quad , \quad (4.51d)$$

$$\begin{aligned} \sigma_{13}^E = \frac{1}{D} & (\xi_{1,1}\xi_{3,1}\sigma_{11} + \xi_{1,2}\xi_{3,2}\sigma_{22} + \xi_{1,3}\xi_{3,3}\sigma_{33} \\ & + (\xi_{1,2}\xi_{3,3} + \xi_{1,3}\xi_{3,2})\sigma_{23} + (\xi_{1,1}\xi_{3,3} + \xi_{1,3}\xi_{3,1})\sigma_{13} \\ & + (\xi_{1,1}\xi_{3,2} + \xi_{1,2}\xi_{3,1})\sigma_{12}) \end{aligned} \quad , \quad (4.51e)$$

$$\begin{aligned} \sigma_{12}^E = \frac{1}{D} & (\xi_{1,1}\xi_{2,1}\sigma_{11} + \xi_{1,2}\xi_{2,2}\sigma_{22} + \xi_{1,3}\xi_{2,3}\sigma_{33} \\ & + (\xi_{1,2}\xi_{2,3} + \xi_{1,3}\xi_{2,2})\sigma_{23} + (\xi_{1,1}\xi_{2,3} + \xi_{1,3}\xi_{2,1})\sigma_{13} \\ & + (\xi_{1,1}\xi_{2,2} + \xi_{1,2}\xi_{2,1})\sigma_{12}) \end{aligned} \quad (4.51f)$$

or in matrix form

$$\begin{pmatrix} \sigma_{11}^E \\ \sigma_{22}^E \\ \sigma_{33}^E \\ \sigma_{23}^E \\ \sigma_{13}^E \\ \sigma_{12}^E \end{pmatrix} = \frac{1}{D} \begin{bmatrix} (\xi_{1,1})^2 & (\xi_{1,2})^2 & (\xi_{1,3})^2 \\ (\xi_{2,1})^2 & (\xi_{2,2})^2 & (\xi_{2,3})^2 \\ (\xi_{3,1})^2 & (\xi_{3,2})^2 & (\xi_{3,3})^2 \\ \xi_{2,1}\xi_{3,1} & \xi_{2,2}\xi_{3,2} & \xi_{2,3}\xi_{3,3} \\ \xi_{1,1}\xi_{3,1} & \xi_{1,2}\xi_{3,2} & \xi_{1,3}\xi_{3,3} \\ \xi_{1,1}\xi_{2,1} & \xi_{1,2}\xi_{2,2} & \xi_{1,3}\xi_{2,3} \end{bmatrix} \quad (4.52a)$$

$$\begin{bmatrix} 2\xi_{1,2}\xi_{1,3} & 2\xi_{1,1}\xi_{1,3} & 2\xi_{1,1}\xi_{1,2} \\ 2\xi_{2,2}\xi_{2,3} & 2\xi_{2,1}\xi_{2,3} & 2\xi_{2,1}\xi_{2,2} \\ 2\xi_{3,2}\xi_{3,3} & 2\xi_{3,1}\xi_{3,3} & 2\xi_{3,1}\xi_{3,2} \\ \xi_{2,2}\xi_{3,3} + \xi_{2,3}\xi_{3,2} & \xi_{2,1}\xi_{3,3} + \xi_{2,3}\xi_{3,1} & \xi_{2,1}\xi_{3,2} + \xi_{2,2}\xi_{3,1} \\ \xi_{1,2}\xi_{3,3} + \xi_{1,3}\xi_{3,2} & \xi_{1,1}\xi_{3,3} + \xi_{1,3}\xi_{3,1} & \xi_{1,1}\xi_{3,2} + \xi_{1,2}\xi_{3,1} \\ \xi_{1,2}\xi_{2,3} + \xi_{1,3}\xi_{2,2} & \xi_{1,1}\xi_{2,3} + \xi_{1,3}\xi_{2,1} & \xi_{1,1}\xi_{2,2} + \xi_{1,2}\xi_{2,1} \end{bmatrix} \begin{pmatrix} \sigma_{11} \\ \sigma_{22} \\ \sigma_{33} \\ \sigma_{23} \\ \sigma_{13} \\ \sigma_{12} \end{pmatrix} \quad (4.52b)$$

Using contracted notation ($\sigma_{11} = \sigma_1$, $\sigma_{22} = \sigma_2$, $\sigma_{23} = \sigma_4$, $\sigma_{13} = \sigma_5$, $\sigma_{12} = \sigma_6$) and applying the shell theory assumption of $\sigma_3 \approx 0$ to Eqs (4.52a) & (4.52b), one obtains

$$\begin{pmatrix} \sigma_1^E \\ \sigma_2^E \\ \sigma_4^E \\ \sigma_5^E \\ \sigma_6^E \end{pmatrix} = \frac{1}{D} \begin{bmatrix} (\xi_{1,1})^2 & (\xi_{1,2})^2 & 2\xi_{1,2}\xi_{1,3} \\ (\xi_{2,1})^2 & (\xi_{2,2})^2 & 2\xi_{2,2}\xi_{2,3} \\ \xi_{2,1}\xi_{3,1} & \xi_{2,2}\xi_{3,2} & \xi_{2,2}\xi_{3,3} + \xi_{2,3}\xi_{3,2} \\ \xi_{1,1}\xi_{3,1} & \xi_{1,2}\xi_{3,2} & \xi_{1,2}\xi_{3,3} + \xi_{1,3}\xi_{3,2} \\ \xi_{1,1}\xi_{2,1} & \xi_{1,2}\xi_{2,2} & \xi_{1,2}\xi_{2,3} + \xi_{1,3}\xi_{2,2} \end{bmatrix} \quad (4.53a)$$

$$\begin{bmatrix} 2\xi_{1,1}\xi_{1,3} & 2\xi_{1,1}\xi_{1,2} \\ 2\xi_{2,1}\xi_{2,3} & 2\xi_{2,1}\xi_{2,2} \\ \xi_{2,1}\xi_{3,3} + \xi_{2,3}\xi_{3,1} & \xi_{2,1}\xi_{3,2} + \xi_{2,2}\xi_{3,1} \\ \xi_{1,1}\xi_{3,3} + \xi_{1,3}\xi_{3,1} & \xi_{1,1}\xi_{3,2} + \xi_{1,2}\xi_{3,1} \\ \xi_{1,1}\xi_{2,3} + \xi_{1,3}\xi_{2,1} & \xi_{1,1}\xi_{2,2} + \xi_{1,2}\xi_{2,1} \end{bmatrix} \begin{pmatrix} \sigma_1 \\ \sigma_2 \\ \sigma_4 \\ \sigma_5 \\ \sigma_6 \end{pmatrix} \quad (4.53b)$$

We can develop a similar strain-state transformation matrix given as (in contracted notation)

$$\begin{pmatrix} e_1 \\ e_2 \\ e_3 \\ e_4 \\ e_5 \\ e_6 \end{pmatrix} = \frac{1}{D^2} \begin{bmatrix} (\chi_{1,1})^2 & (\chi_{1,2})^2 & (\chi_{1,3})^2 \\ (\chi_{2,1})^2 & (\chi_{2,2})^2 & (\chi_{2,3})^2 \\ (\chi_{3,1})^2 & (\chi_{3,2})^2 & (\chi_{3,3})^2 \\ \chi_{2,1}\chi_{3,1} & \chi_{2,2}\chi_{3,2} & \chi_{2,3}\chi_{3,3} \\ \chi_{1,1}\chi_{3,1} & \chi_{1,2}\chi_{3,2} & \chi_{1,3}\chi_{3,3} \\ \chi_{1,1}\chi_{2,1} & \chi_{1,2}\chi_{2,2} & \chi_{1,3}\chi_{2,3} \end{bmatrix}, \quad (4.54a)$$

$$\begin{bmatrix} 2\chi_{1,2}\chi_{1,3} & 2\chi_{1,1}\chi_{1,3} & 2\chi_{1,1}\chi_{1,2} \\ 2\chi_{2,2}\chi_{2,3} & 2\chi_{2,1}\chi_{2,3} & 2\chi_{2,1}\chi_{2,2} \\ 2\chi_{3,2}\chi_{3,3} & 2\chi_{3,1}\chi_{3,3} & 2\chi_{3,1}\chi_{3,2} \\ \chi_{2,2}\chi_{3,3} + \chi_{2,3}\chi_{3,2} & \chi_{2,1}\chi_{3,3} + \chi_{2,3}\chi_{3,1} & \chi_{2,1}\chi_{3,2} + \chi_{2,2}\chi_{3,1} \\ \chi_{1,2}\chi_{3,3} + \chi_{1,3}\chi_{3,2} & \chi_{1,1}\chi_{3,3} + \chi_{1,3}\chi_{3,1} & \chi_{1,1}\chi_{3,2} + \chi_{1,2}\chi_{3,1} \\ \chi_{1,2}\chi_{2,3} + \chi_{1,3}\chi_{2,2} & \chi_{1,1}\chi_{2,3} + \chi_{1,3}\chi_{2,1} & \chi_{1,1}\chi_{2,2} + \chi_{1,2}\chi_{2,1} \end{bmatrix} \begin{pmatrix} \varepsilon_1 \\ \varepsilon_2 \\ \varepsilon_3 \\ \varepsilon_4 \\ \varepsilon_5 \\ \varepsilon_6 \end{pmatrix} \quad (4.54b)$$

Recall, for shell theory, $\sigma_3 \approx 0$. We assume, that none of the Eulerian strains, e_i , depend upon the Lagrangian strain, ε_3 . We can determine e_3 , by dependency, through the constitutive relations. For transversely isotropic materials

$$\sigma_3^E = 0 = C_{13}e_1 + C_{23}e_2 + C_{33}e_3 \quad (4.55)$$

Solving for e_3 results in

$$\begin{aligned}
 e_3 &= -\left(\left(\frac{C_{13}}{C_{33}} \right) e_1 + \left(\frac{C_{23}}{C_{33}} \right) e_2 \right) \\
 &= -\left(\frac{E_1 \nu_{21} (1 - \nu_{23})}{E_2 (1 - \nu_{12} \nu_{21})} e_1 + \frac{E_2 \nu_{23} \nu_{12} \nu_{21}}{E_2 (1 - \nu_{12} \nu_{21})} e_2 \right) \\
 &= -\left(\frac{E_1 \nu_{21} (1 - \nu_{23})}{E_2 (1 - \nu_{12} \nu_{21})} e_1 + \frac{\nu_{23} \nu_{12} \nu_{21}}{(1 - \nu_{12} \nu_{21})} e_2 \right) \\
 &= \left(\frac{C_{13}}{C_{33}} \right) [(\chi_{1,1})^2 \epsilon_1 + (\chi_{1,2})^2 \epsilon_2 + 2\chi_{1,2}\chi_{1,3}\epsilon_4 \\
 &\quad + 2\chi_{1,1}\chi_{1,3}\epsilon_5 + 2\chi_{1,1}\chi_{1,2}\epsilon_6] \\
 &\quad - \left(\frac{C_{23}}{C_{33}} \right) [(\chi_{2,1})^2 \epsilon_1 + (\chi_{2,2})^2 \epsilon_2 + 2\chi_{2,2}\chi_{2,3}\epsilon_4 \\
 &\quad + 2\chi_{2,1}\chi_{2,3}\epsilon_5 + 2\chi_{2,1}\chi_{1,2}\epsilon_6]
 \end{aligned} \tag{4.56}$$

For isotropic materials, the constitutive relations yield

$$\sigma_3^E = 0 = C_{12} (e_1 + e_2) + C_{11} e_3 \quad , \tag{4.57}$$

and solving for e_3 results in

$$\begin{aligned}
 e_3 &= -\frac{C_{12}}{C_{11}} (e_1 + e_2) = -\frac{(1 - \nu)}{2} (e_1 + e_2) \\
 &= -\frac{(1 - \nu)}{2} [(\chi_{1,1})^2 \epsilon_1 + (\chi_{1,2})^2 \epsilon_2 + 2\chi_{1,2}\chi_{1,3}\epsilon_4 \\
 &\quad + 2\chi_{1,1}\chi_{1,3}\epsilon_5 + 2\chi_{1,1}\chi_{1,2}\epsilon_6] \\
 &\quad - \frac{(1 - \nu)}{2} [(\chi_{2,1})^2 \epsilon_1 + (\chi_{2,2})^2 \epsilon_2 + 2\chi_{2,2}\chi_{2,3}\epsilon_4 \\
 &\quad + 2\chi_{2,1}\chi_{2,3}\epsilon_5 + 2\chi_{2,1}\chi_{1,2}\epsilon_6]
 \end{aligned} \tag{4.58}$$

Due to the assumption of no dependency of e_i with respect to ϵ_3 , the strain-state transformation matrix reduces to a 5×5 form shown below

$$\begin{pmatrix} e_1 \\ e_2 \\ e_4 \\ e_5 \\ e_6 \end{pmatrix} = \frac{1}{D^2} \begin{bmatrix} (\chi_{1,1})^2 & (\chi_{1,2})^2 & 2\chi_{1,2}\chi_{1,3} \\ (\chi_{2,1})^2 & (\chi_{2,2})^2 & 2\chi_{2,2}\chi_{2,3} \\ \chi_{2,1}\chi_{3,1} & \chi_{2,2}\chi_{3,2} & \chi_{2,2}\chi_{3,3} + \chi_{2,3}\chi_{3,2} \\ \chi_{1,1}\chi_{3,1} & \chi_{1,2}\chi_{3,2} & \chi_{1,2}\chi_{3,3} + \chi_{1,3}\chi_{3,2} \\ \chi_{1,1}\chi_{2,1} & \chi_{1,2}\chi_{2,2} & \chi_{1,2}\chi_{2,3} + \chi_{1,3}\chi_{2,2} \end{bmatrix} \quad (4.59a)$$

$$\begin{bmatrix} 2\chi_{1,1}\chi_{1,3} & 2\chi_{1,1}\chi_{1,2} \\ 2\chi_{2,1}\chi_{2,3} & 2\chi_{2,1}\chi_{2,2} \\ \chi_{2,1}\chi_{3,3} + \chi_{2,3}\chi_{3,1} & \chi_{2,1}\chi_{3,2} + \chi_{2,2}\chi_{3,1} \\ \chi_{1,1}\chi_{3,3} + \chi_{1,3}\chi_{3,1} & \chi_{1,1}\chi_{3,2} + \chi_{1,2}\chi_{3,1} \\ \chi_{1,1}\chi_{2,3} + \chi_{1,3}\chi_{2,1} & \chi_{1,1}\chi_{2,2} + \chi_{1,2}\chi_{2,1} \end{bmatrix} \begin{pmatrix} \epsilon_1 \\ \epsilon_2 \\ \epsilon_4 \\ \epsilon_5 \\ \epsilon_6 \end{pmatrix} \quad (4.59b)$$

If we apply the definition of $\xi_{k,l}$ given in Eq (4.46) to Eqs (4.40), (4.49a) - (4.49i), and (4.53), and due to the shell theory assumption $u_{3,3} \approx 0$, we have

$$D = 1 + u_{1,1} + u_{2,2} + u_{1,1}u_{2,2} + u_{1,2}u_{2,3}u_{3,1} + u_{1,3}u_{2,1}u_{3,2} - u_{1,2}u_{2,1} - u_{1,3}u_{3,1} - u_{2,3}u_{3,2} - u_{1,1}u_{2,3}u_{3,2} - u_{1,3}u_{2,2}u_{3,1} \quad (4.60)$$

with

$$\chi_{1,1} = (1 + u_{2,2} - u_{2,3}u_{3,2})/D \quad , \quad (4.61a)$$

$$\chi_{1,2} = (u_{1,3}u_{3,2} - u_{1,2})/D \quad , \quad (4.61b)$$

$$\chi_{1,3} = (u_{1,2}u_{2,3} - u_{1,3}(1 + u_{2,2}))/D \quad , \quad (4.61c)$$

$$\chi_{2,1} = (u_{2,3}u_{3,1} - u_{2,1})/D \quad , \quad (4.61d)$$

$$\chi_{2,2} = (1 + u_{1,1} - u_{1,3}u_{3,1})/D \quad , \quad (4.61e)$$

$$\chi_{2,3} = (u_{1,3}u_{2,1} - u_{2,3}(1 + u_{1,1}))/D \quad , \quad (4.61f)$$

$$\chi_{3,1} = (u_{2,1}u_{3,2} - u_{3,1}(1 + u_{2,2}))/D \quad , \quad (4.61g)$$

$$\chi_{3,2} = (u_{1,2}u_{3,1} - u_{3,2}(1 + u_{1,1}))/D \quad , \quad (4.61h)$$

$$\chi_{3,3} = ((1 + u_{1,1})(1 + u_{2,2}) - u_{1,2}u_{2,1})/D \quad , \quad (4.61i)$$

Thus, from Eqs (4.52a) and (4.52b), one obtains

$$\begin{pmatrix} \sigma_1^E \\ \sigma_2^E \\ \sigma_4^E \\ \sigma_5^E \\ \sigma_6^E \end{pmatrix} = \frac{1}{D} \begin{bmatrix} (1+u_{1,1})^2 & (u_{1,2})^2 & 2u_{1,2}u_{1,3} \\ (u_{2,1})^2 & (1+u_{2,2})^2 & 2(1+u_{2,2})u_{2,3} \\ u_{2,1}u_{3,1} & (1+u_{2,2})u_{3,2} & (1+u_{2,2}) + u_{2,3}u_{3,2} \\ (1+u_{1,1})u_{3,1} & u_{1,2}u_{3,2} & u_{1,2} + u_{1,3}u_{3,2} \\ (1+u_{1,1})u_{2,1} & u_{2,1}(1+u_{2,2}) & u_{1,2}u_{2,3} + u_{1,3}(1+u_{2,2}) \end{bmatrix} \quad (4.62a)$$

$$\begin{bmatrix} 2(1+u_{1,1})u_{1,3} & 2(1+u_{1,1})u_{1,2} \\ 2u_{2,1}u_{2,3} & 2u_{2,1}(1+u_{2,2}) \\ u_{2,1} + u_{2,3}u_{3,1} & u_{2,1}u_{3,2} + (1+u_{2,2})u_{3,1} \\ (1+u_{1,1}) + u_{1,3}u_{3,1} & (1+u_{1,1})u_{3,2} + u_{1,2}u_{3,2} \\ (1+u_{1,1})u_{2,3} + u_{1,3}u_{2,1} & (1+u_{1,1})(1+u_{2,2}) + u_{1,2}u_{2,1} \end{bmatrix} \begin{pmatrix} \sigma_1 \\ \sigma_2 \\ \sigma_4 \\ \sigma_5 \\ \sigma_6 \end{pmatrix} \quad (4.62b)$$

For the transformation between stress-states, we assume that rotations of the normal ($u_{3,1}$ or $u_{3,2}$) and rotations about the normal ($u_{1,3}$ or $u_{2,3}$) are small for each increment. Products of these terms are considered higher-order and are neglected. Thus, Eqs (4.60), (4.61a) - (4.61i), (4.62a) and (4.62b) become

$$\begin{aligned} D &= 1 + u_{1,1} + u_{2,2} + u_{1,1}u_{2,2} - u_{1,2}u_{2,1} \\ &= (1 + u_{1,1})(1 + u_{2,2}) - u_{1,2}u_{2,1} \end{aligned} \quad (4.63)$$

with

$$\chi_{1,1} = (1 + u_{2,2})/D \quad (4.64a)$$

$$\chi_{1,2} = -u_{1,2}/D \quad (4.64b)$$

$$\chi_{1,3} = -u_{1,3}/D \quad (4.64c)$$

$$\chi_{2,1} = -u_{2,1}/D \quad (4.64d)$$

$$\chi_{2,2} = (1 + u_{1,1})/D \quad (4.64e)$$

$$\chi_{2,3} = -u_{2,3}/D \quad (4.64f)$$

$$\chi_{3,1} = -u_{3,1}/D \quad , \quad (4.64g)$$

$$\chi_{3,2} = -u_{3,2}/D \quad , \quad (4.64h)$$

$$\chi_{3,3} = ((1 + u_{1,1})(1 + u_{2,2}) - u_{1,2}u_{2,1})/D \approx D/D = 1 \quad , \quad (4.64i)$$

$$\begin{pmatrix} \sigma_1^E \\ \sigma_2^E \\ \sigma_4^E \\ \sigma_5^E \\ \sigma_6^E \end{pmatrix} = \frac{1}{D} \begin{bmatrix} (1 + u_{1,1})^2 & (u_{1,2})^2 & 0 \\ (u_{2,1})^2 & (1 + u_{2,2})^2 & 2u_{2,3} \\ 0 & u_{3,2} & (1 + u_{2,2}) \\ u_{3,1} & 0 & u_{1,2} \\ (1 + u_{1,1})u_{2,1} & u_{2,1}(1 + u_{2,2}) & u_{1,3} \end{bmatrix} \quad (4.65a)$$

$$\begin{bmatrix} 2u_{1,3} & 2(1 + u_{1,1})u_{1,2} \\ 0 & 2u_{2,1}(1 + u_{2,2}) \\ u_{2,1} & u_{3,1} \\ (1 + u_{1,1}) & u_{3,2} \\ u_{2,3} & D' \end{bmatrix} \begin{pmatrix} \sigma_1 \\ \sigma_2 \\ \sigma_4 \\ \sigma_5 \\ \sigma_6 \end{pmatrix} \quad , \quad (4.65b)$$

where

$$D' = (1 + u_{1,1})(1 + u_{2,2}) + u_{1,2}u_{2,1} \quad . \quad (4.66)$$

If Eqs (4.63) - (4.64i) are substituted into Eq (4.59) then, in terms of displacement, a new strain-state transformation matrix results. By applying the same assumptions as in the stress-state relations (Eqs (4.65a) and (4.65b)) concerning rotations of the normal ($u_{3,1}$ or $u_{3,2}$) and rotations about the normal ($u_{1,3}$ or $u_{2,3}$). Multiples of these terms are higher-order and can be neglected. Thus, Eq (4.59) becomes

$$\begin{pmatrix} e_1 \\ e_2 \\ e_4 \\ e_5 \\ e_6 \end{pmatrix} = \frac{1}{D^2} \begin{bmatrix} (1 + u_{2,2})^2 & (u_{1,2})^2 & 0 \\ (u_{2,1})^2 & (1 + u_{1,1})^2 & -2u_{2,3} \\ 0 & -u_{3,2} & (1 + u_{1,1})D \\ -u_{3,1} & 0 & -u_{1,2}D \\ -(1 + u_{1,1})u_{2,1} & -u_{2,1}(1 + u_{2,2}) & -u_{1,3} \end{bmatrix} \quad (4.67a)$$

$$\begin{bmatrix} -2u_{1,3} & -2(1+u_{1,1})u_{1,2} \\ 0 & -2u_{2,1}(1+u_{2,2}) \\ (-u_{2,1})D & -u_{3,1} \\ (1+u_{2,2})D & -u_{3,2} \\ -u_{2,3} & D' \end{bmatrix} \begin{bmatrix} \epsilon_1 \\ \epsilon_2 \\ \epsilon_4 \\ \epsilon_5 \\ \epsilon_6 \end{bmatrix} \quad (4.67b)$$

It should be noted the $1/D^2$ terms appears due to the products of $\chi_{k,l}$. The transverse normal strain, e_3 , for transversely isotropic materials become

$$\begin{aligned} e_3 = & -\frac{E_1\nu_{21}(1-\nu_{23})}{E_2(1-\nu_{12}\nu_{21})} \left[(1+u_{2,2})^2 \epsilon_1 + (u_{1,2})^2 \epsilon_2 - 2u_{1,2}(1+u_{2,2}) \epsilon_6 \right] \\ & -\frac{\nu_{23}\nu_{12}\nu_{21}}{(1-\nu_{12}\nu_{21})} \left[(u_{2,1})^2 \epsilon_1 + (1+u_{1,1})^2 \epsilon_2 - 2(1+u_{1,1})u_{2,1} \epsilon_6 \right] \end{aligned} \quad (4.68)$$

and for isotropic materials

$$\begin{aligned} e_3 = & -\frac{(1-\nu)}{2} \left[(1+u_{2,2})^2 \epsilon_1 + (u_{1,2})^2 \epsilon_2 - 2u_{1,2}(1+u_{2,2}) \epsilon_6 \right] \\ & -\frac{(1-\nu)}{2} \left[(u_{2,1})^2 \epsilon_1 + (1+u_{1,1})^2 \epsilon_2 - 2(1+u_{1,1})u_{2,1} \epsilon_6 \right] \end{aligned} \quad (4.69)$$

Finally, if we consider the magnitude of the terms $u_{1,3}$, $u_{2,3}$, $u_{3,1}$, and $u_{3,2}$ with respect to D , then the stress-state and strain-state relations become

$$\begin{pmatrix} \sigma_1^E \\ \sigma_2^E \\ \sigma_4^E \\ \sigma_5^E \\ \sigma_6^E \end{pmatrix} = \frac{1}{D} \begin{bmatrix} (1+u_{1,1})^2 & (u_{1,2})^2 & 0 \\ (u_{2,1})^2 & (1+u_{2,2})^2 & 0 \\ 0 & 0 & (1+u_{2,2}) \\ 0 & 0 & u_{1,2} \\ (1+u_{1,1})u_{2,1} & u_{2,1}(1+u_{2,2}) & 0 \end{bmatrix} \quad (4.70a)$$

$$\begin{bmatrix} 0 & 2(1+u_{1,1})u_{1,2} \\ 0 & 2u_{2,1}(1+u_{2,2}) \\ u_{2,1} & 0 \\ (1+u_{1,1}) & 0 \\ 0 & D' \end{bmatrix} \begin{bmatrix} \sigma_1 \\ \sigma_2 \\ \sigma_4 \\ \sigma_5 \\ \sigma_6 \end{bmatrix}, \quad (4.70b)$$

and

$$\begin{bmatrix} e_1 \\ e_2 \\ e_4 \\ e_5 \\ e_6 \end{bmatrix} = \frac{1}{D^2} \begin{bmatrix} (1+u_{2,2})^2 & (u_{1,2})^2 & 0 \\ (u_{2,1})^2 & (1+u_{1,1})^2 & 0 \\ 0 & 0 & (1+u_{1,1})D \\ 0 & 0 & -u_{1,2}D \\ -(1+u_{1,1})u_{2,1} & -u_{2,1}(1+u_{2,2}) & 0 \end{bmatrix} \quad (4.71a)$$

$$\begin{bmatrix} 0 & -2(1+u_{1,1})u_{1,2} \\ 0 & -2u_{2,1}(1+u_{2,2}) \\ (-u_{2,1})D & 0 \\ (1+u_{2,2})D & 0 \\ 0 & D' \end{bmatrix} \begin{bmatrix} \varepsilon_1 \\ \varepsilon_2 \\ \varepsilon_4 \\ \varepsilon_5 \\ \varepsilon_6 \end{bmatrix}. \quad (4.71b)$$

Now we can write the transformation from 2nd Piola Kirchhoff stress to Cauchy stress coordinates as

$$(\sigma^E) = \frac{1}{D} [T_1] (\sigma), \quad (4.72)$$

and for the transformation from Green's strain to Cauchy strain as

$$(e) = \frac{1}{D^2} [T_2] (\varepsilon), \quad (4.73)$$

where $[T_1]$ is defined by

$$[T_1] = \begin{bmatrix} (1+u_{1,1})^2 & (u_{1,2})^2 & 0 & 0 & 2(1+u_{1,1})u_{1,2} \\ (u_{2,1})^2 & (1+u_{2,2})^2 & 0 & 0 & 2u_{2,1}(1+u_{2,2}) \\ 0 & 0 & (1+u_{2,2}) & u_{2,1} & 0 \\ 0 & 0 & u_{1,2} & (1+u_{1,1}) & 0 \\ (1+u_{1,1})u_{2,1} & u_{1,2}(1+u_{2,2}) & 0 & 0 & D' \end{bmatrix}, \quad (4.74)$$

and $[T_2]$ is defined by

$$[T_2] = \begin{bmatrix} (1+u_{2,2})^2 & (u_{1,2})^2 & 0 & 0 & -2u_{1,2}(1+u_{2,2}) \\ (u_{2,1})^2 & (1+u_{1,1})^2 & 0 & 0 & -2(1+u_{1,1})u_{2,1} \\ 0 & 0 & (1+u_{1,1})D & -u_{2,1}D & 0 \\ 0 & 0 & -u_{1,2}D & (1+u_{2,2})D & 0 \\ -u_{2,1}(1+u_{2,2}) & -(1+u_{1,1})u_{1,2} & 0 & 0 & D' \end{bmatrix}. \quad (4.75)$$

Recall, in Eulerian coordinates, we express the Cauchy stress-strain relations as

$$(\sigma^E) = [A] (e), \quad (4.76)$$

where $[A]$ is the Eulerian constitutive matrix. For a large-strain, total Lagrangian formulation, we write

$$\frac{1}{D} [T_1] \{\sigma\} = \frac{1}{D^2} [A] [T_2] \{\varepsilon\}, \quad (4.77)$$

or

$$\{\sigma\} = \frac{1}{D} [T_1]^{-1} [A] [T_2] \{\varepsilon\} = [D] \{\varepsilon\}, \quad (4.78)$$

where $[D]$ is the Lagrangian constitutive matrix required for a large-strain analysis. It should be noted that $[T_1]$ and $[T_2]$ are inverses of each other by the definition given in Eq (4.78). Thus, the symmetry of $[D]$ is maintained. It should be noted that Eq (4.78) follows the formulation of

$$\sigma_{ij} = D_{ijkl} \varepsilon_{kl}, \quad (4.79)$$

where

$$D_{ijkl} = \frac{1}{D} \frac{\partial x_i}{\partial X_m} \frac{\partial x_j}{\partial X_n} \frac{\partial x_k}{\partial X_o} \frac{\partial x_l}{\partial X_p} A_{mnop} \quad (4.80)$$

A_{mnop} is the constitutive relations of the Cauchy (Eulerian) coordinate system only. Thus, for a total Lagrangian formulation, these relations must always be transformed into D_{ijkl} when the small strain assumption is no longer valid (i.e. when rotations and/or displacements become significantly large). This usually occurs when rotations reach the magnitude of 15° (0.263 rad) or if the magnitude of displacement is greater than five times the shell's thickness ($d < 5h$). Results in Sections 5.1, 5.3, and 5.5 demonstrate how the material transformations alone do not reflect greater flexibility in the shell's response. Such problems are considered plates or shallow shells when comparing their depth (δ) versus shell thickness (h). However, Eq (4.78) incorporates the assumptions of shell theory which degenerates the analysis to a quasi two-dimensional form.

It should be noted that these transformations relate the Cauchy constitutive relations to the Lagrangian constitutive relations, only. The implication of this becomes more clear for fiber-oriented materials such as laminated composites than for isotropic materials. Since these transformations relate only the constitutive relations between 2nd Piola stress-Green strain and Cauchy stress-strain relations, an implicit assumption is made. The assumption is that the fiber orientation is maintained during each increment, i.e., a 45° oriented fiber will always be 45° in the Cauchy reference frame, and not rotate. In order to capture fiber movement, a second transformation is required to quantify the change in fiber-orientation between each increment. Thus, the implied assumption is that changes in fiber-orientation *between increments* of displacement are negligible. This is verified in Section 6.5 by comparing experimental results of a Gr/PEEK tensile coupon to the analytical model.

Once yielding occurs at a specified point in the layer, the elastic constitutive matrix is replaced with the elastic-plastic constitutive matrix. Also, it is assumed that strains are large enough such that the deformed and the undeformed structural axes are not co-located. A transformation for both the stress-state and strain-state from Eulerian components to the Lagrangian components is required to ensure the constitutive relations are in a total Lagrangian form. Finally, for simplicity, the transformation matrices of the middle layer of the shell is used for the remaining layers of the shell. Using this layered approach allows for direct comparison with several pub-

lished studies [67, 97, 102, 135, 137, 144 - 146, 153, 189, 205, 206].

4.3 Element Independent Stiffness Formulation

The theory of the previous sections dealt with displacement fields, constitutive relations, and strain-displacement relations for curved shells with a nonlinear HTSD theory. The next step required, to create a suitable research tool for the investigation of (1) spherical geometry, (2) nonlinear material effects, and (3) large-strain formulation, is the development and solution of the governing differential equations for shell problems. Since the author is specifically interested in the nonlinear phenomena of large displacements and rotations, no analytical or linear solutions are desired. Furthermore, to provide a suitable comparison to previously published methods, the author has chosen to develop the governing differential equations and solve these in a manner consistent with that of Dennis [48]. In his development, Dennis used an "element independent" finite element formulation for an incremental/iterative solution based upon the principle of stationary potential energy of a linear-elastic laminated shell [48:78-95]. This method is employed for the elastic and large strain formulations. However, since plasticity is unconservative, the stationary potential energy formulation is incorrect. Thus, for the elasto-plastic formulation an incremental elasto-plastic potential energy formulation is developed.

4.3.1 Elastic Formulation: The finite element technique is a powerful numerical method capable of solving many coupled partial differential equations over a certain domain. In this research, the domain is a spherical shell, shown in Figure 4.1, and the equations are based upon the variation of the total potential energy, Π_p , of the elastic body. Specifically, the principal of stationary potential energy is used where $\delta\Pi_p = 0$. The potential energy expression is found by first examining the equilibrium state of the body. For a body of volume V with prescribed forces F^i on part of its surface S_1 and prescribed boundary conditions on the remaining part of the surface S_2 , the equation of equilibrium for an infinitesimal virtual displacement Δu is given by

$$\Pi_p = \int_V \left(\sigma^{ij} \delta \gamma_{ij} - P^k \delta u^k \right) dV - \int_{S_1} (F^k \delta u^k) dS = 0 \quad , \quad (4.81)$$

where

$\sigma^{ij} \equiv$ the components of the Second Piola-Kirchhoff stress tensor (for the orthogonal coordinate system chosen, $\sigma^{ij} = \sigma_{ij}$)

$\gamma^{ij} \equiv$ the Green strain components expressed in the body's coordinate system

$P^k \equiv$ components of body forces, and

$F^k \equiv$ components of prescribed surface forces.

For a conservative system, one where the forces F^k do not vary during virtual displacement, there exists a strain energy density function W^* , such that

$$\sigma_{ij} = \frac{\partial W^*}{\partial \gamma_{ij}} \quad (4.82)$$

Assuming strains are small, then one can express the stress in terms of strain as

$$\sigma_{ij} = C_{ijkl} \gamma_{kl} \quad (4.83)$$

where C_{ijkl} are constants in the Eulerian elastic tensor. Thus, the strain energy density becomes

$$W^* = \frac{1}{2} C_{ijkl} \gamma_{ij} \gamma_{kl} \quad (4.84)$$

The first variation of the potential energy for the case with zero body forces is given by

$$\delta \Pi = \delta \int_V W^* (u^k) dV - \int_{S_1} F^k \delta u^k dS = 0 \quad (4.85)$$

To evaluate Eq (4.85), a suitable reference frame must be chosen. A typical method is to assume a total Lagrangian approach where the strain tensor, elasticity tensor, and all other components are described in terms of coordinates of the original undeformed body.

For a laminated orthotropic material, the stress components can be written in terms of the reduced structural stiffness of the lamina as in Eq (3.61). Substituting Eq (3.61) into Eq (4.84) and integrating over the volume of the body, one obtains the strain energy as $U_1 + U_2$, where

$$\begin{aligned} U_1 &= \frac{1}{2} \int_V (\bar{Q}_{11} \epsilon_1^2 + \bar{Q}_{22} \epsilon_2^2 + 2\bar{Q}_{12} \epsilon_1 \epsilon_2 + 2\bar{Q}_{16} \epsilon_1 \epsilon_6 + 2\bar{Q}_{26} \epsilon_2 \epsilon_6 + \bar{Q}_{66} \epsilon_6^2) dV \\ U_2 &= \frac{1}{2} \int_V (\bar{Q}_{44} \epsilon_4^2 + 2\bar{Q}_{45} \epsilon_4 \epsilon_5 + \bar{Q}_{55} \epsilon_5^2) dV \end{aligned} \quad (4.86)$$

The ε_i in Eq (4.86) depend on the thickness coordinate and the midsurface coordinates y_1 and y_2 . The \bar{Q}_{ij} , defined by Eqs (3.60) and (3.62), however, depend only on the thickness coordinate. Thus, these equations can be reduced to an integral over the midsurface of the shell. This is done by first assuming displacement components u_1 , u_2 , and u_3 vary in the form of a series expansion with respect to the thickness coordinate. Then, one can directly integrate the \bar{Q}_{ij} expressions through the thickness of the shell. The integral through the thickness of $\bar{Q}_{ij}y_3^r$ defines an elasticity array, say C_{ij} . These arrays are the familiar A_{ij} , B_{ij} , D_{ij} , ... associated with macro-mechanical behavior of laminated composite plates [94:154-155]. For the laminated composite, the integral is replaced by summation over the number of plies as shown below

$$\begin{aligned}
 C_{ij_1} &= A_{ij} = \sum_{k=1}^N (\bar{Q}_{ij})_k (y_{3_k} - y_{3_{k-1}}) \\
 C_{ij_2} &= B_{ij} = \sum_{k=1}^N (\bar{Q}_{ij})_k (y_{3_k}^2 - y_{3_{k-1}}^2) \\
 C_{ij_3} &= D_{ij} = \sum_{k=1}^N (\bar{Q}_{ij})_k (y_{3_k}^3 - y_{3_{k-1}}^3) \\
 &\dots \\
 C_{ij_{15}} &= T_{ij} = \sum_{k=1}^N (\bar{Q}_{ij})_k (y_{3_k}^{15} - y_{3_{k-1}}^{15})
 \end{aligned} \tag{4.87}$$

It should be noted that even though y_3^n where $n = 1, 15$, T_{ij} is of the same relative order of magnitude as A_{ij} . Recall, from Eq (4.1), the kinematics for a general spherical shell. Notice that a y_3^3 term appears in both u_1 and u_2 . Also note that $k = -(4/3)h^2$ which implies the last term in both u_1 and u_2 is of the same relative order of magnitude as the middle term. Thus, T_{ij} is of the same relative order of magnitude as A_{ij} .

The previous expression for the variation of total potential energy Πp gives five coupled non-

linear partial differential equations which govern the equilibrium of the system. These expressions contain 18 displacement parameters: $u, u_1, u_2, v, v_1, v_2, w, w_1, w_2, w_{11}, w_{22}, w_{12}, \psi_1, \psi_{1,1}, \psi_{1,2}, \psi_2, \psi_{2,1},$ and $\psi_{2,2}$. The array of these terms is called the displacement gradient vector, $\{d\}$. These parameters include the seven displacement parameters in Eq (4.72) and their derivatives. Since the equilibrium equations are nonlinear in terms of the displacement parameters, an incremental-iterative approach is typically used to solve a system of linearized equations which yields an equivalent solution. These linearized equations are found by differentiating the expression for Πp with respect to the displacement functions. For simple theories, such as a Donnell theory or a linear FTSD theory where relatively few terms are included, the first variation of Πp and its linearization, can be explicitly developed, term by term. For more complete theories, such as the quasi-nonlinear HTSD theory [48] or a fully nonlinear theory, the expression of Πp has several hundred terms. Its first variation would include, perhaps, thousands of terms and the subsequent linear equilibrium equations would be quite lengthy.

Rajasekaran and Murray [173] developed a formal procedure for finite elements, which defines the total potential energy, its first variation, and the linear incremental equilibrium equations in terms of three stiffness matrices. Specifically, the total potential energy is given by

$$\Pi_p = \frac{\{q\}^T}{2} \left[[K] + \frac{1}{3} [N_1] + \frac{1}{6} [N_2] \right] \{q\} - \{q\}^T \{P\} \quad , \quad (4.88)$$

where

$\{q\} \equiv$ a column array of nodal displacement parameters

$\{P\} \equiv$ a column array of nodal loads

$[K] \equiv$ an array of constant stiffness coefficients

$[N_1] \equiv$ an array of nonlinear coefficients with each term dependent on one of the displacement parameters ($[N_1]$ is linear in terms of displacement), and

$[N_2] \equiv$ an array of nonlinear coefficients with each term dependent on the product of two displacement parameters ($[N_2]$ is quadratic in terms of displacement).

By carrying out the variation of Eq (4.88), one obtains the virtual work expression (and the equilibrium equations, F) as shown in Eqs (4.89) & (4.90). In Eq (4.89) note that K , N_1 , and N_2 of Eq (4.88) are duplicated as a result of carrying out the variation of Eq (4.88).

$$\begin{aligned}\delta \Pi_p &= \delta q^T \left[\left(K + \frac{1}{2} N_1 + \frac{1}{3} N_2 \right) q - P \right] = 0 \\ &= \delta q^T F(q) = 0\end{aligned}\tag{4.89}$$

Then, for an arbitrary and independent δq ,

$$F(q) = 0\tag{4.90}$$

Eq (4.90) represents the nonlinear algebraic equations in the nodal degrees of freedom(dof) q . Solutions to Eq (4.90) are found iteratively through the linearized incremental equations. These are derived by expanding Eq (4.90) into a Taylor series as shown in Eq (4.91), where the higher order terms are neglected since Δq is assumed to be small.

$$F(q + \Delta q) = F(q) + \frac{\partial F}{\partial q} \Delta q + \dots = 0\tag{4.91}$$

Rearranging Eq (4.91) and letting $K_T = K + N_1 + N_2$ gives Eq (4.93) where the stiffness arrays K , N_1 , and N_2 are duplicated as a result of taking partial derivatives of F .

$$\begin{aligned}\frac{\partial F}{\partial q} \Delta q &= -F(q) \\ [K + N_1 + N_2] (\Delta q) &= -F(q)\end{aligned}\tag{4.92}$$

$$[K_T] \Delta q = -F(q)\tag{4.93}$$

Eq (4.93) gives solutions in an iterative manner via a Newton-Raphson technique. The current values of q are substituted into N_1 and N_2 resulting in an array of constants for K_T . The set of linear equations are then solved for Δq , which is then added to q giving the updated nodal displacements. Assuming the solution is not yet converged, the right hand side (RHS) of Eq (4.93) is nonzero. Iteration continues until F becomes arbitrarily small, signifying equilibrium is satisfied.

The equilibrium equation, then is given by

$$\left[[K] + \frac{1}{2}[N_1] + \frac{1}{3}[N_2] \right] \{q\} - \{P\} = \{0\} \quad , \quad (4.94)$$

and the linear incremental equilibrium equation is given by

$$\left[[K] + [N_1] + [N_2] \right] \{\Delta q\} - \{\Delta P\} = \{0\} \quad . \quad (4.95)$$

According to Rajasekaran and Murray, this notation was introduced by Mallett and Marcel in 1968 [173]. To assure the formalism of Eqs (4.88) - (4.95) holds, the stiffness matrices $[K]$, $[N_1]$, and $[N_2]$ must be derived in a specific way. Rajasekaran and Murray showed that by expressing strain components as follows

$$\{\epsilon_i\} = \{L_i\}^T \{d\} + \frac{1}{2} \{d\}^T [H_i] \{d\} \quad , \quad (4.96)$$

and then redefining the terms of $[K]$, $[N_1]$, and $[N_2]$ the formalism of Eqs (4.88) - (4.95) would always be valid for any finite element representation of elastic continuum. In Eq (4.96) the terms are defined as:

$\epsilon_i \equiv$ a particular strain component

$\{d\} \equiv$ a column array of continuum displacement parameters is the 18×1 displacement gradient vector

$\{L_i\} \equiv$ a column array of the constant coefficients of terms in ϵ_i containing only one displacement parameter (the terms are linear with respect to displacement), and

$[H_i] \equiv$ a symmetric array of constant coefficients of terms in ϵ_i containing the product of two displacement parameters (the terms are quadratic with respect to displacement).

Using Eq (4.96) and defining the terms for a specific ϵ_i as $\epsilon_i^L + \epsilon_i^{NL}$, the expression for potential energy of an elastic material can be written as

$$\Pi_p = \frac{1}{2} \int_V C_{ij} \left(\epsilon_i^L \epsilon_j^L + 2 \epsilon_i^L \epsilon_j^{NL} + \epsilon_i^{NL} \epsilon_j^{NL} \right) dV - \{d\}^T \{P\} \quad , \quad (4.97)$$

where C_{ij} is the symmetric array of elasticity constants and summation on $i = 1, \dots, 6$ and $j = 1, \dots,$

6 is implied by the repeated subscripts. Introducing Eq (4.96) into Eq (4.97) yields

$$\begin{aligned} \Pi_p = \frac{1}{2} \int_V \left(C_{ij} \{d\}^T \left[(L_i) (L_j)^T + (L_i) \{d\}^T [H_j] \right. \right. \\ \left. \left. + \frac{1}{4} [H_i] \{d\} \{d\}^T [H_j] \right] \{d\} \right) dV - \{d\}^T \{P\} \end{aligned} \quad (4.98)$$

Notice at this point, Eqs (4.96), (4.97), & (4.98) are expressed in terms of $\{d\}$, the continuum displacement gradient vector. No finite element discretization has been used. Thus, these equations represent an element independent formulation. By defining an element approximation for the continuum displacements $\{d\}$ in terms of nodal displacements $\{q\}$, one defines a specific formulation. To provide a general formulation, however, the stiffness matrices of Eqs (4.88) - (4.95) can be developed in terms of the element independent formulation of Eqs (4.96) - (4.98). In this fashion, we seek definitions for $[K]$, $[N_1]$, and $[N_2]$, such that Eqs (4.88) - (4.95) will hold. Rajasekaran and Murray showed that the direct comparison of the terms of Eq (4.98) and those of Eq (4.88) will yield arrays $[K]$, $[N_1]$, and $[N_2]$ which satisfy Eq (4.98). Unfortunately, these arrays *will not* satisfy the formalism of Eq (4.95). In some cases, they will not even satisfy Eq (4.94). They showed that consistent representations of these arrays are given by the following expressions

$$[\hat{K}] = C_{ij} \{L_i\} \{L_j\}^T, \quad (4.99)$$

$$\begin{aligned} [\hat{N}_1] = C_{ij} \left(\{L_i\} \{d\}^T [H_j] + \{d\}^T \{L_i\} [H_j] \right. \\ \left. + [H_i] \{d\} \{L_j\}^T \right), \end{aligned} \quad (4.100)$$

$$[\hat{N}_2] = C_{ij} \left([H_i] \{d\} \{d\}^T [H_j] + \frac{1}{2} \{d\}^T [H_j] \{d\} [H_i] \right). \quad (4.101)$$

Rajasekaran and Murray's formulation was for finite elements where strains do not vary through the thickness of the element. This formulation is extended to account for variation of strain through the thickness [48:79-91]. To do this, one assumes strains at a point in the shell are represented by the following series expansion

$$\varepsilon_i(y_1, y_2, y_3) = \varepsilon_i(y_1, y_2) + \sum_{p=1}^{2d+g} \chi_i^p y_3^p, \quad (4.102)$$

where

$y_3 \equiv$ the distance from the midsurface in the \vec{e}_3 direction

$\chi_i^p(y_1, y_2) \equiv$ the coefficients of y_3^p appearing in the strain expression

$d \equiv$ the degree of the displacement field expression, and

$g \equiv$ the degree of the series expansion approximation of shell shape factor functions appearing in the strain tensor.

Rewriting Eq (4.102) consistent with Eq (4.96), one obtains

$$\varepsilon_i = \sum_{p=0}^n \left(\left(L_i^p \right)^T \{d\} + \frac{1}{2} \{d\}^T \left[H_i^p \right] \{d\} \right) y_3^p, \quad (4.103)$$

where

$(L_i^p) \equiv$ a row array of the constant coefficients of terms in ε_i containing only one displacement parameter and the thickness coordinate y_3 to the power p , and

$[H_i^p] \equiv$ a symmetric array of the coefficients for terms in ε_i containing products of displacement parameters and the thickness coordinate y_3 to the power p .

With this power series expansion of strains, for an elastic analysis, the terms of Eq (4.98) are written as

$$[\hat{K}] = \sum_{p=0}^n \sum_{r=0}^n \frac{1}{2} C_{ij} \left(\left(L_i^p \right) \left(L_j^r \right)^T + \left(L_j^r \right) \left(L_i^p \right)^T \right), \quad (4.104)$$

$$[\hat{N}_1] = C_{ij} \left(\{L_i^p\} \{d\}^T [H_j^r] + \{d\}^T \{L_i^p\} [H_j^r] + [H_i^p] \{d\} \{L_j^r\}^T \right), \quad (4.105)$$

$$\begin{aligned} \left[\hat{N}_2 \right] = & \sum_{p=0}^n \sum_{r=0}^n \frac{1}{2} C_{ij} \left[\left[H_i^p \right] \{d\} \{d\}^T \left[H_j^r \right] \right. \\ & \left. + \left[H_i^r \right] \{d\} \{d\}^T \left[H_j^p \right] \right] \end{aligned} \quad (4.106)$$

where

$$C_{ij} = \int_h \left(\bar{Q}_{ij} y_3^{(p+r)} \right) dy_3 \quad , \quad (4.107)$$

are the higher order elasticity arrays and summation on $i, j = 1, 2, 4-6$ is implied. Notice that these equations are a result of directly substituting definitions of (L_i) and $[H_i]$ into Eqs (4.100) - (4.101). These expressions do not satisfy the formalism of Eqs (4.88) - (4.95). In a fashion similar to Rajasekaran and Murray's formulation, Eqs (4.104) - (4.106) can be manipulated to yield new definitions for arrays $[K]$, $[N_I]$, and $[N_2]$ that satisfy the formalism of Eqs (4.88) - (4.95)

$$\left[\hat{K} \right] = \sum_{p=0}^n \sum_{r=0}^n \frac{1}{2} C_{ij} \left(\left(L_i^p \right) \left(L_j^r \right)^T + \left(L_i^r \right) \left(L_j^p \right)^T \right) \quad , \quad (4.108)$$

$$\begin{aligned} \left[\hat{N}_1 \right] = & \sum_{p=0}^n \sum_{r=0}^n C_{ij} \left[\left(L_i^p \right) \{d\}^T \left[H_j^r \right] + \left(L_i^r \right) \{d\}^T \left[H_j^p \right] \right. \\ & + \{d\}^T \left(L_i^p \right) \left[H_j^r \right] + \{d\}^T \left(L_i^r \right) \left[H_j^p \right] + \left[H_i^p \right] \{d\} \left(L_j^r \right)^T \\ & \left. + \left[H_i^r \right] \{d\} \left(L_j^p \right)^T \right] \end{aligned} \quad (4.109)$$

$$\begin{aligned}
 [\hat{N}_2] = & \sum_{p=0}^n \sum_{r=0}^n \frac{1}{2} C_{ij} \left[\left[H_i^p \right] \{d\} \{d\}^T \left[H_j^r \right] \right. \\
 & + \left[H_i^r \right] \{d\} \{d\}^T \left[H_j^p \right] + \frac{1}{2} \left(\{d\}^T \left[H_j^p \right] \{d\} \left[H_i^r \right] \right. \\
 & \left. \left. + \{d\}^T \left[H_j^r \right] \{d\} \left[H_i^p \right] \right) \right]
 \end{aligned} \quad (4.110)$$

Equation (4.109) can be simplified and still retain the formalism of Eqs (4.88) - (4.95) (see [48:87-89] for the exact discussion concerning this simplification). The simplified version of Eq (4.109) is

$$\begin{aligned}
 [\hat{N}_1] = & \sum_{p=0}^n \sum_{r=0}^n C_{ij} \left[\left(L_i^p \right) \{d\}^T \left[H_j^r \right] \right. \\
 & \left. + \{d\}^T \left(L_i^p \right) \left[H_j^r \right] + \left[H_i^r \right] \{d\} \left(L_j^p \right)^T \right]
 \end{aligned} \quad (4.111)$$

With the definitions of (L_i^p) , $[H_i^p]$, $[\hat{K}]$, $[\hat{N}_1]$, and $[\hat{N}_2]$, one can now form the element independent stiffness arrays given by Eqs (4.108), (4.110), & (4.111). This formulation requires literally hundreds of matrix multiplications to evaluate these equations. MACSYMA, a symbolic solver/generator program, was used to accomplish this task.

4.3.2 Large Strain Formulation: To consider a large-strain analysis, the potential energy equations (Eqs (4.97) & (4.98)) remain in the same form. The strains are given in the total Lagrangian form of Eqs (4.102) & (4.103). Thus, refer back to Eqs (4.108), (4.110), & (4.111) to determine

$$[\hat{K}] = \sum_{p=0}^n \sum_{r=0}^n \frac{1}{2} C_{ij(p+r)}^* \left(\left(L_i^p \right) \left(L_j^r \right)^T + \left(L_i^r \right) \left(L_j^p \right)^T \right) \quad (4.112)$$

$$\begin{aligned} \left[\hat{N}_1 \right] = \sum_{p=0}^n \sum_{r=0}^n C^*_{ij(p+r)} \left[\left(L_i^p \right) \{d\}^T \left[H_j^r \right] \right. \\ \left. + \{d\}^T \left(L_i^p \right) \left[H_j^r \right] + \left[H_i^r \right] \{d\} \left(L_j^p \right)^T \right] \end{aligned} \quad (4.113)$$

$$\begin{aligned} \left[\hat{N}_2 \right] = \sum_{p=0}^n \sum_{r=0}^n \frac{1}{2} C^*_{ij(p+r)} \left[\left[H_i^p \right] \{d\} \{d\}^T \left[H_j^r \right] \right. \\ \left. + \left[H_i^r \right] \{d\} \{d\}^T \left[H_j^p \right] + \frac{1}{2} \left(\{d\}^T \left[H_j^p \right] \{d\} \left[H_i^r \right] \right. \right. \\ \left. \left. + \{d\}^T \left[H_j^r \right] \{d\} \left[H_i^p \right] \right) \right] \end{aligned} \quad (4.114)$$

where

$$C^*_{ij(p+r)} = \int_h \left(\frac{1}{D} \left(T_{1ij} \right)^{-1} \bar{Q}_{ij} \left(T_{2ij} \right) y_3^{(p+r)} \right) dy_3 \quad (4.115)$$

are the higher-order elasticity arrays, with the material transformation matrices (T_1) and (T_2) included, and summation $ij = 1, 2, 4-6$ is implied.

4.3.3 Elastic-Plastic Formulation: Since plasticity is unconservative from a total potential energy formulation, an alternative approach is considered. Hill [79] and Washizu [229] showed that from an incremental formulation, plasticity is considered to be conservative for the incremental since plasticity is considered to be conservative from an incremental potential energy expression. Thus, recalling the form of Eq (4.86) we have, for an orthotropic lamina

$$\begin{aligned} \Delta U_1 = \frac{1}{2} \int_V \left(\bar{Q}_{11}^{ep} \Delta \epsilon_1^2 + \bar{Q}_{22}^{ep} \Delta \epsilon_2^2 + 2 \bar{Q}_{12}^{ep} \Delta \epsilon_1 \Delta \epsilon_2 \right. \\ \left. + 2 \bar{Q}_{16}^{ep} \Delta \epsilon_1 \Delta \epsilon_6 + 2 \bar{Q}_{26}^{ep} \Delta \epsilon_2 \Delta \epsilon_6 + \bar{Q}_{66}^{ep} \Delta \epsilon_6^2 \right) dV \\ \Delta U_2 = \frac{1}{2} \int_V \left(\bar{Q}_{44}^{ep} \Delta \epsilon_4^2 + 2 \bar{Q}_{45}^{ep} \Delta \epsilon_4 \Delta \epsilon_5 + \bar{Q}_{55}^{ep} \Delta \epsilon_5^2 \right) dV \end{aligned} \quad (4.116)$$

such that $\Delta U = \Delta U_1 + \Delta U_2$. From Eq (4.87) one develops an elasto-plastic array, C_{ij}^{ep} , of the form

$$\begin{aligned}
 C_{ij_1}^{ep} &= A_{ij}^{ep} = \sum_{k=1}^N (\bar{Q}_{ij}^{ep})_k (y_{3_k} - y_{3_{k-1}}) \\
 C_{ij_2}^{ep} &= B_{ij}^{ep} = \sum_{k=1}^N (\bar{Q}_{ij}^{ep})_k (y_{3_k}^2 - y_{3_{k-1}}^2) \\
 C_{ij_3}^{ep} &= D_{ij}^{ep} = \sum_{k=1}^N (\bar{Q}_{ij}^{ep})_k (y_{3_k}^3 - y_{3_{k-1}}^3) \\
 &\dots \\
 C_{ij_{15}}^{ep} &= T_{ij}^{ep} = \sum_{k=1}^N (\bar{Q}_{ij}^{ep})_k (y_{3_k}^{15} - y_{3_{k-1}}^{15})
 \end{aligned} \tag{4.117}$$

The incremental strain components follow the format of Eq (4.96) and are given by

$$\Delta \epsilon_i = (L_i)^T \{\Delta d\} + \frac{1}{2} \{\Delta d\}^T [H_i] \{\Delta d\} \quad , \tag{4.118}$$

where

$\Delta \epsilon_i \equiv$ a particular incremental strain component

$\{\Delta d\} \equiv$ a column array of incremental continuum displacement parameters

$(L_i) \equiv$ a column array of the constant coefficients of terms in $\Delta \epsilon_i$ containing only one displacement parameter (the terms are linear with respect to displacement), and
 $[H_i] \equiv$ a symmetric array of constant coefficients of terms in $\Delta \epsilon_i$ containing the product of two displacement parameters (the terms are quadratic with respect to displacement).

Using Eq (4.118) and defining the terms for a specific $\Delta \epsilon_i$ as $\Delta \epsilon_i^L + \Delta \epsilon_i^{NL}$, the expression for incremental potential energy of an elasto-plastic material is written as (following the format of Eq (4.97))

$$\Delta \Pi_p = \frac{1}{2} \int_V C_{ij}^{ep} \left(\Delta \varepsilon_i^L \Delta \varepsilon_j^L + 2 \Delta \varepsilon_i^L \Delta \varepsilon_j^{NL} + \Delta \varepsilon_i^{NL} \Delta \varepsilon_j^{NL} \right) dV - \{\Delta d\}^T \{P\} \quad (4.119)$$

where C_{ij}^{ep} is the symmetric array of elasto-plastic coefficients, determined at each increment of displacement or load. Introducing Eq (4.118) into Eq (4.119) yields

$$\Delta \Pi_p = \frac{1}{2} \int_V \left(C_{ij} \{\Delta d\}^T \left[(L_i) (L_j)^T + (L_i) \{\Delta d\}^T [H_j] + \frac{1}{4} [H_i] \{\Delta d\} \{\Delta d\}^T [H_j] \right] \{\Delta d\} \right) dV - \{\Delta d\}^T \{P\} \quad (4.120)$$

The incremental elasto-plastic forms of the $[\hat{K}]$, $[\hat{N}_1]$, and $[\hat{N}_2]$ arrays, similar to Eqs (4.99) - (4.101) (the generalized Rajasakeren and Murray equations), are

$$[\hat{K}^{ep}] = \frac{1}{2} C_{ij}^{ep} \left(L_i^p \right) \left(L_j^r \right)^T \quad (4.121)$$

$$[\hat{N}_1^{ep}] = \frac{1}{2} C_{ij}^{ep} \left((L_i) (\Delta d)^T [H_j] + (\Delta d)^T (L_i) [H_j] + [H_i] (\Delta d) (L_i)^T \right) \quad (4.122)$$

$$[\hat{N}_2^{ep}] = \frac{1}{2} C_{ij}^{ep} \left([H_i] \{\Delta d\} \{\Delta d\}^T [H_j] + \frac{1}{2} \{\Delta d\}^T [H_j] \{\Delta d\} [H_i] \right) \quad (4.123)$$

Since the strains do vary through-the-thickness, a consistent incremental expression (following Eq (4.103)) is given by

$$\Delta \varepsilon_i = \sum_{p=0}^n \left((L_i^p)^T \{\Delta d\} + \frac{1}{2} \{\Delta d\}^T [H_i^p] \{\Delta d\} \right) y_3^p \quad (4.124)$$

where

$(L_i^p) \equiv$ a row array of the constant coefficients of terms in $\Delta \varepsilon_i$ containing only one displacement parameter and the thickness coordinate y_3 to the power p , and

$[H_i^p] \equiv$ a symmetric array of the coefficients for terms in $\Delta \varepsilon_i$ containing products of displacement parameters and the thickness coordinate y_3 to the power p .

To consider an elastic-plastic analysis, referring back to Eqs (4.108), (4.110), & (4.111) determines that including Eq (4.124) in Eqs (4.121) - (4.123) yields

$$[\hat{K}^{ep}] = \sum_{p=0}^n \sum_{r=0}^n \frac{1}{2} C_{ij(p+r)}^{ep} \left((L_i^p)(L_j^r)^T + (L_i^r)(L_j^p)^T \right), \quad (4.125)$$

$$\begin{aligned} [\hat{N}_1^{ep}] &= \sum_{p=0}^n \sum_{r=0}^n C_{ij(p+r)}^{ep} \left[(L_i^p) \{ \Delta d \}^T [H_j^r] \right. \\ &\quad \left. + \{ \Delta d \}^T (L_i^p) [H_j^r] + [H_i^r] \{ \Delta d \} (L_j^p)^T \right] \end{aligned}, \quad (4.126)$$

$$\begin{aligned} [\hat{N}_2^{ep}] &= \sum_{p=0}^n \sum_{r=0}^n \frac{1}{2} C_{ij(p+r)}^{ep} \left[[H_i^p] \{ \Delta d \} \{ \Delta d \}^T [H_j^r] \right. \\ &\quad \left. + [H_i^r] \{ \Delta d \} \{ \Delta d \}^T [H_j^p] + \frac{1}{2} \left(\{ \Delta d \}^T [H_j^p] \{ \Delta d \} [H_i^r] \right. \right. \\ &\quad \left. \left. + \{ \Delta d \}^T [H_j^r] \{ \Delta d \} [H_i^p] \right) \right] \end{aligned}, \quad (4.127)$$

where

$$C_{ij(p+r)}^{ep} = \int_h \left(\frac{1}{D} (T_{1ij})^{-1} \bar{Q}_{ij}^{ep} (T_{2ij}) y_3^{(p+r)} \right) dy_3 \quad (4.128)$$

are the higher-order elastic-plastic arrays, with the material transformation matrices (T_1) and (T_2) included, and summation $i, j = 1, 2, 4-6$ is implied.

4.4 Symbolic Generation of the Elemental Codes

A significant accomplishment of this research was the development of a tool to generate comparable versions of "elemental code". The results comparing various theoretical attributes would be meaningless if undetected errors were present in some variations, or if different finite element models or discretization schemes were used. For this research, a reliable system of generating different, but comparable, versions of code was required. A MACSYMA routine was developed from previous work in Smith [207] to symbolically generate the assumed displacement field, determine the strain components, determine the shell shape factor approximations, determine the elements of the strain definition arrays, and finally generate the Fortran code for the elements of the $[\hat{K}]$, $[\hat{K}_s]$, $[\hat{N}_1]$, $[\hat{N}_{1s}]$, $[\hat{N}_2]$, and $[\hat{N}_{2s}]$ stiffness arrays which includes spherical geometry. Development of this routine was crucial aspect of this research. With elemental codes approaching 40,000 lines in length, the detection of errors by "hand generation" would have been virtually impossible. The symbolic generation of codes assures reliability and comparability not achievable by other means. By using these codes in an element independent formulation, the accuracy of each version of theory could be compared using the same finite element model and main program (SHELL). This further assured a fair comparison of the various theoretical attributes of each version. The only variables were the displacement field (Donnell approximation, modified Donnell approximation with linear transverse shear, or the cubic displacement field of Eq (3.72)), constitutive relations (elastic or elastic-plastic) and whether the choice to include the material coordinate transformations. The theoretical attributes of the elemental codes used for this research are summarized in Table 1.

The MACSYMA routine for generating elemental codes is included as Appendix E. The routine includes comment statements to explain some special functions, called macros, and a few comments to explain the steps in the process. The generation of each version of elemental code follows the same steps listed in Reference [207:Chap 4,20-24].

Table 1 Definitions of Elemental Codes for Variations of Theory

Code Name GXYZ	Displacement Assumption Field	Constitutive Relations Analyzed	Material Coordinate Transformations	Equations Given in Appendix
S000	Donnell (1)	Elastic	Not Included	C
S001	Donnell	Elastic	Included	C
S011	Donnell	Elastic-Plastic	Included	C
S100	modified Donnell (2)	Elastic	Not Included	D
S101	modified Donnell	Elastic	Included	D
S111	modified Donnell	Elastic-Plastic	Included	D
S200	Cubic Nonlinear (3)	Elastic	Not Included	E
S201	Cubic Nonlinear	Elastic	Included	E
S211	Cubic Nonlinear	Elastic-Plastic	Included	E

(1) u_i defined in Eq (C.2)

(2) u_i defined in Eq (D.2)

(3) u_i defined in Eq (E.2)

The codes are identified by a symbol "GXYZ", where

$G = P$ for plate, C for cylindrical, S for spherical, or A for arbitrary shell geometry Appendix A lists relations for arbitrary shells and Appendices B through D list relations for spherical shells. The plate and cylindrical shell relations are embedded within the spherical shell relations. They are derived by setting the parameters D and/or C to zero,

$X = 0$ for the Donnell approximation displacement field of Eq (B.2), 1 for the modified Donnell approximation displacement field of Eq (C.2), or 2 for the cubic displacement field of Eq (D.2),

$Y = 0$ for an elastic analysis, or 1 for an elastic-plastic analysis, and

$Z = 0$ for no material coordinate transformations, or 1 to include material coordinate transformations from Eulerian to Lagrangian coordinates.

4.5 Finite Element Solution

The element independent stiffness matrices of Eqs (4.108), (4.110), & (4.111) depend upon the continuum displacement gradient vector $\{d\}$. This vector includes the following functions: $u, u_{,1}, u_{,2}, v, v_{,1}, v_{,2}, w, w_{,1}, w_{,2}, w_{,11}, w_{,22}, w_{,12}, \psi_1, \psi_{1,1}, \psi_{1,2}, \psi_2, \psi_{2,1},$ and $\psi_{2,2}$. Likewise, the potential energy of Eqs (4.97) & (4.98) also depend upon these functions. Using a standard displacement-based finite element method, the 18 two-dimensional functions of the continuum displacement gradient vector $\{d(y_1, y_2)\}$ are approximated by interpolation from discrete values of nodal displacement parameters. These nodal parameters or degrees of freedom (dof), are defined only at a finite number of points or nodes and are denoted by $\{q\}$ in Eq (4.129)

$$\{d(y_1, y_2)\} = [\hat{D}(s_1, s_2)] \{q\} \quad , \quad (4.129)$$

where $[\hat{D}(s_1, s_2)]$ is an array of nodal interpolation functions and (s_1, s_2) are the local coordinates of a two-dimensional rectangular finite element.

4.5.1 Elastic Finite Element Solution: If one substitutes Eqs (4.108), (4.110), (4.111), & (4.129) into Eq (4.88) and rewrites the expression in terms of $\{q\}$, the one obtains for the elastic potential energy

$$\Pi_p = \frac{\{q\}^T}{2} \left[[K] + \frac{1}{3} [N_1] + \frac{1}{6} [N_2] \right] \{q\} - \{q\}^T \{P\} \quad , \quad (4.130)$$

where

$$\begin{aligned} [K] &= \int_V [\hat{D}]^T [\hat{K}] [\hat{D}] dV \\ [N_1] &= \int_V [\hat{D}]^T [\hat{N}_1] [\hat{D}] dV \\ [N_2] &= \int_V [\hat{D}]^T [\hat{N}_2] [\hat{D}] dV \end{aligned} \quad . \quad (4.131)$$

The finite element method generally requires the computation of the stiffness matrices of Eq (4.131) for each element independently. These elemental stiffnesses are then assembled according

to their relationship to global nodes of the structure. In this manner, Eq (4.130) represents the potential energy of a single element. The total energy of the system is then found by summing the energies of each element.

4.5.2 Large Strain Finite Element Solution: The large strain potential energy is given by incorporating Eqs (4.112), (4.113), (4.114), and (4.129) into Eq (4.98), and rewriting in terms of $\{q\}$. Thus,

$$\Pi_p = \frac{\{q\}^T}{2} \left[[K^*] + \frac{1}{3} [N^*_1] + \frac{1}{6} [N^*_2] \right] \{q\} - \{q\}^T \{P\} \quad , \quad (4.132)$$

where

$$\begin{aligned} [K^*] &= \int_V [\hat{D}]^T [\hat{K}^*] [\hat{D}] dV \\ [N^*_1] &= \int_V [\hat{D}]^T [\hat{N}^*_1] [\hat{D}] dV \\ [N^*_2] &= \int_V [\hat{D}]^T [\hat{N}^*_2] [\hat{D}] dV \end{aligned} \quad (4.133)$$

4.5.3 Elastic-Plastic Finite Element Solution: The incremental elastic-plastic potential energy is given by [229]

$$\Delta U = \frac{1}{2} \int_V (\{ \Delta \epsilon \}^T \{ \Delta \sigma \}) dV \quad , \quad (4.134)$$

or, following the format of Eq (4.97), the incremental elastic-plastic potential energy becomes

$$\begin{aligned} \Delta \Pi_p &= \frac{1}{2} \int_V C_{ij}^{ep} \left(\Delta \epsilon_i^L \Delta \epsilon_j^L + 2 \Delta \epsilon_i^L \Delta \epsilon_j^{NL} + \Delta \epsilon_i^{NL} \Delta \epsilon_j^{NL} \right) dV \\ &\quad - \{ \Delta d \}^T \{ P \} \end{aligned} \quad , \quad (4.135)$$

where C_{ij}^{ep} is the symmetric array of elastic-plastic constants and summation on $i, j = 1, 2, 4-6$ is implied by the repeated subscripts. Introducing Eq (4.96) into Eq (4.135) yields

$$\Delta \Pi_p = \frac{1}{2} \int_V \left(C_{ij} \{ \Delta d \}^T \left[(L_i) (L_j)^T + (L_i) \{ \Delta d \}^T [H_j] + \frac{1}{4} [H_i] \{ \Delta d \} \{ \Delta d \}^T [H_j] \right] \{ \Delta d \} \right) dV - \{ \Delta d \}^T \{ P \} \quad (4.136)$$

Eq (4.129) must be modified to represent this incremental formulation. Thus, the nodal dof take on an incremental formulation, and are defined by

$$\{ \Delta d(y_1, y_2) \} = \left[\hat{D}(s_1, s_2) \right] \{ \Delta q \} \quad (4.137)$$

Incorporating Eqs (4.125), (4.126), (4.127), & (4.137) into Eq (4.136), and rewriting in terms of $\{ \Delta q \}$. Thus, the final form of the incremental elastic-plastic potential energy takes the form

$$\Delta \Pi_p = \frac{\{ \Delta q \}^T}{2} \left[[K^{ep}] + \frac{1}{3} [N_1^{ep}] + \frac{1}{6} [N_2^{ep}] \right] \{ \Delta q \} - \{ \Delta q \}^T \{ P \} , \quad (4.138)$$

where

$$\begin{aligned} [K^{ep}] &= \int_V [\hat{D}]^T [\hat{K}^{ep}] [\hat{D}] dV \\ [N_1^{ep}] &= \int_V [\hat{D}]^T [\hat{N}_1^{ep}] [\hat{D}] dV \\ [N_2^{ep}] &= \int_V [\hat{D}]^T [\hat{N}_2^{ep}] [\hat{D}] dV \end{aligned} \quad (4.139)$$

Carrying out the variation of Eq (4.139), one obtains

$$\begin{aligned} \delta(\Delta \Pi_p) &= \delta(\{ \Delta q \}^T) \left(\left([K^{ep}] + \frac{1}{3} [N_1^{ep}] + \frac{1}{6} [N_2^{ep}] \right) \{ \Delta q \} \right. \\ &\quad \left. - \{ P \} \right) = \delta(\{ \Delta q \}^T) F(\Delta q) = 0 \end{aligned} \quad (4.140)$$

Then for an arbitrary and independent $\delta(\Delta q)$, and following the derivations of Eqs (4.90)-(4.92), the solution for an iterative manner via a Newton-Raphson technique is given by

$$\begin{aligned} \left(\left[K^{ep} \right] + \left[N_1^{ep} \right] + \left[N_2^{ep} \right] \right) (\Delta(\Delta q)) &= [K_T] (\Delta(\Delta q)) \\ &= -F(\Delta q) \end{aligned} \quad (4.141)$$

Thus, incremental elastic-plastic equilibrium equation is given by

$$\left(\left[K^{ep} \right] + \frac{1}{2} \left[N_1^{ep} \right] + \frac{1}{3} \left[N_2^{ep} \right] \right) \{\Delta q\} - \{P\} = \{0\} \quad , \quad (4.142)$$

and the linearized incremental elastic-plastic equilibrium equation is given by

$$\left(\left[K^{ep} \right] + \left[N_1^{ep} \right] + \left[N_2^{ep} \right] \right) \{\Delta \{\Delta q\}\} - \{P\} = \{0\} \quad . \quad (4.143)$$

4.6 The 36 Degree-of-Freedom Finite Element

Defining the terms of Eqs (4.130), (4.132), and (4.138) requires definition of the specific element, since the nodal parameters $\{q\}$ and the associated nodal interpolation array $[\hat{D}(s_1, s_2)]$ are element specific. Recall, the three stiffness arrays $[\hat{K}]$, $[\hat{N}_1]$, and $[\hat{N}_2]$ of Eq (4.131), the three stiffness arrays $[\hat{K}^*]$, $[\hat{N}_1^*]$, and $[\hat{N}_2^*]$ of Eq (4.133), and the three stiffness arrays $[\hat{K}^{ep}]$, $[\hat{N}_1^{ep}]$, and $[\hat{N}_2^{ep}]$ of Eq (4.139) are element independent. The choices of the number of nodes per element and the nodal degrees of freedom at each node have not been specified at this point. In fact, virtually any two-dimensional element that will provide values of the 18 functions of the continuum displacement gradient vector $\{d\}$ could be used.

The author's research objective is to investigate structural phenomena. Thus, an existing, proven finite element model for laminated cylindrical and spherical shells was used for this research. For the S1XX and S2XX elemental codes, the element chosen was the 36 degree of freedom (DOF) quadrilateral curved shell element described in Reference [48:95-III]. This element has been used for many investigations of static and dynamic response of plates, arches, and cylindrical shells undergoing large displacements with an elastic cubic-nonlinear HTSD theory [49-51, 159, 160, 197, 198, 204, 207, 208, 217, 223, 224]. In addition to these investigations, many linear

problems were used to validate the element's performance. These problems included typical flat plate and patch tests used to show convergence as the number of elements in a mesh is increased [160]. These patch test problems were based upon a linear analysis, not a nonlinear analysis. This is because the patch test is based upon the mathematical theory of *linear* partial differential equations. Since the element stiffness array includes nonlinear terms, the element will not pass the usual definitions of the patch test unless the nonlinear terms are eliminated. For the nonlinear problem, convergence cannot be proven by a simple patch test. Convergence must be demonstrated. The 36 DOF element is shown in Figure 4.5. This element has eight nodes with seven degrees of freedom $u, v, w, w_{,1}, w_{,2}, \psi_1$, and ψ_2 , at each corner nodes and two degrees of freedom, u and v , at the four midside nodes. The two degrees of freedom at the midside nodes allow for quadratic interpolation of in-plane displacements of u and v . This is important for shells due to the curvature-induced coupling of bending and membrane activity in shells.

The continuum values of u and v are interpolated from the nodal values u_k and v_k , using Eq (4.144) where Q_k are quadratic Lagrangian interpolation functions given in Eq (4.145) [48:110]

$$\left(u = \sum_{k=1}^8 Q_k u_k \right), \left(v = \sum_{k=1}^8 Q_k v_k \right), \quad (4.144)$$

$$\begin{aligned} Q_k &= \frac{1}{4} (1 - \eta_k \eta) (\xi_k \xi + \eta_k \eta - 1), \quad (k = 1 - 4) \\ Q_k &= \frac{1}{2} (1 - \xi^2) (1 + \eta_k \eta), \quad (k = 6, 8) \\ Q_k &= \frac{1}{2} (1 - \eta^2) (1 + \xi_k \xi), \quad (k = 5, 7) \end{aligned} \quad (4.145)$$

where the k^{th} node has natural coordinates $\xi_k = s_{1k}/a$ and $\eta_k = s_{2k}/b$. The natural coordinates correspond to global coordinates (s_1, s_2) is the longitudinal and circumferential directions shown in Figure 4.5.

The continuum displacement gradient vector $\{d\}$ includes rotational degrees of freedom ψ_1

and ψ_2 and the first derivatives of these parameters. The parameters ψ_1 and ψ_2 are shown in Figure 4.6. Linear interpolation can be used for these parameters, since only C^0 continuity is required. The interpolation functions of ψ_1 and ψ_2 are given by Eq (4.146) with the linear Lagrangian interpolation functions of Eq (4.147) [48:103].

$$\left(\psi_1 = \sum_{k=1}^4 N_k \psi_{1k} \right), \left(\psi_2 = \sum_{k=1}^4 N_k \psi_{2k} \right) \quad , \quad (4.146)$$

$$N_k = \frac{1}{4} (1 + \xi_k \xi) (1 + \eta_k \eta) \quad . \quad (4.147)$$

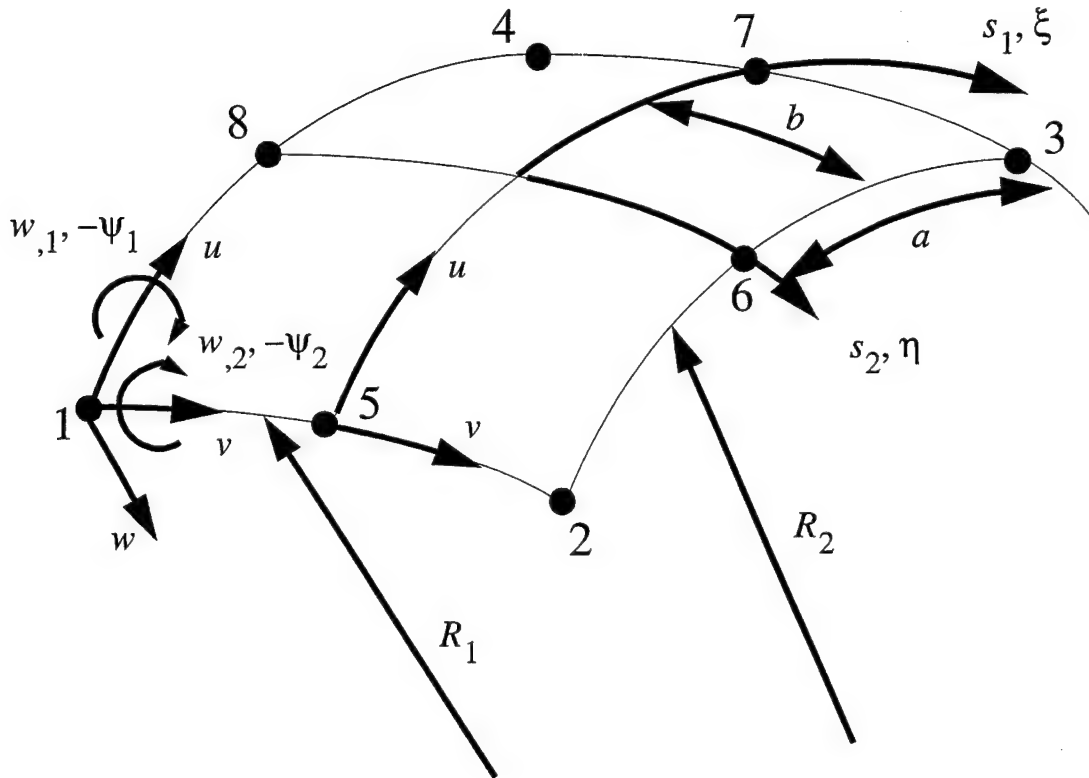


Figure 4.5 36 DOF Spherical Shell Finite Element - For S1XX & S2XX Codes

The continuum displacement gradient variables associated with transverse displacement w , include w and its first and second derivatives. Figure 4.6 shows w , $w_{,1}$, and $w_{,2}$ (for moderately large rotation theory only). Nodal parameters associated with transverse displacement include

only the values w_k , $w_{,1k}$, and $w_{,2k}$ at the four corner nodes where $k = 1 - 4$. Interpolation of w is accomplished using Eq (4.148) and the Hermitian shape functions of Eq (4.149) [48:103].

$$w(s_1, s_2) = \sum_{k=1}^4 (H1_k w_k + H2_k w_{,1k} + H3_k w_{,2k}) \quad , \quad (4.148)$$

$$\begin{aligned} H1_k &= \frac{1}{8} (1 + \xi_k \xi) (1 + \eta_k \eta) \left(2 + \xi_k \xi + \eta_k \eta - \xi^2 - \eta^2 \right) \\ H2_k &= \frac{a}{8} (1 + \xi_k \xi)^2 (\xi_k \xi - 1) (1 + \eta_k \eta) \xi_k \\ H3_k &= \frac{b}{8} (1 + \xi_k \xi) (\eta_k \eta - 1) (1 + \eta_k \eta)^2 \eta_k \end{aligned} \quad (4.149)$$

The approximate continuum values for derivatives of u , v , w , ψ_1 , and ψ_2 , at any point (ξ, η) in the element, are also found by interpolation. This is accomplished by using the corresponding derivatives of the interpolation functions. Thus, the approximate continuum displacement vector is related to the array of discrete nodal degrees of freedom as shown below

$$\{d(\xi, \eta)\} = [\hat{D}(\xi, \eta)] \{q\} \quad , \quad (4.150)$$

where

$$[\hat{D}(\xi, \eta)] = \begin{bmatrix} [Q_1] & 0 & 0 & \dots & [Q_4] & 0 & 0 & [Q_5] & \dots & [Q_8] \\ 0 & [H_1] & 0 & \dots & 0 & [H_4] & 0 & 0 & \dots & 0 \\ 0 & 0 & [N_1] & \dots & 0 & 0 & [N_4] & 0 & \dots & 0 \end{bmatrix} \quad , \quad (4.151)$$

and

$$[Q_k] = \begin{bmatrix} Q & 0 \\ Q_\xi & 0 \\ Q_\eta & 0 \\ 0 & Q \\ 0 & Q_\xi \\ 0 & Q_\eta \end{bmatrix}, [N_k] = \begin{bmatrix} N & 0 \\ N_\xi & 0 \\ N_\eta & 0 \\ 0 & N \\ 0 & N_\xi \\ 0 & N_\eta \end{bmatrix}, \quad (4.152)$$

$$[H_k] = \begin{bmatrix} H1 & H2 & H3 \\ H1_\xi & H2_\xi & H3_\xi \\ H1_\eta & H2_\eta & H3_\eta \\ H1_{\xi\xi} & H2_{\xi\xi} & H3_{\xi\xi} \\ H1_{\eta\eta} & H2_{\eta\eta} & H3_{\eta\eta} \\ H1_{\xi\eta} & H2_{\xi\eta} & H3_{\xi\eta} \end{bmatrix} \quad (4.153)$$

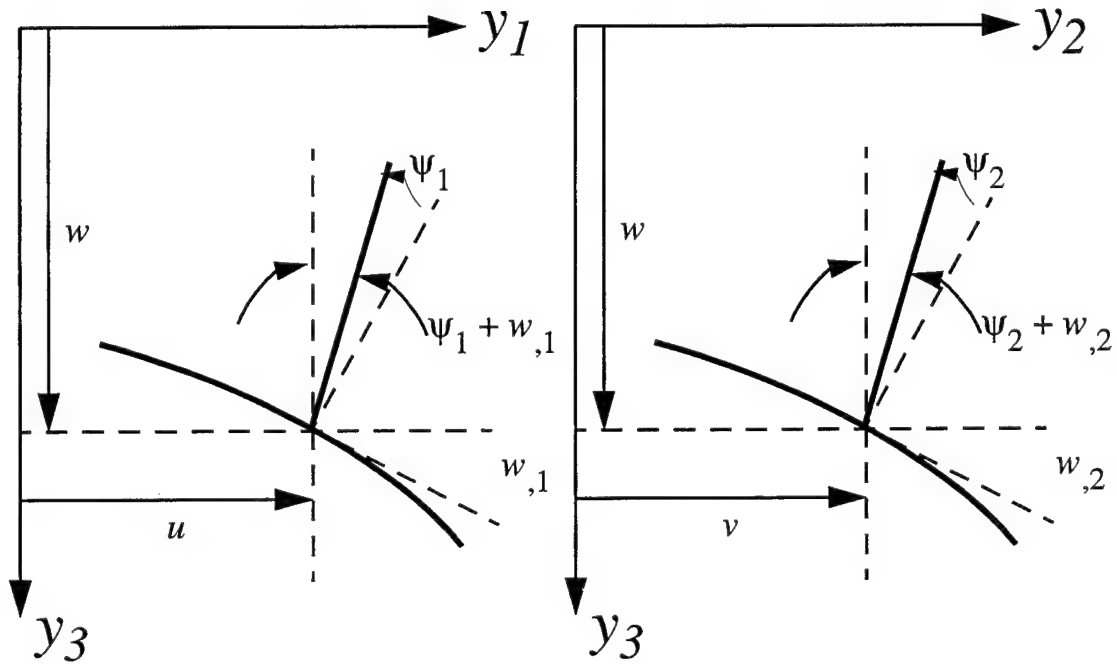


Figure 4.6 Rotational DOF Definitions for the 36 DOF Spherical Shell Element

In Eq (4.151), the numerical subscripts refer to node numbers. In Eqs (4.152) & (4.153), the Greek subscripts imply differentiation with respect to the indicated natural coordinate variable. The k subscript implies that natural coordinates ξ_k and η_k appearing in each interpolation functions are to be assigned values corresponding to the natural coordinates of the k^{th} node. In Eq (4.150), notice that $\{q\}$ is an 36×1 array of nodal displacements, $[\hat{D}]$ is an 18×36 array, and the resulting array $\{d(\xi, \eta)\}$ is an 18×1 array as expected. Transformation of coordinates using the inverse of the Jacobian matrix, $[J]$, as shown in Eq (4.154), completes the definition of the element interpolation scheme

$$[\hat{D}(s_1, s_2)] = [J]^{-1} [\hat{D}(\xi, \eta)] \quad , \quad (4.154)$$

where $[J]^{-1}$ is a diagonal matrix for the transformation of coordinates used in this research. Note that $[J]^{-1}$ is given by

$$[J]^{-1} = \begin{bmatrix} \Gamma_1 & 0 & 0 \\ 0 & \Gamma_2 & 0 \\ 0 & 0 & \Gamma_1 \end{bmatrix} \quad , \quad (4.155)$$

where

$$\Gamma_1 = \begin{bmatrix} 1 & 0 & 0 & 0 & 0 & 0 \\ 0 & 1/a & 0 & 0 & 0 & 0 \\ 0 & 0 & 1/b & 0 & 0 & 0 \\ 0 & 0 & 0 & 1 & 0 & 0 \\ 0 & 0 & 0 & 0 & 1/a & 0 \\ 0 & 0 & 0 & 0 & 0 & 1/b \end{bmatrix} \quad , \quad (4.156)$$

and

$$\Gamma_2 = \begin{bmatrix} 1 & 0 & 0 & 0 & 0 & 0 \\ 0 & 1/a & 0 & 0 & 0 & 0 \\ 0 & 0 & 1/b & 0 & 0 & 0 \\ 0 & 0 & 0 & 1/a^2 & 0 & 0 \\ 0 & 0 & 0 & 0 & 1/b^2 & 0 \\ 0 & 0 & 0 & 0 & 0 & 1/(ab) \end{bmatrix}, \quad (4.157)$$

where a and b are defined in Figure 4.5.

With this finite element discretization, Eq (4.95) is written for an elastic formulation as

$$\begin{aligned} & \left[\sum_{n=1}^m \left[\int_{dA_n} [\hat{D}]^T \left[[\hat{K}] + [\hat{N}_1] + [\hat{N}_2] \right] [\hat{D}] dA_n \right]_n \right] \{\Delta q\} \\ & = \{P\} - \left[\sum_{n=1}^m \left[\int_{dA_n} [\hat{D}]^T \left[[\hat{K}] + \frac{1}{2}[\hat{N}_1] + \frac{1}{3}[\hat{N}_2] \right] [\hat{D}] dA_n \right]_n \right] \{q\} \end{aligned}, \quad (4.158)$$

where

$dA_n \equiv$ the two-dimensional domain of an individual element n

$\equiv [J]dA_n$ in the natural coordinate system

$m \equiv$ the total number of elements in the mesh

$\{\Delta q\} \equiv$ the global column array of nodal displacement parameters assembled from elemental array $\{\Delta q\}_n$

$\{q\} \equiv$ the global column array of nodal displacement parameters assembled from elemental array $\{q\}_n$

$\{q\}_n \equiv$ a 36×1 nodal displacement array for element n

$\{\Delta q\}_n \equiv$ a 36×1 incremental nodal displacement array for element n , and

$\{R\} \equiv$ the global load array which has the same dimension as the global displacement arrays $\{\Delta q\}$ and $\{q\}$.

The integrations of Eq (4.158) are approximated by numerical integration using Gaussian quadrature. Using one of the terms of the first summation of Eq (4.158) as an example, the integral I_n shown in Eq (4.159), can be transformed to natural coordinates as shown in Eq (4.160). Next, the integration of Eq (4.160) are approximated numerically by a double summation of weighting factors at the corresponding Gaussian integration points. This is shown in Eq (4.161).

$$I_n = \int_{dA_n} [\hat{D}]^T \left[[\hat{K}] + [\hat{N}_1] + [\hat{N}_2] \right] [\hat{D}] dA_n \quad , \quad (4.159)$$

$$I_n = \int_{-1}^1 \int_{-1}^1 [\hat{D}]^T \left[[\hat{K}] + [\hat{N}_1] + [\hat{N}_2] \right] [\hat{D}] \det [J] d\xi d\eta \quad , \quad (4.160)$$

$$I_n = \sum_{i=1}^p \sum_{j=1}^r W_i W_j I(\xi, \eta) \quad , \quad (4.161)$$

where

$\det [J] \equiv$ the determinant of the Jacobian matrix

$I(\xi, \eta) = [\hat{D}]^T \{ [\hat{K}] + [\hat{N}_1] + [\hat{N}_2] \} [\hat{D}] \det [J] \equiv$ evaluated at Gauss integration points (ξ, η)

$W_i W_j \equiv$ the weighting factors

$p \equiv$ number of Gauss points in ξ -direction

$q \equiv$ number of Gauss points in η -direction.

The arranged indices i and j define the order of numerical integration. When $m = n$ the integration is called uniform. An $n \times n$ integration will exactly integrate a polynomial integrand of order $2n-1$ [44:172]. For this effort, a 36-dof element would require a 7×7 Gauss quadrature (49 Gauss points) for an exact integration. However, Dennis [51, 160], Smith [207, 208], and Tsai [223] have shown that a 5×5 Gauss quadrature (25 Gauss points) yields accurate results for the higher-order element (see Figure 4.7). The reduced Gauss quadrature yields a dramatic decrease (~50%) in the computational requirements needed for the element. Thus, for this research, the reduced Gauss quadrature was incorporated into the formulation. It should also be pointed out

that this array of integration points are used in the determination of the appropriate Jacobian transformations, for the entire thickness, incorporated in the Lagrangian-Eulerian relationships.

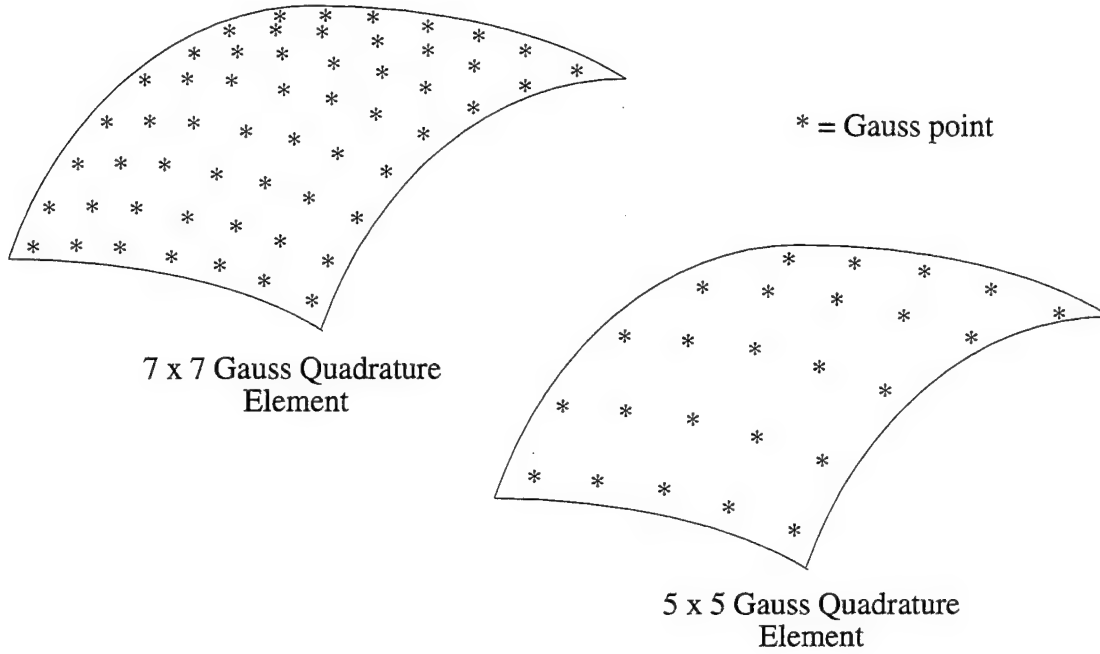


Figure 4.7 7 x 7 and 5 x 5 Gauss Quadrature Elements

The solution of Eq (4.158) is accomplished by an incremental-iterative technique commonly called the Newton-Raphson method [48:115-127]. The parameters to be incremented are the elements of the array $\{q\}$ containing global degrees of freedom. For the first iteration of the first increment, all elements of $\{q\}$ are assumed to be zero and a linear solution of Eq (4.158), one involving only $[\hat{K}]$, is found by Gauss elimination. This solution, call it $\{q\}_1$, is used during the next iteration to compute $[\hat{N}_1]$ and $[\hat{N}_2]$. Equation (4.158) is then solved using $[\hat{K}]$, $[\hat{N}_1]$, and $[\hat{N}_2]$ to generate a new solution, call it $\{q\}_2$. This process continues until the solution for $\{q\}$ has converged. The following criterion is used to determine convergence

$$\frac{\left(\sum \left(\{q_i\}_r\right)^2\right)^{1/2} - \left(\sum \left(\{q_i\}_{r-1}\right)^2\right)^{1/2}}{\left(\sum \left(\{q_i\}_1\right)^2\right)^{1/2}} \times 100 \leq \nabla, \quad (4.162)$$

where $\{q_i\}_r$, $\{q_i\}_{r-1}$, and $\{q_i\}_1$ are the elements of $\{q_i\}$ for the r^{th} , $(r-1)^{th}$, and first iterations, respectively, for a given increment. The criterion is satisfied when the left hand side of Eq (4.162) is less than or equal to ∇ , a user specified percentage tolerance. Values of ∇ ranging from 0.01 to 0.5 percent were chosen for the problems investigated. For each solution discussed in Chapter 5, values of ∇ are specified. The increment of displacement is chosen to be $1/10^{th}$ - $1/15^{th}$ of the total displacement desired for the particular problem of interest.

For an elasto-plastic approach, an incremental formulation is incorporated. The incremental forms of Eqs (4.144), (4.146), & (4.148) are

$$\left(\Delta u = \sum_{k=1}^8 Q_k \Delta u_k \right), \left(\Delta v = \sum_{k=1}^8 Q_k \Delta v_k \right) , \quad (4.163)$$

$$\left(\Delta \psi_1 = \sum_{k=1}^4 N_k \Delta \psi_{1k} \right), \left(\Delta \psi_2 = \sum_{k=1}^4 N_k \Delta \psi_{2k} \right) , \quad (4.164)$$

$$\Delta w(s_1, s_2) = \sum_{k=1}^4 (H1_k \Delta w_k + H2_k \Delta w_{,1k} + H3_k \Delta w_{,2k}) \quad (4.165)$$

where Eqs (4.145), (4.147), & (4.149) hold for Q_k , N_k , & H_k respectively. Thus, the approximate incremental continuum displacement vector is given as

$$\{\Delta d(\xi, \eta)\} = [\hat{D}(\xi, \eta)] \{\Delta q\} , \quad (4.166)$$

where $[\hat{D}](\xi, \eta)$ is defined by Eq (4.151) and Eqs (4.152), (4.153), & (4.154) hold.

With this finite element discretization, Eq (4.95) is written for an elasto-plastic formulation (following the form of Eq (4.158)) as

$$\begin{aligned}
 & \left[\sum_{n=1}^m \left[\int_{dA_n} [\hat{D}]^T \left[[\hat{K}^{ep}] + [\hat{N}_1^{ep}] + [\hat{N}_2^{ep}] \right] [\hat{D}] dA_n \right]_n \right] \{ \Delta(\Delta q) \} \\
 & = \{ \Delta P \} - \left[\sum_{n=1}^m \left[\int_{dA_n} [\hat{D}]^T \left[[\hat{K}^{ep}] + \frac{1}{2} [\hat{N}_1^{ep}] + \frac{1}{3} [\hat{N}_2^{ep}] \right] [\hat{D}] dA_n \right]_n \right] \{ \Delta q \}
 \end{aligned} \tag{4.167}$$

where $[\hat{K}]$, $[\hat{N}_1]$, and $[\hat{N}_2]$ are dependent on $\{\Delta q\}$.

The solution of Eq (4.167) is accomplished in the same manner as for Eq (4.158). However, instead of iterating to a converged solution for the array $\{q\}$, the solution converges for the array $\{\Delta q\}$. Thus, Eq (4.162) takes on the incremental form of

$$\frac{\left(\sum \left(\{ \Delta q_i \}_r \right)^2 \right)^{1/2} - \left(\sum \left(\{ \Delta q_i \}_{r-1} \right)^2 \right)^{1/2}}{\left(\sum \left(\{ \Delta q_i \}_1 \right)^2 \right)^{1/2}} \times 100 \leq \nabla, \tag{4.168}$$

where $\{\Delta q_i\}_r$, $\{\Delta q_i\}_{r-1}$, and $\{\Delta q_i\}_1$ are the elements of $\{\Delta q\}$ for the r^{th} , $(r-1)^{th}$, and first iterations respectively, for a given increment. The criterion is satisfied when the left hand side of Eq (4.168) is less than or equal to ∇ , a user specified percentage tolerance. Values of ∇ ranging from 0.01 to 0.05 percent were chosen for the problems investigated. For each solution discussed in Chapter 6, values of ∇ are specified. For same value of ∇ specified for the elastic solution, the increment of displacement was chosen to be the same as the elastic solution. However, once approximately 20% of the outer surface exhibited strains greater than 2.5%, the displacement increment was halved to maintain the same convergence tolerance for equilibrium.

At this time, a brief discussion regarding the through-the-thickness, elastic-plastic analysis is presented by referring back to Figure 4.2, along with Figure 4.8 above. For every Gauss point considered in a 5×5 Gauss quadrature elastic-plastic solution (refer to Figure 4.7), it assumed that the Gauss point extends through the element and a Gauss point is given for each layer considered. Thus, at each iteration of every increment of displacement, the stress-strain state is tracked for every Gauss point, at each separate layer, within the element. Thus, referring back to Figure 4.2, as the outer layers become plastic, the associated Gauss points' stress state within those layers

exceeds the yield stress, $\sigma > \sigma_Y$ and are behaving in an elastic-plastic manner. The remaining Gauss points for the other layers are still considered to behave in an elastic manner since they have not reach the condition $\sigma > \sigma_Y$. For the Gauss point(s) in the layer(s) where $\sigma > \sigma_Y$ the constitutive relations are modified to follow Eqs (4.10a) or (4.21a) for isotropic or orthotropic material, respectively. Then, the constitutive relations are integrated through-the-thickness to generate the elasticity arrays $A_{ij} - T_{ij}$ discussed in Eq (4.117). These in turn, are used to calculate the stiffness arrays, $[\hat{K}]^{ep}$, $[\hat{N}_1]^{ep}$, and $[\hat{N}_2]^{ep}$.

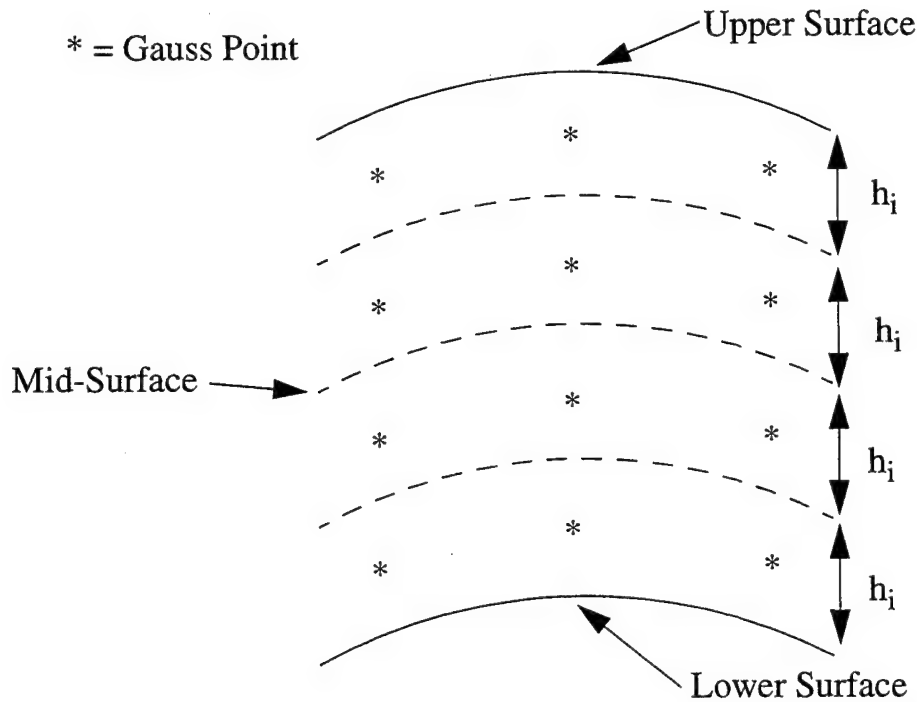


Figure 4.8 Integration of Gauss Points Through the Element's Layers

4.7 The 28 Degree-of-Freedom Finite Element

4.7.1 S1XX & S2XX Codes: For the S1XX & S2XX codes, when the in-plane continuum displacement dof, u and v , are not directly coupled to the transverse displacement dof as in a linear

analysis of a cylindrical or spherical shell, or if a flat plate is being analyzed, then a simpler finite element may be used. By removing the additional dof, u and v , at each of the midside nodes, a 28 DOF finite element is developed with linear approximations for the in-plane dof u and v (see Figure 4.9).

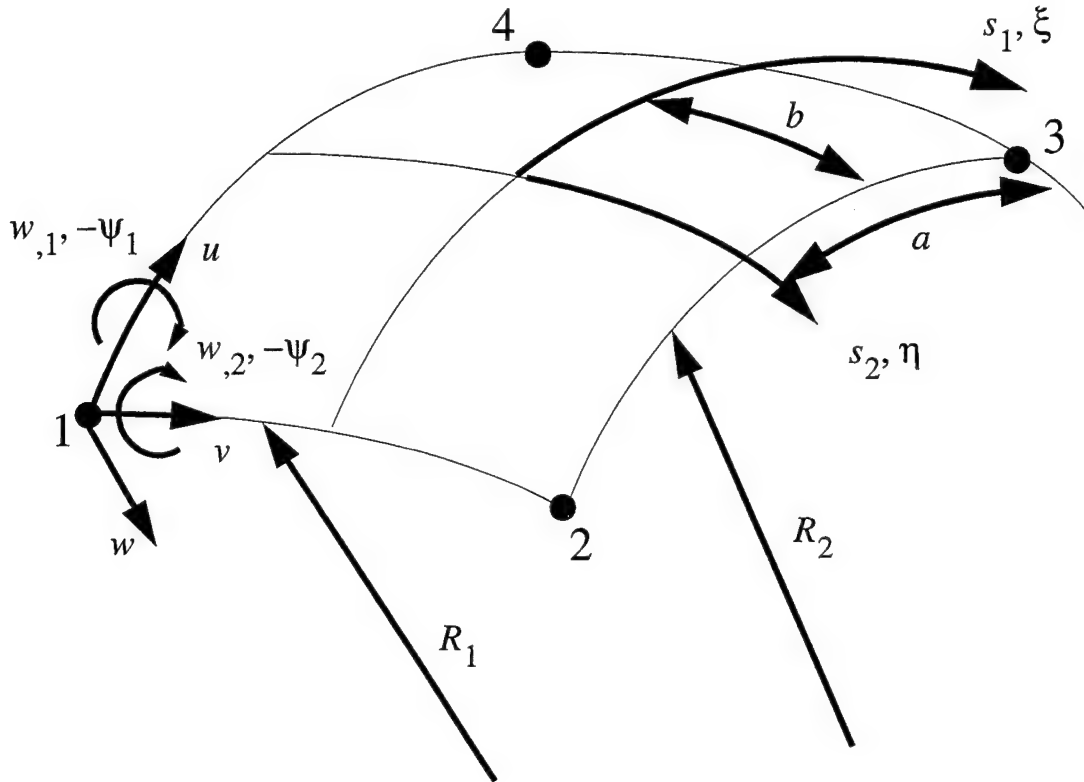


Figure 4.9 28 DOF Spherical Shell Finite Element - For S1XX & S2XX Codes

Thus, Eqs (4.144) & (4.145) become

$$\begin{pmatrix} u \\ v \end{pmatrix} = \begin{pmatrix} \sum_{k=1}^8 N_k u_k \\ \sum_{k=1}^8 N_k v_k \end{pmatrix}, \quad (4.169)$$

$$N_k = \frac{1}{4} (1 + \xi_k \xi) (1 + \eta_k \eta), \quad (4.170)$$

where N_k are linear Lagrangian interpolation functions [48:103]. Then Eq (4.151) becomes for the linear 28 DOF element

$$[\hat{D}(\xi, \eta)] = \begin{bmatrix} [N_1] & 0 & 0 & \dots & [N_4] & 0 & 0 \\ 0 & [H_1] & 0 & \dots & 0 & [H_4] & 0 \\ 0 & 0 & [N_1] & \dots & 0 & 0 & [N_4] \end{bmatrix}, \quad (4.171)$$

where N_k is defined by Eq (4.152) and H_k is defined by Eq (4.153). Recalling Eq (4.150), notice that $\{q\}$ is a 28×1 array of nodal displacements, $[\hat{D}]$ is an 18×28 array, and the resulting array $\{d(\xi, \eta)\}$ is an 18×1 array as expected. Eqs (4.154) - (4.162) remain the same as before.

4.7.2 S0XX Code: To develop a quadratic element for the classical thin shell S0XX code similar to the 36 DOF element discussed previously in Section 4.6, a 28 DOF spherical finite element was developed (see Figure 4.10). The in-plane dof u and v are interpolated with the quadratic Lagrangian approximations of Eqs (4.144) & (4.145). In the classical thin shell theory, the dof y_i and its derivatives are neglected. Thus, there are five dof per corner node ($u, v, w, w_{,1}, w_{,2}$) and two dof at the midside nodes (u & v). The dof w and its derivatives are interpolated by the Hermitian functions listed in Eqs (4.148) & (4.149). Then Eq (4.151) becomes for the quadratic 28 DOF element

$$[\hat{D}(\xi, \eta)] = \begin{bmatrix} [Q_1] & 0 & 0 & \dots & [Q_4] & 0 & [Q_5] & \dots & [Q_8] \\ 0 & [H_1] & 0 & \dots & 0 & [H_4] & 0 & \dots & 0 \end{bmatrix}, \quad (4.172)$$

where

$$[Q_k] = \begin{bmatrix} Q_\xi & 0 \\ Q_\eta & 0 \\ 0 & Q_\xi \\ 0 & Q_\eta \end{bmatrix}, \quad (4.173)$$

and H_k is defined by Eq (4.153).

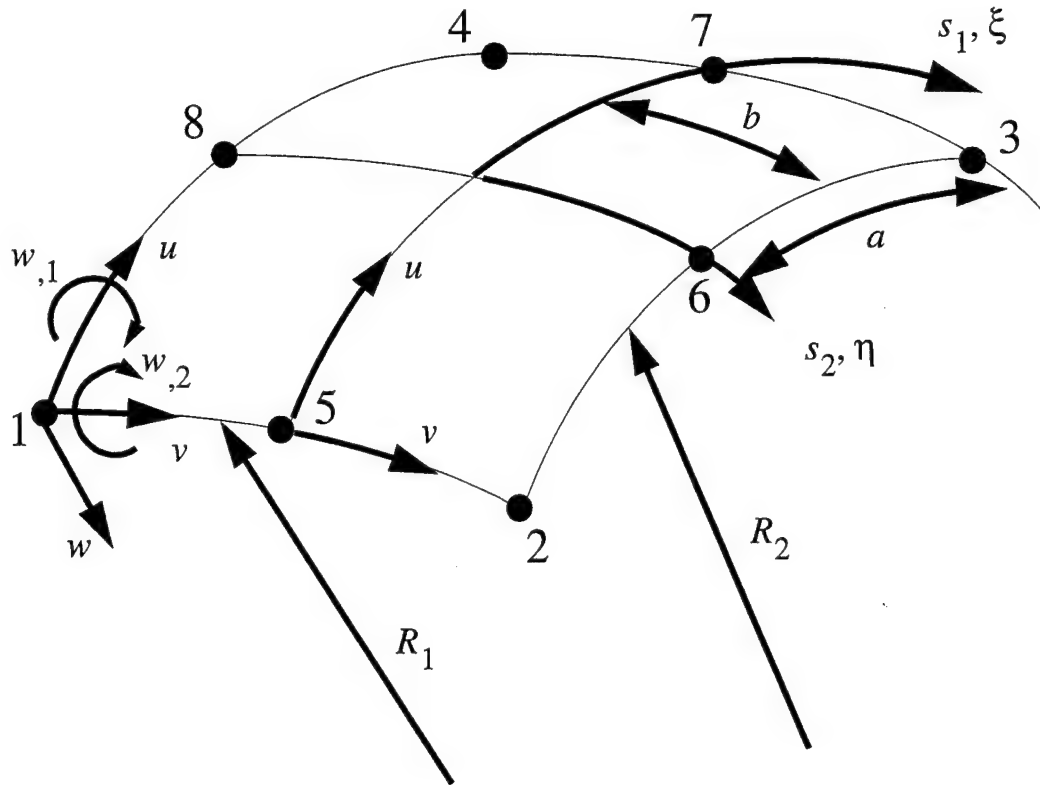


Figure 4.10 28 DOF Spherical Shell Element - For S0XX Code

Recalling Eq (4.150), notice that $\{q\}$ is a 28×1 array of nodal displacements, $[\hat{D}]$ is an 10×28 array, and the resulting array $\{d(\xi, \eta)\}$ is an 10×1 array as expected. Eq (4.155) takes the form

$$[J]^{-1} = \begin{bmatrix} \Gamma_1 & 0 \\ 0 & \Gamma_2 \end{bmatrix}, \quad (4.174)$$

where

$$\Gamma_1 = \begin{bmatrix} 1/a & 0 & 0 & 0 \\ 0 & 1/b & 0 & 0 \\ 0 & 0 & 1/a & 0 \\ 0 & 0 & 0 & 1/b \end{bmatrix}, \quad (4.175)$$

and

$$\Gamma_2 = \begin{bmatrix} 1 & 0 & 0 & 0 & 0 & 0 \\ 0 & 1/a & 0 & 0 & 0 & 0 \\ 0 & 0 & 1/b & 0 & 0 & 0 \\ 0 & 0 & 0 & 1/a^2 & 0 & 0 \\ 0 & 0 & 0 & 0 & 1/b^2 & 0 \\ 0 & 0 & 0 & 0 & 0 & 1/(ab) \end{bmatrix}, \quad (4.176)$$

where a and b are defined in Figure 4.10. Eqs (4.158) - (4.162) remain the same as before.

4.8 The 20 Degree-of-Freedom Finite Element

For the S0XX code a linear version of the finite element discussed in Section 4.7.2 is given by removing the midside nodes and the in-plane dof u and v are approximated by linear Lagrangian interpolation functions defined in Eqs (4.169) & (4.170) (see Figure 4.11). Then Eq (4.172) becomes

$$[\hat{D}(\xi, \eta)] = \begin{bmatrix} [N_1] & 0 & 0 & \dots & [N_4] & 0 \\ 0 & [H_1] & 0 & \dots & 0 & [H_4] \end{bmatrix}, \quad (4.177)$$

where

$$[N_k] = \begin{bmatrix} N_\xi & 0 \\ N_\eta & 0 \\ 0 & N_\xi \\ 0 & N_\eta \end{bmatrix}, \quad (4.178)$$

and H_k is defined by Eq (4.153). Recalling Eq (4.150), notice that $\{q\}$ is a 20×1 array of nodal displacements, $[\hat{D}]$ is an 10×20 array, and the resulting array $\{d(\xi, \eta)\}$ is an 10×1 array as expected. Eqs (4.158) - (4.162) and (4.174) - (4.176) remain the same as before.

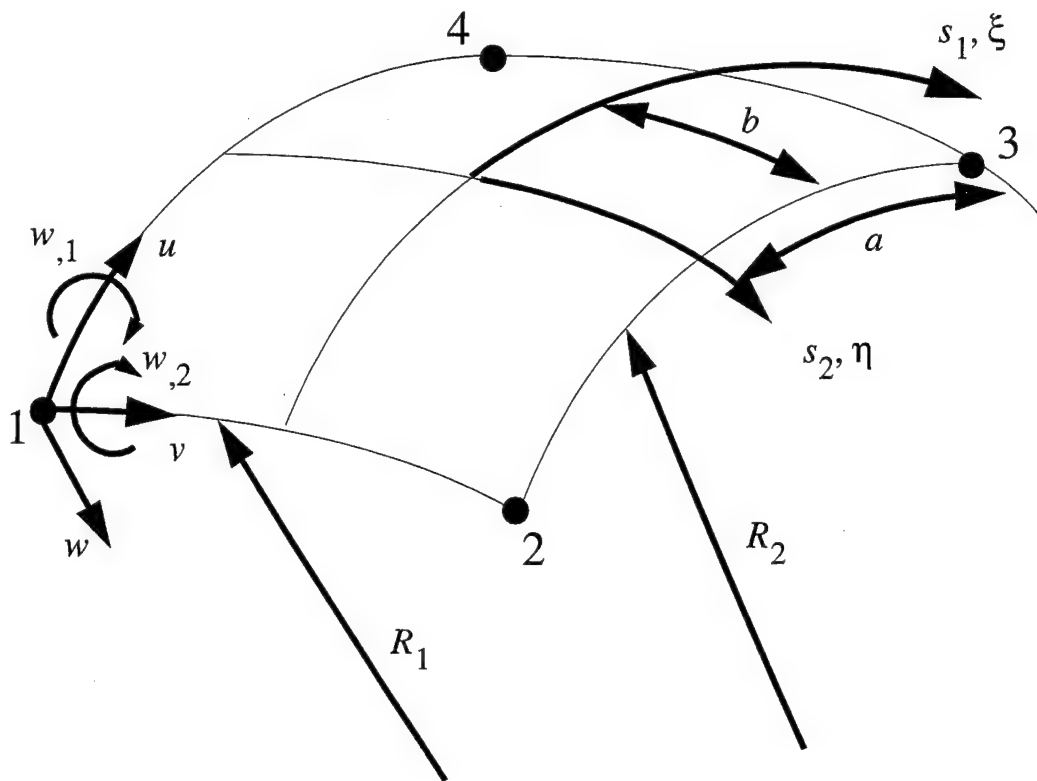


Figure 4.11 20 DOF Spherical Shell Element - For S0XX Code

4.9 The Incremental, Displacement-Control, Elastic-Plastic Algorithm

To understand the elasto-plastic formulation of the Newton-Raphson nonlinear solution algorithm, a discussion is given of the Newton-Raphson algorithm from a load-control approach, then a displacement-control approach, and finally the incremental, displacement-control, elasto-plastic approach.

4.9.1 The Load-Control, Newton-Raphson Algorithm:

Recall from Eq (4.93)

$$[K_T(d)] \{\Delta d\} = -F(d) \quad (4.93)$$

or, in terms of the Rajasekaran & Murray formulation

$$\begin{aligned} & \left[[K] + [N_1(d)] + [N_2(d^2)] \right] \{\Delta d\} = \\ & \{P\} - \left[[K] + \frac{1}{2} [N_1(d)] + \frac{1}{3} [N_2(d^2)] \right] \{q\} \end{aligned} \quad (4.179)$$

As described in [162:Chap 3], for a given first increment in load, P_1 , Eq (4.179) reduces to

$$[K(d)] \{d_1\} = \{P_1\} \quad (4.180)$$

Now d_1 is substituted into the stiffness arrays N_1 and N_2 and the updated tangent stiffness array, K_T , is given by

$$[K_T] = \left[[K] + [N_1(d_1)] + [N_2(d_1^2)] \right] \quad (4.181)$$

The tangent stiffness array, K_T , is comprised of constants after the d substitution and represents the local slope at d_1 of the actual load versus displacement relationship (see Figure 4.12). After similarly substituting d_1 into the right-hand side of Eq (4.179) for the incremental displacement, Δd_1

$$\begin{aligned} & \left[[K] + [N_1(d_1)] + [N_2(d_1^2)] \right] \{\Delta d_1\} = \\ & \{P_1\} - \left[[K] + \frac{1}{2} [N_1(d_1)] + \frac{1}{3} [N_2(d_1^2)] \right] \{d_1\} \end{aligned} \quad (4.182)$$

The right-hand side of Eq (4.182) is the residual force vector ΔR_1 shown in Figure 4.12.

The displacement d is updated as in Eq (4.183) and illustrated in Figure 4.12

$$\{d_2\} = \{d_1\} + \{\Delta d_1\} \quad (4.183)$$

Iteration continues using the recursive relationships of Eqs (4.184)-(4.185) until the residual force vector ΔR_n becomes small, signifying that the equilibrium equations $F(d_n)$ are satisfied

$$\begin{aligned} & \left[[K] + [N_1(d_{n-1})] + [N_2(d_{n-1}^2)] \right] \{\Delta d_{n-1}\} = \\ & \{P_1\} - \left[[K] + \frac{1}{2} [N_1(d_{n-1})] + \frac{1}{3} [N_2(d_{n-1}^2)] \right] \{d_{n-1}\} \end{aligned} \quad (4.184)$$

$$\{d_n\} = \{d_{n-1}\} + \{\Delta d_{n-1}\} \quad (4.185)$$

The converged displacement is the d_n of Figure 4.12, and point A is the first point of the actual load versus displacement path found.

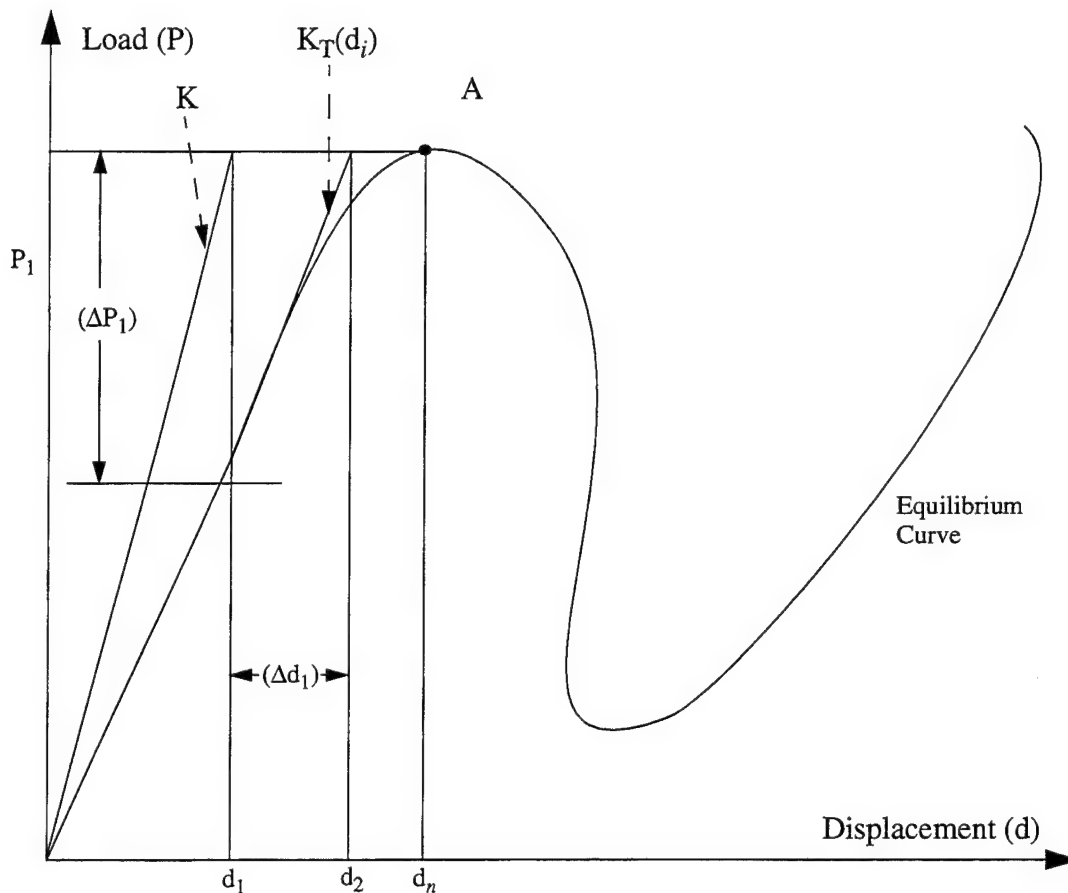


Figure 4.12 Load-Control Solution Algorithm

The process is repeated for the next load increment, R_2 , of Figure 4.13. Upon convergence, point B is determined.

For the usual case of more than one degree of freedom, instead of only one load versus displacement curve, there are as many curves as there are degrees of freedom. A global convergence criterion such as that given in Eq (4.162)

$$\frac{\left(\sum \left(\{d_i\}_r\right)^2\right)^{1/2} - \left(\sum \left(\{d_i\}_{r-1}\right)^2\right)^{1/2}}{\left(\sum \left(\{d_i\}_1\right)^2\right)^{1/2}} \times 100 \leq \nabla \quad (4.162)$$

where $\{d_i\}_r$, $\{d_i\}_{r-1}$, and $\{d_i\}_1$ are the elements of $\{d\}$ for the r^{th} , $(r-1)^{th}$, and first iterations respectively, for a given increment. The criterion is satisfied when the left hand side of Eq (4.168) is less than or equal to ∇ , a user specified percentage tolerance. Values of ∇ ranging from 0.01 to 0.05 % were chosen for the problems investigated.

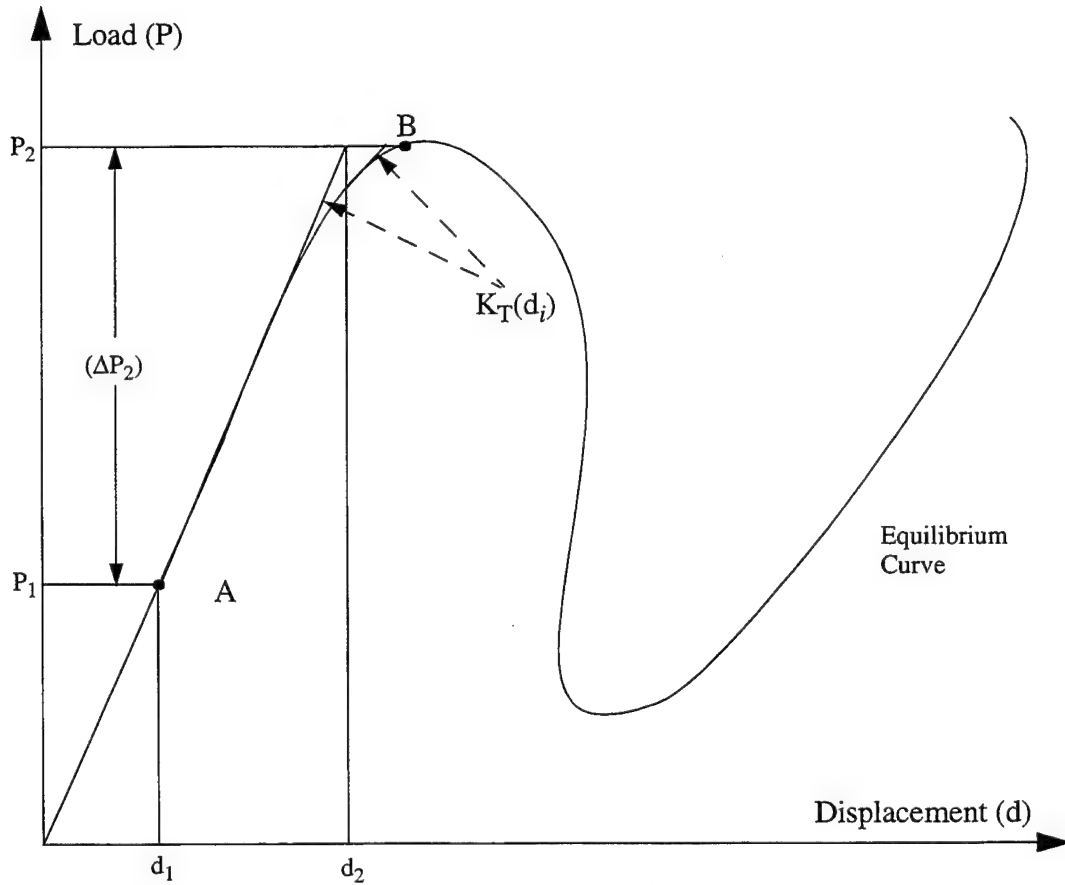


Figure 4.13 Second Increment of Load-Control Solution Algorithm

A drawback of the preceding method is its inability to traverse limit points. A limit point occurs whenever the slope of the load versus displacement curve is zero. At that point, the tan-

gent stiffness becomes singular, and Eq (4.93) cannot be solved. Transversely loaded flat plates typically do not exhibit limit points. However, transversely loaded thin shells often do. Consequently, a variation of the previously described technique is employed which takes the form of the displacement-control Newton-Raphson algorithm.

4.9.2 The Displacement-Control, Newton-Raphson Algorithm:

The displacement control solution method is very similar to the recursive relations of Eqs (4.184)-(4.185) except a single component of displacement is prescribed and incremented, and its corresponding load component becomes unknown. This allows traversing the limit points as the coefficient matrix of the incremental/iterative equations is no longer singular. A simple displacement control approach, but limited in application, only permits stepping of certain displacement components. That is, one application is a structure that only has a single point load acting on it. For this case, the displacement corresponding to that single point load must be the degree of freedom that is incremented. In addition, the simple approach solves the situation where all the edge displacements on an axially compressed plate or shell are identically prescribed. This simple method does not destroy symmetry or bandedness of the equations as more general methods do.

Basically the simple method is described as follows. For the first iteration of a given displacement increment, a displacement component is prescribed, d_p , and Eq (4.180) is solved

$$[K_T(d_p)] \{\tilde{d}_1\} = \{P_1\} \quad (4.180)$$

then $d_p - \tilde{d}_1$ represents an *out of balanced* displacement from the prescribed displacement component, d_p . Thus, Eqs (4.184)-(4.185) take on the form of

$$\begin{aligned} \Delta P_n = & \left[[K] + [N_1(\tilde{d}_n)] + \left[N_2 \left((\tilde{d}_n)^2 \right) \right] \right] \{d_p - \tilde{d}_n\} \\ & + \{P_n\} - \left[[K] + \frac{1}{2} [N_1(\tilde{d}_n)] + \frac{1}{3} \left[N_2 \left((\tilde{d}_n)^2 \right) \right] \right] \{\tilde{d}_n\} \end{aligned} \quad (4.186)$$

$$\{d_p\} = \{d_p\} + \{\tilde{d}_n\} \quad (4.187)$$

This technique is a simple modifications of Eqs (4.184)-(4.185), but only specific applications are

effectively solved. In the load versus displacement space, for a prescribed displacement degree of freedom, the method is graphically portrayed in Figure 4.14.

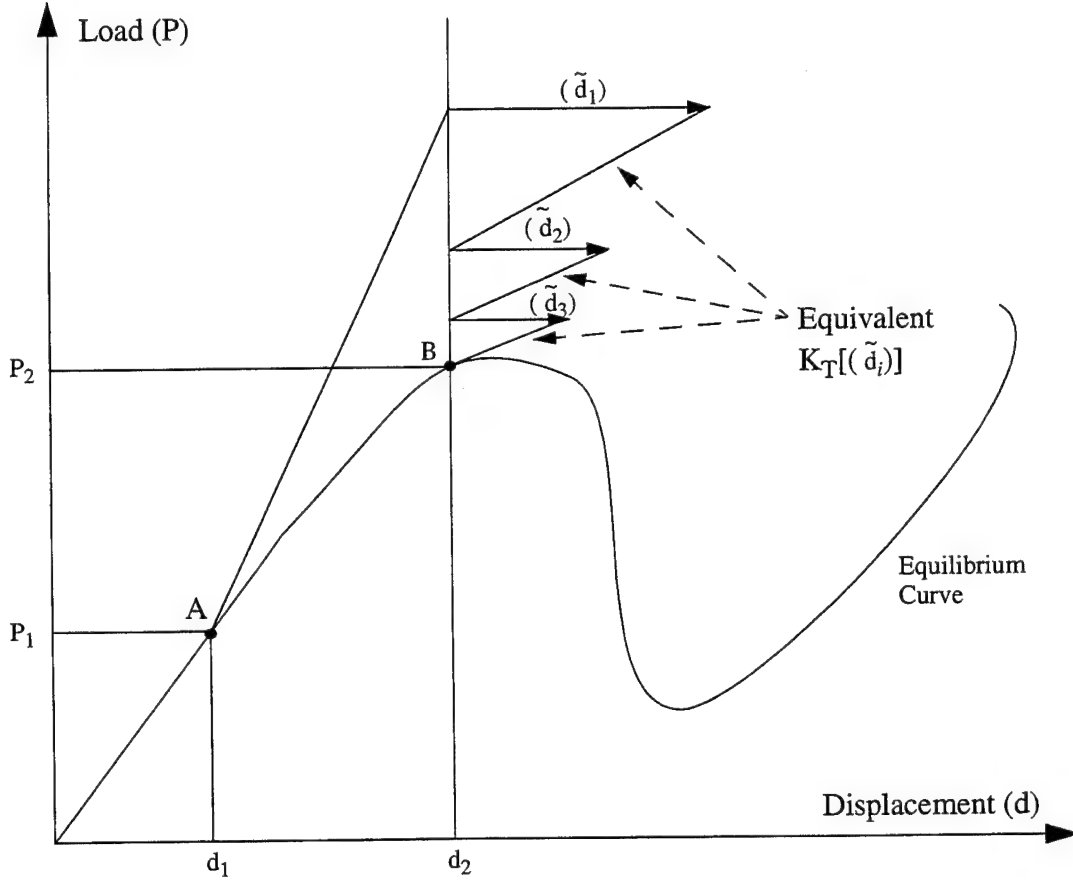


Figure 4.14 Displacement Control Solution Algorithm

The displacement is incremented from that at point A, d_1 , to that at point B, d_2 . Figure 4.14 shows the vertical line of $d_2 = \text{constant}$, becomes a "constraint" line. In the load control solution algorithm, a horizontal line (actually the constraint lines are general surfaces) was the constraint (see $P_1 = \text{constant}$ in Figure 4.12). The different constraint surfaces constrain the solution techniques. A global convergence criterion similar to Eq (4.162) is given by

$$\frac{\left(\sum \left(\{\tilde{d}_i\}_r\right)^2\right)^{1/2} - \left(\sum \left(\{\tilde{d}_i\}_{r-1}\right)^2\right)^{1/2}}{\left(\sum \left(\{\tilde{d}_i\}_1\right)^2\right)^{1/2}} \times 100 \leq \nabla \quad (4.188)$$

where $\{d_i\}_r$, $\{d_i\}_{r-1}$, and $\{d_i\}_1$ are the elements of $\{d\}$ for the r^{th} , $(r-1)^{th}$, and first iterations respectively, for a given increment. The criterion is satisfied when the left hand side of Eq (4.188) is less than or equal to ∇ , a user specified percentage tolerance.

4.9.3 The Incremental, Displacement-Control, Elasto-Plastic, Newton-Raphson Algorithm:

The incremental form of Eq (4.93) is given by

$$[K_T(\Delta d)] \{\Delta(\Delta d)\} = -F(\Delta d) \quad (4.189)$$

or, in terms of the Rajasekaran & Murray formulation

$$\begin{aligned} & \left[[K] + [N_1(\Delta d)] + [N_2(\Delta d^2)] \right] \{\Delta(\Delta d)\} = \\ & \{\Delta P\} - \left[[K] + \frac{1}{2}[N_1(\Delta d)] + \frac{1}{3}[N_2(\Delta d^2)] \right] \{\Delta d\} \end{aligned} \quad (4.190)$$

or in terms of Eq (4.186)

$$\begin{aligned} \Delta(\Delta P_n) &= \left[[K] + [N_1(\Delta \tilde{d}_n)] + [N_2((\Delta \tilde{d}_n)^2)] \right] \{\Delta d_p - \Delta \tilde{d}_n\} \\ &+ \{\Delta P_n\} - \left[[K] + \frac{1}{2}[N_1(\Delta \tilde{d}_n)] + \frac{1}{3}[N_2((\Delta \tilde{d}_n)^2)] \right] \{\Delta \tilde{d}_n\} \end{aligned} \quad (4.191)$$

and Eq (4.187) takes the form

$$\{\Delta d_p\} = \{\Delta d_p\} + \{\Delta \tilde{d}_n\} \quad (4.192)$$

For the first prescribed increment, $\Delta d_p = \Delta d_1$, solve

$$\Delta P_1 = [K] \{\Delta d_1\} \quad (4.193)$$

Then calculate $[K]$, $[N_1]$, and $[N_2]$ based on Δd_1 and solve $\Delta \tilde{d}_1$ from

$$[K_T(\Delta d_1)] \{\Delta \tilde{d}_1\} = \{\Delta P_1\} \quad (4.194)$$

The out of balance displacement term, $\Delta d_1 - \Delta \tilde{d}_1$ is determined and now Eq (4.191) takes on the form

$$\Delta(\Delta P_1) = [[K] + [N_1(\Delta \tilde{d}_1)] + [N_2((\Delta \tilde{d}_1)^2)]] \{\Delta d_1 - \Delta \tilde{d}_1\} \quad , \quad (4.195)$$

$$+ \{\Delta P_1\} - \left[[K] + \frac{1}{2} [N_1(\Delta \tilde{d}_1)] + \frac{1}{3} [N_2((\Delta \tilde{d}_1)^2)] \right] \{\Delta \tilde{d}_1\}$$

and is solved for $\Delta(\Delta P_1)$. ΔP_1 is updated and Eqs (4.194) and (4.195) are solved iteratively until convergence is achieved. The global convergence criterion takes on the incremental form of Eq (4.188) and is given by

$$\frac{\left(\sum \left(\{\Delta \tilde{d}_i\}_r \right)^2 \right)^{1/2} - \left(\sum \left(\{\Delta \tilde{d}_i\}_{r-1} \right)^2 \right)^{1/2}}{\left(\sum \left(\{\Delta \tilde{d}_i\}_1 \right)^2 \right)^{1/2}} \times 100 \leq \nabla \quad . \quad (4.196)$$

Evaluate $\Delta \sigma$ for every Gauss point at each layer through

$$\begin{aligned} \{\Delta \epsilon\} &= [B] \{\Delta d\} \\ \{\Delta \sigma\} &= \frac{1}{D} [T_1]^{-1} [a] [T_2] \{\Delta \epsilon\} = [D] \{\Delta \epsilon\} \quad , \end{aligned} \quad (4.197)$$

where $[B]$ represents the Green's strain-displacement relations, $[a]$ is the Cauchy constitutive relations matrix, $[T_1]$ is the Jacobian transformation matrix for the Cauchy stress-state, $[T_2]$ is the Jacobian transformation matrix for the Cauchy strain state, D is the determinant of the Jacobian transformation matrix, and $[D]$ is the Lagrangian constitutive relations matrix.

The global stress array is updated for each Gauss point, at each layer, by

$$\{\sigma_n\} = \{\sigma_{n-1}\} + \{\Delta \sigma_{n-1}\} \quad , \quad (4.198)$$

and then the desired yield criteria is checked for the updated stress state. If a Gauss point's stress state exceeds the desired yield criterion, then it's flagged as behaving plastic and the constitutive relations are then modelled as elasto-plastic for the remaining analysis.

For the second prescribed increment, $\Delta d_p = \Delta d_2$, calculate $[K]$, $[N_1]$, and $[N_2]$ based on Δd_2 and solve for ΔP_2 from

$$[K_T(\Delta d_1)] \{\Delta d_2\} = \{\Delta P_2\} \quad (4.199)$$

and then solve for $\Delta \tilde{d}_2$ from

$$[K_T(\Delta d_2)] \{\Delta \tilde{d}_2\} = \{\Delta P_2\} \quad . \quad (4.200)$$

The out of balance displacement term, $\Delta d_2 - \Delta \tilde{d}_2$ is determined and now Eq (4.191) takes on the form

$$\Delta(\Delta P_2) = [[K] + [N_1(\Delta \tilde{d}_2)] + [N_2((\Delta \tilde{d}_2)^2)]] \{ \Delta d_2 - \Delta \tilde{d}_2 \} + \{ \Delta P_2 \} - \left[[K] + \frac{1}{2} [N_1(\Delta \tilde{d}_2)] + \frac{1}{3} [N_2((\Delta \tilde{d}_2)^2)] \right] \{ \Delta \tilde{d}_2 \} \quad (4.201)$$

and is solved for $\Delta(\Delta P_2)$. ΔP_2 is updated and Eqs (4.200)-(4.201) are solved iteratively until convergence is achieved. The global convergence criterion takes on the incremental form of Eq (4.196). For each Gauss point that behaves elasto-plastically, Eq (4.201) takes the form

$$\Delta(\Delta P_2) = [[K^{ep}] + [N_1^{ep}(\Delta \tilde{d}_2)] + [N_2^{ep}((\Delta \tilde{d}_2)^2)]] \{ \Delta d_2 - \Delta \tilde{d}_2 \} + \{ \Delta P_2 \} - \left[[K^{ep}] + \frac{1}{2} [N_1^{ep}(\Delta \tilde{d}_2)] + \frac{1}{3} [N_2^{ep}((\Delta \tilde{d}_2)^2)] \right] \{ \Delta \tilde{d}_2 \} \quad (4.202)$$

where $[K^{ep}]$, $[N_1^{ep}]$, and $[N_2^{ep}]$ are based on the elasto-plastic constitutive relations and take the form of Eqs (4.125)-(4.128). A detailed flow chart and discussion of the algorithm is given in Appendix G.

5. Discussion of Elastic Shell Analysis

Chapters 3 and 4 presented the development of three basic geometrical and material variations of theory for plates and shells. The first variation concerns the inclusion of spherical geometry in the kinematic field and the strain-displacement relations. The second variation addresses the transformation of constitutive relations from the Cauchy stress-strain (Eulerian) coordinates to the 2nd Piola stress-Green strain (Lagrangian) coordinate. Finally, the third variation is the inclusion of nonlinear material effects. This chapter discusses the elastic analysis of plates and shells with the inclusion of the material transformation matrices. Results for an elastic-plastic analysis of plates and shells (including the material transformation matrices) are discussed in Chapter 6. One objective of this research was to evaluate the accuracy of including the variations of the HTSD theory with elastic or elastic-plastic material properties listed in Table 5.1, another objective was to assess their limitations. The first step in achieving these objectives was the verification of the computational tools used to achieve results. This verification process included verification of the MACSYMA routines used to generate the elemental codes (this process is discussed in Reference [209:Section 4.6]), verification of the finite element program, and finally verification of numerical analysis.

Several test problems were solved to verify the MACSYMA generated Fortran codes. These test problems were classical flat plate and thin shell problems with known solutions. In all of these test problems, the various elemental codes should give results equivalent to the classical von Karman plate (P000) code or the classical Donnell shell (C000 & S000) codes. This result is expected since the additional terms of the higher-order codes include radius in the denominator. Thus, these terms are zero for a flat plate and negligible for the classical thin shell. In addition, these results should correspond closely to those produced by Dennis [48]. Investigations of the limitations of elastic quasi-nonlinear HTSD theory were based on the shallow isotropic shell panel problems and a deep isotropic arch problem. The shallow shell problems were thin 254.0-cm radius hinged-free cylindrical shell panels with a transverse point load, or thin 12.09-cm radius hinged-hinged spherical shell caps with a transverse point load. The 50.8-cm \times 50.8-cm cylindrical shell panels studied were 0.64-cm thick. The 4.62-cm \times 4.62-cm spherical shell cap studied was 0.04-cm thick. The method used to solve each case was the nonlinear, displacement-controlled method. This method allows for convergence past the buckling or snapping phase within each problem [162:9, 134]. The convergence tolerance, ∇ , unless otherwise specified, for each problem was

0.01. All problems were run on a SUN SPARCstation 10/80 workstation.

Table 5.1 Definitions of Elemental Codes for Variations of Elastic Theory

Code Name GXYZ	Displacement Assumption Field	Constitutive Relations Analyzed	Material Coordinate Transformation	Equations Given in Appendix
G000	Donnell (1)	Elastic	Not Included	C
G001	Donnell	Elastic	Included	C
G100	modified Donnell(2)	Elastic	Not Included	D
G101	modified Donnell	Elastic	Included	D
G200	Cubic Nonlinear (3)	Elastic	Not Included	E
G201	Cubic Nonlinear	Elastic	Included	E

where

(1) u_i defined in Eq (C.2)

(2) u_i defined in Eq (D.2)

(3) u_i defined in Eq (E.2)

$G \equiv P$ for a plate, C for a cylindrical shell, S for a spherical shell, or A for an arbitrary shell geometry. Appendix A lists relations for arbitrary shells, Appendix B lists relation for general spherical shells, and Appendices C through E list relations for spherical shells. The plate and cylindrical shell relations are embedded within the spherical shell relations. They are derived by setting the parameters D and/or C to zero.

5.1 Flat, Quasi-Isotropic Panel with Uniform Pressure Point Load

A transversely-loaded flat plate problem was used to test the MACSYMA generated elemental codes and the modified finite element program. The plate chosen was an 8-ply quasi-isotropic

laminated square plate with simple boundary conditions along each of its 40.64-cm long sides (see Figure 5.1). The plate was loaded with a uniform transverse pressure load. The plate thickness was 4.064-cm. The plate was analyzed by discretizing one quadrant into a 4×4 mesh of uniform elements. Only one quadrant was analyzed because symmetric response is known to occur [48:221]. The problem was solved by incrementing the load in five equal increments of 51.71×10^6 Pa. Boundary conditions and material properties are, respectively:

$$\begin{aligned} s_1 &= 0 & v = w_{,2} = \psi_2 &= 0 & (\text{symmetry}) \\ s_2 &= 0 & u = w_{,1} = \psi_1 &= 0 & (\text{symmetry}) \\ s_1 &= \pm a & v = w = \psi_2 &= 0 & (\text{simple}) \\ s_2 &= \pm b & u = w = \psi_1 &= 0 & (\text{simple}) \\ a &= b = 40.64 \text{ cm} & h &= 4.064 \text{ cm} \end{aligned}$$

$$\begin{aligned} E_1 &= 41.37 \times 10^{10} \text{ Pa} & E_2 &= 1.03 \times 10^{10} \text{ Pa} \\ G_{23} &= 5.17 \times 10^9 \text{ Pa} & G_{12} = G_{13} &= 6.21 \times 10^9 \text{ Pa} \\ \nu &= 0.3 \end{aligned}$$

Transverse displacements at the center of the plate, as predicted by the PXXX codes and several other references are listed in Table 5.2. The results shown on the first line of the table were those reported by Dennis [48:236]. The final line of the table includes the results reported by Putcha and Reddy [172]. They used a mixed finite element model with parabolic transverse shear deformation to solve the von Karman plate equations. The lines labeled P000-P201 are the three geometrical variations with or without the material transformation matrices. These problems were run on the SUN SPARCstation 10MP/80. This workstation provided improved precision to that of the VAX 8550 that Dennis used for his analysis. From Table 5.2, one can see that the six quasi-nonlinear codes provided nearly identical results. This close agreement shows that the author's theories correctly degenerate to flat plate solutions when curvature is not a factor in the problem. Graphical results are shown in Figure 5.2 for the six variations compared and Dennis results given in Table 5.2. Five increments of load (33.34×10^3 N) were applied. For the P00X & P10X

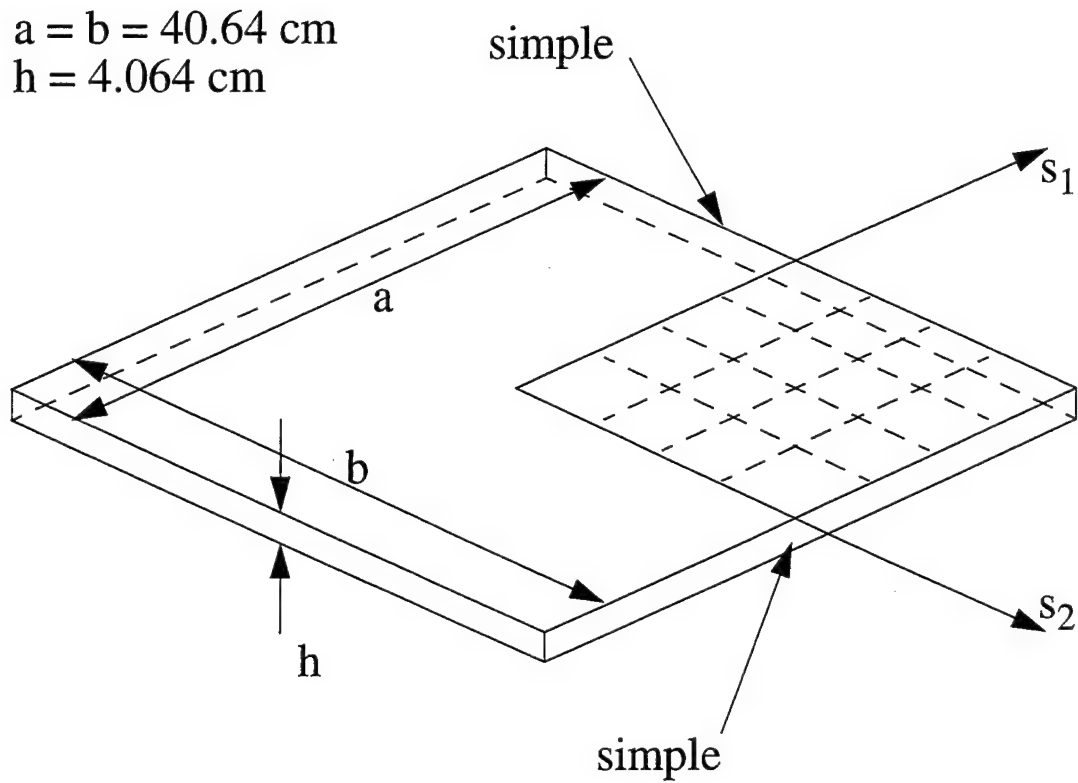


Figure 5.1 4.064 cm Thick, Hinged-Hinged Plate with Uniform Pressure Load

Table 5.2 Comparison of Flat Plate Displacement (cm) Results for Various Geometric Nonlinear Theories

Total Load (10^3 N)	33.34	66.68	100.03	133.37	166.71
Ref [48:236]	1.1212	1.9804	2.6314	3.1496	3.5865
P000	0.7882	1.4567	0.8074	2.5578	2.9947
P001	0.7882	1.4552	0.8060	2.5527	2.9896
P100	1.1212	1.9799	2.6314	3.1496	3.5865
P101	1.1212	1.9738	2.6187	3.1318	3.5611
P200	1.1229	1.9891	2.6492	3.1826	3.6322
P201	1.1229	1.9822	2.6340	3.1598	3.5992
Ref [172:537]	1.143	2.032	2.794	3.302	3.810

theories, solutions took 36.1 cpu seconds. For the P20X theories, solutions required 43.2 cpu seconds.

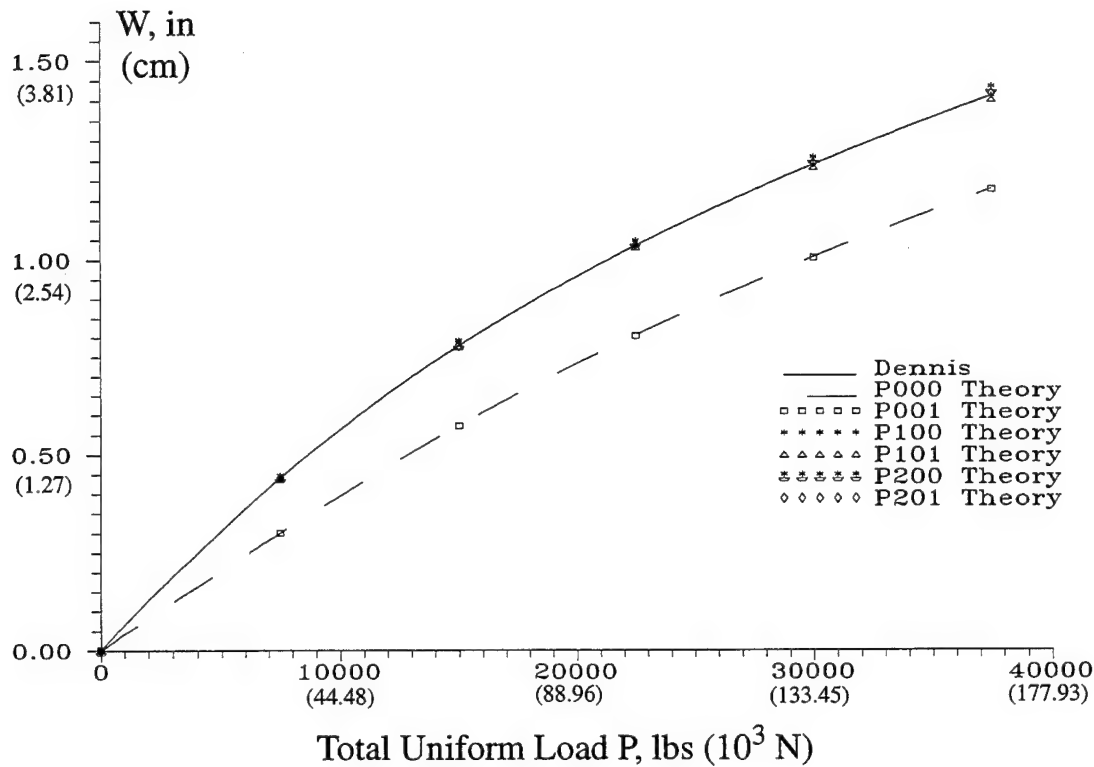


Figure 5.2 Comparison of Flat Plate Displacement Results for Variations of Geometric Nonlinearity

5.2 Simply Supported, Isotropic Deep Arches

Deep circular arches can be used to demonstrate a theory's ability to predict large displacements and rotations. Many variations of transversely-loaded deep arch problems have been reported in the literature [45, 88, 202, 216]. The problem chosen here is a 254.0-cm radius isotropic arch with a 2.54-cm square cross section and an opening angle of 0.92 radians (106°). The arch configuration is shown in Figure 5.3. The geometric and material data are shown below:

$$\begin{aligned}
 s_1 &= 0 & u = w_{,1} = \psi_1 &= 0 & (\text{symmetry}) \\
 s_2 &= 0 & v = w_{,2} = \psi_2 &= 0 & (\text{symmetry}) \\
 s_1 &= \pm 1.27 \text{ cm} & & & (\text{free}) \\
 s_2 &= \pm 235.94 \text{ cm} & u = v = w = \psi_1 &= 0 & (\text{hinged}) \\
 E &= 3.103 \times 10^{10} \text{ Pa} & \theta &= 0.92 \text{ radians} \\
 \text{width} &= 2.54 \text{ cm} & R &= 254.0 \text{ cm} \\
 h &= 2.54 \text{ cm} & L &= 406.4 \text{ cm} \\
 \delta &= 101.6 \text{ cm} & \nu &= 0.0
 \end{aligned}$$

Solutions for this problem were computed using C000 - C201 codes and a 1×40 mesh of elements to represent one quadrant of the arch. Data from the various geometrical theories are shown in Table 5.3 & Table 5.4. The higher-order cubic-nonlinear theories (C200 & C201) in this case predict a more dramatic collapse of the arch than the classical Donnell or the psuedo-Donnell codes (C0XX & C1XX). Dennis explained this difference was due to the "many nonlinear in-plane displacement terms in the strain definitions that are not included in the Donnell equations" [48:260]. He reasoned that these additional terms become more important as displacements become large. A representation that measures the movement of the Cauchy stress-strain axis with respect to the 2nd Piola stress-Green strain axis should produce more flexible results. Figure 5.4 shows the load versus crown displacement predicted by the C10X theories. Figure 5.5 shows the load versus crown displacement predicted by the C100 & C20X theories. As was expected, due to the large movement and rotations near the arch crown, the inclusion of the material transformation matrices created a more flexible response for the model.

Figure 5.6 shows the two-dimensional (2D) view of the arch at four points along the load-displacement curve for the C201 analysis, as indicated in Figure 5.5. Figure 5.7 shows the rotation dof, ψ_2 , along the meridian of the arch. It is important to note that at

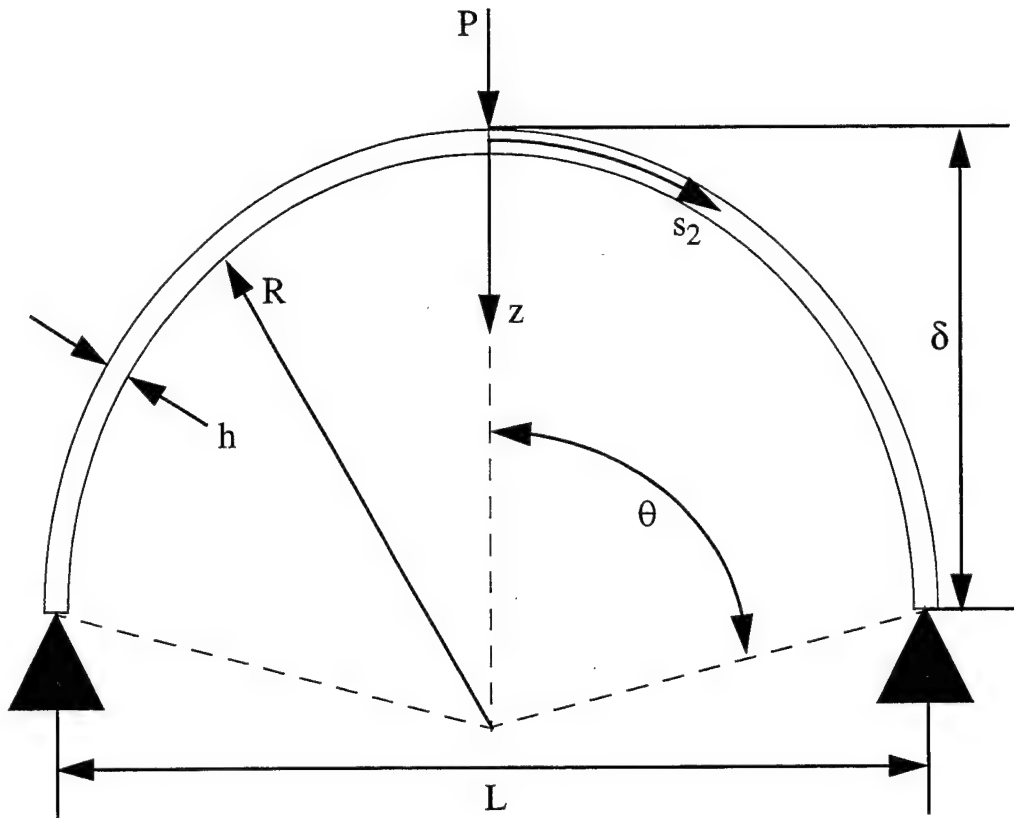


Figure 5.3 Hinged Transverse Point-Loaded Isotropic Cylindrical Arch

Table 5.3 Equilibrium Point Load ($10^3 N$) Predicted for Prescribed Transverse Displacement of Isotropic Cylindrical Arch ($w = 10.16 - 40.64 \text{ cm}$)

Disp (cm)	10.16	20.32	30.48	40.64
Donnell*	2.762	3.973	4.571	4.837
C000	2.760	3.963	4.551	4.807
C001	2.760	3.764	4.201	4.302
C100	2.749	3.954	4.453	4.800
C101	2.749	3.767	4.204	4.305
SLR*	2.832	4.034	4.479	4.441
C200	2.819	4.018	4.463	4.429
C201	2.819	3.832	4.132	3.975

* Ref [53:207]

Table 5.4 Equilibrium Point Load ($10^3 N$) Predicted for Prescribed Transverse Displacement of Isotropic Cylindrical Arch ($w = 50.8 - 71.12 \text{ cm}$)

Disp (cm)	50.8	60.96	71.12
Donnell*	4.893	4.795	4.577
C000	4.853	4.745	4.520
C001	4.199	3.963	5.630
C100	4.864	4.739	4.514
C101	4.204	3.967	3.634
SLR*	4.039	3.486	2.283
C200	4.035	3.330	2.276
C201	3.519	2.435	2.077

* Ref [49:207]

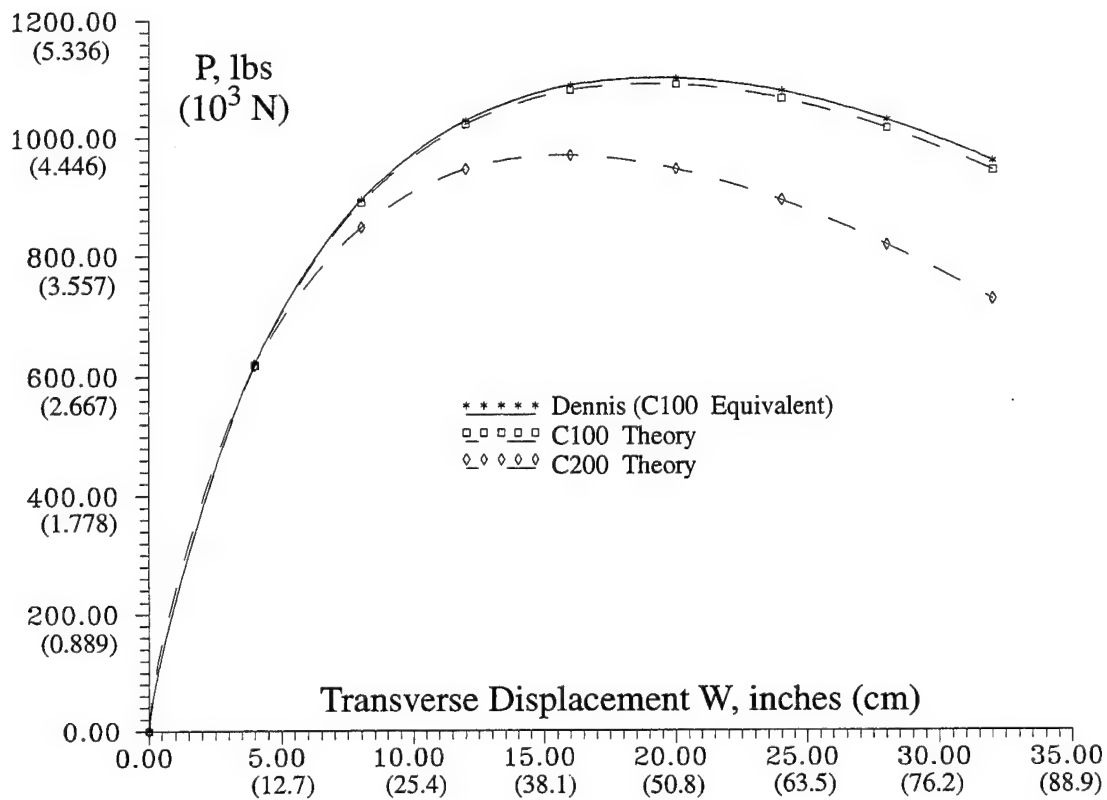


Figure 5.4 Deep Arch Crown Displacement vs Load - C10X Theory

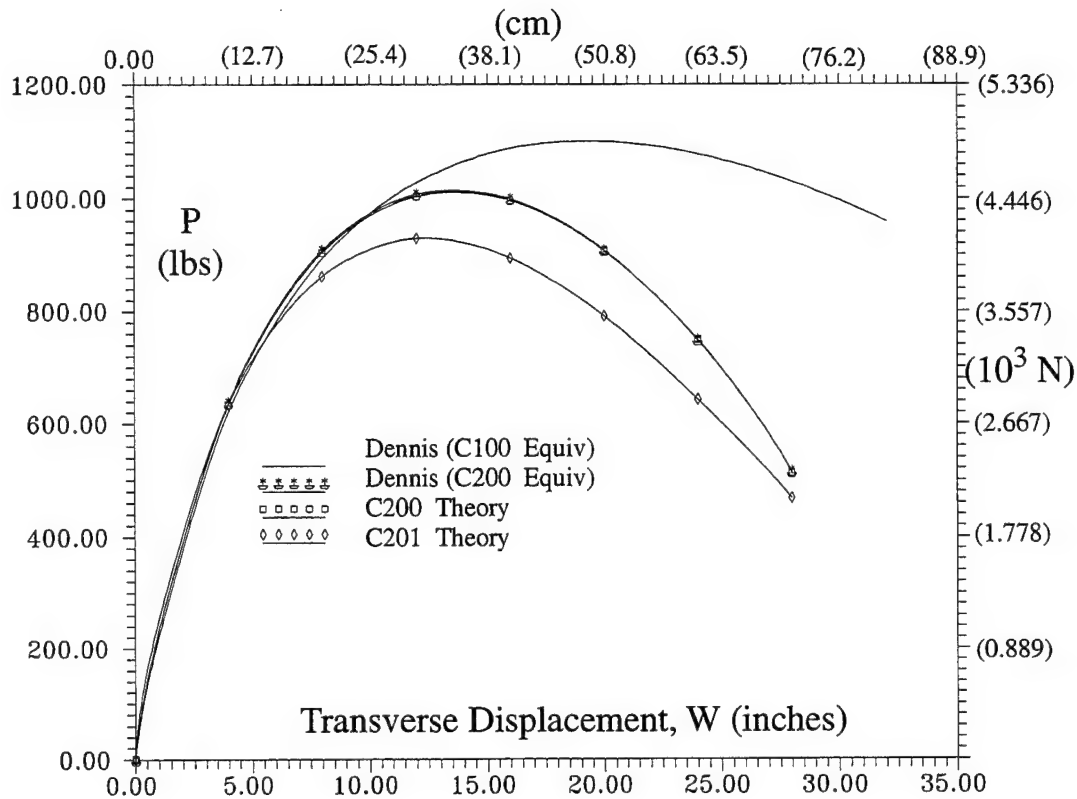
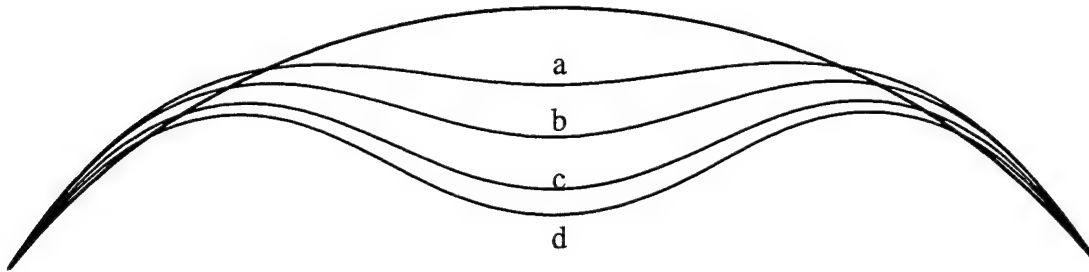


Figure 5.5 Deep Arch Crown Displacement vs Load - C100 & C20X Theory

the collapse load the crown is undergoing large displacement ($w = 30.48 - 71.12$ cm) versus the shell thickness ($h = 2.54$ cm) and moderate rotations. When the prescribed transverse displacement reaches 30.48-cm, the maximum rotation of ψ_2 reached 20.3° , and over 32% of shell surface saw rotations of 9.8° . The classical Donnell theory (C000 & C001) does not include rotations of the normal (i.e. $\psi_2 = w_{,2}$ is assumed) in the kinematics (see Appendix C, Eq (C.2)). While the modified Donnell theory does include rotations of the normal, ψ_2 , in the kinematics (see Appendix D, Eq (D.2)), it ignores most of the in-plane nonlinear strain-displacement relations (see Appendix D, Eq (D.3)). The cubic-nonlinear HTSD (C200 & C201) theory includes the cubic displacement field and all of the nonlinear strain-displacement terms for the in-plane strains (Appendix E, Eqs (E.2) & (E.3)). Thus, the cubic-nonlinear theory most accurately describes a shell behavior when it undergoes large movements and rotations. When the crown displacement reaches 50.8-cm the maximum rotation of ψ_2 reached 30.4° , and over 38% of shell surface saw rotations of 13.2° . At this point, the C201 theory is predicting an equilibrium load 12.8% less than

Dennis' SLR theory, and 28.1% less than Dennis' CDON theory. Clearly, with large movements and moderate rotations of a deep shell structure such as in this arch, the assumption of Cauchy stress-strain and 2nd Piola stress-Green strain axes being co-located is no longer valid. The inclusion of the constitutive transformation matrices causes the material properties (i.e. E , E_{ij} , ν , ν_{ij}) to become increasingly flexible (increasingly anisotropic) as displacements and rotations become relatively significant.



$$a) w = 30.48 \text{ cm}, \quad \psi_2 = 20.3^0$$

$$b) w = 60.96 \text{ cm}, \quad \psi_2 = 30.4^0$$

$$c) w = 71.12 \text{ cm}, \quad \psi_2 = 39.0^0$$

$$d) w = 81.28 \text{ cm}, \quad \psi_2 = 44.5^0$$

Figure 5.6 Two-Dimensional View of Deformation of Hinged Isotropic Deep Circular Arch at Four Specified Increments of Transverse Displacement - C201 Theory

As the prescribed crown displacement is increased to 60.96-cm, the maximum rotation of ψ_2 reached 35.1°, and over 39.2% of shell surface saw rotations of 15.0°. At this point, the C201 theory is predicting an equilibrium load 30.2% less than Dennis' SLR theory, and 49.2% less than Dennis' CDON theory. When the displacement is increased to 71.12-cm, the arch has reached a point where the center of the arch is returning to tension, and resistance begins. Hence, the change in the equilibrium curve for the C201 theory. For a prescribed convergence tolerance, ∇

$= 0.005$, the C100 and C101 theory code required 453.3 cpu and 477.8 cpu seconds, respectively. The C200 theory codes required 11,945.3 cpu seconds and the C201 theory required 12,207.6 cpu seconds.

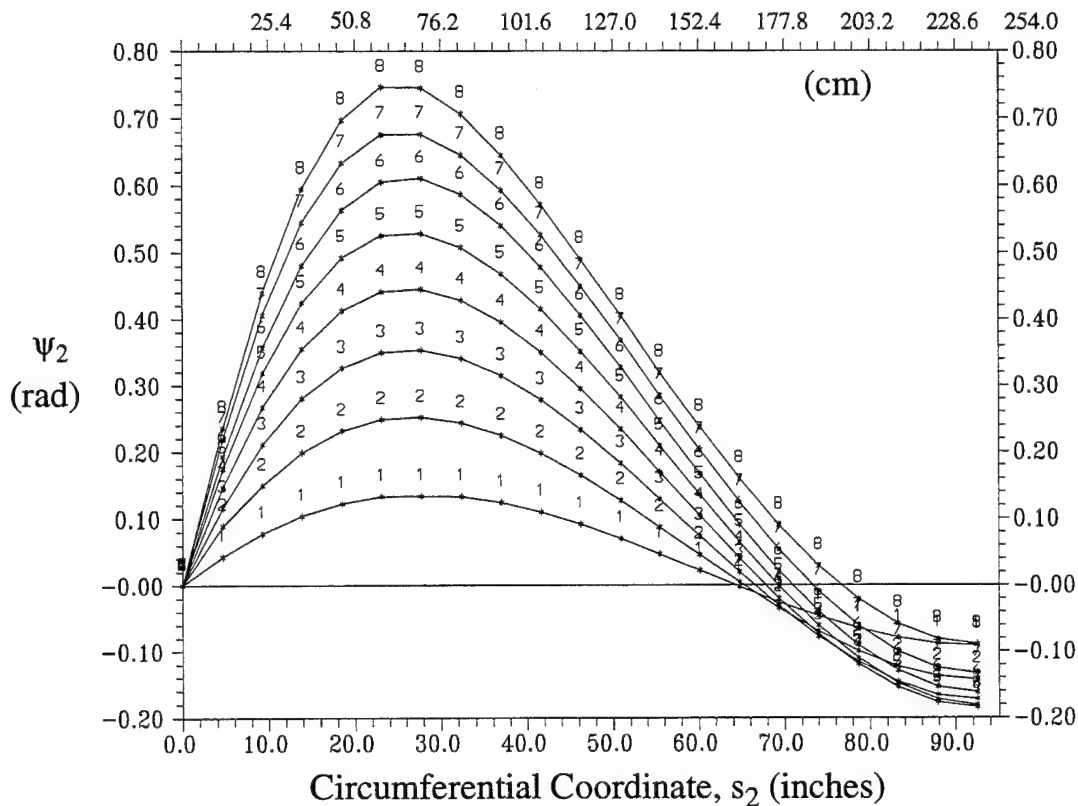


Figure 5.7 Meridian Values of ψ_2 for 8 Increment, 10.16-cm each, of Transverse Displacement of Hinged Isotropic Deep Circular Arch - C201 Theory

5.3 Hinged-Free Cylindrical Shell Panel, 0.635-cm Thick, with Transverse Point Load

The third class of problems investigated was a thin, shallow hinged-free cylindrical shell with a transverse point load. The first problem was a 0.635-cm thick shell of isotropic material. The second problem was a 0.635-cm thick shell of quasi-isotropic material. The 0.635-cm shell is shown in Figure 5.8. Geometric & material properties for the isotropic problem are given below:

$$\begin{aligned}
 s_1 = 0 \quad u = w_{,1} = \psi_1 = 0 & \quad (\text{symmetry}) \\
 s_2 = 0 \quad v = w_{,2} = \psi_2 = 0 & \quad (\text{symmetry}) \\
 s_1 = \pm 25.4 \text{ cm} & \quad (\text{free}) \\
 s_2 = \pm 25.4 \text{ cm} \quad u = v = w = \psi_1 = 0 & \quad (\text{hinged})
 \end{aligned}$$

$$\begin{aligned}
 E = 3.103 \times 10^{10} \text{ Pa} \quad \theta = 0.1 \text{ radians} \\
 h = 0.635 \text{ cm} \quad R = 254.0 \text{ cm} \\
 L = 50.8 \text{ cm} \quad \nu = 0.3
 \end{aligned}$$

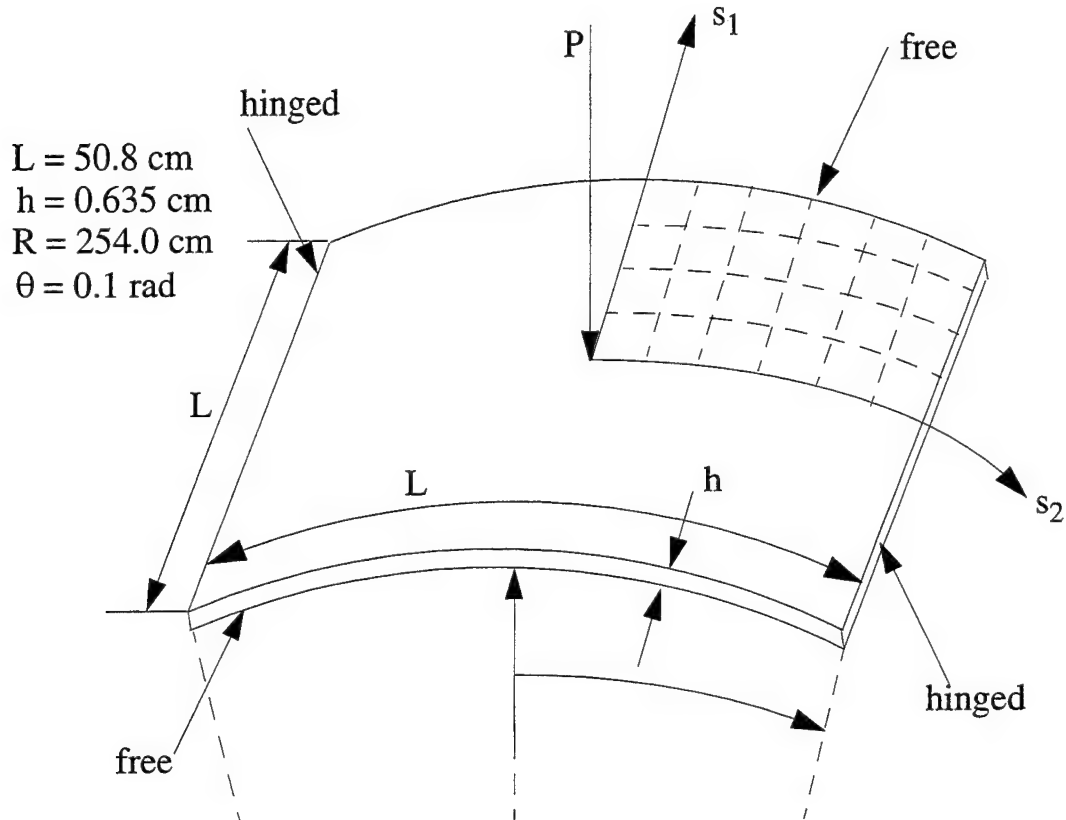


Figure 5.8 0.635-cm Hinged-Free Transversely Point-Loaded Isotropic Cylindrical Shell

Solutions were computed using a 4×6 mesh of elements to model one quadrant of the shell. Convergence studies by Dennis [48:247] showed little difference between a 4×6 and 8×8 element meshes. Significant computational savings result when the 24 element mesh is used instead of the 64 element mesh. Table 5.5 & Table 5.5 shows the results of equilibrium load predictions, for increments of transverse displacement from 0.254 to 2.54 centimeters, for the various CXXX codes. The values of load shown are four times the equilibrium load of the quarter shell. This load

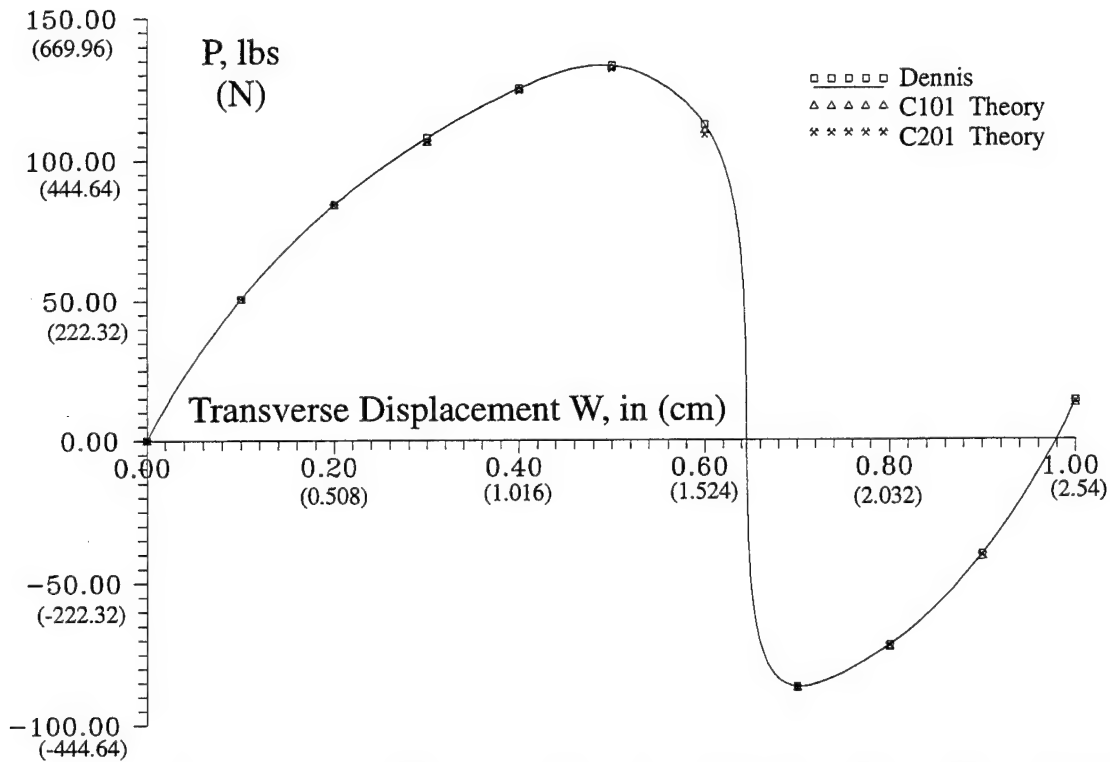
represents the total load on the entire shell panel. Values were computed using 10 increments of center point transverse displacement. One quadrant of the shell was modelled using a 24 element mesh with 4 elements in the lateral direction and 6 elements in the circumferential direction. From this table, one observes the cubic-nonlinear HTSD theory with material transformation (C201 code) provides the most flexibility. This is due primarily to the combination of higher-order nonlinear terms in the in-plane strain-displacement relations, and the transformation of the constitutive relations from Eulerian to Lagrangian coordinates. Figure 5.9 shows the equilibrium curves for the CDON, the modified Donnell (C100 & C101), and the cubic-nonlinear HTSD (C200 & C201) theories. The variance between the various theories is negligible due to the relatively small movement (maximum displacement was only four times the shell thickness) and small rotations (less than 0.15 radians (8.59°)). Figure 5.10 shows the development of the rotational dof, ψ_2 , along the shell meridian for increments of displacement.

Table 5.5 Predicted Load (N) for Prescribed Center Transverse Displacement (cm) of 0.635-cm Hinged-Free Isotropic Cylindrical Shell Panel ($w = 0.254 - 1.27$ cm)

Disp	0.254	0.508	0.762	1.016	1.270
CDON	225.0	374.4	478.9	555.8	591.3
C000	225.0	374.8	480.1	555.8	591.3
C001	225.0	374.6	478.9	555.3	590.9
C100	225.0	374.7	480.1	555.8	591.3
C101	225.0	374.5	473.1	554.4	589.6
C200	225.0	374.2	480.1	554.0	589.6
C201	225.0	374.0	474.0	552.6	586.9

Table 5.6 Predicted Load (N) for Prescribed Center Transverse Displacement (cm) of 0.635- cm Hinged-Free Isotropic Cylindrical Shell Panel ($w = 1.524 - 2.54\text{ cm}$)

Disp	1.524	1.778	2.032	2.286	2.540
CDON	494.4	-385.1	-320.1	-179.2	61.8
C000	494.4	-385.1	-320.1	-179.2	62.2
C001	493.1	-385.1	-321.0	-181.0	61.1
C100	494.4	-385.1	-319.7	-179.2	62.2
C101	491.8	-386.4	-322.3	-182.3	55.4
C200	491.8	-385.1	-317.5	-176.1	65.5
C201	488.5	-386.8	-320.1	-179.6	60.7

Figure 5.9 Equilibrium Curves for Transverse Point Loaded 0.635- cm Hinged-Free Isotropic Cylindrical Shell--CDON, C101, & C201 Theories

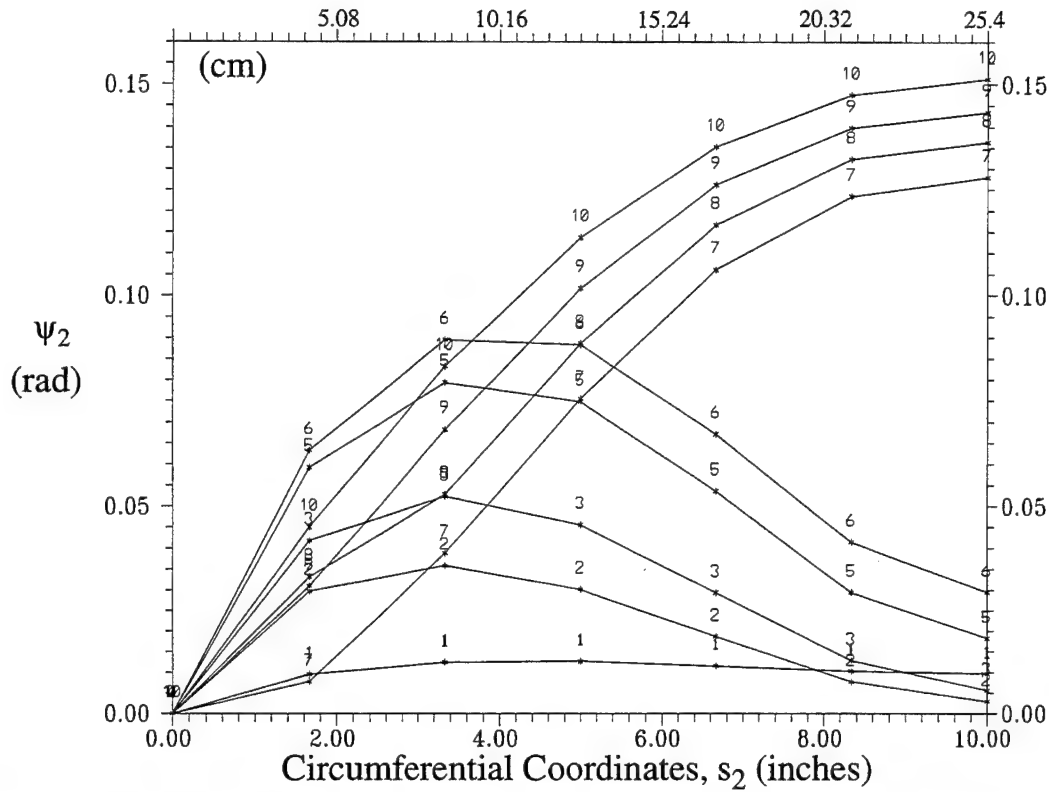


Figure 5.10 Meridian Values of ψ_2 for 10 Increments, 0.254-cm each, of Transverse Displacement of 0.0635-cm Hinged-Free Isotropic Cylindrical Shell - C201 Theory

For a prescribed convergence tolerance, $\nabla = 0.1$ the C100 and C101 theory code required 497.2 cpu and 523.1 cpu seconds, respectively. The C200 theory codes required 2657.9 cpu seconds and the C201 theory required 2801.1 cpu seconds.

The second problem is a 0.635-cm thick cylindrical shell of quasi-isotropic material (see Figure 5.11). This problem was chosen to determine the effect of including the material transformation matrices when analyzing shallow quasi-isotropic shells. Geometric and material properties for the quasi-isotropic problem are given below:

$$\begin{aligned}
 s_1 &= 0 & u &= w_{,1} = \psi_1 = 0 & (\text{symmetry}) \\
 s_2 &= 0 & v &= w_{,2} = \psi_2 = 0 & (\text{symmetry}) \\
 s_1 &= \pm 25.4 \text{ cm} & & & (\text{free}) \\
 s_2 &= \pm 25.4 \text{ cm} & u &= v = w = \psi_1 = 0 & (\text{hinged})
 \end{aligned}$$

$$\begin{aligned}
 E_1 &= 14.109 \times 10^{10} \text{ Pa} & E_2 &= 9.243 \times 10^9 \text{ Pa} \\
 G_{12} &= G_{13} = 5.957 \times 10^9 \text{ Pa} & G_{23} &= 2.965 \times 10^9 \text{ Pa} \\
 \nu_{12} &= 0.313 & \theta &= 0.1 \text{ radians} \\
 h &= 0.635 \text{ cm} & R &= 254.0 \text{ cm} \\
 L &= 50.8 \text{ cm} & \text{Ply Layup} &= [0/-45/45/90]_s
 \end{aligned}$$

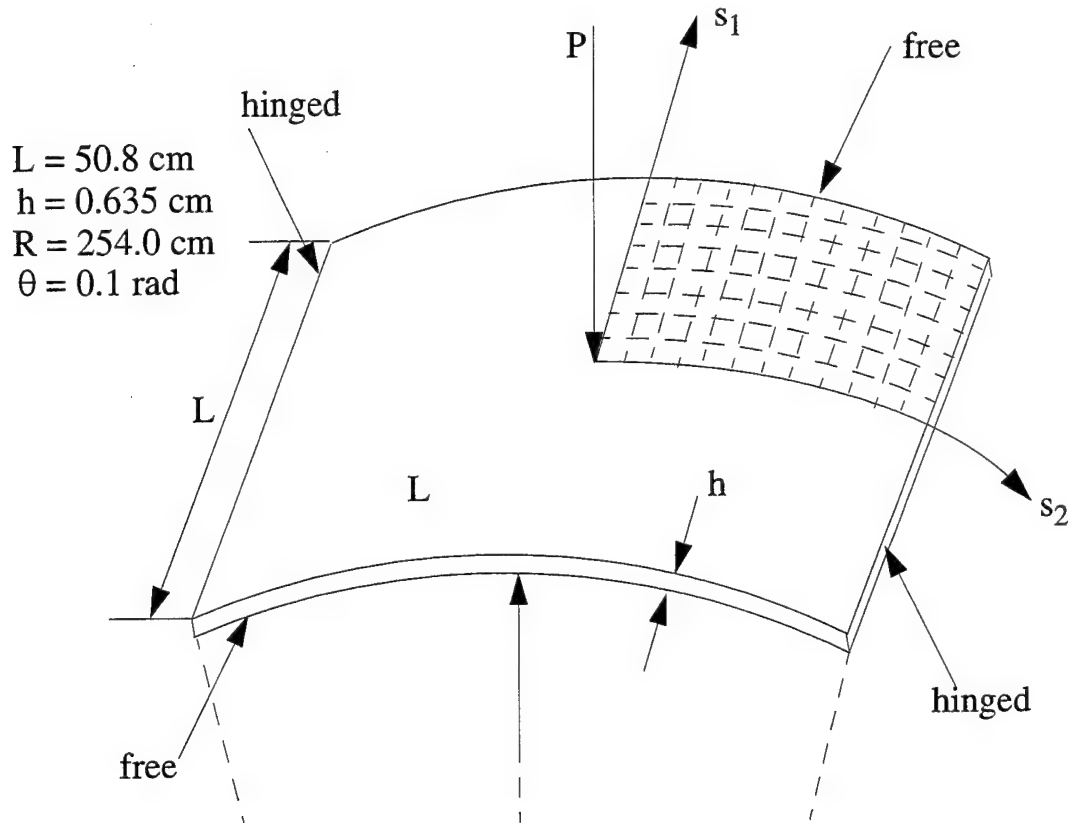


Figure 5.11 0.635-cm Hinged Free Transversely Point-Loaded Quasi-isotropic Cylindrical Shell

Solutions were computed using a 8×12 mesh of elements to model one quadrant of the shell. This mesh was used by Tsai and Palazotto [226] to model a deep clamped-free quasi-isotropic shell. Palazotto and others [161, 163, 225, 226] investigated shells of this configuration and compared static and dynamic results for different material properties and ply lay-ups. Their work is based on a 96 element model of a quadrant of the shell. This mesh was chosen based on the results of their convergence studies summarized in Table 5.7. Tsai and Palazotto concluded that the 8×12 mesh results were acceptable considering the CPU consumption was about 70% less

than the 11×16 mesh [226:69]. Another recent study by Silva, however, revealed that the quasi-isotropic panel with transverse load does not deform in a symmetric manner [206:3-6]. According to Smith [209:Chap 6:1-4], there is negligible difference between the transverse load versus displacement curves for the full shell 16×24 mesh and the quarter shell 8×12 mesh. Since this research is primarily concerned with load-displacement behavior, and due to this being a shallow shell problem, i.e. $\delta/h < 1$, a quarter shell mesh was chosen for the analysis.

Table 5.7 Convergence Study for Quasi-Isotropic Shell Panel

Mesh	Load at Onset of Instability (N)
4×6	515.8
8×12	249.0
11×16	235.7

[226:69]

Transverse load values versus prescribed increments of displacement were computed for a $[0/-45/45/90]_s$ ply layup, using the modified Donnell (C100 & C101) and the cubic-nonlinear HTSD (C200 & C201) theories. Table 5.8 shows values of the transverse load predicted by the various theories. The C201 HTSD theory predicted the most flexible results, due to incorporating the higher-order nonlinear terms for the in-plane strain-displacement relations and the material transformation matrices. Figure 5.12 shows the equilibrium curves of load versus transverse displacement for the modified Donnell (C100 & C101) and the quasi-nonlinear HTSD (C200 & C201) theories. As expected, the C201 theory yields the greatest flexible response.

Figure 5.13 shows the development of the rotational dof, ψ_2 , along the shell's s_2 -axis for increments of displacement. As in the previous problem, the displacements and rotations are small (maximum transverse displacement was only four times the shell thickness and the rotations were less than 0.17 radians (9.74°)). These results imply that transforming the constitutive relations from Eulerian to Lagrangian coordinates make negligible contributions to the equilibrium

analysis. For a prescribed convergence tolerance, $\nabla = 0.1$, along with 10 increments of center point transverse displacement, the C100 and C101 theory code required 207.2 CPU and 233.3 CPU seconds, respectively. The C200 theory codes required 431.4 CPU seconds and the C201 theory required 498.3 CPU seconds. Thus, one can conclude the C100 theory is the most cost efficient, in terms of CPU usage, for this problem of a shallow shell.

Table 5.8 Transverse Center Point Load ($10^3 N$) Predicted for Prescribed Transverse Displacement of a 0.635-cm Hinged-Free Quasi-Isotropic Cylindrical Shell Panel

Disp	C100	C101	C200	C201
0.254	2.680	2.679	2.679	2.679
0.508	4.207	4.204	4.204	4.217
0.762	5.101	5.091	5.091	5.083
1.016	5.230	5.205	5.205	5.190
1.270	4.254	4.204	4.204	4.183
1.524	2.500	2.436	2.436	2.417
1.778	0.116	0.059	0.059	0.052
2.032	-4.218	-4.042	-4.042	-4.108
2.226	-2.710	-2.605	-2.605	-2.676
2.540	0.380	0.451	0.451	0.381

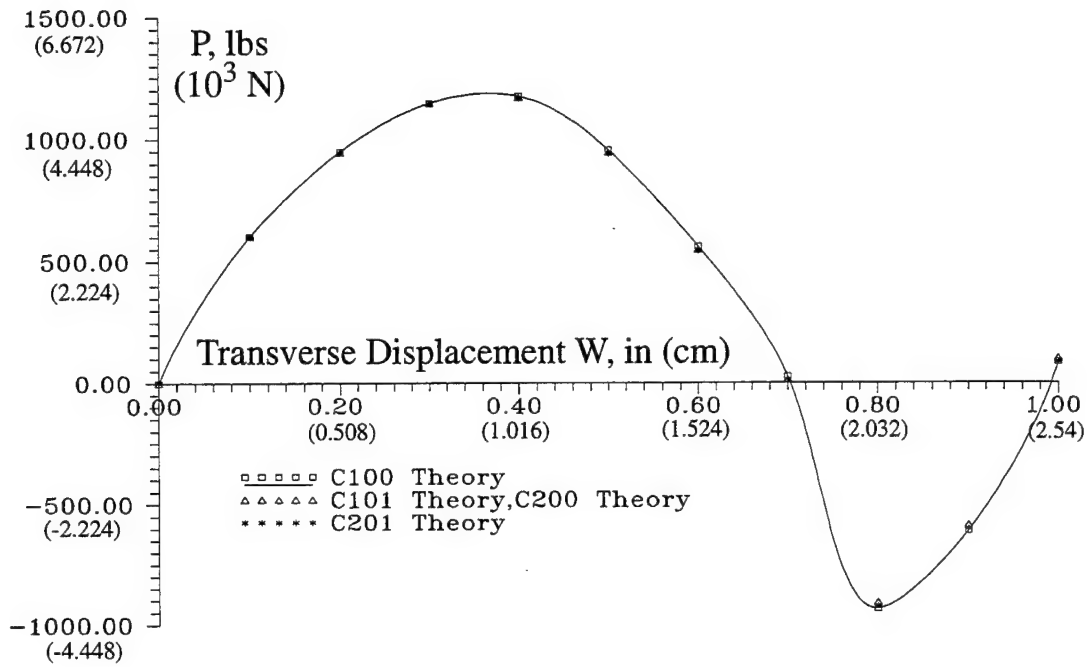


Figure 5.12 Equilibrium Curves for Transverse Point Loaded 0.635-cm Hinged-Free Isotropic Cylindrical Shell - C10X & C20X Theories

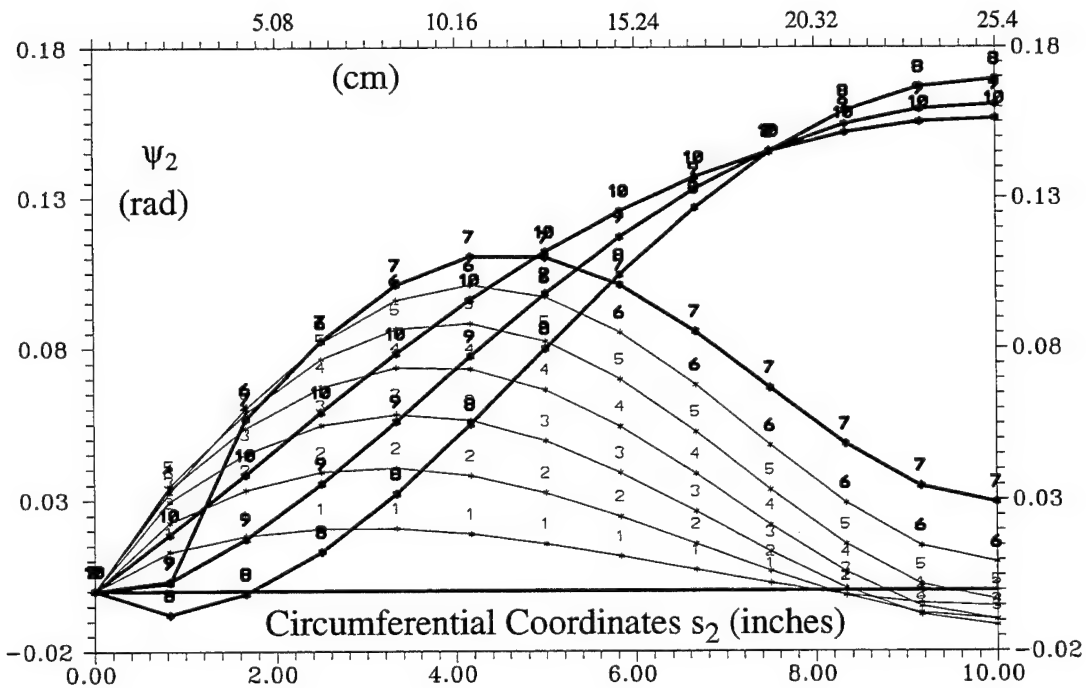


Figure 5.13 Meridian Values of ψ_2 for 10 Increments, 0.254-cm each, of Transverse Displacement of 0.635-cm Quasi-Isotropic Hinged-Free Cylindrical Shell - C201 Theory

5.4 Clamped-Free Quasi-Isotropic Cylindrical Shell Panel with Transverse Point Load

The second deep shell problem, after the isotropic cylindrical arch, was a deep composite shell panel with transverse point load. This problem demonstrates a severe test of an HTSD theory due to the shell's depth, thickness, and quasi-isotropic properties. A deep 30.48-cm radius quasi-isotropic 27.94-cm \times 30.48-cm cylindrical panel was clamped on its lateral boundaries and free on the circumferential boundaries. The shell configuration is shown in Figure 5.14. Geometric and material properties are listed below. A transverse point load was applied at the center of the 0.102-cm thick panel until the panel center displaced over 5.72-cm. This distance is significantly greater than the 4.83-cm depth of the shell. Results for the transversely-loaded panel are compared with the computational results of Tsai [225]. The material properties and geometry are listed below:

$$s_1 = \pm 13.97 \text{ cm} \quad (\text{free})$$

$$s_2 = \pm 15.24 \text{ cm} \quad u = v = w = w_{,1} = w_{,2} = \psi_1 = \psi_2 = 0 \quad (\text{hinged})$$

Material AS4-3501 Graphite Epoxy

$$E_1 = 14.11 \times 10^{10} \text{ Pa} \quad E_2 = 9.243 \times 10^9 \text{ Pa}$$

$$G_{12} = G_{13} = 5.955 \times 10^9 \text{ Pa} \quad G_{23} = 2.965 \times 10^9 \text{ Pa}$$

$$\nu_{12} = 0.313 \quad \theta = 1.0 \text{ radians}$$

$$h = 0.102 \text{ cm} \quad R = 30.48 \text{ cm}$$

$$A = 27.94 \text{ cm} \quad B = 30.48 \text{ cm}$$

$$\delta = 4.83 \text{ cm} \quad \text{Ply Layups } [0/-45/45/90]_s, [0_2/90_2]_s, [0_8], [90_8]$$

As mentioned previously, Smith [209] determined that the load versus transverse displacement curves for a quarter shell mesh and a full shell mesh were negligibly different. However, he did show the transverse displacement along the circumferential coordinate (s_2) did vary significantly between the quarter shell mesh and the full shell mesh. Since the author is primarily concerned with shell response, and with the constitutive relations transformed to Lagrangian coordinates for this deep shell, a quarter mesh (8×12) instead of a full mesh (16×24) is not

used. Transverse load values versus displacement of the center of the shell were computed for $[0/-45/45/90]_s$, $[0_2/90_2]_s$, $[0_8]$, and $[90_8]$ ply layups. The cubic-nonlinear HTSD (C200 & C201) theories were considered. Table 5.8 shows values of transverse load predicted by the various theories for the $[0/-45/45/90]_s$ ply layup.

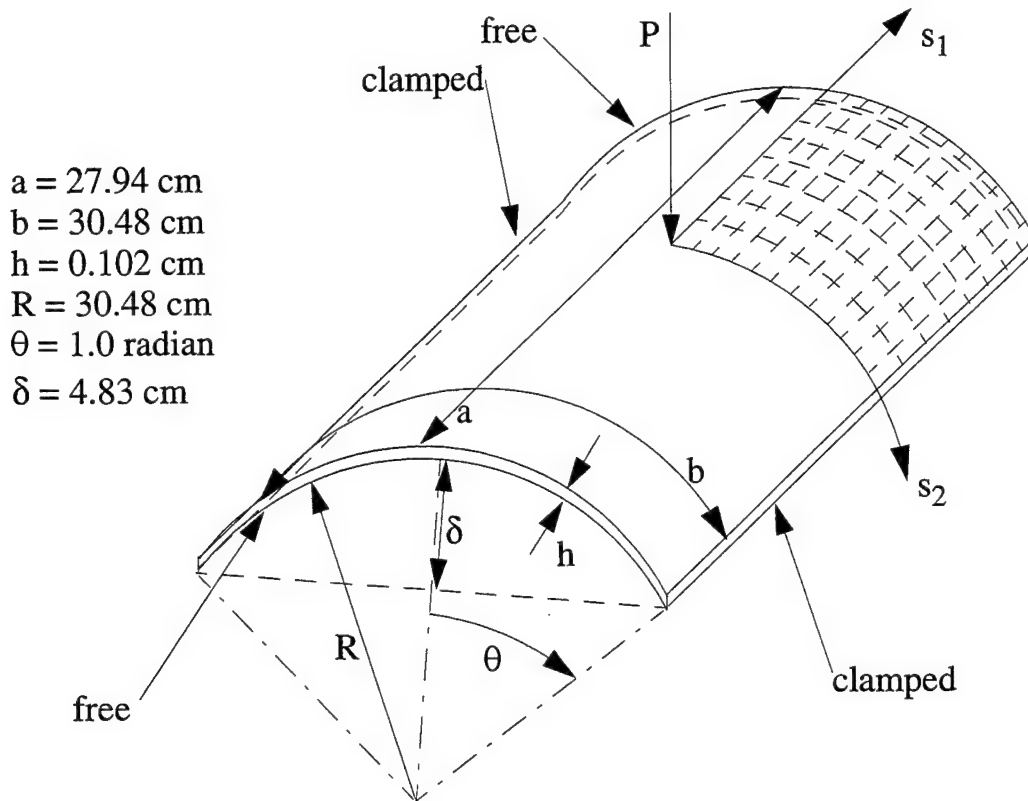


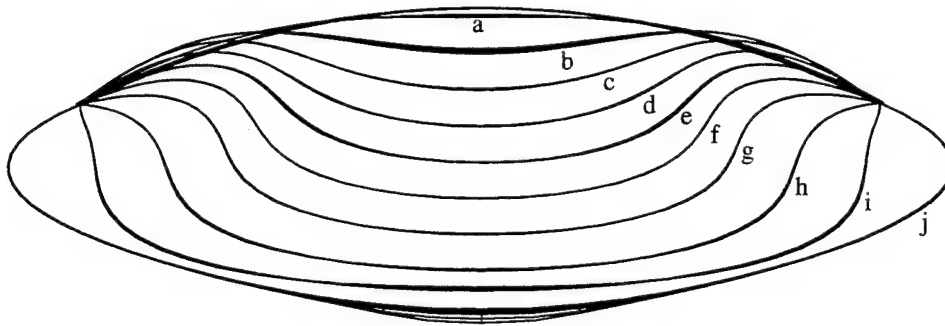
Figure 5.14 Clamped-Free Composite Shell with Transverse Point Load

Figure 5.15 shows a 2D view of the cylindrical shell for several prescribed transverse displacements for the $[0/-45/45/90]_s$ ply layup. As the shell displaces from $w = 1.191\text{-cm}$ to $w = 1.667\text{-cm}$, the deflection about the central point load has reached the lateral edges ($s_1 = \pm A/2$). This is usually indicated in the equilibrium load-displacement curve with the onset of the "snap-through" phase exhibited by these shells. As the displacement is increased to $w = 5.954\text{-cm}$, the shell is "softening" or usually requires smaller loads to increase deflection. However, as displacement continues through $w = 6.906\text{-cm}$ to $w = 7.384\text{-cm}$, the outer circumferential edges ($s_2 = \pm B/2$) have finished the "snap-through" process and the shell is entering a tensile state. This requires

more energy (or load) to increase deflection and is usually represented by an increase in the equilibrium load-displacement curve. Figures 5.16 & 5.17 shows a three-dimensional (3D) view of the shell as it begins the "snap-through" and finishes in a tensile loading state. In Figure 5.16, the 3D views of the shell clearly show the development of the central deflection that leads to the onset of "snap-through". At this point on the load-displacement path ($w = 1.429\text{-cm}$), the maximum rotation of ψ_2 reaches 0.15 radians (8.59°), and over 15% of the shell surface saw rotations of 0.10 radians (5.73°). Figure 5.17 shows the continued 3D shell deformation until the entire shell enters a tensile state (when $w = 6.906\text{-cm}$) At this point, the maximum rotation of ψ_2 reaches 0.57 radians (32.66°), and over 53% of the shell surface saw rotations of 0.26 radians (14.9°). Figure 5.18 shows the equilibrium values of a transverse center point load of the modified Donnell (C100 & C101) theories and the cubic-nonlinear HTSD (C200 & C201) theories for the $[0/-45/45/90]_s$ ply layup. The cubic-nonlinear HTSD theory with material transformations predicted the most flexible shell structure. Figure 5.19 shows the development of the rotational dof, ψ_2 along the shell meridian for prescribed increments of displacement. As in the isotropic arch problem, as displacements and rotations become significantly large, the constitutive transformation matrices reflect the increased flexibility in the material properties with respect to the undeformed axis system.

Figures 5.20, 5.22, and 5.24 show the equilibrium load vs transverse displacement values at the center point of the cubic-nonlinear (C200 & C201) theories for the $[0_8]$, $[0_2/90_2]_s$, $[90_8]$ ply lay-ups respectively. Figures 5.21, 5.23, and 5.25 show the equilibrium load vs transverse displacement values at the center point of the cubic-nonlinear (C200 & C201) theories for the $[0_8]$, $[0_2/90_2]_s$, $[90_8]$ ply lay-ups respectively. It should be noted that the constitutive transformation matrices of Eqs (4.74) and (4.75) reflect greater flexibility at the onset of snapping and during the snap-through phase. In particular, the χ_i terms of Eqs (4.64a)-(4.64i) become significantly greater than unity. These transformation matrices tend to "soften" the shells' response. This is accomplished by the constitutive transformation matrices smoothing the transition of the shells' response from bending to tension in the snap-through (predominantly to bending resistance) to recovery (predominantly membrane resistance). By comparing the three-dimensional shell deformations shown in Figures 5.16-5.17, along with the various equilibrium load-transverse displacement curves shown in Figures 5.18, 5.20, 5.22, and 5.24, it is possible to observe the shell(s)' change in

response to the transverse loading from purely bending (up to the snapping load), to a combination of bending and tension as the shell begins to unload (snap-through phase), to a pure tensile response (recovery phase).



a) $w = 0.239$ cm
b) $w = 1.191$ cm
c) $w = 2.144$ cm
d) $w = 3.096$ cm
e) $w = 4.049$ cm

f) $w = 5.001$ cm
g) $w = 5.594$ cm
h) $w = 6.906$ cm
i) $w = 7.381$ cm
j) $w = 7.859$ cm

Figure 5.15 Two-Dimensional (2D) Profiles of Clamped-Free Laminated Composite Cylindrical Shells at Various Prescribed Transverse Displacements

Table 5.9 Center Point Load (N) Predicted for Prescribed Transverse Displacement (cm) of a 0.102- cm , Clamped-Free, Quasi-Isotropic, Cylindrical Shell Panel, $[0/-45/45/90]_5$

Disp	CDON*	C100	C101	C200	C201
0.4763	116.3	116.3	115.5	116.6	115.9
0.9525	239.2	238.8	237.0	237.7	236.2
1.4288	225.7	225.3	216.5	216.6	208.5
1.9050	205.2	205.1	194.8	187.5	177.5
2.3813	181.5	181.5	169.7	154.6	144.8
2.8575	154.0	154.1	137.6	117.7	99.0
3.3338	125.5	125.4	113.8	93.5	80.5
3.8100	98.3	98.3	92.1	79.1	67.7
4.2863	76.0	75.9	59.1	54.4	52.9
4.7625	62.8	62.8	53.7	52.0	48.0
5.2358	67.5	67.5	60.5	54.9	53.4
2.2500	110.8	110.5	92.5	84.1	74.7

* Computed using Dennis' [48] modified Donnell theory code.

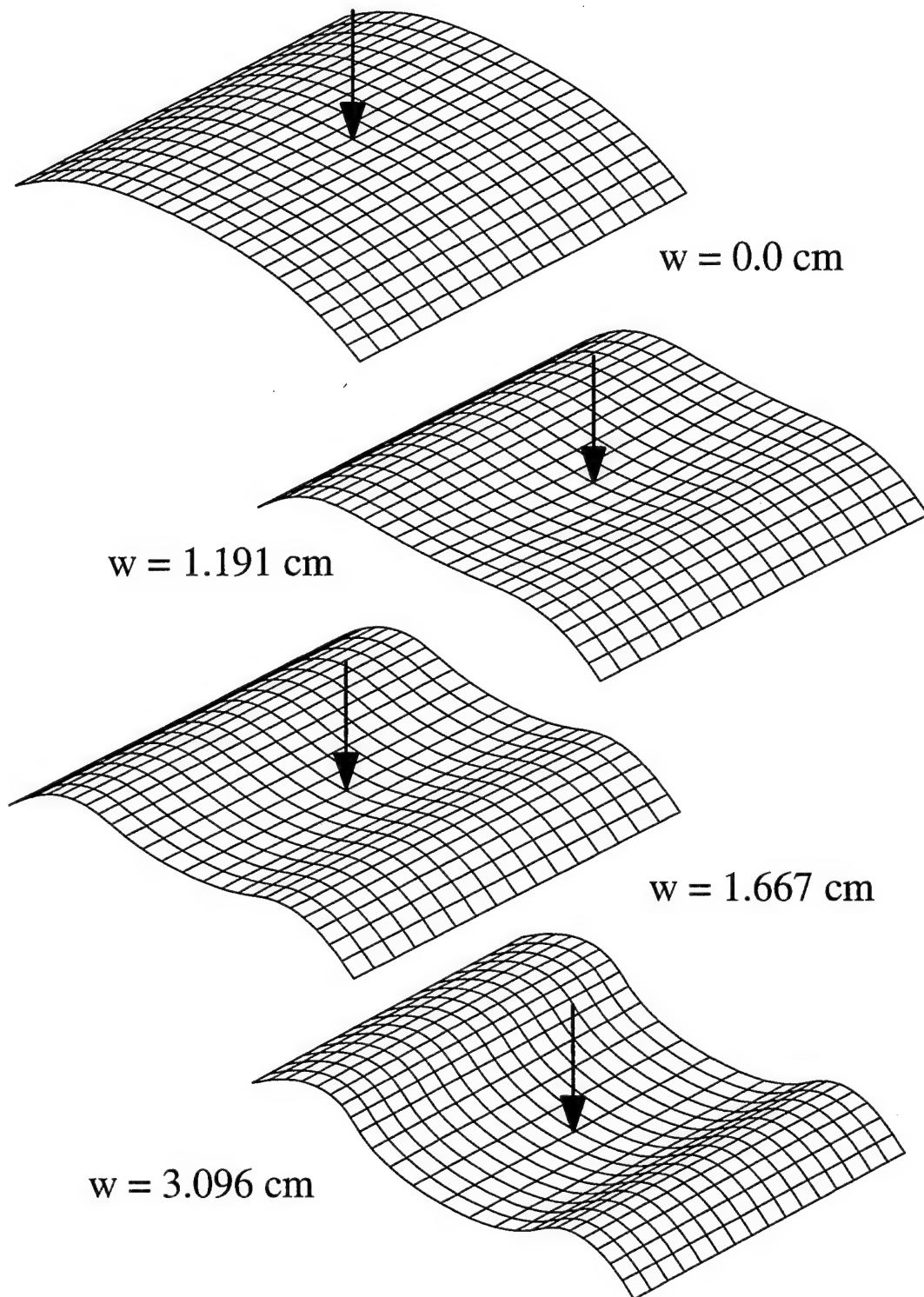
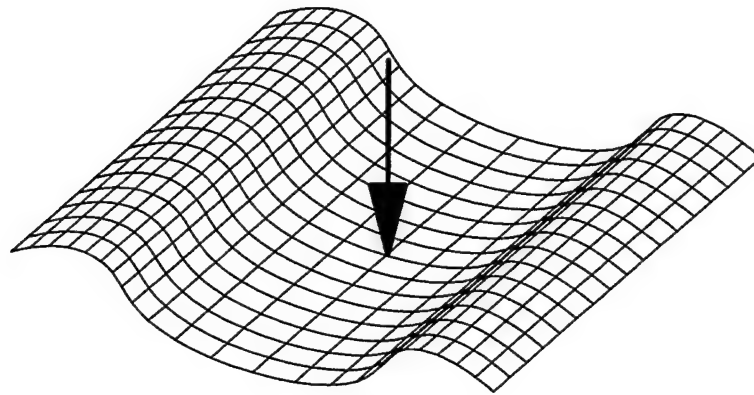
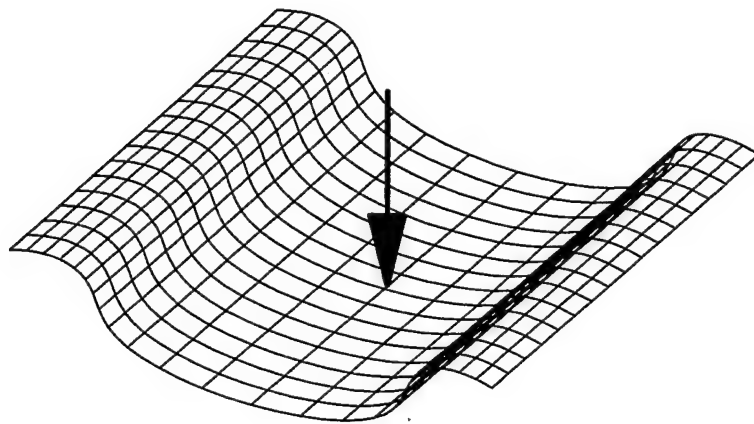


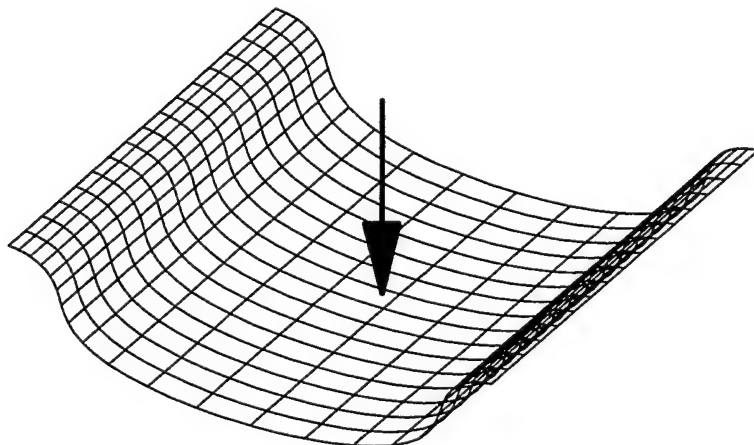
Figure 5.16 Three-Dimensional Views of 0.102-cm Clamped-Free Quasi-Isotropic Cylindrical Shell at Specified Transverse Displacements - C201 Theory



$w = 4.286 \text{ cm}$



$w = 5.953 \text{ cm}$



$w = 6.906 \text{ cm}$

Figure 5.17 Three-Dimensional Views of 0.102-cm Clamped-Free Quasi-Isotropic Cylindrical Shell at Specified Transverse Displacements - C201 Theory

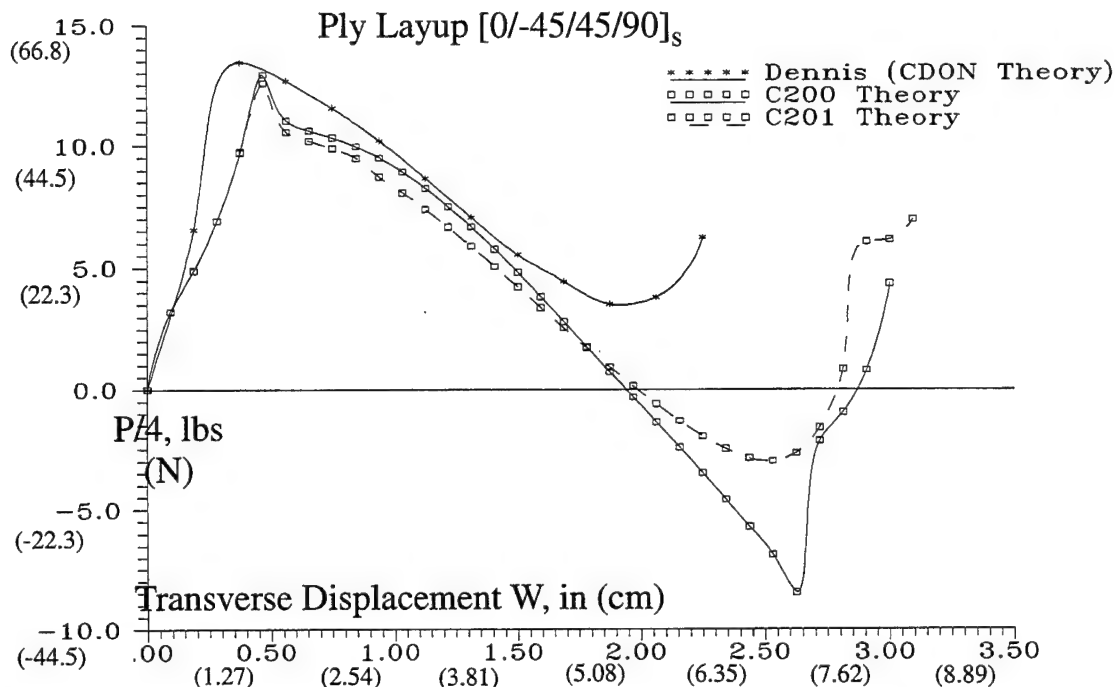


Figure 5.18 Equilibrium Path Comparisons for Transverse Center Point Loaded 0.102-cm Clamped-Free Quasi-Isotropic $[0/-45/45/90]_s$ Cylindrical Shell - CDON, C200 & C201 Theories

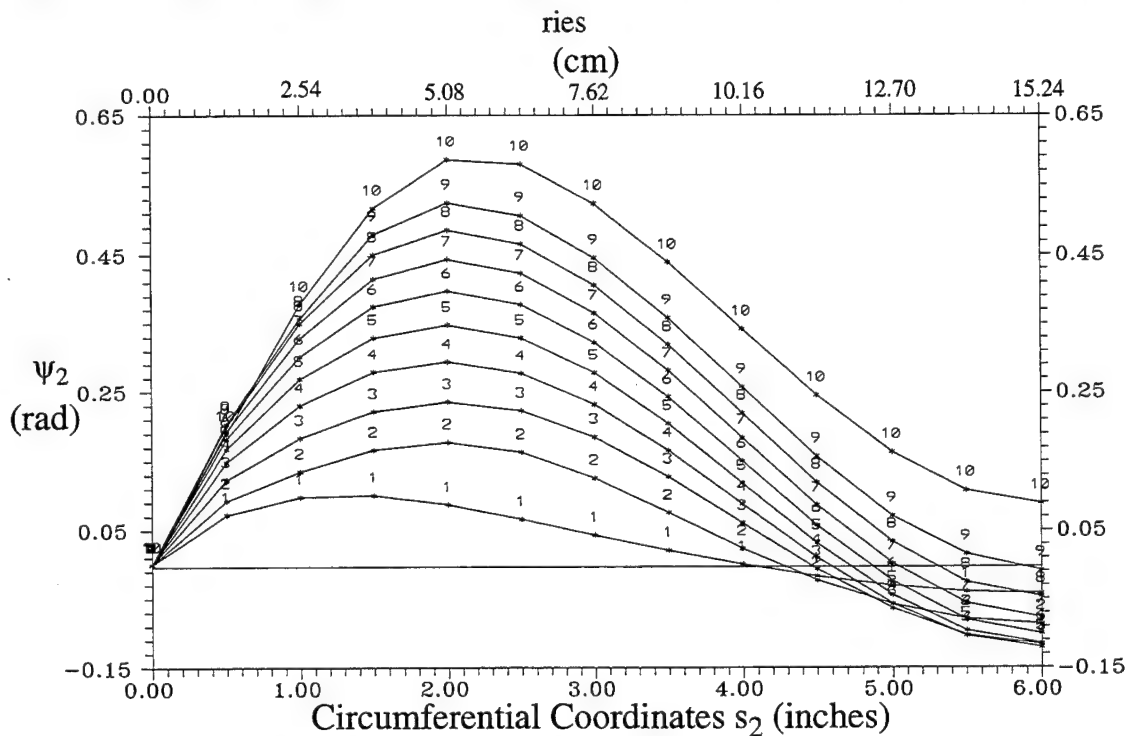


Figure 5.19 Meridian Values of ψ_2 for 10 Increments, 0.476-cm each, of Transverse Displacement of 0.102-cm Hinged-Free Quasi-Isotropic $[0/-45/45/90]_s$ Cylindrical Shell - C201 Theory

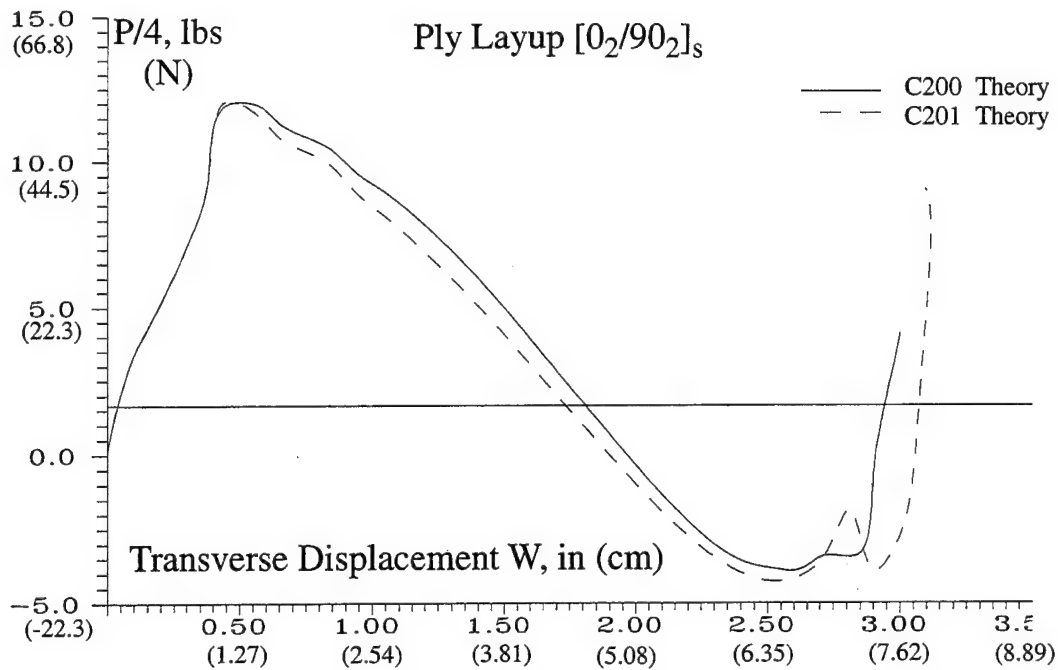


Figure 5.20 Equilibrium Path Comparisons for Transverse Center Point Loaded 0.102cm Clamped-Free Quasi-Isotropic ($[0_2/90_2]_s$) Cylindrical Shell - C201 Theory

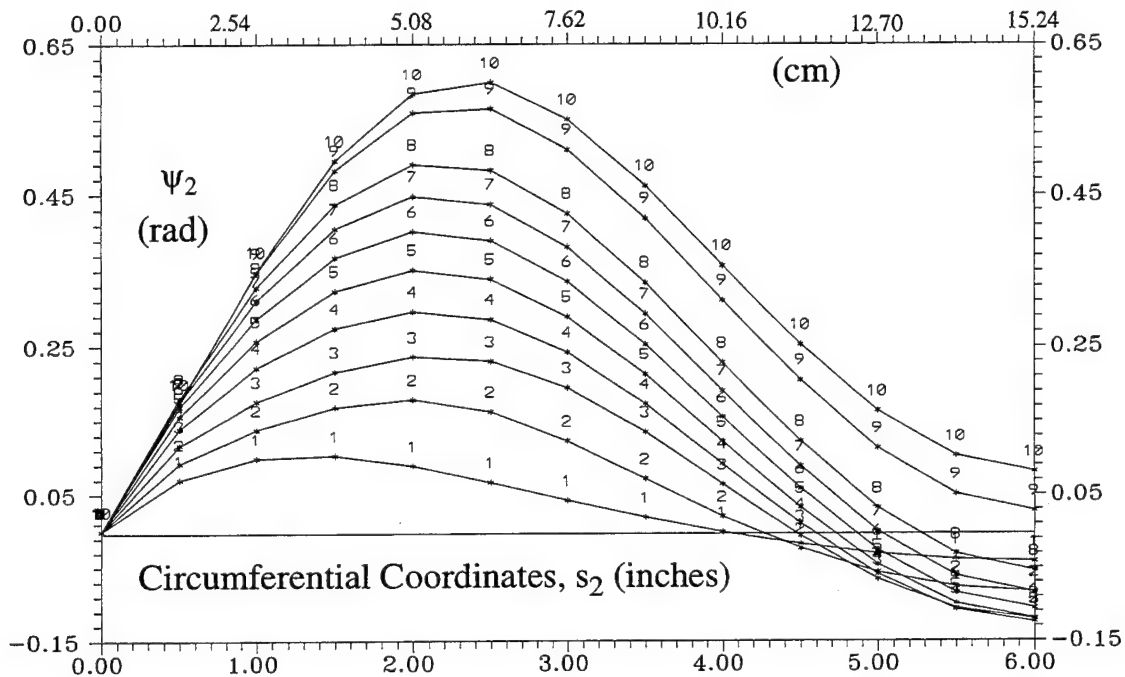


Figure 5.21 Meridian Values of ψ_2 for 10 Increments, 0.476-cm each, of Transverse Displacement of 0.102-cm Hinged-Free Quasi-Isotropic ($[0_2/90_2]_s$) Cylindrical Shell- C201 Theory

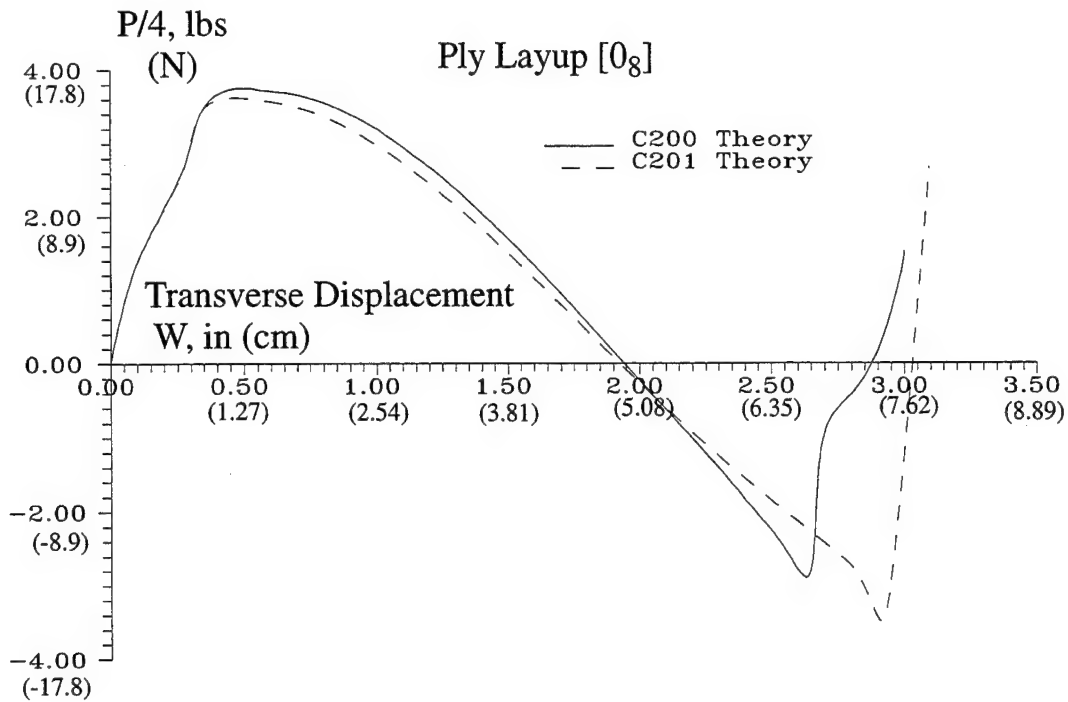


Figure 5.22 Equilibrium Path Comparisons for Transverse Center Point Loaded 0.102-cm Clamped-Free Quasi-Isotropic ($[0_8]$) Cylindrical Shell - C201 Theory

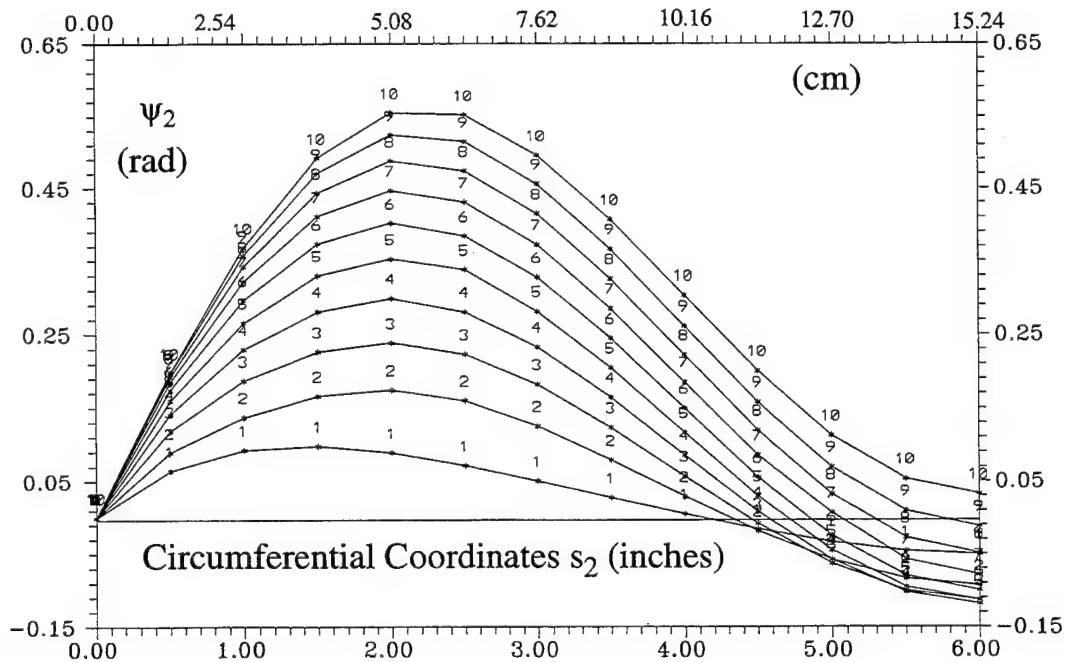


Figure 5.23 Meridian Values of ψ_2 for 10 Increments, 0.476-cm each, of Transverse Displacement of 0.102-cm Clamped-Free Quasi-Isotropic ($[0_8]$) Cylindrical Shell - C201 Theory

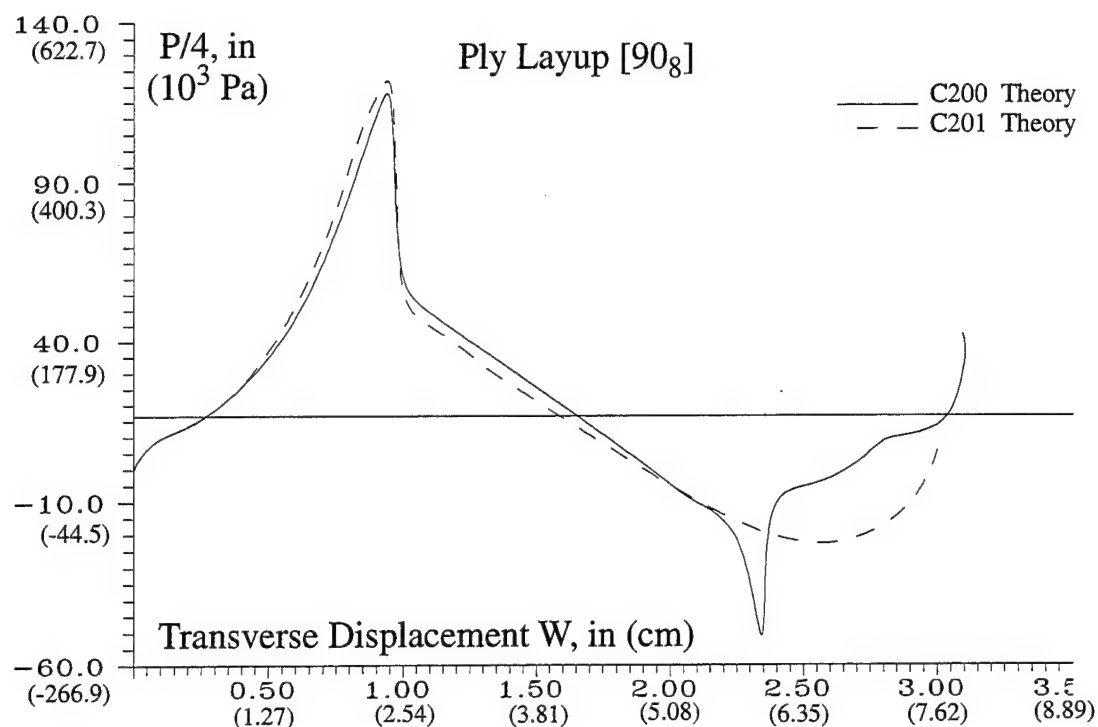


Figure 5.24 Equilibrium Path Comparisons for Transverse Center Point Loaded 0.102-cm Clamped-Free Quasi-Isotropic ($[90_8]$) Cylindrical Shell - C201 Theory

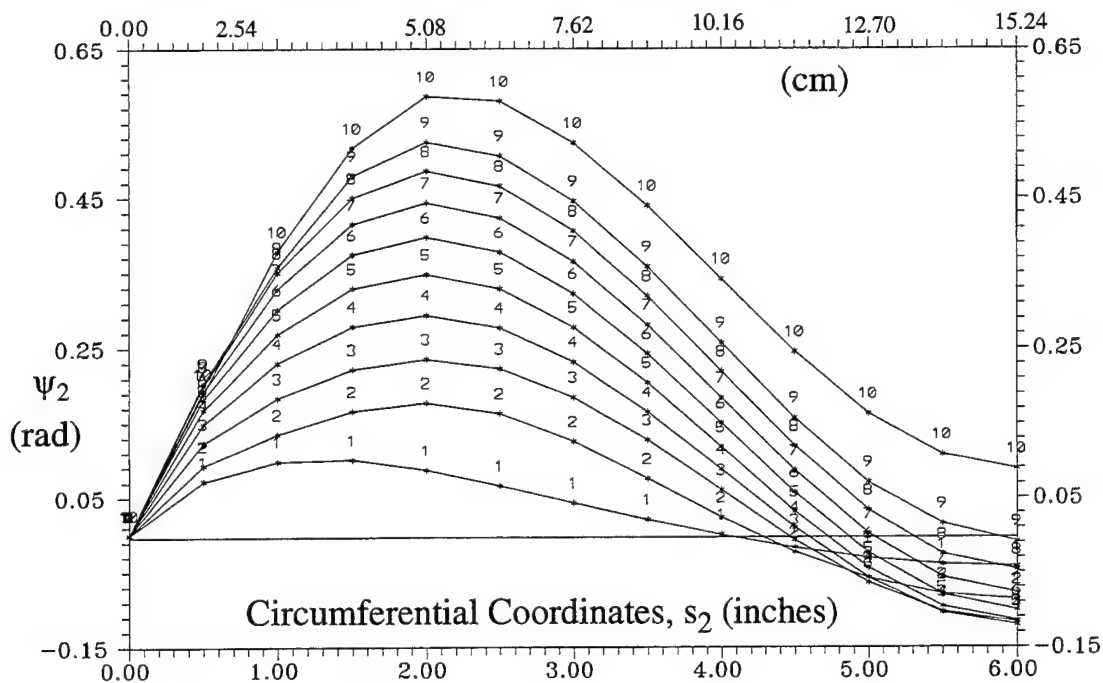


Figure 5.25 Meridian Values of ψ_2 for 10 Increments, 0.476-cm each, of Transverse Displacement of 0.102-cm Clamped-Free Quasi-Isotropic ($[90_8]$) Cylindrical Shell - C201 Theory

Observing the quasi-isotropic, $[0/-45/45/90]_s$, shell's equilibrium response shown in Figure 5.18, yields the conclusion that the material transformation matrices shown in Eqs (4.74)-(4.75) enhance the anisotropy of the laminate. This enhancement is the "softening", or the increase in flexibility, the shell exhibits once the displacements ($w \geq 5h$) and/or rotations ($\psi_i \geq 15^\circ$) become significant. As the shell approaches a purely tensile response to the transverse loading (when w approaches 2.3in) for the C200 theory, the shell snaps into a purely concave position (see Figure 5.17, middle display) with significant inflection points near the clamped boundary conditions. Due to the sharp inflection points in the curvature being near these boundaries, the shell exhibits an initially sharp transition to a membrane (tensile) loading response. As the displacement is increased, the shell then gradually transitions through the inflection points until the entire shell is in tension (recovery phase). The C201 theory, with the $[T_1]$ and $[T_2]$ arrays, softens the transition of these inflection points from the bending-tensile loading to the pure tensile loading phase. Thus, the sharp transition point at the bottom of the equilibrium curve is removed. This is observed similarly for the $[90_8]$ panel, but not for the $[0_8]$ or for the $[0_2/90_2]_s$ panels. The fiber orientation of the $[90_8]$ panel is in the circumferential direction resists the snapping phenomena, whereas the stiffness of the $[0_8]$ panel is in the longitudinal direction and therefore does nothing to inhibit the snapping process. The tensile recovery phase observed for the $[0_8]$ panel is immediate with no gradual recovery as observed in the $[90_8]$ panel.

The $[0_2/90_2]_s$ panel is mixture of the other two and this exhibited by the C20X analysis. The equilibrium path at the onset of tensile recovery oscillates, partly in due to the 0° and 90° fibers conflicting in the shell's response to the added displacement. Notice in Figure 5.21 the change in ψ_2 from the eight to the ninth displacement increment. The magnitude of change is significant when compared to the previous displacement increments. It appears the panel is beginning to respond as the $[0/-45/45/90]_s$ or the $[90_8]$ but is inhibited by the presence of the 0° fibers. Thus, the panels equilibrium is adjusted for the movement of both 0° and 90° fibers within the shell's thickness.

For a prescribed convergence tolerance, $\nabla = 0.001$, along with 25 prescribed center transverse displacement increments of 0.2382-cm, the C100 and C101 theory code required 8424 CPU and 9723 CPU seconds, respectively. The C200 theory codes required 65472 CPU seconds and the C201 theory required 70356 CPU seconds. A comparison of these results with the C211 theory will be accomplished in Section 6.6.

5.5 Clamped-Free Quasi-Isotropic Cylindrical Shell Panel with Axial Compression Load

The earlier quasi-isotropic plate and shell results indicate the cubic-nonlinear HTSD theory, with the transformation of the constitutive relations included (C201), predicted a more flexible response than the simpler geometrical variants. Similarly, for the collapse of thin isotropic cylindrical shells, the cubic-nonlinear HTSD theory also predicted a slightly more flexible response than the classical Donnell or modified Donnell theories. In both cases, the more exact geometric theory predicted responses nearly identical to those of the simplest elemental codes. Problems combining the quasi-isotropic material and a smaller radius of curvature with large displacements and rotations should provide more interesting results. The deeper shells, such as those of the transversely point-loaded hinged isotropic cylindrical arch and the transversely point-loaded clamped-free deep cylindrical quasi-isotropic shell, demonstrate the ability of the quasi-nonlinear HTSD theory with the constitutive transformations to predict more flexible structures. By accurately modelling the large displacements and rotations, and correctly modelling the rotation of the Lagrangian coordinates with respect to the Eulerian coordinates, this theory allows the shells to collapse at lower equilibrium loads.

In addition to the transversely loaded quasi-isotropic cylindrical shells, an axially loaded clamped-free quasi-isotropic cylindrical shell panel with and without a centrally located cut-outs were studied. Figure 5.26 shows the shell configuration. The boundary conditions and material properties are listed below. Panels of this general configuration have been the subject of many AFIT research projects, conducted in cooperation with the Wright Laboratory at Wright-Patterson AFB, Ohio. Panels of this material and configuration were recently tested experimentally, as part of a Master's thesis by Hatfield [77]. The experimental procedures used for these experiments were similar to those used by Becker [19], Janisse [93], Tisler [158, 159, 222], and Schimmels [199, 200] at Wright-Patterson AFB. Results of Tisler were used by Dennis for his comparison of the linear HTSD theory he developed [48, 51]. According to Palazotto and Dennis [162], Tisler had problems with the experimental measurements and with the panels not being properly seated in the test fixtures [51:1087]. These particular problems were avoided during later series of experiments [77, 199, 200]. The geometrical and material properties are listed below:

$$\begin{aligned}
 s_1 &= 0.0 \text{ cm} & u = v = w = w_{,1} = w_{,2} = \psi_1 = \psi_2 &= 0 & (\text{clamped}) \\
 s_1 &= 27.94 \text{ cm} & v = w = w_{,1} = w_{,2} = \psi_1 = \psi_2 &= 0 & (\text{clamped, } u \text{ free}) \\
 s_2 &= 0.0 \text{ cm} & & & (\text{free}) \\
 s_2 &= 30.48 \text{ cm} & & & (\text{free})
 \end{aligned}$$

Material AS4-3501 Graphite Epoxy

$$\begin{aligned}
 E_1 &= 14.109 \times 10^{10} \text{ Pa} & E_2 &= 9.243 \times 10^9 \text{ Pa} \\
 G_{12} &= G_{13} = 5.957 \times 10^9 \text{ Pa} & G_{23} &= 2.965 \times 10^9 \text{ Pa} \\
 \nu_{12} &= 0.301 & \theta &= 1.0 \text{ radians} \\
 h &= 0.102 \text{ cm} & R &= 30.48 \text{ cm} \\
 A &= 30.48 \text{ cm} & B &= 30.48 \text{ cm} \\
 \text{Ply Layup: } &[0/-45/45/90]_s
 \end{aligned}$$

Table 5.10 shows the results for total-applied compression load versus axial displacement u computed with the C10X and C20X theories for the quasi-isotropic cylindrical shell panel with a cutout. Values of transverse displacement w are also shown in this table. As shown in the table, the quasi-nonlinear HTSD (C200 & C201) theory gives more flexible results to the modified Donnell (C100 & C101) theory. Figure 5.27 shows predicted total equilibrium axial load versus axial displacement u for the C101 and C201 theories. Table 5.11 shows the results for total-applied compression load versus axial displacement u computed with the C10X and C20X theories for the quasi-isotropic cylindrical shell panel with no cutout. Values of transverse displacement w are also shown in this table. As shown in the table, the quasi-nonlinear HTSD (C200 & C201) theory gives more flexible results to the modified Donnell (C100 & C101) theory. Figure 5.28 shows predicted total equilibrium axial load along the top edge versus axial displacement u for the C101 and C201 theories.

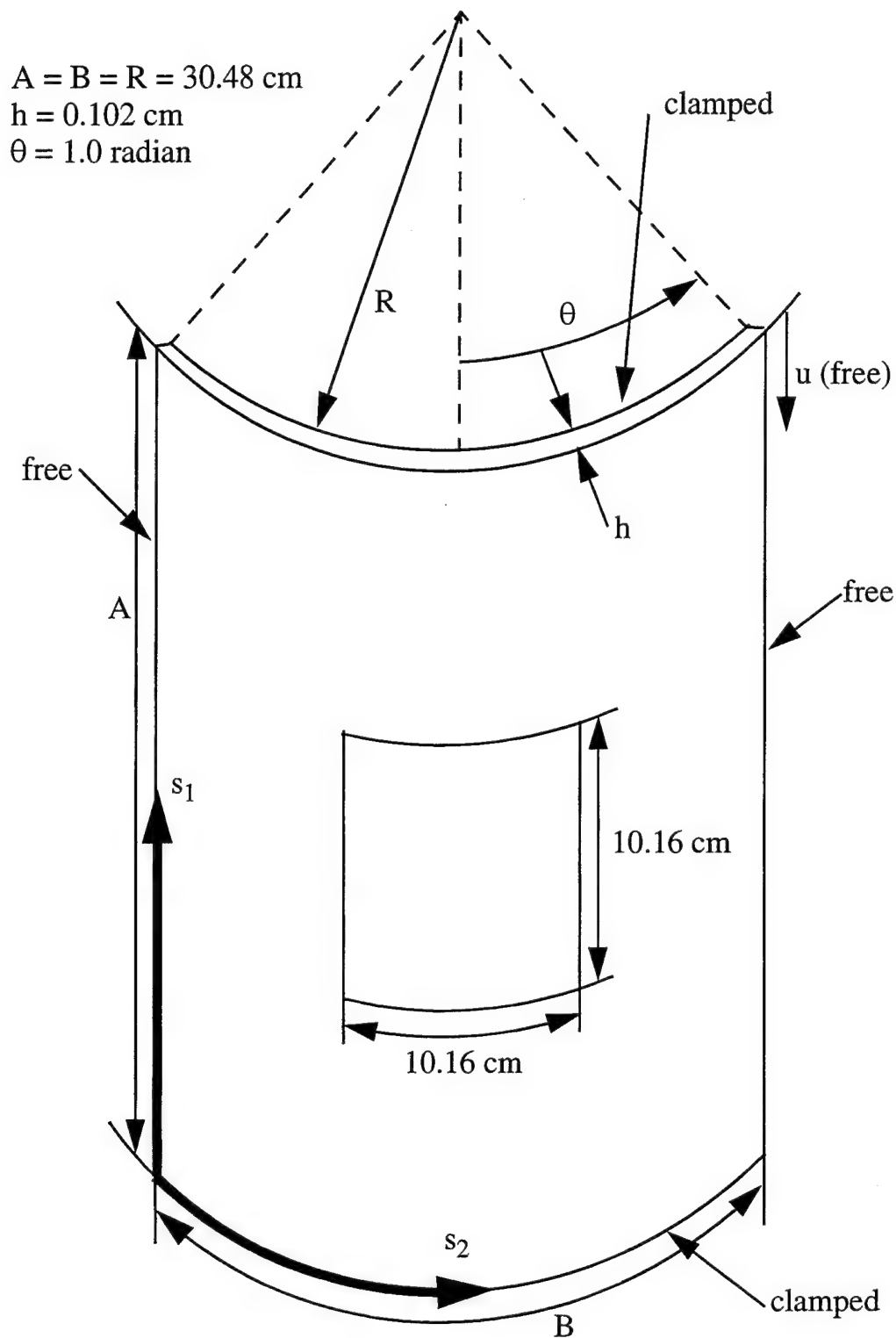


Figure 5.26 Quasi-Isotropic 30.48-cm Radius Cylindrical Composite Shell with Centered 4-Inch Cutout and Free Edges Loaded in Axial Compression

Table 5.10 Axial Displacement vs Transverse Displacement and Load for a 30.48-cm Radius, 30.48-cm \times 30.48-cm, Quasi-Isotropic Cylindrical Shell Panel with Centered 10.16-cm Cutout under Axial Compression Load - C101 and C201 Theories

Axial Disp (cm)	C200 W \dagger (cm)	C200 Load (10^3 N)	C201 W \dagger (cm)	C201 Load (10^3 N)
0.0025	-0.0041	1.041	-0.0041	1.041
0.0051	-0.0105	2.120	-0.0105	2.074
0.0076	-0.0210	3.141	-0.0232	2.936
0.0102	-0.0620	4.110	-0.0681	4.066
0.0127	-0.1745	4.790	-0.1953	4.711
0.0254	-0.4166	6.309	-0.5004	6.153
0.0279	-0.4648	6.335	-0.5334	6.156
0.0305	-0.5004	6.235	-0.5613	6.084

\dagger W is measured at (15.24,3.81)

Table 5.11 Axial Displacement vs Transverse Displacement and Load for a 30.48-cm Radius 30.48-cm \times 30.48-cm Quasi-Isotropic Cylindrical Shell Panel under Axial Compression Load - C101 and C201 Theories

Axial Disp (cm)	C200 W \dagger (cm)	C200 Load (10^3 N)	C201 W \dagger (cm)	C201 Load (10^3 N)
0.0051	-0.0011	2.986	-0.0011	2.990
0.0102	-0.0045	5.968	-0.0046	5.975
0.0152	-0.0055	8.922	-0.1212	8.806
0.0203	-0.2675	11.128	-0.2685	11.151
0.0254	-0.3741	13.279	-0.3752	13.310
0.0305	-0.4663	15.072	-0.4674	14.874
0.0356	-0.1696	9.111	-0.2083	8.825

\dagger W is measured at (15.24,3.81)

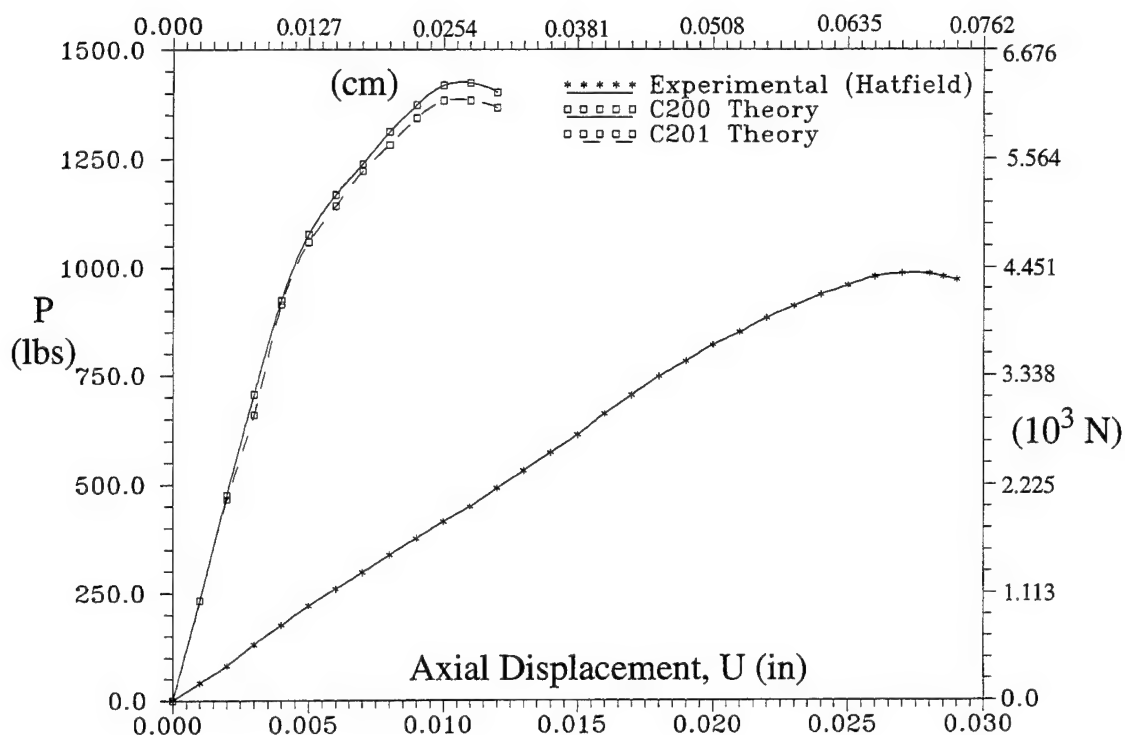


Figure 5.27 Total Equilibrium Load vs Axial Displacement for a Quasi-Isotropic Cylindrical Shell Panel with a Centered 10.16-cm Cutout.

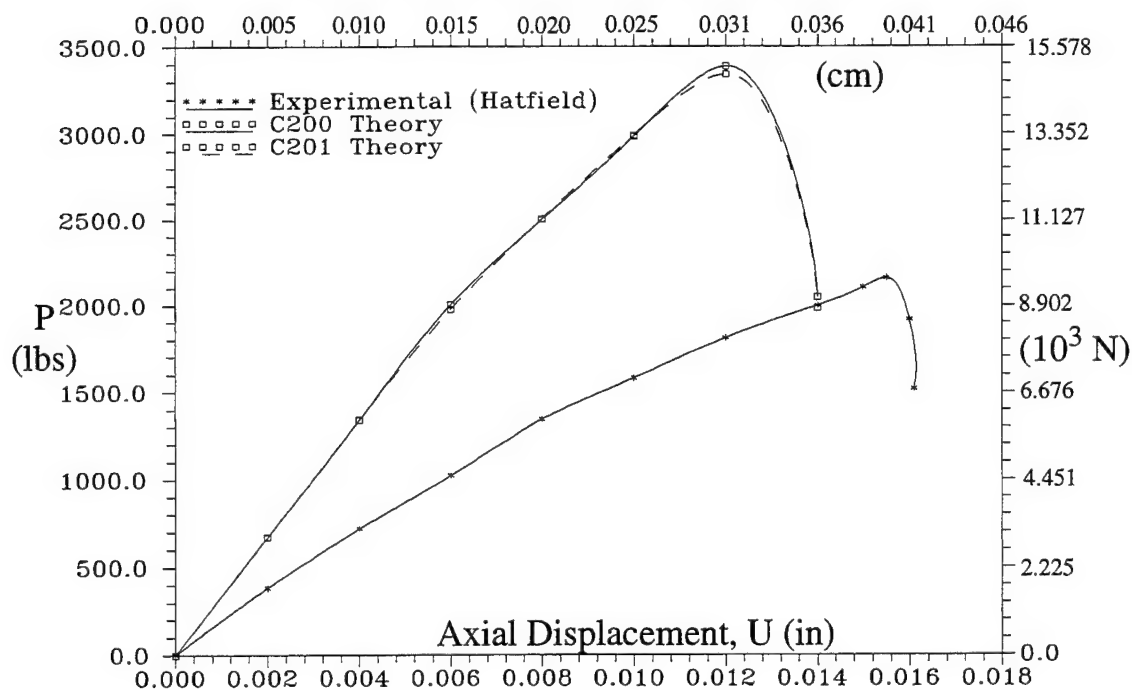


Figure 5.28 Total Equilibrium Load vs Axial Displacement for a Quasi-Isotropic Cylindrical Shell Panel without Cutout

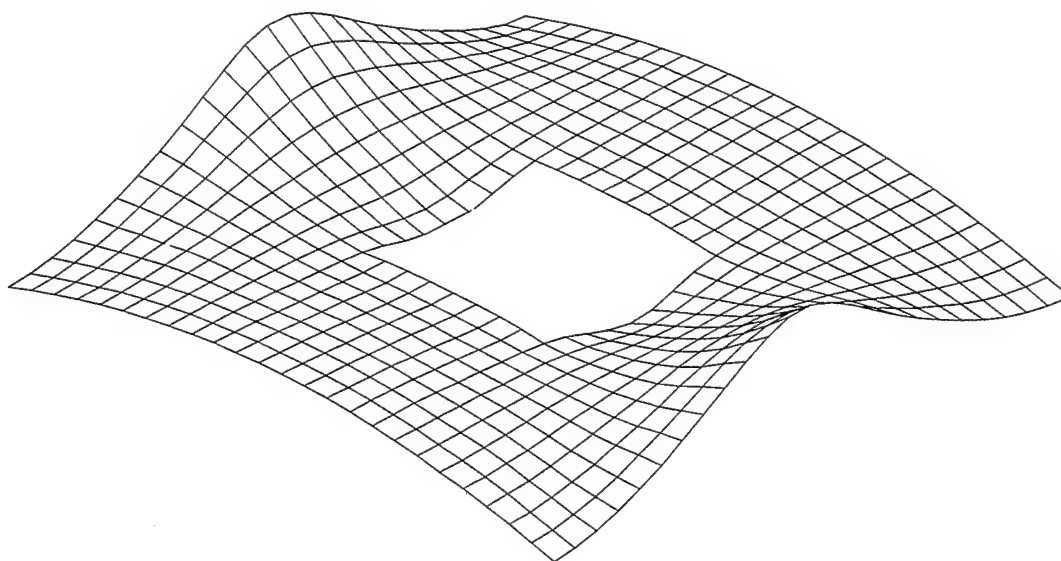


Figure 5.29 Quasi-Isotropic Cylindrical Shell Under Axial Load, Clamped-Free, with 10.16-cm Centered Cutout, ($u = 0.0279$ cm)

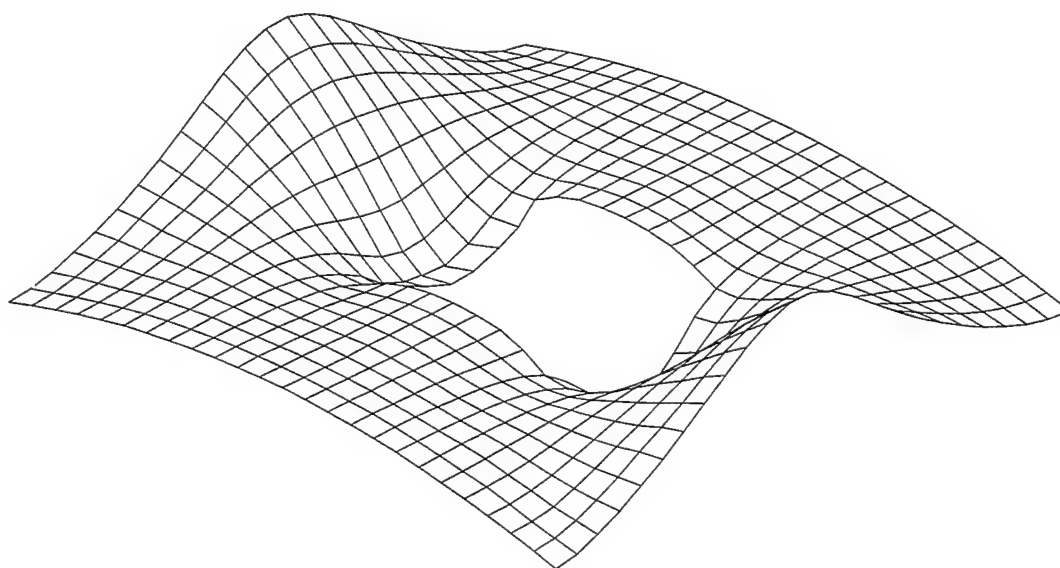


Figure 5.30 Quasi-Isotropic Cylindrical Shell Under Axial Load, Clamped-Free, with 10.16-cm Centered Cutout, ($u = 0.0305$ cm)

Figures 5.29-5.30 show the 30.58-cm \times 30.58-cm cylindrical panel with a 10.16-cm centered cutout just prior to collapse ($u = 0.0279$ cm) and just after collapse ($u = 0.0305$ cm). The shapes shown in Figures 5.29-5.30 are similar in orientation and magnitude to those observed in experiments [77, 199, 200]. At collapse, the maximum rotation of ψ_2 reached 7.8° , and occurred at the middle of the free edges. Only 14.7% of the shell surface saw rotations greater than 4° . After the shell collapsed, the maximum rotation of ψ_2 reached 9.5° and 17.2% of the shell surface saw rotations greater than 4° . Clearly, for this problem, the inclusion of transformation matrices has a negligible improvement in the shell's response to the loading. Considering the relative magnitude of transverse deflection, and the relation of the depth of the shell to shell thickness, these axial panels represent a rather shallow shell when compared to the previous transverse point load, clamped-free quasi-isotropic, cylindrical shell problem. For the cylindrical shell without a cutout, using a prescribed convergence tolerance, $\nabla = 0.0001$, with 15 prescribed axial displacements of 0.0254-cm, the C100 and C101 theory code required 12435 CPU and 17654 CPU seconds, respectively. The C200 theory codes required 77403 CPU seconds and the C201 theory required 83001 CPU seconds. Further comparisons between Hatfield's experimental results and the elastic-plastic theory are made in Section 6.7 where improvement in the analytical predictions are expected.

5.6 Hinged, Isotropic, Spherical Shell Cap

One of the tasks of this research was to incorporate spherical geometry into the classical Donnell, the modified Donnell, and the quasi-nonlinear HTSD theory. Thus, a baseline comparison is made with the published results of Argyris et al. [6] and Parisch [150]. A spherical cap is loaded at the apex and supported on a fixed hinge at the circumference (see Figure 5.31). Note the mesh shown in Figure 5.31 is for one quadrant only and is included **only** to illustrate the mesh density used for this problem and not the actual mesh used for this particular problem. The geometry and material properties are listed below:

$$\begin{aligned}
 s_1 &= 0 & u = w_{,1} = \psi_1 &= 0 & (\text{symmetry}) \\
 s_2 &= 0 & v = w_{,2} = \psi_2 &= 0 & (\text{symmetry}) \\
 s_1 &= \pm 2.301 \text{ cm} & u = v = w = \psi_2 &= 0 & (\text{hinged}) \\
 s_2 &= \pm 2.301 \text{ cm} & u = v = w = \psi_1 &= 0 & (\text{hinged}) \\
 E &= 6.90 \times 10^{10} \text{ Pa} & \nu &= 0.3 \\
 h &= 0.040 \text{ cm} & R_1 = R_2 = R &= 12.09 \text{ cm} \\
 \theta_1 = \theta_2 = \theta &= 0.19024 \text{ radians} & a = b &= 4.6002 \text{ cm} \\
 L &= 4.5725 \text{ cm} & \delta &= 2.1814 \text{ cm}
 \end{aligned}$$

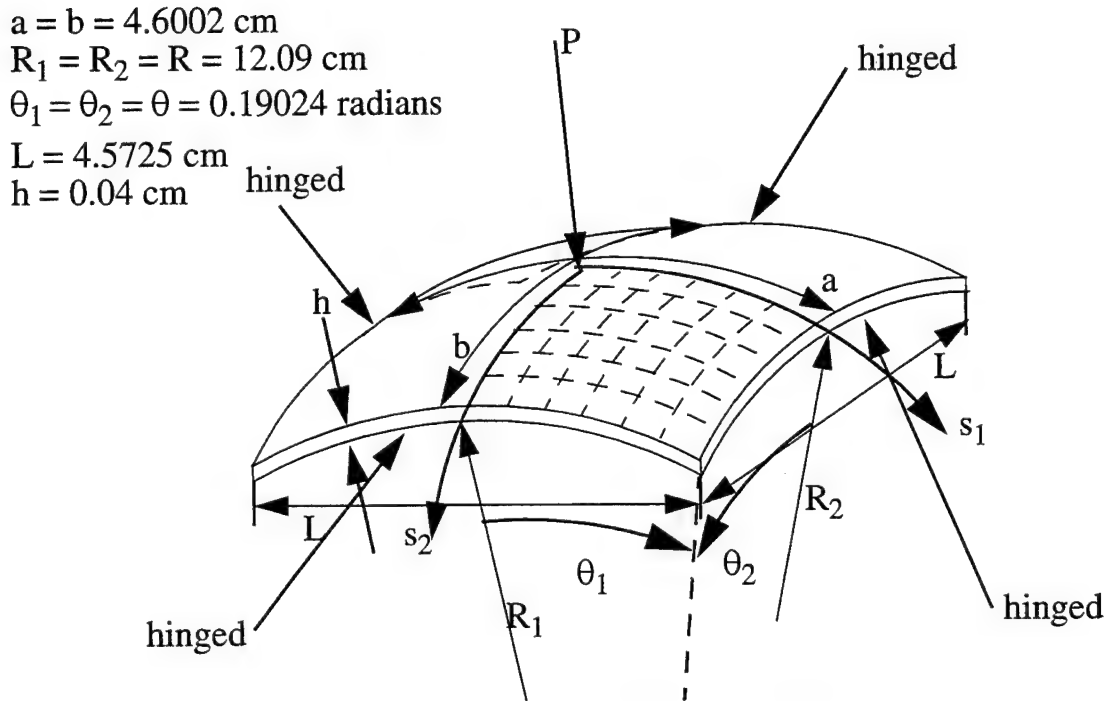


Figure 5.31 Hinged Apex-Loaded Isotropic Spherical Cap

A 12×12 mesh is used to model the entire shell cap. Due to the singularity at the central node, where the transverse load is applied to the spherical shell cap, modelling just one quadrant of the shell was impractical. Flugge [68:350-4] and Krause [100:257-8] showed that for a linear elastic, the closed form solution of the partial differential equations (PDEs) of a spherical shell under a transverse loading at the apex, the shear forces, Q_i , and moments, M_i , at the apex

approach infinity. While this is important to recognize, it is not necessarily the issue at hand when considering a finite element solution. Finite elements are imperfect when compared to the closed form solutions of the PDE. In addition, the finite elements incorporated by the author couples membrane and bending through shell theory. This coupling, along with the imperfections of the element, should "soften" the singularity condition noted by Flugge and Krause. However, by applying symmetry, in both directions (s_1 and s_2) to the element with the apex node, all degrees of freedom (dof) are removed except for the transverse displacement, w . Since this is in the same direction as the load that is applied, the element becomes overly stiff when predicting the shell response due to the lack of sufficient dof to "soften" the element and remove the singularity condition.

To circumvent this singularity condition, the node requires at least four elements [68, 231, 240] to contribute enough energy to the node in the stiffness array. Table 5.12 shows the predicted transverse equilibrium loads for prescribed transverse displacement of the apex. The first column is taken from Reference [6]. Argyris et. al. used a four-noded TRUMP element using classical Donnell shell equations. It is interesting to note the classical Donnell HTSD theories (S000 & S001), which are the linear elastic theories with Hermitian shape functions for w , agree quite well with the TRUMP element but still predict a slightly more flexible shell response. This is attributed to the Hermitian shape functions approximating the transverse displacement, w . The Hermitian shape functions, first proposed by Reddy [172, 179] for plate problems, allows the element to pass the patch test and solve nonlinear problems. This shape functions allows coupling of membrane and bending activity in the shell to be more flexible than the four-noded, TRUMP element. The TRUMP element is a bi-linear element with only linear Lagrangian interpolation functions for the dof u , v , and w . As expected, the modified Donnell HTSD (S10X) and the cubic-nonlinear HTSD (S20X) theories predict a more flexible shell response. Figure 5.32 shows the predicted equilibrium load at the apex versus the prescribed transverse displacement for various theories and from Argyris [6].

Figure 5.33 shows a 2D view of the spherical cap at various points along the load-displacement curve for the C201 analysis. Figure 5.34 shows the rotational dof, ψ_2 , along the meridian of the shell in the s_2 -direction. It should be noted that the same results occur for ψ_1 in the s_1 -direction due to symmetry of curvature in both directions. When the prescribed transverse displace-

ment, w , reaches 0.1905-cm , the maximum rotation of ψ_2 reaches 10.16° and over 13% of the shell surface saw rotations of 4.8° . When the prescribed transverse displacement reaches the collapse point of the shell ($w = 0.381\text{ cm}$), the maximum rotation of ψ_2 reaches 15.68° and over 16% of the of the shell surface saw rotations of 9.7° . As was observed in Section 5.4, when the onset of snapping occurred, and during the snap-through phase, the constitutive transformation matrices of Eqs (4.74) and (4.75) predicted a more flexible shell response than was observed in the standard cubic-nonlinear HTSD (S200) theory. As the transverse displacements, w , approach 10^*h , the combinations of large displacement (w) and moderate rotations (ψ_i) allow the constitutive transformation matrices to change the isotropic material into a psuedo-anisotropic material. In particular, the χ terms of Eqs (4.46a)-(4.64i) become significantly greater than unity.

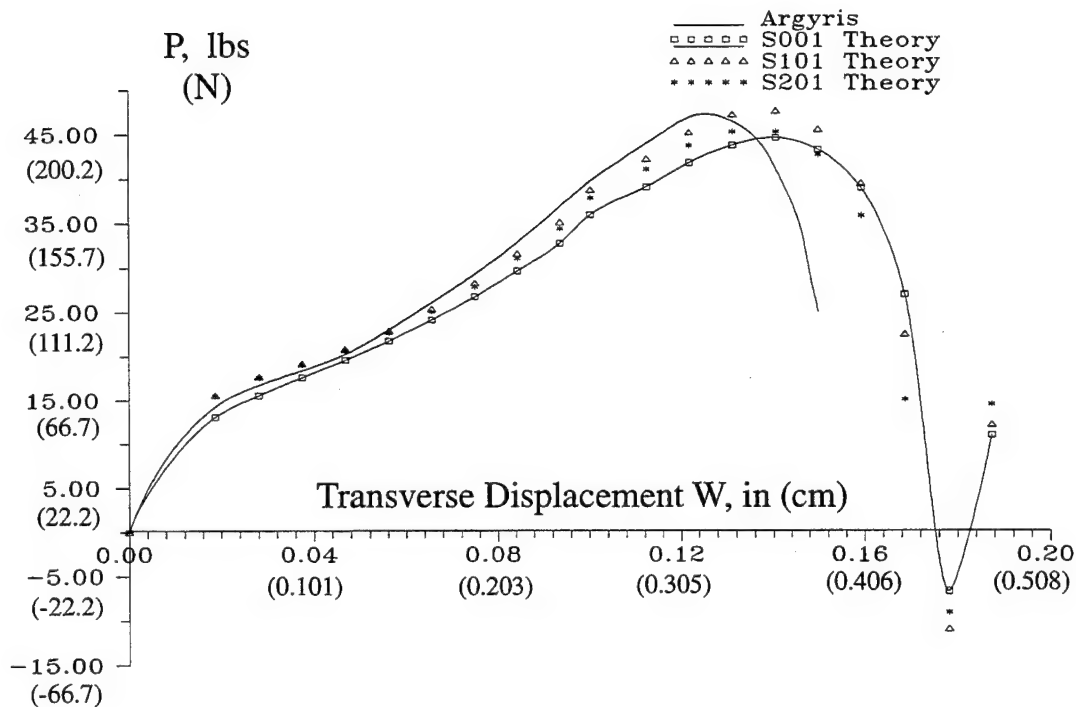


Figure 5.32 Equilibrium Curves for Transverse Point Loaded 0.04-cm Hinged Isotropic Spherical Shell Cap - Ref [6] & SXX1 Theories

Table 5.12 Predicted Load (N) for Prescribed Center Transverse Displacement (cm) of 0.04-cm, Hinged, Isotropic, Spherical Shell Cap

Disp	S000	S001	S100	S101	S200	S201
0.0476	69.7	69.4	69.4	69.4	69.3	69.3
0.0953	87.7	87.2	85.8	85.4	85.2	84.8
0.1429	108.1	107.3	102.5	101.7	101.4	100.6
0.1905	133.1	119.8	127.0	125.9	125.2	124.0
0.2381	162.0	160.0	158.1	156.3	154.7	153.2
0.2858	189.0	186.0	190.6	187.9	185.0	182.8
0.3334	202.1	198.5	213.7	210.0	204.5	201.7
0.3810	197.0	192.6	206.9	202.8	192.3	190.0
0.4286	116.8	120.2	92.5	100.1	96.3	67.2
0.4524	-23.2	-29.8	-40.8	-48.7	-34.7	-40.6
0.4763	57.6	49.2	62.9	54.5	70.4	64.8

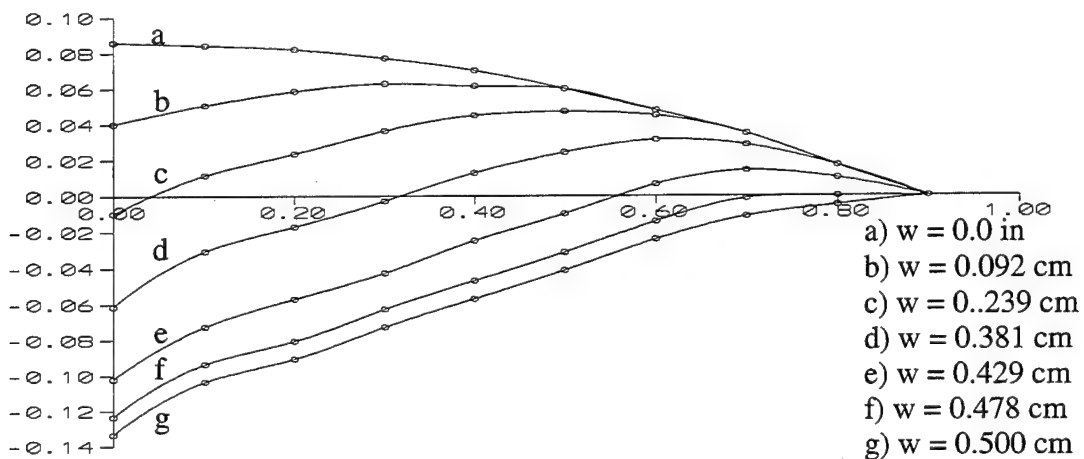


Figure 5.33 Two-Dimensional (2D) Profiles of Hinged Isotropic Spherical Shell Cap at Various Prescribed Transverse Displacements

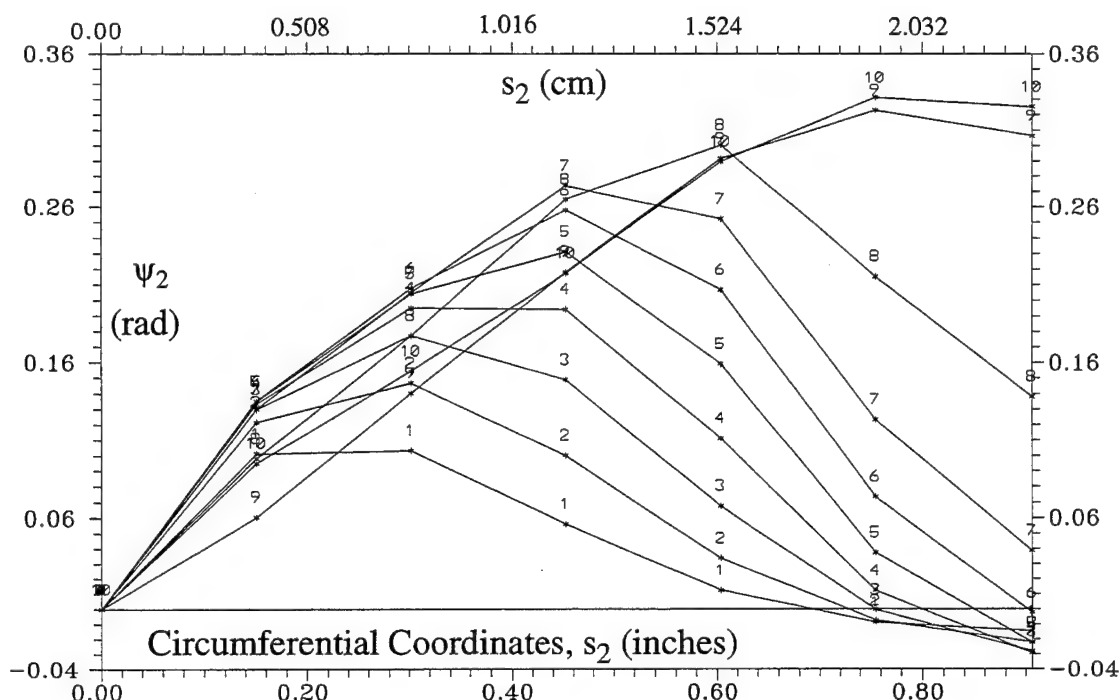


Figure 5.34 Meridian Values of ψ_2 for 10 Increments, 0.0476-cm each, of Transverse Displacement of Hinged Isotropic Spherical Shell - C201 Theory

For a prescribed convergence tolerance, $\nabla = 0.01$, along with 20 increments of prescribed transverse displacement (0.00238-cm), the S000 and S001 theory code required 4428 CPU and 4653 CPU seconds, respectively. The S100 theory codes required 4532 CPU seconds and the S101 theory required 4801 CPU seconds. The S200 theory codes required 40356 CPU seconds and the S201 theory required 43178 CPU seconds.

5.7 Hinged-Hinged Quasi-Isotropic Spherical Shell Cap

To analyze the effect of quasi-isotropic material in a spherical geometry, the model from Section 5.6 (Figure 5.31) is used with some minor modification. Three sample problems were conducted of various ply lay-ups. These were $[0_8]$, $[0_2/90_2]_s$, and a quasi-isotropic lay-up $[0/-45/45/90]_s$. The author determined early on that ply lay-ups of $[0_8]$ and $[90_8]$ produce identical results. The same occurs for ply lay-ups $[0_2/90_2]_s$ and $[90_2/0_2]_s$. The author realizes that the last problem

([0/-45/45/90]_s) is impracticable from an experimental view because of the difficulties of maintaining a true 45° fiber orientation throughout the spherical cap. However, this analysis provides a unique comparison with the other problems and with an isotropic model of the same geometry. The geometric and material properties are listed below:

$$\begin{aligned}
 s_1 &= 0 & u &= w_{,1} = \psi_1 = 0 & (\text{symmetry}) \\
 s_2 &= 0 & v &= w_{,2} = \psi_2 = 0 & (\text{symmetry}) \\
 s_1 &= \pm 2.301 \text{ cm} & u &= v = w = \psi_2 = 0 & (\text{hinged}) \\
 s_2 &= \pm 2.301 \text{ cm} & u &= v = w = \psi_1 = 0 & (\text{hinged}) \\
 E_1 &= 14.120 \times 10^{10} \text{ Pa} & E_2 &= 9.250 \times 10^9 \text{ Pa} \\
 G_{12} &= G_{13} = 5.961 \times 10^9 \text{ Pa} & G_{23} &= 2.967 \times 10^9 \text{ Pa} \\
 v_{12} &= 0.301 & \theta_1 &= \theta_2 = \theta = 0.19024 \text{ radians} \\
 h &= 0.04 \text{ cm} & R_1 &= R_2 = R = 12.09 \text{ cm} \\
 L &= 4.573 \text{ cm} & \delta &= 2.181 \text{ cm} \\
 \text{Ply Layup } [0/-45/45/90]_s & & a &= b = 4.6002 \text{ cm}
 \end{aligned}$$

Table 5.13 shows the predicted transverse equilibrium loads for prescribed transverse displacement of the apex of a [0₈] or [90₈] ply layup with the S200 and S201 theories. As expected, the S201 theory predicts a slightly more flexible shell. Figure 5.35 shows equilibrium path for the S200 and S201 theories. Figure 5.36 shows the rotational dof, ψ_2 , along the meridian of the shell in the s_2 -direction.

Table 5.14 shows the predicted transverse equilibrium loads for prescribed transverse displacement of the apex of a [0₂/90₂]_s or [90₂/0₂]_s ply layup with the S200 and S201 theories. As before, the S201 theory predicts a slightly more flexible shell. Figure 5.37 shows the equilibrium path for the S200 and S201 theories. Figure 5.38 shows the rotational dof, ψ_2 , along the meridian of the shell in the s_2 -direction.

Table 5.15 shows the predicted transverse equilibrium loads for prescribed transverse displacement of the apex of a [0/-45/45/90]_s ply layup with the S200 and S201 theories. As before, the S201 theory predicts a slightly more flexible shell. Figure 5.39 shows the equilibrium path for

the S200 and S201 theories. Figure 5.40 shows the rotational dof, ψ_2 , along the meridian of the shell in the s_2 -direction.

In all three classes of problems (Figures 5.35, 5.37, and 5.39), once the snapping occurs, the transverse displacements, w , become significantly large ($w > 5h$). Referring back to Eqs (4.74)-(4.75), the Cauchy stress-strain constitutive transformation matrices, $[T_1]$ and $[T_2]$, enhance the "softening" or the increasing flexibility of the composite shell once snapping occurs. Along the same lines of discussion as previously mentioned in Section 5.4, as the shell transitions from a purely bending response (load is increasing) to a bending-tension response (load is decreasing), transverse displacement is increasing and the matrices $[T_1]$ and $[T_2]$ reduce the shell's stiffness. This occurs by the "smearing" or blending effect on the stiffness terms in Eqs (4.112)-(4.115) due to these transformation arrays. Thus, in Figure 5.35, after the peak loading is reached, the S201 theory predicts a more flexible shell as the prescribed transverse displacement is increased. Eventually, the shell transitions into a pure tension load due to the shell becoming inverted. This phenomena is observed for Figures 5.37 and 5.39 as well. Figures 5.36, 5.38, and 5.40 show that rotations of the normal (ψ_2) increase smoothly. This is due partly to the dual curvature symmetry of the spherical shell and the hinged (simply supported) boundary conditions. In addition, the spherical shell is considered shallow by the parameters specified by Muc [129, 130]. He identified a shallowness parameter, λ , for isotropic or orthotropic shells:

$$\lambda = \sqrt[4]{12(1 - \nu_{12}\nu_{21})} \frac{a}{\sqrt{Rt}} \quad (5.1)$$

where a is the shell base radius, R is the shell radius of curvature, t is the shell thickness, and ν_{ij} are the Poisson's ratios in the 1- and 2-directions respectively. For these problems the shallowness parameter, λ , is 12.25 indicating, according to Muc, a very shallow shell.

Table 5.13 Predicted Load ($10^3 N$) for Prescribed Transverse Displacement (cm) of Hinged Quasi-Isotropic $[0_8]$ Spherical Shell Cap

Disp	S200	S201
0.0476	0.477	0.510
0.0953	0.835	0.829
0.1429	1.053	1.043
0.1905	1.209	1.170
0.2381	1.306	1.283
0.2858	1.326	1.252
0.3334	1.234	1.193
0.3810	0.973	0.914
0.4286	0.620	0.527
0.4524	0.656	0.595
0.4763	0.889	0.861

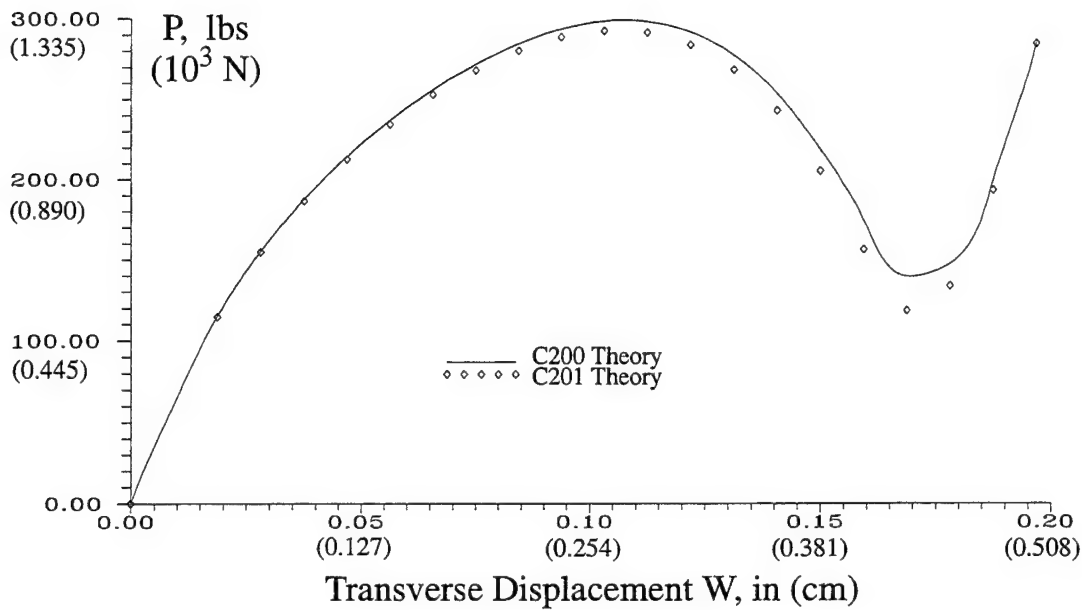


Figure 5.35 Equilibrium Curves for Transverse Point Loaded Hinged Quasi-Isotropic $[0_8]$ Spherical Shell Cap - C200 & C201 Theories

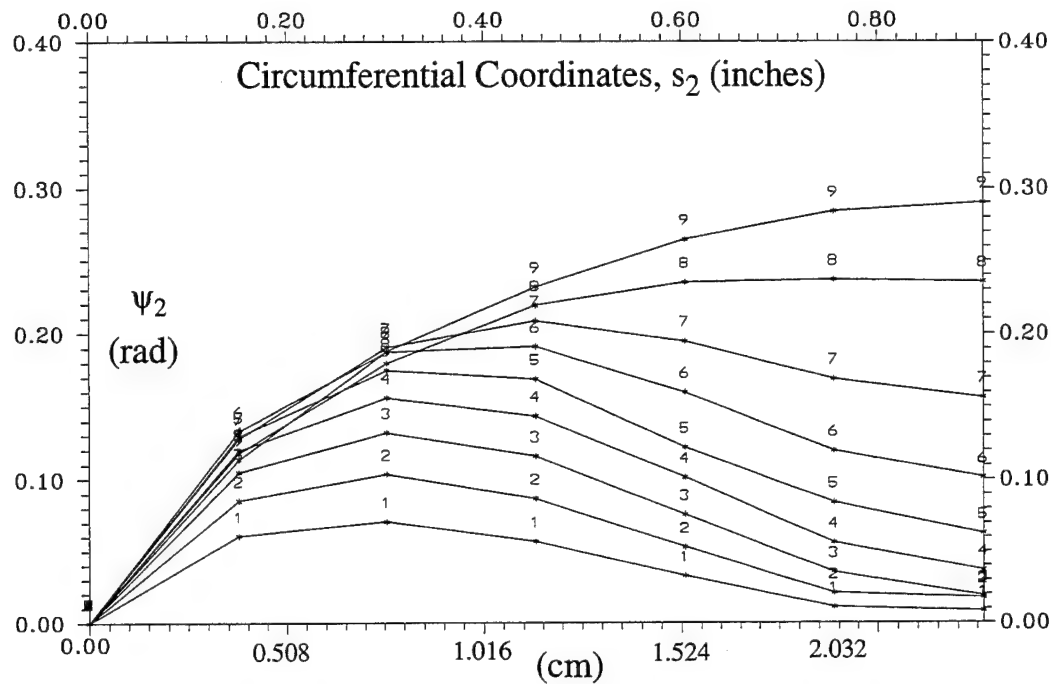


Figure 5.36 Meridian Values of ψ_2 for 10 Increments, 0.01875-Inch each, of Transverse Displacement of Hinged Quasi-Isotropic $[0_8]$ Spherical Shell Cap - C201 Theory

Table 5.14 Predicted Load ($10^3 N$) for Prescribed Transverse Displacement (cm) of Quasi-Isotropic $[0_2/90_2]_s$ Spherical Shell Cap

Disp	S200	S201
0.0476	0.530	0.528
0.0953	0.859	0.854
0.1429	1.082	1.070
0.1905	1.232	1.212
0.2381	1.305	1.279
0.2858	1.281	1.246
0.3334	1.119	1.072
0.3810	0.823	0.744
0.4286	0.681	0.604
0.4524	0.786	0.728
0.4763	1.028	0.992

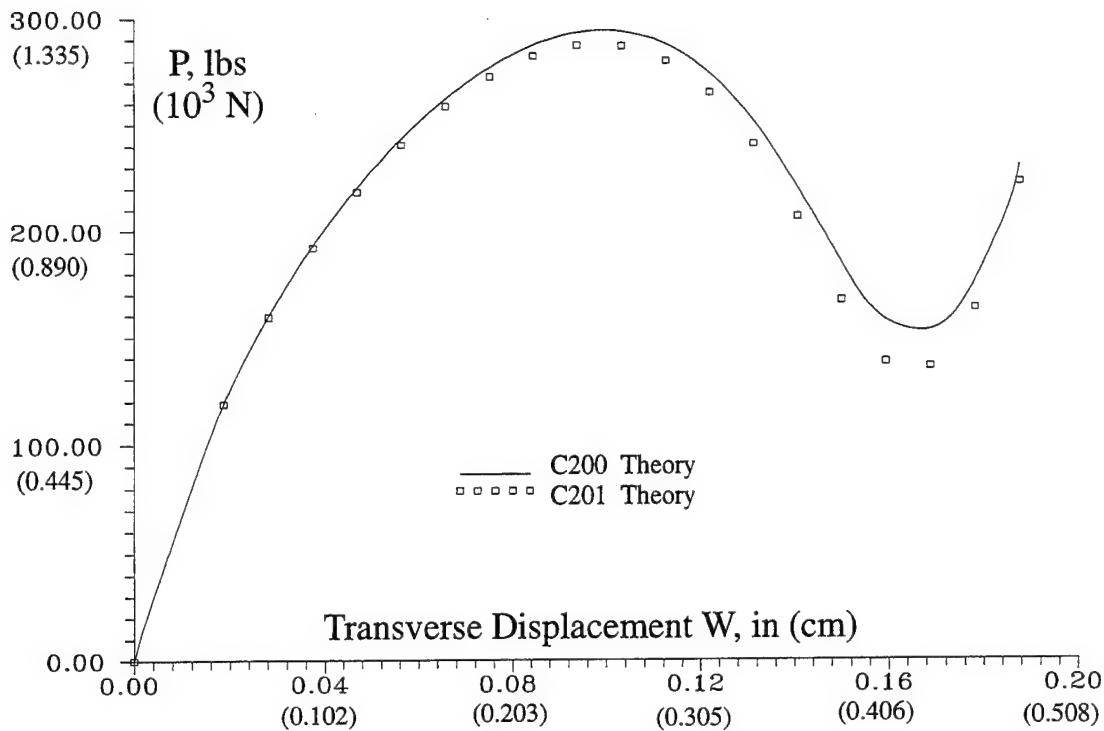


Figure 5.37 Equilibrium Curves for Transverse Point Loaded Hinged Quasi-Isotropic $[0_2/90_2]_s$ Spherical Shell Cap - C200 & C201 Theories

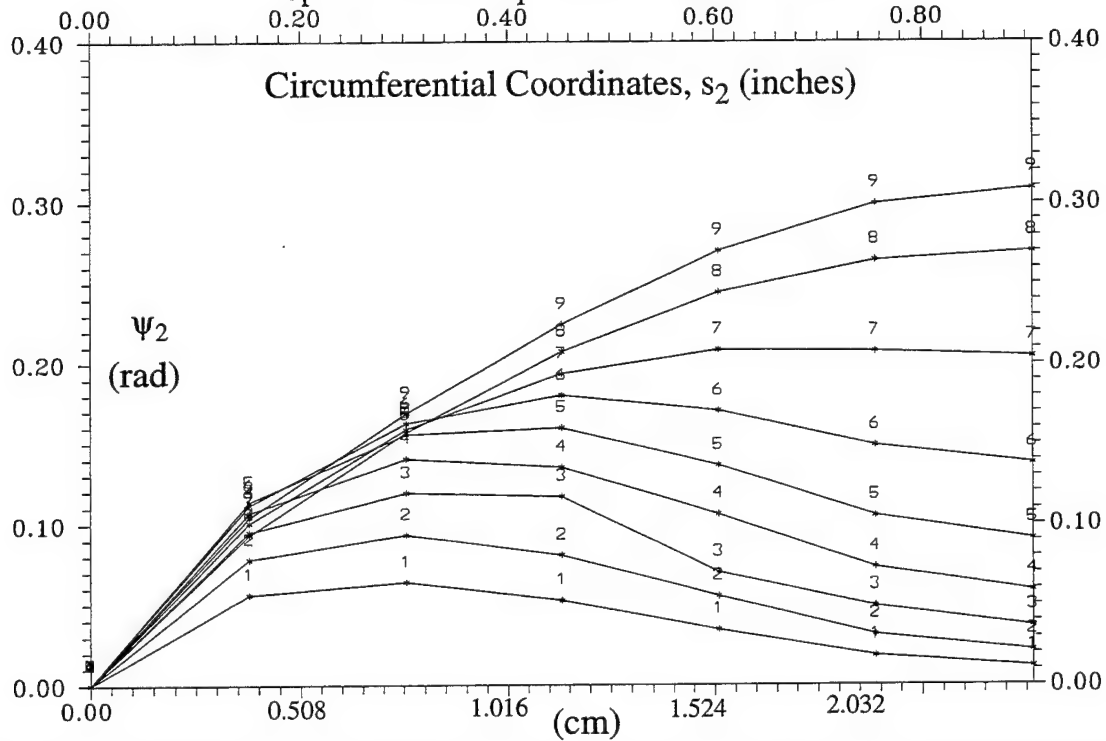
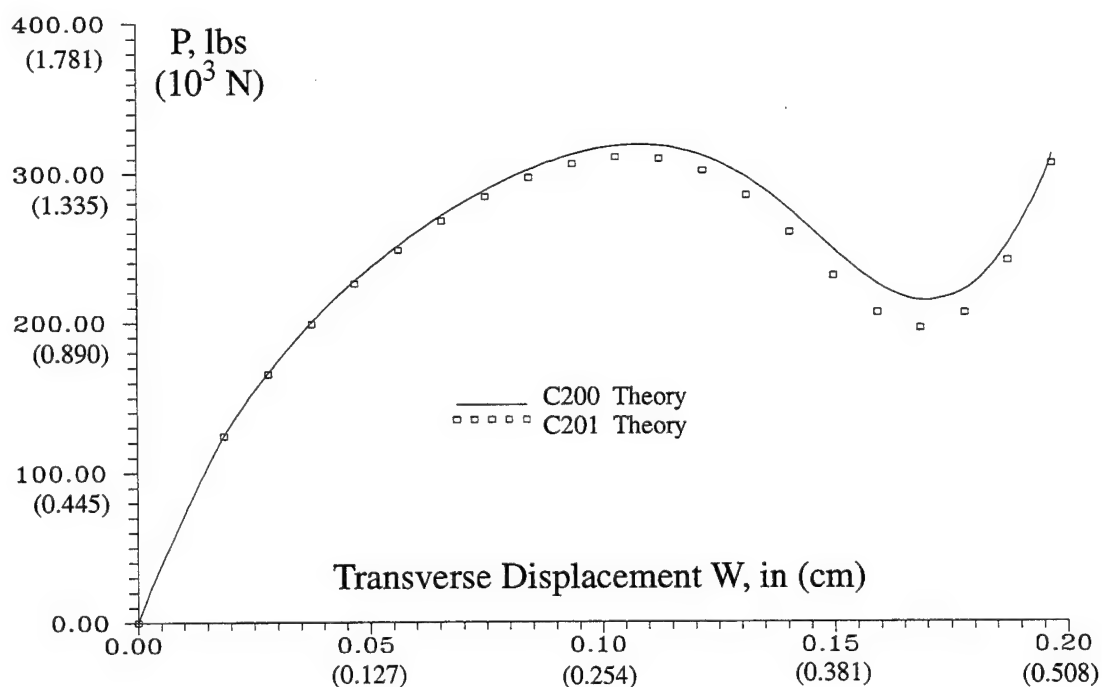


Figure 5.38 Meridian Values of ψ_2 for 10 Increments, 0.01875-Inch each, of Transverse Displacement of Quasi-Isotropic $[0_2/90_2]_s$ Spherical Shell - C201 Theory

Table 5.15 Predicted Load (10^3 N) for Prescribed Transverse Displacement (cm) of Quasi-Isotropic $[0/-45/45/90_2]_s$ Spherical Shell Cap

Disp	S200	S201
0.0476	0.552	0.553
0.0953	0.884	0.881
0.1429	1.105	1.098
0.1905	1.263	1.251
0.2381	1.361	1.344
0.2858	1.377	1.355
0.3334	1.267	1.245
0.3810	1.026	1.006
0.4048	0.917	0.895
0.4286	0.871	0.845
0.4524	0.916	0.883

Figure 5.39 Equilibrium Curves for Transverse Point Load Hinged Quasi-Isotropic $[0/-45/45/90]_s$ Spherical Shell Cap - C200 & C201 Theories

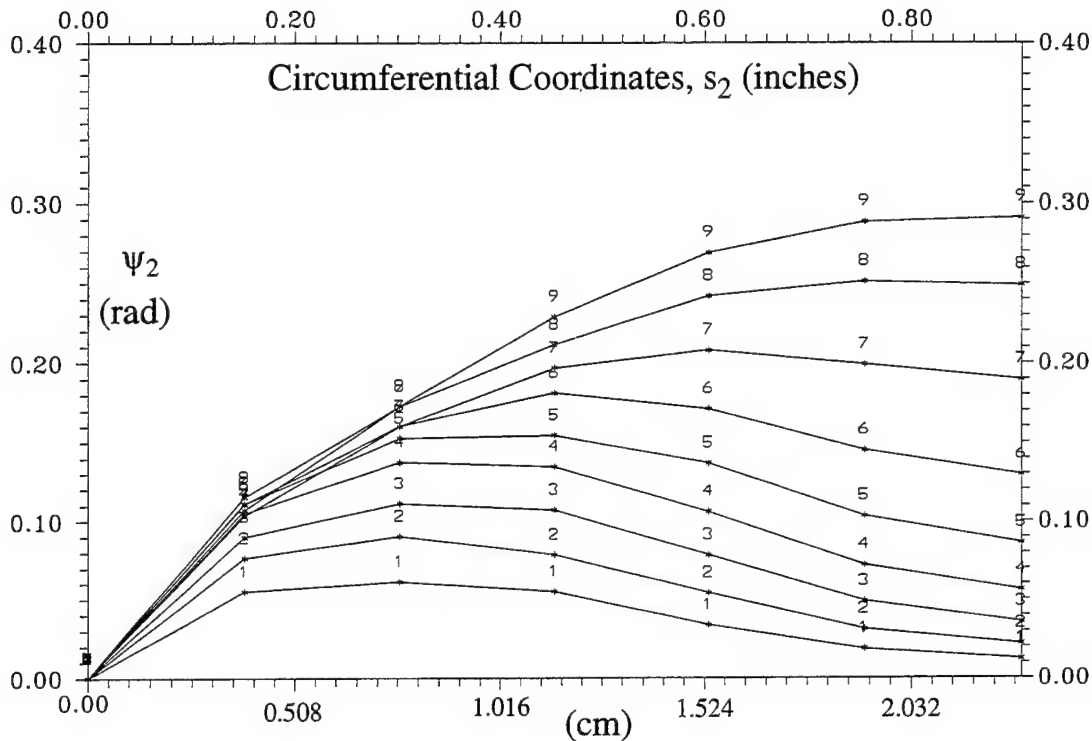


Figure 5.40 Meridian Values of ψ_2 for 10 Increments, 0.01875-Inch each, of Transverse Displacement of Quasi-Isotropic $[0/-45/45/90]_s$ Spherical Shell - C201 Theory

It has been shown that for both isotropic and quasi-isotropic shells, the requirement for the Cauchy stress-strain constitutive transformations matrices occurs when displacements and/or rotations become significant. This usually occurs when the prescribed displacement exceeds the von Karman plate or Donnell thin shell assumption of $5h$. When rotations become excessively large, such as for the deep, isotropic arch or the quasi-isotropic clamped-free, transversely point-loaded, quasi-isotropic shell, and the classical Donnell or the modified Donnell HTSD theories predict an overly stiff shell response, then the constitutive transformation matrices of Eqs (4.74) and (4.75) must be employed for the total Lagrangian formulation discussed herein. For those shell such as the axially loaded quasi-isotropic, cylindrical shell or the spherical shell (isotropic or quasi-isotropic) with a point load at the apex the determination is not so clear. In both problems, the rotations were relatively insignificant. However, for the spherical shells, the transverse displacement were relatively large, when compared to the shell thickness, and therefore indicated the use of Eqs (4.74) and (4.75) was appropriate. The additional CPU burden of including Eqs (4.74) and (4.75) in the analysis was relatively modest. The increase in CPU time, for a converged solution to be achieved, was usually under 10%.

6. Discussion of Elastic-Plastic Shell Analysis

As mentioned in Chapter 5, Chapters 3 & 4 presented the development of three basic material and geometric variations of theory for plates and shells. Results for an elastic analysis of plates and shells (including the material transformation matrices) are discussed in Chapter 5. This chapter discusses the elastic-plastic analysis of plates and shells with the inclusion of the material transformation matrices. One objective of this research was to evaluate the accuracy of including the variations of the HTSD theory with the elastic-plastic material properties listed in Table 6.1, another objective was to assess their limitations. The first step in achieving these objectives was the verification of the computational tools used to achieve results. This verification process included verification of the MACSYMA routines used to generate the elemental codes (this process is discussed in Reference [209:Section 4.6]), verification of the finite element program, and finally verification of numerical analysis.

Several test problems were solved to verify the MACSYMA generated Fortran codes. These test problems were classical flat plate and thin shells with known solutions. In all of the plate and shallow shell test problems, the various elemental codes should give results equivalent to the classical von Karman plate (P010) code or the classical Donnell shell (C010 & S010) codes. This result is expected since the additional terms of the higher-order codes include radius in the denominator. Thus, these terms are zero for a flat plate and negligible for the classical thin shell. Investigations of the limitations of elastic-plastic cubic-nonlinear HTSD theory were based on the shallow isotropic shell panel problems and a deep isotropic arch problem. For the pinched cylinder and sphere problems, the cubic-nonlinear shell (C211 & S211) codes were considered. Due to the large rotations and based on the deep arch solution, it is expected that the classical Donnell and modified Donnell codes were insufficient for modelling these shells. In addition, several quasi-isotropic cylindrical and spherical shell problems were considered. The shallow shell problems were thin 254.0-cm radius hinged-free cylindrical shell panels with a transverse point load, or thin 12.09-cm radius hinged-hinged spherical shell caps with a transverse point load. The 50.8-cm \times 50.8-cm cylindrical shell panels studied were 0.635-cm thick. The 4.623-cm \times 4.62-cm isotropic or quasi-isotropic spherical shell caps studied were 0.04-cm thick. The deep shell problems included an isotropic 254.0-cm radius cylindrical arch with hinged-free boundary

conditions. Another deep shell was a clamped-free quasi-isotropic shell under a transverse point load. The $27.94\text{-cm} \times 27.94\text{-cm}$ cylindrical shell was 0.102-cm thick. The method used to solve each case was the nonlinear, displacement-controlled method. This method allows for convergence past the buckling or snapping phase within each problem [162:9, 134]. The convergence tolerance, ∇ , unless otherwise specified, for each problem was 0.005. The increment of displacement, and the number of increments, is specified for each problem. All problems were run on a SUN SPARCstation 10/80 workstation.

Table 6.1: Definitions of Elemental Codes for Variations of Plastic Theory

Code Name GXYZ	Displacement Assumption Field	Material Coordinate Transformation	Equations Given in Appendix
G011	Donnell (1)	Included	C
G111	modified Donnell (2)	Included	D
G211	Cubic Nonlinear (3)	Included	E

where

- (1) u_i defined in Eq (C.2)
- (2) u_i defined in Eq (D.2)
- (3) u_i defined in Eq (E.2)

$\mathbf{G} \equiv P$ for a plate, C for a cylindrical shell, S for a spherical shell, or A for an arbitrary shell geometry. Appendix A lists relations for arbitrary shells, Appendix B lists relation for general spherical shells, and Appendices C through E list relations for spherical shells. The plate and cylindrical shell relations are embedded within the spherical shell relations. They are derived by setting the parameters D and/or C to zero in the kinematic listed in Eqs (C.2), (D.2), and (E.2).

6.1 Point-Loaded, Simply Supported, Perfectly Plastic, Isotropic Plate

To validate the program, an elastic-perfectly plastic, simply supported $2.54\text{-cm} \times 2.54\text{-cm}$ plate with a point load at its center is considered to test the P2XX theories. This problem was solved by Owen and Hinton [146:370-371]. Due to symmetry, only one quadrant of the 0.0254-cm thick plate is modelled with an 8×8 mesh of elements. The material properties and geometry are listed below:

$$\begin{aligned}
 s_1 &= 0 & v = w_{,2} = \psi_2 &= 0 & (\text{symmetry}) \\
 s_2 &= 0 & u = w_{,1} = \psi_1 &= 0 & (\text{symmetry}) \\
 s_1 &= \pm 1.27 \text{ cm} & v = w = \psi_2 &= 0 & (\text{simple}) \\
 s_2 &= \pm 1.27 \text{ cm} & u = w = \psi_1 &= 0 & (\text{simple}) \\
 a &= b = 2.54 \text{ cm} & h &= 0.0254 \text{ cm} \\
 E &= 7.529 \times 10^{10} \text{ Pa} & \nu &= 0.3 \\
 \sigma_Y &= 11.032 \times 10^6 \text{ Pa} & H' &= 0.0 \\
 M_p &= 275.79 \text{ Pa} & D &= (Eh^3) / (12(1 - \nu^2)) = 11.298 \text{ N-m}
 \end{aligned}$$

Figure 6.1 shows the finite element model. The problem is solved by incrementing transverse displacement at the center of the plate and then calculating the associated load. The objective is to compare the shell response to the predictions of the elementary bending dominated load analysis within the context of Kirchhoff-Love kinematic hypothesis and beyond with the cubic-nonlinear HTSD theory. Owen & Hinton [146:Chapter 9] incorporated a stress resultant, updated Lagrangian formulation that addresses a layered elastic-plastic analysis of Mindlin bending plates. Their model ignored large strains and large displacements, and has no membrane capability (i.e., u and v are not included in the element). In order to obtain results similar to those of Owen & Hinton, the membrane stiffnesses (A_{ij}) must be minimized. Due to the type of response by the plate for the loading and boundary conditions considered, membrane activity dominates the plate's response. The appropriate response was finally achieved by constraining the u and v degrees of freedom from the model, for every node in each element. This constraint effectively removed any membrane activity from the element. The flexure stiffnesses (D_{ij}) dominate the analysis, thereby allowing the plate response to be purely bending. To model nonlinear mate-

rial behavior, a von Mises yield criteria within the Prandtl-Reuss flow theory is incorporated. Figure 6.2 shows the predicted equilibrium load for the prescribed transverse displacement for the various theories and the results published by Owen & Hinton [146]. Note that the load values shown in this figure are 1/4 of the load applied to the corresponding full plate due to the enforcement of the symmetry conditions. As shown in the figure, the elastic solution matches the elementary Kirchhoff-Love plate theory solution identically (see [220:24]). The physical influence of the plate yield criterion is to provide a smooth transition between the elastically dominated and plastically dominated solutions.

Table 6.2: Predicted Normalized Load for Prescribed Normalized Transverse Displacement of Simply Supported, Perfectly Plastic, Isotropic Plate

Disp	Ref [146]	P011	P111	P211
2.5	6.078	6.078	6.078	6.078
5.0	11.962	11.963	11.963	11.963
7.5	17.373	17.378	17.378	17.378
10.0	20.000	20.007	20.005	20.005
12.5	21.804	21.834	21.830	21.830
15.0	22.745	22.769	22.764	22.764
17.5	23.333	23.391	23.381	23.381
20.0	23.922	23.772	23.761	23.761
22.5	24.020	24.013	24.001	24.001
25.0	24.275	24.063	24.050	24.050

The evolution of plastic zones in the plate are depicted in Figures 6.3-6.6 for increasing displacement. These zones are determined by the presence of plastic strain at the Gauss points for each element at the layer being considered. When the normalized displacement reaches $w^* = 8.0$, approximately 25% of the plate's outer surface is exhibiting strain greater than 2.5%. This is reflected in the load-displacement curve by transition from an elastic to an elasto-plastic response in the plate. It is interesting to note that only 8% the middle surface of the plate is only exhibiting strains greater than 2.5%. When the

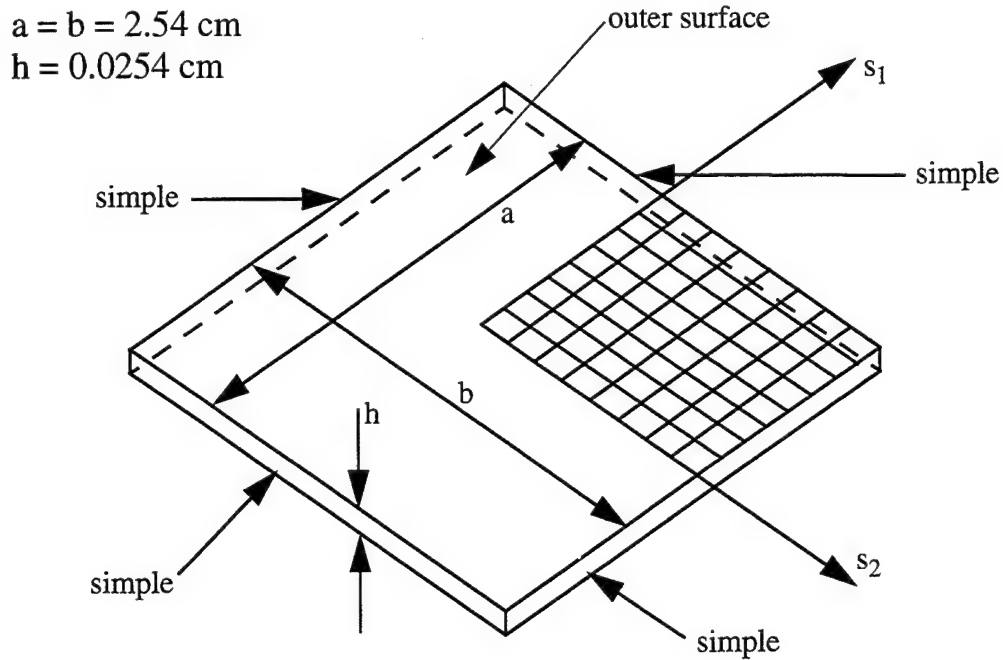


Figure 6.1 Simply Supported Isotropic Plate with Transverse Point Load with no Work Hardening

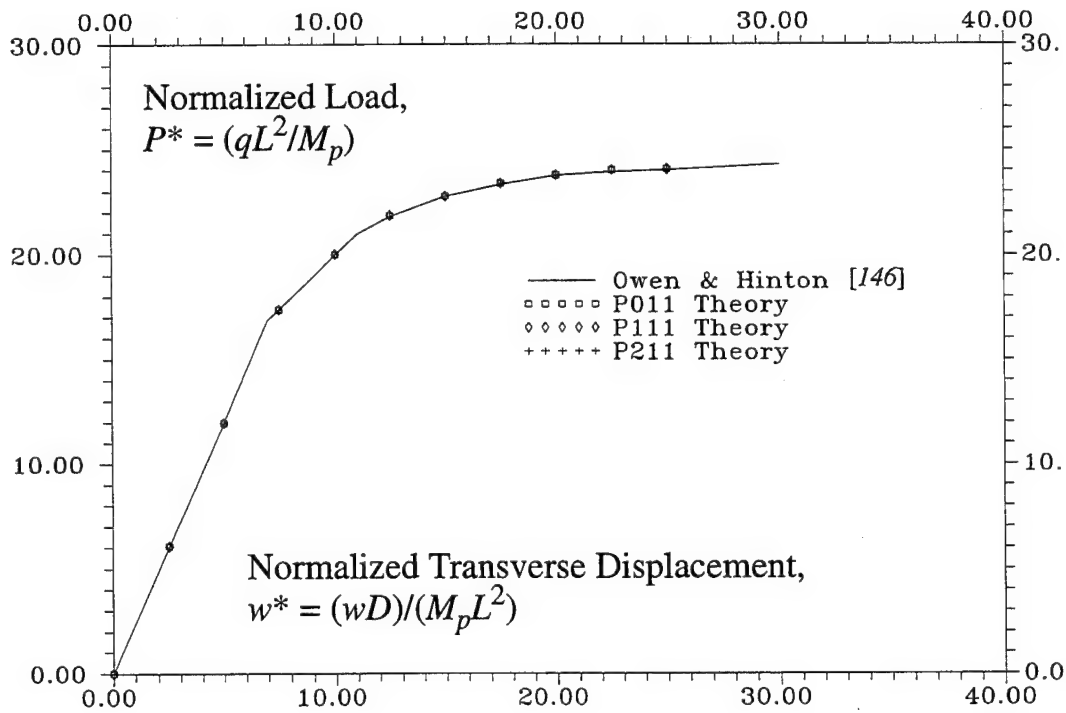


Figure 6.2 Load-Displacement Curves for Simply Supported Isotropic Plate with no Work Hardening. Owen & Hinton [146:370-371] & PX11 results.

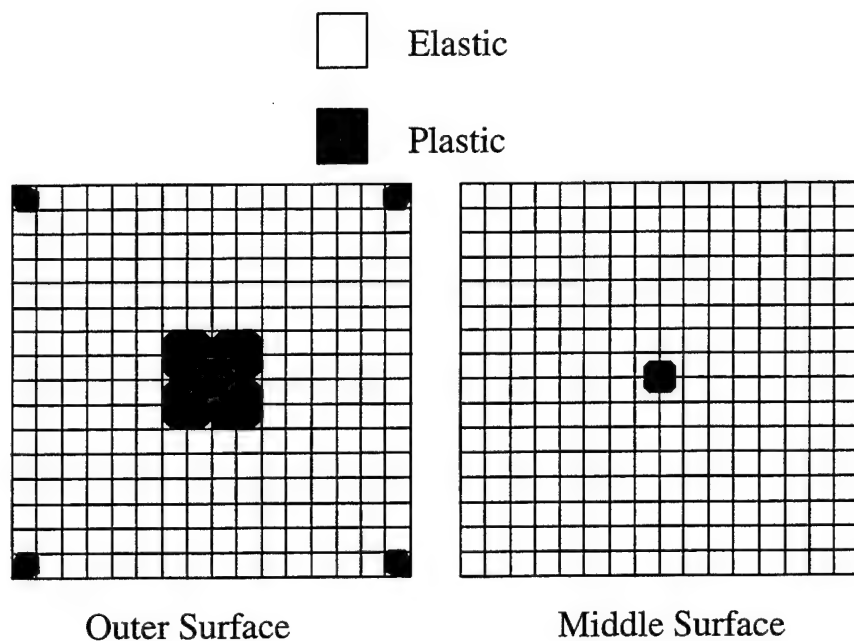


Figure 6.3 Evolution of Plastic Zone in Simply Supported Isotropic Plate with no Work Hardening: $w^* = 5.0$

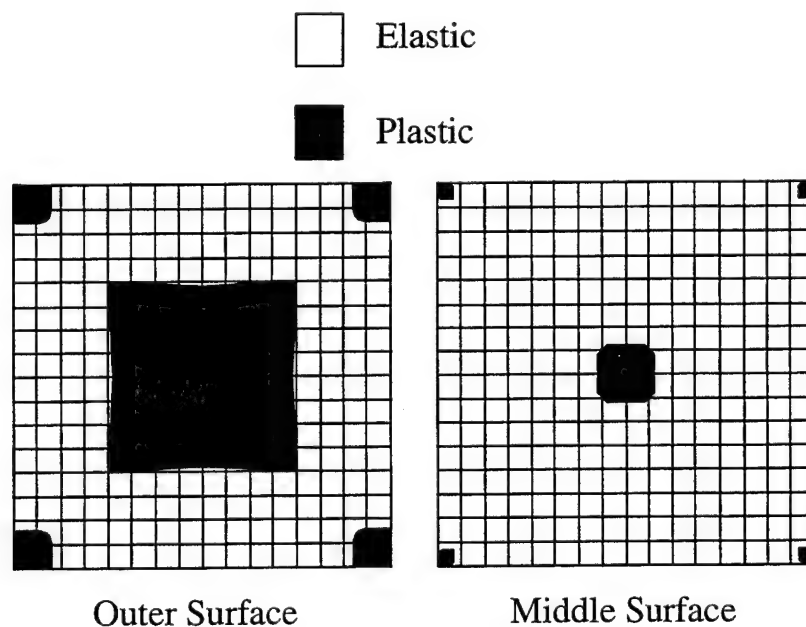


Figure 6.4 Evolution of Plastic Zone in Simply Supported Isotropic Plate with no Work Hardening: $w^* = 10.0$

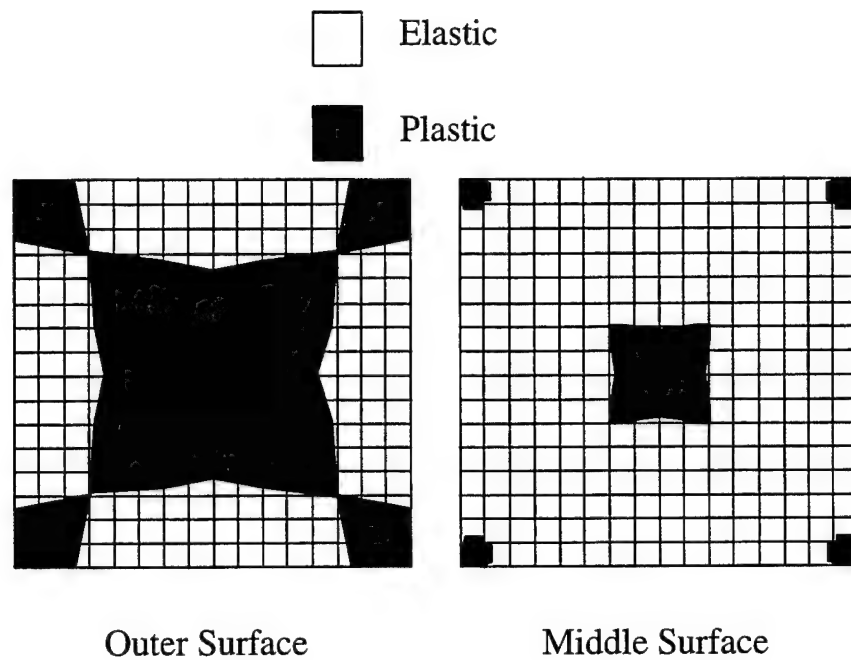


Figure 6.5 Evolution of Plastic Zone in Simply Supported Isotropic Plate with no Work Hardening: $w^* = 15.0$

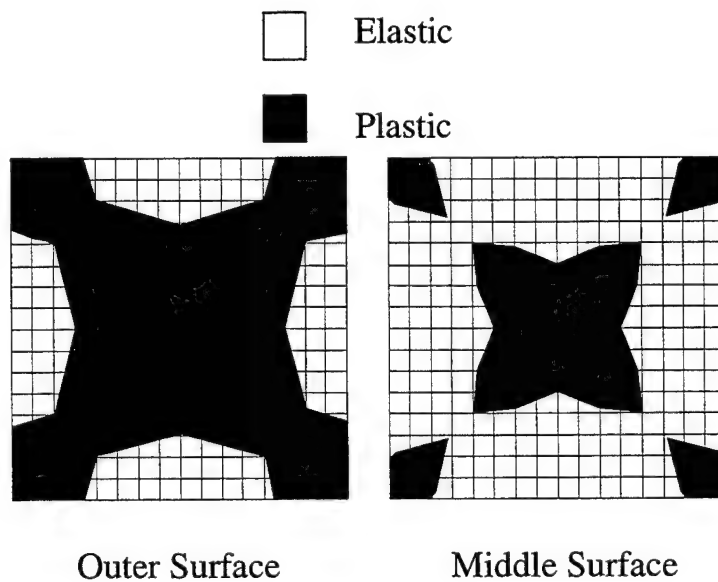


Figure 6.6 Evolution of Plastic Zone in Simply Supported Isotropic Plate with no Work Hardening: $w^* = 20.0$

normalized displacement reaches $w^* = 15.0$ (Figure 6.5) the classical plastic hinge lines appear (exhibited by the plastic zones). Note the plate model predicts finite width plastic zones neighboring each hinge. These plastic zones have considerable width in comparison to the plate thickness as is shown for displacements $w^* > 15.0$ (Figure 6.5 through Figure 6.6). Nevertheless, there is good quantitative agreement between the author's solution and those of Owen & Hinton [146] for the equilibrium load-displacement curve. Owen & Hinton never displayed their plasticity regions for this particular problem. The plastic zones, for each layer of interest, are determined by calculating the stresses at each Gauss point, transforming them into the Cauchy reference frame, and then determining if the yield function was exceeded for this Gauss point. If this occurs, the Gauss point was identified as having yielded for the remainder of the analysis and the Prandtl-Reuss flow relations were followed regarding the elastic and plastic strain increments. For a nonlinear, displacement-control solution with a prescribed tolerance, $\nabla = 0.01$, the P011 theory code required 2030.7 CPU seconds, the P111 theory required 2250.3 CPU seconds, and the P211 required 3243.9 CPU seconds. The normal displacement, w , was initially incremented at 1.27-cm until

6.2 Deep, Hinged, Perfectly-Plastic, Isotropic, Cylindrical Arch with Transverse Point Load

To determine the effect of including an elastic perfectly-plastic material analysis for cylindrical shells, the deep isotropic arch problem from Section 5.2 is studied. It is a 254.0-cm radius arch with a 2.54-cm square cross section and an opening angle of 0.92 radians (106.0°). The arch configuration is shown in Figure 6.7. The geometric and material data are shown below:

$$\begin{aligned}
 s_1 &= 0 & v &= w_{,2} = \psi_2 = 0 & (\text{symmetry}) \\
 s_2 &= 0 & u &= w_{,1} = \psi_1 = 0 & (\text{symmetry}) \\
 s_1 &= \pm 1.27 \text{ cm} & & & (\text{free}) \\
 s_2 &= \pm 234.95 \text{ cm} & u &= v = w = \psi_1 = 0 & (\text{simple})
 \end{aligned}$$

$$\begin{aligned}
 E &= 3.103 \times 10^{10} \text{ Pa} & \theta &= 0.92 \text{ radians} \\
 \text{width} &= 2.54 \text{ cm} & \nu &= 0.3 \\
 h &= 2.54 \text{ cm} & L &= 406.4 \text{ cm} \\
 \delta &= 101.6 \text{ cm} & \nu &= 0.0 \\
 \sigma_Y &= 11.032 \times 10^6 \text{ Pa} & H' &= 0.0
 \end{aligned}$$

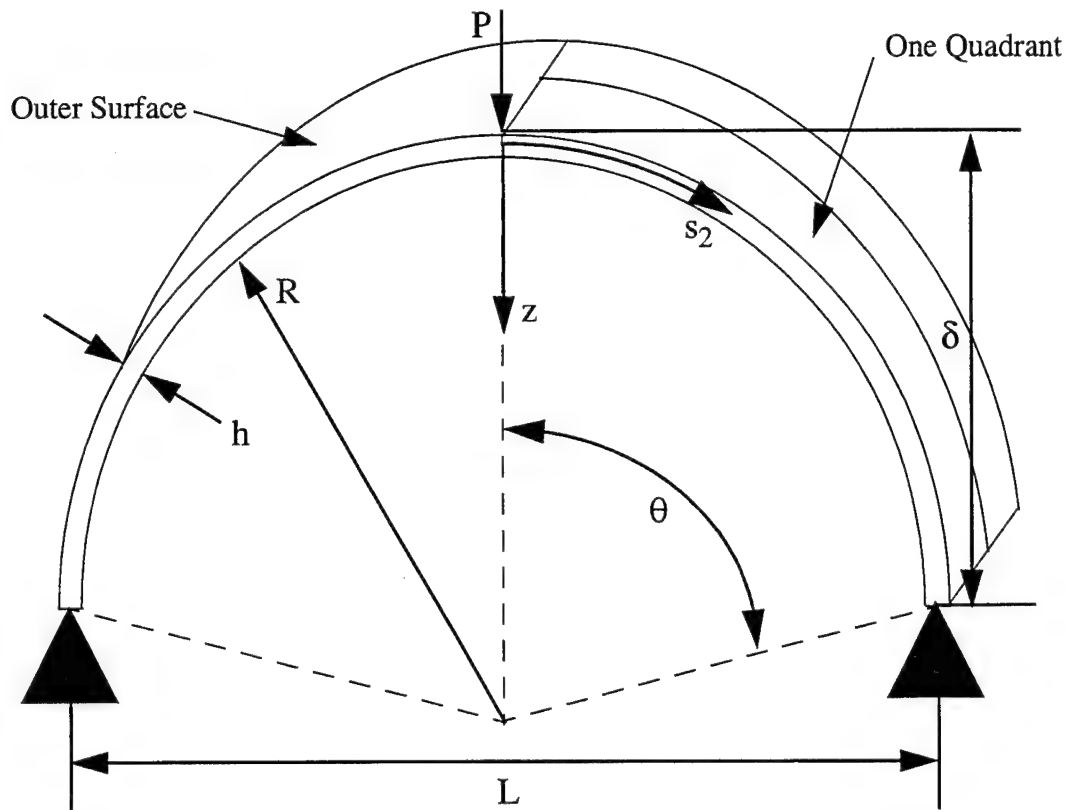


Figure 6.7 Hinged, Point-Loaded, Perfectly Plastic Isotropic Cylindrical Arch

It should be noted that the values for σ_y and H' are arbitrarily chosen for this problem. They were chosen to establish an elastic-perfectly plastic isotropic cylindrical arch analysis. Solutions for this problem were compared using C2XX codes and a 1×40 element mesh to model one quadrant of the arch. Data from the various geometrical theories are shown in Table 6.3. When the elastic-perfectly plastic material analysis is included, the quasi-nonlinear theory (C211) predicts a more dramatic collapse than the elastic analysis. Figure 6.8 shows the load versus crown displacement predicted by the C2XX theories.

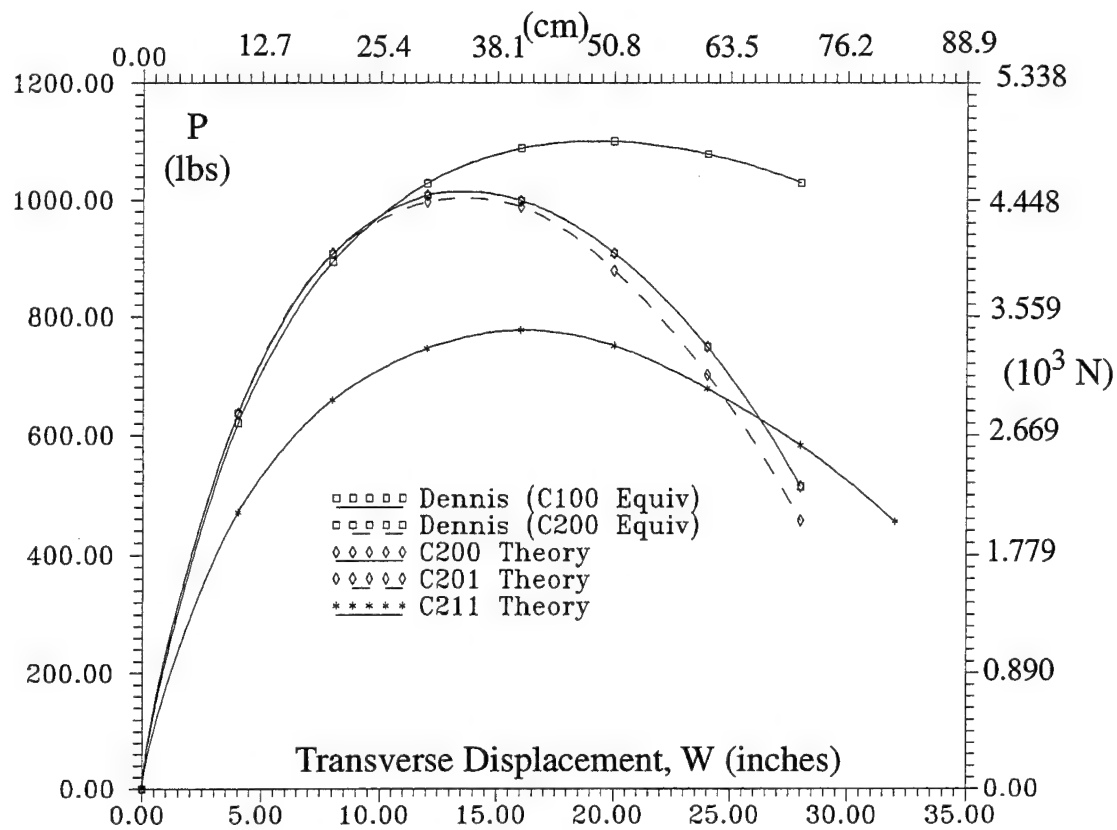


Figure 6.8 Deep Arch Crown Displacement vs Load - C100 & C2XX Theory

Table 6.3: Equilibrium Point Load (10^3 N) for Prescribed Transverse Displacement (cm) of Perfectly Plastic Isotropic Cylindrical Arch

Disp	Donnell*	SLR*	C200	C201	C211
10.16	2.763	2.834	2.823	2.821	2.096
20.32	3.975	4.038	4.021	3.834	2.932
30.48	4.573	4.481	4.464	4.133	3.317
40.64	4.841	4.443	4.431	3.977	3.454
50.80	4.876	4.041	4.037	3.521	3.338
60.96	4.808	3.488	3.532	2.881	2.793
71.12	4.579	2.284	2.277	2.077	2.592
81.28	N/A	N/A	N/A	N/A	2.026

*Ref [162:207]

Along with the large movement and rotations, the changing constitutive relations near the arch crown creates a more flexible response for the model.

Figures 6.9-6.13 show the development of the plastic zones along the arch surface and mid-surface. As expected, plasticity occurs along the counter-flexure points of the arch and at the location of the loading. By the end of the analysis, the entire outer (convex) surface of the arch is behaving plastically (see Figure 6.13), along with the middle surface. This allows for the significantly more flexible shell response observed in Figure 6.8. This is a relatively deep shell with the values of δ/b and θ over five times larger than a typical shallow arch [162:205]. The boundary conditions and loading result in a symmetric response where the arch crown displaces only radially. Previously, the results from the elastic solutions (i.e. C00X, C10X, and C20X) were compared with the inextensible solution of Huddleston [88]. Huddleston provided closed-form solutions for an arch with an extensible midsurface. He defines the extensibility of the arch by a factor, c , as shown in the following

$$c = \frac{I}{A(2b)^2} \quad (6.1)$$

where I is the area moment of inertia, A cross-sectional area, and b is given in Figure 6.7. The inextensible solution is represented by $c = 0$ since the bending EI is very small compared to the axial stiffness EA . The geometry of the arch for the present formulation gives an extensibility factor of $c = 3.255 \times 10^{-6}$.

Solutions were obtained and compared to Huddleston results for $c = 0.0$ and 0.01 . The collapse load for the Donnell arch (C001) is approximately 13% below that for the inextensible solution ($c = 0.0$), yet is much larger than the published extensible solution ($c = 0.01$). The extensibility of the middle is seen to increase the deflection of the arch under the load, as is expected since the arch is in compression. The parameter c for the present case is very small. Therefore, the results tend to follow the $c = 0.0$ results closely until near the peak load. The C001, C101, and C201 responses fall between the curves in the postcollapse regions and gives an expected response for the extensibility factor for the present arch geometry. The C101 collapse load is approximately 15% and the C201 collapse load is approximately 20% less than the inextensible solution. Additionally, the

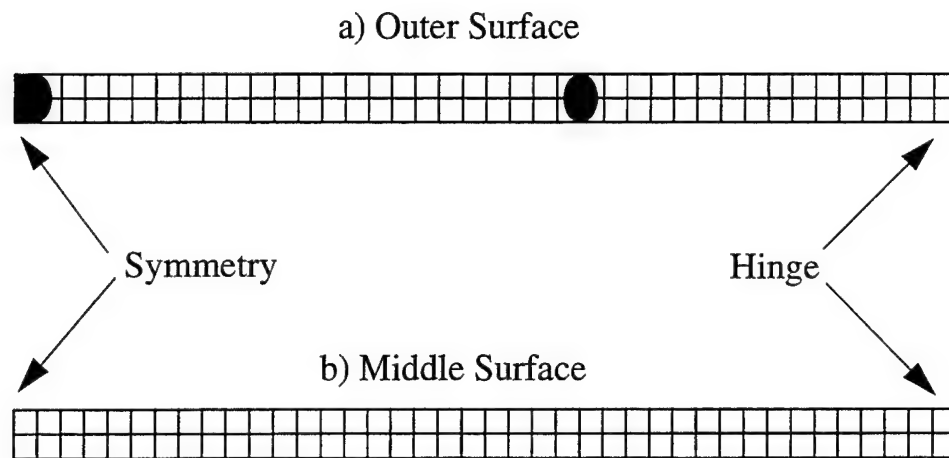


Figure 6.9 Evolution of Plastic Zones for Perfectly Plastic Isotropic Cylindrical Arch: $w = 20.32 \text{ cm}$

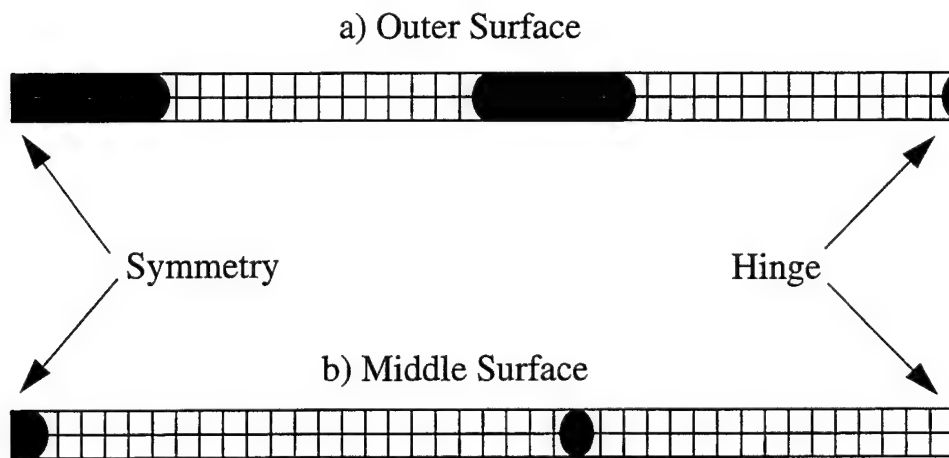


Figure 6.10 Evolution of Plastic Zones for Perfectly Plastic Isotropic Cylindrical Arch: $w = 30.48 \text{ cm}$

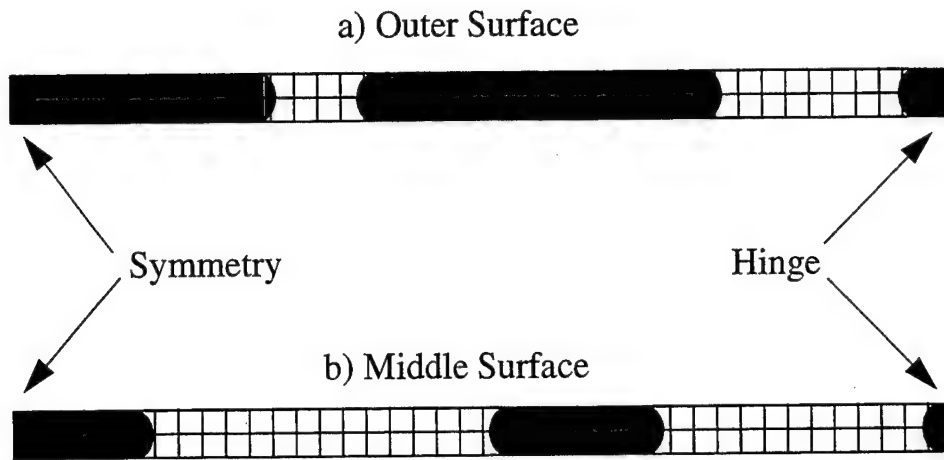


Figure 6.11 Evolution of Plastic Zones for Perfectly Plastic Isotropic Cylindrical Arch: $w = 40.64 \text{ cm}$

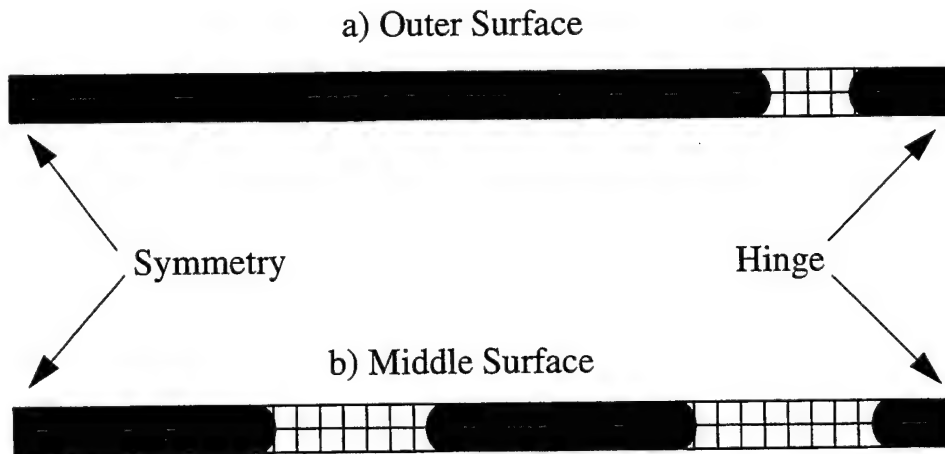


Figure 6.12 Evolution of Plastic Zones for Perfectly Plastic Isotropic Cylindrical Arch: $w = 50.8 \text{ cm}$

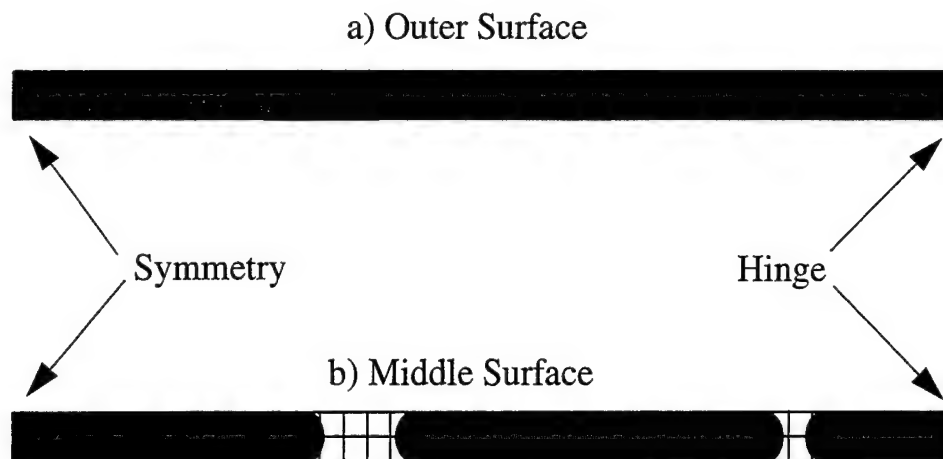


Figure 6.13 Evolution of Plastic Zones for Perfectly Plastic Isotropic Cylindrical Arch: $w = 60.96 \text{ cm}$

post-collapse response of the C201 model, and the entire response of the C211 model, are different from that of the C001 and inextensible results in that it does not fall between the $c = 0.0$ and 0.01 curves. This is attributed to the higher-order representation of the deformation of the mid-surface of the arch and due to the continually changing properties of the elastic-perfectly plastic material. Recall that the C201 formulation included many nonlinear in-plane displacement terms in the strain definitions that are not included in the C001 and C101 formulations. In addition, the C211 formulation allows the material to behave nonlinearly. Therefore, one might expect a greater effect of extensibility in the C201 & C211 formulations compared to the C001 & C101 formulations as the displacements become large, i.e., where the additional terms become more important. Almroth & Brogan [3] saw a similar effect compared to the inextensible solution of a deep arch. Their finite element formulation allows nonzero midplane straining, and their results were consistently more flexible compare to the inextensible results. The transverse shear degrees of freedom have a small effect but also increase the displacement under the load compared to the

inextensible solution [202].

For a nonlinear, displacement-control solution, with a prescribed tolerance, $\nabla = 0.005$, along with 3 prescribed transverse displacements of 10.16-cm and 10 prescribed transverse displacements of 5.08-cm, the C211 theory required 35479.4 CPU seconds. To ensure convergence at this prescribed tolerance, the increments of displacement were half of those used for the C201 theory when approximately 15% of the convex surface saw strains greater than 2.5%. The CPU time is a significant increase, for the same tolerance, when compared to C201 theory in generating a solution.

6.3 Pinched, Perfectly Plastic, Isotropic Cylinder with Rigid Membranes and Two Transverse Point Loads

To test the plasticity model for cylindrical shells, a short isotropic cylinder bounded by two rigid diaphragms at its ends, loaded with two transverse pinching loads at the middle section, and characterized with no kinematic hardening, is considered. Simo & Kennedy [207] published results for this model using their total Lagrangian, large strain formulation. Due to symmetry, only one octant of the cylinder is modelled. The 3-units thick cylinder is 180-units in length with a 300-unit radius. Note: Simo & Kennedy used non-dimensionalized units. The geometry and material properties are listed below. The finite element model is given in Figure 6.14. Because of the geometry, and the difficulty of predicting stress in a displacement-based finite element formulation, a heavily refined 8×36 element mesh is used to model the octant with symmetry about the s_2 -axis and along one edge of the s_1 -axis. The other edge of the s_1 -axis models the rigid diaphragm. The material and geometrical properties are listed below:

$$\begin{array}{lll}
 s_1 = 0.0 & v = w = w_{,2} = \psi_2 = 0 & (\text{rigid membrane}) \\
 s_2 = 0.0 & v = w_{,2} = \psi_2 = 0 & (\text{symmetry}) \\
 s_1 = 90.0 & u = w_{,1} = \psi_1 = 0 & (\text{symmetry}) \\
 s_2 = 471.24 & v = w_{,2} = \psi_2 = 0 & (\text{symmetry})
 \end{array}$$

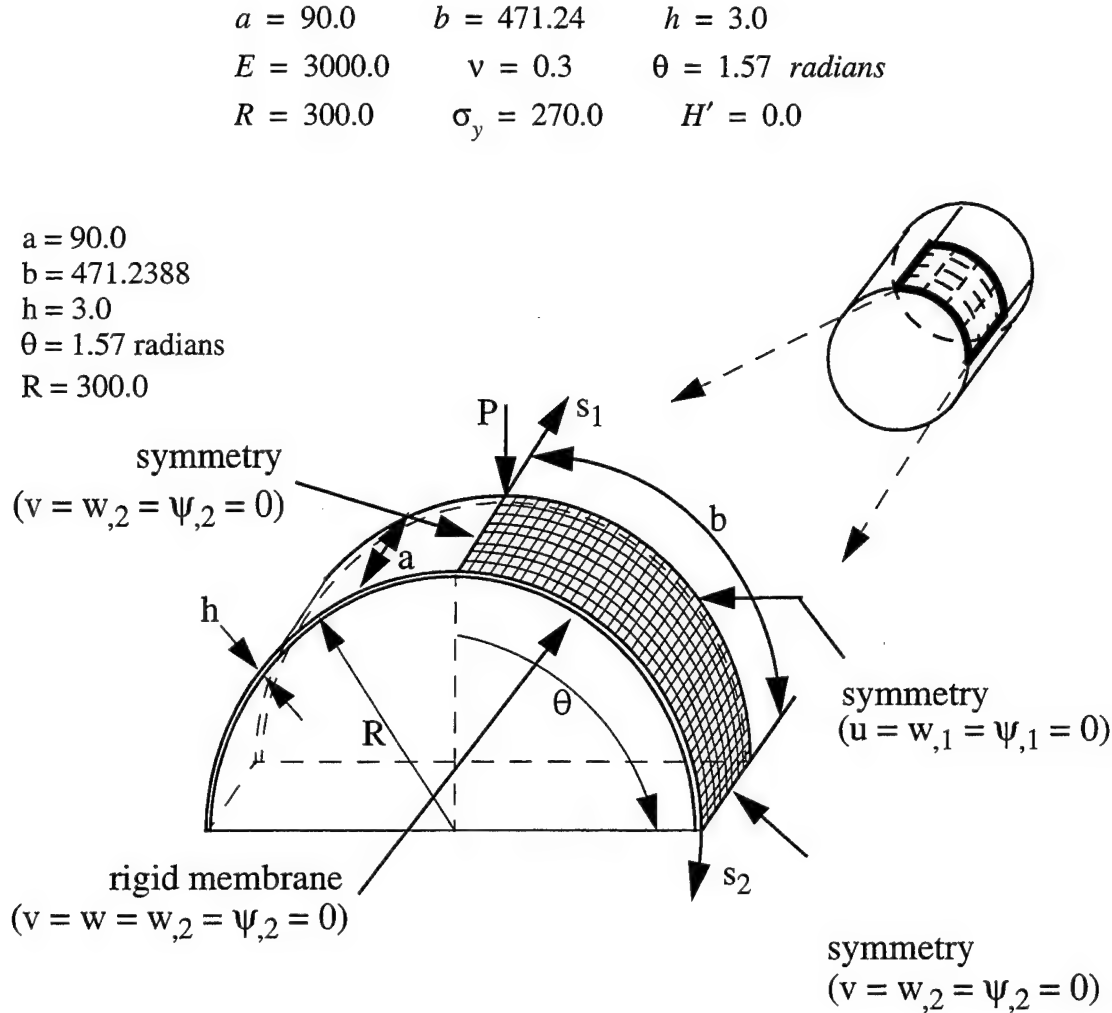


Figure 6.14 Pinched, Perfectly Plastic, Isotropic Cylinder Bounded with Rigid Membranes under Transverse Point Loads.

Table 6.4 shows the predicted equilibrium load for the prescribed transverse displacement for the C201 theories and compared to the results from Simo & Kennedy [207]. The predicted equilibrium load versus prescribed transverse displacement is shown in Figure 6.15 for the C201 & C211 theories and compared with the results published by Simo & Kennedy.

Simo & Kennedy noted that the step-like regions (see Figure 6.15) in their load-displacement curve is due to snap-through mechanisms which arise due to the relatively coarse mesh in comparison to the width of the indentation ridge forming about point load upon loading [207:162-164]. In other words, such regions are due to the nature in which the ridge, or the point of inflection point of the cylinder, passes through the elements as the inflection point moves outward.

This inflection point, in their model, is of equal width to or below the element width. The evolving plastic zones for the convex surface of the pinched cylinder are shown in Figures 6.16-6.20. The corresponding evolving plastic zones for the middle surface of the pinched cylinder, at $w = 150$ and $w = 250$, are shown in Figures 6.21-6.22.

Table 6.4: Predicted Equilibrium Load (10^3 Units) for Prescribed Transverse Displacement of Pinched, Perfectly Plastic, Isotropic Cylinder

Disp	Ref [207]	C201	C211
25.0	0.119	0.365	0.142
50.0	0.201	0.534	0.253
75.0	0.298	0.796	0.296
100.0	0.391	1.068	0.361
125.0	0.452	1.565	0.438
150.0	0.524	N/A	0.531
175.0	0.629	4.823	0.657
200.0	0.927	N/A	0.950
225.0	1.427	N/A	1.587
250.0	2.376	N/A	2.553
275.0	4.976	N/A	5.112

It should be noted that the stress develops along the hinge line of the cylinder (where the cylinder develops an inflection point) and where the load is applied. By the end of the analysis, as the cylinder undergoes pure membrane response, the entire convex surface is behaving plastically. However, the middle surface (Figures 6.21-6.22) is still behaving elastically (except at the load point and the point of inflection in Figure 6.22). For a nonlinear, displacement-control solution, with a prescribed tolerance, $\nabla = 0.005$, and 11 prescribed transverse displacements of 25.0, the C201 theory required 23663.2 CPUseconds to generate a solution while the C211 theory required 127891.3 CPU seconds. The

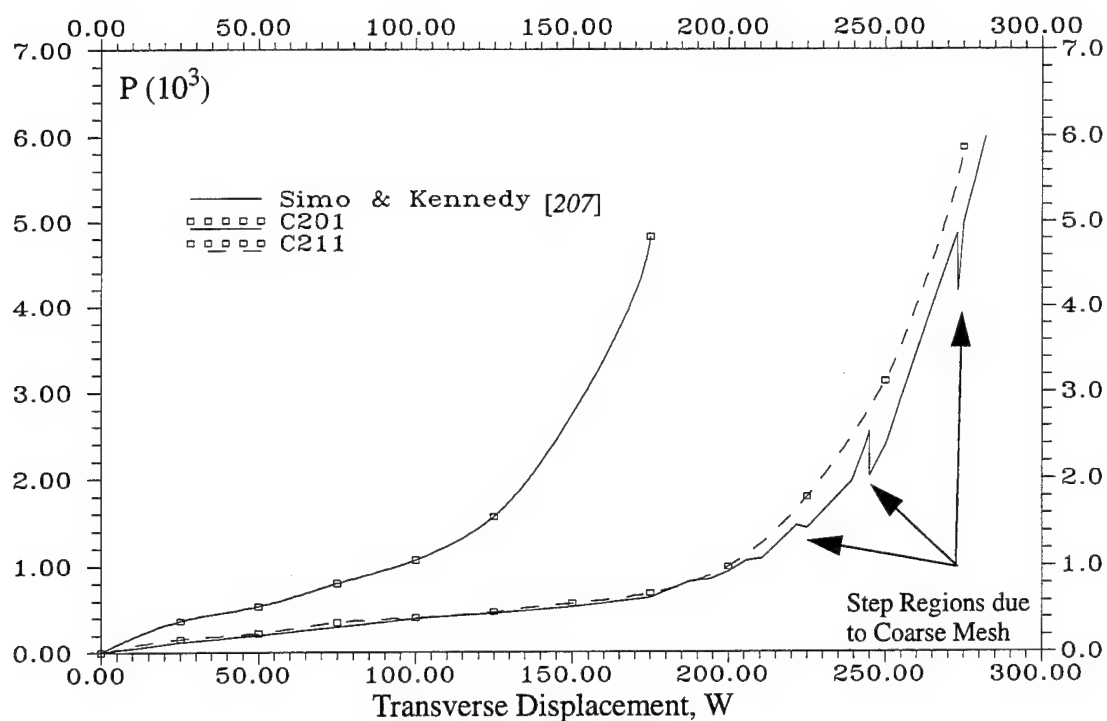


Figure 6.15 Predicted Equilibrium Load for Prescribed Transverse Displacement for Pinched, Perfectly Plastic, Isotropic Cylinder with Rigid Membrane

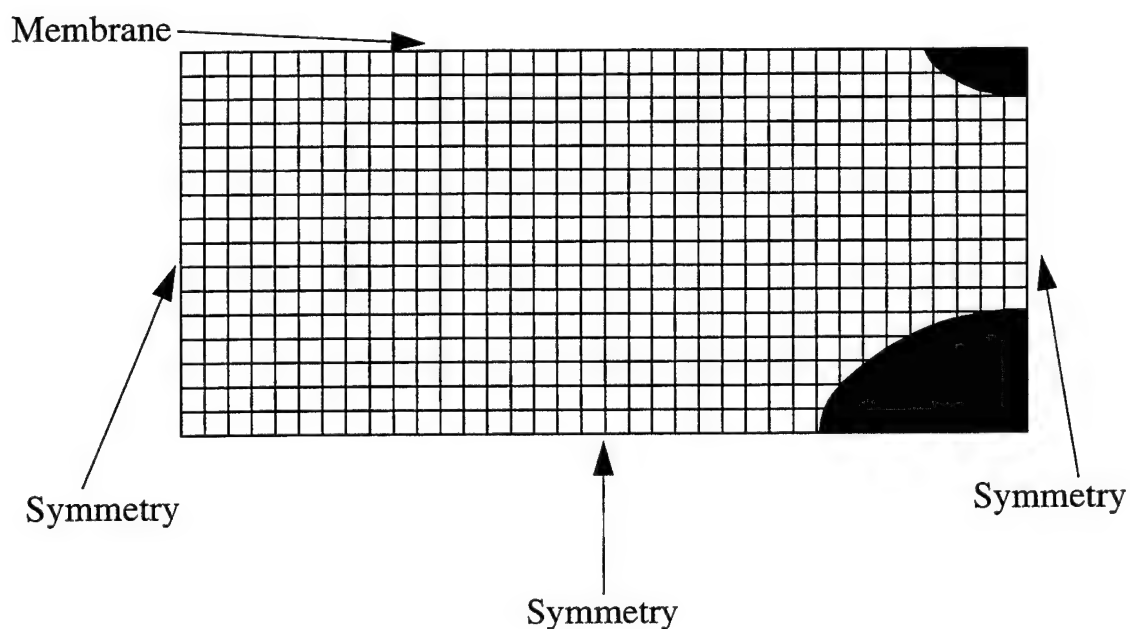


Figure 6.16 Evolution of Plastic Zone for Convex Surface in Pinched, Perfectly Plastic, Isotropic Cylinder: $w = 50.0$

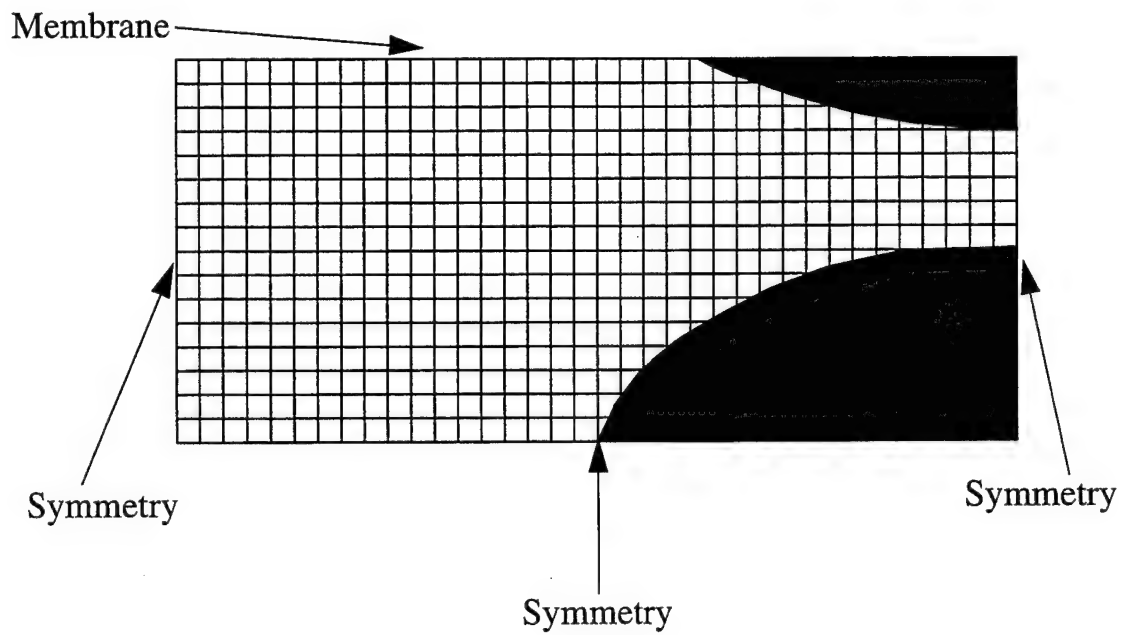


Figure 6.17 Evolution of Plastic Zone for Convex Surface in Pinched, Perfectly Plastic, Isotropic Cylinder: $w = 100.0$

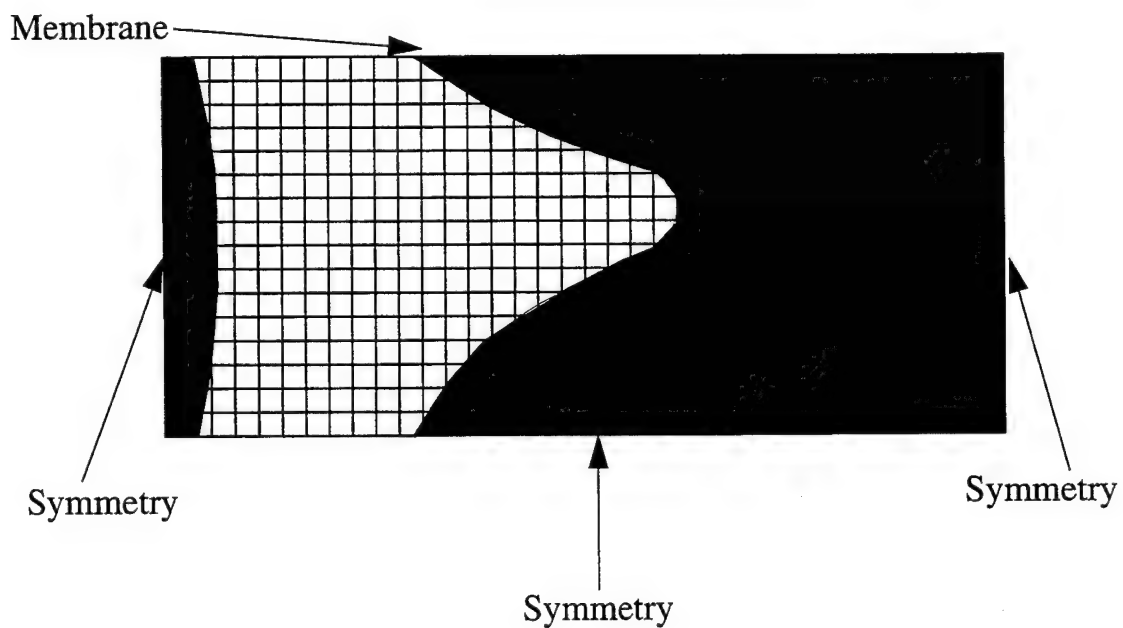


Figure 6.18 Evolution of Plastic Zone for Convex Surface in Pinched, Perfectly Plastic, Isotropic Cylinder: $w = 150.0$

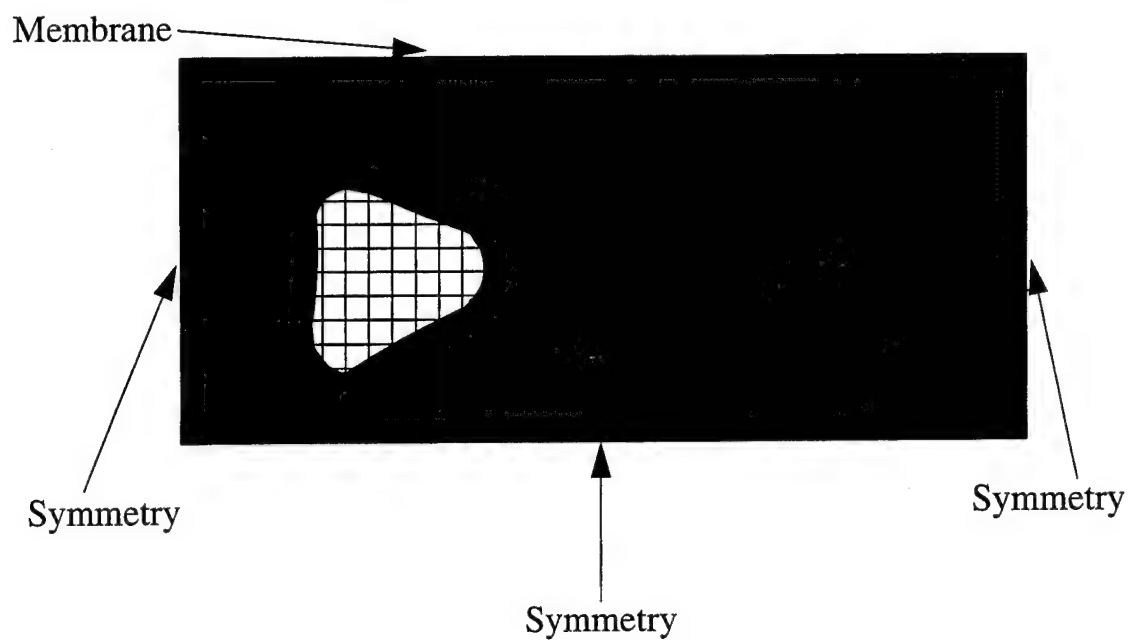


Figure 6.19 Evolution of Plastic Zone for Convex Surface in Pinched, Perfectly Plastic, Isotropic Cylinder: $w = 200$

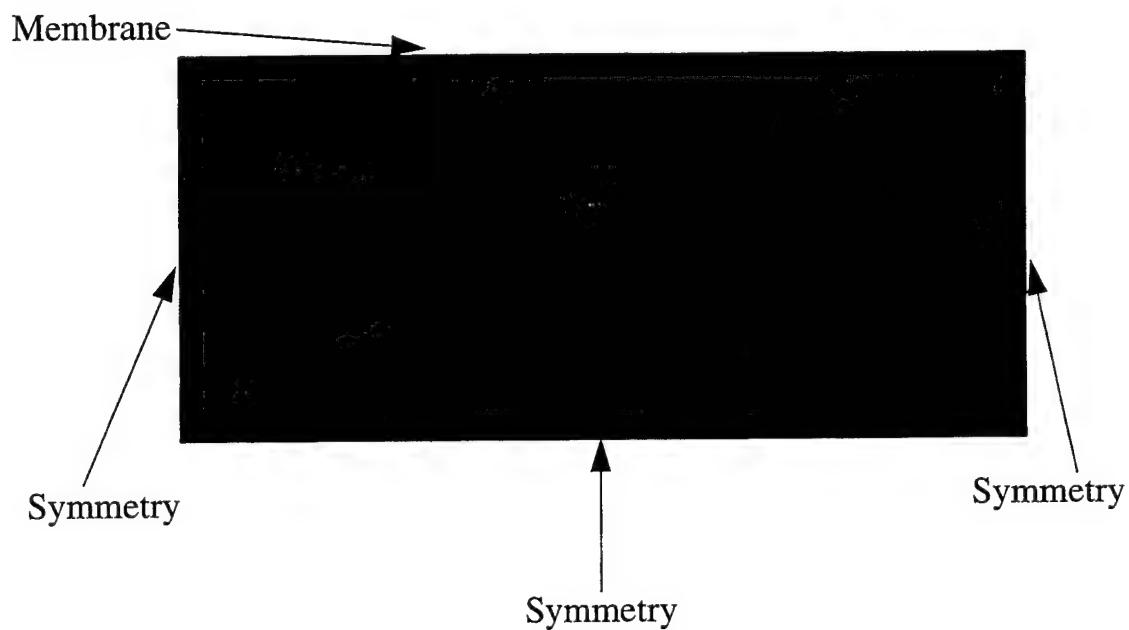


Figure 6.20 Evolution of Plastic Zone for Convex Surface in Pinched, Perfectly Plastic, Isotropic Cylinder: $w = 250$

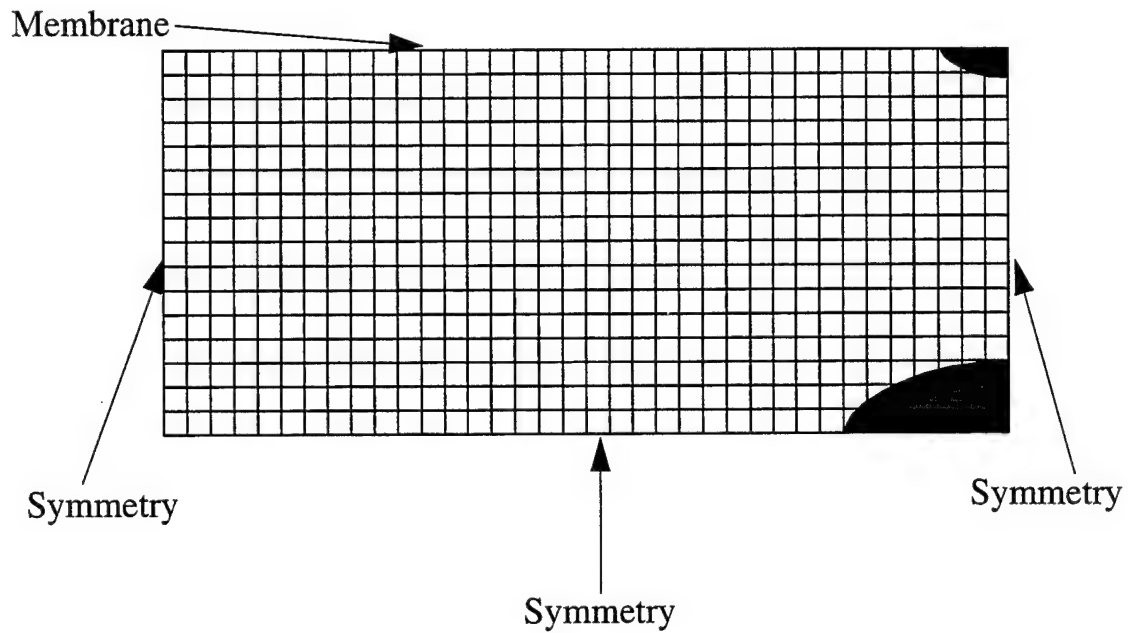


Figure 6.21 Evolution of Plastic Zone for Middle Surface in Pinched, Perfectly Plastic, Isotropic Cylinder: $w = 150$

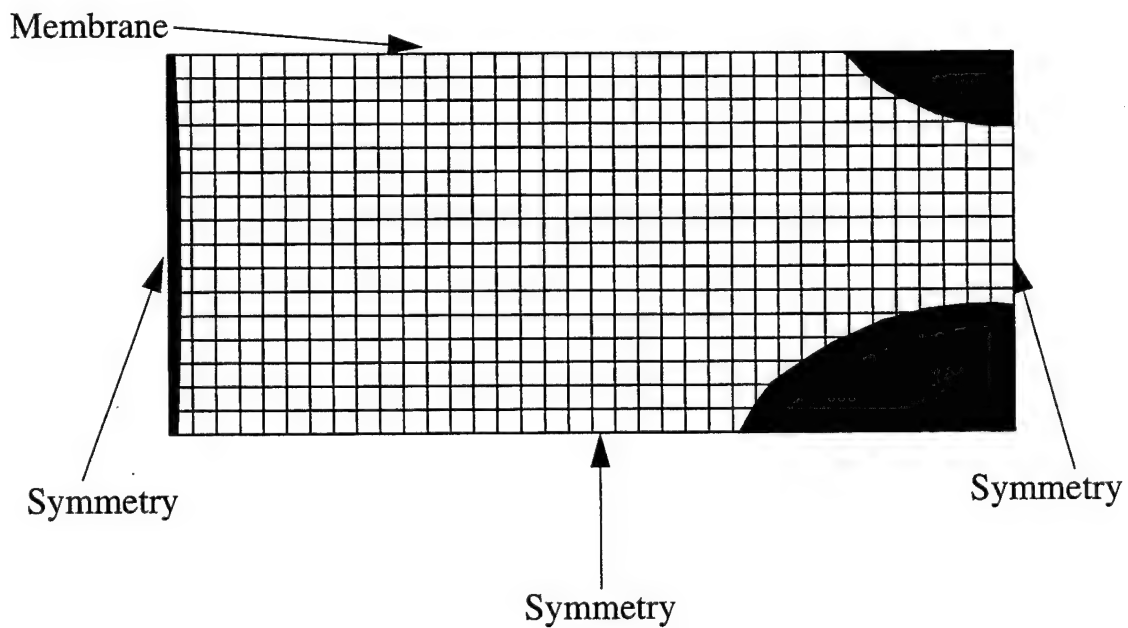


Figure 6.22 Evolution of Plastic Zone for Middle Surface in Pinched, Perfectly Plastic, Isotropic Cylinder: $w = 250$

increase in CPU time is attributed to the significant requirement of resolving the stress field (an eight increment step - Eq (G.4)) for each Gauss point in each layer (for an isotropic shell the default is eight layers).

6.4 Hinged, Perfectly-Plastic, Isotropic, Spherical Cap with Apex Load

A logical extension of the elastic-plastic analysis is to consider a spherical shell geometry. One well documented problem is the elastic-plastic model of the isotropic spherical shell cap discussed in Section 5.6. This problem has been previously analyzed by several authors [166,238], the first being Argyris et. al. [8]. It is an 0.04-cm thick isotropic spherical shell cap, hinged on the boundaries with a transverse point load at the apex. The shell is considered to be perfectly plastic and has a 12.09-cm radius of curvature with a depth of 2.181-cm. Figure 6.23 shows the spherical shell problem. The mesh shown is for one quadrant only, to demonstrate the mesh density, not the actual mesh used. Refer to Section 5.6 for the discussion regarding the singularity condition of a point load applied at the apex of a spherical shell. The boundary conditions and material properties are listed below.

$$\begin{aligned}
 s_1 &= 0.0 \text{ cm} & u = w_{,1} = \psi_1 &= 0 & (\text{symmetry}) \\
 s_2 &= 0.0 \text{ cm} & v = w_{,2} = \psi_2 &= 0 & (\text{symmetry}) \\
 s_1 &= \pm 2.301 \text{ cm} & u = v = w = \psi_2 &= 0 & (\text{hinged}) \\
 s_2 &= \pm 2.301 \text{ cm} & u = v = w = \psi_1 &= 0 & (\text{hinged}) \\
 a = b &= 4.60 \text{ cm} & R_1 = R_2 = R &= 12.09 \text{ cm} & h = 0.04 \text{ cm} \\
 E &= 6.895 \times 10^{10} \text{ Pa} & \nu &= 0.3 & \theta_1 = \theta_2 = \theta = 1.57 \text{ radians} \\
 L &= 4.753 \text{ cm} & \delta &= 2.181 \text{ cm} & \sigma_Y = 1.379 \times 10^{10} \text{ psi} & H' = 0.0
 \end{aligned}$$

The spherical shell cap is modelled with a 12×12 element mesh for the entire shell and eight layers are used to model through-the-thickness plasticity. The results are compared to the TRUMP solution of [8]. Table 6.5 shows the predicted equilibrium loads for prescribed increments of transverse displacement for the S2XX theories. Figure 6.24 shows the equilibrium curves for the S200, S201, and S211 theories as compared to the results from Argyris et. al. [8] and Parish [166].

As expected the elastic perfectly-plastic (S211) shell exhibits a greater flexible response than the purely elastic shell. This flexibility is shown by a reduction in the snap load, and an increase in displacement during the

$$\begin{aligned} a &= b = 4.60 \text{ cm} \\ R_1 &= R_2 = R = 12.09 \text{ cm} \\ \theta_1 &= \theta_2 = \theta = 0.19024 \text{ radians} \\ L &= 4.753 \text{ cm} \\ h &= 0.04 \text{ cm} \end{aligned}$$

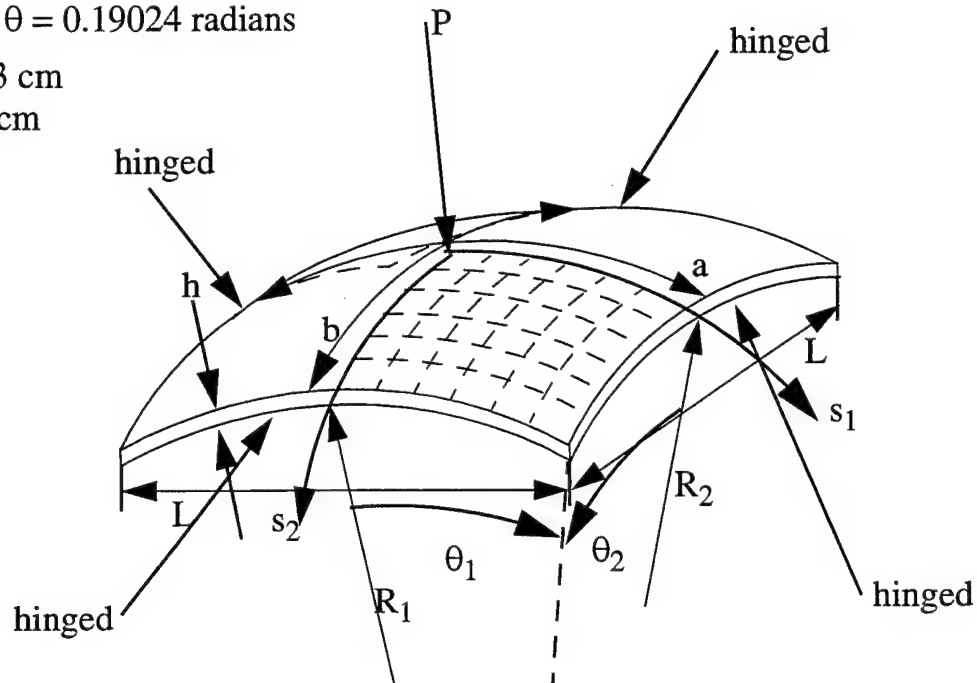


Figure 6.23 Hinged Apex-Loaded Isotropic Elastic Perfectly-Plastic Spherical Cap

snap-through and recovery phases. Figures 6.25-6.27 show the evolution of the plastic zones on the concave surface of the spherical shell. The plastic zones are determined by the presence of plastic strain at the Gauss points, hence the ability for part of an element to be behaving elastically and plastically. As expected, plasticity develops early at the apex of the shell, where the incremental displacement is applied, and at the corners due to the hinged boundary conditions from both sides. With further displacement, bending stresses develop and increase in magnitude as does the plasticity on the shell. At the point of snapping (Figure 6.26) approximately 18% of the shell surface is exhibiting strains greater than 2.5%. However, Figures 6.28-6.29 show how little plasticity develops at the shell's midsurface. For the same point of the onset of snapping, only 6% the shell's midsurface is exhibiting strains greater than 2.5%. This correlates well with results pub-

lished by Yuan [238]. The author's equilibrium load versus transverse displacement results agree very well with those published by Argyris and Parish. The inclusion of the transformation matrices for the elastic-plastic constitutive relations, along with the eight-noded quadratic element and the cubic-nonlinear HTSD theory yields a more flexible shell response than the TRUMP element of Argyris [8] or the QUAD4 element of Yuan [238]. For a nonlinear, displacement-control solution, with a prescribed tolerance, $\nabla = 0.01$, along with 30 prescribed transverse displacement increments (0.0238-cm), the S211 theory required 121547.0 CPU seconds. The increase in CPU time is again attributed to the significant requirement of resolving the stress field after plasticity occurs.

Table 6.5 Predicted Equilibrium Load (N) for Prescribed Transverse Displacement (cm) of a Hinged Isotropic Elastic-Perfectly Plastic Spherical Shell Cap

Disp	S200	S201	S211
0.0476	69.21	69.21	37.60
0.0954	85.19	84.78	46.73
0.1429	101.33	100.55	58.76
0.1905	124.84	123.93	72.51
0.2381	154.57	153.06	86.56
0.2858	184.82	182.58	102.13
0.3334	204.40	201.59	114.77
0.3810	192.12	189.85	127.08
0.4286	96.21	67.08	130.69
0.4365	-34.65	-40.52	N/A
0.4763	70.33	64.72	82.12
0.5001	N/A	N/A	-9.08
0.5239	N/A	N/A	-50.04
0.5477	N/A	N/A	20.10
0.5715	N/A	N/A	108.85

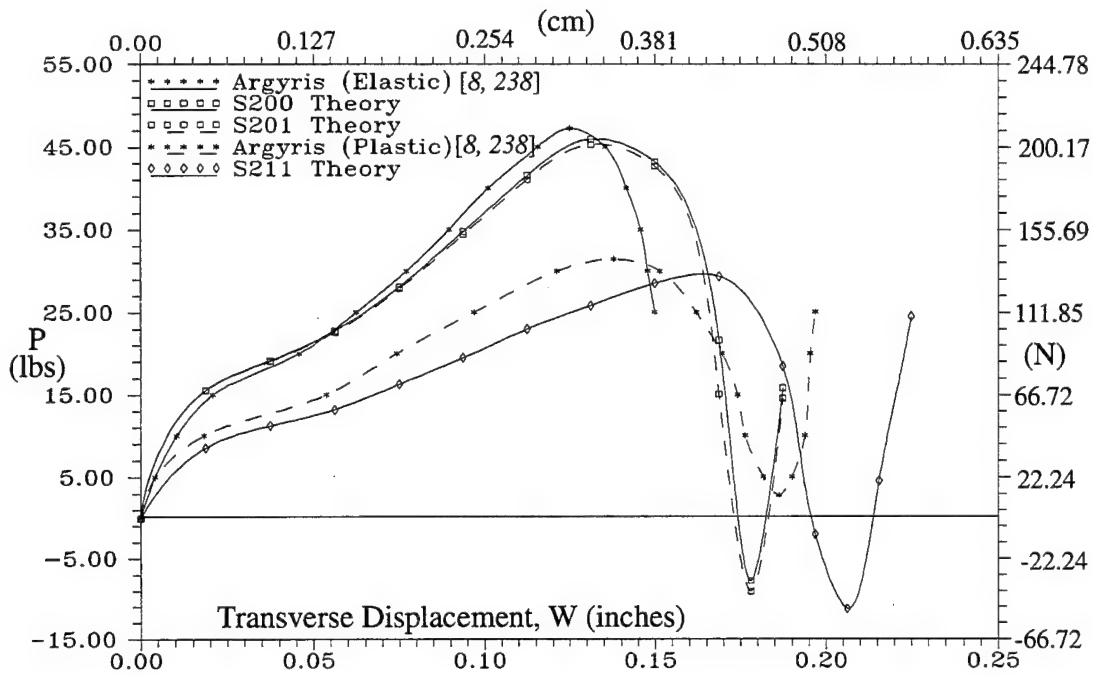


Figure 6.24 Load-Displacement Equilibrium Curves for Hinged Isotropic Elastic-Perfectly Plastic Spherical Shell Cap

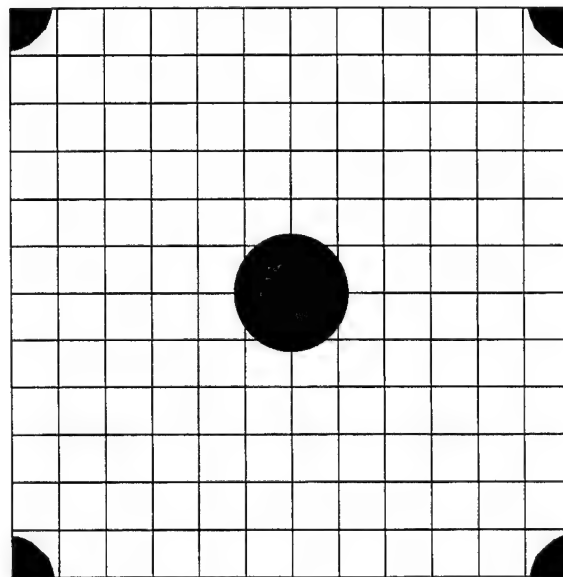


Figure 6.25 Evolution of Plastic Zones for Concave Surface of Hinged Isotropic Elastic-Perfectly Plastic Spherical Shell Cap: $w = 0.0478 \text{ cm}$

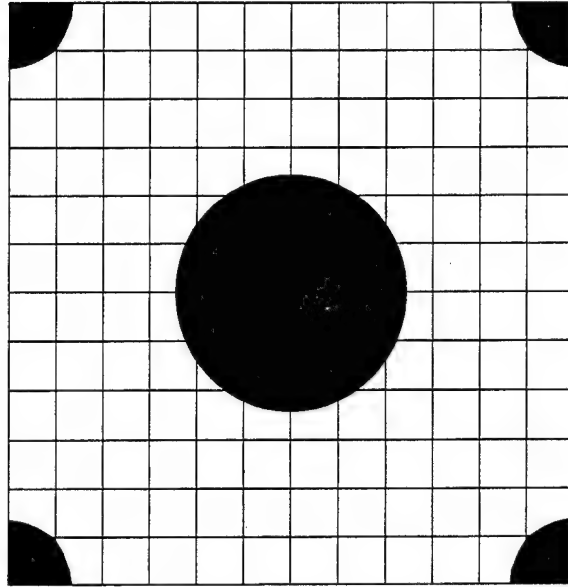


Figure 6.26 Evolution of Plastic Zones for Concave Surface of Hinged Isotropic Elastic-Perfectly Plastic Spherical Shell Cap: $w = 0.429 \text{ cm}$

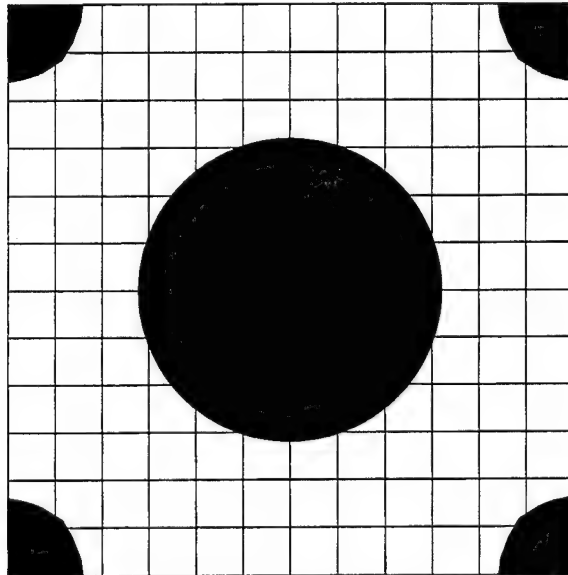


Figure 6.27 Evolution of Plastic Zones for Concave Surface of Hinged Isotropic Elastic-Perfectly Plastic Spherical Shell Cap: $w = 0.523 \text{ cm}$

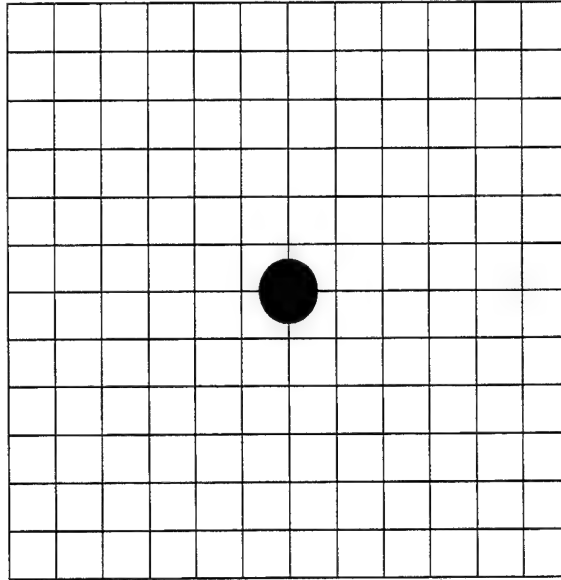


Figure 6.28 Evolution of Plastic Zones for Middle Surface of Hinged Isotropic Elastic-Perfectly Plastic Spherical Shell Cap: $w = 0.0478 \text{ cm}$

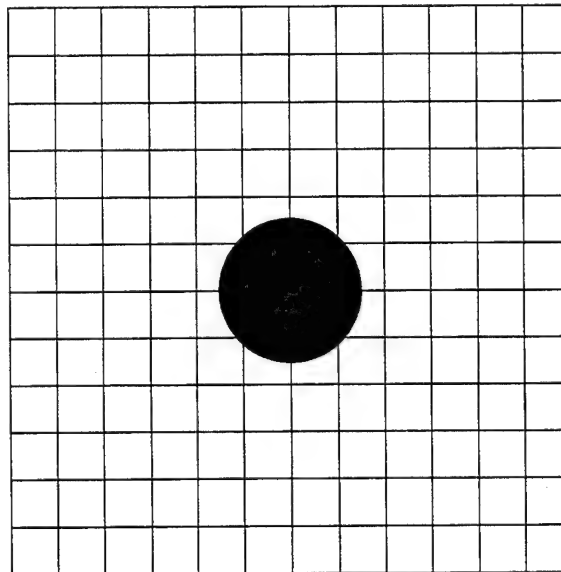


Figure 6.29 Evolution of Plastic Zones for Middle Surface of Hinged Isotropic Elastic-Perfectly Plastic Spherical Shell Cap: $w = 0.429 \text{ cm}$

6.5 Axially Loaded, Graphite Polyetherether Ketone (Gr/PEEK) Tensile Coupon

A relatively simple method of validating the theoretical and analytical models for laminated composite structures is to compare against experimental tensile coupon data. Gould [71] ran several Gr/Peek $\pm 45^\circ$ tensile coupon tests. He then compared an analytical model's predictions with these experimental results. We are only interested in comparing the author's analytical model with Gould's experimental data as a means of validating the nonlinear anisotropic material characterization, including a large strain formulation. The tensile coupon is 2.54-cm wide and 25.4-cm in length with a thickness of 2.134-cm. A ply lay-up of $[45/-45]_{4S}$ is modelled with a 2×20 element mesh. The finite element model is given in Figure 6.30. Since the ply lay-up consists of only $\pm 45^\circ$ oriented plies, symmetry cannot be used. The geometric and material properties are listed below:

$$\begin{aligned}
 s_1 &= b/2 & v &= w = w_{,1} = w_{,2} = \psi_1 = \psi_2 = 0 & (clamped) \\
 s_1 &= -b/2 & u &= v = w = w_{,1} = w_{,2} = \psi_1 = \psi_2 = 0 & (clamped) \\
 s_2 &= \pm a/2 \text{ in} & u &= v = w = w_{,1} = w_{,2} = \psi_1 = \psi_2 & (free) \\
 a &= 2.54 \text{ cm} & b &= 25.4 \text{ cm} & h = 2.134 \text{ cm} \\
 E_1 &= 13.552 \times 10^{10} \text{ Pa} & E_2 &= 1.069 \times 10^{10} \text{ Pa} \\
 G_{12} &= G_{13} = 5.602 \times 10^9 \text{ Pa} & G_{23} &= 4.482 \times 10^9 \text{ Pa} \\
 \nu_{12} &= 0.305 & \sigma_{Y_{11}} &= 2.199 \times 10^9 \text{ Pa} \\
 \sigma_{Y_{22}} &= 8.635 \times 10^7 \text{ Pa} & \sigma_{Y_{12}} &= 5.339 \times 10^7 \text{ Pa} \\
 k_1 &= 0.0 \text{ 1/Pa} & k_2 &= 1.827 \times 10^{-17} \text{ 1/Pa} \\
 k_3 &= 1.189 \times 10^{-16} \text{ 1/Pa} & n &= 2.862
 \end{aligned}$$

The values for $\sigma_{Y_{11}}$, $\sigma_{Y_{22}}$, $\sigma_{Y_{12}}$, k_1 , k_2 , k_3 , n for the Graphite/PEEK material referenced in [71] were determined from the experimental stress-strain curves shown in Figures 6.31-6.33. Predicted load versus prescribed results are shown in Table 6.6. Figure 6.34 shows the predicted equilibrium load vs prescribed axial displacement for the P200,

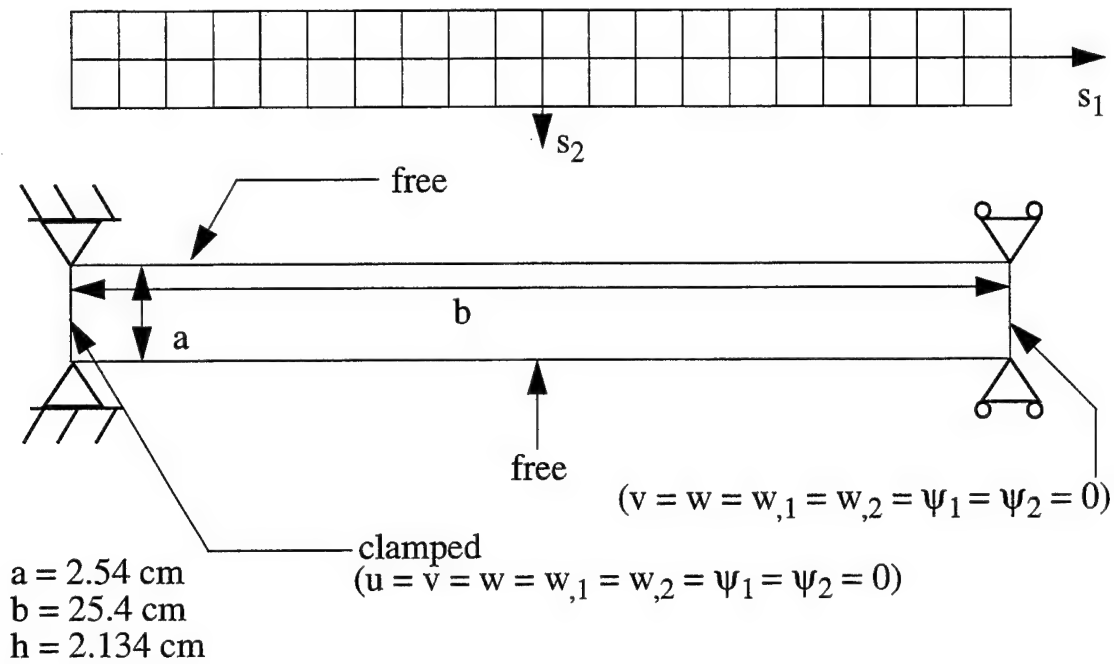


Figure 6.30 $\pm 45^\circ$ Axially Loaded Gr/PEEK Tensile Coupon

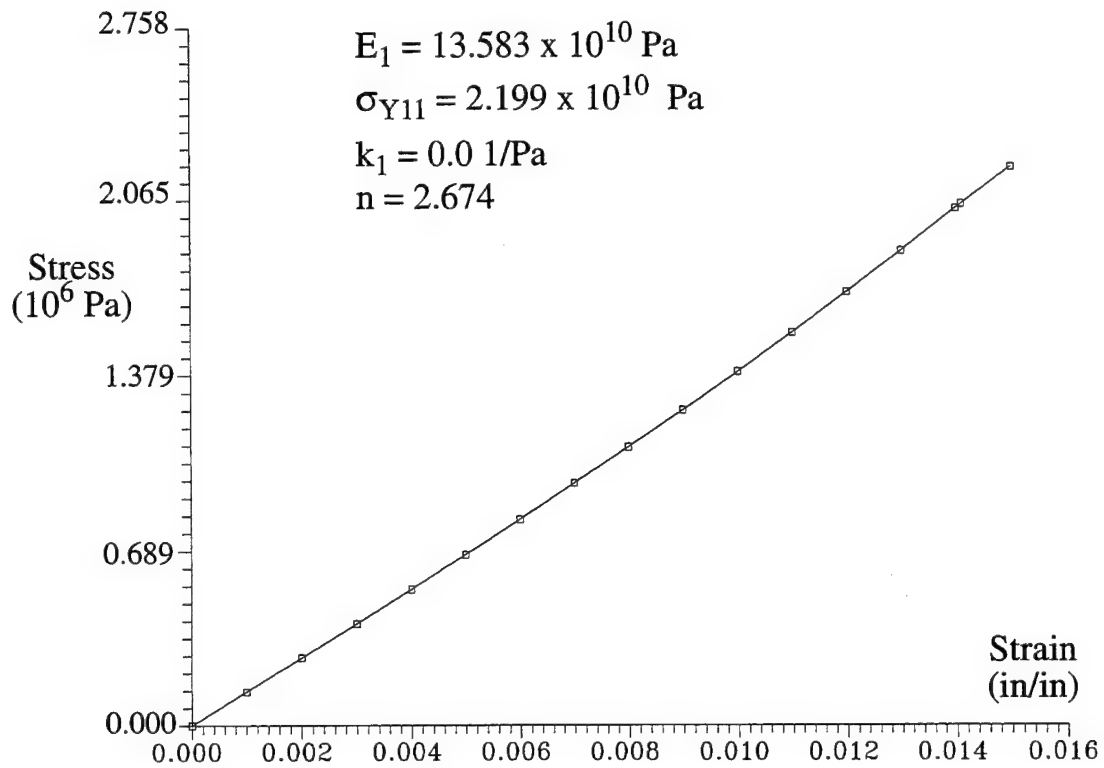


Figure 6.31 Experimental $\sigma_{11} - \epsilon_{11}$ Curves for Gr/PEEK [71]

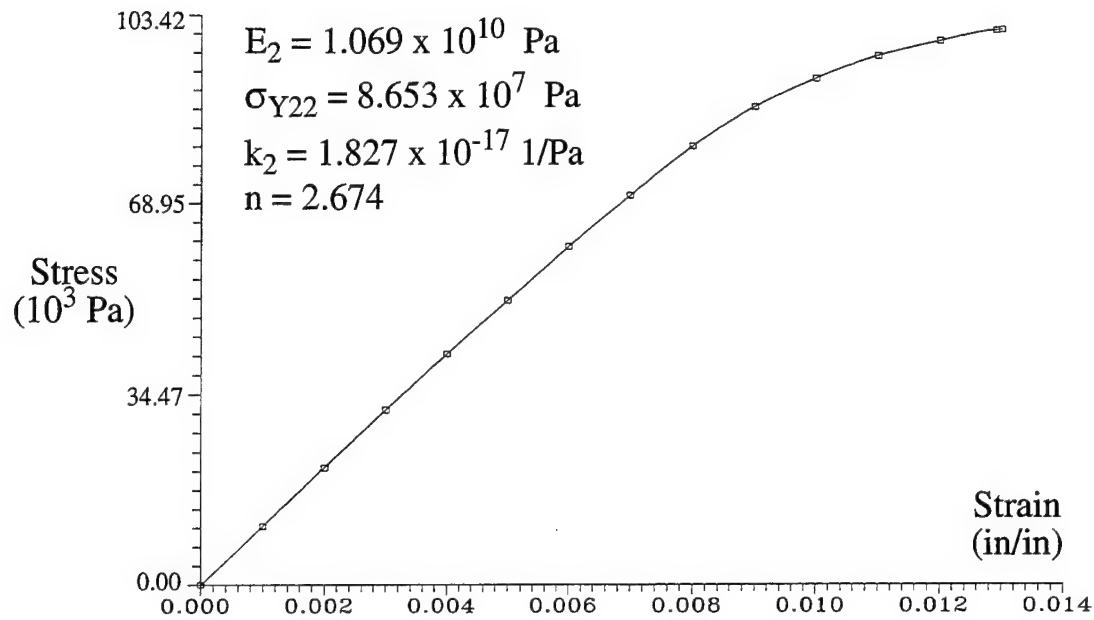


Figure 6.32 Experimental $\sigma_{22} - \epsilon_{22}$ Curves for Gr/PEEK [71]

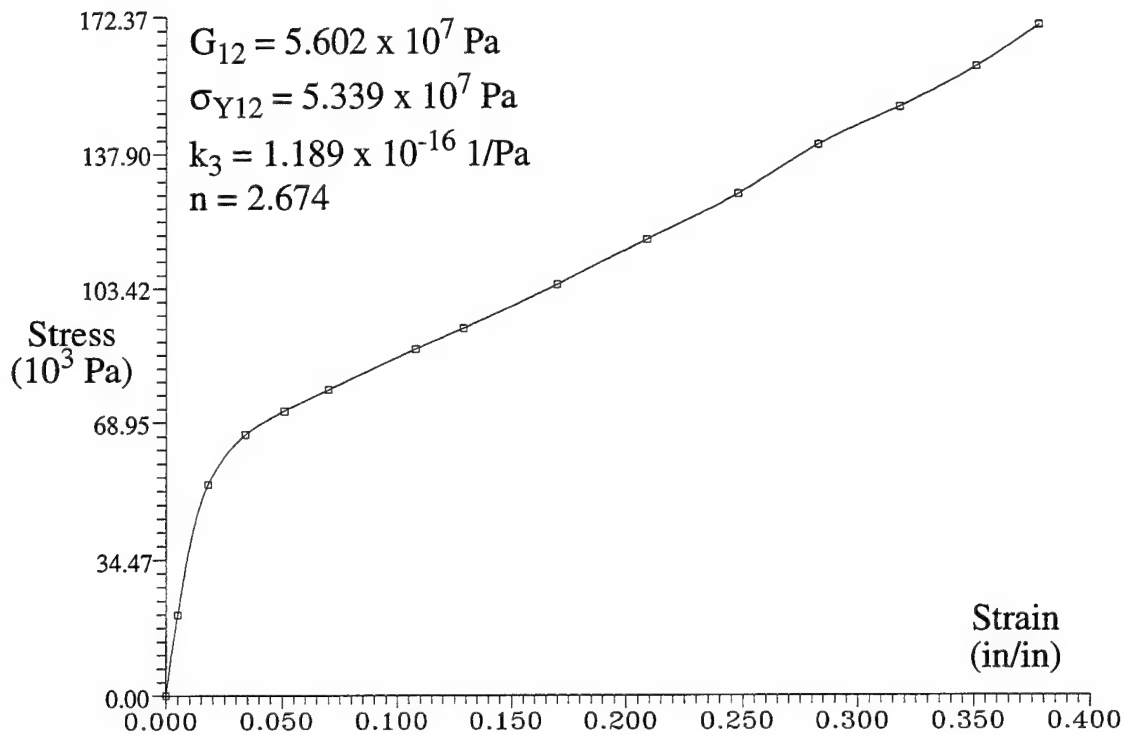


Figure 6.33 Experimental $\sigma_{12} - \epsilon_{12}$ Curves for Gr/PEEK [71]

Table 6.6 Predicted Equilibrium Load (10^3 N) for Prescribed Axial Displacement (cm) of a 2.134-cm Clamped-Free Quasi-Isotropic Gr/PEEK Tensile Coupon

Disp	Gould*	P200	P201	P210	P211
0.254	6.222	10.699	7.257	5.931	5.931
0.508	7.281	20.204	14.489	7.908	7.739
0.762	8.246	29.221	21.650	8.969	8.703
1.016	8.945	N/A	29.211	9.810	9.568
1.270	9.567	N/A	N/A	11.455	10.420
1.524	10.124	N/A	N/A	12.309	11.313
1.778	11.090	N/A	N/A	13.223	12.002
2.032	11.760	N/A	N/A	14.198	12.979
2.286	12.558	N/A	N/A	15.169	13.832
2.540	13.466	N/A	N/A	16.071	14.685
2.794	14.198	N/A	N/A	17.142	15.538
3.048	15.173	N/A	N/A	18.158	16.513
3.302	16.026	N/A	N/A	19.072	17.366
3.556	16.878	N/A	N/A	20.109	18.095
3.810	17.793	N/A	N/A	21.022	19.662
4.064	18.707	N/A	N/A	22.363	19.682
4.318	19.438	N/A	N/A	22.362	20.665
4.572	20.230	N/A	N/A	N/A	N/A
4.826	20.657	N/A	N/A	N/A	N/A
5.080	20.778	N/A	N/A	N/A	N/A
5.205	20.596	N/A	N/A	N/A	N/A

*See Ref [71].

P201, P210, P211 theories and how these various theories compared with Gould's experimental data. It should be noted that the P210 theory was a purely an exercise in code development and was never used again in this research effort. As expected, the P211 theory provides the closest prediction to the experimental results from Gould. The evolving plastic zones of the tensile cou-

pon model, for the middle and upper surfaces, are shown in Figures 6.35-6.37. The solution for P211 stopped at $u = 4.572\text{-cm}$ (Figure 6.34). This was due to the significant reduction in stiffness by the presence of plastically behaving Gauss points across the width of the tensile coupon (Figure 6.37). Up until this increment of displacement, the plasticity provided a "softening" or reduction in equilibrium load for each prescribed increment of displacement in the coupon's response. Once plasticity was spread across the width, the loss in stiffness was so significant, for the step size of displacement increment, that the code diverged. A refinement in the mesh in this region, and a reduction in the displacement increment beyond $u = 4.064\text{-cm}$ would provide a means of progressing beyond this point. It is interesting to note that only 7.5% of the coupon is exhibiting strains greater than 2.125%.

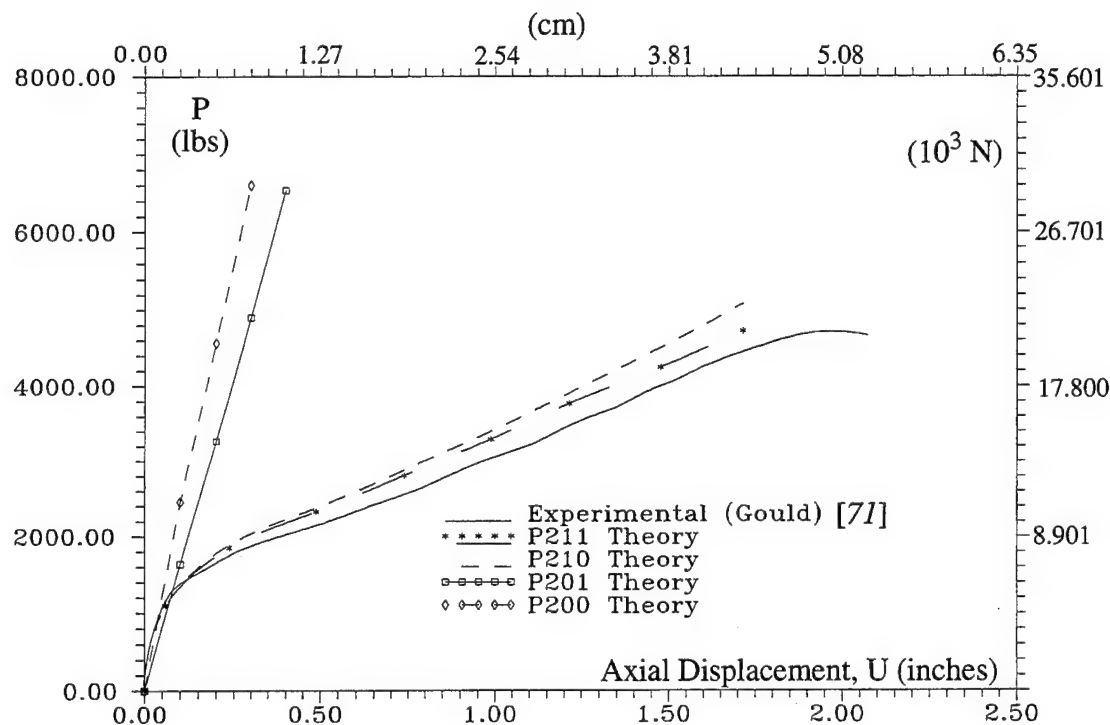


Figure 6.34 Predicted Equilibrium Load for Prescribed Axial Displacement for Gr/PEEK Tensile Coupon - Experimental [7], PX11 Theories

Because of the $\pm 45^\circ$ orientation, plasticity occurs almost instantaneously on the outer and middle surfaces, with only a negligible difference in the amount of area behaving plastically. From Figures 6.34-6.37 one would expect the load-displacement curve to be

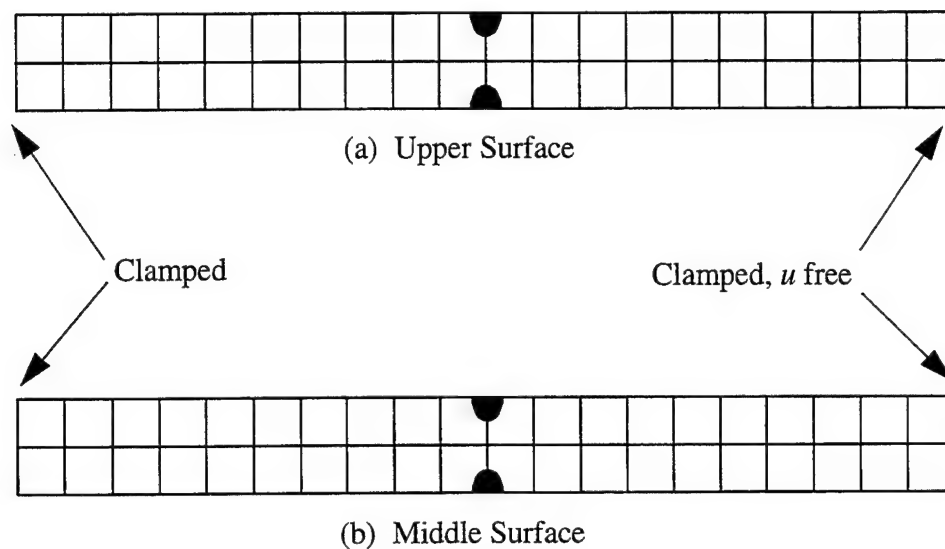


Figure 6.35 Evolution of Plastic Zones in Gr/PEEK Tensile Coupon: $u = 0.254$ cm

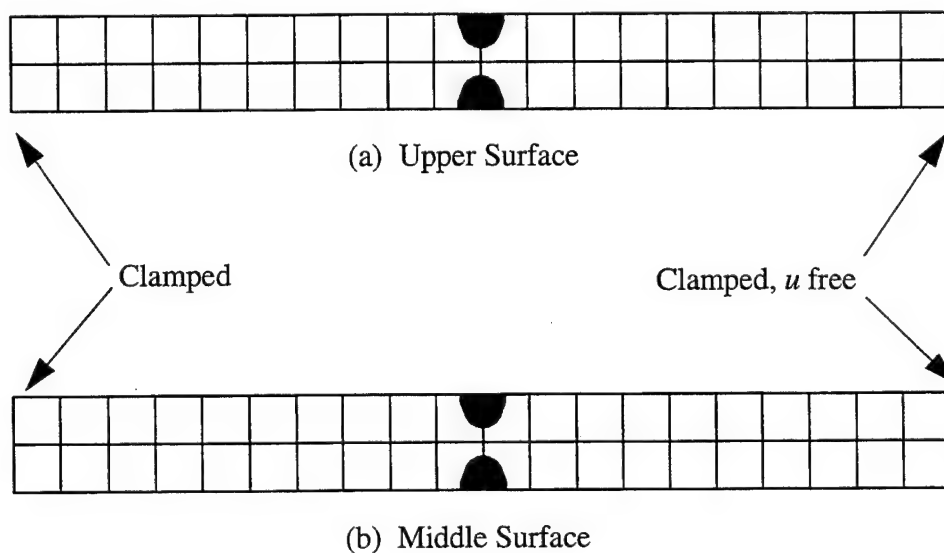


Figure 6.36 Evolution of Plastic Zones in Gr/PEEK Tensile Coupon: $u = 2.54$ cm

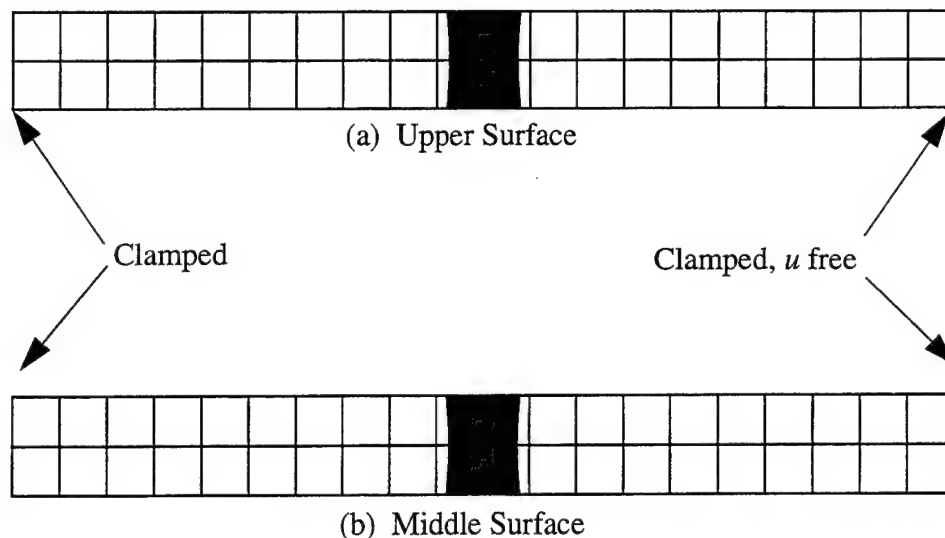


Figure 6.37 Evolution of Plastic Zones in Gr/PEEK Tensile Coupon: $u = 4.572 \text{ cm}$

significantly altered from the elastic solution, which is observed in Figure 6.34. This "material softening" effect allows for a significantly reduced ultimate load (predicted failure) and an increase in displacement. The "material softening" effect is attributed to the highly nonlinear shear stress-strain curve. The yield stress for $\sigma_{12} - \epsilon_{12}$ curve is 2.43% the magnitude of the yield stress for the $\sigma_{12} - \epsilon_{12}$ curve. Note: due to the restraints shown in Figure 6.30 the stress field is non-homogeneous producing the varying stress results shown in Figures 6.35-6.37. Thus, for a $\pm 45^\circ$ coupon, it is not unexpected to see a significant dependence on the shear strain material properties. For a nonlinear, displacement-control solution, with a prescribed tolerance, $\nabla = 0.001$, along with 18 prescribed axial displacements of 0.254-cm , the P201 theory required 32912.3 CPU seconds while the P211 theory required 78341.9 CPU seconds. The displacement increments were one-quarter to one-half the magnitude of the displacement increments used for the P201 analysis. The increase in CPU time is again attributed to the significant requirement of resolving the stress field after plasticity occurs.

6.6 Clamped-Free, Quasi-Isotropic, Cylindrical Shell Panel with Transverse Point Load

The first graphite epoxy, quasi-isotropic shell problem, chosen for this research, was a deep, cylindrical shell panel with a transverse point load. This problem demonstrates a severe test of an HTSD theory, including large strain theory, because of the shell's depth, thickness, and quasi-isotropic properties. A deep 30.48-cm radius quasi-isotropic 27.94-cm by 30.48-cm cylindrical shell panel was clamped at its lateral boundaries and free on the circumferential boundaries. The shell configuration is shown in Figure 6.38. The geometric and material properties are listed below

$$\begin{aligned} s_1 &= b/2 & u &= v = w = w_{,1} = w_{,2} = \psi_1 = \psi_2 = 0 & (\text{clamped}) \\ s_1 &= -b/2 & u &= v = w = w_{,1} = w_{,2} = \psi_1 = \psi_2 = 0 & (\text{clamped}) \\ s_2 &= \pm a/2 & u &= v = w = w_{,1} = w_{,2} = \psi_1 = \psi_2 & (\text{free}) \\ a &= 27.94 \text{ cm} & b &= 30.48 \text{ cm} & h &= 0.102 \text{ cm} \\ R &= 30.48 \text{ cm} & \theta &= 1.0 \text{ radians} \end{aligned}$$

Material AS4-3501 Graphite Epoxy

$$\begin{aligned} E_1 &= 14.114 \times 10^{10} \text{ Pa} & E_2 &= 9.246 \times 10^9 \text{ Pa} \\ G_{12} &= G_{13} = 5.958 \times 10^9 \text{ Pa} & G_{23} &= 2.966 \times 10^{10} \text{ Pa} \\ \nu_{12} &= 0.313 & \sigma_{Y_{11}} &= 1.553 \times 10^9 \text{ Pa} \\ \sigma_{Y_{22}} &= 4.548 \times 10^7 \text{ Pa} & \sigma_{Y_{12}} &= 3.932 \times 10^7 \text{ Pa} \\ k_1 &= 0.0 \text{ 1/Pa} & k_2 &= 7.753 \times 10^{-23} \text{ 1/Pa} \\ k_3 &= 1.606 \times 10^{-18} \text{ 1/Pa} & n &= 3.060 \\ \text{Ply Lay-ups} &[0/-45/45/90]_s \end{aligned}$$

The 0.102-cm thickness is significantly lesser than the 4.826-cm depth of the shell. Results for the transversely-loaded shell were compared with computational results of Tsai and Palazotto [225, 226] and those shown in Section 5.4. Palazotto and others [161-163] investigated shells of this configuration and compared static and dynamic results for different material properties and ply lay-ups. Their work was typically based on a 96 element model of a quadrant of the shell. This mesh was chosen based on the results of their convergence studies summarized in Section 5.4. Tsai and Palazotto [225] concluded that the 8×12 mesh results were acceptable considering

the CPU consumption was about 70% less than the 11×16 mesh. The finite element model is given in Figure 6.38. The values for σ_{Y11} , σ_{Y22} , σ_{Y12} , k_1 , k_2 , k_3 , n for AS4-3501 graphite epoxy were determined from the experimental stress-strain curves shown in Figures 6.39-6.41.

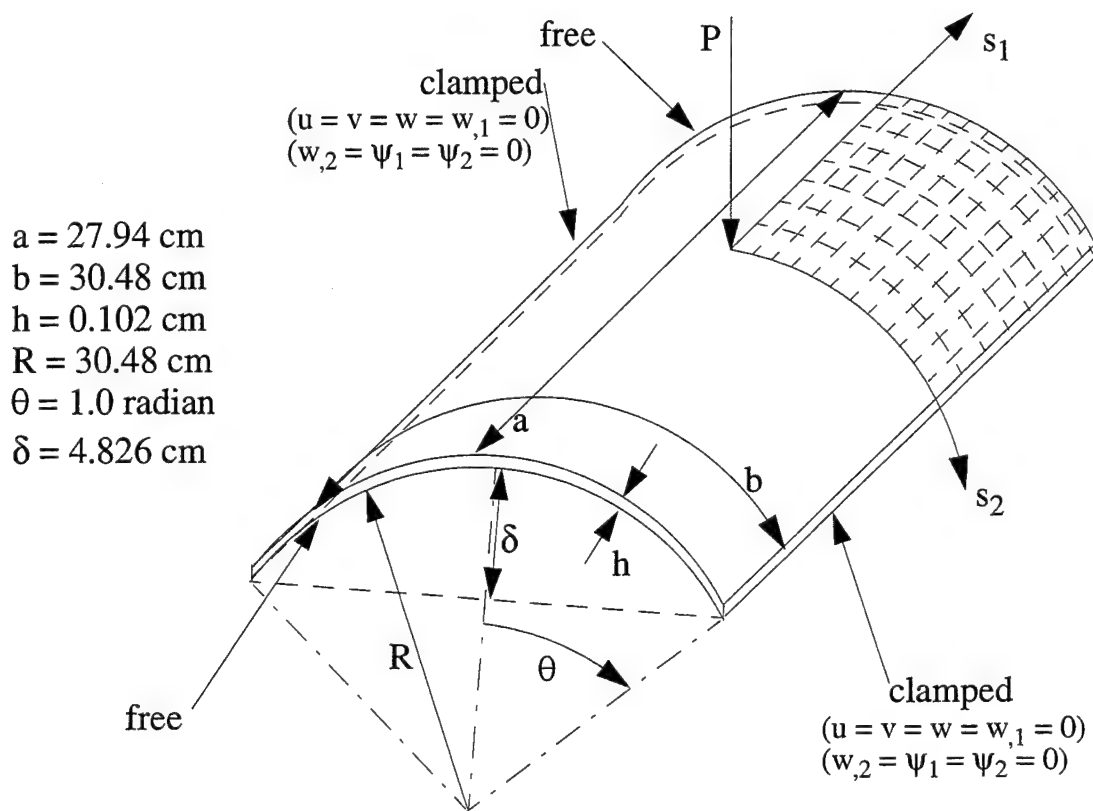


Figure 6.38 Clamped-Free Graphite Epoxy Shell with Transverse Point Load

Transverse load values versus displacements were computed for a ply lay-up of $[0/-45/45/90]_5$, using the modified Donnell (CDON), fully-nonlinear HTSD (C200), fully-nonlinear HTSD with material transformation (C201), and the fully-nonlinear HTSD with large strain (C211) theories. The cubic-nonlinear HTSD elemental codes predicted identical results, comparable to those of Tsai. Figure 6.42 shows the equilibrium values of transverse load for the CDON, C200, C201, and C211 theories. The elastic-plastic, cubic-nonlinear HTSD theory predicted a significantly more flexible structure with a marked difference in the snapping and snap-through behavior as compared to the cubic-nonlinear HTSD theories. As w increased, the fully-nonlinear codes predicted an increasingly more flexible structure for snapping and until snap-through is achieved. In

these portions of equilibrium, the shell is primarily in bending due to the clamped boundary conditions. Once snap-through is achieved, the shell then returns to a membrane-dominated behavior and acts under tension.

The elastic-plastic, cubic-nonlinear HTSD theory and both the elastic cubic-nonlinear HTSD theories predicted snapping occurs at approximately $w = 1.27\text{-cm}$. Palazotto et.al. [161, 225, 226] used the cubic-nonlinear HTSD theory developed by Dennis [48]. Their results showed snapping for many variations of material and geometric parameters [161:703-705]. The ratio of thickness to characteristic length of this problem is even smaller than any of the problems analyzed earlier. This ratio is equal to $1/300$. Therefore, transverse shear is expected to be totally insignificant. The effect of allowing the in-plane ϵ_i 's and σ_i 's to behave nonlinearly was expected to dramatically alter the global displacement response of the shell. This is significant when considering the effect of large rotations. For the ply lay-up of $[0/-45/45/90]_S$, ψ_2 reaches a maximum of 0.57 radians (32.66°) and 53% of the shell surface saw rotations of 0.26 radians (14.9°). The problem is further compounded by the predominance of a relatively weak material in the circumferential direction, compared to the lateral direction. The quasi-isotropic shell with the $[0/-45/45/90]_S$ ply lay-up has a ratio of $E_1/E_2 = 15$ and a transverse shear modulus less than E_2 . The primary cause of deformation for this problem is bending activity. The outer plies of this laminated panel are the only plies oriented in the transverse direction. This implies that 75% of the material of this shell has a stiffness in the circumferential direction that is significantly less than the outer plies. This panel is only 0.102-cm thick, thus, the outer plies may not be very effective in resisting bending, since they are so close to the mid-surface of the shell. With the lateral supports of this shell clamped, the final deformed shape of the shell exhibits both positive and negative curvatures. Thus, severity of bending is characterized by the distance between counterflexure points of the final deformed shape (see Figures 5.16 and 5.17). For this shell, this is a distance of about 5.08-cm. The bending activity of the clamped composite shell is more severe than that of the hinged isotropic shell.

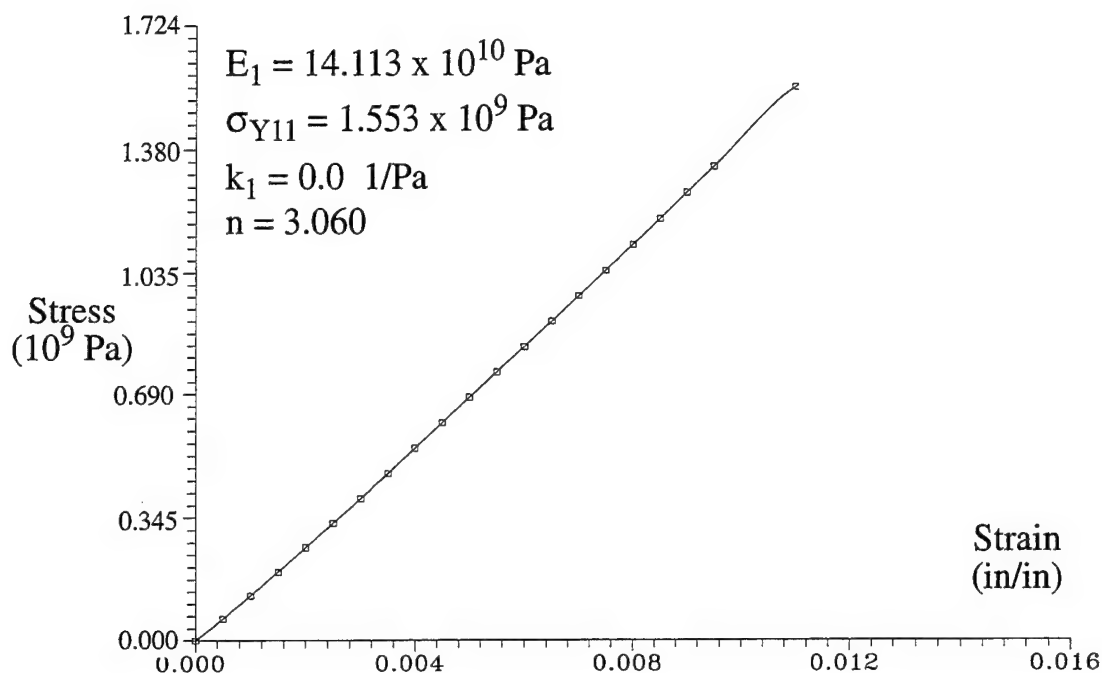


Figure 6.39 Experimental $\sigma_{11} - \epsilon_{11}$ Curves for Graphite Epoxy

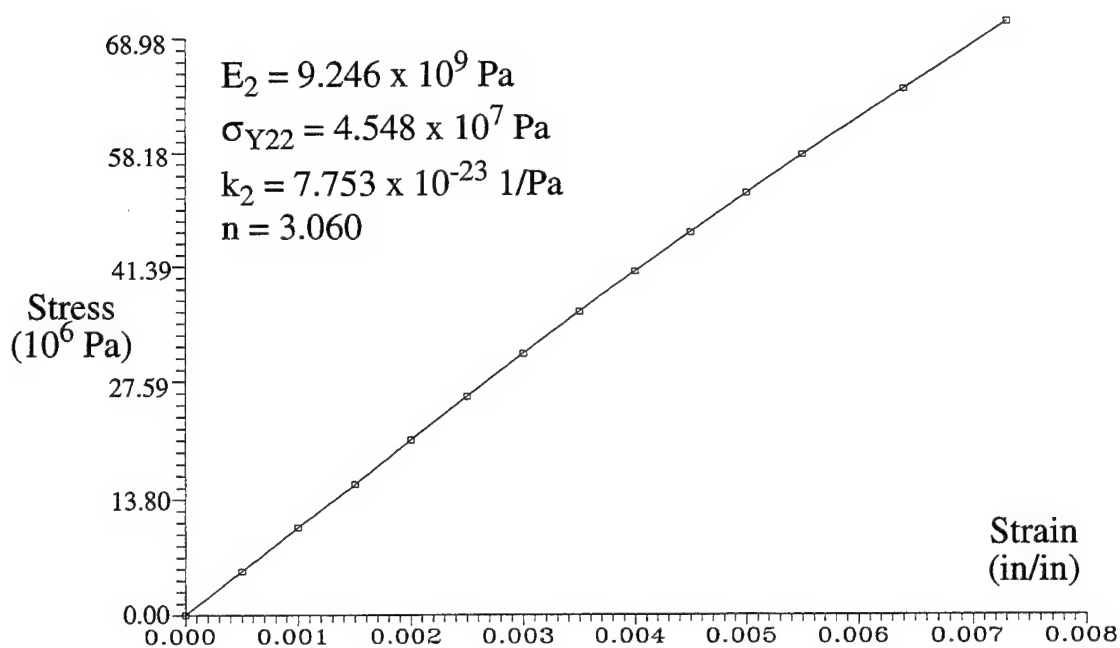


Figure 6.40 Experimental $\sigma_{22} - \epsilon_{22}$ Curves for Graphite Epoxy

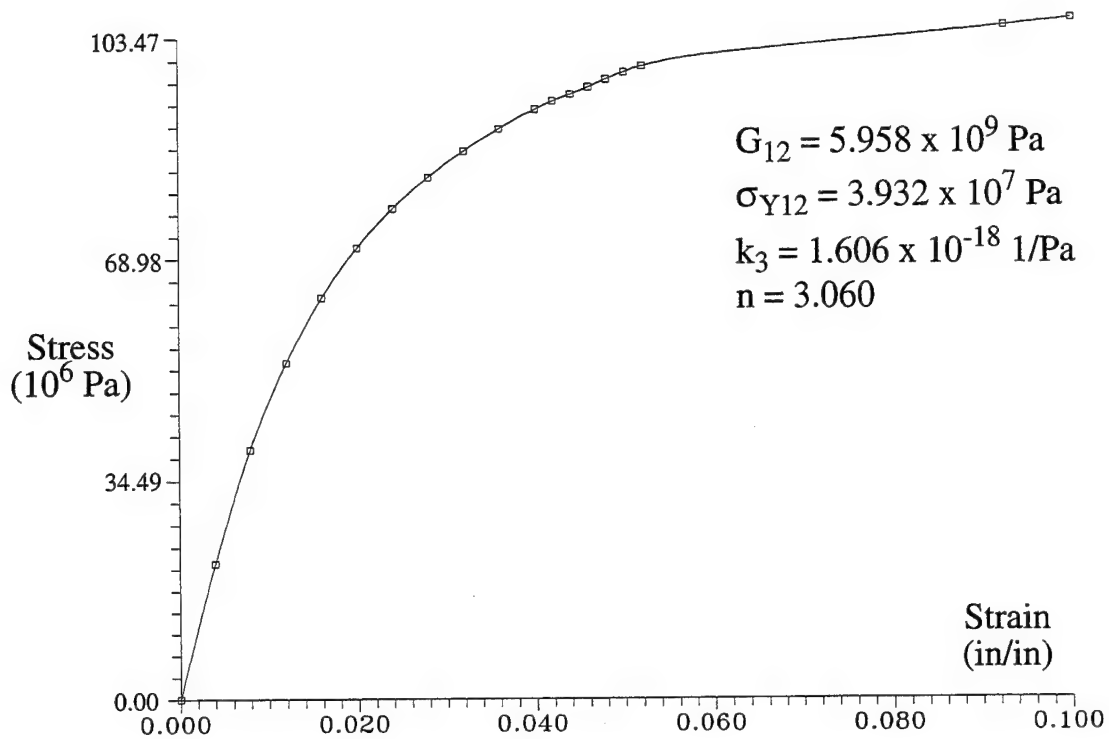


Figure 6.41 Experimental $\sigma_{12} - \epsilon_{12}$ Curves for Graphite Epoxy

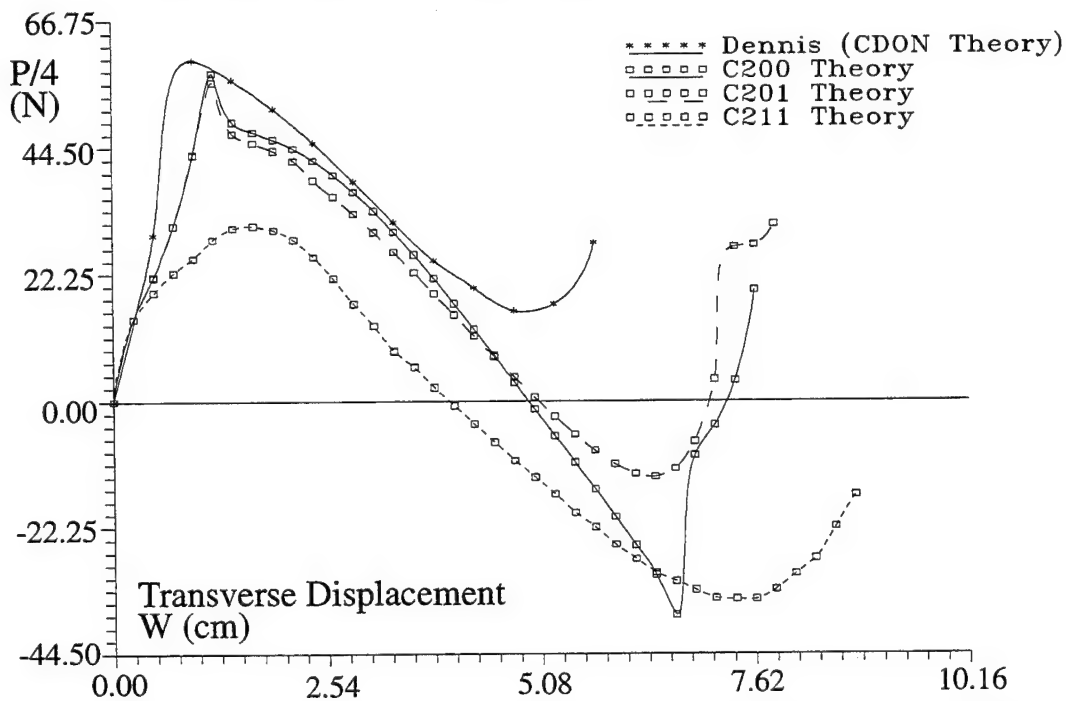


Figure 6.42 Equilibrium Path Comparisons for Transverse Point Loaded 0.04-Inch Clamped-Free Quasi-Isotropic Cylindrical Shell - CDON, C200, C201, & C211 Theories

Table 6.7 Predicted Transverse Equilibrium Load (N) for Prescribed Displacement (cm) of a 0.102-cm Clamped-Free Quasi-Isotropic Cylindrical Shell Panel, $[0/-45/45/90]_s$

Disp	CDON*	C200	C201	C211
0.4763	116.37	87.09	86.52	76.01
0.9525	239.42	172.52	173.22	100.22
1.4288	225.67	196.08	252.44	121.40
1.9050	205.37	183.51	175.79	119.97
2.3813	181.66	169.09	151.81	101.11
2.8575	154.20	147.11	131.53	67.82
3.3338	125.50	118.71	104.57	34.71
3.8100	98.35	85.84	75.22	9.43
4.2863	75.60	50.10	45.43	-16.20
4.7625	62.79	13.00	16.48	-41.83
5.2388	67.55	-5.69	-10.78	-65.51
5.7150	110.81	-43.12	-34.80	-87.15
6.1913	N/A	-101.69	-51.25	-111.43
6.6675	N/A	-150.61	-47.60	-126.74
7.1438	N/A	-16.86	14.92	-139.02
7.6200	N/A	77.39	109.32	-139.56
8.0963	N/A	N/A	N/A	-121.75
8.5723	N/A	N/A	N/A	-88.64
8.8108	N/A	N/A	N/A	-66.40

*Computed using Dennis' [51] modified Donnell theory code.

The inclusion of nonlinear material behavior for the in-plane coordinates is significant due to the relatively low yield stress for G_{12} (see Figure 6.41). The magnitude of the σ_{12Y} is 2.53% the magnitude of σ_{11Y} . Again, the nonlinear shear stiffness material properties have a significant effect on the shell's response when plasticity is included in the analysis. By allowing the material to behave nonlinearly, the reduction to bending stiffness is enhanced, thereby altering the global

equilibrium curve of the shell's displacement response toward a more flexible shell. The softening or reduction in the predicted equilibrium load for a prescribed transverse displacement is observed in Figure 6.42. The C211 theory presents a dramatic change to the shell's response when compared to C200 and C201 results. In addition, this softening or load reduction effect of nonlinear material behavior smears out the bending and tensile loadings within the shell and thereby smooths out the transition from snap-through (unloading) to the recovery (reloading) phase. Thus, as with the C201 theory, there is no sharp transition in the equilibrium path when the shell enters into a fully tensile load as was observed for the C200 results. The inclusion of the nonlinear material resulted in a reduction of the collapse load by 48.7% and an increase in the corresponding collapse displacement of 42.9% as compared to the C200 code's results.

Figures 6.43-6.45 show the evolution of plastic zones in the cylindrical shell on the upper surfaces. At $w = 1.43\text{-cm}$, plasticity is occurring at the point of load application and due to the presence of the clamped boundary conditions. Due to the latter effect, when observing the load-displacement curve in Figure 6.42, the decrease in load occurs due to

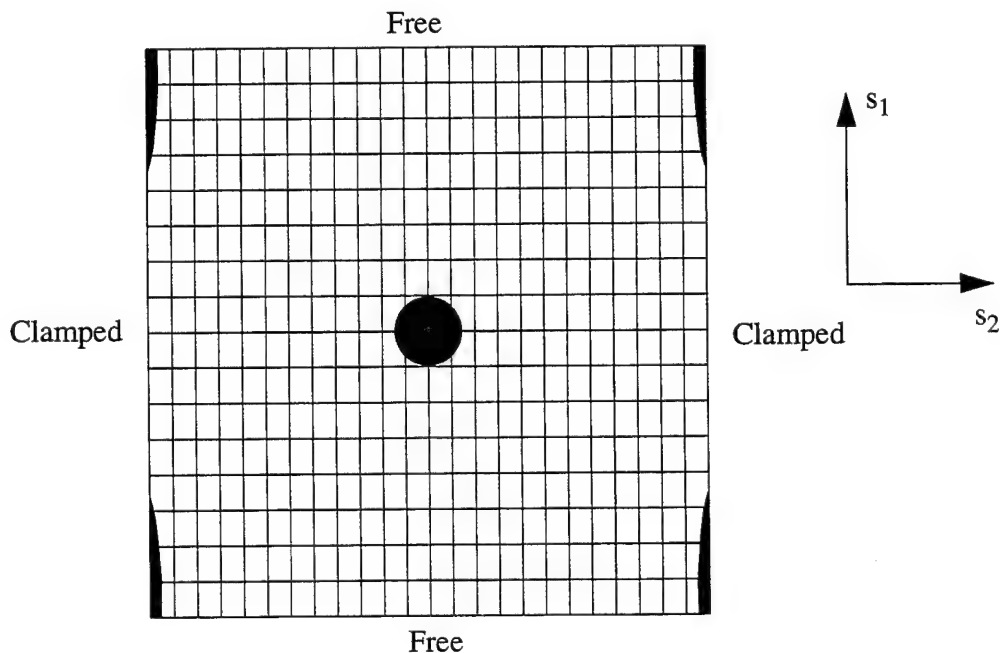


Figure 6.43 Evolution of Plastic Zones in $[0/-45/45/90]_s$, Clamped-Free, Cylindrical Shell with a Transverse Load, $w = 1.43\text{ cm}$

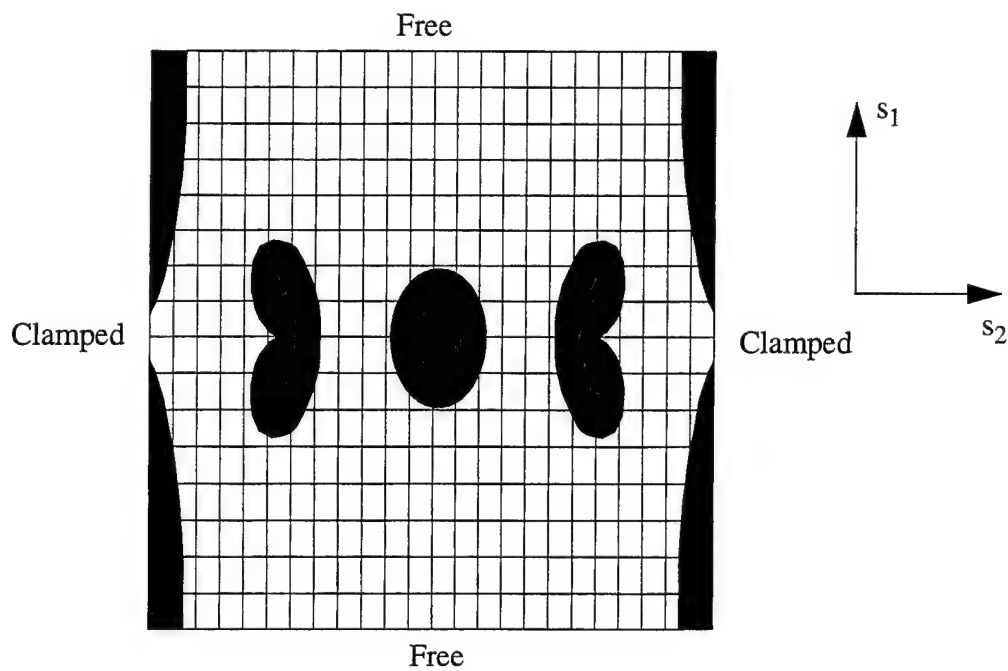


Figure 6.44 Evolution of Plastic Zones in $[0/-45/45/90]_s$, Clamped-Free, Cylindrical Shell with a Transverse Load, $w = 2.858 \text{ cm}$

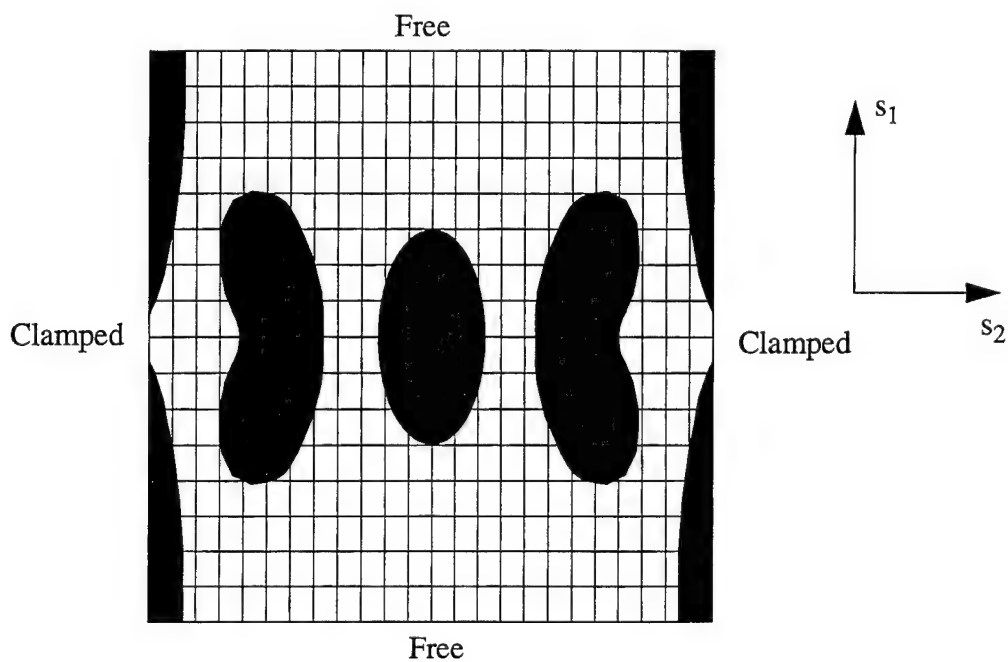


Figure 6.45 Evolution of Plastic Zones in $[0/-45/45/90]_s$, Clamped-Free, Cylindrical Shell with a Transverse Load, $w = 5.715 \text{ cm}$

the relaxing of the shell's stiffness at the boundary. As displacement increases, so too does the regions of plasticity occurring at the upper surface. It is interesting to note the plasticity is orienting along the 0° fibers. The plasticity zone occurring between the load application point and the boundary (Figures 6.44-6.45) is in response to the change in the shell's curvature (slope). When the transverse displacement reaches the onset of snap-through, $w = 1.429\text{-cm}$, approximately 20% of the shell's outer surface is exhibiting strains greater than 1.725% (Figure 6.44). Again due to the plasticity relaxing the shell's stiffness, the load-displacement curve in Figure 6.42 shows a reduction in load, and increase in displacement during the snap-through (bending) and recovery (membrane) phases. For a nonlinear, displacement-control solution, with a prescribed tolerance, $\nabla = 0.001$, along with 40 prescribed transverse displacement increments of 0.2832-cm , the C211 theory required 173952.5 CPU seconds as compared the C201 theory requiring 70356 CPU seconds. The increase in CPU time is attributed to the significant requirement of resolving the stress field through-the-thickness for each layer after plasticity occurred. The number of iterations required for convergence on an increment of displacement rose to as high as 140 for the C211 theory. The C201 theory usually required less than 25 iterations to reach convergence for an increment of displacement.

6.7 Clamped-Free, Quasi-Isotropic, Cylindrical Shell Panel Under Axial Loading (Buckling)

From Section 5.5, the results of the cubic-nonlinear HTSD theory, including the transformation of constitutive relations (C201), predicted only a slightly more flexible shell than the standard elastic cubic-nonlinear HTSD theory. Due to the relatively small magnitudes of transverse displacement, and the small rotations, the C201 theory provided only a small improvement for the elastic analysis. Clearly, when comparing the analytical results with the experimental results, there is other phenomena occurring. The inclusion of nonlinear material response should provide a more flexible shell model. The shell configuration is shown in Figure 6.46. The shells were modelled with a 24×24 mesh (first developed by the author for his master's thesis [199]) with the appropriate elements removed for the model of the shell with a cutout (Figure 6.47). This mesh provided the greatest accuracy of predicting load for the minimum amount of CPU time required. Greater accuracy could be achieved with a finer mesh, but the cost of computational time

becomes exponential due to the exceedingly large arrays required to track stiffness and stress coefficients for the element's Gauss points. The geometry and material properties for this problem are listed below. The nonlinear material properties were taken from Section 6.6 since the laminate material properties were identical.

$$\begin{aligned} s_1 &= 0.0 \text{ cm} & u = v = w = w_{,1} = w_{,2} = \psi_1 = \psi_2 &= 0 & (\text{clamped}) \\ s_1 &= 27.94 \text{ cm} & v = w = w_{,1} = w_{,2} = \psi_1 = \psi_2 &= 0 & (\text{clamped, } u \text{ free}) \\ s_2 &= 0.0 \text{ cm, } 30.48 \text{ cm} & & & (\text{free}) \\ A &= 27.94 \text{ cm} & B &= 30.48 \text{ cm} & h = 0.102 \text{ cm} \\ R &= 30.48 \text{ cm} & \theta &= 1.0 \text{ radians} \end{aligned}$$

Material AS4-3501 Graphite Epoxy

$$\begin{aligned} E_1 &= 14.114 \times 10^{10} \text{ Pa} & E_2 &= 9.246 \times 10^9 \text{ Pa} \\ G_{12} &= G_{13} = 5.958 \times 10^9 \text{ Pa} & G_{23} &= 2.966 \times 10^{10} \text{ Pa} \\ \nu_{12} &= 0.313 & \sigma_{Y_{11}} &= 1.553 \times 10^9 \text{ Pa} \\ \sigma_{Y_{22}} &= 4.548 \times 10^7 \text{ Pa} & \sigma_{Y_{12}} &= 3.932 \times 10^7 \text{ Pa} \\ k_1 &= 0.0 \text{ 1/Pa} & k_2 &= 7.753 \times 10^{-23} \text{ 1/Pa} \\ k_3 &= 1.606 \times 10^{-18} \text{ 1/Pa} & n &= 3.060 \\ \text{Ply Lay-ups} &= [0/-45/45/90]_s \end{aligned}$$

Table 6.8 shows the results for the total applied compression load versus prescribed axial displacement u computed with C200, C201, and C211 theories for the quasi-isotropic shell panel without a cutout. The inclusion of material nonlinearity in the cubic-nonlinear HTSD theory (C211) yields a more flexible shell response than the cubic-nonlinear HTSD (C20X) and the modified Donnell (C10X) theories. Figure 6.48 shows the predicted total equilibrium axial load versus axial displacement u for the C200, C201, and C211 theories and compared against experimental results from Hatfield [77]. Although there is a better approximation of the experimental results, the C211 theory predicts a stiffer shell by 24.1% for buckling load and by 12.5% for the displacement at buckling.

The development of plasticity, as predicted by the cubic-nonlinear HTSD theory (C211), is shown in Figures 6.49-6.51 for the outer convex surface of the composite cylindrical shell without a cutout. As expected, plasticity develops along the free edges, and along the clamped boundary

conditions, and moves toward the center. This plasticity development follows the buckling mode that occurred for the shell along the longitudinal center in the circumferential direction [77, 199]. Due to the compressive loading with the coupling of bending and membrane activity in the shell surface, the plasticity develops in the circumferential direction as the displacement increases and the shell displaces toward the convex surface. This dominates the shell's response over the clamped boundary conditions. Note: the corners at the upper and lower surfaces do not exhibit constant plasticity in the circumferential direction. This is due to the intersection of the free vertical edges with the clamped circumferential edges which reduces the effective stress function for those particular Gauss points below the anisotropic yield criteria in Eq (4.23). This shell's response (in terms of plasticity) is different when comparing to the previous transversely loaded composite cylinder. For the transverse load, the matrix is carrying the majority of the load with the fibers distributing the load away from the point of application. Thus, the plastic strain orients itself with the fibers. For this cylindrical shell, the fibers are carrying the load directly with the matrix distributing the energy away from the fibers. The plastic strain was oriented to the geometry and deformation of the shell, and not the material orientation. When the shell collapsed, at $u = 0.356\text{-cm}$, the majority of the circumferential direction along the center of the shell was behaving in a nonlinear manner (Figure 6.51). The inclusion of the material nonlinearity resulted in a 16.1% reduction in collapse load and a 28.6% increase axial displacement before collapse when comparing the results of the C211 theory with the C201 theory. This clearly indicates the C211 theory is modelling as a more flexible shell, and is responding similarly to the experimental results obtained by Hatfield.

Table 6.9 shows the results for the total applied compression load versus prescribed axial displacement u computed with C200, C201, and C211 theories for the quasi-isotropic shell panel with a cutout. The inclusion of material nonlinearity in the cubic-nonlinear HTSD theory (C211) yields a more flexible shell response than the cubic-nonlinear HTSD (C20X) and the modified Donnell (C10X) theories. Figure 6.52 shows the predicted total equilibrium axial load versus axial displacement u for the C200, C201, and C211 theories and compared against experimental results from Hatfield [77]. As was in the case of the quasi-isotropic shell panel without a cutout, the C211 theory predicts a stiffer shell when compared to Hatfield's experimental results. The buckling load is 12.4% higher than the experimental results and the displacement at buckling is

33.3% less.

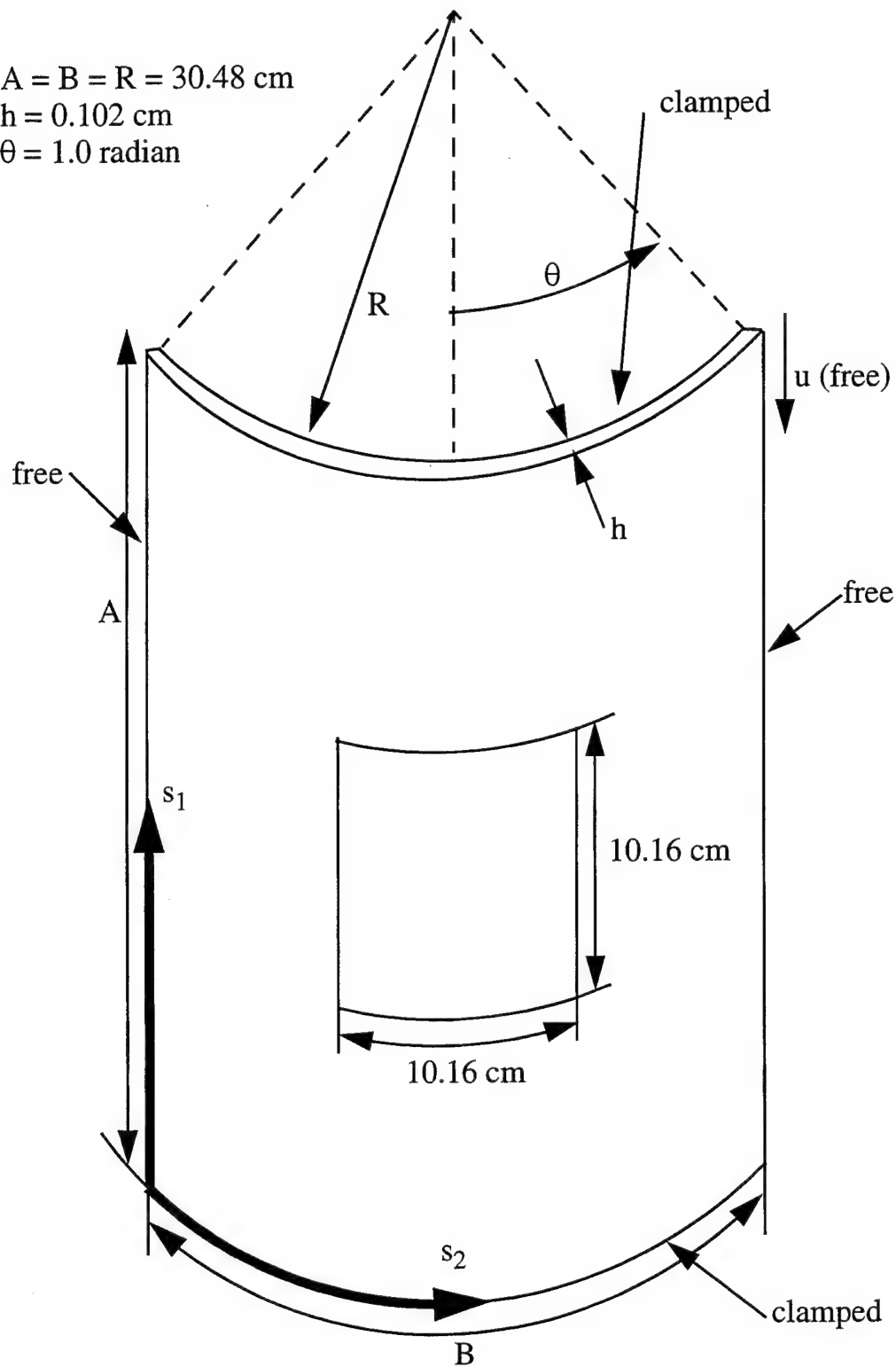


Figure 6.46 Graphite-Epoxy 30.48 cm Radius Cylindrical Shell with Centered 10.16 cm Cutout and Free Edges Loaded in Axial Compression

The development of plasticity, as predicted by the cubic-nonlinear HTSD theory (C211), is shown in Figures 6.53-6.55 for the convex surface of the composite cylindrical shell with a cutout. The plastic strain develops along the free edges and the cutout for this axially loaded shell, and at the clamped boundary conditions. As the displacement increases, the plastic zones move toward the center of each shell section around the cutout. There are stress concentrations occurring at the discontinuous points of the cutout's corners, but from the two-dimensional anisotropic yield criteria these stresses are dominated by the bending stresses generated through the coupling of the shell's membrane response with the compressive loading along the free edges of the shell and the cutout. When the shell collapsed, at $u = 0.457\text{-cm}$, the majority of the circumferential direction along the center of the shell was behaving in a nonlinear manner (see Figure 6.55). Approximately 18% of the shell's surface exhibited strains greater than 1.725%. The inclusion of the material nonlinearity resulted in a 16.1% reduction in collapse load and a 28.6% increase axial displacement before collapse when comparing the results of the C211 theory with the C201 theory. This clearly indicates the C211 theory is modelling as a more flexible shell, and is responding similarly to the experimental results obtained by Hatfield.

Comparing the C211 analytical results with Hatfield's experimental results for both the composite cylinder without, and with, a cutout yielded an interesting question. If the seating problems in the test fixture have been addressed [199] and if anisotropic plasticity is included in the analysis, why is there a significant difference between the analysis and the experiment? There are several possible solutions to this. The first being an obvious one, that is the cylindrical panel is not truly clamped within the test fixture. This is unlikely since 1.27 *cms* of the panel at either longitudinal end are held within the test fixture's clamp (see [222] for greater details on the experimental test fixture and test procedures). However, it is conceivable that in spite of this precaution, the panel is moving within this fixture, thereby relaxing the boundary conditions and allowing the panel to respond in a more flexible manner.

The second possibility is in the fabrication of these panels. When these panels are constructed, they are laid out on a mandrel as part of one very large laminate, usually $365.76\text{-cm} \times 365.76\text{-cm}$. After they are cured in the autoclave, individual panel are then cut from this large laminate. Due to the internal stresses generated in the curing process, when the panels are cut, these stresses are then relieved altering the shape of the panel in a subtle manner. The test fixture

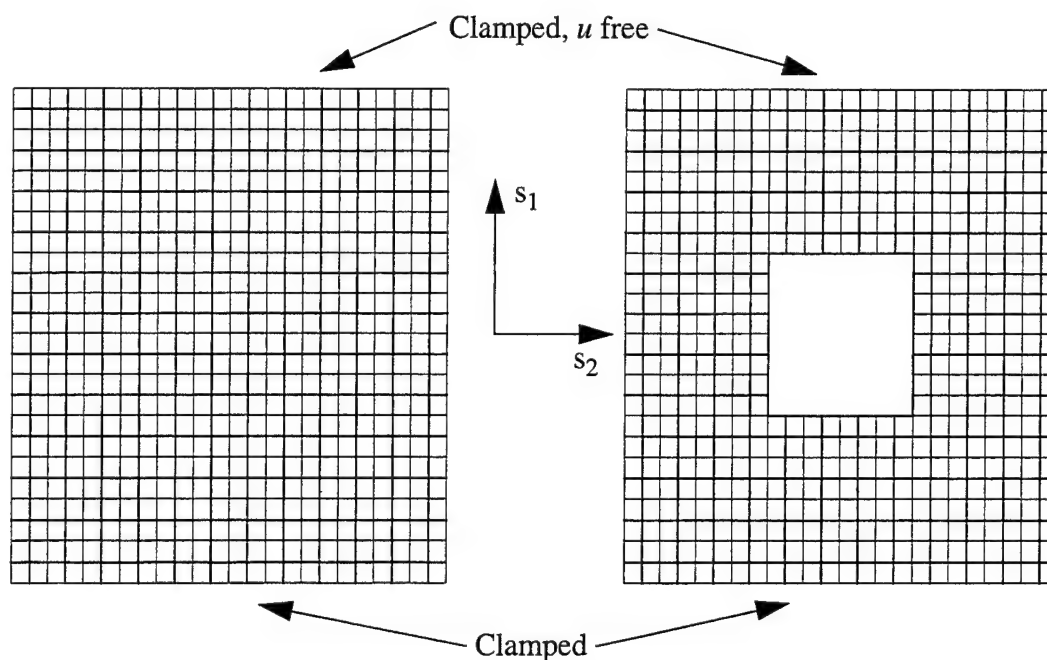


Figure 6.47 24 x 24 Element Meshes for Axially Loaded, Composite, Cylindrical Shell

Table 6.8 Predicted Total Compression Load ($10^3 N$) for Prescribed Axial Displacement (cm) for a Clamped-Free 30.48- cm x 30.48- cm Quasi-Isotropic Cylindrical Shell Panel - Experimental and C2XX Theories

Axial Disp	Hatfield*	C200	C201	C211
0.00508	1.701	2.984	2.984	2.984
0.01016	3.522	5.968	5.975	5.195
0.01524	4.544	8.916	8.805	7.399
0.02032	5.983	11.128	11.472	9.121
0.02540	7.029	15.077	13.308	10.655
0.03048	8.061	9.111	8.821	11.756
0.03556	8.893	N/A	N/A	12.651
0.03810	9.362	N/A	N/A	11.948
0.03937	9.346	N/A	N/A	N/A
0.04064	8.535	N/A	N/A	8.465
0.04089	6.759	N/A	N/A	N/A

* [77]

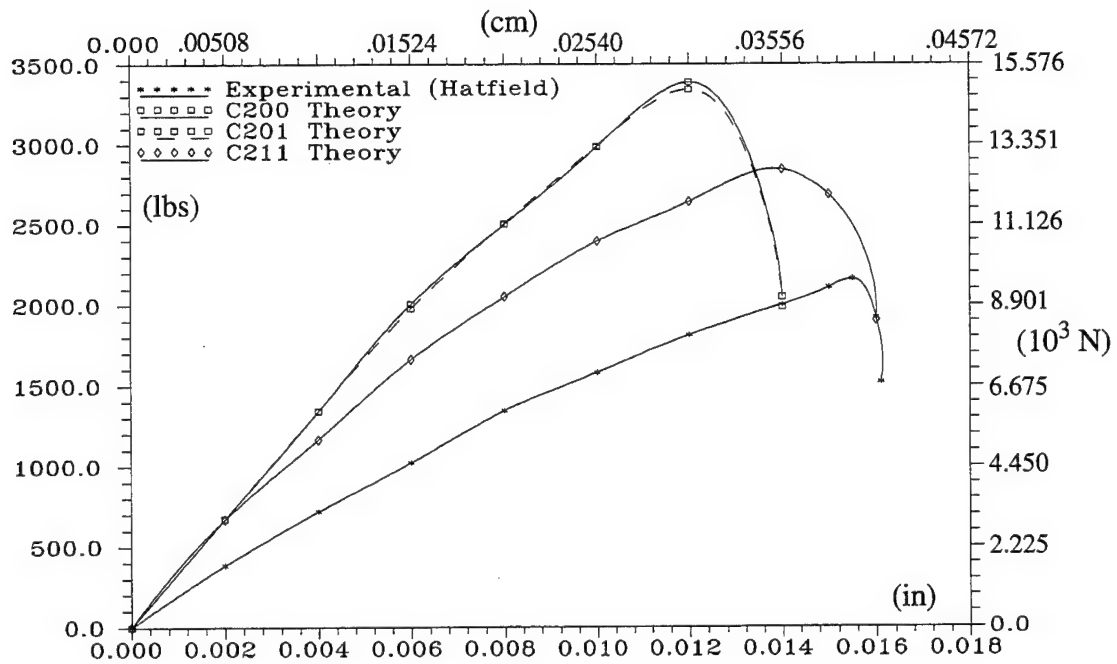


Figure 6.48 Predicted Compressive Load for Prescribed Axial Displacement for Composite Cylindrical Shell Panel [0/-45/45/90]_s without Cutout

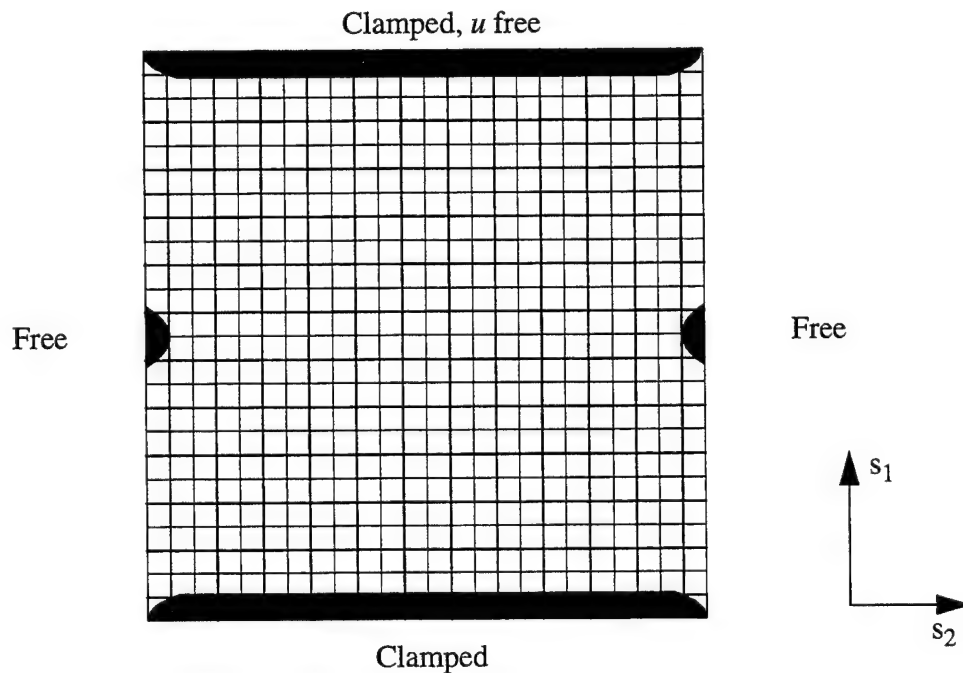


Figure 6.49 Evolution of Plastic Zones for Clamped-Free Composite Cylindrical Shell Panel without Cutout. $w = 0.00508$ cm

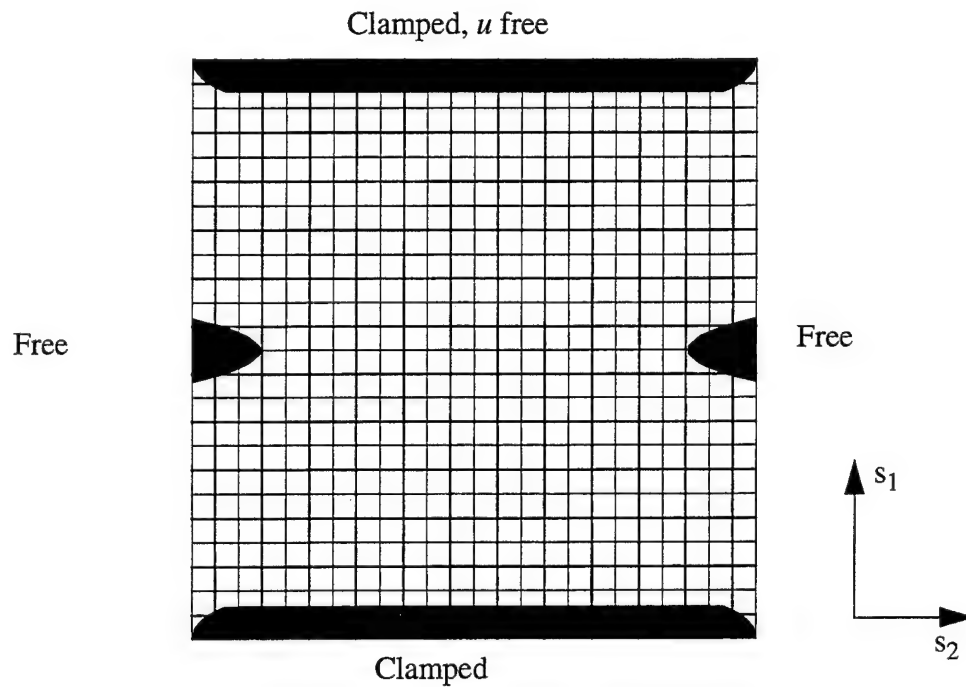


Figure 6.50 Evolution of Plastic Zones for Clamped-Free Composite Cylindrical Shell Panel without Cutout. $w = 0.0254 \text{ cm}$

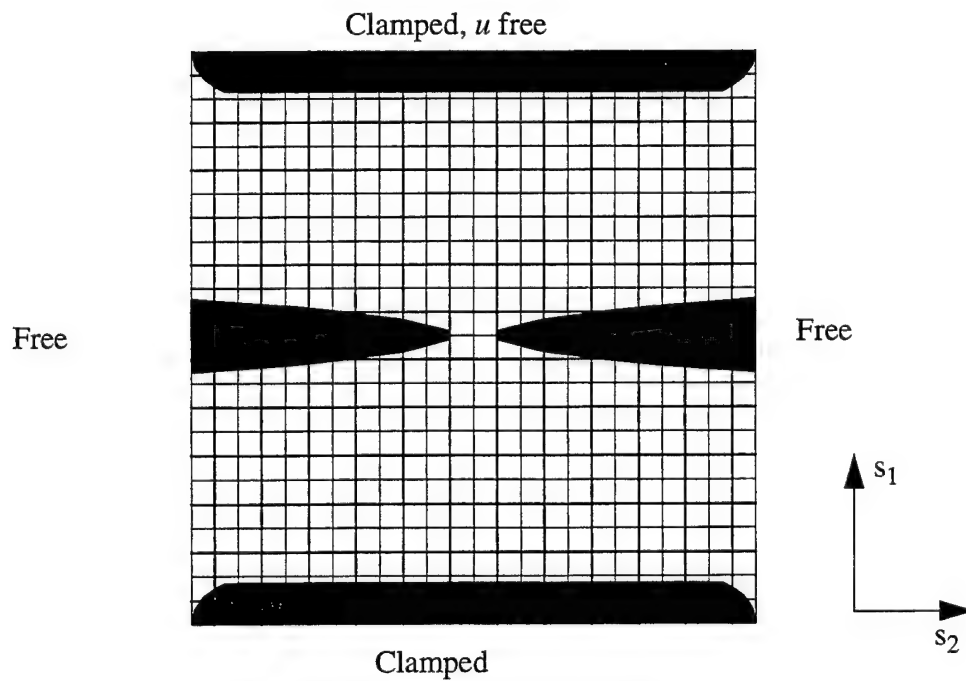


Figure 6.51 Evolution of Plastic Zones for Clamped-Free Composite Cylindrical Shell Panel without Cutout. $w = 0.04572 \text{ cm}$

Table 6.9 Predicted Total Compression Load ($10^3 N$) for Prescribed Axial Displacement (cm) for a Clamped-Free 30.48-cm x 30.48-cm Quasi-Isotropic Cylindrical Shell Panel with Centered 10.16-cm Cutout - Experimental and C2XX Theories

Axial Disp (in)	Hatfield*	C200	C201	C211
0.00254	0.185	1.040	1.040	0.992
0.00508	0.359	2.121	2.074	1.669
0.00762	0.579	3.141	2.875	2.111
0.01016	0.781	4.110	4.066	2.535
0.01270	0.983	4.759	4.711	2.894
0.01524	1.153	5.195	5.083	3.203
0.01778	1.323	5.509	5.437	3.468
0.02032	1.501	5.836	5.706	3.697
0.02286	1.674	6.110	5.975	3.952
0.02500	1.841	6.309	6.153	4.132
0.02794	1.996	6.335	6.156	4.302
0.03048	2.181	6.235	6.083	4.474
0.03302	2.364	N/A	N/A	4.564
0.03556	2.548	N/A	N/A	4.650
0.03810	2.728	N/A	N/A	4.760
0.04064	2.943	N/A	N/A	4.883
0.04318	3.132	N/A	N/A	4.930
0.04572	3.322	N/A	N/A	5.007
0.04826	3.481	N/A	N/A	4.988
0.05080	3.647	N/A	N/A	4.935
0.06604	4.349	N/A	N/A	N/A
0.06858	4.387	N/A	N/A	N/A
0.07112	4.383	N/A	N/A	N/A
0.07239	4.352	N/A	N/A	N/A

* [77]

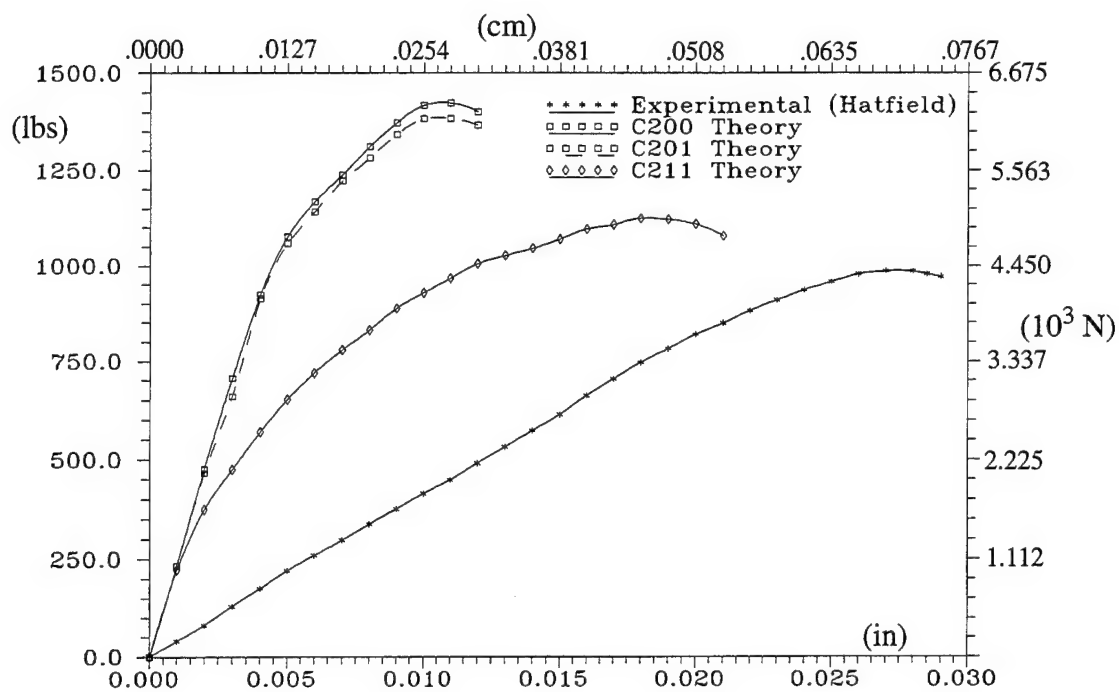


Figure 6.52 Predicted Compressive Load for Prescribed Axial Displacement for Composite Cylindrical Shell Panel $[0/-45/45/90]_s$ with a 10.16 cm Cutout

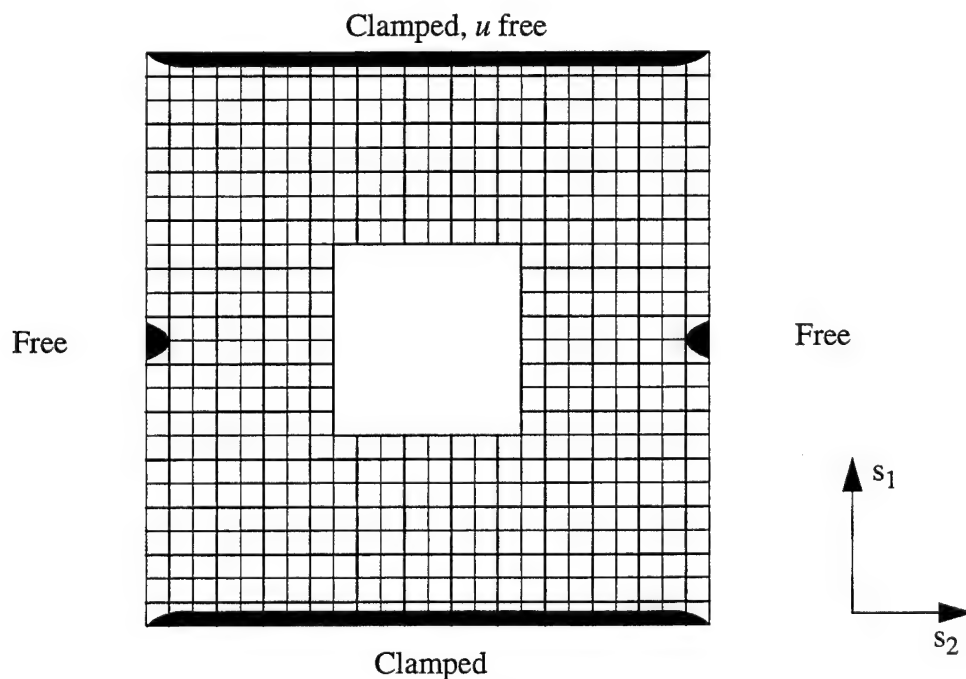


Figure 6.53 Evolution of Plastic Zones for Clamped-Free Composite Cylindrical Shell Panel $[0/-45/45/90]_s$ with a Cutout. $w = 0.00254$ cm

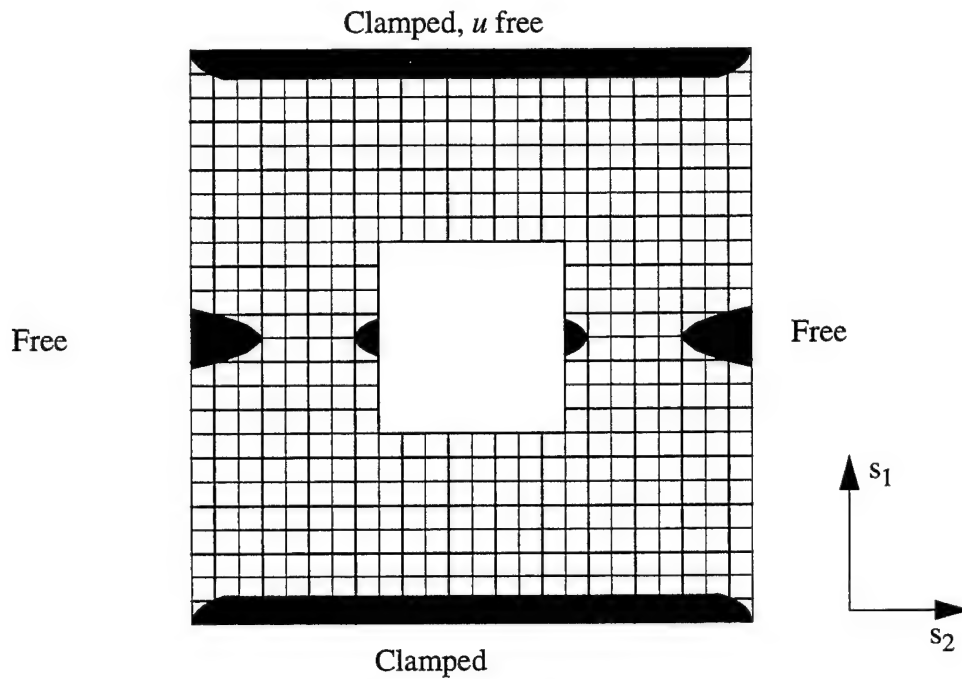


Figure 6.54 Evolution of Plastic Zones for Clamped-Free Composite Cylindrical Shell Panel [0/-45/45/90]_s with a Cutout. $w = 0.0381 \text{ cm}$

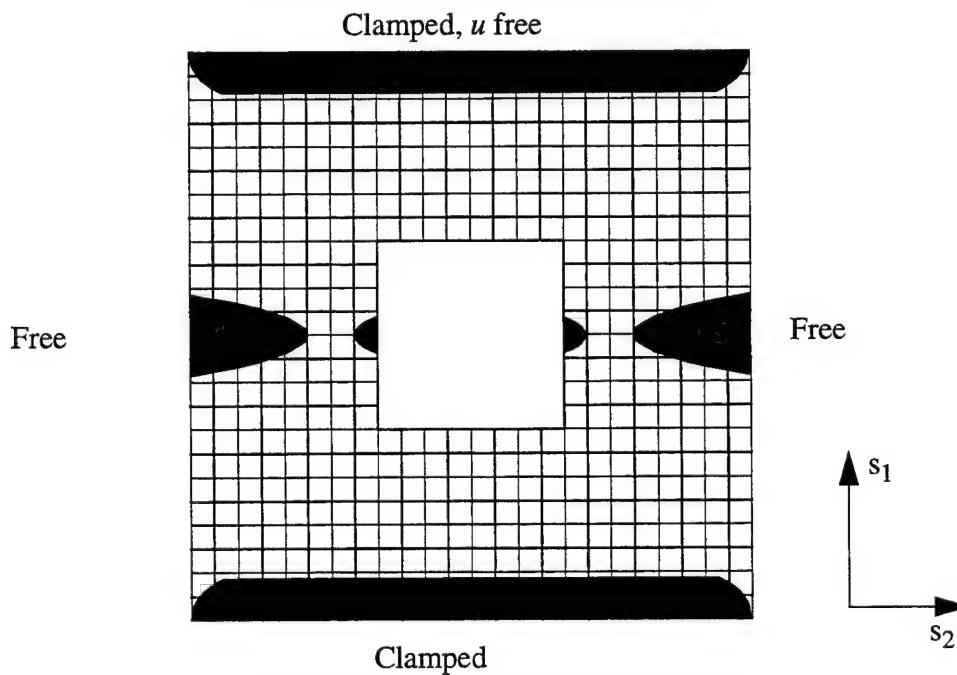


Figure 6.55 Evolution of Plastic Zones for Clamped-Free Composite Cylindrical Shell Panel [0/-45/45/90]_s with a Cutout. $w = 0.0508 \text{ cm}$

is fabricated for a constant 30.48-*cm* radius of curvature. This dimension is fixed and cannot be altered. However, when the author inspected several of the composite panels used for his Master's Thesis [77], he noted that the curvature of the panels varied as much as ± 0.953 -*cm* within the same panel. This variation leads to a built-in imperfection due to the fabrication process when these panels are placed within the fixed 30.48-*cm* radius of curvature in the test apparatus. The analytical model considers the cylindrical shell panel as perfect and the analysis proceeds from this assumption. According to Brush & Almroth [29], an imperfection of .1% can significantly alter the shell's response. The author noted such a response when he incorporated an imperfection in his STAGSC-1 models [199]. The imperfection reduces the predicted buckling load by as much as 40% depending on the dimensions of the shell, the material type, and the ply lay-up. The third alternative is a combination of the first two. The possibility of the boundary conditions being less than clamped (i.e. more flexible) and the imperfections generated due to fabrications would certainly lead to a shell response that is more flexible than is being modelled currently.

For a nonlinear, displacement-control solution, with a prescribed tolerance, $\nabla = 0.0001$, along with 30 prescribed axial displacements of 0.0127-*cm*, the C211 theory required 214578.1 CPU seconds as compared the C201 theory requiring 83001.0 for the cylindrical panel without a cut-out. The increase in CPU time is attributed to the significant requirement of resolving the stress field through-the-thickness for each layer after plasticity occurred. The number of iterations required for convergence on an increment of displacement rose to as high as 200 for the C211 theory. The C201 theory usually required less than 80 iterations to reach convergence for an increment of displacement (0.0254-*cm*). For the cylindrical shell with a cutout, with a prescribed tolerance of $\nabla = 0.0001$, with 40 prescribed axial displacements of 0.00127-*cm*, the C211 theory required 147022.2 CPU seconds as compared the C201 theory requiring 77802.9 CPU seconds.

6.8 Hinged, Quasi-Isotropic, Spherical Shell Cap with Transverse Point Load

The final set of problems considered spherical geometry, quasi-isotropic material, and the nonlinear material behavior. These problems were based on the quasi-isotropic elastic spherical shell analysis discussed in Section 5.7. The two ply lay-ups considered were $[0/-45/45/90]_s$ and $[0_8]$. The geometric and material properties are listed below. It should be noted the anisotropic plasticity parameters were chosen from Section 6.6 since the material properties were identical. The shell configuration is shown in Figure 6.56. Due to some difficulties with the in-plane stress field oscillating near the apex, where the load was applied, no symmetry was used. In addition, a convergence study was required to generate the proper refined mesh needed for a stable solution.

This convergence study needed to satisfy three requirements: (1) an elastic solution was achieved, (2) an adequate stress field was generated for the anisotropic yield criteria (Eq (4.22)), and (3) the displacement function was satisfied. In the previous cases, the meshes used were of an acceptable nature due to previous author's convergence studies [8, 45, 46, 49-51, 71, 129, 146, 161-163, 207, 225, 226]. However, in the spherical composite shell, due to the singularity at the apex, the mesh was refined to generate a non-oscillating stress field. A 12×12 mesh was attempted but the stress field near the apex oscillated which did not allow for convergence. Results were obtained for a refined 18×18 mesh where the stress field remained stable. This is shown in Figure 6.57. A heavily refined 24×24 mesh was solved to compare with the 18×18 mesh results. The equilibrium curve for the heavily refined mesh showed a 3.2% drop in peak load for a significant increase in CPU time (44.5%). Thus, the 18×18 mesh was deemed adequate.

These shells are relatively shallow [129], but provide a good exercise for the nonlinear material portion of the theory since they address spherical geometry and quasi-isotropic material.

$$\begin{aligned}
 s_1 &= 0 & u = w_{,1} = \psi_1 &= 0 & (\text{symmetry}) \\
 s_2 &= 0 & v = w_{,2} = \psi_2 &= 0 & (\text{symmetry}) \\
 s_1 &= \pm 2.301 \text{ cm} & u = v = w = \psi_2 &= 0 & (\text{hinged}) \\
 s_2 &= \pm 2.301 \text{ cm} & u = v = w = \psi_1 &= 0 & (\text{hinged}) \\
 a &= b = 4.60 \text{ cm} & h &= 0.04 \text{ cm} & R = 12.09 \text{ cm} \\
 L &= 4.573 \text{ cm} & \delta &= 2.181 \text{ cm} & \theta = 0.19024 \text{ radians}
 \end{aligned}$$

Material AS4-3501 Graphite Epoxy

$$E_1 = 14.114 \times 10^{10} \text{ Pa} \quad E_2 = 9.246 \times 10^9 \text{ Pa}$$

$$G_{12} = G_{13} = 5.958 \times 10^9 \text{ Pa} \quad G_{23} = 2.966 \times 10^{10} \text{ Pa}$$

$$\nu_{12} = 0.313 \quad \sigma_{Y_{11}} = 1.553 \times 10^9 \text{ Pa}$$

$$\sigma_{Y_{22}} = 4.548 \times 10^7 \text{ Pa} \quad \sigma_{Y_{12}} = 3.932 \times 10^7 \text{ Pa}$$

$$k_1 = 0.0 \text{ 1/Pa} \quad k_2 = 7.753 \times 10^{-23} \text{ 1/Pa}$$

$$k_3 = 1.606 \times 10^{-18} \text{ 1/Pa} \quad n = 3.060$$

Ply Lay-ups $[0/-45/45/90]_s$

$$a = b = 4.60 \text{ cm}$$

$$R_1 = R_2 = R = 12.09 \text{ cm}$$

$$\theta_1 = \theta_2 = \theta = 0.19024 \text{ radians}$$

$$L = 4.573 \text{ cm}$$

$$h = 0.04 \text{ cm}$$

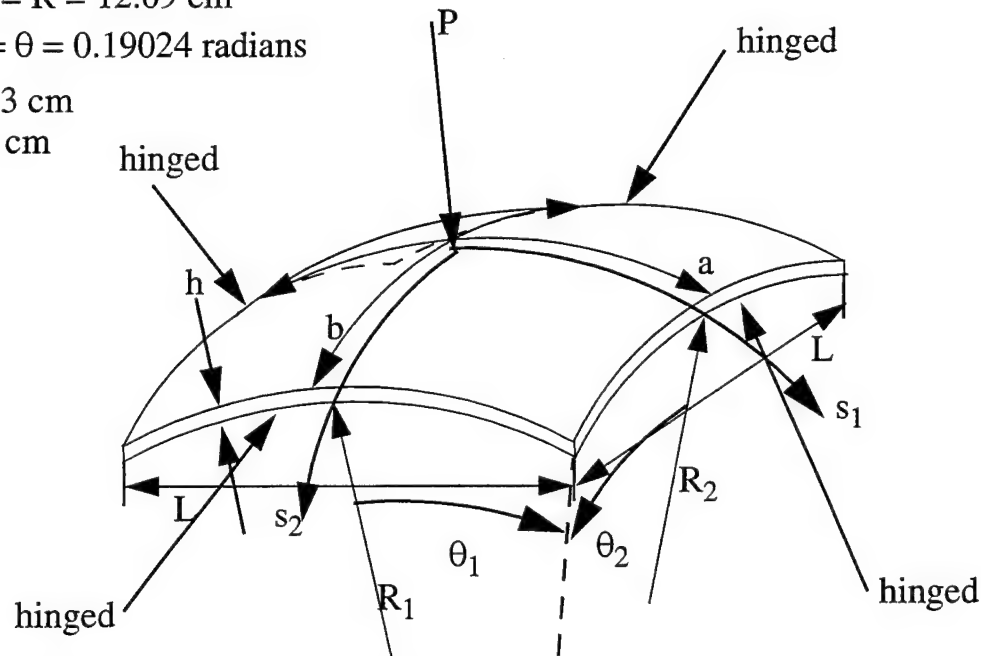


Figure 6.56 Hinged Apex-Loaded Graphite-Epoxy Spherical Shell Cap

Table 6.10 shows the predicted equilibrium loads for prescribed transverse displacement of the apex of a $[0/-45/45/90]_s$ ply lay-up with the S200, S201, and S211 cubic-nonlinear HTSD theories. As expected, the S211 theory predicts the most flexible shell. Figure 6.58 shows the equi-

librium path for the results shown in Table 6.10. The S211 cubic-nonlinear HTSD theory predicts a more flexible shell as loading increases due to the presence of plasticity around the apex (Figure 6.59) and at the corners due to the combined hinged boundary conditions on both sides of the shell cap. As the displacement reaches the peak load, around 32% of the convex shell surface is behaving plastically (Figure 6.60). Then as the shell unloads and reaches the point of pure tension and reloading, a significant portion of the shell's convex surface is exhibiting plasticity.

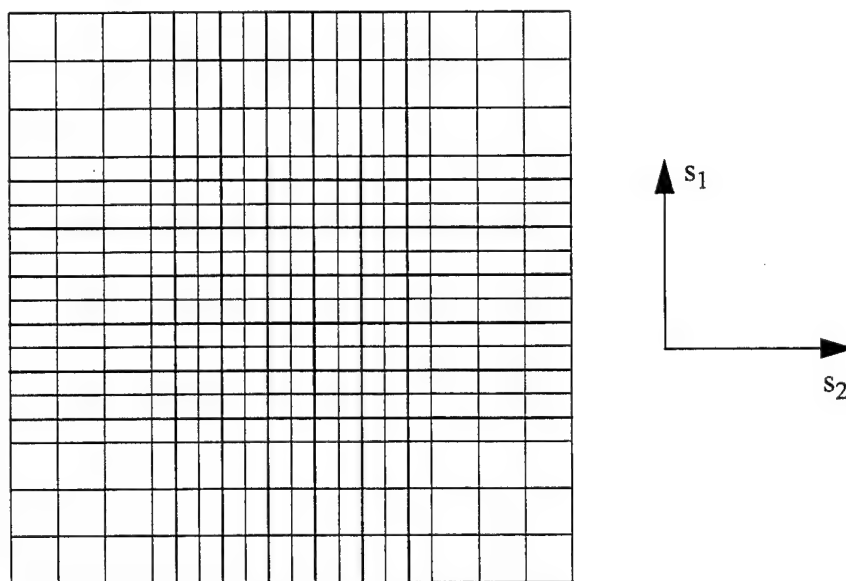


Figure 6.57 Refined Mesh Used for Quasi-Isotropic Hinged Spherical Shell Cap Models

Figures 6.59-6.61 show the evolution of the plastic regions for the convex surface of the $[0/-45/45/90]_s$ spherical shell. It should be noted that the plasticity favors the 0° ply orientation following the discussion of Section 6.6. These plastic zones are determined by analyzing the stress-state at each Gauss point, for each element, at the convex surface layer, and determining which of the Gauss points have exceeded the yield criterion mentioned in Section 4.2.2. Once a Gauss point exceeds the yield criterion, the Prandtl-Reuss flow relations are followed for the remainder of the analysis for that particular Gauss point and a plastic strain pointer is associated with the Gauss point. At the onset of snapping, $w = 0.286\text{-cm}$, approximately 32% of the shell's convex surface

is exhibiting strains greater than 2.125%. When $w = 0.506$ -cm, nearly 45% of the shell's convex surface is exhibiting strains greater than 2.125%

Table 6.11 shows the predicted equilibrium loads for prescribed transverse displacement of the apex of a $[0_8]$ ply lay-up with the S200, S201, and S211 cubic-nonlinear HTSD theories. As expected, the S211 theory predicts the most flexible shell. Figure 6.62 shows the equilibrium path for the results shown in Table 6.11. The S211 theory predicts a more flexible shell as loading increases due to the presence of plasticity around the apex (Figure 6.63). As unloading occurs, the S211 theory allows the $[0_8]$ shell to reduce load-ing more quickly than the $[0/-45/45/90]_s$ shell due to the lack of $\pm 45^\circ$ fibers.

Table 6.10 Predicted Equilibrium Load ($10^3 N$) for Prescribed Transverse Displacement (cm) of Hinged Quasi-Isotropic $[0/-45/45/90]_s$ Spherical Shell Cap

Disp	S200	S201	S211
0.0476	0.552	0.554	0.554
0.0954	0.885	0.881	0.763
0.1429	1.106	1.099	0.930
0.1905	1.263	1.252	1.041
0.2381	1.362	1.345	1.100
0.2858	1.377	1.354	1.132
0.3334	1.268	1.245	1.112
0.3810	1.027	1.006	1.033
0.4098	0.917	0.853	0.923
0.4286	0.872	0.845	0.793
0.4524	0.916	0.884	0.702
0.5061	N/A	N/A	0.808
0.5246	N/A	N/A	0.952
0.5477	N/A	N/A	1.192

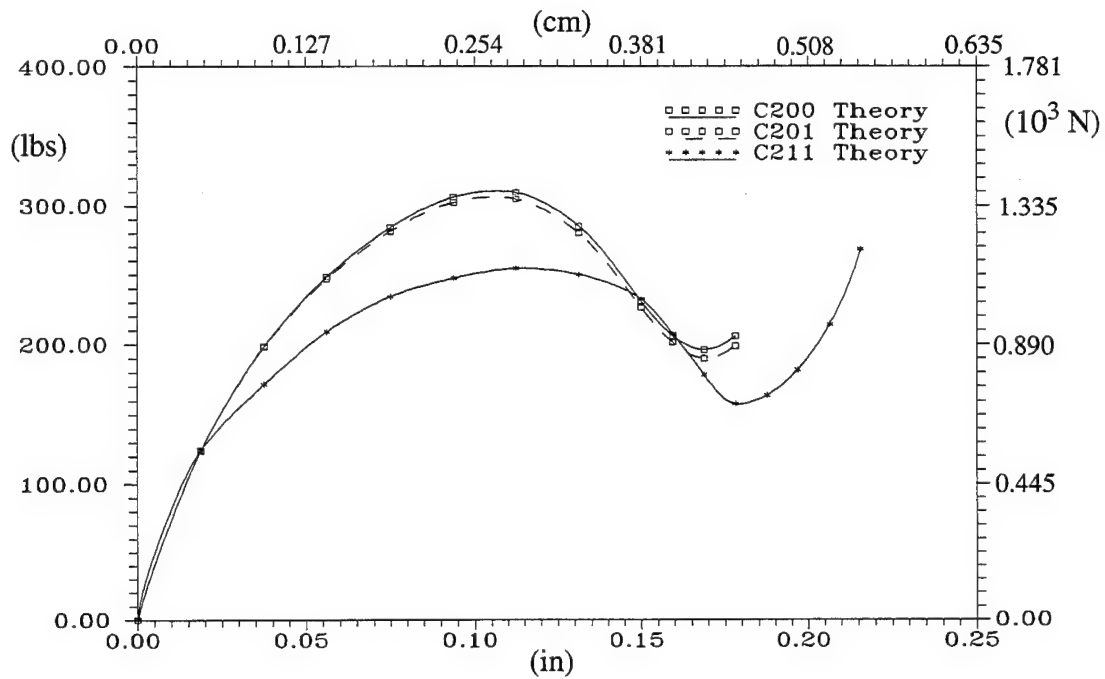


Figure 6.58 Equilibrium Curves for Transverse Point Loaded Quasi-Isotropic $[0/-45/45/90]_s$ Spherical Shell Cap - C200, C201, & C211 Theories

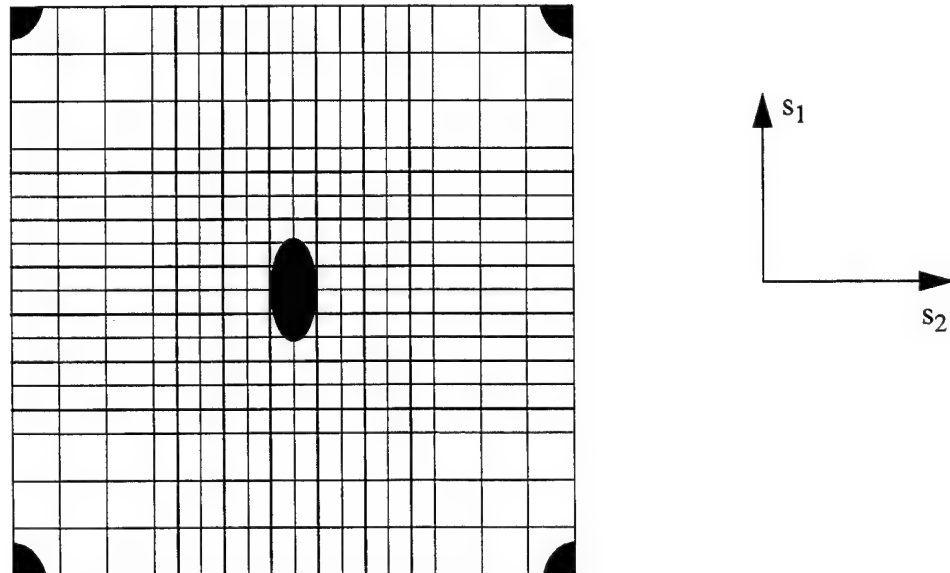


Figure 6.59 Evolution of Plastic Zones for Hinged $[0/-45/45/90]_s$ Composite Spherical Shell Panel. $w = 0.1905 \text{ cm}$

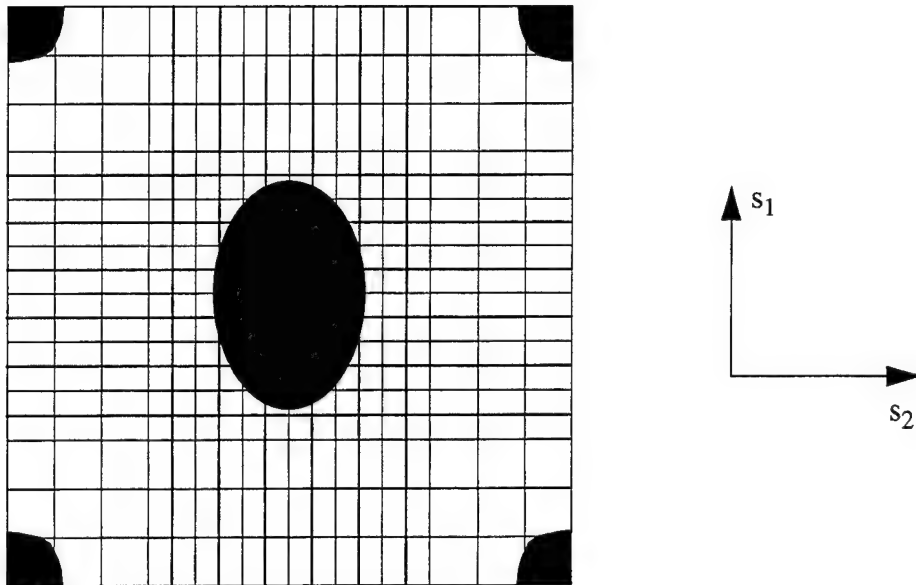


Figure 6.60 Evolution of Plastic Zones for Hinged $[0/-45/45/90]_s$ Composite Spherical Shell
Panel. $w = 0.286 \text{ cm}$

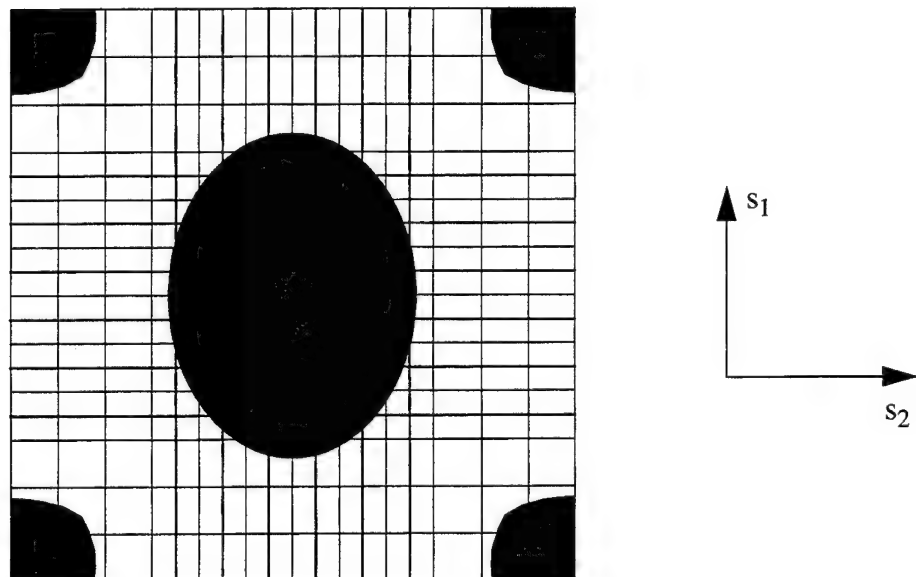


Figure 6.61 Evolution of Plastic Zones for Hinged $[0/-45/45/90]_s$ Composite Spherical Shell
Panel. $w = 0.506 \text{ cm}$

Table 6.11 Predicted Equilibrium Load ($10^3 N$) for Prescribed Transverse Displacement (cm) of Hinged Quasi-Isotropic $[0_8]$ Spherical Shell Cap

Disp	S200	S201	S201
0.0476	0.512	0.510	0.510
0.0954	0.835	0.830	0.713
0.1429	1.054	1.043	0.841
0.1905	1.209	1.170	0.921
0.2381	1.306	1.284	0.970
0.2858	1.327	1.252	1.010
0.3334	1.234	1.194	1.005
0.3810	0.974	0.914	0.935
0.4098	0.621	0.528	0.672
0.4286	0.657	0.596	0.468
0.4763	0.889	0.861	0.346
0.5001	N/A	N/A	0.405
0.5239	N/A	N/A	0.506
0.5477	N/A	N/A	0.759

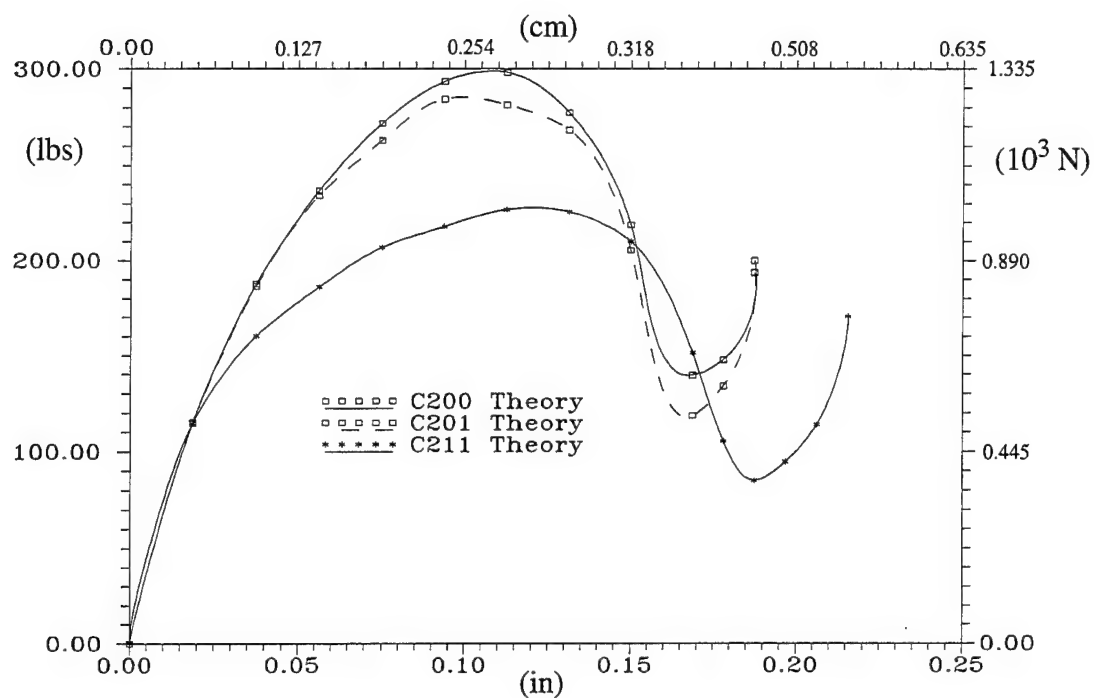


Figure 6.62 Equilibrium Curves for Transverse Point Loaded Quasi-Isotropic $[0_8]$ Spherical Shell Cap - C200, C201, & C211 Theories

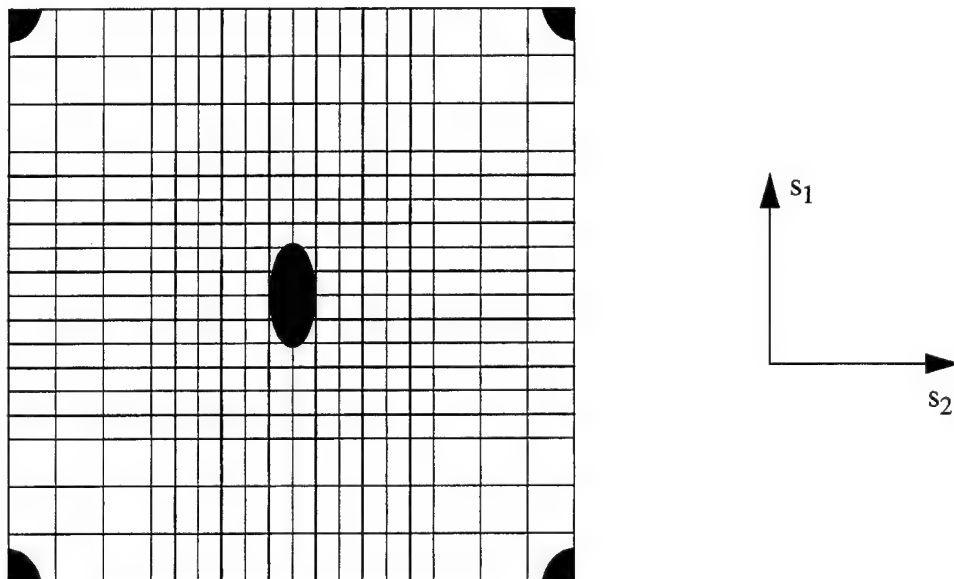


Figure 6.63 Evolution of Plastic Zones for Hinged $[0_8]$ Composite Spherical Shell Panel. $w = 0.1905$ cm

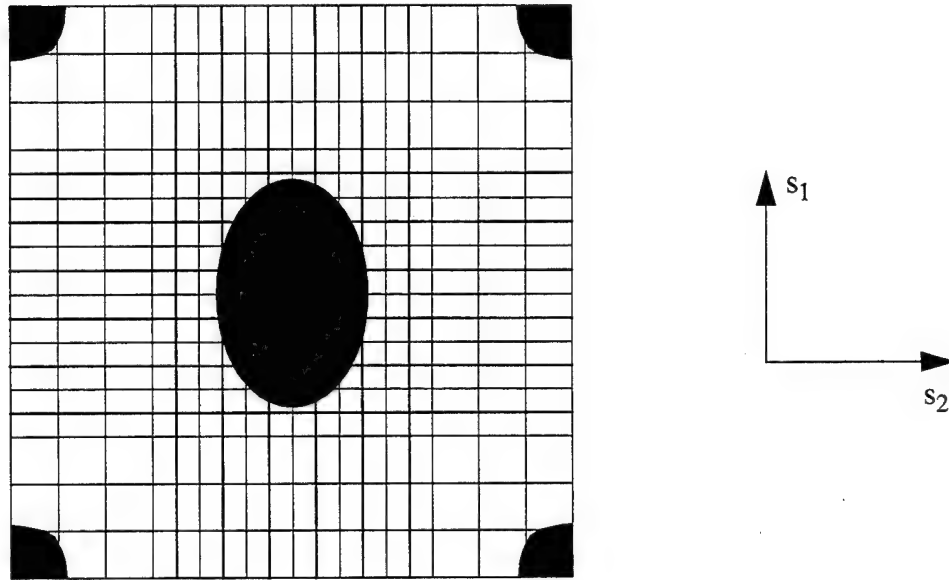


Figure 6.64 Evolution of Plastic Zones for Hinged $[0_8]$ Composite Spherical Shell Panel. $w = 0.286 \text{ cm}$

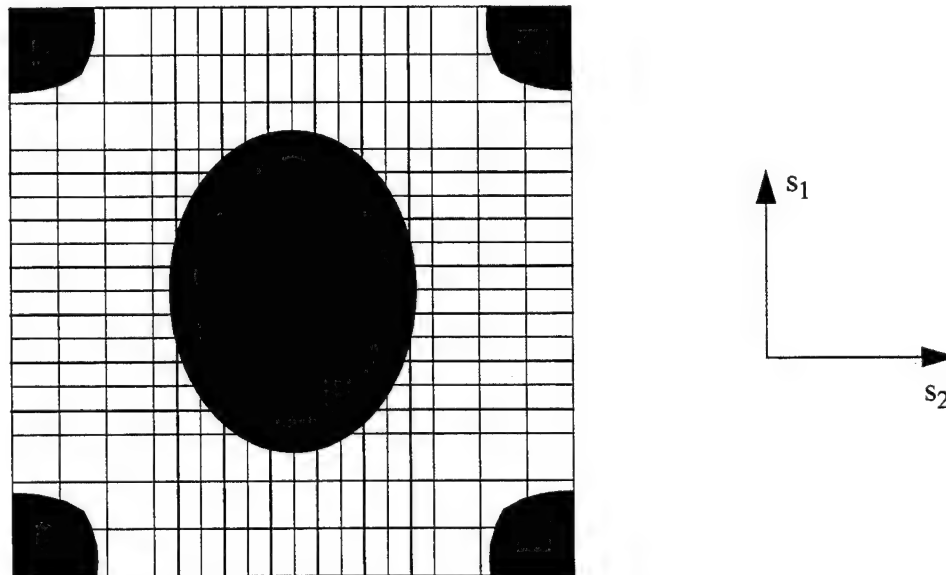


Figure 6.65 Evolution of Plastic Zones for Hinged $[0_8]$ Composite Spherical Shell Panel. $w = 0.506 \text{ cm}$

For the composite spherical shell with a ply lay-up of $[0/-45/45/90]_s$, the S211 theory reduces the snapping load by 17.8% when compared to the S200 theory, and by 16.5% when compared to the S201 theory. For the composite shell with a ply lay-up of $[0_8]$, the S211 theory reduces the snapping load by 23.9% when compared to the S200 theory, and by 19.4% when compared to the S201 theory. Although these composite spherical shells are relatively shallow ($\delta/b = \delta/(L/2) = 0.954$), they provide an excellent comparison for the various theories developed for this research. Due to their relative shallowness, rotations are expected to remain small. Thus, the S201 theory should have a relatively small impact on the global displacement of the shell - a reduction of the snapping load of only 1.56% for the $[0/-45/45/90]_s$ ply lay-up and a reduction of 5.64% for the $[0_8]$ ply lay-up. However, since the prescribed displacement is relatively large when compared to the shell thickness ($w/h = 12.843$), it is probable that the inclusion of nonlinear material behavior would have a significant effect to the global displacement of the shell.

For a nonlinear, displacement-control solution, with a prescribed tolerance, $\nabla = 0.001$, with 28 prescribed transverse displacements of 0.0127-cm, the S211 theory required 104008.2 CPU seconds as compared the S201 theory requiring 44231.4 CPU seconds for the $[0/-45/45/90]_s$ spherical shell. The increase in CPU time is attributed to the significant requirement of resolving the stress field through-the-thickness for each layer after plasticity occurred. The number of iterations required for convergence on an increment of displacement rose to as high as 80 for the S211 theory. The S201 theory usually required less than 15 iterations to reach convergence for an increment of displacement. For the $[0_8]$ spherical shell, with a prescribed tolerance of $\nabla = 0.001$, with 28 prescribed transverse displacements of 0.0127-cm, the S211 theory required 103642.2 CPU seconds as compared the S201 theory requiring 44231.2 CPU seconds for a solution.

It has been shown that for both isotropic and quasi-isotropic plates and shells, the addition of a nonlinear material model significantly alters the the global equilibrium load-displacement curve. For the cases where experimental data was available, the G211 elastic-plastic, cubic-nonlinear HTSD theory predicted a plate or shell response more accurately than the G20X cubic-nonlinear HTSD theories. In all the problems discussed, the G211 theory accurately predicts the development of plastic behavior. That is, plasticity occurs at the outer surfaces first, and depending on geometry and material properties, plasticity eventually occurs at the mid-surface. Although these regions of plasticity were never quantitatively compared with experimental results or any results

published in the literature (primarily due to a lack of data), the author believes from a qualitative view these regions provide some useful insight into the plate or shell's response to the increased displacement and resultant loading.

These regions of plasticity are useful in predicting possible mesh refinement, if necessary, and to demonstrate the through-the-thickness plasticity development by the theory. When a plate or shell exhibits strains greater than 2.125% over 15-20% of the outer surface, along with values of $\psi_i > 12.5-15^\circ$ and displacements greater than five times the thickness, the nonlinear material analysis should be incorporated to accurately predict the global equilibrium curve. For composite materials exhibiting a strong dependence on shear stiffness, G_{12} , material properties, the elastoplastic analysis is required. In the case of the Gr/PEEK, σ_{12Y} was 2.43% the magnitude of σ_{11Y} . For Gr/Ep, σ_{12Y} was 2.54% the magnitude of σ_{11Y} .

There is a significant computational cost associated with using the elastic-plastic, cubic-nonlinear HTSD theory. Due to the requirement of tracking the stress-state at each Gauss point, for every layer, in every element, the arrays developed to track this crucial information were very large. In every problem discussed in Chapter 6, the elastic-plastic theory code took at least 200-300% longer to run, and required 4-6 times the computer memory previously needed to track and calculate the Gauss point stress-state and plasticity strain arrays. By running this code on a SUN SPARC2 work-station, the average time for completion of the smaller problems was on the order of 2-3 days and for the larger problems (quasi-isotropic cylindrical shells, isotropic pinched cylinder) the average time for completion was on the order of 5-8 days.

7. Summary and Conclusions

The goal of the research was to develop a *total Lagrangian* finite element formulation with a quasi-nonlinear higher-order transverse shear deformation (HTSD) theory including transformations of the constitutive relations from the Cauchy stress-strain system 2nd Piola stress-Green strain system and allowing the constitutive relations to become elastic-plastic with work hardening. This formulation was then used in computing solutions for isotropic and quasi-isotropic plates, cylindrical and spherical shells that allows for large displacements, moderate rotations and large strains. The main contributions from this research is: (1) a total Lagrangian finite element formulation with large displacements, moderate rotations, **and large strains** due to the inclusion of transforming the constitutive relations from Eulerian coordinates to Lagrangian coordinates, and (2) an incremental elastic-plastic predictor algorithm for a total Lagrangian finite element formulation, including composite material ply lay-ups. Based on the development from Washizu (1982), a displacement-based transformation matrix was developed for both the stress-states and strain-states. Using incremental Prandtl-Reuss flow theory relations, an elastic-plastic constitutive matrix is developed for isotropic materials based on a von Mises yield criteria. For laminated composite materials, the elastic-plastic constitutive matrix is developed using a modified von Mises criteria with anisotropic interaction parameters to account for material anisotropy. Work hardening for both materials was accomplished by computing the incremental effective stress versus the incremental effective plastic strain at each increment of displacement based on the previously known stress state.

7.1 Theory

A summary of the theory developed for this research follows. Complete details are included in Chapters 3 and 4 of the dissertation. The basic assumptions of a two-dimensional (2D) shell theory are tied to the concepts of a reference surface (the midsurface of the shell) and a local curvilinear coordinate system of principal curvature, which by definition are orthogonal, then the coordinate system is also orthogonal. For this research, the theoretical development was restricted to orthogonal coordinate systems based on lines of constant curvature.

If one uses a Lagrangian description of deformation, all variables are expressed in terms of area and volume conditions prior to deformation. In this system, the displacement vector can be written in terms of orthonormal base vector, \vec{e}_i , ($i = 1-3$). For the shell, the Lamé' parameters A_α , ($\alpha = 1,2$), describe the *two-dimensional* relationship between the orthogonal surface base vectors, \vec{a}_α , and their orthonormal counterparts, \vec{e}_i . The shell shape factors, h_i , ($i = 1-3$), describe the *three-dimensional* relationship between the orthogonal base vectors \vec{g}_i of the three-dimensional orthogonal curvilinear coordinate system, \vec{y}_i , and their orthonormal counterparts \vec{e}_i . For an orthogonal curvilinear coordinate system based upon the lines of principal curvature of a shell, the shape factors are

$$h_1 = A_1 (1 - y_3/R_1), h_2 = A_2 (1 - y_3/R_2), h_3 a = 1, \quad (3.40)$$

where

$$\left(A_1 = \left(\frac{\partial \vec{r}}{\partial \theta_1} \cdot \frac{\partial \vec{r}}{\partial \theta_1} \right)^{1/2} \right), \left(A_2 = \left(\frac{\partial \vec{r}}{\partial \theta_2} \cdot \frac{\partial \vec{r}}{\partial \theta_2} \right)^{1/2} \right). \quad (3.41)$$

Thus, for the case of a spherical shell with radius $R_1 = R_2 = R$ and local coordinates $\theta_1 = s_1$, $\theta_2 = s_2$, z described in an orthogonal space with global coordinates $y_1 = s_1$, $y_2 = s_2$, $y_3 = z$, the position vector $\vec{r}(y_1, y_2, y_3)$ is given by

$$\vec{r} = s_1 \vec{e}_1 + s_2 \vec{e}_2 + s_3 \vec{e}_3, \quad (3.42)$$

and the Lamé parameters reduce to $A_1 = A_2 = 1$.

For this research, the macro-mechanical behavior of a composite lamina was assumed sufficient provided stresses were small enough to assure no material failure occurs. Thus, the material of each lamina was treated as a homogenous anisotropic material. More specifically, the material was assumed to be transversely isotropic. This means the material has properties which are symmetric about two material axes. In this research the effects of transverse shear deformation are considered. Thus, σ_4 and σ_5 are not assumed to be zero. The direct normal stress, σ_3 , however was still assumed to be zero. This assumption was necessary to reduce the three-dimensional problem to a two-dimensional problem. The direct transverse normal strain was assumed to be

given by:

$$\epsilon_{33} = -\frac{C_{13}}{C_{33}}\epsilon_{11} - \frac{C_{23}}{C_{33}}\epsilon_{22} \quad , \quad (3.58)$$

where the C_{ij} were functions of material properties and ply lay-up.

To form a structural component, the lamina are assumed to be perfectly bonded together with their fibers oriented at a particular angle with respect to the structure's reference axis. The stiffness contribution of each lamina in the laminate is transformed to a common reference system of axes. Eq (3.58) relates the direct normal strain ϵ_3 to changes in the direct in-plane strains ϵ_1 and ϵ_2 for the case where σ_3 is equal to zero. The assumption that Eq (3.58) is valid for an arbitrary laminated composite shell is important. Without this assumption, the stress state would be fully three-dimensional and the two-dimensional model's reduced computational effort would be lost. With this assumption, however, the two-dimensional model will not accurately predict the stress distribution within the shell, since σ_3 generally is not zero in the real structure and ϵ_3 may vary considerably from that predicted by Eq (3.58). Research in the 1960's and 1970's by many investigator has validated this assumption.

There are many ways to include transverse shear deformation. Transverse shear effects can be included using a first-order transverse shear deformation (FTSD) theory. In this case, material lines originally normal to the midsurface are allowed to deviate from the normal to the shell midsurface. These lines remain straight and inextensible. Since the angle of deviation is constant, the displacement field varies linearly through the thickness of the shell. The constant angle also implies transverse shear strain is constant, and is not zero at the upper and lower surfaces of the shell. This inconsistent distribution results in a stiff model of the structure. This stiffening effect, called shear locking, becomes more pronounced as the shell thickness approaches zero. The higher-order transverse shear deformation (HTSD) theory allows the normal to rotate and warp. The HSTD theory for a flat plate produces a parabolic distribution of shear strain. This distribution matches the exact distribution of shear strain for the linear infinitesimal case.

For a shell, the FTSD theory is given by the following displacement field

$$\begin{aligned}
 u_1 &= u \left(1 - \frac{y_3}{R_1} \right) + \psi_1 y_3 \\
 u_2 &= v \left(1 - \frac{y_3}{R_2} \right) + \psi_2 y_3 \\
 u_3 &= w
 \end{aligned} \tag{3.64}$$

where the five degrees of freedom u , v , w , ψ_1 , and ψ_2 , are functions of the in-plane curvilinear coordinates (y_1, y_2) . The displacement field of a third-order linear transverse shear deformation theory is given by the following equation

$$\begin{aligned}
 u_1 &= u \left(1 - \frac{y_3}{R_1} \right) + \psi_1 y_3 - \frac{4}{3h^2} \left(\frac{\partial w}{\partial y_1} + \psi_1 \right) y_3^3 \\
 u_2 &= v \left(1 - \frac{y_3}{R_2} \right) + \psi_2 y_3 - \frac{4}{3h^2} \left(\frac{\partial w}{\partial y_2} + \psi_2 \right) y_3^3 \\
 u_3 &= w
 \end{aligned} \tag{3.72}$$

The third-order displacement field has two additional degrees of freedom not present in the first-order theory. These two degrees of freedom are the derivatives of transverse displacement, w . These derivatives are independent degrees of freedom that represent the slope of the elastic curve. The third-order theory allows the slope of the elastic curve to deviate from the bending angles. This deviation is directly related to the transverse shear strains of the structure.

Dennis (1988) used a version of Eq (3.72) to analyze linear and nonlinear plates and cylindrical shells with elastic isotropic and quasi-isotropic materials. His third-order displacement field takes the form of

$$\begin{aligned}
 u_1 &= u + \psi_1 y_3 - \frac{4}{3h^2} \left(\frac{\partial w}{\partial y_1} + \psi_1 \right) y_3^3 \\
 u_2 &= v \left(1 - \frac{y_3}{R_2} \right) + \psi_2 y_3 - \frac{4}{3h^2} \left(\frac{\partial w}{\partial y_2} + \psi_2 \right) y_3^3 \\
 u_3 &= w
 \end{aligned} \tag{7.1}$$

Three extensions of his development are the nucleus of this research effort. The first extension is generating the strain-displacement relations based on Eq (3.72) instead of Eq (3.40). These strain-displacement relations are given by:

$$\begin{aligned} \epsilon_1 = & \frac{u_{1,1}}{h_1} + \frac{u_2 h_{1,2}}{h_1 h_2} + \frac{u_3 h_{1,3}}{h_1 h_3} + \frac{1}{2h_1^2} \left(u_{1,1} + \frac{u_2 h_{1,2}}{h_2} + \frac{u_3 h_{1,3}}{h_3} \right)^2 \\ & + \frac{1}{2h_1^2} \left(u_{2,1} - \frac{u_1 h_{1,2}}{h_2} \right)^2 + \frac{1}{2h_1^2} \left(u_{3,1} - \frac{u_1 h_{1,3}}{h_3} \right)^2 \end{aligned} \quad (4.2a)$$

$$\begin{aligned} \epsilon_2 = & \frac{u_{2,2}}{h_2} + \frac{u_1 h_{2,1}}{h_1 h_2} + \frac{u_3 h_{2,3}}{h_2 h_3} + \frac{1}{2h_2^2} \left(u_{2,2} + \frac{u_1 h_{2,1}}{h_1} + \frac{u_3 h_{2,3}}{h_3} \right)^2 \\ & + \frac{1}{2h_2^2} \left(u_{1,2} - \frac{u_2 h_{2,1}}{h_1} \right)^2 + \frac{1}{2h_2^2} \left(u_{3,2} - \frac{u_2 h_{2,3}}{h_3} \right)^2 \end{aligned} \quad (4.2b)$$

$$\epsilon_4 = \frac{1}{2} \left(\frac{u_{2,3}}{h_3} + \frac{u_{3,2}}{h_2} - \frac{u_3 h_{3,2}}{h_2 h_3} - \frac{u_2 h_{2,3}}{h_2 h_3} \right) \quad (4.2c)$$

$$\epsilon_5 = \frac{1}{2} \left(\frac{u_{1,3}}{h_3} + \frac{u_{3,1}}{h_1} - \frac{u_3 h_{3,1}}{h_1 h_3} - \frac{u_1 h_{1,3}}{h_1 h_3} \right) \quad (4.2d)$$

$$\begin{aligned} \epsilon_6 = & \frac{1}{2} \left(\frac{u_{1,2}}{h_2} + \frac{u_{2,1}}{h_1} - \frac{u_2 h_{2,1}}{h_1 h_2} - \frac{u_1 h_{1,2}}{h_1 h_2} \right) \\ & + \frac{1}{2h_1 h_2} \left(u_{1,2} - \frac{u_1 h_{2,1}}{h_1} \right) \left(u_{1,1} + \frac{u_2 h_{1,2}}{h_2} + \frac{u_3 h_{1,3}}{h_3} \right) \\ & + \frac{1}{2h_1 h_2} \left(u_{2,1} - \frac{u_2 h_{1,2}}{h_2} \right) \left(u_{2,2} + \frac{u_1 h_{2,1}}{h_1} + \frac{u_3 h_{2,3}}{h_3} \right) \\ & + \frac{1}{2h_1 h_2} \left(u_{3,1} - \frac{u_1 h_{1,3}}{h_3} \right) \left(u_{3,2} - \frac{u_2 h_{2,3}}{h_3} \right) \end{aligned} \quad (4.2e)$$

The complete strain-displacement relations for the quasi-nonlinear HTSD theory including spherical geometry are given in Appendix E.

The second extension of the theory from Dennis is the modification of the constitutive relations to include elastic-plastic material behavior with the inclusion of work hardening. For isotropic materials, the incremental elastic-plastic constitutive relations for each layer in the shell are given by

$$\begin{bmatrix} D'_{ep} \end{bmatrix}^k = \begin{bmatrix} (D'_{ep})_f & 0 \\ 0 & D'_s \end{bmatrix}^k, \quad (4.9)$$

where

$$\begin{bmatrix} (D'_{ep})_f \end{bmatrix}^k = \begin{bmatrix} D'_f \end{bmatrix}^k - \frac{\{d_D\} \{d_D\}^T}{A + \{d_D\}^T \{a\}}, \quad (4.10a)$$

$$\{d_D\} = \begin{bmatrix} D'_f \end{bmatrix}^k \{a\}, \quad (4.10b)$$

$$\{a\}^T = \left[\frac{\partial F}{\partial \sigma_{11}}, \frac{\partial F}{\partial \sigma_{22}}, \frac{\partial F}{\partial \sigma_{12}} \right]. \quad (4.10c)$$

The von Mises yield criteria is given by

$$\begin{aligned} F(\sigma) &= \bar{\sigma}^2 = \sqrt{3} (J_2')^{1/2} = \frac{\sqrt{3}}{2} \sigma'_{ij} \sigma'_{ij} \\ &= \frac{\sqrt{3}}{2} \left[(\sigma'_{11})^2 + (\sigma'_{22})^2 + (\sigma'_{33})^2 \right] \\ &\quad + \sqrt{3} \left[(\sigma'_{23})^2 + (\sigma'_{13})^2 + (\sigma'_{12})^2 \right] \end{aligned} \quad (4.11)$$

The strain-hardening effect is found through the scalar A. It has been shown by Owen & Hinton

(1980) that

$$A = H' = \frac{d\sigma_Y}{d\epsilon} = \frac{d\bar{\sigma}}{d\bar{\epsilon}^{-p}} \quad (4.12)$$

By using the Ramberg-Osgood equation to characterize the stress-strain curve, the effective plastic strain can be characterized with effective stress by

$$\bar{\epsilon}_m^{-p} = k\bar{\sigma}_m^{-n-1} \quad (4.15)$$

The differential, $d\bar{\epsilon}_m^{-p}$, can be represented as

$$d\bar{\epsilon}_m^{-p} = kn\bar{\sigma}_m^{-n-1}d\bar{\sigma}_m \quad (4.16)$$

Thus,

$$H' = \frac{d\sigma}{d\epsilon} = \frac{1}{kn\bar{\sigma}^{-n-1}} \quad (4.17)$$

The modified Huber-Mises yield criteria for laminated composite materials is given by

$$F(\sigma) = \frac{\bar{\sigma}^2}{\sigma^2} = a_{12}(\sigma_{11} - \sigma_{12})^2 + a_{23}\sigma_{22}^2 + a_{31}\sigma_{11}^2 + 3a_{44}\sigma_{23}^2 + 3a_{55}\sigma_{13}^2 + 3a_{66}\sigma_{12}^2 = 0 \quad (4.23)$$

where a_{ij} are *anisotropic interaction* parameters determined from experimental yield stress values Y_{ij} . Thus, for transversely isotropic materials the anisotropic interaction parameters are

$$a_{11} = a_{12} + a_{31} = \left(\frac{Y_{11}}{Y_{11}} \right)^2 = 1 \quad (4.26a)$$

$$a_{22} = a_{23} + a_{12} = \left(\frac{Y_{11}}{Y_{22}} \right)^2 \quad (4.26b)$$

$$a_{33} = a_{31} + a_{23} = \left(\frac{Y_{11}}{Y_{33}} \right)^2 = \left(\frac{Y_{11}}{Y_{22}} \right)^2, \quad (4.26c)$$

$$a_{44} = \frac{1}{3} \left(\frac{Y_{11}}{Y_{23}} \right)^2 = \frac{1}{3} \left(\frac{Y_{11}}{(0.8) Y_{12}} \right)^2 = \frac{1}{3(0.64)} \left(\frac{Y_{11}}{Y_{12}} \right)^2, \quad (4.26d)$$

$$a_{55} = \frac{1}{3} \left(\frac{Y_{11}}{Y_{13}} \right)^2 = \frac{1}{3} \left(\frac{Y_{11}}{Y_{12}} \right)^2, \quad (4.26e)$$

$$a_{66} = \frac{1}{3} \left(\frac{Y_{11}}{Y_{12}} \right)^2. \quad (4.26f)$$

The strain-hardening parameter H' for anisotropic materials is found to be

$$H' = d\bar{\sigma}/d\bar{\epsilon}^{-p} = \left[(n-2) \left[k_1 \left(a_{11} \sigma_{11}^2 - 2a_{12} \sigma_{11} \sigma_{22} \right) - k_2 \left(a_{22} \sigma_{22}^2 \right) + 3k_3 \left(a_{44} \sigma_{23}^2 + a_{55} \sigma_{13}^2 + a_{66} \sigma_{12}^2 \right) \right] \bar{\sigma}^{-(n-3)} \right] \quad (4.33)$$

The third extension to Dennis' theory was allowing for a large strain formulation. This implies the Cauchy stress-strain and the Lagrangian stress-strain relations are no longer the same. Thus, for a total Lagrangian formulation, the constitutive relations must be transformed from the Eulerian coordinates to the Lagrangian coordinate axes. Washizu (1982) developed a displacement based transformation between Cauchy strain and Green's strain and between Cauchy stress and Kirchhoff stress. Applying shell theory and assuming rotations of the normals and about the normals to be small these transformation matrices are found to be for the stress state

$$\{\sigma^E\} = \frac{1}{D} [T_1] \{\sigma\}, \quad (4.69)$$

and for the strain state

$$\{e\} = \frac{1}{D^2} [T_2] \{\epsilon\}, \quad (4.70)$$

where

$$[T_1] = \begin{bmatrix} (1+u_{1,1})^2 & (u_{1,2})^2 & 0 & 0 & 2(1+u_{1,1})u_{1,2} \\ (u_{2,1})^2 & (1+u_{2,2})^2 & 0 & 0 & 2u_{2,1}(1+u_{2,2}) \\ 0 & 0 & (1+u_{2,2}) & u_{2,1} & 0 \\ 0 & 0 & u_{1,2} & (1+u_{1,1}) & 0 \\ (1+u_{1,1})u_{2,1} & u_{1,2}(1+u_{2,2}) & 0 & 0 & D' \end{bmatrix}, \quad (4.71)$$

$$[T_2] = \begin{bmatrix} (1+u_{2,2})^2 & (u_{1,2})^2 & 0 & 0 & -2u_{1,2}(1+u_{2,2}) \\ (u_{2,1})^2 & (1+u_{1,1})^2 & 0 & 0 & -2u_{2,1}(1+u_{1,1}) \\ 0 & 0 & (1+u_{1,1})D & u_{2,1}D & 0 \\ 0 & 0 & u_{1,2}D & (1+u_{1,1})D & 0 \\ -u_{2,1}(1+u_{2,2}) & -(1+u_{1,1})u_{1,2} & 0 & 0 & D' \end{bmatrix}, \quad (4.72)$$

$$D' = (1+u_{1,1})(1+u_{2,2}) + u_{1,2}u_{2,1}, \quad (4.63)$$

and

$$D = (1+u_{1,1})(1+u_{2,2}) - u_{1,2}u_{2,1}. \quad (4.60)$$

Thus, for a large-strain total Lagrangian formulation

$$\{\sigma\} = \frac{1}{D} [T_1]^{-1} [A] [T_2] \{\varepsilon\} = [D] \{\varepsilon\}, \quad (4.75)$$

where $[A]$ is the Eulerian constitutive matrix and $[D]$ is the Lagrangian constitutive matrix.

The author's approach of including nonlinear material effects in the cubic nonlinear HTSD theory incorporated several assumptions beyond those of Dennis. First, the author was primarily interested in problems involving large rotations, curvature changes, and large strains for laminated composite shells. Thus, the displacement field of Dennis was used with a minor modification to allow for spherical geometry. The author employed a layered approach to analyzing the nonlinear material effects. This method has been effectively modelled by other researchers in updated Lagrangian stress-resultant formulations. Each layer is allowed to become individually plastic. Thus, the outer layers of the shell are allowed to generate larger plastic strains than the inner layers at each increment of displacement. One simplifying assumption made was to allow the constitutive transformation of the mid-surface be applied to each layer.

Thus, the goal of this research was to evaluate the effects of three theoretical extensions not previously investigated for linear-elastic shells with large displacement, rotations, and curvatures using a higher-order transverse shear deformation theory. These three extensions were the devel-

opment of spherical geometry, the transformation of the constitutive relations from Eulerian coordinates to Lagrangian coordinates, and allowing the constitutive relations to become elastic-plastic with strain hardening. The strain hardening is characterized by using Ramberg-Osgood parameters developed from experimentally derived stress-strain curves.

This previous section of theoretical discussion dealt with the development of the displacement field, the strain-displacement relations, and the constitutive relations for laminated composite shells. The next phase in the research was the development and solution of the governing differential equations for shell problems. Since the author was specifically interested in nonlinear phenomena of large displacements, rotations, and strains, no analytical or linear solutions were desired. The finite element technique is used to obtain numerical solutions for cylindrical and spherical shells. The finite element equations are based upon the total potential energy of the elastic body or the virtual work expression for the elastic-plastic body. Specifically, the principle of stationary potential energy is used where the first variation of potential energy of the system is set equal to zero. The potential energy expression was found by first examining the equilibrium state of the body. For a body with prescribed forces on part of its surface and prescribed boundary conditions on the remaining part of the surface, the equations of equilibrium for an infinitesimal virtual displacement were developed in terms of the Second Piola-Kirchhoff stress tensor and the Green strain components expressed in the body's coordinate system. Assuming strains were small, then the stresses could be written in terms of the strains. For a laminated orthotropic material, the stress components could be written in terms of the reduced structural stiffness of the lamina. These quantities depended only on the thickness coordinate. Thus, they could be written in terms of an integral over the midsurface of the shell, with the integration in the thickness direction performed analytically.

The variation of total potential energy gave five coupled nonlinear partial differential equations which governed the equilibrium of the system. These expressions contained 18 displacement parameters: u , $u_{,1}$, $u_{,2}$, v , $v_{,1}$, $v_{,2}$, w , $w_{,1}$, $w_{,2}$, $w_{,11}$, $w_{,22}$, $w_{,12}$, ψ_1 , $\psi_{1,1}$, $\psi_{1,2}$, ψ_2 , $\psi_{2,1}$, and $\psi_{2,2}$. These parameters included seven displacement parameters of Eq (3.72) and their derivatives. Since the equilibrium equations were nonlinear in terms of the displacement parameters, an incremental-iterative approach is used to solve a system of linearized equations which yields an equivalent solution. For simple theories, such as Donnell's theory or a linear FTSD theory where relatively few terms are included, the first variation of potential energy and its linearization, can

be explicitly developed, term by term. For more complete theories, such as a linear HTSD theory or the fully nonlinear theory, the potential energy expression has several hundred terms. Its first variation could possibly include thousand of terms, and the subsequent linear equilibrium equations would be quite lengthy.

Rajasekaran and Murray (1973) developed a formal procedure for finite elements, which defined the total potential energy, its first variation, and the linear incremental equilibrium equations in terms of three stiffness matrices. Specifically the total potential energy was given by

$$\Pi_p = \{q\}^T \left[\frac{1}{2} [K] + \frac{1}{6} [N_1] + \frac{1}{12} [N_2] \right] \{q\} - \{q\}^T \{P\} \quad , \quad (4.85)$$

where

$\{q\} \equiv$ a column array of nodal displacement parameters

$\{P\} \equiv$ a column array of nodal loads

$[K] \equiv$ an array of constant stiffness coefficients

$[N_1] \equiv$ an array of nonlinear coefficients with each term dependent on one of the displacement parameters ($[N_1]$ is linear in terms of displacement), and

$[N_2] \equiv$ an array of nonlinear coefficients with each term dependent on the product of two displacement parameters ($[N_2]$ is quadratic in terms of displacement).

The first variation of potential energy is then given by

$$\left[[K] + \frac{1}{2} [N_1] + \frac{1}{3} [N_2] \right] \{q\} - \{P\} = \{0\} \quad , \quad (4.86)$$

and the linear incremental equilibrium equation is given by

$$\left[[K] + [N_1] + [N_2] \right] \{\Delta q\} - \{\Delta P\} = \{0\} \quad . \quad (4.87)$$

Rajasekaran and Murray's formulation was for finite elements in which strains did not vary through the thickness of the element. This formulation was extended to account for variation of strain through the thickness of the curved shell. The strain at a point in the shell was developed in terms of a series expansion in the thickness coordinate, and new definitions of $[\hat{K}]$, $[\hat{N}_1]$, and

$[\hat{N}_2]$ were developed for the theory with transverse shear deformation. This formulation required hundreds of matrix multiplications to evaluate these equations. A MACSYMA routine was developed to symbolically generate the assumed displacement field, determine strain components, determine the shell shape factor approximations, determine the elements of the strain definition arrays, form the stiffness arrays, and finally generate the Fortran code for elements of the $[\hat{K}]$, $[\hat{N}_1]$, and $[\hat{N}_2]$ stiffness arrays. Development of this routine was an important part of this research.

The element independent stiffness matrices of this theory depended upon the continuum displacement gradient vector $\{d\}$. Using a standard displacement-based finite element method, the 18 two-dimensional functions of the continuum displacement gradient vector are approximated by interpolation from discrete values of nodal displacement parameters. These nodal parameters, or degrees of freedom, were defined only at a finite number of points or nodes. The finite element method required the computation of the stiffness matrices for each element independently. These elemental stiffnesses were then assembled according to their relationship to global nodes of the structure.

Defining the nodal degrees of freedom required definition for the specific element, since the nodal parameters of $\{q\}$ and the associated nodal interpolation array are element specific. The element of choice is the 36 degree of freedom quadrilateral curved shell element developed by Dennis (1988). This element has been used for many investigations of static and dynamic response of plates, arches, and cylindrical shell undergoing large displacements with linear HTSD theory (von Karman or Donnell theory with HTSD theory included). The element has eight nodes with seven degrees of freedom, u , v , w , $w_{,1}$, $w_{,2}$, ψ_1 , and ψ_2 , at each of the four corner nodes and two degrees of freedom, u and v , at the four midside nodes. The two degrees of freedom at the midside nodes allow for quadratic interpolation of in-plane displacements u and v . This is important for shells, due to the curvature-induced coupling of bending and membrane activity in shells. The continuum values of u and v were interpolated from the nodal values u_k and v_k , using quadratic Lagrangian interpolation functions. The continuum displacement gradient vector $\{d\}$ included ψ_1 and ψ_2 and the first derivatives of these parameters. Thus, linear interpolation could be used for these parameters, since C^0 continuity is required. The interpolations of ψ_1 and ψ_2 were given lin-

ear Lagrangian interpolation functions. Nodal parameters associated with transverse displacement included the values w , $w_{,1}$, and $w_{,2}$ at each of the four corner nodes. Thus, interpolation of w was accomplished using cubic Hermitian shape functions.

The two-dimensional integration of the finite element equations, in the plane of the finite element, was accomplished by numerical integration using Gaussian quadrature. Solution of the resulting equations was accomplished by an incremental-iterative technique commonly called the Newton-Raphson method, in which the solution is either displacement or load controlled. The parameters to be incremented were the elements of the array $\{d\}$, containing global degrees of freedom. A global criterion, written in terms of the norms of all displacement parameters, used to determine convergence.

7.2 Elastic Shell Analysis

One objective of this research was to evaluate the accuracy of the new quasi-nonlinear HTSD theories (spherical geometry and elastic constitutive relations with material transformation matrices). Another objective was to assess their limitations. Shallow shell problems included a thick flat quasi-isotropic plate with uniform transverse pressure load, a thin, deep isotropic cylindrical arch with a transverse point load, a thin isotropic and quasi-isotropic cylindrical shell panels with a transverse point load, a deep, thin laminated composite cylindrical shell panels under a transverse point load with various ply lay-ups, a thin quasi-isotropic cylindrical shell panel with and without a large cut-out and uniform axial compression load, and thin isotropic and laminated composite spherical shells under transverse load with various ply lay-ups.

The transversely-loaded flat plate problem was used to test the MACSYMA generated codes. The plate chosen was an 8-ply quasi-isotropic laminated square plate with total length of 4.064-cm which indicated transverse shear may be important. Solutions were computed using a 4×4 mesh of elements to model one quadrant of the plate. For this problem, the various HTSD elastic theories all gave results within one percent of each other, and predicted significantly more flexible results than the classical von Karman theory code. Although the difference was negligible, all the nonlinear HTSD codes predicted a more flexible response than the linear HTSD codes predicted.

This problem validated the computational algorithms used to develop and solve the linear and nonlinear HTSD finite element equations for laminated composite shells.

The second problem was a thin, deep isotropic cylindrical arch with hinged boundary conditions under a transverse point load at the center of the arch. Deep circular arches can be used to demonstrate a theory's ability to predict large displacements and rotations. Many variations of transversely-loaded deep arch problems have been reported in the literature. The problem chosen for this research was a 254.0-cm radius isotropic arch with a 2.54-cm square cross section and an opening angle of 0.92 radians (106°). Solutions for this problem were computed using all variations of the HTSD theory. A 1×40 mesh of elements was used to represent one quadrant of the arch. The quasi-nonlinear HTSD predicts a more dramatic collapse than the linear Donnell-type solution (even though the Donnell theory was modified to include transverse shear deformation). The divergence between the two theories occur when the transverse displacement, w , reaches 30.48-cm. At this point on the equilibrium path, the maximum rotation of the normal, ψ_2 , reaches 0.354 radians (20.3°) and over 32% of the shell surface see rotations of 0.171 radians (9.8°). This difference in predicted response was due to the many nonlinear in-plane displacement terms in the strain definitions that are not included in the Donnell equations. However, when the material transformations are included in the quasi-nonlinear HTSD theory, a more flexible structure is predicted. This theory diverges from the quasi-nonlinear HTSD theory when the transverse displacement, w , reaches 20.32-cm. At this point on the equilibrium path, the maximum rotation of the normal, ψ_2 , reaches 0.244 radians (14.0°) and over 29% of the arch surface saw rotations of 0.10 radians (5.72°). Due to these rotations, the isotropic material properties are becoming anisotropic due to the movement of the material coordinate system relative to the structural coordinate system. At the point of collapse, $w = 60.96$ -cm, $\psi_2 = 0.531$ radians (30.4°) and over 45% of the arch surface saw rotations of 0.20 radians (14.7°).

The third class of problems investigated were thin shallow hinged-free isotropic or quasi-isotropic cylindrical shells with a transverse point load at the center of the panel. The first problem was a 0.635-cm thick cylindrical shell of isotropic material under a transverse point load with hinged boundary conditions along the axial edges. The shell has a 254.0-cm radius with axial and circumferential lengths of 50.8-cm. Solutions were computed using a 4×6 mesh of elements to

model one quadrant of the shell. For this problem, the linear and quasi-nonlinear HTSD theories all produced the same results. In comparison to the plate problem, the quasi-nonlinear HTSD theories for this problem showed greater flexibility than the linear HTSD variants, but only after the collapse phase. The quasi-nonlinear HTSD with material transformations theory predicted a load about 4 percent less than the modified Donnell theory (with HTSD included) in the range of $0.7 \leq w \leq 0.8$ and about 12 percent less at $w = 0.2.286\text{-cm}$. This is due to the increased coupling of membrane, bending, and transverse shear activity in the quasi-nonlinear HTSD theory.

Values of the rotational term, ψ_2 , for ten increments of transverse displacement, were compared for the cubic-nonlinear HTSD theory with material transformations. The maximum rotation for increments 1-7 never exceeded 0.11 radians (6.3°), before the shell snaps. After the shell snaps, the maximum rotation measured is 0.15 radians (8.6°). These are considered small rotations and the material transformation matrices have a negligible effect when included in the analysis.

The inclusion of laminated composite materials is considered in a 0.635-cm thick quasi-isotropic shell under a transverse point load. The geometry and boundary conditions are the same as the isotropic shell problem. An 8×12 mesh of elements is used to model one quadrant of the shell. The quasi-isotropic shell exhibited a significantly different equilibrium path than the isotropic shell. The peak collapse load is nine times the magnitude of the isotropic problem and the shape of the equilibrium curve is not as dramatic as for the isotropic shell. Interestingly enough, when comparisons were made in the development of the rotational degree of freedom, ψ_2 , the magnitudes of the rotations were similar to those of the isotropic shell. Only the distributions of the ψ_2 rotations differ between the isotropic and quasi-isotropic shells. As before, the magnitude of the rotations are small and the effect of the material transformation matrices was negligible.

A clamped-free cylindrical shell panel with various ply lay-ups under a transverse point load, was chosen to study the effects of material transformation matrices for deep composite shell panels. This shell panel had a 30.48-cm radius, a thickness of 0.102-cm , and dimensions of 27.94-cm (lateral) by 30.48-cm (circumferential). Because of the larger circumferential dimension, this shell was significantly deeper than the previous problems. Tsai and others (1990) investigated shells of this configuration and compared static and dynamic results for different material properties and ply lay-ups. A one quadrant 96 element mesh (8×12) was chosen for this problem. The

cubic-nonlinear HTSD theory predicted results similar to those of Tsai. The cubic-nonlinear HTSD theory with material transformation matrices predicted significantly more flexible results than the other theories. The material transformation theory significantly altered the global displacement response of the shell(s) in the post-snapping behavior when the shell(s) returned to a tensile load state. This is attributed to the majority of shell achieving a deformed shape exhibited in Figure 5.17 where a significant portion of the shell, at least 30%, was undergoing rotations of 0.45 radians (25.78°) or greater.

The 1/4-inch thick isotropic panel has properties that did not vary with orientation of the material. The shear modulus for the isotropic panel was assumed to be one-half the Young's modulus. Since the shell behaved in a flexible manner and snapped through with a relatively low transverse load, the initial severity of bending was characterized by the distance between the lateral supports and the depth of the shell. The quasi-isotropic shell had a $[0/-45/45/90]_s$ ply lay-up with a ratio of $E_1/E_2 = 15$ and a transverse modulus less than E_2 . For the composite shell, the primary cause of deformation was also bending activity. The inner plies of this laminated panel were the only plies in the transverse direction. This implies that 75 % of the material of this shell has a bending stiffness $[D_{ij}]$ in the circumferential direction that was significantly less than the outer plies. This panel was only 0.04-inches thick. Thus, the inner plies may not have been effective in resisting bending, since they were so close to the midsurface of the shell. With the lateral supports of this shell clamped, the final deformed shape of the shell exhibited both positive and negative curvatures. The severity of bending is characterized by the distance of about 2 inches. The bending activity of the clamped composite shell was more severe than that of the hinged isotropic shell.

These problems demonstrated that non-isotropic material properties have a significant effect upon the predicted global response/behavior of shell structures. Because of the reduced stiffness in the circumferential direction, the increased coupling of transverse shear activity and rotations with the in-plane strains, and the significantly lower transverse shear properties of this panel, the incorporation of the material transformations (based on displacement terms) significantly affected the strain energy of the composite shell. This resulted in a more flexible structure at snapping, and in the snap-through phase of the shell's response.

A set of problems with quasi-isotropic material and similar radius of curvature, but a signifi-

cantly altered loading scheme was chosen next. These problems were axially-loaded quasi-isotropic cylindrical shell panels with and without a 10.16-*cm* centered cutout. These panels has a radius of 30.48-*cms*, a thickness of 0.102-*cm*, and dimensions of 30.48-*cm* (lateral) by 30.48-*cm* (circumferential). The cut-out was square, 10.16-*cm* sides, and was centrally located. Due to the possibility of nonsymmetric deformation as discussed by Tisler (1986) and Palazotto & Dennis (1992), the entire panel was modelled with 576 elements. Only the cubic-nonlinear HTSD theory and the cubic-nonlinear HTSD theory including material transformations were evaluated.

When considering the rotations observed in both problems, it was evident that the maximum rotational ψ_2 observed was 9.5° for the cylindrical shell without a cutout and 7.8° for the cylindrical shell with a cutout. In both analyses, less than 18% of the shell surface observed magnitudes of ψ_2 greater than 4° . Thus, the effect of the material transformations on the global displacement behavior of these shells was minimal. Considering the relative magnitude of transverse deflection and circumferential rotation, and the relation of the depth of the shell versus shell thickness, these axial panels represent a rather shallow shell when compared to the previous problem.

Since one of the objectives of this effort was to include spherical geometry, an isotropic spherical shell cap was chosen as the next exercise. This problem was first solved by Argyris (1980) and later by Parisch (1981). This isotropic shell is hinged on all four boundaries and has a depth of 2.181-*cm*. It is 4.60-*cm* along each circumferential direction, has a thickness of 0.0158-inches and a radius of curvature of 12.09-*cm*. The shell was modelled by a 12×12 mesh with the transverse displacement prescribed at the apex. The cubic-nonlinear HTSD and cubic-nonlinear HTSD with material transformation theories compared favorably with Argyris' TRUMP element. Both theories predicted a more flexible shell displacement response than either Argyris or Parisch reported. This is attributed to the eight-noded element used by the author which allows quadratic interpolation of the in-plane degrees of freedom, u and v . This allowed the membrane activity of the shell to behave in a more flexible manner than the four-noded TRUMP element.

The maximum ψ_2 rotation observed in the shell was 15.68° at the collapse point and over 20% of the shell surface saw ψ_2 rotations of 14.9° . These rotations are considered relatively small for shell behavior. Thus, it is not surprising the inclusion of the material transformation matrices in the cubic-nonlinear HTSD theory had minimal effect on altering the shell's global displacement response.

The final set of problems chosen were essentially the isotropic hinged spherical shell cap with the material changed to quasi-isotropic laminates. Three ply lay-ups were considered, $[0/-45/45/90]_s$, $[0_2/90_2]_s$, and $[0_8]$. The author realizes the inclusion of $\pm 45^\circ$ plies is impractical from an experimental point of view owing to the difficulties of maintaining a true 45° fiber orientation throughout the spherical cap. However, the $[0/-45/45/90]_s$ does offer a unique comparison with the other quasi-isotropic and the isotropic spherical shell cap problems. In all three analyses, the cubic-nonlinear HTSD theory with the material transformation matrices had a minimal effect on the shell(s)' global displacement response. This was not surprising considering the relative small ψ_2 rotations (only 12% of the shell surface saw magnitudes of ψ_2 greater than 15°). It was only in the snap-through phase of the equilibrium curve, when ψ_2 exceeded 11.1° , that this theory predicted a more flexible shell response than the cubic-nonlinear HTSD theory. As mentioned in the isotropic spherical shell cap analysis, these types of shells are relatively shallow and only provided a moderate test of the cubic-nonlinear HTSD theory with material transformation matrices included.

7.3 Elastic-Plastic Shell Analysis

A simply-supported, elastic-perfectly plastic plate was considered to exercise and validate the nonlinear material behavior of the theory. The plate is 2.54-cm square with a thickness of 0.01-inches. The results of this problem were compared to Owen & Hinton's published results (1980). One quadrant of the plate was modelled with 64 uniform elements. To accurately predict Owen & Hinton's results, the membrane activity of the plate was minimized to allow bending activity to dominate the plate's response. This was accomplished by removing the in-plane degrees of freedom u and v . This allowed the flexure stiffnesses $[D_{ij}]$ to dominate the analysis, thereby allowing the plate response to be purely bending. The nonlinear material, large strain theory accurately predicted the plate's global displacement response when compared to Owen & Hinton's. Since there is no curvature in the plate, many of the nonlinear displacement terms become zero. In addition, the plate is relatively thin, so transverse shear is negligible also. As expected, the nonlinear material von Karman, nonlinear material modified von Karman, and the nonlinear material cubic-

nonlinear HTSD theories predicted virtually the same equilibrium curve.

The next problem chosen was that of a deep, isotropic cylindrical arch. This problem was identical to the cylindrical arch problem previously discussed in the elastic analysis, Section 7.3. However, the material is allowed to yield and behave perfectly plastic to determine the effect of nonlinear material behavior on a shell's global displacement response. Comparisons between the elastic cubic-nonlinear HTSD theory and the nonlinear material cubic-nonlinear HTSD theories were made. As before, a 1×40 mesh was used to model a quadrant of the arch. The inclusion of nonlinear material behavior significantly altered the arch's global displacement response. The collapse load was reduced by 29.4% when compared to the Donnell theory, 22.3% when compared to the cubic-nonlinear HTSD theory, and 16.4% when compared to the cubic-nonlinear HTSD theory with the material transformation matrices included. As expected, the global displacement response of the arch became more flexible when nonlinear material behavior was included in the analysis.

In the post-collapse response of the nonlinear material model differs from the Donnell, modified Donnell, and Huddelston's inextensible solution (1968) for cylindrical arches. This is attributed to the higher-order representation of the deformation of the midsurface of the arch and the continually changing properties of the elastic perfectly-plastic material. Almroth & Brogan (1980) saw a similar effect to the inextensible solution of a deep arch. Their finite element formulation allows for nonzero straining, and their results were consistently more flexible compared to the inextensible solution.

To test the plasticity model for true cylindrical shells, a short isotropic cylinder bounded by two rigid diaphragms at its ends, loaded with two transverse pinching loads at the middle section, and characterized as elastic perfectly-plastic was chosen. This problem was published by Simo & Kennedy in 1992. The cylinder was 3 non-dimensionalized units thick, 180 non-dimensionalized units in length longitudinally, and had a 300 non-dimensionalized unit radius of curvature. An 8×36 element mesh was used to model one octant of the cylinder. The theory accurately predicted the shell's global displacement response and compares favorably with Simo & Kennedy's results.

The final isotropic shell problem chosen was the spherical shell cap first published by Argyris (1980). The shell is 4.60-cm long in both circumferential directions with hinged boundary conditions. The spherical shell cap is 0.04-cm thick, has a depth of 2.181-cm, a radius of curvature of

12.09-cm, and is loaded transversely at the apex. The material is assumed to behave elastic perfectly-plastic. As expected, the author's theory predicts a more flexible response than Argyris' 4-noded TRUMP element. This is due, primarily, to the 8-noded element, with quadratic interpolation of the in-plane displacement degrees of freedom, the author uses. Since rotations remain small, the only significant effect on the shell's global displacement response was the inclusion of the nonlinear elastic-plastic material behavior. Simply including the material transformation matrices has a minor effect on the equilibrium path of the shell.

To exercise and validate the author's theory for composite laminas, a Graphite Polyetherether Ketone (Gr/PEEK) tensile coupon was chosen. Gould (1990) conducted a series of experiments considering $\pm 45^\circ$ ply lay-ups and then compared a stress-resultant finite element formulation to determine the effect of including material transformation matrices within a nonlinear material theory. The tensile coupon was 2.54-cm in width, 25.4-cm in length, and 2.134-cm thick. The ply lay-up chosen for comparison was $[45/-45]_{4s}$. The anisotropic nonlinear material parameters needed for the analysis were determined from the actual experimental stress-strain curves shown by Gould. The nonlinear material cubic-nonlinear HTSD theory accurately predicted the equilibrium path for the tensile coupon to within 10%. Due to the orientation of the fibers, the matrix appeared to carry much of the load. Since the matrix had a very low yield stress, it was expected to observe a distinct change in the global displacement response when nonlinear material behavior was included in the theory.

The next quasi-isotropic shell problem chosen was a clamped-free, composite cylindrical shell panel under a transverse point load at the middle section. This shell panel had a 30.48-cm radius, a thickness of 0.102-cm, and dimensions of 27.94-cm (lateral) by 30.48-cm (circumferential). Because of the larger circumferential dimension, this shell was significantly deeper than the previous problems. Based on the previous elastic analysis, one quadrant of the shell was modelled with 96 elements (8×12 mesh). Only the $[0/-45/45/90]_s$ ply lay-up was considered. The anisotropic nonlinear material parameters needed for the analysis were determined from the actual experimental stress-strain curves of graphite epoxy tensile coupon tests representative of the material used by Hatfield. The inclusion of the nonlinear material behavior significantly altered the global displacement response of the shell. The collapse load was 46.2% when compared to the Donnell theory, and 38.1% when compared to the cubic-nonlinear HTSD theory. The post-

collapse behavior is significantly more flexible due to the large regions of plasticity occurring across the surface of the shell.

The axially loaded (buckling), clamped-free composite cylindrical shell was considered next. This problem was significant due to the availability of experimental data from Hatfield (1991) for comparison. This shell had a 12-inch radius of curvature, was 12-inches in length longitudinally and circumferentially. The shell's thickness was 0.04-inches and the ply lay-up was $[0/-45/45/90]_5$. The anisotropic nonlinear material parameters needed for the analysis were chosen from the previous clamped-free transversely loaded cylindrical shell problem. The inclusion of the nonlinear material behavior in the model did alter the global displacement response significantly. For the cylindrical panel without a cutout, the predicted collapse load was within 24.1% of Hatfield's experimental results. For the cylindrical panel with a 4-inch centered cutout, the predicted collapse load was within 12.4% of the experimental results recorded by Hatfield. In both problems, the shell's predicted response is more flexible than for the elastic solutions, and behaves similarly to the experimental results observed by Hatfield.

The author proposes two possibilities for the large variance in both collapse load and axial displacement between analysis and the experiment. The first is the possibility that the boundary conditions are not truly clamped. This is a remote possibility considering at least 1.27-cm of the panel is clamped at both the top and bottom, but it is possible the panel is moving within the test fixture's clamps. The other possibility is in the fabrication of the panels. Due to curing stresses generated in the autoclave, when the individual panels are cut from the general laminate, the panels tend to warp. This was observed by the author upon examining panels fabricated for his Master's Thesis (1989). This warping leads to a radius of curvature that is not constant. However, the test fixtures clamps are set for a constant 30.48-cm radius of curvature. Thus, once the panels are seated within the test fixture, it is possible a slight imperfection is being induced. Brush & Almroth (1975) noted that an imperfection of 0.1% is significant and greatly alters the equilibrium path of the shell. The author confirmed this phenomena during his Master's Thesis while using the STAGSC-1 code. Since the author's theory assumes the shell(s) have a constant radii of curvature, it may explain why the theory predicts a stiffer shell, even when nonlinear material behavior is considered.

The final set of problems considered were hinged, quasi-isotropic spherical shell caps. These shells were 4.60-cm in length circumferentially with a radius of curvature of 4.76-inches. The

shell thickness was 0.04-cm and the depth was 2.181-cm. The anisotropic nonlinear material parameters needed for the analysis were chosen from the previous clamped-free transversely loaded cylindrical shell problem. Due to the need for accurately resolving the stress-field near the apex of the spherical shell, a refined 18×18 mesh was used to model the entire shell. Two ply lay-ups were considered, $[0/-45/45/90]_s$ and $[0_8]$. Similarly to the transversely loaded composite cylindrical shell, the nonlinear material theory does predict a more flexible global displacement response. For the $[0/-45/45/90]_s$ ply lay-up, the collapse load was reduced by 17.8% as compared to the elastic cubic-nonlinear HTSD theory. For the $[0_8]$ ply lay-up, the collapse load was reduced by 23.9% as compared to the cubic-nonlinear HTSD theory.

7.4 Conclusions

This research revealed several unique findings to the limitations of a total Lagrangian nonlinear HTSD shell theory employing material transformation matrices and nonlinear material behavior. The magnitudes of the ψ_i rotations and ratio of transverse displacement to depth of the shell were found to be important factors in predicting the applicability of the material transformation nonlinear HTSD theory. If the rotations remained small (less than 15°) the material transformation matrices had no effect on the predicted global displacement response. The plate problem and the 0.25-inch thick hinged-free isotropic shell panel exhibited such a response. When the Donnell approximations are no longer valid (ψ_2 rotations greater than 15°) the material transformations have a minimal effect on the predicted global displacement response. The cylindrical composite shell panels with and without a 4-inch centered cutout under an axial load, and the elastic spherical shell cap problems (isotropic and quasi-isotropic) showed only a marginal increase in flexibility in the shell's global displacement response. If these rotations become very large (ψ_2 rotations greater than 27°), then the material transformation matrices have a significant effect in altering the shell's global displacement response. The cylindrical arch and the deep composite cylindrical shell under a transverse load are examples of this. It should be noted that the greatest change in the global displacement response occurred at the peak loading and during the snap-through behavior.

For nonlinear material behavior, the significant indicator was the yield stress versus Young's modulus for isotropic materials, and the yield stress for the in-plane (σ_{12}) parameter versus the largest elastic moduli, usually E_1 for anisotropic materials. If these ratios remained small (on the order of 10^{-5} to 10^{-3}), plasticity would soon dominate the shell's global displacement response. This was evident in all the quasi-isotropic material models. For the graphite polyetherether ketone (Gr/PEEK) tensile coupon, the ratio is 3.97×10^{-4} . Thus, the tensile coupon behaves materially nonlinear almost from the onset of loading. For the graphite epoxy models, the ratio is 2.79×10^{-3} . Similarly, these problems should exhibit significantly altered global displacement responses due to the inclusion of nonlinear material behavior. When the ratios are larger (on the order of 10^{-1}), plasticity affect the global displacement response to a lesser degree. The pinched isotropic cylinder has a ratio of 0.9 and behaves in a manner dominated by membrane activity.

For those shells or plates exhibiting $\bar{\epsilon} \geq 0.025$ over more than 15-20% of the outer surface, the presence of plasticity dominates their response and reduces their stiffness significantly. Comparing elasto-plastic results to elastic solutions led to a reduction in peak snapping or buckling loads of 18-45% occurred due to plasticity while the displacement associated with the snapping/buckling load increased by 12-27%. The combination of a decrease in load with an increase in the displacement associated with the peak load indicates a significant "softening" effect due to plasticity which is expected.

The additional computational burden of the cubic-nonlinear strain-displacement relations is somewhat significant when spherical geometry is added. The most simple nonlinear HTSD theory is C100 which has 13866 lines of code. By comparison, when spherical geometry is included, the simplest nonlinear HTSD theory is S100 which has 18175 lines of code by including all the curvature terms in the s_I -direction. When the elastic-plastic cubic-nonlinear HTSD theory for spherical geometry (G211) is included, the code has 37856 lines. The resulting computation burden of this additional code is significant in terms of CPU consumption and memory requirement. The elemental independent formulation of stiffness arrays, with Gauss integration in the plane of every element (for the 36 degree of freedom element usually chosen, 25 Gauss points are calculated per element for exact integration) on ever iteration of every load/displacement increment of the nonlinear problem(s). Clearly, this formulation of a higher-order theory is practical for specialized research of this nature, not for routine engineering use. Since the element independent

formulation is based upon arrays of strain coefficients, the possibility of vectorizing the code exists. In this manner, a more efficient higher-order theory may be of practical use.

Due to the total Lagrangian formulation, and the allowance of large strain/nonlinear material behavior, the requirement of transforming the stresses and strains from Lagrangian to Cauchy and back to Lagrangian was necessary. This is due to the assumption of an incremental flow theory which requires a Cauchy reference frame. To accurately predict the stress field, which is secondary in nature for a displacement-based Lagrangian formulation, requires very refined meshes. These refined meshes require a substantial increase in computer times. For the elastic analysis, stress was not usually calculated because of the additional expense in CPU time. To accurately measure the stress at any node, the quasi three-dimensional stress field is calculated at each Gauss point, for every layer, and then integrated to determine the stress at each Gauss point. Thus, for the 36 degree-of-freedom element, with a total of 25 Gauss points per layer, and a minimum of eight layers, led to a total of 40 constitutive Gauss points being calculated. Comparing the run time between an elastic and plastic analysis for the same shell model usually resulted in an increase of CPU time by a factor of 5. This is due to updating the $[\hat{K}]$, $[\hat{N}_1]$, and $[\hat{N}_2]$ stiffness arrays for every iteration in terms of displacement and the constitutive relations. In other words, an elastic problem may take 8 CPU hours to solve on a SPARC10 workstation, the same problem using nonlinear material theory would take at least 40 CPU hours on the same workstation. The author contends using a stress-resultant based finite element formulation with an updated Lagrangian approach would be more efficient. By solving for the stresses directly, and using a Cauchy oriented material system, reduces the computational burden of tracking stresses and transforming them, correctly, between the Cauchy and Lagrangian material axes systems. For each problem presented in Chapter 6, the author has specified the convergence tolerance, ∇ , the element mesh used, and the number of displacement increments (and the increment size) used to achieve a solution. Depending on the geometry of the problem, the material properties and boundary conditions, the development of plasticity varied from problem to problem. Hence, from an elasto-plastic analysis the criteria for the numerics changed from one problem to the next.

The theory developed and presented in this research adequately predicts the changes in global displacement response of isotropic and quasi-isotropic plates, cylindrical and spherical shells. It is a total Lagrangian finite element formulation that incorporates a quasi three-dimensional mate-

rial theory and models orthogonal plates and shells. The inclusion of material transformation matrices within the cubic-nonlinear HTSD theory resulted in a more flexible response prediction for deep shell problems during the collapse phase. Similarly, the nonlinear material cubic-nonlinear HTSD theory provided a more flexible response prediction for both deep and shallow shells, as long as the ratio of yield stress versus modulus of elasticity was greater than 10^{-3} . However, due to requirement of transforming the stress state between Lagrangian and Cauchy reference frames, to satisfy the incremental flow theory requirement, a significant increase in CPU time occurred.

8. Bibliography

1. Aboudi, J. "The Effective Thermomechanical Behavior of Inelastic Fiber-Reinforced Materials", *International Journal of Engineering & Science*, 23:773, 1985.
2. Aboudi, J. "Micromechanical Analysis of Composites by the Method of Cells", *Applied Mechanics Review*, 43:193-221, 1989.
3. Almroth, B.O., & F.A. Brogan. "Numerical Procedures for Analysis of Structural Shells," Air Force Wright Aeronautical Labs, AFWAL-TR-80-3129, Wright-Patterson AFB, OH.
4. Almroth, B.O., F.A. Brogan, & G.M. Stanley. *Structural Analysis of General Shells, Volume II. User Instructions for STAGSC-1 Journal of Mechanical Engineering Science*. Lockheed Palo Alto Research Laboratory, Palo Alto, CA, 1982.
5. Alwar, R.S. & M.C. Narasimhan. "Analysis of Laminated Orthotropic Spherical Shells Subjected to Asymmetric Loads," *Computers & Structures*, 41: 611-620. 1991.
6. Anderson, R.E. *A Variational Theorem for Laminated Composite Plates of Nonlinear Materials and Applications to Postbuckling*. PhD Dissertation, Stanford University, Stanford, CA, 1979.
7. Antman, S.S. "Nonlinear Problems of Geometrically Exact Shell Theories," *Presented at Winter Annual Meeting of ASME, CED-Vol 3:109-131*, San Francisco, CA. 10-15 December 1989.
8. Argyris, J.H., H. Balmer, M. Kleiber, & U. Hindenlang. "Natural Formulation of Large Inelastic Deformation for Shell of Arbitrary shape - Application of the TRUMP Element", *Computer Methods in Applied Mechanics & Engineering*, 22:361-389, 1980.
9. Armen, H. "Assumptions, Models, and Computational Methods for Plasticity", *Computers & Structures*, 10:161-174, 1979.
10. Arnold, R.R. *Buckling, Postbuckling, and Crippling of Materially Nonlinear Composite Plates*. PhD Dissertation, Stanford University, Stanford, CA, 1983.
11. Ashton, J.E., J.C. Halpin, & P.H. Petit. *Primer on Composite Material Analysis*. Stamford, Connecticut: Technomic, 1969.
12. Avery, W.B. & C.T. Herakovich. "Effect of Fiber Anisotropy on Thermal Stresses in Fibrous Composites", *Journal of Applied Mechanics*, 53:318-385, 1987.
13. Banichuk, N.V. & V.V. Kobolev. "Optimal Plastic Anisotropy", *Journal of Applied Mathematics & Mechanics*, 51:381-385, 1987
14. Bank, L.C. & M.P. Bieniek. "A Model for the Nonlinear Response of Composite Laminates", *27th AIAA/ASME/ASCE/AHS Structures, Structural Dynamics and Materials Conference*, Paper

No. AIAA-86-0887-CP, San Antonio, TX, May 19-26, 1986.

15. Bank, L.C. & M.P. Bieniek. "Stress-Resultant Plasticity Theories for Composite Laminated Plates", *International Journal of Plasticity*, 4:317-333, 1988.

16. Bathe, K.J. & L.W. Ho. "Some Results in the Analysis of Thin Shell Structures," in *Finite Element Analysis in Structural Mechanics*, Chapter 2, pages 122-150. Springer-Verlag, NY, 1981.

17. Bathe, K.J. "A Solution Method for Nonlinear Dynamic Analysis of Shell Structures", Technical Report, *BRL-CR-535* (AD-A149846), 1983.

18. Bathe, K.J. & E.N. Dvorkin. "A Formulation of General Shell Elements-The Use of Mixed Interpolation of Tensorial Components", *International Journal of Numerical Methods in Engineering*, 22:697-722, 1986.

19. Becker, M.L, A.N. Palazotto, & N.S. Khot. "Experimental Investigation of the Instability of Composite Cylindrical Panels", *Experimental Mechanics*, 22:372-376, 1982.

20. Belton, J. "Applications of Tensor Functions to Formulation of Yield Criteria for Anisotropic Materials", *International Journal of Plasticity*, 4:29-46, 1988.

21. Belytscho, T. & L. Gaum. "Application of Higher Order Corrotational Stretch Theories to Nonlinear Finite Element Analysis", *Computers & Structures*, 10:175-182, 1979.

22. Belytscho, T., J.S.J. Ong, & W.K. Liu. "Hourglass Control in Linear and Nonlinear Problems", *Computer Methods in Applied Mechanics & Engineering*, 43:251-276, 1984.

23. Belytscho, T. & W.E. Bachrach. "Efficient Implementation of Quadrilaterals with High Course-Mesh Accuracy", *Computer Methods in Applied Mechanics & Engineering*, 54:279-302, 1986.

24. Bishop, A.W. "The Strength of Soils as Engineering Materials," *Geotechnique*, 16:89-130, 1966.

25. Bland, D.R. "The Associated Flow Rule of Plasticity," *Journal of Mechanics and Physics of Solids*, 6:71-78, 1957.

26. Bout, A. & F. van Keulen. "A Mixed Element for Geometrically and Physically Nonlinear Shell Problems", *HERON*, 36:27-35, Edited by Delft University of Technology, Delft, The Netherlands, 1991.

27. Bridgman, P.W. *Studies in Large Plastic Flow and Fracture*, Mcraw-Hill, New York, 1952.

28. Brodland, G.W. & H. Cohen. "Deflection and Snapping of Spherical Caps", *International Journal of Solids & Structures*, 23:1341-1356, 1987.

29. Brush, D.O, & B.O. Almroth. *Buckling of Bars, Plates, & Shells*. McGraw-Hill, London, UK,

1975,

30. Bushnell, D. "Computerized Analysis of Shells-Governing Equations", *Computers & Structures*, 18:471-536, 1984.
31. Calcote, L.R. *The Analysis of Laminated Composite Structures*. Van Nostrand Reinhold Co., Cincinnati, Ohio, 1969.
32. Chandrashakara, K. & J.N. Reddy. "Nonlinear Analysis of Composite Laminates Accounting for Elastic-Plastic Material Behavior", *Proceedings for International Symposium on Composite Materials and Structures*, Beijing, China, June 10-13, 1986.
33. Chang, F. & Z. Kutlu. "Strength and Response of Cylindrical Composite Shells Subjected to Out-of-Plane Loadings", *Journal of Composite Materials*, 23:67-85, 1990.
34. Chang, T.Y. & K. Sawamiphakdi. "Large Deformation Analysis of Laminated Shells by Finite Element Method", *Computers & Structures*, 13:331-340, 1981.
35. Chao, P.C., B.M. McNamee, & D.K. Chou. "The Yield Criterion of Laminated Media," *Journal of Composite Materials*, 7:22-35. January, 1973.
36. Chao, W.C., N.S. Putcha, & J.N. Reddy. "Three-Dimensional Finite Element Analysis of Layered Composite Structures", *Technical Report No. 29*, 1982.
37. Chao, W.C. & J.N. Reddy. "Analysis of Laminated Composite Shells Using a Degenerated 3-D Element", *International Journal of Numerical Mechanical Engineering*, 20:1991-2007, 1984.
38. Chaudhuri, R.A. "An Equilibrium Method for Prediction of Transverse Shear Stresses in a Laminated Shell", *Computers & Structures*, 23:139-146, 1986.
39. Chaudhuri, R.A. & P. Seide. "An Approximate Method for Prediction of Transverse Shear Stresses in a Laminated Shell", *Computers & Structures*, 23:1145-1161, 1987.
40. Chen, H. "The Effect of Nonlinear Behavior of Composite Materials on Load Capacity of the Laminate", *Proceedings of the International Symposium on Composite Materials and Structures*, Beijing, China, pages 163-173, June 1986.
41. Chien, L.S. & A.N. Palazotto. "Dynamics Buckling of Composite Cylindrical Panels with Higher-Order Transverse Shears Subjected to a Transverse Concentrated Load", *International Journal of Non-Linear Mechanics*, 27:719-734, 1992.
42. Chien, L.S. & A.N. Palazotto. "Nonlinear Snapping Considerations for Laminated Cylindrical Panels", *Composites Engineering*, 2:631-639, 1992.
43. Chiou, J.H., J.D. Lee, & A.G. Erdmans. "Development of a Three-Dimensional Finite Element Program for Large Strain Elastic-Plastic Solids", *Computers & Structures*, 36:631-645, 1990.

44. Cook, R.D. *Concepts and Applications of Finite Element Analysis, Third Edition*. John Wiley & Sons, NY, 1989.
45. DaDeppo, D.A. & R. Schmidt. "Instability of Clamped Hinged Circular Arches Subjected to a Point Load", *Journal of Applied Mechanics*:894-896, 1975.
46. Dafalias, Y.F. & M.M. Rashid. *International Journal of Plasticity*, 5:227-246, 1989.
47. Davis, E.M. "Theories of Plasticity and the Failure of Soil Masses", Ch. 6, *Soil Mechanics*, Ed. I.K. Lee, Butterworths, London, 1968.
48. Dennis, S.T. *Large Displacement and Rotational Formulation for Laminated Cylindrical Shells including Parabolic Transverse Shear*. PhD Thesis, AFIT/DS/AA/88-1(AD-A4194871). School of Engineering, Air Force Institute of Technology (AU), Wright-Patterson AFB, Ohio, May 1988.
49. Dennis, S.T. "Two-Dimensional Laminated Shell Theory Including Parabolic Transverse Shear", Technical Report *USAF-A-TR-89-6* (AD-A213817), United States Air Force Academy, Colorado, 1989.
50. Dennis, S.T. & A.N. Palazotto. "Transverse Shear Deformation of Orthotropic Cylindrical Pressure Vessels Using Higher-Order Shear Theory", *AIAA Journal*, 27:1441-1447, 1989.
51. Dennis, S.T. & A.N. Palazotto. "Large Displacements and Rotational Formulation for Laminated Shells Including Parabolic Transverse Shear", *International Journal of Nonlinear Mechanics*, 25:67-85, 1990.
52. Dennis, S.T. B. Horban, & A.N. Palazotto. "Instability in a Cylindrical Panel Subjected to a Normal Pressure", *33rd AIAA/ASME/AHS/ASC Structures, Structural Dynamics and Materials Conference*, Paper No. AIAA-92-2234. Dallas, TX, April 13-15, 1992.
53. Di Scuva, M. "Improved Shear-Deformation Theory for Moderately Thick Multi-Layered Anisotropic Shells and Plates", *Journal of Applied Mechanics*, 54:589-596, 1987.
54. Dodds, Jr., R.H. "Numerical Techniques for Plasticity Computations in Finite Element Analysis", *Computers & Structures*, 26:767-779, 1987.
55. Donnell, L.H. *Stability of Thin Walled Tubes under Torsion*, NACA TR 479, Washington: National Advisory Committee for Aeronautics, 1934.
56. Doxsee, Jr., L.E. "A Higher-Order Theory of Hygrothermal Behavior of Laminated Composite Shells", *International Journal of Solids & Structures*, 25:339-355, 1989.
57. Drucker, D.C. "Conventional and Unconventional Plastic Response and Representation", *Applied Mechanics Review*, 41:151-167, 1988.
58. Dvorak, G.J. "Thermal Expansion of Elastic-Plastic Composite Materials", *Journal of Applied*

Mechanics, 53:737-743, 1986.

59. Dvorkin, E. & K.J. Bathe. "A Continuum Mechanics Based Four-Node Shell Element for General Nonlinear Analysis", *Journal of Engineering Computations*, 1:77-84, 1984.
60. Dubey, R.N. & M.J. Hillier. "Yield Criteria and Bauschinger Effect for a Plastic Solid", *Journal of Basic Engineering*, Paper No. 711-MET-p, March, 1972.
61. Durocher, L. & A.N. Palazotto. "Elastic Plastic Buckling of Anisotropic Plates", *National Science Foundation Grant Report GK-5084*, University of Bridgeport, College of Engineering, Bridgeport, CT, 1971.
62. Eidsheim, O.M. & P.K. Larsen. "A Study of Some General Constitutive Models for Elasto-Plastic Shells", in *Nonlinear Finite Element Analysis in Structural Mechanics*, Chapter 4, pages 364-384. Springer-Verlag, NY, 1981.
63. Engblom, J.J. & O.O. Ochoa. "Finite Element Formulation Including Interlaminar Stress Calculations", *Computers & Structures*, 23:141-249, 1986.
64. Engblom, J.J., J.P. Fuchne, & J.M. Hamdallah. "Transverse Stress Calculations for Laminated Composite Shell Structures Using Plate/Shell Finite Element Formulations", *Journal of Reinforced Plastics & Composites*, 8:446-457, 1989.
65. Fares, N. & G.J. Dvorak. "Large Elastic-Plastic Deformations of Fibrous Metal Matrix Composites". To be published in *Journal of Mechanics & Physical Sciences*.
66. Feldman, E. & J. Aboudi. "Postbuckling Analysis and Imperfection Sensitivity of Metal Matrix Laminated Cylindrical Panels," *Composite Structures*, 25:241-248. 1993.
67. Figueiras, J.A. & D.R.J. Owen. "Analysis of Elasto-Plastic and Geometrically Nonlinear Anisotropic Plates and Shells", in *Finite Element Software for Plates and Shells*, Chapter 4, pages 235-326. Pineridge Press, Swansea, U.K., 1984.
68. Flugge, W. *Stresses in Shells*, 2nd Ed., Spring-Verlag, Berlin/Gottingen/Heidelberg, Germany. 1962.
69. Frederking, R.M.W. & O.M. Sidebottom. "An Experimental Evaluation of Plasticity Theories for Anisotropic Metals", *Journal of Applied Mechanics*, 1971.
70. Ghassemieh, M. & A.R. Kukreti. "An Algorithm for the Analysis of Problems with Combined Material and Geometric Nonlinearities", *Computers & Structures*, 35:579-591, 1990.
71. Gould, S.C. *Investigations of Strain Characteristics of Graphite Polyetherether Ketone using a Nonlinear Analysis and Experimental Methods*. Master's Thesis, AFIT/GAE/ENY/90D-08, School of Engineering, Air Force Institute of Technology (AU), Wright-Patterson AFB, OH, 1990.

72. Graff, E. & G.S. Springer. "Stress Analysis of Thick, Curved Composite Laminates", *Computers & Structures*, 38:41-55, 1991.
73. Griffin, Jr., O.H. "Three-Dimensional Thermal Stresses in Angle-Ply Composite Laminates", *Journal of Composite Materials*, 22:53-70, 1988.
74. Hahn, H.T. & S.W. Tsai. "Nonlinear Elastic Behavior of Unidirectional Composites Laminae", *Journal of Composite Materials*, 7:102, 1973.
75. Hahn, H.T. "Nonlinear Behavior of Laminated Composites", *Journal of Composite Materials*, 7:257, 1973.
76. Hashin, Z. "Failure Criteria for Unidirectional Fiber Composites", *Journal of Applied Mechanics*, 47:329-334, 1980.
77. Hatfield, J. *Effect of Thickness and Ply Layup on the Collapse Characteristics of Cylindrical Composite Shells with Large Cutouts*. Master's Thesis, AFIT/GAE/ENY/92D-20. School of Engineering, Air Force Institute of Technology (AU), Wright-Patterson AFB, OH, 1992.
78. Hildebrand, F.B., E. Reissner, & G.B. Thomas. *Notes on the Foundations of the Theory of Small Displacements of Orthotropic Shells*. Technical Note, NACA TN 1833. Washington D.C.: National Advisory Committee for Aeronautics, 1949.
79. Hill, R. "A Theory of the Yielding and Plastic Flow of Anisotropic Metals", *Proceedings of the Royal Society of London, Series A*, 193:281-297, 1948.
80. Hill, R. *The Mathematical Theory of Plasticity*, Oxford University Press, 1950.
81. Hill, R. "The Plastic Torsion of Anisotropic Bars", *Journal of Mechanics and Physics of Solids*, 2:87-91, 1954.
82. Hinrichsen, R.L. & A.N. Palazotto. "Nonlinear Finite Element Analysis of Thick Composites Plates using a Cubic Spline Function", *AIAA Journal*, 24:11-14, 1986.
83. Hinrichsen, R.L. & A.N. Palazotto. "Use of a Cubic Spline Function in Finite Elements", *Mathematical Computer Modelling*, 10:37-47, 1988.
84. Hoffman, O. & G. Sachs. *Introduction to the Theory of Plasticity for Engineers*, McGraw-Hill, 1953.
85. Hofmeister, L.D., G.A. Greenbaum, & D.A. Evenson. "Large Strain, Elasto-Plastic Finite Element Analysis," *AIAA Journal*, 9: 1248-1254. July, 1971.
86. Hu, L.W. "Studies on Plastic Flow of Anisotropic Metals", *Journal of Applied Mechanics*:444-450, 1956.
87. Huang, H.C. "Elastic and Elastic-Plastic Analysis of Shell Structures Using the Assumed

Strain Elements", *Computers & Structures*, 33:327-336, 1989.

88. Huddleston, J.V. "Finite Deflections and Snap-Through of High Circular Arches", *Journal of Applied Mechanics*:763-769, 1968.

89. Hughes, T.J.R. & W.K. Liu. "Nonlinear Finite Element Analysis of Shells. I - Three-Dimensional Shells", *Computer Methods in Applied Mechanics and Engineering*, 26:331-362, 1981.

90. Hughes, T.J.R. & W.K. Liu. "Nonlinear Finite Element Analysis of Shells. II - Two-Dimensional Shells", *Computer Methods in Applied Mechanics and Engineering*, 27:167-181, 1981.

91. Hughes, T.J.R. & E. Hinton. *Finite Element Methods for plates and Shell Structures. Volume I: Element Technology and Volume II: Formulations and Algorithms*. Pineridge Press, Swansea, U.K., 1986.

92. Hwang, W.C. & C.T. Sun. "Failure Analysis of Laminated Composite by Using Iterative Three-Dimensional Finite Element Method", *Computers and Structures*. 33:41-48, 1989.

93. Janisse, T.C. & A.N. Palazotto. "Collapse Analysis of Cylindrical Composite Panel with Cut-outs", *AIAA Journal*, 21:731-733, 1984.

94. Jensen, W.R., W.E. Falby, & N. Prince. "Matrix Analysis for Anisotropic Inelastic Materials", Technical Report AFFDL-TR-65-220, 1966.

95. Jones, R.M. *Mechanics of Composite Materials*, Washington D.C., Scripta Book Co., 1975.

96. Kaminski, B.E. & R.B. Lantz. "Strength Theories of Failure for Anisotropic Materials", *Composite Materials: Testing and Design*, ASTM STP 460, American Society for Testing and Materials, 160-169, 1969.

97. Kant, T. & M.P. Menon. "Higher-Order Theories for Composite and Sandwich Cylindrical Shells with C^0 Finite Elements", *Computers & Structures*, 33:1191-1204, 1989.

98. Knight, Jr., N.F., J.H. Starnes, Jr., & W.A. Walters, Jr. "Postbuckling Behavior of Selected Graphite-Epoxy Cylindrical Panels Loaded in Axial Compression", in *Proceedings of the 27th Structures, Structural Dynamics, and Materials Conference*, No. 86-0881, pages 142-158, NY:AIAA, 1986.

99. Koiter, W.T. "A Consistent First Approximation in the General Theory of Thin Elastic Shells", *The Theory of Thin Elastic Shells*:12-33. Amsterdam: North Holland, 1960.

100. Krause, H. *Thin Elastic Shells*. John Wiley & Sons, New York, NY. 1967.

101. Kwon, Y.W. & J.E.A. Kin. "Analysis of Layered Composite Plates Using a Higher-Order Deformation Theory", *Computers & Structures*, 27:619-623, 1987.

102. Lee, E.H., R.L. Mallet, & T.B. Werthimer. "Stress Analysis for Kinematic Hardening of

Finite Deformation Plasticity", *Journal of Applied Mechanics*, 50:554-560, 1983.

103. Leissa, A.W. "A Review of Laminated Composite Plate Buckling", *Applied Mechanics Review*, 40:575-591, 1987.

104. Li, Z.H. & D.R.J. Owen. "Elastic-Plastic Analysis of Laminated Anisotropic Shells by a Refined Finite Element Laminated Model", *Computers & Structures*, 32:1005-1024, 1989.

105. Liao, C.L. & J.N. Reddy. "Continuum-based Stiffed Composite Shell Element For Geometrically Nonlinear Analysis", *AIAA Journal*, 27:95-101, 1989.

106. Libai, A. & J.G. Simmonds. "Large-Strain Constitutive Laws for the Cylindrical Deformation of Shells," *International Journal of Non-Linear Mechanics*, 16: 91-103. 1981.

107. Libai, A. & J.G. Simmonds. "Nonlinear Elastic Shell Theory", *Advances in Applied Mechanics*, 23:273- 371, 1983.

108. Libai, A. & J.G. Simmonds. *The Nonlinear Theory of Shells*. Academic Press, NY, 1989.

109. Librescu, L. "Refined Geometrically Nonlinear Theories of Anisotropic Shells", *Quarterly Applied Mechanics*, 45:1-22, 1987.

110. Librescu, L., A.A. Khedir, & D. Fredrick. "Free Vibration and Buckling of Cross-Ply Laminated Shear-Deformable Shallow Shell-Type Panels", in *Recent Advances in Structural Dynamics, Proceedings of the Third International Conference on Structural Dynamics, Volumes I and II*. Technical Report AFWAL-TR-88-3304. Wright Aeronautical Laboratories, Wright-Patterson AFB, OH, 1988.

111. Librescu, L. & R. Schimdt. "Refined Theories of Elastic Anisotropic Shells Accounting for Small Strains and Moderate Rotations", *International Journal of Nonlinear Mechanics*, 23:217-229. 1989.

112. Librescu, L. & M.Y. Chang. "Imperfection Sensitivity and Postbuckling Behavior of Shear Deformable Composite Doubly-Curved Shallow Panels", *International Journal of Solid Structures*, 29:1065-1083, 1992.

113. Lin, J.S. & P.L. Gould. "Shells of Revolution with Local Plasticity", *Computer Methods in Applied Mechanics & Engineering*, 65:127-145, 1987.

114. Lin, K.Y. & I.H. Hwang. "Thermo-Viscoelastic Response of Graphite/Epoxy Composites", *Journal of Engineering Materials & Technology*, 110:113-116, 1988.

115. Loret, B. "On the Effect of Plastic Rotation in the Finite Deformation of Anisotropic Elastic-Plastic Materials", in *Mechanics of Materials, Volume II*:287-304, 1983

116. Love, A.E.H. *A Treatise on the Mathematical Theory of Shells*, 4th Ed., New York:Dover Publications, 1944.

117. Lou, S.Y. & T.W. Chou. "Finite Deformation and Nonlinear Elastic Behavior of Flexible Composites", *Journal of Applied Mechanics*, 55:149-155, 1988.
118. Lou, S.Y. & T.W. Chou. "Elastic Behavior of Laminated Composites Under Finite Deformation", from *Micromechanics and Inhomogeneity-The Toshio Mura Anniversary Volume*, pages 243-256, Springer-Verlag, NY, 1989.
119. Lubahn, J.D. & R.P. Felgar. *Plasticity and Creep of Metals*, Chap. 13, John Wiley and Sons, New York, 1961.
120. Luewood, A.R., J.F. Doule, & C.T. Sun. "Finite Element Program for Analysis of Laminated Anisotropic Elastic-Plastic Materials", *Computers & Structures*, 25:749-758, 1987.
121. *MACSYMA Reference Manual*. Symbolics, Inc. 1988
122. Marcal, V.V. & F.P. King. "Elastic-Plastic Analysis of Two-Dimensional Stress System by the Finite Element Method", *International Journal of Mechanics & Science*, 9:143-155, 1967.
123. Martin, R.J., A.N. Palazotto, & R.S. Sandhu. "Experimental and Analytical Comparisons of Failure in Thermoplastic Composite Laminates". To be published in 1990.
124. Mehan, R.L. "Effect of Combined Stress on Yield and Fracture Behavior of Zircaloy-Z", *Journal of Basic Engineering*, 499-512, 1961.
125. Mendelson, A. & S.S. Manson. "Practical Solutions of Plastic Deformation Problems in Elastic-Plastic Range", Technical Report NASA TR R-28, NASA, Washington D.C., 1959.
126. Mindlin, R.D. "Influence of Rotatory Inertia and Shear on Flexural Motions of Isotropic, Elastic Plates", *Journal of Applied Mechanics*, 18:336-343, 1951.
127. Mohd, S. & D.J. Dawe. "Buckling and Vibration of Thin Laminated Composite, Prismatic Shell Structures," *Composite Structures*, 25:353-362. 1993.
128. Mollmann, H. *Introduction to the Theory of Thin Shells*, New York: John Wiley & Sons, 1981.
129. Muc, A. "Buckling and Post-Buckling Behavior of Laminated Shallow Spherical Shells Subjected to External Pressure," *International Journal of Non-Linear Mechanics*, 27:465-476. 1992.
130. Muc, A., J. Rys, & W. Latas. "Limit Load Carrying Capacity for Spherical Laminated Shells Under External Pressure," *Composite Structures*, 25:295-303. 1993
131. Naghdi, P.M. "The Theory of Plates and Shells", *Encyclopedia of Physics*, 2nd Ed., pages 425-640. Springer-Verlag, NY, 1972.
132. Nahaz, M.N. "Survey of Failure and Post-Failure Theories of Laminated Fiber-Reinforced Composites", *Journal of Composite Technology & Research*, 8:138-153, 1986.

133. Nayak, G.C. & O.C. Zienkiewicz. "Elastic-Plastic Stress Analysis. A Generalization for Various Constitutive Relations Including Strain Softening", *International Journal of Numerical Methods in Engineering*, 5:113-135, 1972.
134. Noor, A.K., J.M. Peters, & C.M. Anderson. "Mixed Models and Reduction Techniques for Large Rotation Nonlinear Problems", *Computer Methods in Applied Mechanics & Engineering*, 44:67-898, 1984.
135. Noor, A.K. & J.M. Peters. "Nonlinear Analysis of Anisotropic Panels", *AIAA Journal*, 24:1545-1553, 1986.
136. Noor, A.K. & S.N. Atluri. "Advances and Trends in Computational Structure Mechanics", *AIAA Journal*, 25:977-995, 1987.
137. Noor, A.K. & W.S. Burton. "Assessment of Shear Deformation Theories for Multi-Layered Composite Plates", *Applied Mechanics Review*, 42:1-14, 1989.
138. Noor, A.K. & W.S. Burton. "Stress and Free Vibration Analysis of Multi-Layered Composite Plates", *Composite Structures*, 11:183-204, 1989.
139. Noor, A.K. & W.S. Burton. "Assessment of Computational Models for Multi-Layered Composite Shells", *Applied Mechanics Review*, 43:67-96, 1990.
140. Noor, A.K. "Mechanics of Anisotropic Plates and Shells--A New Look at an Old Subject," *Computers & Structures*, 44:499-514. 1992.
141. Novozhilov, V.V. *Foundations of the Theory of Nonlinear Elasticity*. Graylock Press, Rochester, NY, 1953.
142. Novozhilov, V.V. *The Theory of Thin Shells*. P. Noordhoff LTD., Groningen, Netherlands, 1959.
143. Neuber, H. "Anisotropic Nonlinear Stress-Strain Laws and Yield Conditions," *International Journal of Solids & Structures*, 5: 1299-1310, 1969.
144. Ochoa, O.O. & J.J. Engblom. "Analysis of Progressive Failure in Composites", *Composite Science & Technology*, 28:87-102, 1984.
145. Ochoa, O.O. & V.M. Marciano. *Journal of Solid Structures*, 3:579-589, 1987.
146. Owen, D.R.J. & E. Hinton. *Finite Elements in Plasticity: Theory and Practice*. Pineridge Press, Swansea, UK, 1980.
147. Owen, D.R.J. & J.A. Figuerias. "Elasto-Plastic Analysis of Anisotropic Plates and Shells by the Semiloof Element", *International Journal of Numerical Methods in Engineering*, 19:521-539, 1983.

148. Owen, D.R.J. & J.A. Figuerias. "Anisotropic Elastic-Plastic Finite Element Analysis of Thick and Thin Plates and Shells", *International Journal of Numerical Methods in Engineering*, 19:541-566, 1983.
149. Owen, D.R.J. & G.Q. Liu. "Elasto-Viscoplastic Analysis of Anisotropic Laminated Plates and Shells", *Engineering Computations*, 2:90-95, 1985.
150. Owens, M.E., A.N. Palazotto, & S.T. Dennis. "Transverse Shear Flexibility in Laminated Plates Undergoing Large Deflections", *Computers & Structures*, 45:69-78, 1992.
151. Padovan, J. & S. Tovchakchaikul. "On the Solution of Elastic-Plastic Static and Dynamic Post-Buckling Collapse of General Structure", *Computers & Structures*, 16, 1983.
152. Padovan, J. & S. Tovchakchaikul. "Algorithms for Elasto-Plastic-Creep Post-Buckling", *Journal of Engineering Mechanics*, 110:911-929, 1984.
153. Padovan, J. & R. Moscarello. "Locally Bound Constrained Newton Raphson Solution Algorithms", *Computers & Structures*, 23:181-197, 1986.
154. Pagano, N.J. & S.R. Soni. "Global-Local Laminate Variational Model", *International Journal of Solids & Structures*, 19:207-228, 1983.
155. Paimushin, V.N. "Generalized Reissner Variational Principle in Nonlinear Mechanics of Three-Dimensional Composite Solid, with Applications to Multi-Layered Shells", *Mechanics of Solids*, 22:16-174, 1987.
156. Palazotto, A.N. & W.P. Witt. "Formulation of a Nonlinear Compatible Finite Element for the Analysis of Laminated Composites", *Computers & Structures*, 21:1213-1234, 1985.
157. Palazotto, A.N. "An Experimental Study of Curved Composite Panel with a Cutout", *ASTM STP 972*, 1988.
158. Palazotto, A.N. & T.W. Tisler. "Considerations of Cutouts in Composite Cylindrical Panels", *Computers & Structures*, 28:1101-1110, 1988.
159. Palazotto, A.N. & T.W. Tisler. "Experimental Collapse Determination of Cylindrical Composite Panels with Large Cutouts Under Axial Loads", *Composite Structures*, 12:61-78, 1989.
160. Palazotto, A.N., R.L. Hinrichsen, & W.P. Witt. "Inter-Ply Rotational Compatibility for Composite Plates", *Composite Structures*, 11:167-182, 1989.
161. Palazotto, A.N., S.T. Dennis, & C.T. Tsai. "Snapping Characteristics in Laminated Cylindrical Panels under Transverse Loading", in *Proceedings of the 31st Structures, Structural Dynamics, and Materials Conference*, 1990.
162. Palazotto, A.N. & S.T. Dennis. *Nonlinear Analysis of Shell Structures*. Edited by J.S. Przemieniecki. American Institute of Aeronautics and Astronautics, Inc., Washington D.C., 1992.

163. Palazotto, A.N., L.S. Chien, & W.W. Taylor. "Stability Characteristics of Laminated Cylindrical Panels Under Transverse Loading", *AIAA Journal*, 30:1649-1653, 1992.
164. Palmerio, A.F., J.N. Reddy, & R. Schmidt. "On a Moderate Rotation Theory of Anisotropic Shells-Part 1: Theory", *International Journal of Nonlinear Mechanics*, 25:687-700, 1990.
165. Palmerio, A.F., J.N. Reddy, & R. Schmidt. "On a Moderate Rotation Theory of Anisotropic Shells-Part 1: Finite Element Analysis", *International Journal of Nonlinear Mechanics*, 25:701-714, 1990.
166. Parisch, H. "Large Displacements of Shells Including Material Nonlinearities", *Computer Methods in Applied Mechanics & Engineering*, 27:183-214, 1981.
167. Pietraszkiewicz, W. & M.L. Szabowicz. "Entirely Lagrangian Nonlinear Theory of Thin Shells", *Archives of Mechanics*, 33:273-288, 1981.
168. Pietraszkiewicz, W. "Lagrangian Description and Incremental Formulation in the Nonlinear Theory of Thin Shells", *International Journal of Nonlinear Mechanics*, 19:115-140, 1984.
169. Popov, E.P. *Introduction to Mechanics of Solids*. Englewood Cliffs, New Jersey: Prentice-Hall, 1968.
170. Prager, W. *An Introduction to Plasticity*, Addison-Wesley, Amsterdam and London, 1959.
171. Prathap, G. & R.P. Naganarayana. "Analysis of Locking and Stress Oscillations in a General Curved Beam Element", *International Journal of Numerical Methods for Engineering*, 30:177-200, 1990.
172. Putcha, N.S. & J.N. Reddy. "A Refined Mixed Shear Flexible Finite Element for Nonlinear Analysis of Laminated Plates", *Computers & Structures*, 22:529-538, 1986.
173. Puppo, A.H. & H.A. Evenson. "Strength of Anisotropic Materials under Combined Stresses," *AIAA Journal*, 10: 468-474. April, 1972.
174. Qian, C. & Z. Demao. "Vibrational Analysis Theory and Application to Elasto-Viscoelastic Composite Structures", *Computers & Structures*, 37:585-593, 1990.
175. Rajasakaran, S. & D.W. Murray. "Incremental Finite Element Matrices", *Journal of the Structures Division*, ASCE, pages 2423-2437, 1973.
176. Reddy, J.N. "Exact and Finite-Element Analysis of Laminated Shells", Technical Report AFOSR-81-0142-B (AD-A135849), 1983.
177. Reddy, J.N. "A Refined Nonlinear Analysis of Laminated Composites Plates and Shells", *International Journal of Solids & Structures*, 23:219-300, 1984.
178. Reddy, J.N. & K. Chandrashekhara. "Nonlinear Analysis of Composite Laminates", *AIAA*

Journal, 23:440-441, 1985.

179. Reddy, J.N. "A Refined Nonlinear Analysis of Laminated Composite Plates and Shells", Technical Report ARO 21203.7-MA (AD-A1844367), 1987.

180. Reddy, J.N. "A Generalization of Two-Dimensional Theories of Laminated Composite Plates", *Communications in Applied Numerical Methods*, 3:173-180, 1987.

181. Reddy, J.N. & A.K. Pandey. "A First Ply Failure Analysis of Composite Laminates", *Computers & Structures*, 25:371-393, 1987.

182. Reddy, J.N. "On the Generalization of Displacement-Based Laminate Theories", *Applied Mechanics Review*, 42:S213-S222, 1989.

183. Reddy, J.N. "A General Nonlinear Third-Order Theory of Plates with Moderate Thickness", *International Journal of Nonlinear Mechanics*, 25:677-686, 1990.

184. Reddy, J.N. & E.J. Barbero. "A Plate Bending Element Based on a Generalized Laminate Plate Theory". *International Journal for Numerical Methods in Engineering* 25:26-34, 1993.

185. Reddy, J.N. "An Evaluation of Equivalent-Single-Layer and Layerwise Theories of Composite Laminates," *Composite Structures*, 25:21-35. 1993.

186. Reed, K.W. & S.N. Atluri. "Analysis of Large Quasi-Static Deformations of Inelastic Bodies by a New Finite Element Algorithm", *Computer Methods in Applied Mechanics & Engineering*, 39:245-295, 1983.

187. Reed, K.W. & S.N. Atluri. "Constitutive Modelling and Computational Implementation of Finite Strain Plasticity", *International Journal of Plasticity*, 1:63-87, 1985.

188. Reissner, E. "The Effect of Transverse Shear Deformation on the Bending of Elastic Plates", *Journal of Applied Mechanics*, 12:69-77, 1945.

189. Reissner, E. "Effect of Transverse Shear Deformability on Stress Concentration Factors for Twisted Shallow Spherical Shells", *Journal of Applied Mechanics*, 53:597-601, 1986.

190. Ren, J.G. "Exact Solutions for Laminated Cylindrical Shells in Cylindrical Bending", *Composite Sciences & Technology*, 29:169-187, 1987.

191. Rourke, D.R. *Geometric and Material Nonlinear Effects in Elastic-Plastic and Failure Analysis of Anisotropic Laminated Structures*. PhD Dissertation, Virginia Polytechnic Institute & State University, Blacksburg, VA, 1986.

192. Rowlands, R.E. "Failure Mechanics of Composites, Strength (Failure) Theories and Their Experimental Correlation", in *Handbook of Composites, Vol 3: Failure Mechanics*, Chapter 2, pages 71-126. North-Holland Publishing Co., NY, 1985.

193. Ruben, M.B. "Elasto-Viscoplastic Model for Large Deformation", *International Journal of Engineering*, 24:1083-1095, 1986.
194. Saada, A.S. *Elasticity Theory and Applications*. Pergamon Press Inc., NY, 1984. Reprinted by Kreigler Publishing Co., Inc., Malabra, FL, 1989.
195. Sabir, A.B. & A.C. Lock. "The Application of Finite Elements to the Large Deflection Geometrically Nonlinear Behavior of Cylindrical Shells", *Variational Methods in Engineering*. Edited by C.A. Brebbia and H. Tottenham. London:Southampton Press, 1972.
196. Saigal, S., R.K. Kapania, & T.Y. Yang. "Geometrically Nonlinear Finite Element Analysis of Imperfect Laminated Shells", *Journal of Composite Materials*, 20:197-214, 1986.
197. Samuelson, A. & M. Froier. "Numerical Methods in Elasto-Plasticity-A Comparative Study", in *Nonlinear Finite Element Analysis in Structural Mechanics*, Chapter 4, pages 274-289, Springer-Verlag, NY, 1981.
198. Sandhu, R.S. *Ultimate Strength Analysis of Symmetric Laminates*. Technical Report (AD-A779927).
199. Schimmels, S.A. *Investigation of Collapse Characteristics of Cylindrical Composite Panels with Large Cutouts*. Master's Thesis, AFIT/GAE/ENY/89D-33, School of Engineering, Air Force Institute of Technology (AU), Wright-Patterson AFB, OH, 1989.
200. Schimmels, S.A. & A.N. Palazotto. "Collapse Characteristics of Cylindrical Composite Panels Under Axial Loads", *AIAA Journal*, 30:1447-1449, 1992.
201. Schimmels, S.A. & A.N. Palazotto. "Nonlinear Geometric and Material Behavior of Shell Structures with Large Strains," *Journal of Engineering Mechanics*, 120:320-345. February, 1994.
202. Schmidt, R. & D.A. DaDeppo. "A Survey of Literature on Large Deflections of Non Shallow Arches", *Journal of Industrial Math Society*, 42 1975.
203. Schmidt, R. "On Geometrically Nonlinear Theories for Thin Elastic Shells", *Flexible Shells Theory and Applications*:76-90. Edited by E.L. Axelrad and F.A. Emmerling, New York:Springer-Verlag,1984.
204. Schmidt, R. & J.N. Reddy. "A Refined Small Strain and Moderate Rotation Theory of Elastic Anisotropic Shells", *Journal of Applied Mechanics*, 55:611-617, 1988.
205. Shih, C.F. & D. Lee. "Further Developments in Anisotropic Plasticity", *Journal of Engineering Materials and Technology*, 100:294, 1978.
206. Silva, K. *Finite Element Investigation of a Composite Cylindrical Shell under Transverse Load with Through the Thickness Shear and Snapping*. Master's thesis, AFIT/GAE/ENY/89D-35. School of Engineering, Air Force Institute of Technology (AU), Wright Patterson AFB, OH, 1989. (AD-A216 377)

207. Simo, J.C. & J.G. Kennedy. "On a Stress Resultant Geometrically Exact Shell Model. Part V. Nonlinear Plasticity: Formulation and Integration Algorithms", *Computer Methods in Applied Mechanics and Engineering*, 96:133-171, 1992.
208. Singh, G. & Y.V.K Sadasiva Rao. "Large Deflection Behavior of Thick Composite Plates", *Composite Structures*, 8:13-29, 1987
209. Smith, R.A. *Higher-Order Thickness Expansion for Cylindrical Shells*. PhD Dissertation, AFIT/DS/ENY/91-1, School of Engineering, Air Force Institute of Technology (AU), Wright-Patterson AFB, OH, 1991.
210. Smith, R.A. & A.N. Palazotto. "Comparison of Eight Variations of a Higher-Order Theory for Cylindrical Shells", *AIAA*, 1125-1132, 1993.
211. Soldatos, K.P. "On Thickness Shear Deformation Theories for Dynamics Analysis of Non-Circular Cylindrical Shells", *International Journal of Solids & Structures*, 22:625-641, 1986.
212. Stricklin, J.A., W.E. Haisler, & W.A. von Riesemann. "Computation and Solution Procedures for Nonlinear Analysis by Combined Finite Element-Finite Difference Methods", *Computers & Structures*, 2:955-974, 1972.
213. Sun, C.T. & K.M. Kao. "A Global-Local Finite Element Method Suitable for Parallel Computations", *Computers & Structures*, 29:309-316, 1988.
214. Sun, C.T. & S.R. Kelly. "Failure in Composite Angle Structure-Part 1: Initial Failure", *Journal of Reinforced Plastics and Composites*, 7:220-232, 1988.
215. Sun, C.T. & J.L. Chen. "A Simple Flow Rule for Characterizing Nonlinear Behavior of Fiber Composites", *Journal of Composite Materials*, 23:1009-1019, 1989.
216. Surana, K.S. "Geometrically Nonlinear Formulation for the Curved Shell Elements", *International Journal of Numerical Methods for Engineering*, 19:581-615, 1983.
217. Takahashi, K. & T. Chou. "Nonlinear Deformation and Failure Behavior of Carbon/Glass Hybrid Laminate", *Journal of Composite Materials*, 21:396-420, 1987.
218. Tay, T.E. & E.H. Lim. "Analysis of Stiffness Loss in Cross-Ply Composite Laminates," *Composite Structures*, 25:419-425. 1993.
219. Taylor, W.W. *Finite Element Investigation into the Dynamic Instability Characteristics of Laminated Composite Panels*. Masters Thesis, AFIT/GAE/AA/90D-. School of Engineering, Air Force Institute of Technology (AU), Wright-Patterson AFB, OH, 1990.
220. Telles, J.C.F. & C.F.A. Brebbia. "Elasto-Plastic Boundary Element Analysis", in *Nonlinear Finite Element Analysis in Structural Mechanics*, Chapter 4, pages 403-433. Springer-Verlag, NY, 1981.

221. Timoshenko, S. & W. Woinowsky-Kreiger. *Theory of Plates and Shells*. 2nd Ed. McGraw-Hill, New York, 1959.
222. Tisler, T.W., Jr. *Collapse Analysis of Cylindrical Composite Panels with Large Cutouts Under Axial Load*. Masters Thesis, AFIT/GAE/AA/86D-18. School of Engineering, Air Force Institute of Technology (AU), Wright-Patterson AFB, OH, 1986. (AD-A179112)
223. Touratier, M. "A Generalization of Shear Deformation Theories for Axisymmetric Multilayered Shells", *International Journal of Solid Structures*, 29:1379-1399, 1992.
224. Touratier, M. "A Refined Theory of Laminated Shallow Shells", *International Journal of Solid Structures*, 29:1401-1415, 1992.
225. Tsai, C.T. & A.N. Palazotto. "A Modified Riks Approach to Composite Shell Snapping Using a Higher-Order Shear Deformation Theory", *Computers & Structures*, 35:221-226, 1990.
226. Tsai, C.T. & A.N. Palazotto. "Large-Rotation Snap-Through Buckling in Laminated Cylindrical Panels", *Finite Elements in Analysis and Design*, 9:65-75, 1991.
227. Vaziri, R., M.D. Olson, & D.L. Anderson. "Finite Element Analysis of Fibrous Composite Structures: A Plasticity Approach," *Computers & Structures*, 44: 103-116. 1992.
228. Verijenko, V.E. "Nonlinear Analysis of Laminated Composite Plates and Shells Including the Effects of Shear and Normal Deformation," *Composite Structures*, 25:297-405. 1993.
229. Vlasov, V.Z. *General Theory of Shells and its Application in Engineering*, Washington D.C.: National Aeronautics and Space Administration, 1964.
230. Wang, H.S. & T.W. Chou. *Journal of Composite Materials*, 19:424-442, 1985.
231. Washizu, K. *Variational Methods in Elasticity and Plasticity*, 3rd Ed. Pergamon Press, NY, 1982.
232. Watanabe, N. & K. Hondo. "New Simplified Finite Element Model for Elasto-Plastic Analysis of Plate Bending", *Computers & Structures*, 28:495-503, 1988.
233. Wempner, G. "Mechanics and Finite Element Solution", *Applied Mechanics Review*, 42:129-142, 1989.
234. Whitney, J.M. *Structural Analysis of Laminated Anisotropic Plates*. Lancaster, Pennsylvania: Technomic, 1987.
235. Wu, C.P. & C.C. Lin. "Analysis of Sandwich Plates Using a Mixed Finite Element," *Composite Structures*, 25:297-405. 1993.
236. Wu, C.P. & C.C. Lin. "A New Local Higher-Order Laminate Theory," *Composite Structures*, 25:297-405. 1993.

237. Yamada, Y., N. Yoshimura, & T. Sakuri. "Plastic Stress-Strain Matrix and its Application for the Solution of Elastic-Plastic Problems by Finite Element Method", *International Journal of Mechanics & Science*, 10:343-354, 1968
238. Yang, T.Y. & D.G. Liaw. "Elastic-Plastic Dynamic Buckling of Thin-Shell Finite Elements with Asymmetric Imperfections", *AIAA Journal*, 26:479-486, 1988.
239. Yuan, K.Y. & C.C. Liang. "Nonlinear Analysis of an Axisymmetric Shell Using Three Noded Degenerated Isoparametric Shell Elements", *Computers & Structures*, 32:1225-1239, 1989.
240. Zienkiewicz, O.C., S. Valliappan, & I.P. King. "Elasto-Plastic Solutions of Engineering Problems; Initial Stress Finite Element Approach", *International Journal of Numerical Methods in Engineering*, 1:75-100, 1969.
241. Zienkiewicz, O.C. *The Finite Element Method*, 4th Ed. McGraw-Hill, London, UK, 1989.

This Page Intentionally Left Blank

Appendix A. Arbitrary Shell Strain-Displacement Relations

The arbitrary shell is described in terms of a curvilinear orthogonal coordinate system aligned with lines of principal curvature. Displacement within the shell is assumed to be of the form

$$\vec{U} = u_1 \vec{e}_1 + u_2 \vec{e}_2 + u_3 \vec{e}_3 \quad (\text{A.1})$$

where the orthonormal \vec{e}_1 and \vec{e}_2 are aligned with principal lines of curvature. The direction of \vec{e}_3 is determined by the cross product of \vec{e}_1 and \vec{e}_2 . The components of displacement in the 1-, 2-, and 3-directions are assumed to be unspecified functions of the curvilinear coordinates y_1 , y_2 , and y_3 . The shell shape factors h_1 and h_2 are general arbitrary functions, specifically: $h_1 = h_1(y_1, y_2, y_3)$, $h_2 = h_2(y_1, y_2, y_3)$, and $h_3 = 1$.

A.1 Midsurface Strain Components for the Arbitrary Shell

The strain equations listed below are the linear and nonlinear parts of the strain components for the case of an arbitrary shell. The ϵ_{33} component is assumed to be zero for this shell formulation. Contracted notation is used, where $\epsilon_1 = \epsilon_{11}$, $\epsilon_2 = \epsilon_{22}$, $\epsilon_4 = \epsilon_{23}$, $\epsilon_5 = \epsilon_{13}$, and $\epsilon_6 = \epsilon_{12}$.

$$\epsilon_{1L} = (u_{1,1} + h_{1,3}u_3)/h_1 + (h_{1,2}u_2)/(h_1h_2) \quad (\text{A.2})$$

$$\epsilon_{2L} = (u_{2,2} + h_{2,3}u_3)/h_2 + (h_{2,1}u_1)/(h_1h_2) \quad (\text{A.3})$$

$$\epsilon_{4L} = u_{2,3} + (u_{3,2} - h_{2,3}u_3)/h_2 \quad (\text{A.4})$$

$$\epsilon_{5L} = u_{1,3} + (u_{3,1} - h_{1,3}u_3)/h_1 \quad (\text{A.5})$$

$$\epsilon_{6L} = u_{1,2}/h_2 + u_{2,1}/h_1 - (h_{1,2}u_1 + h_{2,1}u_2)/(h_1h_2) \quad (\text{A.6})$$

$$\begin{aligned} \epsilon_{1NL} = & (h_{1,3}(u_{1,3}u_3 - u_1u_{3,1})) / (h_1^2) + h_3[u_{1,1}^2 + u_{2,1}^2 + u_{3,1}^2 \\ & + h_{1,3}^2(u_1^2 + u_3^2)] / (2h_1^2) + h_{1,2}(u_{1,1}u_2 - u_1u_{2,1}) \\ & + h_{1,3}u_2u_3 / (h_1^2h_2) + h_{1,2}^2h_3(u_1^2 + u_3^2) / (2h_1^2h_2^2) \end{aligned} \quad (A.7)$$

$$\begin{aligned} \epsilon_{2NL} = & (h_{2,3}(u_{2,3}u_3 - u_2u_{3,2})) / (h_2^2) + h_3[u_{1,2}^2 + u_{2,2}^2 + u_{3,2}^2 \\ & + h_{2,3}^2(u_2^2 + u_3^2)] / (2h_2^2) + h_{2,1}(u_1u_{2,2} - u_{1,2}u_2) \\ & + h_{2,3}u_1u_3 / (h_1h_2^2) + h_{2,1}^2h_3(u_2^2 + u_3^2) / (2h_1^2h_2^2) \end{aligned} \quad (A.8)$$

$$\begin{aligned} \epsilon_{4NL} = & [u_{1,2}u_{1,3} + u_{2,2}u_{2,3} + u_{3,2}u_{3,3} + h_{2,3}(u_{2,3}u_3 \\ & - u_2u_{3,3})] / h_2 + (h_{2,1}(u_1u_{2,3} - u_{1,3}u_2)) / (h_1h_2) \end{aligned} \quad (A.9)$$

$$\begin{aligned} \epsilon_{5NL} = & [u_{1,1}u_{1,3} + u_{2,1}u_{2,3} + u_{3,1}u_{3,3} + h_{1,3}(u_{1,3}u_3 \\ & - u_1u_{3,3})] / h_1 + (h_{1,2}(u_{1,3}u_2 - u_1u_{2,3})) / (h_1h_2) \end{aligned} \quad (A.10)$$

$$\begin{aligned} \epsilon_{6NL} = & [u_{1,1}u_{1,2} + u_{2,1}u_{2,2} + u_{3,1}u_{3,2} \\ & + h_{1,3}(u_{1,2}u_3 - u_1u_{3,2}) + h_{2,3}(u_{2,1}u_3 - u_2u_{3,1}) \\ & + h_{1,3}h_{2,3}u_1u_2] / (h_1h_2) \\ & + (h_{2,1}(u_1u_{2,1} - u_{1,1}u_2 - h_{1,3}u_2u_3)) / (h_1^2h_2) \\ & + (h_{1,2}(u_{1,2}u_2 - u_1u_{2,2} - h_{2,3}u_1u_3)) / (h_1h_2^2) \\ & - (h_{1,2}h_{2,1}(u_1^2 + u_2^2)) / (h_1^2h_2^2) \end{aligned} \quad (A.11)$$

A.2 Mid-Surface Strain Components for the Arbitrary Shell with a Quartic

Displacement Field Assumption

The expressions listed in the previous section represent strain components for an arbitrary shell where displacement components are unspecified functions of the coordinates (y_1, y_2, y_3) . For a shear deformation theory, the displacements are assumed to be functions of the thickness coordinate. Specifically, for a shell with radius R_1 in the y_1 -direction and radius R_2 in the y_2 -direction, we shall assume a quartic series expansion u_1 and u_2 as shown below. The u_3 component is assumed to be constant through-the-thickness of the shell.

$$\begin{aligned} u_1 &= u(1 - y_3/R_1) + \psi_1 y_3 + \phi_1 y_3^2 + \gamma_1 y_3^3 + \theta_1 y_3^4 \\ u_2 &= v(1 - y_3/R_2) + \psi_2 y_3 + \phi_2 y_3^2 + \gamma_2 y_3^3 + \theta_2 y_3^4 \\ u_3 &= w \end{aligned} \quad (A.12)$$

If one substitutes these expressions for the displacements into the previously derived expressions for strain components, the following expressions are obtained for the strain components χ_i^p , where

$$\epsilon_{i_L} = \chi_{i_L} + \sum_{p=1}^n \chi_{i_L}^p y_3^p, \quad (A.13)$$

and

$$\epsilon_{i_{NL}} = \chi_{i_{NL}} + \sum_{p=1}^n \chi_{i_{NL}}^p y_3^p. \quad (A.14)$$

$$\chi_{1_L}^0 = u_{,1}/h_1 + (h_{1,2}v)/(h_1 h_2) \quad (A.15)$$

$$\chi_{1_L}^1 = \left(\psi_{1,1} - u_{,1}/R_1 \right) / h_1 + (h_{1,2}(\psi_2 - v/R_2)) / (h_1 h_2) \quad (A.16)$$

$$\chi_{1_L}^2 = \phi_{1,1}/h_1 + (h_{1,2}\phi_2)/(h_1h_2) \quad (\text{A.17})$$

$$\chi_{1_L}^3 = \gamma_{1,1}/h_1 + (h_{1,2}\gamma_2)/(h_1h_2) \quad (\text{A.18})$$

$$\chi_{1_L}^4 = \theta_{1,1}/h_1 + (h_{1,2}\theta_2)/(h_1h_2) \quad (\text{A.19})$$

$$\chi_{2_L}^0 = v_{,1}/h_1 + (h_{1,2}u)/(h_1h_2) \quad (\text{A.20})$$

$$\chi_{2_L}^1 = \left(\psi_{2,2} - v_{,2}/R_2 \right) / h_2 + (h_{2,1}(\psi_1 - u/R_1)) / (h_1h_2) \quad (\text{A.21})$$

$$\chi_{2_L}^2 = \phi_{2,2}/h_2 + (h_{2,1}\phi_1)/(h_1h_2) \quad (\text{A.22})$$

$$\chi_{2_L}^3 = \gamma_{2,2}/h_2 + (h_{2,1}\gamma_1)/(h_1h_2) \quad (\text{A.23})$$

$$\chi_{2_L}^4 = \theta_{2,2}/h_2 + (h_{2,1}\theta_1)/(h_1h_2) \quad (\text{A.24})$$

$$\chi_{4_L}^0 = (\psi_2 - v/R_2) + w_{,2}/h_2 \quad (\text{A.25})$$

$$\chi_{4_L}^1 = 2\phi_2 - (h_{2,3}(\psi_2 - v/R_2)) / h_2 \quad (\text{A.26})$$

$$\chi_{4_L}^2 = 3\gamma_2 - (h_{2,3}\phi_2) / h_2 \quad (\text{A.27})$$

$$\chi_{4_L}^3 = 4\theta_2 - (h_{2,3}\gamma_2)/h_2 \quad (\text{A.28})$$

$$\chi_{4_L}^4 = -(h_{2,3}\theta_2)/h_2 \quad (\text{A.29})$$

$$\chi_{5_L}^0 = (\psi_1 - u/R_1) + w_{,1}/h_1 \quad (\text{A.30})$$

$$\chi_{5_L}^1 = 2\phi_1 - (h_{1,3}(\psi_1 - u/R_1))/h_1 \quad (\text{A.31})$$

$$\chi_{5_L}^2 = 3\gamma_1 - (h_{1,3}\phi_1)/h_1 \quad (\text{A.32})$$

$$\chi_{5_L}^3 = 4\theta_1 - (h_{1,3}\gamma_1)/h_1 \quad (\text{A.33})$$

$$\chi_{5_L}^4 = -(h_{1,3}\theta_1)/h_1 \quad (\text{A.34})$$

$$\chi_{6_L}^0 = u_{,2}/h_2 + v_{,1}/h_1 - (h_{1,2}u + h_{2,1}v)/(h_1h_2) \quad (\text{A.35})$$

$$\begin{aligned} \chi_{6_L}^1 &= (\psi_{1,2} - u_{,2}/R_1)/h_1 + (\psi_{2,1} - v_{,1}/R_2)/h_2 \\ &- [h_{1,2}(\psi_1 - u/R_1) + h_{2,1}(\psi_2 - v/R_2)]/(h_1h_2) \end{aligned} \quad (\text{A.36})$$

$$\chi_{6_L}^2 = \phi_{1,2}/h_2 + \phi_{2,1}/h_1 - (h_{1,2}\phi_1 + h_{2,1}\phi_2)/(h_1h_2) \quad (\text{A.37})$$

$$\chi_{6_L}^3 = \gamma_{1,2}/h_2 + \gamma_{2,1}/h_1 - (h_{1,2}\gamma_1 + h_{2,1}\gamma_2)/(h_1h_2) \quad (\text{A.38})$$

$$\chi_{6_L}^4 = \theta_{1,2}/h_2 + \theta_{2,1}/h_1 - (h_{1,2}\theta_1 + h_{2,1}\theta_2)/(h_1h_2) \quad (A.39)$$

$$\begin{aligned} \chi_{1_{NL}}^0 &= \left(u_{,1}^2 + v_{,1}^2 + w_{,1}^2 \right) / \left(2h_1^2 \right) + (h_{1,2}(u_{,1}v - uv_{,1})) / \left(h_1^2 h_2 \right) \\ &+ \left(h_{1,2}^2 (u^2 + v^2) \right) / \left(2h_1^2 h_2^2 \right) \end{aligned} \quad (A.40)$$

$$\begin{aligned} \chi_{1_{NL}}^1 &= \left[u_{,1}(\psi_{1,1} - u_{,1}/R_1) + v_{,1}(\psi_{2,1} - v_{,1}/R_2) \right. \\ &+ h_{1,3}(w(\psi_{1,1} - u_{,1}/R_1) - w_{,1}(\psi_1 - u/R_1)) \\ &+ h_{1,3}^2 u(\psi_1 - u/R_1) \left. \right] / h_1^2 + (h_{1,2}[u_{,1}(\psi_2 - v/R_2) \\ &- u(\psi_{2,1} - v_{,1}/R_2) - v_{,1}(\psi_1 - u/R_1) \\ &+ v(\psi_{1,1} - u_{,1}/R_1) + h_{1,3}w(\psi_2 - v/R_2)]) / \left(h_1^2 h_2 \right) \\ &+ \left(h_{1,2}^2 [u(\psi_1 - u/R_1) + v(\psi_2 - v/R_2)] \right) / \left(h_1^2 h_2^2 \right) \end{aligned} \quad (A.41)$$

$$\begin{aligned} \chi_{1_{NL}}^2 &= \left[u_{,1}(\phi_{1,1} - u_{,1}/R_1) + v_{,1}(\phi_{2,1} - v_{,1}/R_2) \right. \\ &+ h_{1,3}(w\phi_{1,1} - w_{,1}\phi_1) + h_{1,3}^2 u(\phi_1 - \psi_1/R_1) \left. \right] / h_1^2 \\ &+ \left[\psi_{1,1}^2 + \psi_{2,1}^2 + u_{,1}^2/R_1 + v_{,1}^2/R_2 + h_{1,3}^2 (\psi_1^2 + u^2/R_1^2) \right] / \left(2h_1^2 \right) \\ &+ (h_{1,2}[\phi_{1,1}(\psi_2 - v/R_2) - \phi_1(\psi_{2,1} - v_{,1}/R_2) \\ &- \phi_{2,1}(\psi_1 - u/R_1) + \phi_{2,1}(\psi_{1,1} - u_{,1}/R_1) + \phi_{1,1}v - \phi_1v_{,1} \\ &- \phi_{2,1}u + \phi_2u_{,1} + (u_{,1}v - uv_{,1})/(R_1R_2) + h_{1,3}\phi_2w]) / \left(h_1^2 h_2 \right) \\ &+ \left(h_{1,2}^2 [u(\phi_1 - \psi_1/R_1) + v(\phi_2 - \psi_2/R_2)] \right) / \left(h_1^2 h_2^2 \right) \\ &+ \left(h_{1,2}^2 (\psi_1^2 + u^2/R_1^2 + \psi_2^2 + v^2/R_2^2) \right) / \left(2h_1^2 h_2^2 \right) \end{aligned} \quad (A.42)$$

$$\begin{aligned}
\chi_{1_{NL}}^3 = & \left[\phi_{1,1} (\psi_{1,1} - u_{,1}/R_1) + \phi_{2,1} (\psi_{2,1} - v_{,1}/R_2) \right. \\
& + \gamma_{1,1} u_{,1} + \gamma_{2,1} v_{,1} + h_{1,3} (\gamma_{1,1} w - \gamma_1 w_{,1}) \\
& + h_{1,3}^2 (\phi_1 (\psi_1 - u/R_1) + \gamma_1 u) \left. \right] / h_1^2 + (h_{1,2} [\phi_{1,1} (\psi_2 - v/R_2) \\
& - \phi_1 (\psi_{2,1} - v_{,1}/R_2) - \phi_{2,1} (\psi_1 - u/R_1) + \phi_2 (\psi_{1,1} - u_{,1}/R_1) \\
& + \gamma_{1,1} v - \gamma_1 v_{,1} - \gamma_{2,1} u + \gamma_2 u_{,1} + h_{1,3} \gamma_2 w]) / (h_1^2 h_2) \\
& + \left(h_{1,2}^2 [\phi_1 (\psi_2 - v/R_2) + \gamma_2 u + \phi_2 (\psi_2 - v/R_2) + \gamma_2 v] \right) / (h_1^2 h_2^2)
\end{aligned} \tag{A.43}$$

$$\begin{aligned}
\chi_{1_{NL}}^4 = & \left[\gamma_{1,1} (\psi_{1,1} - u_{,1}/R_1) + \gamma_{2,1} (\psi_{2,1} - v_{,1}/R_2) + \theta_{1,1} u_{,1} \right. \\
& + \theta_{2,1} v_{,1} + h_{1,3} (\theta_{1,1} w - \theta_1 w_{,1}) + h_{1,3}^2 [\gamma_1 (\psi_1 - u/R_1) + \theta_1 u] \left. \right] / h_1^2 \\
& + \left(\psi_{1,1}^2 + \psi_{2,1}^2 + h_{1,3}^2 \psi_1^2 \right) / (2h_1^2) + (h_{1,2} [\gamma_{1,1} (\psi_2 - v/R_2) \\
& - \gamma_1 (\psi_{2,1} - v_{,1}/R_2) - \gamma_{2,1} (\psi_1 - u/R_1) + \gamma_2 (\psi_{1,1} - u_{,1}/R_1) \\
& + \phi_{1,1} \phi_2 - \phi_1 \phi_{2,1} + \theta_{1,1} v - \theta_1 v_{,1} - \theta_{2,1} u + \theta_2 u_{,1} \\
& + h_{1,3} \theta_2 w]) / (h_1^2 h_2) + \left(h_{1,2}^2 [\gamma_1 (\psi_1 - u/R_1) + \theta_1 u \right. \\
& + \gamma_1 (\psi_2 - v/R_2) + \theta_2 v] \left. \right) / (h_1^2 h_2^2) + \left(h_{1,2}^2 (\psi_1^2 + \psi_2^2) \right) / (2h_1^2 h_2^2)
\end{aligned} \tag{A.44}$$

$$\begin{aligned}
\chi_{1_{NL}}^5 = & \left[\gamma_{1,1} \phi_{1,1} + \gamma_{2,1} \phi_{2,1} + \theta_{1,1} (\psi_{1,1} - u_{,1}/R_1) \right. \\
& + \theta_{2,1} (\psi_{2,1} - v_{,1}/R_2) + h_{1,3}^2 (\gamma_1 \phi_1 + \theta_1 (\psi_1 - u/R_1)) \left. \right] / h_1^2 \\
& + (h_{1,2} [\gamma_{1,1} \phi_2 - \gamma_1 \phi_{2,1} - \gamma_{2,1} \phi_1 + \gamma_2 \phi_{1,1} + \theta_{1,1} (\psi_2 - v/R_2) \\
& - \theta_1 (\psi_{2,1} - v_{,1}/R_2) - \theta_{2,1} (\psi_1 - u/R_1) + \theta_2 (\psi_{1,1} \\
& - u_{,1}/R_1)]) / (h_1^2 h_2) + \left(h_{1,2}^2 [\gamma_1 \phi_1 + \gamma_2 \phi_2 + \theta_1 (\psi_1 - u/R_1) \right. \\
& + \theta_2 (\psi_2 - v/R_2)] \left. \right) / (h_1^2 h_2^2) + \left(h_{1,2}^2 (\gamma_1^2 + \gamma_2^2) \right) / (2h_1^2 h_2^2)
\end{aligned} \tag{A.45}$$

$$\begin{aligned} \chi_{1_{NL}}^6 = & \left(\phi_{1,1} \theta_{1,1} + \phi_{2,1} \theta_{2,1} + h_{1,3}^2 \phi_1 \theta_1 \right) / \left(h_1^2 \right) + \left(\gamma_{1,1}^2 + \gamma_{2,1}^2 \right. \\ & + \left. h_{1,3}^2 \gamma_1^2 \right) / \left(2h_1^2 \right) + \left(h_{1,2} [\gamma_{1,1} \gamma_2 - \gamma_1 \gamma_{2,1} + \phi_{1,1} \theta_2 - \phi_1 \theta_{2,1} \right. \\ & - \left. \phi_{2,1} \theta_1 + \phi_2 \theta_{1,1}] \right) / \left(h_1^2 h_2 \right) + \left(h_{1,2}^2 (\phi_1 \theta_1 + \phi_2 \theta_2) \right) / \left(h_1^2 h_2^2 \right) \\ & + \left(h_{1,2}^2 (\gamma_1^2 + \gamma_2^2) \right) / \left(2h_1^2 h_2^2 \right) \end{aligned} \quad (A.46)$$

$$\begin{aligned} \chi_{1_{NL}}^7 = & \left(\gamma_{1,1} \theta_{1,1} + \gamma_{2,1} \theta_{2,1} + h_{1,3}^2 \gamma_1 \theta_1 \right) / \left(2h_1^2 \right) \\ & + \left(h_{1,2} [\gamma_{1,1} \theta_2 - \gamma_1 \theta_{2,1} - \gamma_{2,1} \theta_1 + \gamma_2 \theta_{1,1}] \right) / \left(h_1^2 h_2 \right) \\ & + \left(h_{1,2}^2 (\gamma_1 \theta_1 + \gamma_2 \theta_2) \right) / \left(h_1^2 h_2^2 \right) \end{aligned} \quad (A.47)$$

$$\begin{aligned} \chi_{1_{NL}}^8 = & \left(\theta_{1,1}^2 + \theta_{2,1}^2 + h_{1,3}^2 \theta_1^2 \right) / \left(2h_1^2 \right) + \left(h_{1,2} [\theta_{1,1} \theta_2 \right. \\ & - \left. \theta_1 \theta_{2,1}] \right) / \left(h_1^2 h_2 \right) + \left(h_{1,2}^2 (\theta_1^2 + \theta_2^2) \right) / \left(h_1^2 h_2^2 \right) \end{aligned} \quad (A.48)$$

$$\begin{aligned} \chi_{2_{NL}}^0 = & \left(u_{,2}^2 + v_{,2}^2 + w_{,2}^2 \right) / \left(2h_2^2 \right) - \left(h_{2,1} (u_{,2} v - u v_{,2}) \right) / \left(h_1^2 h_2 \right) \\ & + \left(h_{2,1}^2 (u^2 + v^2) \right) / \left(2h_1^2 h_2^2 \right) \end{aligned} \quad (A.49)$$

$$\begin{aligned} \chi_{2_{NL}}^1 = & \left[u_{,2} (\psi_{1,2} - u_{,2}/R_1) + v_{,2} (\psi_{2,2} - v_{,2}/R_2) \right. \\ & + h_{2,3} (w (\psi_{2,2} - v_{,2}/R_2) - w_{,2} (\psi_2 - v/R_2)) \\ & + \left. h_{2,3}^2 v (\psi_2 - v/R_2) \right] / h_2^2 - \left(h_{1,2} [u_{,2} (\psi_2 - v/R_2) \right. \\ & - \left. u (\psi_{2,2} - v_{,2}/R_2) - v_{,2} (\psi_1 - u/R_1) \right. \\ & + \left. v (\psi_{1,2} - u_{,2}/R_1) + h_{2,3} w (\psi_1 - u/R_1)] \right) / \left(h_1 h_2^2 \right) \\ & + \left(h_{2,1}^2 [u (\psi_1 - u/R_1) + v (\psi_2 - v/R_2)] \right) / \left(h_1^2 h_2^2 \right) \end{aligned} \quad (A.50)$$

$$\begin{aligned}
 \chi_{2_{NL}}^2 = & \left[u_{,2} (\phi_{1,2} - u_{,2}/R_1) + v_{,2} (\phi_{2,2} - v_{,2}/R_2) + h_{2,3} (w\phi_{2,2} \right. & (A.51) \\
 & - w_{,2}\phi_2) + h_{2,3}^2 v (\phi_2 - \psi_2/R_2) \left. \right] / h_2^2 + \left[\psi_{1,2}^2 + \psi_{2,2}^2 + u_{,2}^2/R_1 \right. \\
 & + v_{,2}^2/R_2 + h_{2,3}^2 (\psi_2^2 + v^2/R_2^2) \left. \right] / (2h_2^2) + (h_{2,1} [\phi_{1,1} (\psi_2 - v/R_2) \\
 & - \phi_1 (\psi_{2,1} - v_{,1}/R_2) - \phi_{2,1} (\psi_1 - u/R_1) + \phi_{2,1} (\psi_{1,1} - u_{,1}/R_1) \\
 & + \phi_{1,1} v - \phi_1 v_{,1} - \phi_{2,1} u + \phi_2 u_{,1} + (u_{,1} v - u v_{,1}) / (R_1 R_2) \\
 & + h_{1,3} \phi_2 w]) / (h_1^2 h_2^2) + \left(h_{1,2}^2 [u (\phi_1 - \psi_1/R_1) + v (\phi_2 \right. \\
 & - \psi_2/R_2)] \left. \right) / (h_1^2 h_2^2) + \left(h_{1,2}^2 (\psi_1^2 + u^2/R_1^2 + \psi_2^2 + v^2/R_2^2) \right) / (2h_1^2 h_2^2)
 \end{aligned}$$

$$\begin{aligned}
 \chi_{2_{NL}}^3 = & \left[\phi_{1,2} (\psi_{1,2} - u_{,2}/R_1) + \phi_{2,2} (\psi_{2,2} - v_{,2}/R_2) + \gamma_{1,2} u_{,2} \right. & (A.52) \\
 & + \gamma_{2,2} v_{,2} + h_{2,3} (\gamma_{2,2} w - \gamma_2 w_{,2}) + h_{2,3}^2 (\phi_2 (\psi_2 - v/R_2) + \gamma_2 v) \left. \right] / h_2^2 \\
 & - (h_{2,1} [\phi_{1,2} (\psi_2 - v/R_2) - \phi_1 (\psi_{2,2} - v_{,2}/R_2) - \phi_{2,2} (\psi_1 - u/R_1) \\
 & + \phi_2 (\psi_{1,2} - u_{,2}/R_1) + \gamma_{1,2} v - \gamma_1 v_{,2} - \gamma_{2,2} u + \gamma_2 u_{,2} \\
 & + h_{2,3} \gamma_1 w]) / (h_1 h_2^2) + \left(h_{2,1}^2 [\phi_1 (\psi_1 - u/R_1) + \gamma_1 u \right. \\
 & + \phi_2 (\psi_2 - v/R_2) + \gamma_2 v] \left. \right) / (h_1^2 h_2^2)
 \end{aligned}$$

$$\begin{aligned}
 \chi_{2_{NL}}^4 = & \left[\gamma_{1,2} (\psi_{1,2} - u_{,2}/R_2) + \gamma_{2,2} (\psi_{2,2} - v_{,2}/R_2) + \theta_{1,2} u_{,2} \right. & (A.53) \\
 & + \theta_{2,2} v_{,2} + h_{2,3} (\theta_{2,2} w - \theta_2 w_{,2}) + h_{2,3}^2 [\gamma_2 (\psi_2 - v/R_2) + \theta_2 v] \left. \right] / h_2^2 \\
 & + \left(\psi_{1,2}^2 + \psi_{2,2}^2 + h_{2,3}^2 \psi_2^2 \right) / (2h_2^2) - (h_{2,1} [\gamma_{1,2} (\psi_2 - v/R_2) \\
 & - \gamma_1 (\psi_{2,2} - v_{,2}/R_2) - \gamma_{2,2} (\psi_1 - u/R_1) + \gamma_2 (\psi_{1,2} - u_{,2}/R_1) \\
 & + \phi_{1,2} \phi_2 - \phi_1 \phi_{2,2} + \theta_{1,2} v - \theta_1 v_{,2} - \theta_{2,2} u + \theta_2 u_{,2} \\
 & + h_{2,3} \theta_1 w]) / (h_1 h_2^2) + \left(h_{2,1}^2 [\gamma_1 (\psi_1 - u/R_1) + \theta_1 u \right. \\
 & + \gamma_1 (\psi_2 - v/R_2) + \theta_2 v] \left. \right) / (h_1^2 h_2^2) + \left(h_{2,1}^2 (\psi_1^2 + \psi_2^2) \right) / (2h_1^2 h_2^2)
 \end{aligned}$$

$$\begin{aligned}
 \chi_{2_{NL}}^5 = & \left[\gamma_{1,2} \phi_{1,2} + \gamma_{2,2} \phi_{2,2} + \theta_{1,2} (\psi_{1,2} - u_{,2}/R_1) \right. \\
 & \left. + \theta_{2,2} (\psi_{2,2} - v_{,2}/R_2) + h_{2,3}^2 (\gamma_2 \phi_2 + \theta_2 (\psi_2 - v/R_2)) \right] / h_2^2 \\
 & - (h_{2,1} [\gamma_{1,2} \phi_2 - \gamma_1 \phi_{2,2} - \gamma_{2,2} \phi_1 + \gamma_2 \phi_{1,2} + \theta_{1,2} (\psi_2 - v/R_2) \\
 & - \theta_1 (\psi_{2,2} - v_{,2}/R_2) - \theta_{2,2} (\psi_1 - u/R_1) + \theta_2 (\psi_{1,2} \\
 & - u_{,2}/R_1)]) / (h_1 h_2^2) + \left(h_{2,1}^2 [\gamma_1 \phi_1 + \gamma_2 \phi_2 + \theta_1 (\psi_1 - u/R_1) \right. \\
 & \left. + \theta_2 (\psi_2 - v/R_2)] \right) / (h_1^2 h_2^2) + \left(h_{2,1}^2 (\gamma_1^2 + \gamma_2^2) \right) / (2 h_1^2 h_2^2)
 \end{aligned} \tag{A.54}$$

$$\begin{aligned}
 \chi_{2_{NL}}^6 = & \left(\phi_{1,2} \theta_{1,2} + \phi_{2,2} \theta_{2,2} + h_{2,3}^2 \phi_2 \theta_2 \right) / (h_2^2) + \left(\gamma_{1,2}^2 + \gamma_{2,2}^2 \right. \\
 & \left. + h_{2,3}^2 \gamma_2^2 \right) / (2 h_2^2) - (h_{2,1} [\gamma_{1,2} \gamma_2 - \gamma_1 \gamma_{2,2} + \phi_{1,2} \theta_2 - \phi_1 \theta_{2,2} \\
 & - \phi_{2,2} \theta_1 + \phi_2 \theta_{1,2}]) / (h_1 h_2^2) + \left(h_{2,1}^2 (\phi_1 \theta_1 + \phi_2 \theta_2) \right) / (h_1^2 h_2^2) \\
 & + \left(h_{2,1}^2 (\gamma_1^2 + \gamma_2^2) \right) / (2 h_1^2 h_2^2)
 \end{aligned} \tag{A.55}$$

$$\begin{aligned}
 \chi_{2_{NL}}^7 = & \left(\gamma_{1,2} \theta_{1,2} + \gamma_{2,2} \theta_{2,2} + h_{2,3}^2 \gamma_2 \theta_2 \right) / (2 h_2^2) \\
 & - (h_{1,2} [\gamma_{1,2} \theta_2 - \gamma_1 \theta_{2,2} - \gamma_{2,2} \theta_1 + \gamma_2 \theta_{1,2}]) / (h_1 h_2^2) \\
 & + \left(h_{2,1}^2 (\gamma_1 \theta_1 + \gamma_2 \theta_2) \right) / (h_1^2 h_2^2)
 \end{aligned} \tag{A.56}$$

$$\begin{aligned}
 \chi_{2_{NL}}^8 = & \left(\theta_{1,2}^2 + \theta_{2,2}^2 + h_{2,3}^2 \theta_2^2 \right) / (2 h_2^2) - (h_{2,1} [\theta_{1,2} \theta_2 \\
 & - \theta_1 \theta_{2,2}]) / (h_1 h_2^2) + \left(h_{2,1}^2 (\theta_1^2 + \theta_2^2) \right) / (h_1^2 h_2^2)
 \end{aligned} \tag{A.57}$$

$$\begin{aligned}
 \chi_{4_{NL}}^0 = & [u_{,2} (\psi_1 - u/R_1) + v_{,2} (\psi_2 - v/R_2)] / h_2 \\
 & - (h_{2,1} [v (\psi_1 - u/R_1) - u (\psi_2 - v/R_2)]) / (h_1 h_2)
 \end{aligned} \tag{A.58}$$

$$\begin{aligned} \chi_{4_{NL}}^1 = & [\psi_{1,2}(\psi_1 - u/R_1) + \psi_{2,2}(\psi_2 - v/R_2) \\ & - u_{,2}(\psi_1 - u/R_1) - v_{,2}(\psi_2 - v/R_2) + 2(\phi_1 u_{,2} + \phi_2 v_{,2}) \\ & + 2h_{2,3}\phi_2 w] / h_2 - (h_{2,1}[2(\phi_1 v - \phi_2 u)]) / (h_1 h_2) \end{aligned} \quad (A.59)$$

$$\begin{aligned} \chi_{4_{NL}}^2 = & [\phi_{1,2}(\psi_1 - u/R_1) + \phi_{2,2}(\psi_2 - v/R_2) + 2(\phi_1(\psi_1 \\ & - u/R_1) + \phi_2(\psi_2 - v/R_2)) + 3(\gamma_1 u_{,2} + \gamma_2 v_{,2}) + 3h_{2,3}\gamma_2 w] / h_2 \\ & - (h_{2,1}[\phi_1(\psi_2 - v/R_2) - \phi_2(\psi_1 - u/R_1) + 3(\gamma_1 u + \gamma_2 v)]) / (h_1 h_2) \end{aligned} \quad (A.60)$$

$$\begin{aligned} \chi_{4_{NL}}^3 = & [\gamma_{1,2}(\psi_1 - u/R_1) + \gamma_{2,2}(\psi_2 - v/R_2) + 2(\phi_1\phi_{1,2} \\ & + \phi_2\phi_{2,2}) + 3(\gamma_1(\psi_{1,2} - u_{,2}/R_1) + \gamma_2(\psi_{2,2} - v_{,2}/R_2)) \\ & + 4(\theta_1 u_{,2} + \theta_2 v_{,2}) + 4h_{2,3}\theta_2 w] / h_2 - (h_{2,1}[2(\gamma_1(\psi_2 - v/R_2) \\ & - \gamma_2(\psi_1 - u/R_1)) + 4(\theta_1 u + \theta_2 v)]) / (h_1 h_2) \end{aligned} \quad (A.61)$$

$$\begin{aligned} \chi_{4_{NL}}^4 = & [\theta_{1,2}(\psi_1 - u/R_1) + \theta_{2,2}(\psi_2 - v/R_2) + 2(\phi_1\gamma_{1,2} + \phi_2\gamma_{2,2}) \\ & + 3(\gamma_1\phi_{1,2} + \gamma_2\phi_{2,2}) + 4(\theta_1(\psi_{1,2} - u_{,2}/R_1) \\ & + \theta_2(\psi_{2,2} - v_{,2}/R_2))] / h_2 - (h_{2,1}[\gamma_1\phi_2 - \gamma_2\phi_1 + 3(\theta_1(\psi_2 - v/R_2) \\ & + \theta_2(\psi_1 - u/R_1))]) / (h_1 h_2) \end{aligned} \quad (A.62)$$

$$\begin{aligned} \chi_{4_{NL}}^5 = & [2(\phi_1\phi_{1,2} + \phi_2\phi_{2,2}) + 3(\gamma_1\gamma_{1,2} + \gamma_2\gamma_{2,2}) + 4(\theta_1\phi_{1,2} \\ & + \theta_2\phi_{2,2})] / h_2 - (h_{2,1}[2(\theta_1\phi_2 - \theta_2\phi_1)]) / (h_1 h_2) \end{aligned} \quad (A.63)$$

$$\chi_{4_{NL}}^6 = [3(\gamma_1\theta_{1,2} + \gamma_2\theta_{2,2}) + 4(\theta_1\gamma_{1,2} + \theta_2\gamma_{2,2})]/h_2 \quad (A.64)$$

$$- (h_{2,1}[\theta_1\gamma_2 - \gamma_2\phi_1])/(h_1h_2)$$

$$\chi_{4_{NL}}^7 = 4(\theta_1\theta_{1,2} + \theta_2\theta_{2,2})/h_2 \quad (A.65)$$

$$\chi_{5_{NL}}^0 = [u_{,1}(\psi_1 - u/R_1) + v_{,1}(\psi_2 - v/R_2)]/h_1 \quad (A.66)$$

$$+ (h_{1,2}[v(\psi_1 - u/R_1) - u(\psi_2 - v/R_2)])/(h_1h_2)$$

$$\chi_{5_{NL}}^1 = [\psi_{1,1}(\psi_1 - u/R_1) + \psi_{2,1}(\psi_2 - v/R_2) - u_{,1}(\psi_1 - u/R_1) \quad (A.67)$$

$$- v_{,1}(\psi_2 - v/R_2) + 2(\phi_1u_{,1} + \phi_2v_{,1}) + 2h_{1,3}\phi_1w]/h_1$$

$$+ (h_{1,2}[2(\phi_1v - \phi_2u)])/(h_1h_2)$$

$$\chi_{5_{NL}}^2 = [\phi_{1,1}(\psi_1 - u/R_1) + \phi_{2,1}(\psi_2 - v/R_2) \quad (A.68)$$

$$+ 2(\phi_1(\psi_1 - u/R_1) + \phi_2(\psi_2 - v/R_2))$$

$$+ 3(\gamma_1u_{,1} + \gamma_2v_{,1}) + 3h_{1,3}\gamma_1w]/h_1 + (h_{1,2}[\phi_1(\psi_2 - v/R_2)$$

$$- \phi_2(\psi_1 - u/R_1) + 3(\gamma_1u + \gamma_2v)])/(h_1h_2)$$

$$\chi_{5_{NL}}^3 = [\gamma_{1,1}(\psi_1 - u/R_1) + \gamma_{2,1}(\psi_2 - v/R_2) + 2(\phi_1\phi_{1,1} \quad (A.69)$$

$$+ \phi_2\phi_{2,1}) + 3(\gamma_1(\psi_{1,1} - u_{,1}/R_1) + \gamma_2(\psi_{2,1} - v_{,1}/R_2))$$

$$+ 4(\theta_1u_{,1} + \theta_2v_{,1}) + 4h_{1,3}\theta_1w]/h_1 + (h_{1,2}[2(\gamma_1(\psi_2 - v/R_2)$$

$$- \gamma_2(\psi_1 - u/R_1)) + 4(\theta_1u + \theta_2v)])/(h_1h_2)$$

$$\begin{aligned} \chi_{5_{NL}}^4 = & [\theta_{1,1}(\psi_1 - u/R_1) + \theta_{2,1}(\psi_2 - v/R_2) + 2(\phi_1\gamma_{1,1} \\ & + \phi_2\gamma_{2,1}) + 3(\gamma_1\phi_{1,1} + \gamma_2\phi_{2,1}) + 4(\theta_1(\psi_{1,1} - u_{,1}/R_1) \\ & + \theta_2(\psi_{2,1} - v_{,1}/R_2))] / h_1 + (h_{1,2}[\gamma_1\phi_2 - \gamma_2\phi_1 \\ & + 3(\theta_1(\psi_2 - v/R_2) + \theta_2(\psi_1 - u/R_1))]) / (h_1 h_2) \end{aligned} \quad (A.70)$$

$$\begin{aligned} \chi_{5_{NL}}^5 = & [2(\phi_1\phi_{1,1} + \phi_2\phi_{2,1}) + 3(\gamma_1\gamma_{1,1} + \gamma_2\gamma_{2,1}) + 4(\theta_1\phi_{1,1} \\ & + \theta_2\phi_{2,1})] / h_1 + (h_{1,2}[2(\theta_1\phi_2 - \theta_2\phi_1)]) / (h_1 h_2) \end{aligned} \quad (A.72)$$

$$\begin{aligned} \chi_{5_{NL}}^6 = & [3(\gamma_1\theta_{1,1} + \gamma_2\theta_{2,1}) + 4(\theta_1\gamma_{1,1} + \theta_2\gamma_{2,1})] / h_1 \\ & + (h_{1,2}[\theta_1\gamma_2 - \gamma_2\phi_1]) / (h_1 h_2) \end{aligned} \quad (A.73)$$

$$\chi_{5_{NL}}^7 = 4(\theta_1\theta_{1,1} + \theta_2\theta_{2,1}) / h_1 \quad (A.74)$$

$$\begin{aligned} \chi_{6_{NL}}^0 = & (u_{,1}u_{,2} + v_{,1}v_{,2} + w_{,1}w_{,2}) / (h_1 h_2) - (h_{2,1}[u_{,1}v \\ & - uv_{,1}]) / (h_1^2 h_2) + (h_{1,2}[u_{,2}v - uv_{,2}]) / (h_1^2 h_2) \\ & - (h_{1,2}h_{2,1}[u^2 + v^2]) / (h_1^2 h_2^2) \end{aligned} \quad (A.75)$$

$$\begin{aligned}
 \chi_{6_{NL}}^1 = & [u_{,1}(\psi_{1,2} - u_{,2}/R_1) + u_{,2}(\psi_{1,1} - u_{,1}/R_1) + v_{,1}(\psi_{2,2} \\
 & - v_{,2}/R_2) + v_{,2}(\psi_{2,1} - v_{,1}/R_2) + h_{1,3}(w(\psi_{1,2} - u_{,2}/R_1) \\
 & - w_{,2}(\psi_1 - u/R_1)) + h_{2,3}(w(\psi_{2,1} - v_{,1}/R_2) - w_{,1}(\psi_2 - v/R_2)) \\
 & - h_{1,3}h_{2,3}(u(\psi_2 - v/R_2) + v(\psi_1 - u/R_1))] / (h_1 h_2) \\
 & - (h_{2,1}[u_{,1}(\psi_2 - v/R_2) - u(\psi_{2,1} - v_{,1}/R_2) - v_{,1}(\psi_1 - u/R_1) \\
 & + v(\psi_{1,1} - u_{,1}/R_1) + h_{1,3}w(\psi_2 - v/R_2)]) / (h_1^2 h_2) \\
 & + (h_{1,2}[u_{,2}(\psi_2 - v/R_2) - u(\psi_{2,2} - v_{,2}/R_2) - v_{,2}(\psi_1 - u/R_1) \\
 & + v(\psi_{1,2} - u_{,2}/R_1) - h_{2,3}w(\psi_1 - u/R_1)]) / (h_1^2 h_2) \\
 & - (h_{1,2}h_{2,1}[2(u(\psi_1 - u/R_1) + v(\psi_2 - v/R_2))]) / (h_1^2 h_2^2)
 \end{aligned} \tag{A.76}$$

$$\begin{aligned}
 \chi_{6_{NL}}^2 = & [u_{,1}(\phi_{1,2} - \psi_{1,2}/R_1) + u_{,2}(\phi_{1,1} - \psi_{1,1}/R_1) + v_{,1}(\phi_{2,2} \\
 & - \psi_{2,2}/R_2) + v_{,2}(\phi_{2,1} - \psi_{2,1}/R_2) + \psi_{1,1}\psi_{1,2} + \psi_{2,1}\psi_{2,2} \\
 & + (u_{,1}u_{,2})/R_1^2 + (v_{,1}v_{,2})/R_2^2 + h_{1,3}(w\phi_{1,2} - w_{,2}\phi_1) \\
 & + h_{2,3}(w\phi_{2,1} - w_{,1}\phi_2) + h_{1,3}h_{2,3}(u(\phi_2 - \psi_2/R_2) + v(\phi_1 - \psi_1/R_1) \\
 & + \psi_1\psi_2 + (uv)/(R_1 R_2))] / (h_1 h_2) - (h_{2,1}[u_{,1}(\phi_2 - \psi_2/R_2) \\
 & - u(\phi_{2,1} - \psi_{2,1}/R_2) - v_{,1}(\phi_1 - \psi_1/R_1) + v(\phi_{1,1} - \psi_{1,1}/R_1) \\
 & + (\psi_{1,1}\psi_2 - \psi_1\psi_{2,1}) + (u_{,1}v - uv_{,1})/(R_1 R_2) + h_{1,3}w\phi_2]) / (h_1^2 h_2) \\
 & + (h_{1,2}[u_{,2}(\phi_2 - \psi_2/R_2) - u(\phi_{2,2} - \psi_{2,2}/R_2) - v_{,2}(\phi_1 - \psi_1/R_1) \\
 & + v(\phi_{1,2} - \psi_{1,2}/R_1) + (\psi_{1,2}\psi_2 - \psi_1\psi_{2,2}) + (u_{,2}v - uv_{,2})/(R_1 R_2) \\
 & + h_{2,3}w\phi_1]) / (h_1^2 h_2) - (h_{1,2}h_{2,1}[2(u(\phi_1 - \psi_1/R_1) \\
 & + v(\phi_2 - \psi_2/R_2)) + u^2/R_1^2 + v^2/R_2^2 + \psi_1^2 + \psi_2^2]) / (h_1^2 h_2^2)
 \end{aligned} \tag{A.77}$$

$$\begin{aligned}
\chi_{6_{NL}}^3 = & [\phi_{1,1}(\psi_{1,2} - u_{,2}/R_1) + \phi_{1,2}(\psi_{1,1} - u_{,1}/R_1) \\
& + \phi_{2,1}(\psi_{2,2} - v_{,2}/R_2) + \phi_{2,2}(\psi_{2,1} - v_{,1}/R_2) + u_{,1}\gamma_{1,2} \\
& + u_{,2}\gamma_{1,1} + v_{,1}\gamma_{2,2} + v_{,2}\gamma_{2,1} + h_{1,3}(w\gamma_{1,2} - w_{,2}\gamma_1) \\
& + h_{2,3}(w\gamma_{2,1} - w_{,1}\gamma_2) + h_{1,3}h_{2,3}(\phi_1(\psi_2 - v/R_2) \\
& + \phi_2(\psi_1 - u/R_1) + u\gamma_2 + v\gamma_1)] / (h_1h_2) - (h_{2,1}[\phi_{1,1}(\psi_2 \\
& - v/R_2) - \phi_1(\psi_{2,1} - v_{,1}/R_2) - \phi_{2,1}(\psi_1 - u/R_1) \\
& + \phi_2(\psi_{1,1} - u_{,1}/R_1) + \gamma_{1,1}v - \gamma_1v_{,1} - \gamma_{2,1}u + \gamma_2u_{,1} \\
& + h_{1,3}w\gamma_2]) / (h_1^2h_2) + (h_{1,2}[\phi_{1,2}(\psi_2 - v/R_2) - \phi_1(\psi_{2,2} \\
& - v_{,2}/R_2) - \phi_{2,2}(\psi_1 - u/R_1) + \phi_2(\psi_{1,2} - u_{,2}/R_1) + \gamma_{1,2}v \\
& - \gamma_1v_{,2} - \gamma_{2,2}u + \gamma_2u_{,2} + h_{2,3}w\gamma_1]) / (h_1^2h_2) \\
& - (h_{1,2}h_{2,1}[2(\phi_1(\psi_1 - u/R_1) + \phi_2(\psi_2 - v/R_2) \\
& - u\gamma_1 - v\gamma_2))] / (h_1^2h_2^2)
\end{aligned}
\tag{A.78}$$

$$\begin{aligned}
 \chi_{6_{NL}}^4 = & [u_{,1}(\theta_{1,2} - \gamma_{1,2}/R_1) + u_{,2}(\theta_{1,1} - \gamma_{1,1}/R_1) \\
 & + v_{,1}(\theta_{2,2} - \gamma_{2,2}/R_2) + v_{,2}(\theta_{2,1} - \gamma_{2,1}/R_2) + \phi_{1,1}\phi_{1,2} \\
 & + \phi_{2,1}\phi_{2,2} + \psi_{1,1}\gamma_{1,2} + \psi_{1,2}\gamma_{1,1} + \psi_{2,2}\gamma_{2,1} + \psi_{2,1}\gamma_{2,2} \\
 & + h_{1,3}(w\theta_{1,2} - w_{,2}\theta_1) + h_{2,3}(w\theta_{2,1} - w_{,1}\theta_2) \\
 & + h_{1,3}h_{2,3}(u(\theta_2 - \gamma_2/R_2) + v(\theta_1 - \gamma_1/R_1) \\
 & + \phi_1\phi_2 + \psi_1\gamma_2 + \psi_2\gamma_1)] / (h_1h_2) - (h_{2,1}[u_{,1}(\theta_2 - \gamma_2/R_2) \\
 & - u(\theta_{2,1} - \gamma_{2,1}/R_2) - v_{,1}(\theta_1 - \gamma_1/R_1) + v(\theta_{1,1} - \gamma_{1,1}/R_1) \\
 & + (\phi_{1,1}\phi_2 - \phi_1\phi_{2,1}) + \psi_{1,1}\gamma_2 - \psi_1\gamma_{2,1} - \psi_{2,1}\gamma_1 + \psi_2\gamma_{1,1} \\
 & + h_{1,3}w\theta_2]) / (h_1^2h_2) + (h_{1,2}[u_{,2}(\theta_2 - \gamma_2/R_2) - u(\theta_{2,2} \\
 & - \gamma_{2,2}/R_2) - v_{,2}(\theta_1 - \gamma_1/R_1) + v(\theta_{1,2} - \gamma_{1,2}/R_1) + (\phi_{1,2}\phi_2 \\
 & - \phi_1\phi_{2,2}) + \psi_{1,2}\gamma_2 - \psi_1\gamma_{2,2} - \psi_{2,2}\gamma_1 + \psi_2\gamma_{1,2} \\
 & + h_{2,3}w\theta_1]) / (h_1^2h_2) - (h_{1,2}h_{2,1}[2(u(\theta_1 - \gamma_1/R_1) \\
 & + v(\theta_2 - \gamma_2/R_2) + \psi_1\gamma_1 + \psi_2\gamma_2) + \phi_1^2 + \phi_2^2]) / (h_1^2h_2^2)
 \end{aligned}$$

(A.79)

$$\chi_{6_{NL}}^5 = [\theta_{1,1}(\psi_{1,2} - u_{,2}/R_1) + \theta_{1,2}(\psi_{1,1} - u_{,1}/R_1) \quad (A.80)$$

$$\begin{aligned} & + \theta_{2,1}(\psi_{2,2} - v_{,2}/R_2) + \theta_{2,2}(\psi_{2,1} - v_{,1}/R_2) + \theta_{1,1}\gamma_{1,2} \\ & + \theta_{1,2}\gamma_{1,1} + \theta_{2,1}\gamma_{2,2} + \theta_{2,2}\gamma_{2,1} + h_{1,3}h_{2,3}(\theta_1(\psi_2 - v/R_2) \\ & + \theta_2(\psi_1 - u/R_1) + \phi_1\gamma_2 + \phi_2\gamma_1)] / (h_1h_2) \\ & - (h_{2,1}[\theta_{1,1}(\psi_2 - v/R_2) - \theta_1(\psi_{2,1} - v_{,1}/R_2) \\ & - \theta_{2,1}(\psi_1 - u/R_1) + \theta_2(\psi_{1,1} - u_{,1}/R_1) + \gamma_{1,1}\phi_2 - \gamma_1\phi_{2,1} \\ & - \gamma_{2,1}\phi_1 + \gamma_2\phi_{1,1}]) / (h_1^2h_2) + (h_{1,2}[\theta_{1,2}(\psi_2 - v/R_2) \\ & - \theta_1(\psi_{2,2} - v_{,2}/R_2) - \theta_{2,2}(\psi_1 - u/R_1) + \theta_2(\psi_{1,2} - u_{,2}/R_1) \\ & + \gamma_{1,2}\phi_2 - \gamma_1\phi_{2,2} - \gamma_{2,2}\phi_1 + \gamma_2\phi_{1,2}]) / (h_1^2h_2) \\ & - (h_{1,2}h_{2,1}[2(\theta_1(\psi_1 - u/R_1) + \theta_2(\psi_2 - v/R_2) \\ & + \gamma_1\phi_1 + \gamma_2\phi_2)]) / (h_1^2h_2^2) \end{aligned}$$

$$\chi_{6_{NL}}^6 = [\gamma_{1,1}\gamma_{1,2} + \gamma_{2,1}\gamma_{2,2} + \phi_{1,1}\theta_{1,2} + \phi_{1,2}\theta_{1,1} + \phi_{2,1}\theta_{2,2} \quad (A.81)$$

$$\begin{aligned} & + \phi_{2,2}\theta_{2,1} + h_{1,3}h_{2,3}(\gamma_1\gamma_2 + \phi_1\theta_2 + \phi_2\theta_1)] / (h_1h_2) \\ & - (h_{2,1}[\gamma_{1,1}\gamma_2 - \gamma_1\gamma_{2,1} + \phi_{1,1}\theta_2 - \phi_1\theta_{2,1} - \phi_{2,1}\theta_1 \\ & + \phi_2\theta_{1,1}]) / (h_1^2h_2) + (h_{1,2}[\gamma_{1,2}\gamma_2 - \gamma_1\gamma_{2,2} + \phi_{1,2}\theta_2 - \phi_1\theta_{2,2} \\ & - \phi_{2,2}\theta_1 + \phi_2\theta_{1,2}]) / (h_1^2h_2) - (h_{1,2}h_{2,1}[\gamma_1^2 + \gamma_2^2 + 2(\phi_1\theta_1 \\ & + \phi_2\theta_2)]) / (h_1^2h_2^2) \end{aligned}$$

$$\begin{aligned} \chi_{6_{NL}}^7 = & [\gamma_{1,1}\theta_{1,2} + \gamma_{1,2}\theta_{1,1} + \gamma_{2,1}\theta_{2,2} + \gamma_{2,2}\theta_{2,1} \\ & + h_{1,3}h_{2,3}(\gamma_{1,1}\theta_{2,2} + \gamma_{2,1}\theta_{1,1})] / (h_1 h_2) - (h_{2,1}[\gamma_{1,1}\theta_{2,2} - \gamma_{1,2}\theta_{2,1} \\ & - \gamma_{2,1}\theta_{1,1} + \gamma_{2,2}\theta_{1,2}]) / (h_1^2 h_2) + (h_{1,2}[\gamma_{1,2}\theta_{2,2} - \gamma_{1,1}\theta_{2,1} - \gamma_{2,2}\theta_{1,1} \\ & + \gamma_{2,1}\theta_{1,2}]) / (h_1^2 h_2) - (h_{1,2}h_{2,1}[2(\gamma_{1,1}\theta_{1,1} + \gamma_{2,2}\theta_{2,2})]) / (h_1^2 h_2^2) \end{aligned} \quad (A.82)$$

$$\begin{aligned} \chi_{6_{NL}}^8 = & [\theta_{1,1}\theta_{1,2} + \theta_{2,1}\theta_{2,2} + h_{1,3}h_{2,3}(\theta_{1,1}\theta_{2,2})] / (h_1 h_2) \\ & - (h_{2,1}[\theta_{1,1}\theta_{2,2} - \theta_{1,2}\theta_{2,1}]) / (h_1^2 h_2) + (h_{1,2}[\theta_{1,2}\theta_{2,2} \\ & - \theta_{1,1}\theta_{2,1}]) / (h_1^2 h_2) - (h_{1,2}h_{2,1}[\theta_{1,1}^2 + \theta_{2,2}^2]) / (h_1^2 h_2^2) \end{aligned} \quad (A.83)$$

A.3 Approximation of 60 Shell Shape Factor Functions with Second Order Taylor's Series Expansions

Most of the expressions listed in the previous section contain shape functions h_1 and h_2 or their derivatives. If one factors out all these functions, there are 60 different combinations possible. For a shell with radius R_1 in the y_1 direction and radius R_2 in the y_2 directions, the shape factors h_1 and h_2 are shown below

$$h_1 = A_1 (1 - y_3/R_1) \quad h_2 = A_2 (1 - y_3/R_2) \quad (A.1)$$

where $A_1 = \sqrt{a_{11}}$ and $A_2 = \sqrt{a_{22}}$ are the Lamé parameters of the surface. The 60 possible combinations of the functions are listed below along with their quadratic Taylor's series approximations.

$$\hat{H}_1 = \frac{h_{1,2}}{h_1} \cong \left[\frac{A_{1,2}}{A_1} \right] + \left[\frac{R_{1,2}}{R_1^2} \right] y_3 + \left[\frac{R_{1,2}}{R_1^3} \right] y_3^2 \quad (A.2)$$

$$\hat{H}_2 = \frac{h_{1,3}}{h_1} \cong \left[\frac{A_{1,3}}{A_1} - \frac{1}{R_1} \right] + \left[\frac{R_{1,3} - 1}{R_1^2} \right] y_3 + \left[\frac{R_{1,3} - 1}{R_1^3} \right] y_3^2 \quad (\text{A.3})$$

$$\hat{H}_3 = \frac{1}{h_1^2} \cong \left[\frac{1}{A_1^2} \right] + \left[\frac{2}{A_1^2 R_1} \right] y_3 + \left[\frac{3}{A_1^2 R_1^2} \right] y_3^2 \quad (\text{A.4})$$

$$\hat{H}_4 = \frac{h_{1,2}^2}{h_1^2} \cong \left[\frac{A_{1,2}^2}{A_1^2} \right] + \left[\frac{2A_{1,2}R_{1,2}}{A_1 R_1^2} \right] y_3 + \left[\frac{R_{1,2}}{R_1^3} \left(\frac{2A_{1,2}}{A_1} + \frac{R_{1,2}}{R_1} \right) \right] y_3^2 \quad (\text{A.5})$$

$$\begin{aligned} \hat{H}_5 = \frac{h_{1,2}^2}{h_2^2} \cong & \left[\frac{A_{1,2}^2}{A_2^2} \right] + \left[\frac{2A_{1,2}}{A_2^2} \left(A_{1,2} \left(\frac{1}{R_2} - \frac{1}{R_1} \right) + \frac{A_1 R_{1,2}}{R_1^2} \right) \right] y_3 \\ & + \left[\frac{A_{1,2}^2}{A_2^2} \left(\frac{1}{R_1} - \frac{3}{R_2} \right)^2 + \frac{A_1 R_{1,2}}{A_2^2 R_1^2} \left(2A_{1,2} \left(\frac{2}{R_2} - \frac{1}{R_1} \right) + \frac{A_1 R_{1,2}}{R_1^2} \right) \right] y_3^2 \end{aligned} \quad (\text{A.6})$$

$$\begin{aligned} \hat{H}_6 = \frac{h_{1,3}^2}{h_1^2} \cong & \left[\left(\frac{A_{1,3}}{A_1} - \frac{1}{R_1} \right)^2 \right] + \left[\frac{(R_{1,3} - 1)}{R_1^2} \left(\frac{2A_{1,3}}{A_1} - \frac{2}{R_1} \right) \right] y_3 \\ & + \left[\frac{(R_{1,3} - 1)}{R_1^3} \left(\frac{2A_{1,3}}{A_1} - \frac{(R_{1,3} - 3)}{R_1} \right) \right] y_3^2 \end{aligned} \quad (\text{A.7})$$

$$\hat{H}_7 = h_{1,3}^2 \equiv \left[\left(A_{1,3} - \frac{1}{R_1} \right)^2 \right] \quad (\text{A.8})$$

$$+ \left[\frac{2}{R_1} \left(\frac{A_1}{R_1} - A_{1,3} \right) \left(A_{1,3} - \frac{A_1 R_{1,3}}{R_1} \right) \right] y_3$$

$$+ \left[\left(\frac{A_{1,3}}{R_1} - \frac{A_1 R_{1,3}}{R_1^2} \right)^2 \right] y_3^2$$

$$\hat{H}_8 = \frac{h_{1,2} h_{1,3}}{h_1^2} \equiv \left[\frac{A_{1,2}}{A_1} \left(\frac{A_{1,3}}{A_1} - \frac{1}{R_1} \right) \right] + \left[\frac{A_{1,2} (R_{1,3} - 1)}{A_1 R_1^2} \right] \quad (\text{A.9})$$

$$+ \frac{R_{1,2}}{R_1^2} \left(\frac{A_{1,3}}{A_1} - \frac{1}{R_1} \right) y_3 + \left[\frac{A_{1,2} (R_{1,3} - 1)}{A_1 R_1^3} \right]$$

$$+ \frac{R_{1,2}}{R_1^3} \left(\frac{A_{1,3}}{A_1} - \frac{(R_{1,3} - 2)}{R_1} \right) y_3^2$$

$$\hat{H}_9 = \frac{h_{2,3}}{h_2} \equiv \left[\frac{A_{2,3}}{A_2} - \frac{1}{R_2} \right] + \left[\frac{R_{2,3} - 1}{R_2^2} \right] y_3 + \left[\frac{R_{2,3} - 1}{R_2^3} \right] y_3^2 \quad (\text{A.10})$$

$$\hat{H}_{10} = \frac{h_{2,1}}{h_2} \equiv \left[\frac{A_{2,1}}{A_2} \right] + \left[\frac{R_{2,1}}{R_2^2} \right] y_3 + \left[\frac{R_{2,1}}{R_2^3} \right] y_3^2 \quad (\text{A.11})$$

$$\hat{H}_{11} = \frac{1}{h_2} \equiv \left[\frac{1}{A_2^2} \right] + \left[\frac{2}{A_2^2 R_2} \right] y_3 + \left[\frac{3}{A_2^2 R_2^2} \right] y_3^2 \quad (\text{A.12})$$

$$\begin{aligned}\hat{H}_{12} = \frac{h_{2,1}^2}{h_2^2} &\cong \left[\frac{A_{2,1}^2}{A_2^2} \right] + \left[\frac{2A_{2,1}R_{2,1}}{A_2R_2^2} \right] y_3 \\ &+ \left[\frac{R_{2,1}}{R_1^3} \left(\frac{2A_{2,1}}{A_2} + \frac{R_{2,1}}{R_2} \right) \right] y_3^2\end{aligned}\quad (\text{A.13})$$

$$\begin{aligned}\hat{H}_{13} = \frac{h_{2,1}^2}{h_1^2} &\cong \left[\frac{A_{2,1}^2}{A_1^2} \right] + \left[\frac{2A_{2,1}}{A_1^2} \left(A_{2,1} \left(\frac{1}{R_1} - \frac{1}{R_2} \right) + \frac{A_2R_{2,1}}{R_2^2} \right) \right] y_3 \\ &+ \left[\frac{A_{2,1}^2}{A_1^2} \left(\frac{1}{R_2} - \frac{3}{R_1} \right)^2 + \frac{A_2R_{2,1}}{A_1^2R_2^2} \left(2A_{2,1} \left(\frac{2}{R_1} - \frac{1}{R_2} \right) + \frac{A_2R_{2,1}}{R_2^2} \right) \right] y_3^2\end{aligned}\quad (\text{A.14})$$

$$\begin{aligned}\hat{H}_{14} = \frac{h_{2,3}^2}{h_2^2} &\cong \left[\left(\frac{A_{2,3}}{A_2} - \frac{1}{R_2} \right)^2 \right] + \left[\frac{(R_{2,3}-1)}{R_2^2} \left(\frac{2A_{2,3}}{A_2} - \frac{2}{R_2} \right) \right] y_3 \\ &+ \left[\frac{(R_{2,3}-1)}{R_2^3} \left(\frac{2A_{2,3}}{A_2} - \frac{(R_{2,3}-3)}{R_2} \right) \right] y_3^2\end{aligned}\quad (\text{A.15})$$

$$\hat{H}_{15} = h_{2,3}^2 \equiv \left[\left(A_{2,3} - \frac{1}{R_2} \right)^2 \right] \quad (\text{A.16})$$

$$+ \left[\frac{2}{R_2} \left(\frac{A_2}{R_2} - A_{2,3} \right) \left(A_{2,3} - \frac{A_2 R_{2,3}}{R_2} \right) \right] y_3$$

$$+ \left[\left(\frac{A_{2,3}}{R_2} - \frac{A_2 R_{2,3}}{R_2^2} \right)^2 \right] y_3^2$$

$$\hat{H}_{16} = \frac{h_{2,1} h_{2,3}}{h_2^2} \equiv \left[\frac{A_{2,1}}{A_2} \left(\frac{A_{2,3}}{A_2} - \frac{1}{R_2} \right) \right] + \left[\frac{A_{2,1} (R_{2,3} - 1)}{A_2 R_2^2} \right] \quad (\text{A.17})$$

$$+ \frac{R_{2,1}}{R_2^2} \left(\frac{A_{2,3}}{A_2} - \frac{1}{R_2} \right) y_3 + \left[\frac{A_{2,1} (R_{2,3} - 1)}{A_2 R_2^3} \right]$$

$$+ \frac{R_{2,1}}{R_2^3} \left(\frac{A_{2,3}}{A_2} - \frac{(R_{2,3} - 2)}{R_2} \right) y_3^2$$

$$\hat{H}_{17} = \frac{1}{h_2} \equiv \left[\frac{1}{A_2} \right] + \left[\frac{1}{A_2 R_2} \right] y_3 + \left[\frac{1}{A_1 R_1^2} \right] y_3^2 \quad (\text{A.18})$$

$$\hat{H}_{18} = \frac{1}{h_1} \equiv \left[\frac{1}{A_1} \right] + \left[\frac{1}{A_1 R_1} \right] y_3 + \left[\frac{1}{A_1 R_1^2} \right] y_3^2 \quad (\text{A.19})$$

$$\begin{aligned}\hat{H}_{19} = \frac{h_{2,1}}{h_1} \cong & \left[\frac{A_{2,1}}{A_1} \right] + \left[\frac{A_{2,1}}{A_1} \left(\frac{1}{R_1} - \frac{1}{R_2} \right) + \frac{A_2 R_{2,1}}{A_1 R_2^2} \right] y_3 \\ & + \left[\frac{A_{2,1}}{A_1 R_1} \left(\frac{1}{R_1} - \frac{1}{R_2} \right) + \frac{A_2 R_{2,1}}{A_1 R_1 R_2^2} \right] y_3^2\end{aligned}\quad (\text{A.20})$$

$$\begin{aligned}\hat{H}_{20} = \frac{h_{1,2}}{h_2} \cong & \left[\frac{A_{1,2}}{A_2} \right] + \left[\frac{A_{1,2}}{A_2} \left(\frac{1}{R_2} - \frac{1}{R_1} \right) + \frac{A_1 R_{1,2}}{A_2 R_1^2} \right] y_3 \\ & + \left[\frac{A_{1,2}}{A_2 R_2} \left(\frac{1}{R_2} - \frac{1}{R_1} \right) + \frac{A_1 R_{1,2}}{A_2 R_1^2 R_2} \right] y_3^2\end{aligned}\quad (\text{A.21})$$

$$\hat{H}_{21} = \frac{1}{h_1 h_2} \cong \left[\frac{1}{A_1 A_2} \right] + \left[\frac{R_1 + R_2}{A_1 A_2 R_1 R_2} \right] y_3 + \left[\frac{R_1^2 + R_1 R_2 + R_2^2}{A_1 A_2 R_1^2 R_2^2} \right] y_3^2 \quad (\text{A.22})$$

$$\begin{aligned}\hat{H}_{22} = \frac{h_{1,3}}{h_2} \cong & \left[\frac{1}{A_2} \left(A_{1,3} - \frac{A_1}{R_1} \right) \right] + \left[\frac{A_{1,3}}{A_2} \left(\frac{1}{R_2} - \frac{1}{R_1} \right) \right. \\ & + \left. \frac{A_1}{A_2 R_1} \left(\frac{R_{1,3}}{R_1} - \frac{1}{R_2} \right) \right] y_3 + \left[\frac{A_{1,3}}{A_2 R_2} \left(\frac{1}{R_2} - \frac{1}{R_1} \right) \right. \\ & + \left. \frac{A_1}{A_2 R_1 R_2} \left(\frac{R_{1,3}}{R_1} - \frac{1}{R_2} \right) \right] y_3^2\end{aligned}\quad (\text{A.23})$$

$$\begin{aligned}\hat{H}_{23} = \frac{h_{2,3}}{h_1} &\equiv \left[\frac{1}{A_1} \left(A_{2,3} - \frac{A_2}{R_2} \right) \right] + \left[\frac{A_{2,3}}{A_1} \left(\frac{1}{R_1} - \frac{1}{R_2} \right) \right. \\ &+ \left. \frac{A_2}{A_1 R_2} \left(\frac{R_{2,3}}{R_2} - \frac{1}{R_1} \right) \right] y_3 + \left[\frac{A_{2,3}}{A_1 R_1} \left(\frac{1}{R_1} - \frac{1}{R_2} \right) \right. \\ &+ \left. \frac{A_2}{A_1 R_1 R_2} \left(\frac{R_{2,3}}{R_2} - \frac{1}{R_1} \right) \right] y_3^2\end{aligned}\quad (A.24)$$

$$\begin{aligned}\hat{H}_{24} = \frac{h_{1,2} h_{1,2}}{h_1^2} &\equiv \left[\frac{A_{1,2} A_{1,2}}{A_1^2} \right] + \left[\frac{A_{1,2} A_{2,1}}{A_1^2} \left(\frac{1}{R_1} - \frac{1}{R_2} \right) \right. \\ &+ \left. \frac{A_{2,1} R_{1,2}}{A_1 R_1^2} + \frac{A_2 A_{1,2} R_{2,1}}{A_1^2 R_2^2} \right] y_3 + \left[\frac{A_{1,2} A_{2,1}}{A_1^2 R_1} \left(\frac{1}{R_1} - \frac{1}{R_2} \right) \right. \\ &+ \left. \frac{A_{2,1} R_{1,2}}{A_1 R_1^2} \left(\frac{2}{R_1} - \frac{1}{R_2} \right) + \frac{A_2 A_{1,2} R_{2,1}}{A_1^2 R_1 R_2^2} \left(\frac{A_{1,2}}{A_1} + \frac{R_{1,2}}{R_1} \right) \right] y_3^2\end{aligned}\quad (A.25)$$

$$\begin{aligned}\hat{H}_{25} = \frac{h_{1,2} h_{2,1}}{h_2^2} &\equiv \left[\frac{A_{1,2} A_{1,2}}{A_2^2} \right] + \left[\frac{A_{1,2} A_{2,1}}{A_2^2} \left(\frac{1}{R_2} - \frac{1}{R_1} \right) \right. \\ &+ \left. \frac{A_{1,2} R_{2,1}}{A_2 R_2^2} + \frac{A_1 A_{2,1} R_{1,2}}{A_2^2 R_1^2} \right] y_3 + \left[\frac{A_{1,2} A_{2,1}}{A_2^2 R_2} \left(\frac{1}{R_2} - \frac{1}{R_1} \right) \right. \\ &+ \left. \frac{A_{1,2} R_{2,1}}{A_2 R_2^2} \left(\frac{2}{R_2} - \frac{1}{R_1} \right) + \frac{A_1 A_{2,1} R_{1,2}}{A_2^2 R_1 R_2^2} \left(\frac{A_{2,1}}{A_2} + \frac{R_{2,1}}{R_2} \right) \right] y_3^2\end{aligned}\quad (A.26)$$

$$\begin{aligned}
 \hat{H}_{26} = h_{1,3}h_{2,3} \cong & \left[A_{1,3}A_{2,3} - \frac{A_1A_{2,3}}{R_1} - \frac{A_2A_{1,3}}{R_2} + \frac{A_1A_2}{R_1R_2} \right] \\
 & - \left[\frac{A_{1,3}A_{2,3}}{A_1A_2} \left(\frac{1}{R_1} + \frac{1}{R_2} \right) - \frac{A_1A_{2,3}}{R_1} \left(\frac{R_{1,3}}{R_1} + \frac{1}{R_2} \right) \right. \\
 & \left. - \frac{A_2A_{1,3}}{R_2} \left(\frac{R_{2,3}}{R_2} + \frac{1}{R_1} \right) + \frac{A_1A_2}{R_1R_2} \left(\frac{R_{1,3}}{R_1} + \frac{R_{2,3}}{R_2} \right) \right] y_3 \\
 & + \left[\frac{A_{1,3}A_{2,3}}{R_1R_2} - \frac{A_1A_{2,3}R_{1,3}}{R_1^2R_2} - \frac{A_2A_{1,3}R_{2,3}}{R_1R_2^2} \right. \\
 & \left. + \frac{A_1A_2R_{1,3}R_{2,3}}{R_1^2R_2^2} \right] y_3^2
 \end{aligned} \tag{A.27}$$

$$\begin{aligned}
 \hat{H}_{27} = \frac{h_{1,3}h_{2,1}}{h_1^2} \cong & \left[\frac{A_{2,1}}{A_1} \left(\frac{A_{1,3}}{A_1} - \frac{1}{R_1} \right) \right] + \left[\frac{A_{1,3}A_{2,1}}{A_1^2} \left(\frac{1}{R_1} - \frac{1}{R_2} \right) \right. \\
 & \left. + \frac{A_{2,1}}{A_1R_1} \left(\frac{(R_{1,3}-2)}{R_1} + \frac{1}{R_2} \right) + \frac{A_2R_{2,1}}{A_1R_2^2} \left(\frac{A_{1,3}}{A_1} - \frac{1}{R_1} \right) \right] y_3 \\
 & + \left[\frac{A_{1,3}A_{2,1}}{A_1^2R_1} \left(\frac{1}{R_1} - \frac{1}{R_2} \right) + \frac{A_{2,1}}{A_1R_1^2} \left(\frac{(2R_{1,3}-3)}{R_1} - \frac{(R_{1,3}-2)}{R_2} \right) \right. \\
 & \left. + \frac{A_2R_{2,1}}{A_1R_1R_2^2} \left(\frac{A_{1,3}}{A_1} + \frac{(R_{1,3}-2)}{R_1} \right) \right] y_3^2
 \end{aligned} \tag{A.28}$$

$$\begin{aligned}
 \hat{H}_{28} = \frac{h_{1,2}h_{2,3}}{h_2^2} \cong & \left[\frac{A_{1,2}}{A_2} \left(\frac{A_{1,2}}{A_2} - \frac{1}{R_2} \right) \right] + \left[\frac{A_{1,2}A_{2,3}}{A_2^2} \left(\frac{1}{R_2} - \frac{1}{R_1} \right) \right. \\
 & + \frac{A_{1,2}}{A_2R_2} \left(\frac{(R_{2,3}-2)}{R_2} + \frac{1}{R_1} \right) + \frac{A_1R_{1,2}}{A_2R_1^2} \left(\frac{A_{2,3}}{A_2} - \frac{1}{R_2} \right) \left. \right] y_3 \\
 & + \left[\frac{A_{1,2}A_{2,3}}{A_2^2R_2} \left(\frac{1}{R_2} - \frac{1}{R_1} \right) + \frac{A_{1,2}}{A_2R_2^2} \left(\frac{(2R_{2,3}-3)}{R_2} - \frac{(R_{2,3}-2)}{R_1} \right) \right. \\
 & + \left. \frac{A_1R_{1,2}}{A_1R_1R_2^2} \left(\frac{A_{1,3}}{A_1} + \frac{(R_{1,3}-2)}{R_1} \right) \right] y_3^2
 \end{aligned} \tag{A.29}$$

$$\begin{aligned}
 \hat{H}_{29} = \frac{h_{1,2}}{h_1h_2} \cong & \left[\frac{A_{1,2}}{A_1A_2} \right] + \left[\frac{1}{A_2} \left(\frac{A_{1,2}}{A_1R_2} + \frac{R_{1,2}}{R_1^2} \right) \right] y_3 + \left[\frac{1}{A_2} \left(\frac{A_{1,2}}{A_1R_2} \right. \right. \\
 & + \left. \left. \frac{R_{1,2}}{R_1^2} \left(\frac{1}{R_1} + \frac{1}{R_2} \right) \right) \right] y_3^2
 \end{aligned} \tag{A.30}$$

$$\begin{aligned}
 \hat{H}_{30} = \frac{h_{1,2}^2}{h_1^2h_2} \cong & \left[\frac{A_{1,2}^2}{A_1^2A_2} \right] + \left[\frac{A_{1,2}}{A_1A_2} \left(\frac{A_{1,2}}{A_1R_2} + \frac{2R_{1,2}}{R_1^2} \right) \right] y_3 \\
 & + \left[\frac{A_{1,2}}{A_1A_2} \left(\frac{A_{1,2}}{A_1R_2^2} + \frac{2R_{1,2}}{R_1^2} \left(\frac{1}{R_1} + \frac{1}{R_2} \right) \right) + \frac{R_{1,2}^2}{A_2R_1^4} \right] y_3^2
 \end{aligned} \tag{A.31}$$

$$\begin{aligned}\hat{H}_{31} = \frac{h_{1,2}^2}{h_1 h_2^2} \cong & \left[\frac{A_{1,2}^2}{A_1 A_2^2} + \left[\frac{A_{1,2}}{A_2^2} \left(\frac{A_{1,2}}{A_1} \left(\frac{2}{R_2} - \frac{1}{R_1} \right) + \frac{2R_{1,2}}{R_1^2} \right) \right] y_3 \right. \\ & \left. + \left[\frac{A_{1,2}}{A_2^2} \left(\frac{A_{1,2}}{A_1 R_2} \left(\frac{3}{R_2} - \frac{2}{R_1} \right) + \frac{4R_{1,2}}{R_1^2 R_2} \right) + \frac{A_1 R_{1,2}^2}{A_2^2 R_1^4} \right] y_3^2 \right]\end{aligned}\quad (\text{A.32})$$

$$\begin{aligned}\hat{H}_{32} = \frac{h_{1,3}^2}{h_1} \cong & \left[A_{1,3} \left(\frac{A_{1,3}}{A_1} - \frac{2}{R_1} \right)^2 + \frac{A_1}{R_1^2} \right] + \left[\frac{A_{1,3}}{R_1} \left(\frac{2R_{1,3}}{R_1} - \frac{A_{1,3}}{R_1} \right) \right. \\ & \left. + \frac{A_1}{R_1^3} (1 - 2R_{1,3}) \right] y_3 + \left[\frac{A_1}{R_1^4} (1 - R_{1,3})^2 \right] y_3^2\end{aligned}\quad (\text{A.33})$$

$$\begin{aligned}\hat{H}_{33} = \frac{h_{1,2}}{h_1^2} \cong & \left[\frac{A_{1,2}}{A_1^2} + \left[\frac{1}{A_1 R_1} \left(\frac{A_{1,2}}{A_1} + \frac{R_{1,2}}{R_1} \right) \right] y_3 + \left[\frac{1}{A_1 R_1^2} \left(\frac{A_{1,2}}{A_1} \right. \right. \right. \\ & \left. \left. + \frac{2R_{1,2}}{R_1} \right) \right] y_3^2\end{aligned}\quad (\text{A.34})$$

$$\begin{aligned}\hat{H}_{34} = \frac{h_{1,3}}{h_1^2} \cong & \left[\frac{1}{A_1} \left(\frac{A_{1,3}}{A_1} - \frac{1}{R_1} \right) \right] \\ & + \left[\frac{1}{A_1 R_1} \left(\frac{A_{1,3}}{A_1} + \frac{(R_{1,3} - 2)}{R_1} \right) \right] y_3 \\ & + \left[\frac{1}{A_1 R_1^2} \left(\frac{A_{1,3}}{A_1} + \frac{(2R_{1,3} - 3)}{R_1} \right) \right] y_3^2\end{aligned}\quad (\text{A.35})$$

$$\begin{aligned}
 \hat{H}_{35} = \frac{h_{1,2}h_{1,3}}{h_1^2h_2} &\equiv \left[\frac{A_{1,2}}{A_1A_2} \left(\frac{A_{1,3}}{A_1} - \frac{1}{R_1} \right) \right] + \left[\frac{A_{1,2}}{A_1A_2} \left(\frac{A_{1,3}}{A_1R_2} \right. \right. \\
 &+ \left. \left. \frac{(R_{1,3}-1)}{R_1^2} - \frac{1}{R_1R_2} \right) + \frac{R_{1,2}}{A_1R_1^2} \left(\frac{A_{1,3}}{A_1} - \frac{1}{R_1} \right) \right] y_3 \\
 &+ \left[\frac{A_{1,2}}{A_1A_2} \left(\frac{A_{1,3}}{A_1R_2^2} + \frac{(R_{1,3}-1)}{R_1^3} + \frac{(R_{1,3}-1)}{R_1^2R_2} - \frac{1}{R_1R_2^2} \right) \right. \\
 &+ \left. \frac{R_{1,2}}{A_2R_1^2} \left(\frac{A_{1,3}}{A_1} \left(\frac{1}{R_1} + \frac{1}{R_2} \right) + \frac{(R_{1,3}-1)}{R_1^2} - \frac{1}{R_1R_2} \right) \right] y_3^2
 \end{aligned} \tag{A.36}$$

$$\begin{aligned}
 \hat{H}_{36} = \frac{h_{2,1}}{h_1h_2} &\equiv \left[\frac{A_{1,2}}{A_1A_2} \right] + \left[\frac{1}{A_1} \left(\frac{A_{2,1}}{A_2R_1} + \frac{R_{2,1}}{R_2^2} \right) \right] y_3 \\
 &+ \left[\frac{1}{A_1} \left(\frac{A_{2,1}}{A_2R_1} + \frac{R_{2,1}}{R_2^2} \left(\frac{1}{R_1} + \frac{1}{R_2} \right) \right) \right] y_3^2
 \end{aligned} \tag{A.37}$$

$$\begin{aligned}
 \hat{H}_{37} = \frac{h_{2,1}^2}{h_1h_2^2} &\equiv \left[\frac{A_{2,1}^2}{A_1A_2^2} \right] + \left[\frac{A_{2,1}}{A_1A_2} \left(\frac{A_{2,1}}{A_2R_1} + \frac{2R_{2,1}}{R_2^2} \right) \right] y_3 \\
 &+ \left[\frac{A_{2,1}}{A_1A_2} \left(\frac{A_{2,1}}{A_2R_1^2} + \frac{2R_{2,1}}{R_2^2} \left(\frac{1}{R_1} + \frac{1}{R_2} \right) \right) + \frac{R_{2,1}^2}{A_1R_2^4} \right] y_3^2
 \end{aligned} \tag{A.38}$$

$$\begin{aligned} \hat{H}_{38} = \frac{h_{2,1}^2}{h_1^2 h_2} \cong & \left[\frac{A_{2,1}^2}{A_1^2 A_2} \right] + \left[\frac{A_{2,1}}{A_1^2} \left(\frac{A_{2,1}}{A_2} \left(\frac{2}{R_1} - \frac{1}{R_2} \right) + \frac{2R_{2,1}}{R_2^2} \right) \right] y_3 \\ & + \left[\frac{A_{2,1}}{A_1^2} \left(\frac{A_{2,1}}{A_2 R_1} \left(\frac{3}{R_1} - \frac{2}{R_2} \right) + \frac{4R_{2,1}}{R_1 R_2^2} \right) + \frac{A_2 R_{2,1}^2}{A_1^2 R_2^4} \right] y_3^2 \end{aligned} \quad (A.39)$$

$$\begin{aligned} \hat{H}_{39} = \frac{h_{2,3}^2}{h_1} \cong & \left[A_{2,3} \left(\frac{A_{2,3}}{A_2} - \frac{2}{R_2} \right)^2 + \frac{A_2}{R_2^2} \right] + \left[\frac{A_{2,3}}{R_2} \left(\frac{2R_{2,3}}{R_2} - \frac{A_{2,3}}{R_2} \right) \right. \\ & \left. + \frac{A_2}{R_2^3} (1 - 2R_{2,3}) \right] y_3 + \left[\frac{A_2}{R_2^4} (1 - R_{2,3})^2 \right] y_3^2 \end{aligned} \quad (A.40)$$

$$\begin{aligned} \hat{H}_{40} = \frac{h_{2,1}}{h_2^2} \cong & \left[\frac{A_{2,1}}{A_2^2} \right] + \left[\frac{1}{A_2 R_2} \left(\frac{A_{2,1}}{A_2} + \frac{R_{2,1}}{R_2} \right) \right] y_3 + \left[\frac{1}{A_2 R_2^2} \left(\frac{A_{2,1}}{A_2} \right. \right. \\ & \left. \left. + \frac{2R_{2,1}}{R_1} \right) \right] y_3^2 \end{aligned} \quad (A.41)$$

$$\begin{aligned}\hat{H}_{41} = \frac{h_{2,1}h_{2,3}}{h_1h_2^2} &\equiv \left[\frac{A_{2,1}}{A_1A_2} \left(\frac{A_{2,3}}{A_2} - \frac{1}{R_2} \right) \right] + \left[\frac{A_{2,1}}{A_1A_2} \left(\frac{A_{2,1}}{A_2R_1} \right. \right. \\ &+ \left. \left. \frac{(R_{2,3}-1)}{R_2^2} - \frac{1}{R_1R_2} \right) + \frac{R_{2,1}}{A_2R_2^2} \left(\frac{A_{2,3}}{A_2} - \frac{1}{R_2} \right) \right] y_3 \\ &+ \left[\frac{A_{2,1}}{A_1A_2} \left(\frac{A_{2,3}}{A_2R_1^2} + \frac{(R_{2,3}-1)}{R_2^3} + \frac{(R_{2,3}-1)}{R_1R_2^2} - \frac{1}{R_1^2R_2} \right) \right. \\ &+ \left. \left. \frac{R_{2,1}}{A_1R_2^2} \left(\frac{A_{2,3}}{A_2} \left(\frac{1}{R_1} + \frac{1}{R_2} \right) + \frac{(R_{2,3}-2)}{R_2^2} - \frac{1}{R_1R_2} \right) \right] y_3^2\end{aligned}\quad (A.42)$$

$$\begin{aligned}\hat{H}_{42} = \frac{h_{2,3}}{h_2^2} &\equiv \left[\frac{1}{A_2} \left(\frac{A_{2,3}}{A_2} - \frac{1}{R_2} \right) \right] \\ &+ \left[\frac{1}{A_2R_2} \left(\frac{A_{2,3}}{A_2} + \frac{(R_{2,3}-2)}{R_2} \right) \right] y_3 \\ &+ \left[\frac{1}{A_2R_2^2} \left(\frac{A_{2,3}}{A_2} + \frac{(2R_{2,3}-3)}{R_2} \right) \right] y_3^2\end{aligned}\quad (A.43)$$

$$\begin{aligned}\hat{H}_{43} = \frac{h_{1,2}}{h_2^2} &\equiv \left[\frac{A_{1,2}}{A_2^2} \right] + \left[\frac{1}{A_2^2} \left(A_{1,2} \left(\frac{2}{R_2} - \frac{1}{R_1} \right) + \frac{A_1R_{1,2}}{R_1^2} \right) \right] y_3 \\ &+ \left[\frac{1}{A_2^2R_2} \left(A_{1,2} \left(\frac{3}{R_2} - \frac{2}{R_1} \right) + \frac{2A_1R_{1,2}}{R_1^2} \right) \right] y_3^2\end{aligned}\quad (A.44)$$

$$\begin{aligned}\hat{H}_{44} = \frac{h_{2,1}}{h_1^2} \cong & \left[\frac{A_{2,1}}{A_1^2} \right] + \left[\frac{1}{A_1^2} \left(A_{2,1} \left(\frac{2}{R_1} - \frac{1}{R_2} \right) + \frac{A_2 R_{2,1}}{R_2^2} \right) \right] y_3 \\ & + \left[\frac{1}{A_1^2 R_1} \left(A_{2,1} \left(\frac{3}{R_1} - \frac{2}{R_2} \right) + \frac{2A_2 R_{2,1}}{R_2^2} \right) \right] y_3^2\end{aligned}\quad (\text{A.45})$$

$$\begin{aligned}\hat{H}_{45} = \frac{h_{1,3}}{h_1 h_2} \cong & \left[\frac{1}{A_2} \left(\frac{A_{1,3}}{A_1} - \frac{1}{R_1} \right) \right] \\ & + \left[\frac{1}{A_2 R_2} \left(\frac{A_{1,3}}{A_1} - \frac{1}{R_1} \right) + \frac{(R_{1,3} - 1)}{A_2 R_1^2} \right] y_3 \\ & + \left[\frac{1}{A_2 R_2^2} \left(\frac{A_{1,3}}{A_1} - \frac{1}{R_1} \right) + \frac{(R_{1,3} - 1)}{A_2 R_1^2} \left(\frac{1}{R_1} + \frac{1}{R_2} \right) \right] y_3^2\end{aligned}\quad (\text{A.46})$$

$$\begin{aligned}\hat{H}_{46} = \frac{h_{2,3}}{h_1 h_2} \cong & \left[\frac{1}{A_1} \left(\frac{A_{2,3}}{A_2} - \frac{1}{R_2} \right) \right] \\ & + \left[\frac{1}{A_1 R_1} \left(\frac{A_{2,3}}{A_2} - \frac{1}{R_2} \right) + \frac{(R_{2,3} - 1)}{A_1 R_2^2} \right] y_3 \\ & + \left[\frac{1}{A_1 R_1^2} \left(\frac{A_{2,3}}{A_2} - \frac{1}{R_2} \right) + \frac{(R_{2,3} - 1)}{A_1 R_2^2} \left(\frac{1}{R_1} + \frac{1}{R_2} \right) \right] y_3^2\end{aligned}\quad (\text{A.47})$$

$$\hat{H}_{47} = \frac{h_{1,2}h_{2,1}}{h_1^2h_2} \equiv \left[\frac{A_{1,2}A_{2,1}}{A_1^2A_2} \right] + \left[\frac{A_{2,1}}{A_1A_2R_1} \left(\frac{A_{1,2}}{A_1} + \frac{R_{1,2}}{R_1} \right) + \frac{A_{1,2}R_{2,1}}{A_1^2R_2^2} \right] y_3 + \left[\frac{A_{2,1}}{A_1A_2R_1^2} \left(\frac{A_{1,2}}{A_1} + \frac{R_{1,2}}{R_1} \right) + \frac{A_{1,2}R_{2,1}}{A_1^2R_2^2} \left(\frac{1}{R_1} + \frac{1}{R_2} \right) \right] y_3^2 \quad (A.48)$$

$$\hat{H}_{48} = \frac{h_{1,2}h_{2,1}}{h_1h_2^2} \equiv \left[\frac{A_{1,2}A_{2,1}}{A_1A_2^2} \right] + \left[\frac{A_{1,2}}{A_1A_2R_2} \left(\frac{A_{2,1}}{A_2} + \frac{R_{2,1}}{R_2} \right) + \frac{A_{2,1}R_{1,2}}{A_2^2R_1^2} \left(\frac{1}{R_1} + \frac{1}{R_2} \right) \right] y_3 + \left[\frac{A_{1,2}}{A_1A_2R_2^2} \left(\frac{A_{2,1}}{A_2} + \frac{R_{2,1}}{R_2} \right) + \frac{A_{2,1}R_{1,2}}{A_2^2R_1^2} \left(\frac{1}{R_1} + \frac{1}{R_2} \right) \right] y_3^2 \quad (A.49)$$

$$\hat{H}_{49} = \frac{h_{1,3}h_{2,1}}{h_1^2h_2} \equiv \left[\frac{A_{2,1}}{A_1A_2} \left(\frac{A_{1,3}}{A_1} - \frac{1}{R_1} \right) \right] + \left[\frac{A_{2,1}}{A_1A_2R_1} \left(\frac{A_{1,3}}{A_1} + \frac{(R_{1,3}-2)}{R_1} \right) + \frac{R_{2,1}}{A_1R_2^2} \left(\frac{A_{1,3}}{A_1} - \frac{1}{R_1} \right) \right] y_3 + \left[\frac{A_{2,1}}{A_1A_2R_1^2} \left(\frac{A_{1,3}}{A_1} - \frac{(2R_{1,3}-3)}{R_1} \right) + \frac{R_{2,1}}{A_1R_1R_2^2} \left(\frac{A_{1,3}}{A_1} - \frac{1}{R_1} \right) + \frac{R_{2,1}}{A_1R_2^3} \left(\frac{A_{1,3}}{A_1} - \frac{1}{R_1} \right) + \frac{R_{1,3}R_{2,1}}{A_1R_1^2R_2^2} \right] y_3^2 \quad (A.50)$$

$$\begin{aligned}
 \hat{H}_{50} = \frac{h_{1,2}h_{2,3}}{h_1h_2^2} \cong & \left[\frac{A_{1,2}}{A_1A_2} \left(\frac{A_{2,3}}{A_2} - \frac{1}{R_2} \right) \right] + \left[\frac{A_{1,2}}{A_1A_2R_2} \left(\frac{A_{2,3}}{A_2} \right. \right. \\
 & \left. \left. + \frac{(R_{2,3}-2)}{R_2} \right) + \frac{R_{1,2}}{A_1R_1^2} \left(\frac{A_{2,3}}{A_2} - \frac{1}{R_2} \right) \right] y_3 + \left[\frac{A_{1,2}}{A_1A_2R_2^2} \left(\frac{A_{2,3}}{A_2} \right. \right. \\
 & \left. \left. - \frac{(2R_{2,3}-3)}{R_2} \right) + \frac{R_{1,2}}{A_1R_1^2R_2} \left(\frac{A_{2,3}}{A_2} - \frac{1}{R_2} \right) + \frac{R_{1,2}}{A_2R_1^3} \left(\frac{A_{2,3}}{A_2} - \frac{1}{R_2} \right) \right. \\
 & \left. \left. + \frac{R_{1,2}R_{2,3}}{A_2R_1^2R_2^2} \right] y_3^2 \right.
 \end{aligned} \tag{A.51}$$

$$\begin{aligned}
 \hat{H}_{51} = \frac{h_{1,3}h_{2,3}}{h_2} \cong & \left[\left(A_{1,3} - \frac{A_1}{R_1} \right) \left(\frac{A_{2,3}}{A_2} - \frac{1}{R_2} \right) \right] - \left[\left(\frac{A_{1,3}}{R_1} \right. \right. \\
 & \left. \left. - \frac{A_1R_{1,3}}{R_1^2} \right) \left(\frac{A_{2,3}}{A_2} - \frac{1}{R_2} \right) - \left(A_{1,3} - \frac{A_1}{R_1} \right) \frac{(R_{2,3}-1)}{R_2^2} \right] y_3 \\
 & + \left[\frac{(A_{1,3}(R_{2,3}-1))}{R_2^2} \left(\frac{1}{R_2} - \frac{1}{R_1} \right) + \frac{(A_1(R_{2,3}-1))}{R_1R_2^2} \left(\frac{R_{1,3}}{R_1} + \frac{1}{R_2} \right) \right] y_3^2
 \end{aligned} \tag{A.52}$$

$$\begin{aligned}
 \hat{H}_{52} = \frac{h_{1,3}h_{2,3}}{h_1} \cong & \left[\left(A_{2,3} - \frac{A_2}{R_2} \right) \left(\frac{A_{1,3}}{A_1} - \frac{1}{R_1} \right) \right] - \left[\left(\frac{A_{2,3}}{R_2} \right. \right. \\
 & \left. \left. - \frac{A_2R_{2,3}}{R_2^2} \right) \left(\frac{A_{1,3}}{A_1} - \frac{1}{R_1} \right) - \left(A_{2,3} - \frac{A_2}{R_2} \right) \frac{(R_{1,3}-1)}{R_1^2} \right] y_3 \\
 & + \left[\frac{(A_{2,3}(R_{1,3}-1))}{R_1^2} \left(\frac{1}{R_1} - \frac{1}{R_2} \right) + \frac{(A_2(R_{1,3}-1))}{R_1^2R_2} \left(\frac{R_{2,3}}{R_2} + \frac{1}{R_1} \right) \right] y_3^2
 \end{aligned} \tag{A.53}$$

$$\hat{H}_{53} = \frac{h_{1,2}^2}{h_1^2 h_2^2} \cong \left[\frac{A_{1,2}^2}{A_1^2 A_2^2} \right] + \left[\frac{2A_{1,2}}{A_1 A_2^2} \left(\frac{A_{1,2}}{A_1 R_2} + \frac{R_{1,2}}{R_1^2} \right) \right] y_3 \quad (A.54)$$

$$+ \left[\frac{A_{1,2}}{A_1 A_2^2} \left(\frac{3A_{1,2}}{A_1 R_2^2} + \frac{2R_{1,2}}{R_1^2} \left(\frac{1}{R_1} + \frac{2}{R_2} \right) \right) + \frac{R_{1,2}^2}{A_2^2 R_1^4} \right] y_3^2$$

$$\hat{H}_{54} = \frac{h_{1,2}}{h_1^2 h_2} \cong \left[\frac{A_{1,2}}{A_1^2 A_2} \right] + \left[\frac{A_{1,2}}{A_1^2 A_2} \left(\frac{1}{R_1} + \frac{1}{R_2} \right) + \frac{R_{1,2}}{A_1 A_2 R_1^2} \right] y_3 \quad (A.55)$$

$$+ \left[\frac{A_{1,2}}{A_1^2 A_2} \left(\frac{1}{R_1^2} + \frac{1}{R_1 R_2} + \frac{1}{R_2^2} \right) + \frac{R_{1,2}}{A_1 A_2 R_1^2} \left(\frac{2}{R_1} + \frac{1}{R_2} \right) \right] y_3^2$$

$$\hat{H}_{55} = \frac{h_{2,1}^2}{h_1^2 h_2^2} \cong \left[\frac{A_{2,1}^2}{A_1^2 A_2^2} \right] + \left[\frac{2A_{2,1}}{A_1^2 A_2} \left(\frac{A_{2,1}}{A_2 R_1} + \frac{R_{2,1}}{R_2^2} \right) \right] y_3$$

$$+ \left[\frac{A_{2,1}}{A_1^2 A_2} \left(\frac{3A_{2,1}}{A_2 R_1^2} + \frac{2R_{2,1}}{R_2^2} \left(\frac{2}{R_1} + \frac{1}{R_2} \right) \right) + \frac{R_{2,1}^2}{A_1^2 R_4^4} \right] y_3^2$$

$$\hat{H}_{56} = \frac{h_{2,1}}{h_1 h_2^2} \cong \left[\frac{A_{2,1}}{A_1 A_2^2} \right] + \left[\frac{A_{2,1}}{A_1 A_2^2} \left(\frac{1}{R_1} + \frac{1}{R_2} \right) + \frac{R_{2,1}}{A_1 A_2 R_2^2} \right] y_3 \quad (A.56)$$

$$+ \left[\frac{A_{2,1}}{A_1 A_2^2} \left(\frac{1}{R_1^2} + \frac{1}{R_1 R_2} + \frac{1}{R_2^2} \right) + \frac{R_{2,1}}{A_1 A_2 R_2^2} \left(\frac{1}{R_1} + \frac{2}{R_2} \right) \right] y_3^2$$

$$\hat{H}_{57} = \frac{h_{1,2}}{h_1 h_2^2} \cong \left[\frac{A_{1,2}}{A_1 A_2^2} \right] + \left[\frac{A_{1,2}}{A_1 A_2^2 R_2} + \frac{R_{1,2}}{A_2^2 R_1^2} \right] y_3 \quad (A.57)$$

$$+ \left[\frac{3A_{1,2}}{A_1 A_2^2 R_2^2} + \frac{R_{1,2}}{A_2^2 R_1^2} \left(\frac{1}{R_1} + \frac{2}{R_2} \right) \right] y_3^2$$

$$\hat{H}_{58} = \frac{h_{2,1}}{h_1 h_2} \cong \left[\frac{A_{2,1}}{A_1 A_2} \right] + \left[\frac{A_{2,1}}{A_1^2 A_2 R_2} + \frac{R_{2,1}}{A_1^2 R_2^2} \right] y_3 \quad (\text{A.58})$$

$$\begin{aligned} \hat{H}_{59} = \frac{h_{1,2} h_{2,1}}{h_1^2 h_2^2} \cong & \left[\frac{A_{1,2} A_{2,1}}{A_1^2 A_2^2} \right] + \left[\frac{A_{1,2} A_{2,1}}{A_1^2 A_2^2} \left(\frac{1}{R_1} + \frac{1}{R_2} \right) \right. \\ & + \frac{A_{1,2} R_{2,1}}{A_1^2 A_2 R_2^2} + \frac{A_{2,1} R_{1,2}}{A_1 A_2^2 R_1^2} \left. \right] y_3 + \left[\frac{A_{1,2} A_{2,1}}{A_1^2 A_2^2} \left(\frac{1}{R_1^2} + \frac{1}{R_1 R_2} + \frac{1}{R_2^2} \right) \right. \\ & + \frac{A_{1,2} R_{2,1}}{A_1 A_2^2 R_1^2} \left(\frac{1}{R_1} + \frac{2}{R_2} \right) + \frac{A_{2,1} R_{1,2}}{A_1 A_2^2 R_1^2} \left(\frac{2}{R_1} + \frac{1}{R_2} \right) + \frac{R_{1,2} R_{2,1}}{A_1 A_2 R_1^2 R_2^2} \left. \right] y_3^2 \end{aligned} \quad (\text{A.59})$$

$$\begin{aligned} \hat{H}_{60} = \frac{h_{1,3} h_{2,3}}{h_1 h_2} \cong & \left[A_{1,3} A_{2,3} - \frac{A_{1,3}}{A_1 R_2} - \frac{A_{2,3}}{A_2 R_1} + \frac{1}{R_1 R_2} \right] \\ & + \left[\left(\frac{(R_{2,3} - 1)}{R_2^2} \right) \left(\frac{A_{1,3}}{A_1} - \frac{1}{R_1} \right) + \left(\frac{(R_{1,3} - 1)}{R_1^2} \right) \left(\frac{A_{2,3}}{A_2} - \frac{1}{R_2} \right) \right] y_3 \\ & + \left[\left(\frac{(R_{2,3} - 1)}{R_2^3} \right) \left(\frac{A_{1,3}}{A_1} - \frac{1}{R_1} \right) + \left(\frac{(R_{1,3} - 1)}{R_1^3} \right) \left(\frac{A_{2,3}}{A_2} - \frac{1}{R_2} \right) \right. \\ & + \left. \frac{(R_{1,2} R_{2,1} - R_{1,3} - R_{2,3} + 1)}{R_1^2 R_2^2} \right] y_3^2 \end{aligned} \quad (\text{A.60})$$

If the standard assumption of no warping through the thickness for shell theory is applied, then $A_{1,3}$, $A_{2,3}$, $R_{1,3}$, and $R_{2,3}$ are all zero. Thus, the 60 independent \hat{H}_i functions reduce to:

$$\hat{H}_1 = \frac{h_{1,2}}{h_1} \cong \left[\frac{A_{1,2}}{A_1} \right] + \left[\frac{R_{1,2}}{R_1^2} \right] y_3 + \left[\frac{R_{1,2}}{R_1^3} \right] y_3^2 \quad (\text{A.61})$$

$$\hat{H}_2 = \frac{h_{1,3}}{h_1} \cong \left[-\left(\frac{1}{R_1} \right) \right] + \left[-\left(\frac{1}{R_1^2} \right) \right] y_3 + \left[-\left(\frac{1}{R_1^3} \right) \right] y_3^2 \quad (\text{A.62})$$

$$\hat{H}_3 = \frac{1}{h_1^2} \cong \left[\frac{1}{A_1^2} \right] + \left[\frac{2}{A_1^2 R_1} \right] y_3 + \left[\frac{3}{A_1^2 R_1^2} \right] y_3^2 \quad (\text{A.63})$$

$$\begin{aligned} \hat{H}_4 = \frac{h_{1,2}^2}{h_1^2} &\cong \left[\frac{A_{1,2}^2}{A_1^2} \right] + \left[\frac{2A_{1,2}R_{1,2}}{A_1 R_1^2} \right] y_3 \\ &+ \left[\frac{R_{1,2}}{R_1^3} \left(\frac{2A_{1,2}}{A_1} + \frac{R_{1,2}}{R_1} \right) \right] y_3^2 \end{aligned} \quad (\text{A.64})$$

$$\begin{aligned} \hat{H}_5 = \frac{h_{1,2}^2}{h_2^2} &\cong \left[\frac{A_{1,2}^2}{A_2^2} \right] + \left[\frac{2A_{1,2}}{A_2^2} \left(A_{1,2} \left(\frac{1}{R_2} - \frac{1}{R_1} \right) + \frac{A_1 R_{1,2}}{R_1^2} \right) \right] y_3 \\ &+ \left[\frac{A_{1,2}^2}{A_2^2} \left(\frac{1}{R_1} - \frac{3}{R_2} \right)^2 + \frac{A_1 R_{1,2}}{A_2^2 R_1^2} \left(2A_{1,2} \left(\frac{2}{R_2} - \frac{1}{R_1} \right) + \frac{A_1 R_{1,2}}{R_1^2} \right) \right] y_3^2 \end{aligned} \quad (\text{A.65})$$

$$\hat{H}_6 = \frac{h_{1,3}^2}{h_1^2} \cong \left[\frac{1}{R_1^2} \right] + \left[\frac{2}{R_1^3} \right] y_3 + \left[\frac{3}{R_1^4} \right] y_3^2 \quad (\text{A.66})$$

$$\hat{H}_7 = h_{1,3}^2 \cong \left[\frac{1}{R_1^2} \right] \quad (\text{A.67})$$

$$\begin{aligned} \hat{H}_8 = \frac{h_{1,2}h_{1,3}}{h_1^2} \cong & \left[-\left(\frac{A_{1,2}}{A_1 R_1} \right) \right] + \left[-\left(\frac{A_{1,2}}{A_1 R_1^2} + \frac{R_{1,2}}{R_1^3} \right) \right] y_3 \\ & + \left[-\left(\frac{A_{1,2}}{A_1 R_1^3} + \frac{2R_{1,2}}{R_1^4} \right) \right] y_3^2 \end{aligned} \quad (\text{A.68})$$

$$\hat{H}_9 = \frac{h_{2,3}}{h_2} \cong \left[-\left(\frac{1}{R_2} \right) \right] + \left[-\left(\frac{1}{R_2^2} \right) \right] y_3 + \left[-\left(\frac{1}{R_2^3} \right) \right] y_3^2 \quad (\text{A.69})$$

$$\hat{H}_{10} = \frac{h_{2,1}}{h_2} \cong \left[\frac{A_{2,1}}{A_2} \right] + \left[\frac{R_{2,1}}{R_2^2} \right] y_3 + \left[\frac{R_{2,1}}{R_2^3} \right] y_3^2 \quad (\text{A.70})$$

$$\hat{H}_{11} = \frac{1}{h_2^2} \cong \left[\frac{1}{A_2^2} \right] + \left[\frac{2}{A_2^2 R_2} \right] y_3 + \left[\frac{3}{A_2^2 R_2^2} \right] y_3^2 \quad (\text{A.71})$$

$$\begin{aligned} \hat{H}_{12} = \frac{h_{2,1}^2}{h_2^2} \cong & \left[\frac{A_{2,1}^2}{A_2^2} \right] + \left[\frac{2A_{2,1}R_{2,1}}{A_2^2 R_2^2} \right] y_3 \\ & + \left[\frac{R_{2,1}^2}{R_1^3} \left(\frac{2A_{2,1}}{A_2} + \frac{R_{2,1}}{R_2} \right) \right] y_3^2 \end{aligned} \quad (\text{A.72})$$

$$\hat{H}_{13} = \frac{h_{2,1}^2}{h_1^2} \equiv \left[\frac{A_{2,1}^2}{A_1^2} \right] + \left[\frac{2A_{2,1}}{A_1^2} \left(A_{2,1} \left(\frac{1}{R_1} - \frac{1}{R_2} \right) + \frac{A_2 R_{2,1}}{R_2^2} \right) \right] y_3 \quad (A.73)$$

$$+ \left[\frac{A_{2,1}^2}{A_1^2} \left(\frac{1}{R_2} - \frac{3}{R_1} \right)^2 + \frac{A_2 R_{2,1}}{A_1^2 R_2^2} \left(2A_{2,1} \left(\frac{2}{R_1} - \frac{1}{R_2} \right) + \frac{A_2 R_{2,1}}{R_2^2} \right) \right] y_3^2$$

$$\hat{H}_{14} = \frac{h_{2,3}^2}{h_2^2} \equiv \left[\frac{1}{R_2^2} \right] + \left[\frac{2}{R_2^3} \right] y_3 + \left[\frac{3}{R_2^3} \right] y_3^2 \quad (A.74)$$

$$\hat{H}_{15} = h_{2,3}^2 \equiv \left[\frac{1}{R_2^2} \right] \quad (A.75)$$

$$\hat{H}_{16} = \frac{h_{2,1} h_{2,3}}{h_2^2} \equiv \left[- \left(\frac{A_{2,1}}{A_2 R_2} \right) \right] + \left[- \left(\frac{A_{2,1}}{A_2 R_2^2} + \frac{R_{2,1}}{R_2^3} \right) \right] y_3 \quad (A.76)$$

$$+ \left[- \left(\frac{A_{2,1}}{A_2 R_2^3} + \frac{R_{2,1}}{R_2^4} \right) \right] y_3^2$$

$$\hat{H}_{17} = \frac{1}{h_2} \equiv \left[\frac{1}{A_2} \right] + \left[\frac{1}{A_2 R_2} \right] y_3 + \left[\frac{1}{A_1 R_1^2} \right] y_3^2 \quad (A.77)$$

$$\hat{H}_{18} = \frac{1}{h_1} \equiv \left[\frac{1}{A_1} \right] + \left[\frac{1}{A_1 R_1} \right] y_3 + \left[\frac{1}{A_1 R_1^2} \right] y_3^2 \quad (A.78)$$

$$\hat{H}_{19} = \frac{h_{2,1}}{h_1} \equiv \left[\frac{A_{2,1}}{A_1} \right] + \left[\frac{A_{2,1}}{A_1} \left(\frac{1}{R_1} - \frac{1}{R_2} \right) + \frac{A_2 R_{2,1}}{A_1 R_2^2} \right] y_3 \quad (\text{A.79})$$

$$+ \left[\frac{A_{2,1}}{A_1 R_1} \left(\frac{1}{R_1} - \frac{1}{R_2} \right) + \frac{A_2 R_{2,1}}{A_1 R_1 R_2^2} \right] y_3^2$$

$$\hat{H}_{20} = \frac{h_{1,2}}{h_2} \equiv \left[\frac{A_{1,2}}{A_2} \right] + \left[\frac{A_{1,2}}{A_2} \left(\frac{1}{R_2} - \frac{1}{R_1} \right) + \frac{A_1 R_{1,2}}{A_2 R_1^2} \right] y_3 \quad (\text{A.80})$$

$$+ \left[\frac{A_{1,2}}{A_2 R_2} \left(\frac{1}{R_2} - \frac{1}{R_1} \right) + \frac{A_1 R_{1,2}}{A_2 R_1^2 R_2} \right] y_3^2$$

$$\hat{H}_{21} = \frac{1}{h_1 h_2} \equiv \left[\frac{1}{A_1 A_2} \right] + \left[\frac{R_1 + R_2}{A_1 A_2 R_1 R_2} \right] y_3 + \left[\frac{R_1^2 + R_1 R_2 + R_2^2}{A_1 A_2 R_1^2 R_2^2} \right] y_3^2 \quad (\text{A.81})$$

$$\hat{H}_{22} = \frac{h_{1,3}}{h_2} \equiv \left[-\left(\frac{A_1}{A_2 R_1} \right) \right] + \left[-\left(\frac{A_1}{A_2 R_1 R_2} \right) \right] y_3 + \left[-\left(\frac{A_1}{A_2 R_1 R_2^2} \right) \right] y_3^2 \quad (\text{A.82})$$

$$\hat{H}_{23} = \frac{h_{2,3}}{h_1} \equiv \left[-\left(\frac{A_2}{A_1 R_2} \right) \right] + \left[-\left(\frac{A_2}{A_1 R_1 R_2} \right) \right] y_3 + \left[-\left(\frac{A_2}{A_1 R_1^2 R_2} \right) \right] y_3^2 \quad (\text{A.83})$$

$$\hat{H}_{24} = \frac{h_{1,2} h_{1,2}}{h_1^2} \equiv \left[\frac{A_{1,2} A_{1,2}}{A_1^2} \right] + \left[\frac{A_{1,2} A_{2,1}}{A_1^2} \left(\frac{1}{R_1} - \frac{1}{R_2} \right) \right] \quad (\text{A.84})$$

$$+ \frac{A_{2,1} R_{1,2}}{A_1 R_1^2} + \frac{A_2 A_{1,2} R_{2,1}}{A_1^2 R_2^2} \left] y_3 + \left[\frac{A_{1,2} A_{2,1}}{A_1^2 R_1} \left(\frac{1}{R_1} - \frac{1}{R_2} \right) \right. \right. \\ \left. \left. + \frac{A_{2,1} R_{1,2}}{A_1 R_1^2} \left(\frac{2}{R_1} - \frac{1}{R_2} \right) + \frac{A_2 A_{1,2} R_{2,1}}{A_1^2 R_1 R_2^2} \left(\frac{A_{1,2}}{A_1} + \frac{R_{1,2}}{R_1} \right) \right] y_3^2$$

$$\begin{aligned}\hat{H}_{25} = \frac{h_{1,2}h_{2,1}}{h_2^2} \cong & \left[\frac{A_{1,2}A_{1,2}}{A_2^2} \right] + \left[\frac{A_{1,2}A_{2,1}}{A_2^2} \left(\frac{1}{R_2} - \frac{1}{R_1} \right) \right. \\ & + \frac{A_{1,2}R_{2,1}}{A_2R_2^2} + \frac{A_1A_{2,1}R_{1,2}}{A_2^2R_1^2} \left. \right] y_3 + \left[\frac{A_{1,2}A_{2,1}}{A_2^2R_2} \left(\frac{1}{R_2} - \frac{1}{R_1} \right) \right. \\ & + \frac{A_{1,2}R_{2,1}}{A_2R_2^2} \left(\frac{2}{R_2} - \frac{1}{R_1} \right) + \frac{A_1A_{2,1}R_{1,2}}{A_2^2R_1^2R_2} \left(\frac{A_{2,1}}{A_2} + \frac{R_{2,1}}{R_2} \right) \left. \right] y_3^2\end{aligned}\quad (A.85)$$

$$\hat{H}_{26} = h_{1,3}h_{2,3} \cong \left[\frac{A_1A_2}{R_1R_2} \right] \quad (A.86)$$

$$\begin{aligned}\hat{H}_{27} = \frac{h_{1,3}h_{2,1}}{h_1^2} \cong & \left[-\left(\frac{A_{2,1}}{A_1R_1} \right) \right] + \left[\frac{A_{2,1}}{A_1R_1} \left(\frac{1}{R_2} - \frac{2}{R_1} \right) \right. \\ & - \frac{A_2R_{2,1}}{A_1R_1R_2^2} \left. \right] y_3 + \left[\frac{A_{2,1}}{A_1R_1^2} \left(\frac{2}{R_2} - \frac{3}{R_1} \right) - \frac{2A_2R_{2,1}}{A_1R_1^2R_2^2} \right] y_3^2\end{aligned}\quad (A.87)$$

$$\begin{aligned}\hat{H}_{28} = \frac{h_{1,2}h_{2,3}}{h_2^2} \cong & \left[-\left(\frac{A_{1,2}}{A_2R_2} \right) \right] + \left[\frac{A_{1,2}}{A_2R_2} \left(\frac{1}{R_1} - \frac{2}{R_2} \right) \right. \\ & - \frac{A_1R_{1,2}}{A_2R_1^2R_2} \left. \right] y_3 + \left[\frac{A_{1,2}}{A_2R_2^2} \left(\frac{2}{R_1} - \frac{3}{R_2} \right) - \frac{2A_1R_{1,2}}{A_2R_1^2R_2^2} \right] y_3^2\end{aligned}\quad (A.88)$$

$$\begin{aligned}\hat{H}_{29} = \frac{h_{1,2}}{h_1h_2} \cong & \left[\frac{A_{1,2}}{A_1A_2} \right] + \left[\frac{1}{A_2} \left(\frac{A_{1,2}}{A_1R_2} + \frac{R_{1,2}}{R_1^2} \right) \right] y_3 \\ & + \left[\frac{1}{A_2} \left(\frac{A_{1,2}}{A_1R_2} + \frac{R_{1,2}}{R_1^2} \left(\frac{1}{R_1} + \frac{1}{R_2} \right) \right) \right] y_3^2\end{aligned}\quad (A.89)$$

$$\hat{H}_{30} = \frac{h_{1,2}^2}{h_1^2 h_2} \cong \left[\frac{A_{1,2}^2}{A_1^2 A_2} \right] + \left[\frac{A_{1,2}}{A_1 A_2} \left(\frac{A_{1,2}}{A_1 R_2} + \frac{2R_{1,2}}{R_1^2} \right) \right] y_3 \quad (\text{A.90})$$

$$+ \left[\frac{A_{1,2}}{A_1 A_2} \left(\frac{A_{1,2}}{A_1 R_2^2} + \frac{2R_{1,2}}{R_1^2} \left(\frac{1}{R_1} + \frac{1}{R_2} \right) \right) + \frac{R_{1,2}^2}{A_2 R_1^4} \right] y_3^2$$

$$\hat{H}_{31} = \frac{h_{1,2}^2}{h_1 h_2^2} \cong \left[\frac{A_{1,2}^2}{A_1 A_2^2} \right] + \left[\frac{A_{1,2}}{A_2^2} \left(\frac{A_{1,2}}{A_1} \left(\frac{2}{R_2} - \frac{1}{R_1} \right) + \frac{2R_{1,2}}{R_1^2} \right) \right] y_3 \quad (\text{A.91})$$

$$+ \left[\frac{A_{1,2}}{A_2^2} \left(\frac{A_{1,2}}{A_1 R_2} \left(\frac{3}{R_2} - \frac{2}{R_1} \right) + \frac{4R_{1,2}}{R_1^2 R_2} \right) + \frac{A_1 R_{1,2}^2}{A_2^2 R_1^4} \right] y_3^2$$

$$\hat{H}_{32} = \frac{h_{1,3}^2}{h_1} \cong \left[\frac{A_1}{R_1^2} \right] + \left[\frac{A_1}{R_1^3} \right] y_3 + \left[\frac{A_1}{R_1^4} \right] y_3^2 \quad (\text{A.92})$$

$$\hat{H}_{33} = \frac{h_{1,2}}{h_1^2} \cong \left[\frac{A_{1,2}}{A_1^2} \right] + \left[\frac{1}{A_1 R_1} \left(\frac{A_{1,2}}{A_1} + \frac{R_{1,2}}{R_1} \right) \right] y_3 \quad (\text{A.93})$$

$$+ \left[\frac{1}{A_1 R_1^2} \left(\frac{A_{1,2}}{A_1} + \frac{2R_{1,2}}{R_1} \right) \right] y_3^2$$

$$\hat{H}_{34} = \frac{h_{1,3}}{h_1^2} \cong \left[-\left(\frac{1}{A_1 R_1} \right) \right] + \left[-\left(\frac{2}{A_1 R_1^2} \right) \right] y_3 + \left[-\left(\frac{3}{A_1 R_1^3} \right) \right] y_3^2 \quad (\text{A.94})$$

$$\begin{aligned}\hat{H}_{35} = \frac{h_{1,2}h_{1,3}}{h_1^2h_2} \cong & \left[-\left(\frac{A_{1,2}}{A_1A_2R_1} \right) \right] - \left[\frac{A_{1,2}}{A_1A_2R_1} \left(\frac{1}{R_1} + \frac{1}{R_2} \right) \right. \\ & \left. + \frac{R_{1,2}}{A_1R_1^3} \right] y_3 - \left[\frac{A_{1,2}}{A_1A_2R_1R_2} \left(\frac{1}{R_1} + \frac{1}{R_2} \right) + \frac{R_{1,2}}{A_2R_1^3} \left(\frac{1}{R_1} + \frac{1}{R_2} \right) \right] y_3^2\end{aligned}\quad (A.95)$$

$$\begin{aligned}\hat{H}_{36} = \frac{h_{2,1}}{h_1h_2} \cong & \left[\frac{A_{1,2}}{A_1A_2} \right] + \left[\frac{1}{A_1} \left(\frac{A_{2,1}}{A_2R_1} + \frac{R_{2,1}}{R_2^2} \right) \right] y_3 \\ & + \left[\frac{1}{A_1} \left(\frac{A_{2,1}}{A_2R_1} + \frac{R_{2,1}}{R_2^2} \left(\frac{1}{R_1} + \frac{1}{R_2} \right) \right) \right] y_3^2\end{aligned}\quad (A.96)$$

$$\begin{aligned}\hat{H}_{37} = \frac{h_{2,1}^2}{h_1h_2^2} \cong & \left[\frac{A_{2,1}^2}{A_1A_2^2} \right] + \left[\frac{A_{2,1}}{A_1A_2} \left(\frac{A_{2,1}}{A_2R_1} + \frac{2R_{2,1}}{R_2^2} \right) \right] y_3 \\ & + \left[\frac{A_{2,1}}{A_1A_2} \left(\frac{A_{2,1}}{A_2R_1^2} + \frac{2R_{2,1}}{R_2^2} \left(\frac{1}{R_1} + \frac{1}{R_2} \right) \right) + \frac{R_{2,1}^2}{A_1R_2^4} \right] y_3^2\end{aligned}\quad (A.97)$$

$$\begin{aligned}\hat{H}_{38} = \frac{h_{2,1}^2}{h_1^2h_2} \cong & \left[\frac{A_{2,1}^2}{A_1^2A_2} \right] + \left[\frac{A_{2,1}}{A_1^2} \left(\frac{A_{2,1}}{A_2} \left(\frac{2}{R_1} - \frac{1}{R_2} \right) + \frac{2R_{2,1}}{R_2^2} \right) \right] y_3 \\ & + \left[\frac{A_{2,1}}{A_1^2} \left(\frac{A_{2,1}}{A_2R_1} \left(\frac{3}{R_1} - \frac{2}{R_2} \right) + \frac{4R_{2,1}}{R_1R_2^2} \right) + \frac{A_2R_{2,1}^2}{A_1^2R_2^4} \right] y_3^2\end{aligned}\quad (A.98)$$

$$\hat{H}_{39} = \frac{h_{2,3}^2}{h_1} \cong \left[\frac{A_2}{R_2^2} \right] + \left[\frac{A_2}{R_2^3} \right] y_3 + \left[\frac{A_2}{R_2^4} \right] y_3^2\quad (A.99)$$

$$\begin{aligned}\hat{H}_{40} = \frac{h_{2,1}}{h_2^2} &\cong \left[\frac{A_{2,1}}{A_2^2} \right] + \left[\frac{1}{A_2 R_2} \left(\frac{A_{2,1}}{A_2} + \frac{R_{2,1}}{R_2} \right) \right] y_3 \\ &+ \left[\frac{1}{A_2 R_2^2} \left(\frac{A_{2,1}}{A_2} + \frac{2R_{2,1}}{R_1} \right) \right] y_3^2\end{aligned}\quad (\text{A.100})$$

$$\begin{aligned}\hat{H}_{41} = \frac{h_{2,1}h_{2,3}}{h_1 h_2^2} &\cong \left[-\left(\frac{A_{2,1}}{A_1 A_2 R_2} \right) \right] - \left[\frac{A_{2,1}}{A_1 A_2 R_2} \left(\frac{1}{R_1} + \frac{1}{R_2} \right) \right. \\ &+ \left. \frac{R_{2,1}}{A_1 R_2^3} \right] y_3 - \left[\frac{A_{2,1}}{A_1 A_2 R_1 R_2} \left(\frac{1}{R_1} + \frac{1}{R_2} \right) + \frac{R_{1,2}}{A_2 R_2^3} \left(\frac{1}{R_1} + \frac{1}{R_2} \right) \right] y_3^2\end{aligned}\quad (\text{A.101})$$

$$\hat{H}_{42} = \frac{h_{2,3}}{h_2^2} \cong \left[-\left(\frac{1}{A_2 R_2} \right) \right] + \left[-\left(\frac{2}{A_2 R_2^2} \right) \right] y_3 + \left[-\left(\frac{3}{A_2 R_2^3} \right) \right] y_3^2\quad (\text{A.102})$$

$$\begin{aligned}\hat{H}_{43} = \frac{h_{1,2}}{h_2^2} &\cong \left[\frac{A_{1,2}}{A_2^2} \right] + \left[\frac{1}{A_2^2} \left(A_{1,2} \left(\frac{2}{R_2} - \frac{1}{R_1} \right) + \frac{A_1 R_{1,2}}{R_1^2} \right) \right] y_3 \\ &+ \left[\frac{1}{A_2^2 R_2} \left(A_{1,2} \left(\frac{3}{R_2} - \frac{2}{R_1} \right) + \frac{2A_1 R_{1,2}}{R_1^2} \right) \right] y_3^2\end{aligned}\quad (\text{A.103})$$

$$\begin{aligned}\hat{H}_{44} = \frac{h_{2,1}}{h_1^2} &\cong \left[\frac{A_{2,1}}{A_1^2} \right] + \left[\frac{1}{A_1^2} \left(A_{2,1} \left(\frac{2}{R_1} - \frac{1}{R_2} \right) + \frac{A_2 R_{2,1}}{R_2^2} \right) \right] y_3 \\ &+ \left[\frac{1}{A_1^2 R_1} \left(A_{2,1} \left(\frac{3}{R_1} - \frac{2}{R_2} \right) + \frac{2A_2 R_{2,1}}{R_2^2} \right) \right] y_3^2\end{aligned}\quad (\text{A.104})$$

$$\begin{aligned}
 \hat{H}_{45} = \frac{h_{1,3}}{h_1 h_2} &\equiv \left[-\left(\frac{1}{A_2 R_1} \right) \right] - \left[\frac{1}{A_2 R_1 R_2} + \frac{1}{A_2 R_1^2} \right] y_3 \\
 &- \left[\frac{1}{A_2 R_1 R_2^2} + \frac{1}{A_2 R_1^2} \left(\frac{1}{R_1} + \frac{1}{R_2} \right) \right] y_3^2 \\
 \hat{H}_{46} = \frac{h_{2,3}}{h_1 h_2} &\equiv \left[-\left(\frac{1}{A_1 R_2} \right) \right] - \left[\frac{1}{A_1 R_1 R_2} + \frac{1}{A_1 R_2^2} \right] y_3 \\
 &- \left[\frac{1}{A_1 R_1 R_2^2} + \frac{1}{A_1 R_2^2} \left(\frac{1}{R_1} + \frac{1}{R_2} \right) \right] y_3^2
 \end{aligned} \tag{A.105}$$

$$\begin{aligned}
 \hat{H}_{47} = \frac{h_{1,2} h_{2,1}}{h_1^2 h_2} &\equiv \left[\frac{A_{1,2} A_{2,1}}{A_1^2 A_2} \right] + \left[\frac{A_{2,1}}{A_1 A_2 R_1} \left(\frac{A_{1,2}}{A_1} + \frac{R_{1,2}}{R_1} \right) \right. \\
 &+ \left. \frac{A_{1,2} R_{2,1}}{A_1^2 R_2^2} \right] y_3 + \left[\frac{A_{2,1}}{A_1 A_2 R_1^2} \left(\frac{A_{1,2}}{A_1} + \frac{R_{1,2}}{R_1} \right) \right. \\
 &+ \left. \frac{A_{1,2} R_{2,1}}{A_1^2 R_2^2} \left(\frac{1}{R_1} + \frac{1}{R_2} \right) \right] y_3^2
 \end{aligned} \tag{A.106}$$

$$\begin{aligned}
 \hat{H}_{48} = \frac{h_{1,2} h_{2,1}}{h_1 h_2^2} &\equiv \left[\frac{A_{1,2} A_{2,1}}{A_1 A_2^2} \right] + \left[\frac{A_{1,2}}{A_1 A_2 R_2} \left(\frac{A_{2,1}}{A_2} + \frac{R_{2,1}}{R_2} \right) \right. \\
 &+ \left. \frac{A_{2,1} R_{1,2}}{A_2^2 R_1^2} \right] y_3 + \left[\frac{A_{1,2}}{A_1 A_2 R_2^2} \left(\frac{A_{2,1}}{A_2} + \frac{R_{2,1}}{R_2} \right) \right. \\
 &+ \left. \frac{A_{2,1} R_{1,2}}{A_2^2 R_1^2} \left(\frac{1}{R_1} + \frac{1}{R_2} \right) \right] y_3^2
 \end{aligned} \tag{A.107}$$

$$\begin{aligned}\hat{H}_{49} = \frac{h_{1,3}h_{2,1}}{h_1^2h_2} &\cong \left[-\left(\frac{A_{2,1}}{A_1A_2R_1} \right) \right] - \left[\frac{2A_{2,1}}{A_1A_2R_1^2} + \frac{R_{2,1}}{A_1R_1R_2^2} \right] y_3 \\ &- \left[\frac{3A_{2,1}}{A_1A_2R_1^3} + \frac{R_{2,1}}{A_1R_1^2R_2^2} + \frac{R_{2,1}}{A_1R_1R_2^3} \right] y_3^2\end{aligned}\quad (\text{A.108})$$

$$\begin{aligned}\hat{H}_{50} = \frac{h_{1,2}h_{2,3}}{h_1h_2^2} &\cong \left[-\left(\frac{A_{1,2}}{A_1A_2R_2} \right) \right] - \left[\frac{2A_{1,2}}{A_1A_2R_2^2} + \frac{R_{1,2}}{A_1R_1^2R_2} \right] y_3 \\ &- \left[\frac{3A_{1,2}}{A_1A_2R_2^3} + \frac{R_{1,2}}{A_1R_1^2R_2^2} + \frac{R_{1,2}}{A_2R_1^3R_2} \right] y_3^2\end{aligned}\quad (\text{A.109})$$

$$\hat{H}_{51} = \frac{h_{1,3}h_{2,3}}{h_2} \cong \left[\frac{A_1}{R_1R_2} \right] + \left[\frac{A_1}{R_1R_2^2} \right] y_3 + \left[\frac{A_1}{R_1R_2^3} \right] y_3^2\quad (\text{A.110})$$

$$\hat{H}_{52} = \frac{h_{1,3}h_{2,3}}{h_1} \cong \left[\frac{A_2}{R_1R_2} \right] + \left[\frac{A_2}{R_1^2R_2} \right] y_3 + \left[\frac{A_2}{R_1^3R_2} \right] y_3^2\quad (\text{A.111})$$

$$\begin{aligned}\hat{H}_{53} = \frac{h_{1,2}^2}{h_1^2h_2} &\cong \left[\frac{A_{1,2}^2}{A_1^2A_2^2} \right] + \left[\frac{2A_{1,2}}{A_1A_2^2} \left(\frac{A_{1,2}}{A_1R_2} + \frac{R_{1,2}}{R_1^2} \right) \right] y_3 \\ &+ \left[\frac{A_{1,2}}{A_1A_2^2} \left(\frac{3A_{1,2}}{A_1R_2^2} + \frac{2R_{1,2}}{R_1^2} \left(\frac{1}{R_1} + \frac{2}{R_2} \right) \right) + \frac{R_{1,2}^2}{A_2^2R_1^4} \right] y_3^2\end{aligned}\quad (\text{A.112})$$

$$\begin{aligned}\hat{H}_{54} = \frac{h_{1,2}}{h_1 h_2} &\equiv \left[\frac{A_{1,2}}{A_1^2 A_2} \right] + \left[\frac{A_{1,2}}{A_1^2 A_2} \left(\frac{1}{R_1} + \frac{1}{R_2} \right) + \frac{R_{1,2}}{A_1 A_2 R_1^2} \right] y_3 \\ &+ \left[\frac{A_{1,2}}{A_1^2 A_2} \left(\frac{1}{R_1^2} + \frac{1}{R_1 R_2} + \frac{1}{R_2^2} \right) + \frac{R_{1,2}}{A_1 A_2 R_1^2} \left(\frac{2}{R_1} + \frac{1}{R_2} \right) \right] y_3^2\end{aligned}\quad (A.113)$$

$$\begin{aligned}\hat{H}_{55} = \frac{h_{2,1}^2}{h_1 h_2} &\equiv \left[\frac{A_{2,1}^2}{A_1^2 A_2} \right] + \left[\frac{2A_{2,1}}{A_1^2 A_2} \left(\frac{A_{2,1}}{A_2 R_1} + \frac{R_{2,1}}{R_2^2} \right) \right] y_3 \\ &+ \left[\frac{A_{2,1}}{A_1^2 A_2} \left(\frac{3A_{2,1}}{A_2 R_1^2} + \frac{2R_{2,1}}{R_2^2} \left(\frac{2}{R_1} + \frac{1}{R_2} \right) \right) + \frac{R_{2,1}^2}{A_1^2 R_4^4} \right] y_3^2\end{aligned}$$

$$\begin{aligned}\hat{H}_{56} = \frac{h_{2,1}}{h_1 h_2} &\equiv \left[\frac{A_{2,1}}{A_1 A_2^2} \right] + \left[\frac{A_{2,1}}{A_1 A_2^2} \left(\frac{1}{R_1} + \frac{1}{R_2} \right) + \frac{R_{2,1}}{A_1 A_2 R_2^2} \right] y_3 \\ &+ \left[\frac{A_{2,1}}{A_1 A_2^2} \left(\frac{1}{R_1^2} + \frac{1}{R_1 R_2} + \frac{1}{R_2^2} \right) + \frac{R_{2,1}}{A_1 A_2 R_2^2} \left(\frac{1}{R_1} + \frac{2}{R_2} \right) \right] y_3^2\end{aligned}\quad (A.114)$$

$$\begin{aligned}\hat{H}_{57} = \frac{h_{1,2}}{h_1 h_2} &\equiv \left[\frac{A_{1,2}}{A_1 A_2^2} \right] + \left[\frac{A_{1,2}}{A_1 A_2^2 R_2} + \frac{R_{1,2}}{A_2^2 R_1^2} \right] y_3 \\ &+ \left[\frac{3A_{1,2}}{A_1 A_2^2 R_2^2} + \frac{R_{1,2}}{A_2^2 R_1^2} \left(\frac{1}{R_1} + \frac{2}{R_2} \right) \right] y_3^2\end{aligned}\quad (A.115)$$

$$\begin{aligned}\hat{H}_{58} = \frac{h_{2,1}}{h_1 h_2} &\equiv \left[\frac{A_{2,1}}{A_1^2 A_2} \right] + \left[\frac{A_{2,1}}{A_1^2 A_2 R_2} + \frac{R_{2,1}}{A_1^2 R_2^2} \right] y_3 \\ &+ \left[\frac{3A_{2,1}}{A_1^2 A_2 R_1^2} + \frac{R_{2,1}}{A_1^2 R_2^2} \left(\frac{2}{R_1} + \frac{1}{R_2} \right) \right] y_3^2\end{aligned}\quad (A.116)$$

$$\begin{aligned}
 \hat{H}_{59} = \frac{h_{1,2}h_{2,1}}{h_1^2 h_2^2} \cong & \left[\frac{A_{1,2}A_{2,1}}{A_1^2 A_2^2} \right] + \left[\frac{A_{1,2}A_{2,1}}{A_1^2 A_2^2} \left(\frac{1}{R_1} + \frac{1}{R_2} \right) \right. \\
 & + \frac{A_{1,2}R_{2,1}}{A_1^2 A_2 R_2^2} + \frac{A_{2,1}R_{1,2}}{A_1 A_2^2 R_1^2} \left. \right] y_3 + \left[\frac{A_{1,2}A_{2,1}}{A_1^2 A_2^2} \left(\frac{1}{R_1^2} + \frac{1}{R_1 R_2} + \frac{1}{R_2^2} \right) \right. \\
 & + \frac{A_{1,2}R_{2,1}}{A_1 A_2^2 R_1^2} \left(\frac{1}{R_1} + \frac{2}{R_2} \right) + \frac{A_{2,1}R_{1,2}}{A_1 A_2^2 R_1^2} \left(\frac{2}{R_1} + \frac{1}{R_2} \right) \\
 & \left. + \frac{R_{1,2}R_{2,1}}{A_1 A_2 R_1^2 R_2^2} \right] y_3^2
 \end{aligned} \tag{A.117}$$

$$\begin{aligned}
 \hat{H}_{60} = \frac{h_{1,3}h_{2,3}}{h_1 h_2} \cong & \left[\frac{1}{R_1 R_2} \right] + \left[\frac{1}{R_1 R_2} \left(\frac{1}{R_1} + \frac{1}{R_2} \right) \right] y_3 \\
 & + \left[\frac{1}{R_1 R_2} \left(\frac{1}{R_1^2} + \frac{1}{R_2^2} \right) + \frac{(R_{1,2}R_{2,1} + 1)}{R_1^2 R_2^2} \right] y_3^2
 \end{aligned} \tag{A.118}$$

This Page Intentionally Left Blank

Appendix B. Strain-Displacement Relations for a General Spherical Shell Elemental Code

The strain-displacement relations of this appendix are for the case of a spherical shell with a radius of $R_1 = R_2 = R$. The y_1 coordinate is the circumferential distance $dy_1 = R_1 d\theta_1 = R d\theta$ and the y_2 coordinate is the circumferential distance $dy_2 = R_2 d\theta_2 = R d\theta$. The kinematic displacements within the shell are assumed to be of the form

$$\vec{U} = u_1 \vec{e}_1 + u_2 \vec{e}_2 + u_3 \vec{e}_3, \quad (\text{B.1})$$

where

$$\begin{aligned} u_1(y_1, y_2, y_3) &= u(1 - Dy_3) + \psi_1 y_3 + k(w_{,1} + \psi_1) y_3^3 \\ u_2(y_1, y_2, y_3) &= v(1 - Cy_3) + \psi_2 y_3 + k(w_{,2} + \psi_2) y_3^3 \\ u_3(y_1, y_2) &= w \end{aligned} \quad (\text{B.2})$$

The seven degrees of freedom $u, v, w, w_{,1}, w_{,2}, \psi_1$, and ψ_2 are functions of midsurface coordinates (y_1, y_2) only. The y_i are rotations about the normal and $D = 1/R_1 = 1/R$, $C = 1/R_2 = 1/R$, and $k = -4/(3h^2)$. The full in-plane nonlinear spherical shell strain-displacement relations with transverse shear flexibility are shown in Eqs (B.3a)-(B.3e).

$$\begin{aligned} \epsilon_1 &= \hat{H}_{18} u_{1,1} + \hat{H}_{29} u_2 + \hat{H}_{20} u_3 + \left(\frac{\hat{H}_3}{2} \right) (u_{1,1} + \hat{H}_{19} u_2 + D u_3)^2 \\ &+ \left(\frac{\hat{H}_3}{2} \right) (u_{2,1} - \hat{H}_{19} u_1)^2 + \left(\frac{\hat{H}_3}{2} \right) (u_{3,1} - D u_1)^2 \end{aligned} \quad (\text{B.3a})$$

$$\begin{aligned} \epsilon_2 &= \hat{H}_{17} u_{2,2} + \hat{H}_{36} u_1 + \hat{H}_9 u_3 + \left(\frac{\hat{H}_{11}}{2} \right) (u_{2,2} + \hat{H}_{20} u_1 + C u_3)^2 \\ &+ \left(\frac{\hat{H}_{11}}{2} \right) (u_{1,2} - \hat{H}_{20} u_2)^2 + \left(\frac{\hat{H}_{11}}{2} \right) (u_{3,2} - C u_2)^2 \end{aligned} \quad (\text{B.3b})$$

$$\varepsilon_4 = \hat{H}_{17} \left[Cu_{3,2} + (1 - Cy_3) u_{2,3} + Cu_2 \right] \quad (B.3c)$$

$$\varepsilon_5 = \hat{H}_{18} \left[Cu_{3,1} + (1 - Dy_3) u_{1,3} + Du_1 \right] \quad (B.3d)$$

$$\begin{aligned} \varepsilon_6 = & \hat{H}_{17}u_{1,2} + \hat{H}_{18}u_{2,1} - \hat{H}_{36}u_2 - \hat{H}_{29}u_1 \\ & + \left(\frac{\hat{H}_{21}}{2} \right) (u_{1,2} - \hat{H}_{20}u_2) (u_{1,1} + \hat{H}_{19}u_2 + Du_3) \\ & + \left(\frac{\hat{H}_{21}}{2} \right) (u_{2,1} - \hat{H}_{19}u_1) (u_{2,2} + \hat{H}_{20}u_1 + Cu_3) \\ & + \left(\frac{\hat{H}_{21}}{2} \right) (u_{3,1} - Du_1) (u_{3,2} - Cu_2) \end{aligned} \quad (B.3e)$$

where u_1 , u_2 , and u_3 are given in Eq (B.2). For this case, the 60 shell geometric functions \hat{H}_i are simplified, because $h_3 = 1$ and the quadratic terms of the expansions are neglected. The simplified nonzero functions of Appendix A are listed in Eq (B.4).

The strain equations listed below are the parts of the linear and nonlinear strain components for the general spherical elemental codes. Contracted notation is used, where $\varepsilon_1 = \varepsilon_{11}$, $\varepsilon_2 = \varepsilon_{22}$, $\varepsilon_3 = \varepsilon_{33}$, $\varepsilon_4 = \varepsilon_{23}$, $\varepsilon_5 = \varepsilon_{13}$, and $\varepsilon_6 = \varepsilon_{12}$. The strain components ε_i are given by the series expansion shown in Eq (B.5).

$$\begin{aligned}
 \hat{H}_2 &= -D(1 + Dy_3) & \hat{H}_3 &= 1 + 2Dy_3 \\
 \hat{H}_6 &= D^2(1 + 2Dy_3) & \hat{H}_7 &= D^2 \\
 \hat{H}_9 &= -C(1 + Cy_3) & \hat{H}_{11} &= 1 + 2Cy_3 \\
 \hat{H}_{14} &= C^2(1 + 2Cy_3) & \hat{H}_{15} &= C^2 \\
 \hat{H}_{17} &= 1 + Cy_3 & \hat{H}_{18} &= 1 + Dy_3 \\
 \hat{H}_{21} &= 1 + (C + D)y_3 & \hat{H}_{22} &= -D(1 + Cy_3) \\
 \hat{H}_{23} &= -C(1 + Dy_3) & \hat{H}_{26} &= CD \\
 \hat{H}_{32} &= D^2(1 + Dy_3) & \hat{H}_{24} &= -D(1 + 2Dy_3) \\
 \hat{H}_{39} &= C^2(1 + Cy_3) & \hat{H}_{42} &= -C(1 + 2Cy_3) \\
 \hat{H}_{45} &= -D(1 + (C + D)y_3) & \hat{H}_{46} &= -C(1 + (C + D)y_3) \\
 \hat{H}_{51} &= CD(1 + Cy_3) & \hat{H}_{52} &= CD(1 + Dy_3) \\
 \hat{H}_{60} &= CD(1 + (C + D)y_3)
 \end{aligned} \tag{B.4}$$

$$\epsilon_i = \sum_{p=0}^n \chi_i^p y_3^p \tag{B.5}$$

The nonzero χ_i^p are listed below for each component of the general spherical shell theory code. The general cylindrical shell theory is given by setting $R_1 = \infty$ thereby causing $D = 0$. Thus, all terms containing D are neglected. The general plate theory is given by setting $R_1 = \infty$ and $R_2 = \infty$, thereby $D = 0$ and $C = 0$ result. Thus, all terms containing D and C are neglected. Note: for shell theory, $\epsilon_3 \approx 0$

$$\begin{aligned}\chi_1^0 &= \frac{D^2}{2} (u^2 + w^2) + D [uw_{,1} - (1 + u_{,1}) w] \\ &+ \frac{1}{2} (u_{,1}^2 + v_{,1}^2 + w_{,1}^2) + u_{,1}\end{aligned}\quad (\text{B.6})$$

$$\begin{aligned}\chi_1^1 &= D^3 w^2 + D^2 [u (w_{,1} + \psi_1) - (1 + u_{,1}) w] \\ &+ D [w_{,1} (w_{,1} + \psi_1) - w \psi_{1,1}] + (D - C) v_{,1}^2 \\ &+ (1 + u_{,1}) \psi_{1,1} + v_{,1} \psi_{2,1}\end{aligned}\quad (\text{B.7})$$

$$\begin{aligned}\chi_1^2 &= -\frac{3}{2} D^4 u^2 + D^3 [2 (u_{,1} w - u w_{,1}) + u \psi_1] \\ &+ D^2 \left[2 (w_{,1} \psi_1 - w \psi_{1,1}) - (1 + u_{,1}) u_{,1} + \frac{1}{2} (\psi_1^2 - u_{,1}^2) \right] \\ &+ \frac{C}{2} (C - 4D) v_{,1}^2 + D [(1 + u_{,1}) \psi_{1,1}] \\ &+ (2D - C) v_{,1} \psi_{2,1} + \frac{1}{2} (\psi_{1,1}^2 + \psi_{2,1}^2)\end{aligned}\quad (\text{B.8})$$

$$\begin{aligned}\chi_1^3 &= D^5 u^2 - 2D^4 u \psi_1 + D \left[D^2 (u_{,1}^2 + \psi_1^2) + C^2 v_{,1}^2 \right] \\ &- 2D (D u_{,1} \psi_{1,1} + C v_{,1} \psi_{2,1}) + D^2 k u (w_{,1} + \psi_1) \\ &+ D (\psi_{1,1}^2 + \psi_{2,1}^2) + D k [w_{,1} (w_{,1} + \psi_1) - w (w_{,11} + \psi_{1,1})] \\ &+ k [(1 + u_{,1}) (w_{,11} + \psi_{1,1}) + v_{,1} (w_{,12} + \psi_{2,1})]\end{aligned}\quad (\text{B.9})$$

$$\begin{aligned}\chi_1^4 &= D^3 k [u (w_{,1} + \psi_1)] + D^2 k [(2w_{,1} + \psi_1) (w_{,1} + \psi_1) \\ &- 2w (w_{,11} + \psi_{1,1})] + D k [(1 + u_{,1}) (w_{,11} + \psi_{1,1})] \\ &+ (2D - C) k [v_{,1} (w_{,12} + \psi_{2,1})] + k [\psi_{1,1} (w_{,11} + \psi_{1,1}) \\ &+ \psi_{2,1} (w_{,12} + \psi_{2,1})]\end{aligned}\quad (\text{B.10})$$

$$\begin{aligned}\chi_1^5 = & -2D^4ku(w_{,1} + \psi_1) + 2D^3k[\psi_1(w_{,1} + \psi_1)] \\ & + 2Dk[(\psi_{1,1} - Du_{,1})(w_{,11} + \psi_{1,1}) \\ & + (\psi_{2,1} - Cv_{,1})(w_{,12} + \psi_{2,1})]\end{aligned}\quad (B.11)$$

$$\begin{aligned}\chi_1^6 = & \frac{(Dk)^2}{2}(w_{,1} + \psi_1)^2 + \frac{k^2}{2}[(w_{,11} + \psi_{1,1})^2 \\ & + (w_{,12} + \psi_{2,1})^2]\end{aligned}\quad (B.12)$$

$$\begin{aligned}\chi_1^7 = & D^3k^2(w_{,1} + \psi_1)^2 + Dk^2[(w_{,11} + \psi_{1,1})^2 \\ & + (w_{,12} + \psi_{2,1})^2]\end{aligned}\quad (B.13)$$

$$\begin{aligned}\chi_2^0 = & \frac{C^2}{2}(v^2 + w^2) + C[vw_{,2} - (1 + v_{,2})w] \\ & + \frac{1}{2}(u_{,2}^2 + v_{,2}^2 + w_{,2}^2) + v_{,2}\end{aligned}\quad (B.14)$$

$$\begin{aligned}\chi_2^1 = & C^3w^2 + C^2[v(w_{,2} + \psi_2) - (1 + v_{,2})w] \\ & + C[w_{,2}(w_{,2} + \psi_2) - w\psi_{2,2}] + (C - D)u_{,2}^2 \\ & + u_{,2}\psi_{1,2} + (1 + v_{,2})\psi_{2,2}\end{aligned}\quad (B.15)$$

$$\begin{aligned}
 \chi_2^2 = & -\frac{3}{2}C^4 v_{,2}^2 + C^3 [2(v_{,2}w - vw_{,2}) + v\psi_2] \\
 & + C^2 \left[2(w_{,2}\psi_2 - w\psi_{2,2}) - (1 + v_{,2})v_{,2} + \frac{1}{2}(\psi_2^2 - v_{,2}^2) \right] \\
 & + \frac{D}{2}(D - 4C)u_{,2}^2 + C[(1 + v_{,2})\psi_{2,2}] \\
 & + (2C - D)u_{,2}\psi_{1,2} + \frac{1}{2}(\psi_{1,2}^2 + \psi_{2,2}^2)
 \end{aligned} \tag{B.16}$$

$$\begin{aligned}
 \chi_2^3 = & C^5 v_{,2}^2 - 2C^4 v\psi_2 + C \left[C^2(v_{,2}^2 + \psi_2^2) + D^2 u_{,2}^2 \right] \\
 & - 2C(Cv_{,2}\psi_{2,2} + Du_{,2}\psi_{1,2}) + C^2 kv(w_{,2} + \psi_2) \\
 & + D(\psi_{1,2}^2 + \psi_{2,2}^2) + Ck[w_{,2}(w_{,2} + \psi_2) \\
 & - w(w_{,22} + \psi_{2,2})] + k[u_{,2}(w_{,12} + \psi_{1,2}) \\
 & + (1 + v_{,2})(w_{,22} + \psi_{2,2})]
 \end{aligned} \tag{B.17}$$

$$\begin{aligned}
 \chi_2^4 = & C^3 k[v(w_{,2} + \psi_2)] + C^2 k[(2w_{,2} + \psi_2)(w_{,2} + \psi_2) \\
 & - 2w(w_{,22} + \psi_{2,2})] + Ck[(1 + v_{,2})(w_{,22} + \psi_{2,2})] \\
 & + (2C - D)k[u_{,2}(w_{,12} + \psi_{1,2})] + k[\psi_{1,2}(w_{,12} + \psi_{1,2}) \\
 & + \psi_{2,2}(w_{,22} + \psi_{2,2})]
 \end{aligned} \tag{B.18}$$

$$\begin{aligned}
 \chi_2^5 = & -2C^4 kv(w_{,2} + \psi_2) + 2C^3 k[\psi_2(w_{,2} + \psi_2)] \\
 & + 2Ck[(\psi_{2,2} - Cv_{,2})(w_{,22} + \psi_{2,2}) \\
 & + (\psi_{1,2} - Du_{,2})(w_{,12} + \psi_{1,2})]
 \end{aligned} \tag{B.19}$$

$$\chi_2^6 = \frac{(Ck)^2}{2} (w_{,2} + \psi_2)^2 + \frac{k^2}{2} \left[(w_{,12} + \psi_{1,2})^2 + (w_{,22} + \psi_{2,2})^2 \right] \quad (B.20)$$

$$\chi_2^7 = C^3 k^2 (w_{,2} + \psi_2)^2 + Ck^2 \left[(w_{,12} + \psi_{1,2})^2 + (w_{,22} + \psi_{2,2})^2 \right] \quad (B.21)$$

$$\chi_4^0 = w_{,2} + \psi_2 \quad (B.22)$$

$$\chi_4^2 = 3k (w_{,2} + \psi_2) \quad (B.23)$$

$$\chi_5^0 = w_{,1} + \psi_1$$

$$\chi_5^2 = 3k (w_{,1} + \psi_1) \quad (B.24)$$

$$\chi_6^0 = CDuv + D(uw_{,2} - u_{,2}w) + C(vw_{,1} - v_{,1}w) + (u_{,1}u_{,2} + v_{,1}v_{,2} + w_{,1}w_{,2}) + u_{,2} + v_{,1} \quad (B.25)$$

$$\begin{aligned} \chi_6^1 = & CD[u(w_{,2} + \psi_2) + v(w_{,1} + \psi_1) - w(u_{,2} + v_{,1})] \\ & + (C - D)[(1 + u_{,1})u_{,2} - v_{,1}(1 + v_{,2})] + (C + D)w_{,1}w_{,2} \\ & + D(w_{,2}\psi_1 - w\psi_{1,2}) + C(w_{,1}\psi_2 - w\psi_{2,1}) \\ & + (1 + u_{,1})\psi_{1,2} + u_{,2}\psi_{1,1} + v_{,1}\psi_{2,2} + (1 + v_{,2})\psi_{2,1} \end{aligned} \quad (B.26)$$

$$\begin{aligned}
 \chi_6^2 = & -CD(C^2 + CD + D^2)uv + (C + D)[D(uw_{,2} - u_{,2}w) \\
 & + C(vw_{,1} - v_{,1}w)] + CD(Cu\psi_2 + Dv\psi_1) \\
 & + (C + D)[D(u_{,1}u_{,2} + w_{,2}\psi_1 - w\psi_{1,2}) + C(v_{,1}v_{,2} + w_{,1}\psi_2 \\
 & - w\psi_{2,1})] - CD[(1 + u_{,1})u_{,2} + v_{,1}(1 + v_{,2})] \\
 & + C[(1 + u_{,1})\psi_{1,2} + u_{,2}\psi_{1,1}] + D[v_{,1}\psi_{2,2} + (1 + v_{,2})\psi_{2,1}] \\
 & + \psi_{1,1}\psi_{1,2} + \psi_{2,1}\psi_{2,2}
 \end{aligned} \tag{B.27}$$

$$\begin{aligned}
 \chi_6^3 = & C^2D^2(C + D)uv + (C + D)[D^2u_{,1}u_{,2} + C^2v_{,1}v_{,2}] \\
 & - CD[(C^2 + D^2)(u\psi_2 + v\psi_1)] - (C + D)[D(u_{,1}\psi_{1,2} \\
 & + u_{,2}\psi_{1,1}) + C(v_{,1}\psi_{2,2} + v_{,2}\psi_{1,2})] + CD(C + D)\psi_1\psi_2 \\
 & + CDk[u(w_{,2} + \psi_2) + v(w_{,1} + \psi_1)] + (C + D)(\psi_{1,1}\psi_{1,2} \\
 & + \psi_{2,1}\psi_{2,2}) + (C + D)k(w_{,1}w_2 - ww_{1,2}) \\
 & + Ck(w_{,1}\psi_2 - w\psi_{2,1}) + Dk(w_{,2}\psi_1 - w\psi_{1,2}) \\
 & + k[(1 + u_{,1})(w_{,12} + \psi_{1,2}) + u_{,2}(w_{,11} + \psi_{1,1}) \\
 & + v_{,1}(w_{,22} + \psi_{2,2}) + (1 + v_{,2})(w_{,12} + \psi_{2,1})]
 \end{aligned} \tag{B.28}$$

$$\begin{aligned}\chi_6^4 = & CDk [Cu(w_{,2} + \psi_2) + Dv(w_{,1} + \psi_1)] \\ & + (C+D)^2 k (w_{,1}w_{,2} - ww_{1,2}) + (C+D)k [C(w_{,1}\psi_2 \\ & - w\psi_{2,1}) + D(w_{,2}\psi_1 - w\psi_{1,2})] + CDk [\psi_1(w_{,2} + \psi_2) \\ & + \psi_2(w_{,1} + \psi_1)] + Ck [(1+u_{,1})(w_{,12} + \psi_{1,2}) \\ & + u_{,2}(w_{,11} + \psi_{1,1})] + Dk [v_{,1}(w_{,22} + \psi_{2,2}) \\ & + (1+v_{,2})(w_{,12} + \psi_{2,1})] + k [\psi_{1,1}(w_{,12} + \psi_{1,2}) \\ & + \psi_{1,2}(w_{,11} + \psi_{1,1}) + \psi_{2,1}(w_{,22} + \psi_{2,2}) \\ & + \psi_{2,2}(w_{,12} + \psi_{2,1})]\end{aligned}\tag{B.29}$$

$$\begin{aligned}\chi_6^5 = & -CD(C+D)k [Du(w_{,2} + \psi_2) + Cv(w_{,1} + \psi_1)] \\ & + CD(C+D)k [\psi_1(w_{,2} + \psi_2) + \psi_2(w_{,1} + \psi_1)] \\ & - D(C+D)k [(1+u_{,1})(w_{,12} + \psi_{1,2}) + u_{,2}(w_{,11} + \psi_{1,1})] \\ & - C(C+D)k [v_{,1}(w_{,22} + \psi_{2,2}) + (1+v_{,2})(w_{,12} + \psi_{2,1})] \\ & + (C+D)k [\psi_{1,1}(w_{,12} + \psi_{1,2}) + \psi_{1,2}(w_{,11} + \psi_{1,1}) \\ & + \psi_{2,1}(w_{,22} + \psi_{2,2}) + \psi_{2,2}(w_{,12} + \psi_{2,1})]\end{aligned}\tag{B.30}$$

$$\begin{aligned}\chi_6^6 = & CDk [(w_{,1} + \psi_1)(w_{,2} + \psi_2)] \\ & + k^2 [(w_{,12} + \psi_{1,2})(w_{,11} + \psi_{1,1}) \\ & + (w_{,22} + \psi_{2,2})(w_{,12} + \psi_{2,1})]\end{aligned}\tag{B.31}$$

$$\begin{aligned}\chi_6^7 = & CD(C+D)k [(w_{,1} + \psi_1)(w_{,2} + \psi_2)] \\ & + (C+D)k^2 [(w_{,12} + \psi_{1,2})(w_{,11} + \psi_{1,1}) \\ & + (w_{,22} + \psi_{2,2})(w_{,12} + \psi_{2,1})]\end{aligned}\tag{B.32}$$

This Page Intentionally Left Blank

Appendix C. Strain-Displacement Relations for Classical Donnell (SOXX) Elemental Codes

The strain-displacement relations of this appendix are for the case of a spherical shell with a radius of $R_1 = R_2 = R$. The y_1 coordinate is the circumferential distance $dy_1 = R_1 d\theta_1 = R d\theta$ and the y_2 coordinate is the circumferential distance $dy_2 = R_2 d\theta_2 = R d\theta$. The kinematic displacements within the shell are assumed to be classical Donnell relations with a first-order transverse shear deformation theory (FTSD) and of the form

$$\vec{U} = u_1 \vec{e}_1 + u_2 \vec{e}_2 + u_3 \vec{e}_3, \quad (C.1)$$

where

$$\begin{aligned} u_1(y_1, y_2, y_3) &= u(1 - Dy_3) + w_{,1}y_3 \\ u_2(y_1, y_2, y_3) &= v(1 - Cy_3) + w_{,2}y_3 \\ u_3(y_1, y_2) &= w \end{aligned} \quad (C.2)$$

The five degrees of freedom u , v , w , $w_{,1}$, and $w_{,2}$ are functions of midsurface coordinates (y_1, y_2) only. There are no y_i (rotations about the normal) due to the classical theory, and $D = 1/R_1 = 1/R$ and $C = 1/R_2 = 1/R$. The classical Donnell spherical shell strain-displacement relations are shown in Eq (C.3).

$$\begin{aligned} \varepsilon_1 &= u_{1,1} - Du_3 + u_{3,1}^2/2 \\ \varepsilon_2 &= u_{2,2} - Cu_3 + u_{3,2}^2/2 \\ \varepsilon_6 &= u_{1,2} + u_{2,1} + u_{3,1}u_{3,2} \end{aligned} \quad (C.3)$$

where u_1 , u_2 , and u_3 are given in Eq (C.16). For this case, the 60 shell geometric functions \hat{H}_i are simplified, because $h_3 = 1$ and the quadratic terms of the expansions are neglected. The simplified nonzero functions of Appendix A are listed in Eq (C.4).

$$\begin{aligned}
 \hat{H}_2 &= -D(1 + Dy_3) & \hat{H}_3 &= 1 + 2Dy_3 \\
 \hat{H}_6 &= D^2(1 + 2Dy_3) & \hat{H}_7 &= D^2 \\
 \hat{H}_9 &= -C(1 + Cy_3) & \hat{H}_{11} &= 1 + 2Cy_3 \\
 \hat{H}_{14} &= C^2(1 + 2Cy_3) & \hat{H}_{15} &= C^2 \\
 \hat{H}_{17} &= 1 + Cy_3 & \hat{H}_{18} &= 1 + Dy_3 \\
 \hat{H}_{21} &= 1 + (C + D)y_3 & \hat{H}_{22} &= -D(1 + Cy_3) \\
 \hat{H}_{23} &= -C(1 + Dy_3) & \hat{H}_{26} &= CD \\
 \hat{H}_{32} &= D^2(1 + Dy_3) & \hat{H}_{24} &= -D(1 + 2Dy_3) \\
 \hat{H}_{39} &= C^2(1 + Cy_3) & \hat{H}_{42} &= -C(1 + 2Cy_3) \\
 \hat{H}_{45} &= -D(1 + (C + D)y_3) & \hat{H}_{46} &= -C(1 + (C + D)y_3) \\
 \hat{H}_{51} &= CD(1 + Cy_3) & \hat{H}_{52} &= CD(1 + Dy_3) \\
 \hat{H}_{60} &= CD(1 + (C + D)y_3)
 \end{aligned} \tag{C.4}$$

The strain equations listed below are the parts of the linear and nonlinear strain components for the S0XX elemental codes. Contracted notation is used, where $\epsilon_1 = \epsilon_{11}$, $\epsilon_2 = \epsilon_{22}$, $\epsilon_3 = \epsilon_{33}$, $\epsilon_4 = \epsilon_{23}$, $\epsilon_5 = \epsilon_{13}$, and $\epsilon_6 = \epsilon_{12}$. The strain components ϵ_i are given by the series expansion shown in Eq (C.5).

$$\epsilon_i = \sum_{p=0}^n \chi_i^p y_3^p \tag{C.5}$$

The nonzero χ_i^p are listed below for each component of the S0XX classical Donnell spherical shell theory code. The C0XX general cylindrical shell theory is given by setting $R_1 = \infty$ thereby

causing $D = 0$. Thus, all terms containing D are neglected. The P0XX classical von Karman plate theory is given by setting $R_1 = \infty$ and $R_2 = \infty$, thereby $D = 0$ and $C = 0$ result. Thus, all terms containing D and C are neglected. Note: for shell theory, $\epsilon_3 \approx 0$ and due to classical FTSD theory, transverse shear is ignored. Thus, $\epsilon_4 \approx 0$ and $\epsilon_5 \approx 0$.

$$\chi_1^0 = u_{,1} - Dw + w_{,1}^2/2 \quad (C.6)$$

$$\chi_1^1 = w_{,11} - Du_{,1} \quad (C.7)$$

$$\chi_2^0 = v_{,2} - Cw + w_{,2}^2/2 \quad (C.8)$$

$$\chi_2^1 = w_{,22} - Cv_{,2} \quad (C.9)$$

$$\chi_6^0 = u_{,2} + v_{,1} + w_{,1}w_{,2} \quad (C.10)$$

$$\chi_6^1 = 2w_{,12} - Du_{,2} - Cv_{,1} \quad (C.11)$$

This Page Intentionally Left Blank

Appendix D. Strain-Displacement Relations for Modified Donnell (S1XX) Elemental Codes

The strain-displacement relations of this appendix are for the case of a spherical shell with a radius of $R_1 = R_2 = R$. The y_1 coordinate is the circumferential distance $dy_1 = R_1 d\theta_1 = R d\theta$ and the y_2 coordinate is the circumferential distance $dy_2 = R_2 d\theta_2 = R d\theta$. The kinematic displacements within the shell are assumed to be a modified Donnell relations with a higher-order (parabolic) transverse shear distribution (HTSD) theory, and take the form

$$\vec{U} = u_1 \vec{e}_1 + u_2 \vec{e}_2 + u_3 \vec{e}_3, \quad (\text{D.1})$$

where

$$\begin{aligned} u_1(y_1, y_2, y_3) &= u(1 - Dy_3) + \psi_1 y_3 + k(w_{,1} + \psi_1) y_3^3 \\ u_2(y_1, y_2, y_3) &= v(1 - Cy_3) + \psi_2 y_3 + k(w_{,2} + \psi_2) y_3^3 \\ u_3(y_1, y_2) &= w \end{aligned} \quad (\text{D.2})$$

The seven degrees of freedom $u, v, w, w_{,1}, w_{,2}, \psi_1$, and ψ_2 are functions of midsurface coordinates (y_1, y_2) only. The ψ_i are rotations about the normal and $D = 1/R_1 = 1/R$, $C = 1/R_2 = 1/R$, and $k = -4/(3h^2)$. The modified Donnell spherical shell strain-displacement relations with transverse shear flexibility are shown in Eqs (D.3a)-(D.3e).

$$\begin{aligned} \epsilon_1 &= \hat{H}_{18} u_{1,1} + \hat{H}_{29} u_2 + \hat{H}_{20} u_3 + \left(\frac{\hat{H}_3}{2} \right) (u_{1,1} + \hat{H}_{19} u_2 + D u_3)^2 \\ &+ \left(\frac{\hat{H}_3}{2} \right) (u_{2,1} - \hat{H}_{19} u_1)^2 + \left(\frac{\hat{H}_3}{2} \right) (u_{3,1} - D u_1)^2 \end{aligned} \quad (\text{D.3a})$$

$$\begin{aligned} \epsilon_2 &= \hat{H}_{17} u_{2,2} + \hat{H}_{36} u_1 + \hat{H}_9 u_3 + \left(\frac{\hat{H}_{11}}{2} \right) (u_{2,2} + \hat{H}_{20} u_1 + C u_3)^2 \\ &+ \left(\frac{\hat{H}_{11}}{2} \right) (u_{1,2} - \hat{H}_{20} u_2)^2 + \left(\frac{\hat{H}_{11}}{2} \right) (u_{3,2} - C u_2)^2 \end{aligned} \quad (\text{D.3b})$$

$$\varepsilon_4 = \hat{H}_{17} \left[C u_{3,2} + (1 - C y_3) u_{2,3} + C u_2 \right] \quad (D.3c)$$

$$\varepsilon_5 = \hat{H}_{18} \left[C u_{3,1} + (1 - D y_3) u_{1,3} + D u_1 \right] \quad (D.3d)$$

$$\begin{aligned} \varepsilon_6 = & \hat{H}_{17} u_{1,2} + \hat{H}_{18} u_{2,1} - \hat{H}_{36} u_2 - \hat{H}_{29} u_1 \\ & + \left(\frac{\hat{H}_{21}}{2} \right) (u_{1,2} - \hat{H}_{20} u_2) (u_{1,1} + \hat{H}_{19} u_2 + D u_3) \\ & + \left(\frac{\hat{H}_{21}}{2} \right) (u_{2,1} - \hat{H}_{19} u_1) (u_{2,2} + \hat{H}_{20} u_1 + C u_3) \\ & + \left(\frac{\hat{H}_{21}}{2} \right) (u_{3,1} - D u_1) (u_{3,2} - C u_2) \end{aligned} \quad (D.3e)$$

where u_1 , u_2 , and u_3 are given in Eq (D.2). For this case, the 60 shell geometric functions \hat{H}_i are simplified, because $h_3 = 1$ and the quadratic terms of the expansions are neglected. The simplified nonzero functions of Appendix A are listed in Eq (D.4).

The strain equations listed below are the parts of the linear and nonlinear strain components for the S1XX elemental codes. Contracted notation is used, where $\varepsilon_1 = \varepsilon_{11}$, $\varepsilon_2 = \varepsilon_{22}$, $\varepsilon_3 = \varepsilon_{33}$, $\varepsilon_4 = \varepsilon_{23}$, $\varepsilon_5 = \varepsilon_{13}$, and $\varepsilon_6 = \varepsilon_{12}$. The strain components ε_i are given by the series expansion shown in Eq (D.5).

$$\begin{aligned}
\hat{H}_2 &= -D(1 + Dy_3) & \hat{H}_3 &= 1 + 2Dy_3 \\
\hat{H}_6 &= D^2(1 + 2Dy_3) & \hat{H}_7 &= D^2 \\
\hat{H}_9 &= -C(1 + Cy_3) & \hat{H}_{11} &= 1 + 2Cy_3 \\
\hat{H}_{14} &= C^2(1 + 2Cy_3) & \hat{H}_{15} &= C^2 \\
\hat{H}_{17} &= 1 + Cy_3 & \hat{H}_{18} &= 1 + Dy_3 \\
\hat{H}_{21} &= 1 + (C + D)y_3 & \hat{H}_{22} &= -D(1 + Cy_3) \\
\hat{H}_{23} &= -C(1 + Dy_3) & \hat{H}_{26} &= CD \\
\hat{H}_{32} &= D^2(1 + Dy_3) & \hat{H}_{24} &= -D(1 + 2Dy_3) \\
\hat{H}_{39} &= C^2(1 + Cy_3) & \hat{H}_{42} &= -C(1 + 2Cy_3) \\
\hat{H}_{45} &= -D(1 + (C + D)y_3) & \hat{H}_{46} &= -C(1 + (C + D)y_3) \\
\hat{H}_{51} &= CD(1 + Cy_3) & \hat{H}_{52} &= CD(1 + Dy_3) \\
\hat{H}_{60} &= CD(1 + (C + D)y_3)
\end{aligned} \tag{D.4}$$

$$\epsilon_i = \sum_{p=0}^n \chi_i^p y_3^p \tag{D.5}$$

The nonzero χ_i^p are listed below for each component of the S1XX modified Donnell spherical theory code. The C1XX modified Donnell cylindrical shell theory is given by setting $R_1 = \infty$ thereby causing $D = 0$. Thus, all terms containing D are neglected. The P1XX modified von Karman plate theory is given by setting $R_1 = \infty$ and $R_2 = \infty$, thereby $D = 0$ and $C = 0$ result. Thus, all terms containing D and C are neglected. Note: for shell theory, $\epsilon_3 \approx 0$

$$\chi_1^0 = u_{,1} - Dw + w_{,1}^2 \quad (D.6)$$

$$\chi_1^1 = \psi_{1,1} - Du_{,1} \quad (D.7)$$

$$\chi_1^3 = k(w_{,11} + \psi_{1,1}) \quad (D.8)$$

$$\chi_2^0 = v_{,2} - Cw + w_{,2}^2 \quad (D.9)$$

$$\chi_2^1 = \psi_{2,2} - Cv_{,2} \quad (D.10)$$

$$\chi_2^3 = k(w_{,22} + \psi_{2,2}) \quad (D.11)$$

$$\chi_4^0 = w_{,2} + \psi_2 \quad (D.12)$$

$$\chi_4^2 = 3k(w_{,2} + \psi_2) \quad (D.13)$$

$$\chi_5^0 = w_{,1} + \psi_1 \quad (D.14)$$

$$\chi_5^2 = 3k(w_{,1} + \psi_1) \quad (D.15)$$

$$\chi_6^0 = u_{,2} + v_{,1} + w_{,1}w_{,2} \quad (D.16)$$

$$\chi_6^1 = \psi_{1,2} + \psi_{2,1} - Du_{,2} - Cv_{,1} \quad (D.17)$$

$$\chi_6^3 = k(2w_{,12} + \psi_{1,2} + \psi_{2,1}) \quad (\text{D.18})$$

Appendix E. Strain-Displacement Relations for a Full Nonlinear (S2XX) Elemental Codes

The strain-displacement relations of this appendix are for the case of a spherical shell with a radius of $R_1 = R_2 = R$. The y_1 coordinate is the circumferential distance $dy_1 = Rd\theta_1 = Rd\theta$ and the y_2 coordinate is the circumferential distance $dy_2 = Rd\theta_2 = Rd\theta$. The kinematic displacements within the shell are assumed to be of the form

$$\vec{U} = u_1 \vec{e}_1 + u_2 \vec{e}_2 + u_3 \vec{e}_3, \quad (E.1)$$

where

$$\begin{aligned} u_1(y_1, y_2, y_3) &= u(1 - Dy_3) + \psi_1 y_3 + k(w_{,1} + \psi_1) y_3^3 \\ u_2(y_1, y_2, y_3) &= v(1 - Cy_3) + \psi_2 y_3 + k(w_{,2} + \psi_2) y_3^3 \\ u_3(y_1, y_2) &= w \end{aligned} \quad (E.2)$$

The seven degrees of freedom $u, v, w, w_{,1}, w_{,2}, \psi_1$, and ψ_2 are functions of midsurface coordinates (y_1, y_2) only. The ψ_i are rotations about the normal and $D = 1/R_1 = 1/R$, $C = 1/R_2 = 1/R$, and $k = -4/(3h^2)$. The full in-plane nonlinear spherical shell strain-displacement relations with a higher-order (parabolic) transverse shear theory (HTSD) are shown in Eqs (E.3a)-(E.3e).

$$\begin{aligned} \varepsilon_1 &= \hat{H}_{18} u_{1,1} + \hat{H}_{29} u_2 + \hat{H}_{20} u_3 + \left(\frac{\hat{H}_3}{2} \right) (u_{1,1} + \hat{H}_{19} u_2 + Du_3)^2 \\ &+ \left(\frac{\hat{H}_3}{2} \right) (u_{2,1} - \hat{H}_{19} u_1)^2 + \left(\frac{\hat{H}_3}{2} \right) (u_{3,1} - Du_1)^2 \end{aligned} \quad (E.3a)$$

$$\begin{aligned} \varepsilon_2 &= \hat{H}_{17} u_{2,2} + \hat{H}_{36} u_1 + \hat{H}_9 u_3 + \left(\frac{\hat{H}_{11}}{2} \right) (u_{2,2} + \hat{H}_{20} u_1 + Cu_3)^2 \\ &+ \left(\frac{\hat{H}_{11}}{2} \right) (u_{1,2} - \hat{H}_{20} u_2)^2 + \left(\frac{\hat{H}_{11}}{2} \right) (u_{3,2} - Cu_2)^2 \end{aligned} \quad (E.3b)$$

$$\varepsilon_4 = \hat{H}_{17} [Cu_{3,2} + (1 - Cy_3) u_{2,3} + Cu_2] \quad (E.3c)$$

$$\varepsilon_5 = \hat{H}_{18} [Cu_{3,1} + (1 - Dy_3) u_{1,3} + Du_1] \quad (E.3d)$$

$$\begin{aligned} \varepsilon_6 = & \hat{H}_{17} u_{1,2} + \hat{H}_{18} u_{2,1} - \hat{H}_{36} u_2 - \hat{H}_{29} u_1 \\ & + \left(\frac{\hat{H}_{21}}{2} \right) (u_{1,2} - \hat{H}_{20} u_2) (u_{1,1} + \hat{H}_{19} u_2 + Du_3) \\ & + \left(\frac{\hat{H}_{21}}{2} \right) (u_{2,1} - \hat{H}_{19} u_1) (u_{2,2} + \hat{H}_{20} u_1 + Cu_3) \\ & + \left(\frac{\hat{H}_{21}}{2} \right) (u_{3,1} - Du_1) (u_{3,2} - Cu_2) \end{aligned} \quad (E.3e)$$

where u_1 , u_2 , and u_3 are given in Eq (E.2). For this case, the 60 shell geometric functions \hat{H}_i are simplified, because $h_3 = 1$ and the quadratic terms of the expansions are neglected. The simplified nonzero functions of Appendix A are listed in Eq (E.4).

The strain equations listed below are the parts of the linear and nonlinear strain components for the S2XX elemental codes. Contracted notation is used, where $\varepsilon_1 = \varepsilon_{11}$, $\varepsilon_2 = \varepsilon_{22}$, $\varepsilon_3 = \varepsilon_{33}$, $\varepsilon_4 = \varepsilon_{23}$, $\varepsilon_5 = \varepsilon_{13}$, and $\varepsilon_6 = \varepsilon_{12}$. The strain components ε_i are given by the series expansion shown in Eq (E.5).

$$\begin{aligned}
 \hat{H}_2 &= -D(1 + Dy_3) & \hat{H}_3 &= 1 + 2Dy_3 \\
 \hat{H}_6 &= D^2(1 + 2Dy_3) & \hat{H}_7 &= D^2 \\
 \hat{H}_9 &= -C(1 + Cy_3) & \hat{H}_{11} &= 1 + 2Cy_3 \\
 \hat{H}_{14} &= C^2(1 + 2Cy_3) & \hat{H}_{15} &= C^2 \\
 \hat{H}_{17} &= 1 + Cy_3 & \hat{H}_{18} &= 1 + Dy_3 \\
 \hat{H}_{21} &= 1 + (C + D)y_3 & \hat{H}_{22} &= -D(1 + Cy_3) \\
 \hat{H}_{23} &= -C(1 + Dy_3) & \hat{H}_{26} &= CD \\
 \hat{H}_{32} &= D^2(1 + Dy_3) & \hat{H}_{24} &= -D(1 + 2Dy_3) \\
 \hat{H}_{39} &= C^2(1 + Cy_3) & \hat{H}_{42} &= -C(1 + 2Cy_3) \\
 \hat{H}_{45} &= -D(1 + (C + D)y_3) & \hat{H}_{46} &= -C(1 + (C + D)y_3) \\
 \hat{H}_{51} &= CD(1 + Cy_3) & \hat{H}_{52} &= CD(1 + Dy_3) \\
 \hat{H}_{60} &= CD(1 + (C + D)y_3)
 \end{aligned} \tag{E.4}$$

$$\epsilon_i = \sum_{p=0}^n \chi_i^p y_3^p \tag{E.5}$$

The nonzero χ_i^p are listed below for each component of the S2XX general spherical shell theory code. The C2XX general cylindrical shell theory is given by setting $R_1 = \infty$ thereby causing $D = 0$. Thus, all terms containing D are neglected. The P2XX general plate theory is given by setting $R_1 = \infty$ and $R_2 = \infty$, thereby $D = 0$ and $C = 0$ result. Thus, all terms containing D and C are neglected. Note: for shell theory, $\epsilon_3 \approx 0$

$$\begin{aligned}\chi_1^0 &= \frac{D^2}{2} (u^2 + w^2) + D [uw_{,1} - (1 + u_{,1}) w] \\ &+ \frac{1}{2} (u_{,1}^2 + v_{,1}^2 + w_{,1}^2) + u_{,1}\end{aligned}\quad (\text{E.6})$$

$$\begin{aligned}\chi_1^1 &= D^3 w^2 + D^2 [u (w_{,1} + \psi_1) - (1 + u_{,1}) w] \\ &+ D [w_{,1} (w_{,1} + \psi_1) - w \psi_{1,1}] + (D - C) v_{,1}^2 \\ &+ v_{,1} \psi_{2,1} + (1 + u_{,1}) \psi_{1,1}\end{aligned}\quad (\text{E.7})$$

$$\begin{aligned}\chi_1^2 &= D^3 u \psi_1 + \frac{D^2}{2} (\psi_1^2 + 4w_{,1} \psi_1 - 4w \psi_{1,1}) + \frac{C^2}{2} v_{,1}^2 - 2CD v_{,1}^2 \\ &+ D [(1 + u) \psi_{1,1}] + (2D - C) v_{,1} \psi_{2,1} + \frac{1}{2} (\psi_{1,1}^2 + \psi_{2,1}^2)\end{aligned}\quad (\text{E.8})$$

$$\begin{aligned}\chi_1^3 &= D^3 \psi_1^2 + D (\psi_{1,1}^2 + \psi_{2,1}^2) + k [(1 + u_{,1}) (w_{,11} + \psi_{1,1}) \\ &+ v_{,1} (w_{,12} + \psi_{2,1})]\end{aligned}\quad (\text{E.9})$$

$$\begin{aligned}\chi_1^4 &= D^3 k [u (w_{,1} + \psi_1)] - D^2 k [2w (w_{,11} + \psi_{1,1}) \\ &- (2w_{,1} + \psi_1) (w_{,1} + \psi_1)] + Dk [(1 + u_{,1}) (w_{,11} + \psi_{1,1})] \\ &+ (2D - C) k [v_{,1} (w_{,12} + \psi_{2,1})] \\ &+ k [\psi_{1,1} (w_{,11} + \psi_{1,1}) + \psi_{2,1} (w_{,12} + \psi_{2,1})]\end{aligned}\quad (\text{E.10})$$

$$\begin{aligned}\chi_1^5 &= 2D^3 k [\psi_1 (w_{,1} + \psi_1)] + 2Dk [\psi_{1,1} (w_{,11} + \psi_{1,1}) \\ &+ \psi_{2,1} (w_{,12} + \psi_{2,1})]\end{aligned}\quad (\text{E.11})$$

$$\chi_1^6 = \frac{(Dk)^2}{2} (w_{,1} + \psi_1)^2 + \frac{k^2}{2} \left[(w_{,11} + \psi_{1,1})^2 + (w_{,12} + \psi_{2,1})^2 \right] \quad (\text{E.12})$$

$$\chi_1^7 = D^3 k^2 (w_{,1} + \psi_1)^2 + Dk^2 \left[(w_{,11} + \psi_{1,1})^2 + (w_{,12} + \psi_{2,1})^2 \right] \quad (\text{E.13})$$

$$\begin{aligned} \chi_2^0 &= \frac{C^2}{2} (v^2 + w^2) + C[vw_{,2} - (1 + v_{,2})w] \\ &+ \frac{1}{2} \left(u_{,2}^2 + v_{,2}^2 + w_{,2}^2 \right) + v_{,2} \end{aligned} \quad (\text{E.14})$$

$$\begin{aligned} \chi_2^1 &= C^3 w^2 + C^2 [v(w_{,2} + \psi_2) - (1 + v_{,2})w] \\ &+ C[w_{,2}(w_{,2} + \psi_2) - w\psi_{2,2}] + (C - D)u_{,2}^2 \\ &+ u_{,2}\psi_{1,2} + (1 + v_{,2})\psi_{2,2} \end{aligned} \quad (\text{E.15})$$

$$\begin{aligned} \chi_2^2 &= c^3 v\psi_2 + \frac{C^2}{2} \left(\psi_2^2 + 4w_{,2}\psi_2 - 4w\psi_{2,2} \right) + \frac{D^2}{2} u_{,2}^2 - 2CDu_{,2}^2 \\ &+ C[(1 + v)\psi_{2,2}] + (2C - d)u_{,2}\psi_{1,2} + \frac{1}{2} \left(\psi_{1,2}^2 + \psi_{2,2}^2 \right) \end{aligned} \quad (\text{E.16})$$

$$\begin{aligned} \chi_2^3 &= C^3 \psi_2^2 + C \left(\psi_{1,2}^2 + \psi_{2,2}^2 \right) + k[(1 + v_{,2})(w_{,22} + \psi_{2,2}) \\ &+ u_{,2}(w_{,12} + \psi_{1,2})] \end{aligned} \quad (\text{E.17})$$

$$\begin{aligned} \chi_2^4 &= C^3 k[v(w_{,2} + \psi_2)] - C^2 k[2w(w_{,22} + \psi_{2,2}) \\ &- (2w_{,2} + \psi_2)(w_{,2} + \psi_2)] + Ck[(1 + v_{,2})(w_{,22} + \psi_{2,2})] \\ &+ (2C - D)k[u_{,2}(w_{,12} + \psi_{1,2})] \\ &+ k[\psi_{1,2}(w_{,12} + \psi_{1,2}) + \psi_{2,2}(w_{,22} + \psi_{2,2})] \end{aligned} \quad (\text{E.18})$$

$$\begin{aligned} \chi_2^5 = & 2C^3k[\psi_2(w_{,2} + \psi_2)] + 2Ck[\psi_{1,2}(w_{,12} + \psi_{1,2}) \\ & + \psi_{2,2}(w_{,22} + \psi_{2,2})] \end{aligned} \quad (E.19)$$

$$\chi_2^6 = \frac{(Ck)^2}{2}(w_{,2} + \psi_2)^2 + \frac{k^2}{2}[(w_{,12} + \psi_{1,2})^2 + (w_{,22} + \psi_{2,2})^2] \quad (E.20)$$

$$\chi_1^7 = C^3k^2(w_{,2} + \psi_2)^2 + Ck^2[(w_{,12} + \psi_{1,2})^2 + (w_{,22} + \psi_{2,2})^2] \quad (E.21)$$

$$\chi_4^0 = w_{,2} + \psi_2 \quad (E.22)$$

$$\chi_4^2 = 3k(w_{,2} + \psi_2) \quad (E.23)$$

$$\chi_5^0 = w_{,1} + \psi_1 \quad (E.24)$$

$$\chi_5^2 = 3k(w_{,1} + \psi_1) \quad (E.25)$$

$$\begin{aligned} \chi_6^0 = & CDuv + D(uw_{,2} - u_{,2}w) + C(vw_{,1} - v_{,1}w) + u_{,1}u_{,2} + v_{,1}v_{,2} \\ & + w_{,1}w_{,2} + u_{,2} + v_{,1} \end{aligned} \quad (E.26)$$

$$\begin{aligned} \chi_6^1 = & CD[u(w_{,2} + \psi_2) + v(w_{,1} + \psi_1) - w(u_{,2} + v_{,1})] \\ & + D[w_{,2}(w_{,1} + \psi_1)] + C[w_{,1}(w_{,2} + \psi_2)] \\ & - (C + D)[w(\psi_{1,2} + \psi_{2,1})] + (D - C)[(1 + u_{,1})u_{,2} \\ & - v_{,1}(1 + v_{,2})] + (1 + u_{,1})\psi_{1,2} + (1 + v_{,2})\psi_{2,1} \end{aligned} \quad (E.27)$$

$$\begin{aligned}
\chi_6^2 = & D^2 (w_{,2}\psi_1 - w\psi_{1,2}) + C^2 (w_{,1}\psi_2 - w\psi_{2,1}) \\
& + CD (w_{,2}\psi_1 - w\psi_{1,2} + w_{,1}\psi_2 - w\psi_{2,1} + \psi_1\psi_2) \\
& + D [(1 + \nu_{,2})\psi_{2,1} + \nu_{,1}\psi_{2,2}] + C [(1 + u_{,1})\psi_{1,2} + u_{,2}\psi_{1,1}] \\
& + \psi_{1,1}\psi_{1,2} + \psi_{2,1}\psi_{2,2}
\end{aligned} \tag{E.28}$$

$$\begin{aligned}
\chi_6^3 = & (C + D)k (w_{,1}w_{,2} - ww_{,12}) + (C + D) (\psi_{1,1}\psi_{1,2} \\
& + \psi_{2,1}\psi_{2,2}) + Dk (w_{,2}\psi_1 - w\psi_{1,2}) + Ck (w_{,1}\psi_2 - w\psi_{2,1}) \\
& + k [(1 + u_{,1}) (w_{,12} + \psi_{1,2}) + u_{,2} (w_{,11} + \psi_{1,1}) \\
& + \nu_{,1} (w_{,22} + \psi_{2,2}) + (1 + \nu_{,2}) (w_{,12} + \psi_{2,1})]
\end{aligned} \tag{E.29}$$

$$\begin{aligned}
\chi_6^4 = & (C + D)^2 k (w_{,1}w_{,2} - ww_{,12}) \\
& + D(C + D)k (w_{,2}\psi_1 - w\psi_{1,2}) \\
& + C(C + D)k (w_{,1}\psi_2 - w\psi_{2,1}) \\
& + CDk [\psi_1 (w_{,2} + \psi_2) + \psi_2 (w_{,1} + \psi_1)] \\
& + Dk [(1 + \nu_{,2}) (w_{,12} + \psi_{2,1})] \\
& + Ck [(1 + u_{,1}) (w_{,12} + \psi_{1,2})] \\
& + k [\psi_{1,1} (w_{,12} + \psi_{1,2}) + \psi_{1,2} (w_{,11} + \psi_{1,1}) \\
& + \psi_{2,1} (w_{,22} + \psi_{2,2}) + \psi_{2,2} (w_{,12} + \psi_{2,1})]
\end{aligned} \tag{E.30}$$

$$\begin{aligned}
\chi_6^5 = & (C + D)k [\psi_{1,1} (w_{,12} + \psi_{1,2}) + \psi_{1,2} (w_{,11} + \psi_{1,1}) \\
& + \psi_{2,1} (w_{,22} + \psi_{2,2}) + \psi_{2,2} (w_{,12} + \psi_{2,1})]
\end{aligned} \tag{E.31}$$

$$\begin{aligned}\chi_6^6 = & k^2 [(w_{,12} + \psi_{1,2}) (w_{,11} + \psi_{1,1}) \\ & + (w_{,22} + \psi_{2,2}) (w_{,12} + \psi_{2,1})]\end{aligned}\tag{E.32}$$

$$\begin{aligned}\chi_6^7 = & (C + D) k^2 [(w_{,12} + \psi_{1,2}) (w_{,11} + \psi_{1,1}) \\ & + (w_{,22} + \psi_{2,2}) (w_{,12} + \psi_{2,1})]\end{aligned}\tag{E.33}$$

Appendix F. MACSYMA Routine for Elemental Code Generation

F.1 SPHSTRN.MAC Input Deck

The MACSYMA input deck, SPHSTRN.MAC, accomplishes several steps: (1) symbolically generating the appropriate strain-displacement relations, (2) symbolically generating the Taylor series approximations for the 60 shell shape functions (\hat{H}_i), (3) inserting the shell shape functions into the strain-displacement relations, and (4) determining the χ_j^i components for each strain-displacement relation ϵ_j .

```

/*.....*/
/*.....*/
/*  MACSYMA ROUTINE FOR ELEMENTAL CODE GENERATION BY S. A. SCHIMMELS */
/*  CREATED AS A PART OF AN AIR FORCE INSTITUTE OF TECHNOLOGY (AFIT) */
/*  PhD PROGRAM IN AERONAUTICAL ENGINEERING (MATERIAL AND GEOMETRIC */
/*  NONLINEARITY OF COMPOSITE SHELL STRUCTURES) ---- MARCH 1993 */
/*          MACSYMA IS A REGISTERED TRADEMARK OF */
/*          THE MASSACHUSETTS INSTITUTE OF TECHNOLOGY */
/*          */
/*  PROGRAM SPHSTRN.MAC: FOR A SPHERICAL SHELL.  CREATES THE */
/*  STRAIN-DISPLACEMENT RELATIONS BASED ON THE PRESCRIBED */
/*  DISPLACEMENT FIELD AND THEN GENERATES AND SAVES THE APPROPRIATE */
/*  CHI COMPONENTS FOR EACH STRAIN TERM. */
/*.....*/
/*.....*/

/*.....*/
/*  INITIALIZE THE MACSYMA PARAMETERS AND DECLARE THE VARIABLE */
/*  PROPERTIES */
/*.....*/
[DYNAMALLOC:TRUE,DISKGC:TRUE,DERIVABBREV:TRUE,POWERDISP:TRUE];
DEPENDS([U1D,U1R,U2D,U2R,P1,P2,R1,R2,M1,M2,H1,H2],[Y1,Y2,Y3]);
DEPENDS([PSI1,PSI2,PHI1,PHI2,GAMMA1,GAMMA2],[Y1,Y2]);
DEPENDS([THETA1,THETA2,U,V,W,U3],[Y1,Y2]);
DECLARE([R,C,D,AR1,AR2,AR3,AR4,H3],CONSTANT);

/*.....*/
/*  SET THE THEORETICAL ATTRIBUTES FOR A SPECIFIC ELEMENTAL CODE */
/*.....*/

```



```

/*.....*/
/*  H3 = 1 FOR A SHELL */
/*.....*/
H3:1;
/*.....*/
/*  AR1 = 0 FOR A INCOMPLETE CUBIC KINEMATICS */
/*  AR1 = 1 FOR THE COMPLETE QUARTIC KINEMATICS */
/*.....*/
AR1:0;

/*.....*/
/*  AR2 = 0 FOR A LINEAR H1/H2 APPROXIMATIONS */
/*  AR2 = 1 FOR THE QUADRATIC APPROXIMATIONS */
/*.....*/
AR2:0;
/*.....*/
/*  AR3 = 0 FOR LINEAR TRANSVERSE STRAIN */
/*  AR3 = 1 FOR NONLINEAR TRANSVERSE STRAIN */
/*.....*/
AR3:0;

/*.....*/
/*  SUBLIST IS A VARIABLE CONTAINING THE DEFINITIONS OF DISPLACEMENT */
/*  PARAMETERS Q(1) THROUGH Q(18). ALL SYMBOLIC MANIPULATION OF STRAIN */
/*  COMPONENTS IS DONE WITH THE NAMES TO THE LEFT OF THE EQUAL SIGNS IN */
/*  THE SUBLIST. THE Q(XX) DEFINITIONS ARE REQUIRED ONLY FOR GENERATION */
/*  OF ELEMENT INDEPENDENT STRAIN DEFINITION ARRAYS L0 THROUGH SS12, */
/*  ETC. */
/*.....*/

SUBLIST:[DIFF(U,Y1)=Q(2),DIFF(U,Y2)=Q(3),U=Q(1),DIFF(V,Y1)=Q(5),
DIFF(V,Y2)=Q(6),V=Q(4),DIFF(W,Y1,2)=Q(10),DIFF(W,Y2,2)=Q(11),
DIFF(W,Y1,1,Y2,1)=Q(12),DIFF(W,Y1)=Q(8),DIFF(W,Y2)=Q(9),W=Q(7),
DIFF(PSI1,Y1)=Q(14),DIFF(PSI1,Y2)=Q(15),PSI1=Q(13),
DIFF(PSI2,Y1)=Q(17),DIFF(PSI2,Y2)=Q(18),PSI2=Q(16)];

/*.....*/
/*  BEGIN GENERATING THE DISPLACEMENT FIELD COMPONENTS U1, U2, U3 THESE */
/*  NEXT STEPS HAVE BEEN SPECIALIZED FOR A SPHERICAL SHELL R1 = 1/D, */
/*  R2 = 1/C, K = -4/(3*H^2). THE VALUES OF D, C, AND K WILL BE INPUT */
/*  AS PART OF THE FORTRAN PROGRAM. THEY ARE UNSPECIFIED CONSTANTS AS */
/*  FAR AS MACSYMA IS CONCERNED */
/*.....*/
P1:U*(1-Y3*D);

```

```

P2:V*(1-Y3*C);
P11:DIFF(U,Y1)*(1-Y3*D);
P12:DIFF(U,Y2)*(1-Y3*D);
P21:DIFF(V,Y1)*(1-Y3*C);
P22:DIFF(V,Y2)*(1-Y3*C);
L11:DIFF(PSI1,Y1);
L12:DIFF(PSI1,Y2);
L21:DIFF(PSI2,Y1);
L22:DIFF(PSI2,Y2);
M1:K*(DIFF(W,Y1)+PSI1);
M2:K*(DIFF(W,Y2)+PSI2);

/*.....*/
/* INCOMPLETE CUBIC U1 DISPLACEMENT */
/* OF DENNIS. */
/*.....*/
U1D:P1+Y3*PSI1+Y3^3*M1;
/*.....*/
/* INCOMPLETE CUBIC U2 DISPLACEMENT */
/* OF DENNIS. */
/*.....*/
U2D:P2+Y3*PSI2+Y3^3*M2;

/*.....*/
/* COMPLETE QUARTIC U1 & U2 OF SMITH IS GIVEN BY U1 = U1D + U1R & U2 = */
/* U2D + U2R, WHERE U1R & U2R ARE THE CURVATURE CORRECTION TERMS. */
/*.....*/
U1R:(-M1*(1+K*Y3^2)*Y3^2/(K/D));
U2R:(-M2*(1+K*Y3^2)*Y3^2/(K/C));
U1:U1D+U1R*AR1;
U2:U2D+U2R*AR1;
U3:W;

/*.....*/
/* SYMBOLICALLY THE DERIVATIONS OF U1, U2, AND U3. */
/*.....*/
DU11:P11+Y3*L11+Y3^3*DIFF(M1,Y1)+AR1*DIFF(U1R,Y1);
DU12:P12+Y3*L12+Y3^3*DIFF(M1,Y2)+AR1*DIFF(U1R,Y2);
DU21:P21+Y3*L21+Y3^3*DIFF(M2,Y1)+AR1*DIFF(U2R,Y1);
DU22:P22+Y3*L22+Y3^3*DIFF(M2,Y2)+AR1*DIFF(U2R,Y2);
DU31:DIFF(U3,Y1);
DU32:DIFF(U3,Y2);

```

```

/*.....*/
/* SYMBOLICALLY GENERATE THE LAGRANGIAN GREEN-STRAIN COMPONENTS */
/* DIVIDED BY THE APPROPRIATE SHELL LAME' PARAMETERS H1, H2, TO GIVE THE */
/* PHYSICAL STRAINS EPSILON11, EPSILON22, EPSILON12, EPSILON23, */
/* EPSILON13, EPSILON33 */
/*.....*/

/*.....*/
/* EPSILON11 COMPONENT OF STRAIN. LINE 1 IS THE LINEAR TERMS. LINES 2 */
/* THROUGH 4 ARE THE NONLINEAR TERMS */
/*.....*/
ER[1]: ((H1*DU11+DIFF(H1,Y2)*H1*U2/H2+DIFF(H1,Y3)*H1*U3/H3)+
1/2*(DU11+DIFF(H1,Y2)*U2/H2+DIFF(H1,Y3)*U3/H3)^2+
1/2*(DU21-DIFF(H1,Y2)*U1/H2)^2+
1/2*(DU31-DIFF(H1,Y3)*U1/H3)^2)/H1^2;

/*.....*/
/* EPSILON22 COMPONENT OF STRAIN. LINE 1 IS THE LINEAR TERMS. LINES 2 */
/* THROUGH 4 ARE THE NONLINEAR TERMS */
/*.....*/
ER[2]: ((H2*DU22+DIFF(H2,Y1)*H2*U1/H1+DIFF(H2,Y3)*H2*U3/H3)+
1/2*(DU22+DIFF(H2,Y1)*U1/H1+DIFF(H2,Y3)*U3/H3)^2+
1/2*(DU12-DIFF(H2,Y1)*U2/H1)^2+
1/2*(DU32-DIFF(H2,Y3)*U2/H3)^2)/H2^2;

/*.....*/
/* EPSILON12 COMPONENT OF STRAIN. LINE 1 IS THE LINEAR TERMS. LINES 2 */
/* THROUGH 4 ARE THE NONLINEAR TERMS */
/*.....*/
ER[6]: ((H1*DU12+H2*DU21-DIFF(H2,Y1)*U2-DIFF(H1,Y2)*U1)+
(DU12-DIFF(H2,Y1)*U2/H1)*(DU11+DIFF(H1,Y2)*U2/H2+DIFF(H1,Y3)*U3/H3)+
(DU21-DIFF(H1,Y2)*U1/H2)*(DU22+DIFF(H2,Y1)*U1/H1+DIFF(H2,Y3)*U3/H3)+
(DU31-DIFF(H1,Y3)*U1/H3)*(DU32-DIFF(H2,Y3)*U2/H3))/(H1*H2);

/*.....*/
/* EPSILON23 COMPONENT OF STRAIN. LINE 1 IS THE LINEAR TERMS. LINES 2 */
/* THROUGH 8 ARE THE NONLINEAR TERMS. FORCING FUNCTION F(Z)=1+ 3*K*Y3^2 */
/* IS USED. THIS PARABOLIC FORCING FUNCTION APPLIED ONLY TO NONLINEAR */
/* TERMS. */
/*.....*/
ER[4]: (DU32+(1-C*Y3)*DIFF(U2,Y3)-U2*(-C))/(H2*H3);
ERNL[4]: (1+3*K*Y3^2)*
(DIFF(U2,Y3)-DIFF(H3,Y2)*U3/H2)*
(DIFF(U2,Y2)+DIFF(H2,Y1)*U1/H1+DIFF(H2,Y3)*U3/H3)+

```

```

(DIFF(U3,Y2)-DIFF(H2,Y3)*U2/H3)*
(DIFF(U3,Y3)+DIFF(H3,Y1)*U1/H1+DIFF(H3,Y2)*U2/H2)+
(DIFF(U1,Y2)-DIFF(H2,Y1)*U2/H1)*
(DIFF(U1,Y3)-DIFF(H3,Y1)*U3/H1))/(H2*H3);
ER[4]:ER[4]+ERNL[4]*AR3;

/*.....*/
/* EPSILON13 COMPONENT OF STRAIN. LINE 1 IS THE LINEAR TERMS. LINES 2 */
/* THROUGH 8 ARE THE NONLINEAR TERMS. FORCING FUNCTION F(Z) =1+3*K*Y3^2 */
/* IS USED. THIS PARABOLIC FORCING FUNCTION APPLIED ONLY TO NONLINEAR */
/* TERMS. */
/*.....*/
ER[5]:(DU31+(1-D*Y3)*DIFF(U1,Y3)-U1*(-D))/(H1*H3);
ERNL[5]:(1+3*K*Y3^2)*
(DIFF(U1,Y3)-DIFF(H3,Y1)*U3/H1)*
(DIFF(U1,Y1)+DIFF(H1,Y2)*U2/H2+DIFF(H1,Y3)*U3/H3)+
(DIFF(U3,Y1)-DIFF(H1,Y3)*U1/H3)*
(DIFF(U3,Y3)+DIFF(H3,Y1)*U1/H1+DIFF(H3,Y2)*U2/H2)+
(DIFF(U2,Y1)-DIFF(H1,Y2)*U1/H2)*
(DIFF(U2,Y3)-DIFF(H3,Y2)*U3/H2))/(H1*H3);
ER[5]:ER[5]+ERNL[5]*AR3;

/*.....*/
/* EPSILON33 COMPONENT OF STRAIN IS ZERO. IT IS, HOWEVER, INCLUDED IN */
/* THE CONSTITUTIVE RELATIONS THROUGH THE ELASTICITY SUBROUTINE OF THE */
/* CODE WRITTEN BY DENNIS. */
/*.....*/
ER[3]:0;

/*.....*/
/* SUBSTITUTE THE Q(1) THROUGH Q(18) DEFINITIONS OF SUBLIST AND DISPLAY */
/* THE STRAIN COMPONENTS INDIVIDUALLY. */
/*.....*/
FOR I THRU 6 DO (ER[I]:EXPAND(ER[I]),
ER[I]:EXPAND(SUBST(SUBLIST,ER[I]),DISPLAY(ER[I])));

/*.....*/
/* THE NEXT 60 EXPRESSIONS ARE THE POSSIBLE COMBINATIONS OF THE LAME' */
/* PARAMETERS APPEARING IN THE STRAIN EXPRESSIONS FOR AN ARBITRARY */
/* SHELL, WHERE H3 = 1, AND H1, H2 DEPEND UPON Y1, Y2, AND Y3. */
/*.....*/
HREXP[1]:(DIFF(H1,Y2)/H1);
HREXP[2]:(DIFF(H1,Y3)/H1);
HREXP[3]:(1/(H1^2));
HREXP[4]:(DIFF(H1,Y2)^2/(H1^2));

```

```

HREXP[5] : (DIFF (H1, Y2) ^2 / (H2 ^2));
HREXP[6] : (DIFF (H1, Y3) ^2 / (H1 ^2));
HREXP[7] : (DIFF (H1, Y3) ^2);
HREXP[8] : (DIFF (H1, Y2) *DIFF (H1, Y3) / (H1 ^2));
HREXP[9] : (DIFF (H2, Y3) / H2);
HREXP[10] : (DIFF (H2, Y1) / H2);
HREXP[11] : (1 / (H2 ^2));
HREXP[12] : (DIFF (H2, Y1) ^2 / (H2 ^2));
HREXP[13] : (DIFF (H2, Y1) ^2 / (H1 ^2));
HREXP[14] : (DIFF (H2, Y3) ^2 / (H2 ^2));
HREXP[15] : (DIFF (H2, Y3) ^2);
HREXP[16] : (DIFF (H2, Y3) *DIFF (H2, Y1) / (H2 ^2));
HREXP[17] : (1 / H2);
HREXP[18] : (1 / H1);
HREXP[19] : (DIFF (H2, Y1) / H1);
HREXP[20] : (DIFF (H1, Y2) / H2);
HREXP[21] : (1 / (H1 * H2));
HREXP[22] : (DIFF (H1, Y3) / H2);
HREXP[23] : (DIFF (H2, Y3) / H1);
HREXP[24] : (DIFF (H2, Y1) *DIFF (H1, Y2) / (H1 ^2));
HREXP[25] : (DIFF (H2, Y1) *DIFF (H1, Y2) / (H2 ^2));
HREXP[26] : (DIFF (H1, Y3) *DIFF (H2, Y3));
HREXP[27] : (DIFF (H1, Y3) *DIFF (H2, Y1) / (H1 ^2));
HREXP[28] : (DIFF (H2, Y3) *DIFF (H1, Y2) / (H2 ^2));
HREXP[29] : (DIFF (H1, Y2) / (H1 * H2));
HREXP[30] : (DIFF (H1, Y2) ^2 / (H1 ^2 * H2));
HREXP[31] : (DIFF (H1, Y2) ^2 / (H2 ^2 * H1));
HREXP[32] : (DIFF (H1, Y3) ^2 / H1);
HREXP[33] : (DIFF (H1, Y2) / (H1 ^2));
HREXP[34] : (DIFF (H1, Y3) / (H1 ^2));
HREXP[35] : (DIFF (H1, Y2) *DIFF (H1, Y3) / (H1 ^2 * H2));
HREXP[36] : (DIFF (H2, Y1) / (H1 * H2));
HREXP[37] : (DIFF (H2, Y1) ^2 / (H1 * H2 ^2));
HREXP[38] : (DIFF (H2, Y1) ^2 / (H2 * H1 ^2));
HREXP[39] : (DIFF (H2, Y3) ^2 / H2);
HREXP[40] : (DIFF (H2, Y1) / (H2 ^2));
HREXP[41] : (DIFF (H2, Y3) *DIFF (H2, Y1) / (H1 * H2 ^2));
HREXP[42] : (DIFF (H2, Y3) / (H2 ^2));
HREXP[43] : (DIFF (H1, Y2) / (H2 ^2));
HREXP[44] : (DIFF (H2, Y1) / (H1 ^2));
HREXP[45] : (DIFF (H1, Y3) / (H1 * H2));
HREXP[46] : (DIFF (H2, Y3) / (H1 * H2));
HREXP[47] : (DIFF (H2, Y1) *DIFF (H1, Y2) / (H1 ^2 * H2));
HREXP[48] : (DIFF (H1, Y2) *DIFF (H2, Y1) / (H2 ^2 * H1));
HREXP[49] : (DIFF (H1, Y3) *DIFF (H2, Y1) / (H1 ^2 * H2));
HREXP[50] : (DIFF (H2, Y3) *DIFF (H1, Y2) / (H2 ^2 * H1));

```

```

HREXP[51]:(DIFF(H1,Y3)*DIFF(H2,Y3)/H2);
HREXP[52]:(DIFF(H1,Y3)*DIFF(H2,Y3)/H1);
HREXP[53]:(DIFF(H1,Y2)^2/(H1^2*H2^2));
HREXP[54]:(DIFF(H1,Y2)/(H1^2*H2));
HREXP[55]:(DIFF(H2,Y1)^2/(H1^2*H2^2));
HREXP[56]:(DIFF(H2,Y1)/(H2^2*H1));
HREXP[57]:(DIFF(H1,Y2)/(H1*H2^2));
HREXP[58]:(DIFF(H2,Y1)/(H2*H1^2));
HREXP[59]:(DIFF(H2,Y1)*DIFF(H1,Y2)/(H1^2*H2^2));
HREXP[60]:(DIFF(H1,Y3)*DIFF(H2,Y3)/(H1*H2));

/*.....*/
/* THE MACRO HRTAY(X,I)::= GENERATES THE COEFFICIENTS F, G, AND H OF THE*/
/* TAYLOR'S SERIES EXPANSION OF THE EXPRESSION X ABOUT THE POINT Y3 = 0 */
/* FOR A SPHERICAL SHELL WITH H1 = 1 - Y3/R1 AND H2 = 1 - Y3/R2.      */
/*.....*/
HRTAY(X,I):=BUILDQ([X,I],(
PRINT(" THE TAYLOR SERIES EXPANSION OF "),DISPLAY(X),
PRINT(" IS EQUAL TO F + G*Y3 + H*Y3^2 + H.O.T., WHERE "),
(X:TAYLOR(FACTOROUT(EXPAND(RAT(EV(X,H1=(1-Y3*D),
H2=(1-Y3*C),DIFF))),C,D),Y3,0,3)),
F[I]:EXPAND(COEFF(X,Y3,0)),DISPLAY(F[I]),
G[I]:EXPAND(COEFF(X,Y3,1)),DISPLAY(G[I]),
H[I]:EXPAND(COEFF(X,Y3,2)),DISPLAY(H[I])));

/*.....*/
/* COMPUTE THE COEFFICIENTS F, G, AND H FOR ALL 60 HREXP EXPRESSIONS. */
/*.....*/
FOR I THRU 60 DO HRTAY(HREXP[I],I);

/*.....*/
/* THE MACRO HRSUB(X)::= TAKES ANY ONE-TERM EXPRESSION X, (PRODUCTS ARE */
/* OK, BUT [+ -] OPERATORS ARE NOT) AND SUBSTITUTES THE APPROXIMATE */
/* SERIES EXPANSION F + G*Y3 + H*Y3^2 FOR THE FUNCTION OF LAME'      */
/* PARAMETERS.                                                         */
/*.....*/
HRSUB(X):=BUILDQ([X],(
XO:X,
X:NUM(X)/SUBST(D[1],H1,DENOM(X)),
X:NUM(X)/SUBST(D[2],H2,DENOM(X)),
X:NUM(X)/RATSUBST(D[3],D[1]*D[1],DENOM(X)),
X:NUM(X)/RATSUBST(D[4],D[2]*D[2],DENOM(X)),
X:NUM(X)/RATSUBST(D[5],D[1]*D[2],DENOM(X)),
X:NUM(X)/RATSUBST(D[6],D[1]*D[4],DENOM(X)),
X:NUM(X)/RATSUBST(D[7],D[2]*D[3],DENOM(X)),
X:NUM(X)/RATSUBST(D[8],D[3]*D[4],DENOM(X)),

```

```

XD:X,
X:NUM(X)/RATSUBST(1/D[1],D[1],DENOM(X)),
X:NUM(X)/RATSUBST(1/D[2],D[2],DENOM(X)),
X:NUM(X)/RATSUBST(1/D[3],D[3],DENOM(X)),
X:NUM(X)/RATSUBST(1/D[4],D[4],DENOM(X)),
X:NUM(X)/RATSUBST(1/D[5],D[5],DENOM(X)),
X:NUM(X)/RATSUBST(1/D[6],D[6],DENOM(X)),
X:NUM(X)/RATSUBST(1/D[7],D[7],DENOM(X)),
X:NUM(X)/RATSUBST(1/D[8],D[8],DENOM(X)),
XN:X,
X:RATSUBST(F[59]+Y3*G[59]+Y3^2*AR2*H[59],'DIFF(H2,Y1)*DIFF(H1,Y2)*D[8],X),
X:RATSUBST(F[55]+Y3*G[55]+Y3^2*AR2*H[55],'DIFF(H2,Y1)^2*D[8],X),
X:RATSUBST(F[53]+Y3*G[53]+Y3^2*AR2*H[53],'DIFF(H1,Y2)^2*D[8],X),
X:RATSUBST(F[50]+Y3*G[50]+Y3^2*AR2*H[50],'DIFF(H2,Y3)*DIFF(H1,Y2)*D[6],X),
X:RATSUBST(F[49]+Y3*G[49]+Y3^2*AR2*H[49],'DIFF(H1,Y3)*DIFF(H2,Y1)*D[7],X),
X:RATSUBST(F[48]+Y3*G[48]+Y3^2*AR2*H[48],'DIFF(H1,Y2)*DIFF(H2,Y1)*D[6],X),
X:RATSUBST(F[47]+Y3*G[47]+Y3^2*AR2*H[47],'DIFF(H2,Y1)*DIFF(H1,Y2)*D[7],X),
X:RATSUBST(F[41]+Y3*G[41]+Y3^2*AR2*H[41],'DIFF(H2,Y3)*DIFF(H2,Y1)*D[6],X),
X:RATSUBST(F[38]+Y3*G[38]+Y3^2*AR2*H[38],'DIFF(H2,Y1)^2*D[7],X),
X:RATSUBST(F[37]+Y3*G[37]+Y3^2*AR2*H[37],'DIFF(H2,Y1)^2*D[6],X),
X:RATSUBST(F[35]+Y3*G[35]+Y3^2*AR2*H[35],'DIFF(H1,Y2)*DIFF(H1,Y3)*D[7],X),
X:RATSUBST(F[31]+Y3*G[31]+Y3^2*AR2*H[31],'DIFF(H1,Y2)^2*D[6],X),
X:RATSUBST(F[30]+Y3*G[30]+Y3^2*AR2*H[30],'DIFF(H1,Y2)^2*D[7],X),
X:RATSUBST(F[58]+Y3*G[58]+Y3^2*AR2*H[58],'DIFF(H2,Y1)*D[7],X),
X:RATSUBST(F[57]+Y3*G[57]+Y3^2*AR2*H[57],'DIFF(H1,Y2)*D[6],X),
X:RATSUBST(F[56]+Y3*G[56]+Y3^2*AR2*H[56],'DIFF(H2,Y1)*D[6],X),
X:RATSUBST(F[54]+Y3*G[54]+Y3^2*AR2*H[54],'DIFF(H1,Y2)*D[7],X),
X:RATSUBST(F[60]+Y3*G[60]+Y3^2*AR2*H[60],'DIFF(H1,Y3)*DIFF(H2,Y3)*D[5],X),
X:RATSUBST(F[28]+Y3*G[28]+Y3^2*AR2*H[28],'DIFF(H2,Y3)*DIFF(H1,Y2)*D[4],X),
X:RATSUBST(F[27]+Y3*G[27]+Y3^2*AR2*H[27],'DIFF(H1,Y3)*DIFF(H2,Y1)*D[3],X),
X:RATSUBST(F[25]+Y3*G[25]+Y3^2*AR2*H[25],'DIFF(H2,Y1)*DIFF(H1,Y2)*D[4],X),
X:RATSUBST(F[24]+Y3*G[24]+Y3^2*AR2*H[24],'DIFF(H2,Y1)*DIFF(H1,Y2)*D[3],X),
X:RATSUBST(F[16]+Y3*G[16]+Y3^2*AR2*H[16],'DIFF(H2,Y3)*DIFF(H2,Y1)*D[4],X),
X:RATSUBST(F[8]+Y3*G[8]+Y3^2*AR2*H[8],'DIFF(H1,Y2)*DIFF(H1,Y3)*D[3],X),
X:RATSUBST(F[14]+Y3*G[14]+Y3^2*AR2*H[14],'DIFF(H2,Y3)^2*D[4],X),
X:RATSUBST(F[13]+Y3*G[13]+Y3^2*AR2*H[13],'DIFF(H2,Y1)^2*D[3],X),
X:RATSUBST(F[12]+Y3*G[12]+Y3^2*AR2*H[12],'DIFF(H2,Y1)^2*D[4],X),
X:RATSUBST(F[6]+Y3*G[6]+Y3^2*AR2*H[6],'DIFF(H1,Y3)^2*D[3],X),
X:RATSUBST(F[5]+Y3*G[5]+Y3^2*AR2*H[5],'DIFF(H1,Y2)^2*D[4],X),
X:RATSUBST(F[4]+Y3*G[4]+Y3^2*AR2*H[4],'DIFF(H1,Y2)^2*D[3],X),
X:RATSUBST(F[46]+Y3*G[46]+Y3^2*AR2*H[46],'DIFF(H2,Y3)*D[5],X),
X:RATSUBST(F[45]+Y3*G[45]+Y3^2*AR2*H[45],'DIFF(H1,Y3)*D[5],X),
X:RATSUBST(F[44]+Y3*G[44]+Y3^2*AR2*H[44],'DIFF(H2,Y1)*D[3],X),
X:RATSUBST(F[43]+Y3*G[43]+Y3^2*AR2*H[43],'DIFF(H1,Y2)*D[4],X),
X:RATSUBST(F[42]+Y3*G[42]+Y3^2*AR2*H[42],'DIFF(H2,Y3)*D[4],X),
X:RATSUBST(F[40]+Y3*G[40]+Y3^2*AR2*H[40],'DIFF(H2,Y1)*D[4],X),

```

```

X:RATSUBST(F[36]+Y3*G[36]+Y3^2*AR2*H[36], 'DIFF(H2,Y1)*D[5],X),
X:RATSUBST(F[34]+Y3*G[34]+Y3^2*AR2*H[34], 'DIFF(H1,Y3)*D[3],X),
X:RATSUBST(F[33]+Y3*G[33]+Y3^2*AR2*H[33], 'DIFF(H1,Y2)*D[3],X),
X:RATSUBST(F[29]+Y3*G[29]+Y3^2*AR2*H[29], 'DIFF(H1,Y2)*D[5],X),
X:RATSUBST(F[3]+Y3*G[3]+Y3^2*AR2*H[3],1*D[3],X),
X:RATSUBST(F[21]+Y3*G[21]+Y3^2*AR2*H[21],1*D[5],X),
X:RATSUBST(F[11]+Y3*G[11]+Y3^2*AR2*H[11],1*D[4],X),
X:RATSUBST(F[52]+Y3*G[52]+Y3^2*AR2*H[52], 'DIFF(H1,Y3)*DIFF(H2,Y3)*D[1],X),
X:RATSUBST(F[51]+Y3*G[51]+Y3^2*AR2*H[51], 'DIFF(H1,Y3)*DIFF(H2,Y3)*D[2],X),
X:RATSUBST(F[39]+Y3*G[39]+Y3^2*AR2*H[39], 'DIFF(H2,Y3)^2*D[2],X),
X:RATSUBST(F[32]+Y3*G[32]+Y3^2*AR2*H[32], 'DIFF(H1,Y3)^2*D[1],X),
X:RATSUBST(F[23]+Y3*G[23]+Y3^2*AR2*H[23], 'DIFF(H2,Y3)*D[1],X),
X:RATSUBST(F[22]+Y3*G[22]+Y3^2*AR2*H[22], 'DIFF(H1,Y3)*D[2],X),
X:RATSUBST(F[20]+Y3*G[20]+Y3^2*AR2*H[20], 'DIFF(H1,Y2)*D[2],X),
X:RATSUBST(F[19]+Y3*G[19]+Y3^2*AR2*H[19], 'DIFF(H2,Y1)*D[1],X),
X:RATSUBST(F[10]+Y3*G[10]+Y3^2*AR2*H[10], 'DIFF(H2,Y1)*D[2],X),
X:RATSUBST(F[9]+Y3*G[9]+Y3^2*AR2*H[9], 'DIFF(H2,Y3)*D[2],X),
X:RATSUBST(F[1]+Y3*G[1]+Y3^2*AR2*H[1], 'DIFF(H1,Y2)*D[1],X),
X:RATSUBST(F[2]+Y3*G[2]+Y3^2*AR2*H[2], 'DIFF(H1,Y3)*D[1],X),
X:RATSUBST(F[17]+Y3*G[17]+Y3^2*AR2*H[17],1*D[2],X),
X:RATSUBST(F[18]+Y3*G[18]+Y3^2*AR2*H[18],1*D[1],X),
X:RATSUBST(F[15]+Y3*G[15]+Y3^2*AR2*H[15], 'DIFF(H2,Y3)^2,X),
X:RATSUBST(F[7]+Y3*G[7]+Y3^2*AR2*H[7], 'DIFF(H1,Y3)^2,X),
X:RATSUBST(F[26]+Y3*G[26]+Y3^2*AR2*H[26], 'DIFF(H1,Y3)*DIFF(H2,Y3),X));

```

```

/*.....*/
/* THE MACRO PICK(XXX) ::= TAKES ANY EXPRESSION XXX (PREVIOUSLY EXPANDED)*/
/* AND SEPARATES IT INTO SINGLE EXPRESSIONS LABELED E(I). IT THEN CALLS*/
/* MACRO HRSUB(X) TO FIND THE APPROPRIATE LAME' PARAMETERS APPROXIMATION */
/* FOR EACH EXPRESSION AND THEN SUMS ALL THE EXPRESSIONS TO YIELD THE */
/* EXPRESSION XXX WITH ALL THE TERMS FULLY APPROXIMATED. */
/*.....*/

```

```

E(I):=CONCAT(E,I);
PICK(XXX):=BUILDQ([XXX],(I1:LINENUM,NT:NTERMS(XXX),I2:I1+NT-1,
PRINT(" THIS EXPRESSION HAS ",NT," TERMS TO BE RESOLVED "),
PICKAPART(XXX,1),FOR K:I1 THRU I2 DO EXH[K]:EV(E(K),EVAL),
FOR K:I1 THRU I2 DO HRSUB(EXH[K]),XXX:=SUM(EXH[K],K,I1,I2),
DISPLAY(XXX)));

```

```

/*.....*/
/* USE THE MACRO PICK(XXX) TO APPROXIMATE LAME' PARAMETER FUNCTIONS OF */
/* THE STRAIN COMPONENTS. */
/*.....*/
ERR4:ER[4];
ERR5:ER[5];
PICK(ERR4);

```



```
PICK(ERR5);
ER[4]:ERR4;
ER[5]:ERR5;
ERR1:ER[1];
ERR2:ER[2];
ERR6:ER[6];
PICK(ERR1);
PICK(ERR2);
PICK(ERR6);
ER[1]:ERR1;
ER[2]:ERR2;
ER[6]:ERR6;

SAVE("SPH-ER.SV",ER);

/*.....*/
/* THE MACRO, CHIFORM(XX,YY,K):= EXPANDS A 6x1 VECTOR CALLED XX, THEN */
/* DETERMINES AND DISPLAYS THE COEFFICIENTS OF Y3 UPTO THE Kth POWER. */
/* THESE ARE CALLED YY[I,K]. */
/*.....*/
CHIFORM(XX,YY,K):=BUILDQ([XX,YY,K],(FOR I THRU 6 DO FOR JJ THRU K+1 DO
(XY[I]:FACTOROUT(EXPAND(RAT(XX[I])),[H1,H2]),
YY[I,JJ-1]:COEFF(XY[I],Y3,JJ-1),DISPLAY(YY[I,JJ-1]))));
POWERDISP:TRUE;
CHIFORM(ER,XR,12);
KILL(ER);

SAVE("SPH-XR.SV",XR);

CLOSEFILE();
QUIT()
```

F.2 SPHINIT.MAC Input Deck

The MACSYMA input deck, SPHINIT.MAC, generates the $(L^P)_i$ column arrays and the $[H^P]_i$ matrices for each strain component, ϵ_i .

```

WRITEFILE("SPH-INIT.WF");
/*****
/*****
/*  MACSYMA ROUTINE FOR ELEMENTAL CODE GENERATION BY S. A. SCHIMMELS  */
/*  CREATED AS A PART OF AN AIR FORCE INSTITUTE OF TECHNOLOGY (AFIT)  */
/*      PhD PROGRAM IN AERONAUTICAL ENGINEERING --- MARCH 1993      */
/*      MACSYMA IS A REGISTERED TRADEMARK OF                        */
/*      THE MASSACHUSETTS INSTITUTE OF TECHNOLOGY                  */
/*                                                                    */
/*  PROGRAM SPHINIT.MAC: FOR A SPHERICAL SHELL.  CREATES THE LHMAT,  */
/*  LSMAT, HMAT, & SSMAT ARRAYS.                                    */
/*****
/*****

/*****
/*  INITIALIZE MACSYMA PARAMETERS AND DECLARE VARIABLE PROPERTIES  */
/*****
[DYNAMALLOC:TRUE,DISKGC:TRUE,DERIVABBREV:TRUE,POWERDISP:TRUE]$

/*****
/*  THE MACRO DECOMPOSE(XR):= DETERMINES AND DISPLAYS THE COEFFICIENTS OF */
/*  DISPLACEMENT VARIABLES Q(1) THROUGH Q(18) AND CREATES A 6x13x18 ARRAY */
/*  CALLED LMAT OF THE CONSTANT COEFFICIENTS OF LINEAR DISPLACEMENT TERMS, */
/*  AND A 6x13x18x18 ARRAY CALLED HMAT OF THE CONSTANT COEFFICIENTS OF THE */
/*  CONSTANT COEFFICIENTS OF THE QUADRATIC DISPLACEMENT TERMS.          */
/*****
LOADFILE("SPH-XRNEW.SV");

FOR I THRU 6 DO FOR JJ THRU 13 DO (DISPLAY (XR[I,JJ-1]))$
DECOMPOSE(XR):=BUILDQ([XR],
(FOR I THRU 6 DO (PRINT("DECOMPOSING STRAIN COMPONENT",I),
(FOR J:0 THRU 12 DO (FOR K THRU 18 DO
(IF HIPOW(XR[I,J],Q(K))=2 THEN
XQUAD[I,J,K]:RATCOEFF(XR[I,J],Q(K),2)*Q(K)*2+RATCOEFF(XR[I,J],Q(K),1) ELSE
XQUAD[I,J,K]:RATCOEFF(XR[I,J],Q(K),1),
FOR L THRU 18 DO HMAT[I,J,K,L]:RATCOEFF(XQUAD[I,J,K],Q(L),1),
LMAT[I,J,K]:EXPAND(XQUAD[I,J,K]-SUM(HMAT[I,J,K,L]*Q(L),L,1,18))))))$
DECOMPOSE(XR);
KILL(XR)$

```

```
SAVE ("SPH-LHMAT.SV",LMAT,HMAT);
```

```

/*****
/* GENERATE ELEMENT-INDEPENDENT STRAIN DEFINITION ARRAYS LX AN HXX FOR */
/* IN-PLANE STRAINS AND SX AND SSXX FOR TRANSVERSE SHEAR STRAINS. X AND*/
/* XX REPRESENT THE POWER OF Y3 FOR WHICH THE COEFFICIENTS APPLY. NOTE */
/* LX HAS 3 COLUMNS. COLUMN 1 CONTAINS COEFFICIENTS OF THE EPSILON11 */
/* TERMS WHICH ARE LINEAR IN DISPLACEMENTS Q(1)-Q(18). COLUMN 2 */
/* CONTAINS EPSILON22 TERMS AND COLUMN 3 CONTAINS EPSILON12 TERMS. */
/* LIKEWISE HXX HAS 3 PARTITIONS. COLUMNS 1-18 CONTAINSS COEFFICIENTS */
/* OF EPSILON11 TERMS WHICH ARE QUADRATIC IN DISPLACEMENT. COLUMNS 19- */
/* 36 CONTAIN THE EPSILON22 TERMS AND COLUMNS 37-54 CONTAIN THE */
/* EPSILON12 TERMS. SIMILARLY, SX CONTAINS 2 COLUMNS PERTAINING TO THE */
/* COEFFICIENTS OF LINEAR TERMS OF EPSILON23 AND EPSILON133, */
/* RESPECTIVELY. SSXX HAS 2 PARTITIONS. COLUMNS 1-18 CONTAIN */
/* COEFFICIENTS OF THE QUADRATIC TERMS OF EPSILON23 AND COLUMNS 19-36 */
/* CONTAIN THE QUADRATIC TERMS OF EPSILON13. */
*****/
FOR NN THRU 18 DO (
  L0[NN,1]:LMAT[1,0,NN],L0[NN,2]:LMAT[2,0,NN],L0[NN,3]:LMAT[6,0,NN],
  L1[NN,1]:LMAT[1,1,NN],L1[NN,2]:LMAT[2,1,NN],L1[NN,3]:LMAT[6,1,NN],
  L2[NN,1]:LMAT[1,2,NN],L2[NN,2]:LMAT[2,2,NN],L2[NN,3]:LMAT[6,2,NN],
  L3[NN,1]:LMAT[1,3,NN],L3[NN,2]:LMAT[2,3,NN],L3[NN,3]:LMAT[6,3,NN],
  L4[NN,1]:LMAT[1,4,NN],L4[NN,2]:LMAT[2,4,NN],L4[NN,3]:LMAT[6,4,NN],
  L5[NN,1]:LMAT[1,5,NN],L5[NN,2]:LMAT[2,5,NN],L5[NN,3]:LMAT[6,5,NN],
  L6[NN,1]:LMAT[1,6,NN],L6[NN,2]:LMAT[2,6,NN],L6[NN,3]:LMAT[6,6,NN],
  L7[NN,1]:LMAT[1,7,NN],L7[NN,2]:LMAT[2,7,NN],L7[NN,3]:LMAT[6,7,NN],
  S0[NN,1]:LMAT[4,0,NN],S0[NN,2]:LMAT[5,0,NN],
  S1[NN,1]:LMAT[4,1,NN],S1[NN,2]:LMAT[5,1,NN],
  S2[NN,1]:LMAT[4,2,NN],S2[NN,2]:LMAT[5,2,NN],
  S3[NN,1]:LMAT[4,3,NN],S3[NN,2]:LMAT[5,3,NN],
  S4[NN,1]:LMAT[4,4,NN],S4[NN,2]:LMAT[5,4,NN],
  S5[NN,1]:LMAT[4,5,NN],S5[NN,2]:LMAT[5,5,NN],
  S6[NN,1]:LMAT[4,6,NN],S6[NN,2]:LMAT[5,6,NN],
  S7[NN,1]:LMAT[4,7,NN],S7[NN,2]:LMAT[5,7,NN],
  FOR MM THRU 18 DO (
    H0[NN,MM]:HMAT[1,0,NN,MM],H0[NN,MM+18]:HMAT[2,0,NN,MM],
    H0[NN,MM+36]:HMAT[6,0,NN,MM],
    H1[NN,MM]:HMAT[1,1,NN,MM],H1[NN,MM+18]:HMAT[2,1,NN,MM],
    H1[NN,MM+36]:HMAT[6,1,NN,MM],
    H2[NN,MM]:HMAT[1,2,NN,MM],H2[NN,MM+18]:HMAT[2,2,NN,MM],
    H2[NN,MM+36]:HMAT[6,2,NN,MM],
    H3[NN,MM]:HMAT[1,3,NN,MM],H3[NN,MM+18]:HMAT[2,3,NN,MM],
    H3[NN,MM+36]:HMAT[6,3,NN,MM],
    H4[NN,MM]:HMAT[1,4,NN,MM],H4[NN,MM+18]:HMAT[2,4,NN,MM],

```

```

H4[NN,MM+36]:HMAT[6,4,NN,MM],
H5[NN,MM]:HMAT[1,5,NN,MM],H5[NN,MM+18]:HMAT[2,5,NN,MM],
H5[NN,MM+36]:HMAT[6,5,NN,MM],
H6[NN,MM]:HMAT[1,6,NN,MM],H6[NN,MM+18]:HMAT[2,6,NN,MM],
H6[NN,MM+36]:HMAT[6,6,NN,MM],
H7[NN,MM]:HMAT[1,7,NN,MM],H7[NN,MM+18]:HMAT[2,7,NN,MM],
H7[NN,MM+36]:HMAT[6,7,NN,MM],
H8[NN,MM]:HMAT[1,8,NN,MM],H8[NN,MM+18]:HMAT[2,8,NN,MM],
H8[NN,MM+36]:HMAT[6,8,NN,MM],
H9[NN,MM]:HMAT[1,9,NN,MM],H9[NN,MM+18]:HMAT[2,9,NN,MM],
H9[NN,MM+36]:HMAT[6,9,NN,MM],
H10[NN,MM]:HMAT[1,10,NN,MM],H10[NN,MM+18]:HMAT[2,10,NN,MM],
H10[NN,MM+36]:HMAT[6,10,NN,MM],
H11[NN,MM]:HMAT[1,11,NN,MM],H11[NN,MM+18]:HMAT[2,11,NN,MM],
H11[NN,MM+36]:HMAT[6,11,NN,MM],
H12[NN,MM]:HMAT[1,12,NN,MM],H12[NN,MM+18]:HMAT[2,12,NN,MM],
H12[NN,MM+36]:HMAT[6,12,NN,MM],
SS0[NN,MM]:HMAT[4,0,NN,MM],SS0[NN,MM+18]:HMAT[5,0,NN,MM],
SS1[NN,MM]:HMAT[4,1,NN,MM],SS1[NN,MM+18]:HMAT[5,1,NN,MM],
SS2[NN,MM]:HMAT[4,2,NN,MM],SS2[NN,MM+18]:HMAT[5,2,NN,MM],
SS3[NN,MM]:HMAT[4,3,NN,MM],SS3[NN,MM+18]:HMAT[5,3,NN,MM],
SS4[NN,MM]:HMAT[4,4,NN,MM],SS4[NN,MM+18]:HMAT[5,4,NN,MM],
SS5[NN,MM]:HMAT[4,5,NN,MM],SS5[NN,MM+18]:HMAT[5,5,NN,MM],
SS6[NN,MM]:HMAT[4,6,NN,MM],SS6[NN,MM+18]:HMAT[5,6,NN,MM],
SS7[NN,MM]:HMAT[4,7,NN,MM],SS7[NN,MM+18]:HMAT[5,7,NN,MM],
SS8[NN,MM]:HMAT[4,8,NN,MM],SS8[NN,MM+18]:HMAT[5,8,NN,MM],
SS9[NN,MM]:HMAT[4,9,NN,MM],SS9[NN,MM+18]:HMAT[5,9,NN,MM],
SS10[NN,MM]:HMAT[4,10,NN,MM],SS10[NN,MM+18]:HMAT[5,10,NN,MM],
SS11[NN,MM]:HMAT[4,11,NN,MM],SS11[NN,MM+18]:HMAT[5,11,NN,MM],
SS12[NN,MM]:HMAT[4,12,NN,MM],SS12[NN,MM+18]:HMAT[5,12,NN,MM]))$

```

```

/*****
/*  FORM MACSYMA MATRICES FROM THE ABOVE DEFINED ARRAYS.  */
*****/
L0:GENMATRIX(L0,18,3);
L1:GENMATRIX(L1,18,3);
L2:GENMATRIX(L2,18,3);
L3:GENMATRIX(L3,18,3);
L4:GENMATRIX(L4,18,3);
L5:GENMATRIX(L5,18,3);
L6:GENMATRIX(L6,18,3);
L7:GENMATRIX(L7,18,3);
S0:GENMATRIX(S0,18,2);
S1:GENMATRIX(S1,18,2);
S2:GENMATRIX(S2,18,2);
S3:GENMATRIX(S3,18,2);

```

```
S4:GENMATRIX(S4,18,2);
S5:GENMATRIX(S5,18,2);
S6:GENMATRIX(S6,18,2);
S7:GENMATRIX(S7,18,2);
H0:GENMATRIX(H0,18,54);
H1:GENMATRIX(H1,18,54);
H2:GENMATRIX(H2,18,54);
H3:GENMATRIX(H3,18,54);
H4:GENMATRIX(H4,18,54);
H5:GENMATRIX(H5,18,54);
H6:GENMATRIX(H6,18,54);
H7:GENMATRIX(H7,18,54);
H8:GENMATRIX(H8,18,54);
H9:GENMATRIX(H9,18,54);
H10:GENMATRIX(H10,18,54);
H11:GENMATRIX(H11,18,54);
H12:GENMATRIX(H12,18,54);
SS0:GENMATRIX(SS0,18,36);
SS1:GENMATRIX(SS1,18,36);
SS2:GENMATRIX(SS2,18,36);
SS3:GENMATRIX(SS3,18,36);
SS4:GENMATRIX(SS4,18,36);
SS5:GENMATRIX(SS5,18,36);
SS6:GENMATRIX(SS6,18,36);
SS7:GENMATRIX(SS7,18,36);
SS8:GENMATRIX(SS8,18,36);
SS9:GENMATRIX(SS9,18,36);
SS10:GENMATRIX(SS10,18,36);
SS11:GENMATRIX(SS11,18,36);
SS12:GENMATRIX(SS12,18,36);

SAVE("SPH-LSMAT.SV",L0,L1,L2,L3,L4,L5,L6,L7,S0,S1,S2,S3,S4,S5,S6,S7);
SAVE("SPH-HMAT.SV",H0,H1,H2,H3,H4,H5,H6,H7,H8,H9,H10,H11,H12);
SAVE("SPH-SSMAT.SV",SS0,SS1,SS2,SS3,SS4,SS5,SS6,SS7,SS8,SS9,SS10,SS11,SS12);

KILL(ALL)$

CLOSEFILE();
QUIT();
```

F.3 SPHK.MAC Input Deck

The MACSYMA input deck, SPHK.MAC, generates all the nonzero entries of the $[K]$ matrix for a spherical shell, including transverse shear effects.

```

WRITEFILE("SPH-STK.WF");
/*****
/*****
/*  MACSYMA ROUTINE FOR ELEMENTAL CODE GENERATION BY S. A. SCHIMMELS  */
/*  CREATED AS A PART OF AN AIR FORCE INSTITUTE OF TECHNOLOGY (AFIT)  */
/*      PhD PROGRAM IN AERONAUTICAL ENGINEERING --- MARCH 1993      */
/*      MACSYMA IS A REGISTERED TRADEMARK OF                          */
/*      THE MASSACHUSETTS INSTITUTE OF TECHNOLOGY                    */
/*                                                                    */
/*  PROGRAM SPH-STK.MAC: FOR A SPHERICAL SHELL.  CREATES ELEMENT    */
/*  INDEPENDENT STIFFNESS ARRAYS K & KS.                            */
/*****
/*****

/*****
/*  INITIALIZE MACSYMA PARAMETERS AND DECLARE VARIABLE PROPERTIES  */
/*****
[DYNAMALLOC:TRUE,DISKGC:TRUE,DERIVABBREV:TRUE,POWERDISP:TRUE]$

/*****
/*  GENERATE THE LINEAR ELEMENT-INDEPENDENT STIFFNESS ARRAY K.      */
/*****

/*****
/*  ASSEMBLE MATRIX KO  */
/*****

LOADFILE("SPH-LSMAT.SV");

L0:SUBST([K=K1,C=P1,D=P2],L0);
L1:SUBST([K=K1,C=P1,D=P2],L1);
L2:SUBST([K=K1,C=P1,D=P2],L2);
L3:SUBST([K=K1,C=P1,D=P2],L3);
L4:SUBST([K=K1,C=P1,D=P2],L4);
L5:SUBST([K=K1,C=P1,D=P2],L5);
L6:SUBST([K=K1,C=P1,D=P2],L6);
L7:SUBST([K=K1,C=P1,D=P2],L7);
L0T:TRANPOSE(L0);
L1T:TRANPOSE(L1);
L2T:TRANPOSE(L2);

```

```

L3T:TRANPOSE(L3);
L4T:TRANPOSE(L4);
L5T:TRANPOSE(L5);
L6T:TRANPOSE(L6);
L7T:TRANPOSE(L7);
KM:ZEROMATRIX(18,18)$
FOR II THRU 3 DO FOR JJ THRU 3 DO (PRINT(II,JJ),
KM:KM+A[II,JJ]*(COL(L0,II).ROW(L0T,JJ))+
  DD[II,JJ]*(COL(L1,II).ROW(L1T,JJ)+
    COL(L0,II).ROW(L2T,JJ)+COL(L2,II).ROW(L0T,JJ))+
  F[II,JJ]*(COL(L2,II).ROW(L2T,JJ)+
    COL(L1,II).ROW(L3T,JJ)+COL(L3,II).ROW(L1T,JJ)+
    COL(L0,II).ROW(L4T,JJ)+COL(L4,II).ROW(L0T,JJ))+
  H[II,JJ]*(COL(L3,II).ROW(L3T,JJ)+
    COL(L2,II).ROW(L4T,JJ)+COL(L4,II).ROW(L2T,JJ)+
    COL(L1,II).ROW(L5T,JJ)+COL(L5,II).ROW(L1T,JJ)+
    COL(L0,II).ROW(L6T,JJ)+COL(L6,II).ROW(L0T,JJ))+
  J[II,JJ]*(COL(L4,II).ROW(L4T,JJ)+
    COL(L3,II).ROW(L5T,JJ)+COL(L5,II).ROW(L3T,JJ)+
    COL(L2,II).ROW(L6T,JJ)+COL(L6,II).ROW(L2T,JJ)+
    COL(L1,II).ROW(L7T,JJ)+COL(L7,II).ROW(L1T,JJ))+
  L[II,JJ]*(COL(L5,II).ROW(L5T,JJ)+
    COL(L4,II).ROW(L6T,JJ)+COL(L6,II).ROW(L4T,JJ)+
    COL(L3,II).ROW(L7T,JJ)+COL(L7,II).ROW(L3T,JJ))+
  R[II,JJ]*(COL(L6,II).ROW(L6T,JJ)+
    COL(L5,II).ROW(L7T,JJ)+COL(L7,II).ROW(L5T,JJ)));

SAVE("SPH-K.SV",KM);

```

```

/*****/
/* THE FOLLOWING STATEMENTS GENERATE A FORTRAN STATEMENT FOR EACH */
/* NONZERO ELEMENT OF STK(I,J). THESE STATEMENTS ARE OF THE FORM */
/* STK(2,2)=A(1,1). EACH STATEMENT IS WRITTEN TO A SEPERATE FILE CALLED */
/* TT2XXX, WHERE XXX STARTS AT 001 FOR THE FIRST NONZERO ENTRY AND */
/* CONTINUES SEQUENTIALLY UNTIL ALL NONZERO ENTRIES THROUGH STK(18,18) */
/* ARE GENERATED. THE MACSYMA FUNTION GENTRAN WILL ALSO BREAK */
/* STATEMENTS EXCEEDING 800 INTO SHORTER EXPRESSIONS TO AVOID TOO MANY */
/* CONTINUATION LINES. MACSYMA AUTOMATICALLY MAKES CONTINUATION LINES */
/* COMPLETE WITH A LEGAL CHARACTER IN COLUMN 6. */
/*****/
K0:ZEROMATRIX(18,18)$
FOR III THRU 18 DO FOR JJJ:III THRU 18 DO
K0[III,JJJ]:KM[III,JJJ];
FRAME(I,J):=CONCAT(TK,EV(18*(I-1)+J+1000))$
FOR I THRU 18 DO FOR J:I THRU 18 DO
(IF K0[I,J]#0 THEN (PT:1,GENTRAN(PCSTK[EVAL(I),EVAL(J)]:EVAL(K0[I,J]),

```

```

[EVAL(FRAME(I,J)))]))$
IF PT#1 THEN GENTRAN(PT:EVAL(PT),[TT2000])$

/*****
/* GENERATE THE LINEAR ELEMENT-INDEPENDENT STIFFNESS ARRAY KS.          */
*****/

/*****
/* ASSEMBLE MATRIX KS          */
*****/

LOADFILE("SPH-LSMAT.SV");

S0:SUBST([K=K1,C=P1,D=P2],S0);
S1:SUBST([K=K1,C=P1,D=P2],S1);
S2:SUBST([K=K1,C=P1,D=P2],S2);
S3:SUBST([K=K1,C=P1,D=P2],S3);
S4:SUBST([K=K1,C=P1,D=P2],S4);
S5:SUBST([K=K1,C=P1,D=P2],S5);
S6:SUBST([K=K1,C=P1,D=P2],S6);
S7:SUBST([K=K1,C=P1,D=P2],S7);
S0T:TRANPOSE(S0);
S1T:TRANPOSE(S1);
S2T:TRANPOSE(S2);
S3T:TRANPOSE(S3);
S4T:TRANPOSE(S4);
S5T:TRANPOSE(S5);
S6T:TRANPOSE(S6);
S7T:TRANPOSE(S7);
KS:ZEROMATRIX(18,18)$
FOR II THRU 2 DO FOR JJ THRU 2 DO (PRINT(II,JJ),
KS:KS+AS[II,JJ]*(COL(S0,II).ROW(S0T,JJ))+
    DS[II,JJ]*(COL(S1,II).ROW(S1T,JJ)+
        COL(S0,II).ROW(S2T,JJ)+COL(S2,II).ROW(S0T,JJ))+
    FS[II,JJ]*(COL(S2,II).ROW(S2T,JJ)+
        COL(S1,II).ROW(S3T,JJ)+COL(S3,II).ROW(S1T,JJ)+
        COL(S0,II).ROW(S4T,JJ)+COL(S4,II).ROW(S0T,JJ))+
    HS[II,JJ]*(COL(S3,II).ROW(S3T,JJ)+
        COL(S2,II).ROW(S4T,JJ)+COL(S4,II).ROW(S2T,JJ)+
        COL(S1,II).ROW(S5T,JJ)+COL(S5,II).ROW(S1T,JJ)+
        COL(S0,II).ROW(S6T,JJ)+COL(S6,II).ROW(S0T,JJ))+
    JS[II,JJ]*(COL(S4,II).ROW(S4T,JJ)+
        COL(S3,II).ROW(S5T,JJ)+COL(S5,II).ROW(S3T,JJ)+
        COL(S2,II).ROW(S6T,JJ)+COL(S6,II).ROW(S2T,JJ)+
        COL(S1,II).ROW(S7T,JJ)+COL(S7,II).ROW(S1T,JJ))+
    LS[II,JJ]*(COL(S5,II).ROW(S5T,JJ)+
        COL(S4,II).ROW(S6T,JJ)+COL(S6,II).ROW(S4T,JJ)+

```



```
COL(S3,II).ROW(S7T,JJ)+COL(S7,II).ROW(S3T,JJ))+
RS[II,JJ]*(COL(S6,II).ROW(S6T,JJ)+
COL(S5,II).ROW(S7T,JJ)+COL(S7,II).ROW(S5T,JJ));

SAVE("SPH-KS.SV",KS);

/*****
/* THE FOLLOWING STATEMENTS GENERATE A FORTRAN STATEMENT FOR EACH */
/* NONZERO ELEMENT OF STKS(I,J). THESE STATEMENTS ARE OF THE FORM */
/* STKS(2,2)=A(1,1). EACH STATEMENT IS WRITTEN TO A SEPERATE FILE */
/* CALLED TT2XXX, WHERE XXX STARTS AT 001 FOR THE FIRST NONZERO ENTRY */
/* AND CONTINUES SEQUENTIALLY UNTIL ALL NONZERO ENTRIES THROUGH */
/* STKS(18,18) ARE GENERATED. THE MACSYMA FUNTION GENTRAN WILL ALSO */
/* BREAK STATEMENTS EXCEEDING 800 INTO SHORTER EXPRESSIONS TO AVOID TOO */
/* MANY CONTINUATION LINES. MACSYMA AUTOMATICALLY MAKES CONTINUATION */
/* LINES COMPLETE WITH A LEGAL CHARACTER IN COLUMN 6. */
*****/
K0:ZEROMATRIX(18,18)$
FOR III THRU 18 DO FOR JJJ:III THRU 18 DO
K0[III,JJJ]:KS[III,JJJ];
FRAME(I,J):=CONCAT(TKS,EV(18*(I-1)+J+2000));
FOR I THRU 18 DO FOR J:I THRU 18 DO
(IF K0[I,J]#0 THEN (PT:1,GENTRAN(PCSTKS[EVAL(I),EVAL(J)]:EVAL(K0[I,J]),
[EVAL(FRAME(I,J))]))))$
IF PT#1 THEN GENTRAN(PT:EVAL(PT),[TT2000])$

CLOSEFILE();
QUIT();
```

F.4 SPHN1.MAC Input Deck

The MACSYMA input deck, SPHN1.MAC, generates all the nonzero entries of the $[\hat{N}_1]$ matrix for a spherical shell, including transverse shear effects.

```

WRITEFILE("SPHN1.WF");
/*****
/*****
/*  MACSYMA ROUTINE FOR ELEMENTAL CODE GENERATION BY S. A. SCHIMMELS */
/*  CREATED AS A PART OF AN AIR FORCE INSTITUTE OF TECHNOLOGY (AFIT) */
/*      PhD PROGRAM IN AERONAUTICAL ENGINEERING --- MARCH 1993 */
/*      MACSYMA IS A REGISTERED TRADEMARK OF */
/*      THE MASSACHUSETTS INSTITUTE OF TECHNOLOGY */
/*      */
/*  PROGRAM SPHN1.MAC: FOR A SPHERICAL SHELL.  CREATES ELEMENT */
/*  INDEPENDENT STIFFNESS ARRAYS N1 & N1S. */
/*****
/*****

/*****
/*  INITIALIZE MACSYMA PARAMETERS AND DECLARE VARIABLE PROPERTIES */
/*****
[DYNAMALLOC:TRUE,DISKGC:TRUE,DERIVABBREV:TRUE,POWERDISP:TRUE]$

/*****
/*  GENERATE THE NONLINEAR ELEMENT-INDEPENDENT STIFFNESS ARRAY N1. */
/*****

/*****
/*  ASSEMBLE MATRIX N1 */
/*****
TQ:MATRIX([Q(1),Q(2),Q(3),Q(4),Q(5),Q(6),Q(7),Q(8),Q(9),Q(10),
          Q(11),Q(12),Q(13),Q(14),Q(15),Q(16),Q(17),Q(18)]);
Q:TRANPOSE(TQ);

LOADFILE("SPH-LSMAT.SV");
LOADFILE("SPH-HMAT.SV");

L0:SUBST([K=K1,C=P1,D=P2],L0)$
L1:SUBST([K=K1,C=P1,D=P2],L1)$
L2:SUBST([K=K1,C=P1,D=P2],L2)$
L3:SUBST([K=K1,C=P1,D=P2],L3)$
L4:SUBST([K=K1,C=P1,D=P2],L4)$

```

```

L5:SUBST([K=K1,C=P1,D=P2],L5)$
L6:SUBST([K=K1,C=P1,D=P2],L6)$
L7:SUBST([K=K1,C=P1,D=P2],L7)$
L0T:TRANPOSE(L0)$
L1T:TRANPOSE(L1)$
L2T:TRANPOSE(L2)$
L3T:TRANPOSE(L3)$
L4T:TRANPOSE(L4)$
L5T:TRANPOSE(L5)$
L6T:TRANPOSE(L6)$
L7T:TRANPOSE(L7)$
H0:SUBST([K=K1,C=P1,D=P2],H0)$
H1:SUBST([K=K1,C=P1,D=P2],H1)$
H2:SUBST([K=K1,C=P1,D=P2],H2)$
H3:SUBST([K=K1,C=P1,D=P2],H3)$
H4:SUBST([K=K1,C=P1,D=P2],H4)$
H5:SUBST([K=K1,C=P1,D=P2],H5)$
H6:SUBST([K=K1,C=P1,D=P2],H6)$
H7:SUBST([K=K1,C=P1,D=P2],H7)$
H8:SUBST([K=K1,C=P1,D=P2],H8)$
H9:SUBST([K=K1,C=P1,D=P2],H9)$
H10:SUBST([K=K1,C=P1,D=P2],H10)$
H11:SUBST([K=K1,C=P1,D=P2],H11)$
H12:SUBST([K=K1,C=P1,D=P2],H12)$

N1:ZEROMATRIX(18,18)$

FOR II THRU 3 DO FOR JJ THRU 3 DO (PRINT(II,JJ),
(I1:3*(-9*II^2+33*II-12), J2:3*(9*JJ^2-39*JJ+48),
J1:3*(-9*JJ^2+33*JJ-12), I2:3*(9*II^2-39*II+48),
SUBI0:SUBMATRIX(H0,I1,I1-1,I1-2,I1-3,I1-4,I1-5,I1-6,I1-7,I1-8,I1-9,
I1-10,I1-11,I1-12,I1-13,I1-14,I1-15,I1-16,I1-17,
I2,I2-1,I2-2,I2-3,I2-4,I2-5,I2-6,I2-7,I2-8,I2-9,
I2-10,I2-11,I2-12,I2-13,I2-14,I2-15,I2-16,I2-17),
SUBJ0:SUBMATRIX(H0,J1,J1-1,J1-2,J1-3,J1-4,J1-5,J1-6,J1-7,J1-8,J1-9,
J1-10,J1-11,J1-12,J1-13,J1-14,J1-15,J1-16,J1-17,
J2,J2-1,J2-2,J2-3,J2-4,J2-5,J2-6,J2-7,J2-8,J2-9,
J2-10,J2-11,J2-12,J2-13,J2-14,J2-15,J2-16,J2-17),
PRINT("H0",II,JJ),
SUBI1:SUBMATRIX(H1,I1,I1-1,I1-2,I1-3,I1-4,I1-5,I1-6,I1-7,I1-8,I1-9,
I1-10,I1-11,I1-12,I1-13,I1-14,I1-15,I1-16,I1-17,
I2,I2-1,I2-2,I2-3,I2-4,I2-5,I2-6,I2-7,I2-8,I2-9,
I2-10,I2-11,I2-12,I2-13,I2-14,I2-15,I2-16,I2-17),
SUBJ1:SUBMATRIX(H1,J1,J1-1,J1-2,J1-3,J1-4,J1-5,J1-6,J1-7,J1-8,J1-9,
J1-10,J1-11,J1-12,J1-13,J1-14,J1-15,J1-16,J1-17,
J2,J2-1,J2-2,J2-3,J2-4,J2-5,J2-6,J2-7,J2-8,J2-9,

```

```

J2-10,J2-11,J2-12,J2-13,J2-14,J2-15,J2-16,J2-17) ,
PRINT("H1",II,JJ) ,
SUBI2:SUBMATRIX(H2,I1,I1-1,I1-2,I1-3,I1-4,I1-5,I1-6,I1-7,I1-8,I1-9,
I1-10,I1-11,I1-12,I1-13,I1-14,I1-15,I1-16,I1-17,
I2,I2-1,I2-2,I2-3,I2-4,I2-5,I2-6,I2-7,I2-8,I2-9,
I2-10,I2-11,I2-12,I2-13,I2-14,I2-15,I2-16,I2-17) ,
SUBJ2:SUBMATRIX(H2,J1,J1-1,J1-2,J1-3,J1-4,J1-5,J1-6,J1-7,J1-8,J1-9,
J1-10,J1-11,J1-12,J1-13,J1-14,J1-15,J1-16,J1-17,
J2,J2-1,J2-2,J2-3,J2-4,J2-5,J2-6,J2-7,J2-8,J2-9,
J2-10,J2-11,J2-12,J2-13,J2-14,J2-15,J2-16,J2-17) ,
PRINT("H2",II,JJ) ,
SUBI3:SUBMATRIX(H3,I1,I1-1,I1-2,I1-3,I1-4,I1-5,I1-6,I1-7,I1-8,I1-9,
I1-10,I1-11,I1-12,I1-13,I1-14,I1-15,I1-16,I1-17,
I2,I2-1,I2-2,I2-3,I2-4,I2-5,I2-6,I2-7,I2-8,I2-9,
I2-10,I2-11,I2-12,I2-13,I2-14,I2-15,I2-16,I2-17) ,
SUBJ3:SUBMATRIX(H3,J1,J1-1,J1-2,J1-3,J1-4,J1-5,J1-6,J1-7,J1-8,J1-9,
J1-10,J1-11,J1-12,J1-13,J1-14,J1-15,J1-16,J1-17,
J2,J2-1,J2-2,J2-3,J2-4,J2-5,J2-6,J2-7,J2-8,J2-9,
J2-10,J2-11,J2-12,J2-13,J2-14,J2-15,J2-16,J2-17) ,
PRINT("H3",II,JJ) ,
SUBI4:SUBMATRIX(H4,I1,I1-1,I1-2,I1-3,I1-4,I1-5,I1-6,I1-7,I1-8,I1-9,
I1-10,I1-11,I1-12,I1-13,I1-14,I1-15,I1-16,I1-17,
I2,I2-1,I2-2,I2-3,I2-4,I2-5,I2-6,I2-7,I2-8,I2-9,
I2-10,I2-11,I2-12,I2-13,I2-14,I2-15,I2-16,I2-17) ,
SUBJ4:SUBMATRIX(H4,J1,J1-1,J1-2,J1-3,J1-4,J1-5,J1-6,J1-7,J1-8,J1-9,
J1-10,J1-11,J1-12,J1-13,J1-14,J1-15,J1-16,J1-17,
J2,J2-1,J2-2,J2-3,J2-4,J2-5,J2-6,J2-7,J2-8,J2-9,
J2-10,J2-11,J2-12,J2-13,J2-14,J2-15,J2-16,J2-17) ,
PRINT("H4",II,JJ) ,
SUBI5:SUBMATRIX(H5,I1,I1-1,I1-2,I1-3,I1-4,I1-5,I1-6,I1-7,I1-8,I1-9,
I1-10,I1-11,I1-12,I1-13,I1-14,I1-15,I1-16,I1-17,
I2,I2-1,I2-2,I2-3,I2-4,I2-5,I2-6,I2-7,I2-8,I2-9,
I2-10,I2-11,I2-12,I2-13,I2-14,I2-15,I2-16,I2-17) ,
SUBJ5:SUBMATRIX(H5,J1,J1-1,J1-2,J1-3,J1-4,J1-5,J1-6,J1-7,J1-8,J1-9,
J1-10,J1-11,J1-12,J1-13,J1-14,J1-15,J1-16,J1-17,
J2,J2-1,J2-2,J2-3,J2-4,J2-5,J2-6,J2-7,J2-8,J2-9,
J2-10,J2-11,J2-12,J2-13,J2-14,J2-15,J2-16,J2-17) ,
PRINT("H5",II,JJ) ,
SUBI6:SUBMATRIX(H6,I1,I1-1,I1-2,I1-3,I1-4,I1-5,I1-6,I1-7,I1-8,I1-9,
I1-10,I1-11,I1-12,I1-13,I1-14,I1-15,I1-16,I1-17,
I2,I2-1,I2-2,I2-3,I2-4,I2-5,I2-6,I2-7,I2-8,I2-9,
I2-10,I2-11,I2-12,I2-13,I2-14,I2-15,I2-16,I2-17) ,
SUBJ6:SUBMATRIX(H6,J1,J1-1,J1-2,J1-3,J1-4,J1-5,J1-6,J1-7,J1-8,J1-9,
J1-10,J1-11,J1-12,J1-13,J1-14,J1-15,J1-16,J1-17,
J2,J2-1,J2-2,J2-3,J2-4,J2-5,J2-6,J2-7,J2-8,J2-9,
J2-10,J2-11,J2-12,J2-13,J2-14,J2-15,J2-16,J2-17) ,

```

```
PRINT("H6", II, JJ),
SUBI7: SUBMATRIX(H7, I1, I1-1, I1-2, I1-3, I1-4, I1-5, I1-6, I1-7, I1-8, I1-9,
                 I1-10, I1-11, I1-12, I1-13, I1-14, I1-15, I1-16, I1-17,
                 I2, I2-1, I2-2, I2-3, I2-4, I2-5, I2-6, I2-7, I2-8, I2-9,
                 I2-10, I2-11, I2-12, I2-13, I2-14, I2-15, I2-16, I2-17),
SUBJ7: SUBMATRIX(H7, J1, J1-1, J1-2, J1-3, J1-4, J1-5, J1-6, J1-7, J1-8, J1-9,
                 J1-10, J1-11, J1-12, J1-13, J1-14, J1-15, J1-16, J1-17,
                 J2, J2-1, J2-2, J2-3, J2-4, J2-5, J2-6, J2-7, J2-8, J2-9,
                 J2-10, J2-11, J2-12, J2-13, J2-14, J2-15, J2-16, J2-17),

PRINT("H7", II, JJ),
SUBI8: SUBMATRIX(H8, I1, I1-1, I1-2, I1-3, I1-4, I1-5, I1-6, I1-7, I1-8, I1-9,
                 I1-10, I1-11, I1-12, I1-13, I1-14, I1-15, I1-16, I1-17,
                 I2, I2-1, I2-2, I2-3, I2-4, I2-5, I2-6, I2-7, I2-8, I2-9,
                 I2-10, I2-11, I2-12, I2-13, I2-14, I2-15, I2-16, I2-17),
SUBJ8: SUBMATRIX(H8, J1, J1-1, J1-2, J1-3, J1-4, J1-5, J1-6, J1-7, J1-8, J1-9,
                 J1-10, J1-11, J1-12, J1-13, J1-14, J1-15, J1-16, J1-17,
                 J2, J2-1, J2-2, J2-3, J2-4, J2-5, J2-6, J2-7, J2-8, J2-9,
                 J2-10, J2-11, J2-12, J2-13, J2-14, J2-15, J2-16, J2-17),

PRINT("H8", II, JJ),
SUBI9: SUBMATRIX(H9, I1, I1-1, I1-2, I1-3, I1-4, I1-5, I1-6, I1-7, I1-8, I1-9,
                 I1-10, I1-11, I1-12, I1-13, I1-14, I1-15, I1-16, I1-17,
                 I2, I2-1, I2-2, I2-3, I2-4, I2-5, I2-6, I2-7, I2-8, I2-9,
                 I2-10, I2-11, I2-12, I2-13, I2-14, I2-15, I2-16, I2-17),
SUBJ9: SUBMATRIX(H9, J1, J1-1, J1-2, J1-3, J1-4, J1-5, J1-6, J1-7, J1-8, J1-9,
                 J1-10, J1-11, J1-12, J1-13, J1-14, J1-15, J1-16, J1-17,
                 J2, J2-1, J2-2, J2-3, J2-4, J2-5, J2-6, J2-7, J2-8, J2-9,
                 J2-10, J2-11, J2-12, J2-13, J2-14, J2-15, J2-16, J2-17),

PRINT("H9", II, JJ),
SUBI10: SUBMATRIX(H10, I1, I1-1, I1-2, I1-3, I1-4, I1-5, I1-6, I1-7, I1-8, I1-9,
                 I1-10, I1-11, I1-12, I1-13, I1-14, I1-15, I1-16, I1-17,
                 I2, I2-1, I2-2, I2-3, I2-4, I2-5, I2-6, I2-7, I2-8, I2-9,
                 I2-10, I2-11, I2-12, I2-13, I2-14, I2-15, I2-16, I2-17),
SUBJ10: SUBMATRIX(H10, J1, J1-1, J1-2, J1-3, J1-4, J1-5, J1-6, J1-7, J1-8, J1-9,
                 J1-10, J1-11, J1-12, J1-13, J1-14, J1-15, J1-16, J1-17,
                 J2, J2-1, J2-2, J2-3, J2-4, J2-5, J2-6, J2-7, J2-8, J2-9,
                 J2-10, J2-11, J2-12, J2-13, J2-14, J2-15, J2-16, J2-17),

PRINT("H10", II, JJ),
SUBI11: SUBMATRIX(H11, I1, I1-1, I1-2, I1-3, I1-4, I1-5, I1-6, I1-7, I1-8, I1-9,
                 I1-10, I1-11, I1-12, I1-13, I1-14, I1-15, I1-16, I1-17,
                 I2, I2-1, I2-2, I2-3, I2-4, I2-5, I2-6, I2-7, I2-8, I2-9,
                 I2-10, I2-11, I2-12, I2-13, I2-14, I2-15, I2-16, I2-17),
SUBJ11: SUBMATRIX(H11, J1, J1-1, J1-2, J1-3, J1-4, J1-5, J1-6, J1-7, J1-8, J1-9,
                 J1-10, J1-11, J1-12, J1-13, J1-14, J1-15, J1-16, J1-17,
                 J2, J2-1, J2-2, J2-3, J2-4, J2-5, J2-6, J2-7, J2-8, J2-9,
                 J2-10, J2-11, J2-12, J2-13, J2-14, J2-15, J2-16, J2-17),

PRINT("H11", II, JJ),
```

```

SUBI12:SUBMATRIX(H12,I1,I1-1,I1-2,I1-3,I1-4,I1-5,I1-6,I1-7,I1-8,I1-9,
                I1-10,I1-11,I1-12,I1-13,I1-14,I1-15,I1-16,I1-17,
                I2,I2-1,I2-2,I2-3,I2-4,I2-5,I2-6,I2-7,I2-8,I2-9,
                I2-10,I2-11,I2-12,I2-13,I2-14,I2-15,I2-16,I2-17),
SUBJ12:SUBMATRIX(H12,J1,J1-1,J1-2,J1-3,J1-4,J1-5,J1-6,J1-7,J1-8,J1-9,
                J1-10,J1-11,J1-12,J1-13,J1-14,J1-15,J1-16,J1-17,
                J2,J2-1,J2-2,J2-3,J2-4,J2-5,J2-6,J2-7,J2-8,J2-9,
                J2-10,J2-11,J2-12,J2-13,J2-14,J2-15,J2-16,J2-17),

PRINT("H12",II,JJ),
N1:N1+A[II,JJ]*(
COL(L0,II).TQ.SUBJ0+(TQ.COL(L0,II))*SUBJ0+SUBI0.Q.ROW(L0T,JJ)),
PRINT("N1A",II,JJ),
N1:N1+DD[II,JJ]*(
COL(L0,II).TQ.SUBJ2+(TQ.COL(L0,II))*SUBJ2+SUBI2.Q.ROW(L0T,JJ)+
COL(L1,II).TQ.SUBJ1+(TQ.COL(L1,II))*SUBJ1+SUBI1.Q.ROW(L1T,JJ)+
COL(L2,II).TQ.SUBJ0+(TQ.COL(L2,II))*SUBJ0+SUBI0.Q.ROW(L2T,JJ)),
PRINT("N1DD",II,JJ),
N1:N1+F[II,JJ]*(
COL(L0,II).TQ.SUBJ4+(TQ.COL(L0,II))*SUBJ4+SUBI4.Q.ROW(L0T,JJ)+
COL(L1,II).TQ.SUBJ3+(TQ.COL(L1,II))*SUBJ3+SUBI3.Q.ROW(L1T,JJ)+
COL(L2,II).TQ.SUBJ2+(TQ.COL(L2,II))*SUBJ2+SUBI2.Q.ROW(L2T,JJ)+
COL(L3,II).TQ.SUBJ1+(TQ.COL(L3,II))*SUBJ1+SUBI1.Q.ROW(L3T,JJ)+
COL(L4,II).TQ.SUBJ0+(TQ.COL(L4,II))*SUBJ0+SUBI0.Q.ROW(L4T,JJ)),
PRINT("N1F",II,JJ),
N1:N1+H[II,JJ]*(
COL(L0,II).TQ.SUBJ6+(TQ.COL(L0,II))*SUBJ6+SUBI6.Q.ROW(L0T,JJ)+
COL(L1,II).TQ.SUBJ5+(TQ.COL(L1,II))*SUBJ5+SUBI5.Q.ROW(L1T,JJ)+
COL(L2,II).TQ.SUBJ4+(TQ.COL(L2,II))*SUBJ4+SUBI4.Q.ROW(L2T,JJ)+
COL(L3,II).TQ.SUBJ3+(TQ.COL(L3,II))*SUBJ3+SUBI3.Q.ROW(L3T,JJ)+
COL(L4,II).TQ.SUBJ2+(TQ.COL(L4,II))*SUBJ2+SUBI2.Q.ROW(L4T,JJ)+
COL(L5,II).TQ.SUBJ1+(TQ.COL(L5,II))*SUBJ1+SUBI1.Q.ROW(L5T,JJ)+
COL(L6,II).TQ.SUBJ0+(TQ.COL(L6,II))*SUBJ0+SUBI0.Q.ROW(L6T,JJ)),
PRINT("N1H",II,JJ),
N1:N1+J[II,JJ]*(
COL(L0,II).TQ.SUBJ8+(TQ.COL(L0,II))*SUBJ8+SUBI8.Q.ROW(L0T,JJ)+
COL(L1,II).TQ.SUBJ7+(TQ.COL(L1,II))*SUBJ7+SUBI7.Q.ROW(L1T,JJ)+
COL(L2,II).TQ.SUBJ6+(TQ.COL(L2,II))*SUBJ6+SUBI6.Q.ROW(L2T,JJ)+
COL(L3,II).TQ.SUBJ5+(TQ.COL(L3,II))*SUBJ5+SUBI5.Q.ROW(L3T,JJ)+
COL(L4,II).TQ.SUBJ4+(TQ.COL(L4,II))*SUBJ4+SUBI4.Q.ROW(L4T,JJ)+
COL(L5,II).TQ.SUBJ3+(TQ.COL(L5,II))*SUBJ3+SUBI3.Q.ROW(L5T,JJ)+
COL(L6,II).TQ.SUBJ2+(TQ.COL(L6,II))*SUBJ2+SUBI2.Q.ROW(L6T,JJ)+
COL(L7,II).TQ.SUBJ1+(TQ.COL(L7,II))*SUBJ1+SUBI1.Q.ROW(L7T,JJ)),
PRINT("N1J",II,JJ),
N1:N1+L[II,JJ]*(
COL(L0,II).TQ.SUBJ10+(TQ.COL(L0,II))*SUBJ10+SUBI10.Q.ROW(L0T,JJ)+
COL(L1,II).TQ.SUBJ9+(TQ.COL(L1,II))*SUBJ9+SUBI9.Q.ROW(L1T,JJ)+

```

```

COL(L2,II).TQ.SUBJ8+(TQ.COL(L2,II))*SUBJ8+SUBI8.Q.ROW(L2T,JJ)+
COL(L3,II).TQ.SUBJ7+(TQ.COL(L3,II))*SUBJ7+SUBI7.Q.ROW(L3T,JJ)+
COL(L4,II).TQ.SUBJ6+(TQ.COL(L4,II))*SUBJ6+SUBI6.Q.ROW(L4T,JJ)+
COL(L5,II).TQ.SUBJ5+(TQ.COL(L5,II))*SUBJ5+SUBI5.Q.ROW(L5T,JJ)+
COL(L6,II).TQ.SUBJ4+(TQ.COL(L6,II))*SUBJ4+SUBI4.Q.ROW(L6T,JJ)+
COL(L7,II).TQ.SUBJ3+(TQ.COL(L7,II))*SUBJ3+SUBI3.Q.ROW(L7T,JJ)),
PRINT("N1L",II,JJ),
N1:N1+R[II,JJ]*(
COL(L0,II).TQ.SUBJ12+(TQ.COL(L0,II))*SUBJ12+SUBI12.Q.ROW(L0T,JJ)+
COL(L1,II).TQ.SUBJ11+(TQ.COL(L1,II))*SUBJ11+SUBI11.Q.ROW(L1T,JJ)+
COL(L2,II).TQ.SUBJ10+(TQ.COL(L2,II))*SUBJ10+SUBI10.Q.ROW(L2T,JJ)+
COL(L3,II).TQ.SUBJ9+(TQ.COL(L3,II))*SUBJ9+SUBI9.Q.ROW(L3T,JJ)+
COL(L4,II).TQ.SUBJ8+(TQ.COL(L4,II))*SUBJ8+SUBI8.Q.ROW(L4T,JJ)+
COL(L5,II).TQ.SUBJ7+(TQ.COL(L5,II))*SUBJ7+SUBI7.Q.ROW(L5T,JJ)+
COL(L6,II).TQ.SUBJ6+(TQ.COL(L6,II))*SUBJ6+SUBI6.Q.ROW(L6T,JJ)+
COL(L7,II).TQ.SUBJ5+(TQ.COL(L7,II))*SUBJ5+SUBI5.Q.ROW(L7T,JJ)),
PRINT("N1R",II,JJ),
N1:N1+T[II,JJ]*(
COL(L2,II).TQ.SUBJ12+(TQ.COL(L2,II))*SUBJ12+SUBI12.Q.ROW(L2T,JJ)+
COL(L3,II).TQ.SUBJ11+(TQ.COL(L3,II))*SUBJ11+SUBI11.Q.ROW(L3T,JJ)+
COL(L4,II).TQ.SUBJ10+(TQ.COL(L4,II))*SUBJ10+SUBI10.Q.ROW(L4T,JJ)+
COL(L5,II).TQ.SUBJ9+(TQ.COL(L5,II))*SUBJ9+SUBI9.Q.ROW(L5T,JJ)+
COL(L6,II).TQ.SUBJ8+(TQ.COL(L6,II))*SUBJ8+SUBI8.Q.ROW(L6T,JJ)+
COL(L7,II).TQ.SUBJ7+(TQ.COL(L7,II))*SUBJ7+SUBI7.Q.ROW(L7T,JJ)),
PRINT("N1T",II,JJ),
N1:N1+XH[II,JJ]*(
COL(L4,II).TQ.SUBJ12+(TQ.COL(L4,II))*SUBJ12+SUBI12.Q.ROW(L4T,JJ)+
COL(L5,II).TQ.SUBJ11+(TQ.COL(L5,II))*SUBJ11+SUBI11.Q.ROW(L5T,JJ)+
COL(L6,II).TQ.SUBJ10+(TQ.COL(L6,II))*SUBJ10+SUBI10.Q.ROW(L6T,JJ)+
COL(L7,II).TQ.SUBJ9+(TQ.COL(L7,II))*SUBJ9+SUBI9.Q.ROW(L7T,JJ)),
PRINT("N1XH",II,JJ),
N1:N1+XJ[II,JJ]*(
COL(L6,II).TQ.SUBJ12+(TQ.COL(L6,II))*SUBJ12+SUBI12.Q.ROW(L6T,JJ)+
COL(L7,II).TQ.SUBJ11+(TQ.COL(L7,II))*SUBJ11+SUBI11.Q.ROW(L7T,JJ)),
PRINT("N1XJ",II,JJ),
KILL(SUBJ12,SUBI12,SUBJ11,SUBI11,SUBJ10,SUBI10),
KILL(SUBJ0,SUBJ1,SUBJ2,SUBJ3,SUBJ4,SUBJ5,SUBJ6,SUBJ7,SUBJ8,SUBJ9),
KILL(SUBI0,SUBI1,SUBI2,SUBI3,SUBI4,SUBI5,SUBI6,SUBI7,SUBI8,SUBI9)))$

SAVE("SPH-N1.SV",N1);

KILL(L0,L1,L2,L3,L4,L5,L6,L7,L0T,L1T,L2T,L3T,L4T,L5T,L6T,L7T)$
KILL(H0,H1,H2,H3,H4,H5,H6,H7,H8,H9,H10,H11,H12)$
N1SYM:ZEROMATRIX(18,18)$
FOR II THRU 18 DO FOR JJ:II THRU 18 DO N1SYM[II,JJ]:N1[II,JJ]$
PRINT("SYMMETRIC N1 FORMED")$

```

```

KILL(N1)$
N1:ZEROMATRIX(18,18)$
KILL(Q,TQ)$

/*****
/* THE FOLLOWING STATEMENTS GENERATE A FORTRAN STATEMENT FOR EACH */
/* NONZERO ELEMENT OF SN1(I,J). THESE STATEMENTS ARE OF THE FORM */
/* SN1(2,2)=A(1,1). EACH STATEMENT IS WRITTEN TO A SEPERATE FILE CALLED*/
/* TT2XXX, WHERE XXX STARTS AT 001 FOR THE FIRST NONZERO ENTRY AND */
/* CONTINUES SEQUENTIALLY UNTIL ALL NONZERO ENTRIES THROUGH SN1(18,18) */
/* ARE GENERATED. THE MACSYMA FUNTION GENTRAN WILL ALSO BREAK */
/* STATEMENTS EXCEEDING 800 INTO SHORTER EXPRESSIONS TO AVOID TOO MANY */
/* CONTINUATION LINES. MACSYMA AUTOMATICALLY MAKES CONTINUATION LINES */
/* COMPLETE WITH A LEGAL CHARACTER IN COLUMN 6. */
*****/

FOR II THRU 18 DO FOR JJ:II THRU 18 DO
N1[II,JJ]:FACTOROUT(N1SYM[II,JJ],Q(1),Q(2),Q(3),Q(4),Q(5),Q(6),Q(7),Q(8),
Q(9),Q(10),Q(11),Q(12),Q(13),Q(14),Q(15),Q(16),Q(17),Q(18))$
FRAME(I,J):=CONCAT(TN,EV(18*(I-1)+J+1000))$
FOR I THRU 18 DO FOR J:I THRU 18 DO
(IF N1[I,J]#0 THEN (P1:1,GENTRAN(PCSN1[EVAL(I),EVAL(J)]:EVAL(N1[I,J]),
[EVAL(FRAME(I,J))]))$
IF PT#1 THEN GENTRAN(PT:EVAL(PT),[TT2000])$

/*****
/* GENERATE THE NONLINEAR ELEMENT-INDEPENDENT STIFFNESS ARRAY N1S. */
*****/

/*****
/* ASSEMBLE MATRIX N1S */
*****/

TQ:MATRIX([Q(1),Q(2),Q(3),Q(4),Q(5),Q(6),Q(7),Q(8),Q(9),Q(10),
Q(11),Q(12),Q(13),Q(14),Q(15),Q(16),Q(17),Q(18)]);
Q:TRANPOSE(TQ);

LOADFILE("SPH-LSMAT.SV");

S0:SUBST([K=K1,C=P1,D=P2],S0)$
S1:SUBST([K=K1,C=P1,D=P2],S1)$
S2:SUBST([K=K1,C=P1,D=P2],S2)$
S3:SUBST([K=K1,C=P1,D=P2],S3)$
S4:SUBST([K=K1,C=P1,D=P2],S4)$
S5:SUBST([K=K1,C=P1,D=P2],S5)$
S6:SUBST([K=K1,C=P1,D=P2],S6)$
S7:SUBST([K=K1,C=P1,D=P2],S7)$

```



```
S0T:TRANSPOSE(S0)$
S1T:TRANSPOSE(S1)$
S2T:TRANSPOSE(S2)$
S3T:TRANSPOSE(S3)$
S4T:TRANSPOSE(S4)$
S5T:TRANSPOSE(S5)$
S6T:TRANSPOSE(S6)$
S7T:TRANSPOSE(S7)$

LOADFILE("SPH-SSMAT.SV");

SS0:SUBST([K=K1,C=P1,D=P2],SS0)$
SS1:SUBST([K=K1,C=P1,D=P2],SS1)$
SS2:SUBST([K=K1,C=P1,D=P2],SS2)$
SS3:SUBST([K=K1,C=P1,D=P2],SS3)$
SS4:SUBST([K=K1,C=P1,D=P2],SS4)$
SS5:SUBST([K=K1,C=P1,D=P2],SS5)$
SS6:SUBST([K=K1,C=P1,D=P2],SS6)$
SS7:SUBST([K=K1,C=P1,D=P2],SS7)$
SS8:SUBST([K=K1,C=P1,D=P2],SS8)$
SS9:SUBST([K=K1,C=P1,D=P2],SS9)$
SS10:SUBST([K=K1,C=P1,D=P2],SS10)$
SS11:SUBST([K=K1,C=P1,D=P2],SS11)$
SS12:SUBST([K=K1,C=P1,D=P2],SS12)$

N1S:ZEROMATRIX(18,18)$

FOR II THRU 2 DO FOR JJ THRU 2 DO (PRINT(II,JJ),
J2:3*(9*(JJ+1)^2-39*(JJ+1)+48),
I2:3*(9*(II+1)^2-39*(II+1)+48),
SUBIS0:SUBMATRIX(SS0,I2,I2-1,I2-2,I2-3,I2-4,I2-5,I2-6,I2-7,I2-8,I2-9,
I2-10,I2-11,I2-12,I2-13,I2-14,I2-15,I2-16,I2-17),
SUBJS0:SUBMATRIX(SS0,J2,J2-1,J2-2,J2-3,J2-4,J2-5,J2-6,J2-7,J2-8,J2-9,
J2-10,J2-11,J2-12,J2-13,J2-14,J2-15,J2-16,J2-17),
PRINT("SS0",II,JJ),
SUBIS1:SUBMATRIX(SS1,I2,I2-1,I2-2,I2-3,I2-4,I2-5,I2-6,I2-7,I2-8,I2-9,
I2-10,I2-11,I2-12,I2-13,I2-14,I2-15,I2-16,I2-17),
SUBJS1:SUBMATRIX(SS1,J2,J2-1,J2-2,J2-3,J2-4,J2-5,J2-6,J2-7,J2-8,J2-9,
J2-10,J2-11,J2-12,J2-13,J2-14,J2-15,J2-16,J2-17),
PRINT("SS1",II,JJ),
SUBIS2:SUBMATRIX(SS2,I2,I2-1,I2-2,I2-3,I2-4,I2-5,I2-6,I2-7,I2-8,I2-9,
I2-10,I2-11,I2-12,I2-13,I2-14,I2-15,I2-16,I2-17),
SUBJS2:SUBMATRIX(SS2,J2,J2-1,J2-2,J2-3,J2-4,J2-5,J2-6,J2-7,J2-8,J2-9,
J2-10,J2-11,J2-12,J2-13,J2-14,J2-15,J2-16,J2-17),
PRINT("SS2",II,JJ),
```

```

SUBIS3: SUBMATRIX(SS3, I2, I2-1, I2-2, I2-3, I2-4, I2-5, I2-6, I2-7, I2-8, I2-9,
                  I2-10, I2-11, I2-12, I2-13, I2-14, I2-15, I2-16, I2-17),
SUBJS3: SUBMATRIX(SS3, J2, J2-1, J2-2, J2-3, J2-4, J2-5, J2-6, J2-7, J2-8, J2-9,
                  J2-10, J2-11, J2-12, J2-13, J2-14, J2-15, J2-16, J2-17),
PRINT("SS3", II, JJ),
SUBIS4: SUBMATRIX(SS4, I2, I2-1, I2-2, I2-3, I2-4, I2-5, I2-6, I2-7, I2-8, I2-9,
                  I2-10, I2-11, I2-12, I2-13, I2-14, I2-15, I2-16, I2-17),
SUBJS4: SUBMATRIX(SS4, J2, J2-1, J2-2, J2-3, J2-4, J2-5, J2-6, J2-7, J2-8, J2-9,
                  J2-10, J2-11, J2-12, J2-13, J2-14, J2-15, J2-16, J2-17),
PRINT("SS4", II, JJ),
SUBIS5: SUBMATRIX(SS5, I2, I2-1, I2-2, I2-3, I2-4, I2-5, I2-6, I2-7, I2-8, I2-9,
                  I2-10, I2-11, I2-12, I2-13, I2-14, I2-15, I2-16, I2-17),
SUBJS5: SUBMATRIX(SS5, J2, J2-1, J2-2, J2-3, J2-4, J2-5, J2-6, J2-7, J2-8, J2-9,
                  J2-10, J2-11, J2-12, J2-13, J2-14, J2-15, J2-16, J2-17),
PRINT("SS5", II, JJ),
SUBIS6: SUBMATRIX(SS6, I2, I2-1, I2-2, I2-3, I2-4, I2-5, I2-6, I2-7, I2-8, I2-9,
                  I2-10, I2-11, I2-12, I2-13, I2-14, I2-15, I2-16, I2-17),
SUBJS6: SUBMATRIX(SS6, J2, J2-1, J2-2, J2-3, J2-4, J2-5, J2-6, J2-7, J2-8, J2-9,
                  J2-10, J2-11, J2-12, J2-13, J2-14, J2-15, J2-16, J2-17),
PRINT("SS6", II, JJ),
SUBIS7: SUBMATRIX(SS7, I2, I2-1, I2-2, I2-3, I2-4, I2-5, I2-6, I2-7, I2-8, I2-9,
                  I2-10, I2-11, I2-12, I2-13, I2-14, I2-15, I2-16, I2-17),
SUBJS7: SUBMATRIX(SS7, J2, J2-1, J2-2, J2-3, J2-4, J2-5, J2-6, J2-7, J2-8, J2-9,
                  J2-10, J2-11, J2-12, J2-13, J2-14, J2-15, J2-16, J2-17),
PRINT("SS7", II, JJ),
SUBIS8: SUBMATRIX(SS8, I2, I2-1, I2-2, I2-3, I2-4, I2-5, I2-6, I2-7, I2-8, I2-9,
                  I2-10, I2-11, I2-12, I2-13, I2-14, I2-15, I2-16, I2-17),
SUBJS8: SUBMATRIX(SS8, J2, J2-1, J2-2, J2-3, J2-4, J2-5, J2-6, J2-7, J2-8, J2-9,
                  J2-10, J2-11, J2-12, J2-13, J2-14, J2-15, J2-16, J2-17),
PRINT("SS8", II, JJ),
SUBIS9: SUBMATRIX(SS9, I2, I2-1, I2-2, I2-3, I2-4, I2-5, I2-6, I2-7, I2-8, I2-9,
                  I2-10, I2-11, I2-12, I2-13, I2-14, I2-15, I2-16, I2-17),
SUBJS9: SUBMATRIX(SS9, J2, J2-1, J2-2, J2-3, J2-4, J2-5, J2-6, J2-7, J2-8, J2-9,
                  J2-10, J2-11, J2-12, J2-13, J2-14, J2-15, J2-16, J2-17),
PRINT("SS9", II, JJ),
SUBIS10: SUBMATRIX(SS10, I2, I2-1, I2-2, I2-3, I2-4, I2-5, I2-6, I2-7, I2-8, I2-9,
                  I2-10, I2-11, I2-12, I2-13, I2-14, I2-15, I2-16, I2-17),
SUBJS10: SUBMATRIX(SS10, J2, J2-1, J2-2, J2-3, J2-4, J2-5, J2-6, J2-7, J2-8, J2-9,
                  J2-10, J2-11, J2-12, J2-13, J2-14, J2-15, J2-16, J2-17),
PRINT("SS10", II, JJ),
SUBIS11: SUBMATRIX(SS11, I2, I2-1, I2-2, I2-3, I2-4, I2-5, I2-6, I2-7, I2-8, I2-9,
                  I2-10, I2-11, I2-12, I2-13, I2-14, I2-15, I2-16, I2-17),
SUBJS11: SUBMATRIX(SS11, J2, J2-1, J2-2, J2-3, J2-4, J2-5, J2-6, J2-7, J2-8, J2-9,
                  J2-10, J2-11, J2-12, J2-13, J2-14, J2-15, J2-16, J2-17),
PRINT("SS11", II, JJ),
SUBIS12: SUBMATRIX(SS12, I2, I2-1, I2-2, I2-3, I2-4, I2-5, I2-6, I2-7, I2-8, I2-9,

```

```

I2-10, I2-11, I2-12, I2-13, I2-14, I2-15, I2-16, I2-17),
SUBJS12: SUBMATRIX(SS12, J2, J2-1, J2-2, J2-3, J2-4, J2-5, J2-6, J2-7, J2-8, J2-9,
J2-10, J2-11, J2-12, J2-13, J2-14, J2-15, J2-16, J2-17),
PRINT("SS12", II, JJ),
N1S: N1S+AS[II, JJ]*(
COL(S0, II).TQ.SUBJS0+(TQ.COL(S0, II))*SUBJS0+SUBIS0.Q.ROW(S0T, JJ)),
PRINT("N1AS", II, JJ),
N1S: N1S+DS[II, JJ]*(
COL(S0, II).TQ.SUBJS2+(TQ.COL(S0, II))*SUBJS2+SUBIS2.Q.ROW(S0T, JJ)+
COL(S1, II).TQ.SUBJS1+(TQ.COL(S1, II))*SUBJS1+SUBIS1.Q.ROW(S1T, JJ)+
COL(S2, II).TQ.SUBJS0+(TQ.COL(S2, II))*SUBJS0+SUBIS0.Q.ROW(S2T, JJ)),
PRINT("N1DS", II, JJ),
N1S: N1S+FS[II, JJ]*(
COL(S0, II).TQ.SUBJS4+(TQ.COL(S0, II))*SUBJS4+SUBIS4.Q.ROW(S0T, JJ)+
COL(S1, II).TQ.SUBJS3+(TQ.COL(S1, II))*SUBJS3+SUBIS3.Q.ROW(S1T, JJ)+
COL(S2, II).TQ.SUBJS2+(TQ.COL(S2, II))*SUBJS2+SUBIS2.Q.ROW(S2T, JJ)+
COL(S3, II).TQ.SUBJS1+(TQ.COL(S3, II))*SUBJS1+SUBIS1.Q.ROW(S3T, JJ)+
COL(S4, II).TQ.SUBJS0+(TQ.COL(S4, II))*SUBJS0+SUBIS0.Q.ROW(S4T, JJ)),
PRINT("N1FS", II, JJ),
N1S: N1S+HS[II, JJ]*(
COL(S0, II).TQ.SUBJS6+(TQ.COL(S0, II))*SUBJS6+SUBIS6.Q.ROW(S0T, JJ)+
COL(S1, II).TQ.SUBJS5+(TQ.COL(S1, II))*SUBJS5+SUBIS5.Q.ROW(S1T, JJ)+
COL(S2, II).TQ.SUBJS4+(TQ.COL(S2, II))*SUBJS4+SUBIS4.Q.ROW(S2T, JJ)+
COL(S3, II).TQ.SUBJS3+(TQ.COL(S3, II))*SUBJS3+SUBIS3.Q.ROW(S3T, JJ)+
COL(S4, II).TQ.SUBJS2+(TQ.COL(S4, II))*SUBJS2+SUBIS2.Q.ROW(S4T, JJ)+
COL(S5, II).TQ.SUBJS1+(TQ.COL(S5, II))*SUBJS1+SUBIS1.Q.ROW(S5T, JJ)+
COL(S6, II).TQ.SUBJS0+(TQ.COL(S6, II))*SUBJS0+SUBIS0.Q.ROW(S6T, JJ)),
PRINT("N1HS", II, JJ),
N1S: N1S+JS[II, JJ]*(
COL(S0, II).TQ.SUBJS8+(TQ.COL(S0, II))*SUBJS8+SUBIS8.Q.ROW(S0T, JJ)+
COL(S1, II).TQ.SUBJS7+(TQ.COL(S1, II))*SUBJS7+SUBIS7.Q.ROW(S1T, JJ)+
COL(S2, II).TQ.SUBJS6+(TQ.COL(S2, II))*SUBJS6+SUBIS6.Q.ROW(S2T, JJ)+
COL(S3, II).TQ.SUBJS5+(TQ.COL(S3, II))*SUBJS5+SUBIS5.Q.ROW(S3T, JJ)+
COL(S4, II).TQ.SUBJS4+(TQ.COL(S4, II))*SUBJS4+SUBIS4.Q.ROW(S4T, JJ)+
COL(S5, II).TQ.SUBJS3+(TQ.COL(S5, II))*SUBJS3+SUBIS3.Q.ROW(S5T, JJ)+
COL(S6, II).TQ.SUBJS2+(TQ.COL(S6, II))*SUBJS2+SUBIS2.Q.ROW(S6T, JJ)+
COL(S7, II).TQ.SUBJS1+(TQ.COL(S7, II))*SUBJS1+SUBIS1.Q.ROW(S7T, JJ)),
PRINT("N1JS", II, JJ),
N1S: N1S+LS[II, JJ]*(
COL(S0, II).TQ.SUBJS10+(TQ.COL(S0, II))*SUBJS10+SUBIS10.Q.ROW(S0T, JJ)+
COL(S1, II).TQ.SUBJS9+(TQ.COL(S1, II))*SUBJS9+SUBIS9.Q.ROW(S1T, JJ)+
COL(S2, II).TQ.SUBJS8+(TQ.COL(S2, II))*SUBJS8+SUBIS8.Q.ROW(S2T, JJ)+
COL(S3, II).TQ.SUBJS7+(TQ.COL(S3, II))*SUBJS7+SUBIS7.Q.ROW(S3T, JJ)+
COL(S4, II).TQ.SUBJS6+(TQ.COL(S4, II))*SUBJS6+SUBIS6.Q.ROW(S4T, JJ)+
COL(S5, II).TQ.SUBJS5+(TQ.COL(S5, II))*SUBJS5+SUBIS5.Q.ROW(S5T, JJ)+
COL(S6, II).TQ.SUBJS4+(TQ.COL(S6, II))*SUBJS4+SUBIS4.Q.ROW(S6T, JJ)+

```

```

COL(S7,II).TQ.SUBJS3+(TQ.COL(S7,II))*SUBJS3+SUBIS3.Q.ROW(S7T,JJ)),
PRINT("N1LS",II,JJ),
N1S:N1S+RS[II,JJ]*(
COL(S0,II).TQ.SUBJS12+(TQ.COL(S0,II))*SUBJS12+SUBIS12.Q.ROW(S0T,JJ)+
COL(S1,II).TQ.SUBJS11+(TQ.COL(S1,II))*SUBJS11+SUBIS11.Q.ROW(S1T,JJ)+
COL(S2,II).TQ.SUBJS10+(TQ.COL(S2,II))*SUBJS10+SUBIS10.Q.ROW(S2T,JJ)+
COL(S3,II).TQ.SUBJS9+(TQ.COL(S3,II))*SUBJS9+SUBIS9.Q.ROW(S3T,JJ)+
COL(S4,II).TQ.SUBJS8+(TQ.COL(S4,II))*SUBJS8+SUBIS8.Q.ROW(S4T,JJ)+
COL(S5,II).TQ.SUBJS7+(TQ.COL(S5,II))*SUBJS7+SUBIS7.Q.ROW(S5T,JJ)+
COL(S6,II).TQ.SUBJS6+(TQ.COL(S6,II))*SUBJS6+SUBIS6.Q.ROW(S6T,JJ)+
COL(S7,II).TQ.SUBJS5+(TQ.COL(S7,II))*SUBJS5+SUBIS5.Q.ROW(S7T,JJ)),
PRINT("N1RS",II,JJ),
N1S:N1S+TS[II,JJ]*(
COL(S2,II).TQ.SUBJS12+(TQ.COL(S2,II))*SUBJS12+SUBIS12.Q.ROW(S2T,JJ)+
COL(S3,II).TQ.SUBJS11+(TQ.COL(S3,II))*SUBJS11+SUBIS11.Q.ROW(S3T,JJ)+
COL(S4,II).TQ.SUBJS10+(TQ.COL(S4,II))*SUBJS10+SUBIS10.Q.ROW(S4T,JJ)+
COL(S5,II).TQ.SUBJS9+(TQ.COL(S5,II))*SUBJS9+SUBIS9.Q.ROW(S5T,JJ)+
COL(S6,II).TQ.SUBJS8+(TQ.COL(S6,II))*SUBJS8+SUBIS8.Q.ROW(S6T,JJ)+
COL(S7,II).TQ.SUBJS7+(TQ.COL(S7,II))*SUBJS7+SUBIS7.Q.ROW(S7T,JJ)),
PRINT("N1TS",II,JJ),
N1S:N1S+XHS[II,JJ]*(
COL(S4,II).TQ.SUBJS12+(TQ.COL(S4,II))*SUBJS12+SUBIS12.Q.ROW(S4T,JJ)+
COL(S5,II).TQ.SUBJS11+(TQ.COL(S5,II))*SUBJS11+SUBIS11.Q.ROW(S5T,JJ)+
COL(S6,II).TQ.SUBJS10+(TQ.COL(S6,II))*SUBJS10+SUBIS10.Q.ROW(S6T,JJ)+
COL(S7,II).TQ.SUBJS9+(TQ.COL(S7,II))*SUBJS9+SUBIS9.Q.ROW(S7T,JJ)),
PRINT("N1XHS",II,JJ),
N1S:N1S+XJS[II,JJ]*(
COL(S6,II).TQ.SUBJS12+(TQ.COL(S6,II))*SUBJS12+SUBIS12.Q.ROW(S6T,JJ)+
COL(S7,II).TQ.SUBJS11+(TQ.COL(S7,II))*SUBJS11+SUBIS11.Q.ROW(S7T,JJ)),
PRINT("N1XJS",II,JJ),
KILL(SUBJS12,SUBIS12,SUBJS11,SUBIS11,SUBJS10,SUBIS10),
KILL(SUBJS0,SUBJS1,SUBJS2,SUBJS3,SUBJS4,SUBJS5,SUBJS6),
KILL(SUBJS7,SUBJS8,SUBJS9),
KILL(SUBIS0,SUBIS1,SUBIS2,SUBIS3,SUBIS4,SUBIS5,SUBIS6),
KILL(SUBIS7,SUBIS8,SUBIS9))$

SAVE("SPH-N1S.SV",N1S);

KILL(SS0,SS1,SS2,SS3,SS4,SS5,SS6,SS7,SS8,SS9,SS10,SS1,SS12)$
KILL(S0,S1,S2,S3,S4,S5,S6,S7,S0T,S1T,S2T,S3T,S4T,S5T,S6T,S7T)$
N1SYM:ZEROMATRIX(18,18)$
FOR II THRU 18 DO FOR JJ:II THRU 18 DO N1SYM[II,JJ]:N1S[II,JJ]$
PRINT("SYMMETRIC N1 FORMED")$
KILL(N1,N1S)$
N1:ZEROMATRIX(18,18)$
KILL(Q,TQ)$

```

```

/*****
/* THE FOLLOWING STATEMENTS GENERATE A FORTRAN STATEMENT FOR EACH */
/* NONZERO ELEMENT OF SN1S(I,J). THESE STATEMENTS ARE OF THE FORM */
/* SN1S(2,2)=A(1,1). EACH STATEMENT IS WRITTEN TO A SEPERATE FILE CALLED*/
/* TT2XXX, WHERE XXX STARTS AT 001 FOR THE FIRST NONZERO ENTRY AND */
/* CONTINUES SEQUENTIALLY UNTIL ALL NONZERO ENTRIES THROUGH SN1S(18,18) */
/* ARE GENERATED. THE MACSYMA FUNTION GENTRAN WILL ALSO BREAK */
/* STATEMENTS EXCEEDING 800 INTO SHORTER EXPRESSIONS TO AVOID TOO MANY */
/* CONTINUATION LINES. MACSYMA AUTOMATICALLY MAKES CONTINUATION LINES */
/* COMPLETE WITH A LEGAL CHARACTER IN COLUMN 6. */
*****/

FOR II THRU 18 DO FOR JJ:II THRU 18 DO
N1[II,JJ]:FACTOROUT(N1SYM[II,JJ],Q(1),Q(2),Q(3),Q(4),Q(5),Q(6),Q(7),Q(8),
Q(9),Q(10),Q(11),Q(12),Q(13),Q(14),Q(15),Q(16),Q(17),Q(18))$
FRAME(I,J):=CONCAT(TNS,EV(18*(I-1)+J+1000))$
FOR I THRU 18 DO FOR J:I THRU 18 DO
(IF N1[I,J]#0 THEN(P1:1,GENTRAN(PCSN1S[EVAL(I),EVAL(J)]:EVAL(N1[I,J]),
[EVAL(FRAME(I,J))]))$
IF P1#1 THEN GENTRAN(P1:EVAL(P1),[TT2000])$

CLOSEFILE();
QUIT();

```

F.5 SPHN2.B1 Input Deck

The MACSYMA input deck, SPHN2.B1, generates all the nonzero entries of the $[\hat{N}_2]$ matrix for a spherical shell. Because the $[\hat{N}_2]$ is fully populated, and due to limited disk space on the SPARC2 workstations, this input deck calculates entries for rows 1 through 6 (out of a total of 18) of this matrix.

```

WRITEFILE("SPHN2.WF");
/*****
/*****
/*  MACSYMA ROUTINE FOR ELEMENTAL CODE GENERATION BY S. A. SCHIMMELS */
/*  CREATED AS A PART OF AN AIR FORCE INSTITUTE OF TECHNOLOGY (AFIT) */
/*      PHD PROGRAM IN AERONAUTICAL ENGINEERING --- MARCH 1993 */
/*      MACSYMA IS A REGISTERED TRADEMARK OF */
/*      THE MASSACHUSETTS INSTITUTE OF TECHNOLOGY */
/* */
/*  PROGRAM SPHN2.B1: FOR A SPHERICAL SHELL.  CREATES ELEMENT */
/*  INDEPENDENT STIFFNESS ARRAY N2, ROWS 1-6. */
/*****
/*****

/*****
/*  INITIALIZE MACSYMA PARAMETERS AND DECLARE VARIABLE PROPERTIES */
/*****
[DYNAMALLOC:TRUE,DISKGC:TRUE,DERIVABBREV:TRUE,POWERDISP:TRUE]$

/*****
/*  GENERATE THE NONLINEAR ELEMENT-INDEPENDENT STIFFNESS ARRAY N2. */
/*****

/*****
/*  ASSEMBLE MATRIX N2 */
/*****
TQ:MATRIX([Q(1),Q(2),Q(3),Q(4),Q(5),Q(6),Q(7),Q(8),Q(9),Q(10),
          Q(11),Q(12),Q(13),Q(14),Q(15),Q(16),Q(17),Q(18)]);
Q:TRANPOSE(TQ);

LOADFILE("SPH-HMAT.SV");

H0:SUBST([K=K1,C=P1,D=P2],H0)$
H1:SUBST([K=K1,C=P1,D=P2],H1)$
H2:SUBST([K=K1,C=P1,D=P2],H2)$

```

```

H3:SUBST([K=K1,C=P1,D=P2],H3)$
H4:SUBST([K=K1,C=P1,D=P2],H4)$
H5:SUBST([K=K1,C=P1,D=P2],H5)$
H6:SUBST([K=K1,C=P1,D=P2],H6)$
H7:SUBST([K=K1,C=P1,D=P2],H7)$
H8:SUBST([K=K1,C=P1,D=P2],H8)$
H9:SUBST([K=K1,C=P1,D=P2],H9)$
H10:SUBST([K=K1,C=P1,D=P2],H10)$
H11:SUBST([K=K1,C=P1,D=P2],H11)$
H12:SUBST([K=K1,C=P1,D=P2],H12)$
N2:ZEROMATRIX(18,18)$
CA:1/2;
CB:1/3;
CC:2/3;

FOR II THRU 3 DO FOR JJ THRU 3 DO (PRINT(II,JJ),
(I1:3*(-9*II^2+33*II-12), J2:3*(9*JJ^2-39*JJ+48),
J1:3*(-9*JJ^2+33*JJ-12), I2:3*(9*II^2-39*II+48),
SUBI0:SUBMATRIX(H0,I1,I1-1,I1-2,I1-3,I1-4,I1-5,I1-6,I1-7,I1-8,I1-9,
I1-10,I1-11,I1-12,I1-13,I1-14,I1-15,I1-16,I1-17,
I2,I2-1,I2-2,I2-3,I2-4,I2-5,I2-6,I2-7,I2-8,I2-9,
I2-10,I2-11,I2-12,I2-13,I2-14,I2-15,I2-16,I2-17),
SUBJ0:SUBMATRIX(H0,J1,J1-1,J1-2,J1-3,J1-4,J1-5,J1-6,J1-7,J1-8,J1-9,
J1-10,J1-11,J1-12,J1-13,J1-14,J1-15,J1-16,J1-17,
J2,J2-1,J2-2,J2-3,J2-4,J2-5,J2-6,J2-7,J2-8,J2-9,
J2-10,J2-11,J2-12,J2-13,J2-14,J2-15,J2-16,J2-17),
PRINT("H0",II,JJ),
SUBI1:SUBMATRIX(H1,I1,I1-1,I1-2,I1-3,I1-4,I1-5,I1-6,I1-7,I1-8,I1-9,
I1-10,I1-11,I1-12,I1-13,I1-14,I1-15,I1-16,I1-17,
I2,I2-1,I2-2,I2-3,I2-4,I2-5,I2-6,I2-7,I2-8,I2-9,
I2-10,I2-11,I2-12,I2-13,I2-14,I2-15,I2-16,I2-17),
SUBJ1:SUBMATRIX(H1,J1,J1-1,J1-2,J1-3,J1-4,J1-5,J1-6,J1-7,J1-8,J1-9,
J1-10,J1-11,J1-12,J1-13,J1-14,J1-15,J1-16,J1-17,
J2,J2-1,J2-2,J2-3,J2-4,J2-5,J2-6,J2-7,J2-8,J2-9,
J2-10,J2-11,J2-12,J2-13,J2-14,J2-15,J2-16,J2-17),
PRINT("H1",II,JJ),
SUBI2:SUBMATRIX(H2,I1,I1-1,I1-2,I1-3,I1-4,I1-5,I1-6,I1-7,I1-8,I1-9,
I1-10,I1-11,I1-12,I1-13,I1-14,I1-15,I1-16,I1-17,
I2,I2-1,I2-2,I2-3,I2-4,I2-5,I2-6,I2-7,I2-8,I2-9,
I2-10,I2-11,I2-12,I2-13,I2-14,I2-15,I2-16,I2-17),
SUBJ2:SUBMATRIX(H2,J1,J1-1,J1-2,J1-3,J1-4,J1-5,J1-6,J1-7,J1-8,J1-9,
J1-10,J1-11,J1-12,J1-13,J1-14,J1-15,J1-16,J1-17,
J2,J2-1,J2-2,J2-3,J2-4,J2-5,J2-6,J2-7,J2-8,J2-9,
J2-10,J2-11,J2-12,J2-13,J2-14,J2-15,J2-16,J2-17),
PRINT("H2",II,JJ),
SUBI3:SUBMATRIX(H3,I1,I1-1,I1-2,I1-3,I1-4,I1-5,I1-6,I1-7,I1-8,I1-9,

```

```

I1-10, I1-11, I1-12, I1-13, I1-14, I1-15, I1-16, I1-17,
I2, I2-1, I2-2, I2-3, I2-4, I2-5, I2-6, I2-7, I2-8, I2-9,
I2-10, I2-11, I2-12, I2-13, I2-14, I2-15, I2-16, I2-17),
SUBJ3: SUBMATRIX(H3, J1, J1-1, J1-2, J1-3, J1-4, J1-5, J1-6, J1-7, J1-8, J1-9,
J1-10, J1-11, J1-12, J1-13, J1-14, J1-15, J1-16, J1-17,
J2, J2-1, J2-2, J2-3, J2-4, J2-5, J2-6, J2-7, J2-8, J2-9,
J2-10, J2-11, J2-12, J2-13, J2-14, J2-15, J2-16, J2-17),

PRINT("H3", II, JJ),
SUBI4: SUBMATRIX(H4, I1, I1-1, I1-2, I1-3, I1-4, I1-5, I1-6, I1-7, I1-8, I1-9,
I1-10, I1-11, I1-12, I1-13, I1-14, I1-15, I1-16, I1-17,
I2, I2-1, I2-2, I2-3, I2-4, I2-5, I2-6, I2-7, I2-8, I2-9,
I2-10, I2-11, I2-12, I2-13, I2-14, I2-15, I2-16, I2-17),
SUBJ4: SUBMATRIX(H4, J1, J1-1, J1-2, J1-3, J1-4, J1-5, J1-6, J1-7, J1-8, J1-9,
J1-10, J1-11, J1-12, J1-13, J1-14, J1-15, J1-16, J1-17,
J2, J2-1, J2-2, J2-3, J2-4, J2-5, J2-6, J2-7, J2-8, J2-9,
J2-10, J2-11, J2-12, J2-13, J2-14, J2-15, J2-16, J2-17),

PRINT("H4", II, JJ),
SUBI5: SUBMATRIX(H5, I1, I1-1, I1-2, I1-3, I1-4, I1-5, I1-6, I1-7, I1-8, I1-9,
I1-10, I1-11, I1-12, I1-13, I1-14, I1-15, I1-16, I1-17,
I2, I2-1, I2-2, I2-3, I2-4, I2-5, I2-6, I2-7, I2-8, I2-9,
I2-10, I2-11, I2-12, I2-13, I2-14, I2-15, I2-16, I2-17),
SUBJ5: SUBMATRIX(H5, J1, J1-1, J1-2, J1-3, J1-4, J1-5, J1-6, J1-7, J1-8, J1-9,
J1-10, J1-11, J1-12, J1-13, J1-14, J1-15, J1-16, J1-17,
J2, J2-1, J2-2, J2-3, J2-4, J2-5, J2-6, J2-7, J2-8, J2-9,
J2-10, J2-11, J2-12, J2-13, J2-14, J2-15, J2-16, J2-17),

PRINT("H5", II, JJ),
SUBI6: SUBMATRIX(H6, I1, I1-1, I1-2, I1-3, I1-4, I1-5, I1-6, I1-7, I1-8, I1-9,
I1-10, I1-11, I1-12, I1-13, I1-14, I1-15, I1-16, I1-17,
I2, I2-1, I2-2, I2-3, I2-4, I2-5, I2-6, I2-7, I2-8, I2-9,
I2-10, I2-11, I2-12, I2-13, I2-14, I2-15, I2-16, I2-17),
SUBJ6: SUBMATRIX(H6, J1, J1-1, J1-2, J1-3, J1-4, J1-5, J1-6, J1-7, J1-8, J1-9,
J1-10, J1-11, J1-12, J1-13, J1-14, J1-15, J1-16, J1-17,
J2, J2-1, J2-2, J2-3, J2-4, J2-5, J2-6, J2-7, J2-8, J2-9,
J2-10, J2-11, J2-12, J2-13, J2-14, J2-15, J2-16, J2-17),

PRINT("H6", II, JJ),
SUBI7: SUBMATRIX(H7, I1, I1-1, I1-2, I1-3, I1-4, I1-5, I1-6, I1-7, I1-8, I1-9,
I1-10, I1-11, I1-12, I1-13, I1-14, I1-15, I1-16, I1-17,
I2, I2-1, I2-2, I2-3, I2-4, I2-5, I2-6, I2-7, I2-8, I2-9,
I2-10, I2-11, I2-12, I2-13, I2-14, I2-15, I2-16, I2-17),
SUBJ7: SUBMATRIX(H7, J1, J1-1, J1-2, J1-3, J1-4, J1-5, J1-6, J1-7, J1-8, J1-9,
J1-10, J1-11, J1-12, J1-13, J1-14, J1-15, J1-16, J1-17,
J2, J2-1, J2-2, J2-3, J2-4, J2-5, J2-6, J2-7, J2-8, J2-9,
J2-10, J2-11, J2-12, J2-13, J2-14, J2-15, J2-16, J2-17),

PRINT("H7", II, JJ),
SUBI8: SUBMATRIX(H8, I1, I1-1, I1-2, I1-3, I1-4, I1-5, I1-6, I1-7, I1-8, I1-9,
I1-10, I1-11, I1-12, I1-13, I1-14, I1-15, I1-16, I1-17,

```



```

I2,I2-1,I2-2,I2-3,I2-4,I2-5,I2-6,I2-7,I2-8,I2-9,
I2-10,I2-11,I2-12,I2-13,I2-14,I2-15,I2-16,I2-17),
SUBJ8: SUBMATRIX(H8,J1,J1-1,J1-2,J1-3,J1-4,J1-5,J1-6,J1-7,J1-8,J1-9,
J1-10,J1-11,J1-12,J1-13,J1-14,J1-15,J1-16,J1-17,
J2,J2-1,J2-2,J2-3,J2-4,J2-5,J2-6,J2-7,J2-8,J2-9,
J2-10,J2-11,J2-12,J2-13,J2-14,J2-15,J2-16,J2-17),

PRINT("H8",II,JJ),
SUBI9: SUBMATRIX(H9,I1,I1-1,I1-2,I1-3,I1-4,I1-5,I1-6,I1-7,I1-8,I1-9,
I1-10,I1-11,I1-12,I1-13,I1-14,I1-15,I1-16,I1-17,
I2,I2-1,I2-2,I2-3,I2-4,I2-5,I2-6,I2-7,I2-8,I2-9,
I2-10,I2-11,I2-12,I2-13,I2-14,I2-15,I2-16,I2-17),
SUBJ9: SUBMATRIX(H9,J1,J1-1,J1-2,J1-3,J1-4,J1-5,J1-6,J1-7,J1-8,J1-9,
J1-10,J1-11,J1-12,J1-13,J1-14,J1-15,J1-16,J1-17,
J2,J2-1,J2-2,J2-3,J2-4,J2-5,J2-6,J2-7,J2-8,J2-9,
J2-10,J2-11,J2-12,J2-13,J2-14,J2-15,J2-16,J2-17),

PRINT("H9",II,JJ),
SUBI10: SUBMATRIX(H10,I1,I1-1,I1-2,I1-3,I1-4,I1-5,I1-6,I1-7,I1-8,I1-9,
I1-10,I1-11,I1-12,I1-13,I1-14,I1-15,I1-16,I1-17,
I2,I2-1,I2-2,I2-3,I2-4,I2-5,I2-6,I2-7,I2-8,I2-9,
I2-10,I2-11,I2-12,I2-13,I2-14,I2-15,I2-16,I2-17),
SUBJ10: SUBMATRIX(H10,J1,J1-1,J1-2,J1-3,J1-4,J1-5,J1-6,J1-7,J1-8,J1-9,
J1-10,J1-11,J1-12,J1-13,J1-14,J1-15,J1-16,J1-17,
J2,J2-1,J2-2,J2-3,J2-4,J2-5,J2-6,J2-7,J2-8,J2-9,
J2-10,J2-11,J2-12,J2-13,J2-14,J2-15,J2-16,J2-17),

PRINT("H10",II,JJ),
SUBI11: SUBMATRIX(H11,I1,I1-1,I1-2,I1-3,I1-4,I1-5,I1-6,I1-7,I1-8,I1-9,
I1-10,I1-11,I1-12,I1-13,I1-14,I1-15,I1-16,I1-17,
I2,I2-1,I2-2,I2-3,I2-4,I2-5,I2-6,I2-7,I2-8,I2-9,
I2-10,I2-11,I2-12,I2-13,I2-14,I2-15,I2-16,I2-17),
SUBJ11: SUBMATRIX(H11,J1,J1-1,J1-2,J1-3,J1-4,J1-5,J1-6,J1-7,J1-8,J1-9,
J1-10,J1-11,J1-12,J1-13,J1-14,J1-15,J1-16,J1-17,
J2,J2-1,J2-2,J2-3,J2-4,J2-5,J2-6,J2-7,J2-8,J2-9,
J2-10,J2-11,J2-12,J2-13,J2-14,J2-15,J2-16,J2-17),

PRINT("H11",II,JJ),
SUBI12: SUBMATRIX(H12,I1,I1-1,I1-2,I1-3,I1-4,I1-5,I1-6,I1-7,I1-8,I1-9,
I1-10,I1-11,I1-12,I1-13,I1-14,I1-15,I1-16,I1-17,
I2,I2-1,I2-2,I2-3,I2-4,I2-5,I2-6,I2-7,I2-8,I2-9,
I2-10,I2-11,I2-12,I2-13,I2-14,I2-15,I2-16,I2-17),
SUBJ12: SUBMATRIX(H12,J1,J1-1,J1-2,J1-3,J1-4,J1-5,J1-6,J1-7,J1-8,J1-9,
J1-10,J1-11,J1-12,J1-13,J1-14,J1-15,J1-16,J1-17,
J2,J2-1,J2-2,J2-3,J2-4,J2-5,J2-6,J2-7,J2-8,J2-9,
J2-10,J2-11,J2-12,J2-13,J2-14,J2-15,J2-16,J2-17),

PRINT("H12",II,JJ),
N2:N2+ A[II,JJ]*(SUBI0.Q.TQ.SUBJ0+CA*(TQ.SUBJ0.Q)*SUBI0),
PRINT("N2A",II,JJ),
N2:N2+DD[II,JJ]*(CB*(SUBI0.Q.TQ.SUBJ2+CA*(TQ.SUBI0.Q)*SUBJ2+

```

```

SUBI2.Q.TQ.SUBJ0+CA*(TQ.SUBI2.Q)*SUBJ0)+
SUBI1.Q.TQ.SUBJ1+CA*(TQ.SUBI1.Q)*SUBI1),
PRINT("N2D",II,JJ),
N2:N2+ F[II,JJ]*(CB*(SUBI0.Q.TQ.SUBJ4+CA*(TQ.SUBI0.Q)*SUBJ4+
SUBI4.Q.TQ.SUBJ0+CA*(TQ.SUBI4.Q)*SUBJ0)+
CC*(SUBI1.Q.TQ.SUBJ3+CA*(TQ.SUBI1.Q)*SUBJ3+
SUBI3.Q.TQ.SUBJ1+CA*(TQ.SUBI3.Q)*SUBJ1)+
SUBI2.Q.TQ.SUBJ2+CA*(TQ.SUBI2.Q)*SUBI2),
PRINT("N2F",II,JJ),
N2:N2+ H[II,JJ]*(CB*(SUBI0.Q.TQ.SUBJ6+CA*(TQ.SUBI0.Q)*SUBJ6+
SUBI6.Q.TQ.SUBJ0+CA*(TQ.SUBI6.Q)*SUBJ0)+
CC*(SUBI1.Q.TQ.SUBJ5+CA*(TQ.SUBI1.Q)*SUBJ5+
SUBI5.Q.TQ.SUBJ1+CA*(TQ.SUBI5.Q)*SUBJ1)+
CC*(SUBI2.Q.TQ.SUBJ4+CA*(TQ.SUBI2.Q)*SUBJ4+
SUBI4.Q.TQ.SUBJ2+CA*(TQ.SUBI4.Q)*SUBJ2)+
SUBI3.Q.TQ.SUBJ3+CA*(TQ.SUBI3.Q)*SUBI3),
PRINT("N2H",II,JJ),
N2:N2+ J[II,JJ]*(CB*(SUBI0.Q.TQ.SUBJ8+CA*(TQ.SUBI0.Q)*SUBJ8+
SUBI8.Q.TQ.SUBJ0+CA*(TQ.SUBI8.Q)*SUBJ0)+
CC*(SUBI1.Q.TQ.SUBJ7+CA*(TQ.SUBI1.Q)*SUBJ7+
SUBI7.Q.TQ.SUBJ1+CA*(TQ.SUBI7.Q)*SUBJ1)+
CC*(SUBI2.Q.TQ.SUBJ6+CA*(TQ.SUBI2.Q)*SUBJ6+
SUBI6.Q.TQ.SUBJ2+CA*(TQ.SUBI6.Q)*SUBJ2)+
CC*(SUBI3.Q.TQ.SUBJ5+CA*(TQ.SUBI3.Q)*SUBJ5+
SUBI5.Q.TQ.SUBJ3+CA*(TQ.SUBI5.Q)*SUBJ3)+
SUBI4.Q.TQ.SUBJ4+CA*(TQ.SUBI4.Q)*SUBI4),
PRINT("N2J",II,JJ),
N2:N2+ L[II,JJ]*(CB*(SUBI0.Q.TQ.SUBJ10+CA*(TQ.SUBI0.Q)*SUBJ10+
SUBI10.Q.TQ.SUBJ0+CA*(TQ.SUBI10.Q)*SUBJ0)+
CC*(SUBI1.Q.TQ.SUBJ9+CA*(TQ.SUBI1.Q)*SUBJ9+
SUBI9.Q.TQ.SUBJ1+CA*(TQ.SUBI9.Q)*SUBJ1)+
CC*(SUBI2.Q.TQ.SUBJ8+CA*(TQ.SUBI2.Q)*SUBJ8+
SUBI8.Q.TQ.SUBJ2+CA*(TQ.SUBI8.Q)*SUBJ2)+
CC*(SUBI3.Q.TQ.SUBJ7+CA*(TQ.SUBI3.Q)*SUBJ7+
SUBI7.Q.TQ.SUBJ3+CA*(TQ.SUBI7.Q)*SUBJ3)+
CC*(SUBI4.Q.TQ.SUBJ6+CA*(TQ.SUBI4.Q)*SUBJ6+
SUBI6.Q.TQ.SUBJ4+CA*(TQ.SUBI6.Q)*SUBJ4)+
SUBI5.Q.TQ.SUBJ5+CA*(TQ.SUBI5.Q)*SUBI5),
PRINT("N2L",II,JJ),
N2:N2+ R[II,JJ]*(CB*(SUBI0.Q.TQ.SUBJ12+CA*(TQ.SUBI0.Q)*SUBJ12+
SUBI12.Q.TQ.SUBJ0+CA*(TQ.SUBI12.Q)*SUBJ0)+
CC*(SUBI1.Q.TQ.SUBJ11+CA*(TQ.SUBI1.Q)*SUBJ11+
SUBI11.Q.TQ.SUBJ1+CA*(TQ.SUBI11.Q)*SUBJ1)+
CC*(SUBI2.Q.TQ.SUBJ10+CA*(TQ.SUBI2.Q)*SUBJ10+
SUBI10.Q.TQ.SUBJ2+CA*(TQ.SUBI10.Q)*SUBJ2)+
CC*(SUBI3.Q.TQ.SUBJ9+CA*(TQ.SUBI3.Q)*SUBJ9+

```

```

        SUBI9.Q.TQ.SUBJ3+CA*(TQ.SUBI9.Q)*SUBJ3)+
        CC*(SUBI4.Q.TQ.SUBJ8+CA*(TQ.SUBI4.Q)*SUBJ8+
        SUBI8.Q.TQ.SUBJ4+CA*(TQ.SUBI8.Q)*SUBJ4)+
        CC*(SUBI5.Q.TQ.SUBJ7+CA*(TQ.SUBI5.Q)*SUBJ7+
        SUBI7.Q.TQ.SUBJ5+CA*(TQ.SUBI7.Q)*SUBJ5)+
        SUBI6.Q.TQ.SUBJ6+CA*(TQ.SUBJ6.Q)*SUBI6),
PRINT("N2R",II,JJ),
N2:N2+ T[II,JJ]*(CC*(SUBI2.Q.TQ.SUBJ12+CA*(TQ.SUBI2.Q)*SUBJ12+
        SUBI12.Q.TQ.SUBJ2+CA*(TQ.SUBI12.Q)*SUBJ2)+
        CC*(SUBI3.Q.TQ.SUBJ11+CA*(TQ.SUBI3.Q)*SUBJ11+
        SUBI11.Q.TQ.SUBJ3+CA*(TQ.SUBI11.Q)*SUBJ3)+
        CC*(SUBI4.Q.TQ.SUBJ10+CA*(TQ.SUBI4.Q)*SUBJ10+
        SUBI10.Q.TQ.SUBJ4+CA*(TQ.SUBI10.Q)*SUBJ4)+
        CC*(SUBI5.Q.TQ.SUBJ9+CA*(TQ.SUBI5.Q)*SUBJ9+
        SUBI9.Q.TQ.SUBJ5+CA*(TQ.SUBI9.Q)*SUBJ5)+
        CC*(SUBI6.Q.TQ.SUBJ8+CA*(TQ.SUBI6.Q)*SUBJ8+
        SUBI8.Q.TQ.SUBJ6+CA*(TQ.SUBI8.Q)*SUBJ6)+
        SUBI7.Q.TQ.SUBJ7+CA*(TQ.SUBJ7.Q)*SUBI7),
PRINT("N2T",II,JJ),
N2:N2+XH[II,JJ]*(CC*(SUBI4.Q.TQ.SUBJ12+CA*(TQ.SUBI4.Q)*SUBJ12+
        SUBI12.Q.TQ.SUBJ4+CA*(TQ.SUBI12.Q)*SUBJ4)+
        CC*(SUBI5.Q.TQ.SUBJ11+CA*(TQ.SUBI5.Q)*SUBJ11+
        SUBI11.Q.TQ.SUBJ5+CA*(TQ.SUBI11.Q)*SUBJ5)+
        CC*(SUBI6.Q.TQ.SUBJ10+CA*(TQ.SUBI6.Q)*SUBJ10+
        SUBI10.Q.TQ.SUBJ6+CA*(TQ.SUBI10.Q)*SUBJ6)+
        CC*(SUBI7.Q.TQ.SUBJ9+CA*(TQ.SUBI7.Q)*SUBJ9+
        SUBI9.Q.TQ.SUBJ7+CA*(TQ.SUBI9.Q)*SUBJ7)+
        SUBI8.Q.TQ.SUBJ8+CA*(TQ.SUBJ8.Q)*SUBI8),
PRINT("N2XH",II,JJ),
N2:N2+XJ[II,JJ]*(CC*(SUBI6.Q.TQ.SUBJ12+CA*(TQ.SUBI6.Q)*SUBJ12+
        SUBI12.Q.TQ.SUBJ6+CA*(TQ.SUBI12.Q)*SUBJ6)+
        CC*(SUBI7.Q.TQ.SUBJ11+CA*(TQ.SUBI7.Q)*SUBJ11+
        SUBI11.Q.TQ.SUBJ7+CA*(TQ.SUBI11.Q)*SUBJ7)+
        CC*(SUBI8.Q.TQ.SUBJ10+CA*(TQ.SUBI8.Q)*SUBJ10+
        SUBI10.Q.TQ.SUBJ8+CA*(TQ.SUBI10.Q)*SUBJ8)+
        SUBI9.Q.TQ.SUBJ9+CA*(TQ.SUBJ9.Q)*SUBI9),
PRINT("N2XJ",II,JJ),
N2:N2+XL[II,JJ]*(CC*(SUBI8.Q.TQ.SUBJ12+CA*(TQ.SUBI8.Q)*SUBJ12+
        SUBI12.Q.TQ.SUBJ8+CA*(TQ.SUBI12.Q)*SUBJ8)+
        CC*(SUBI9.Q.TQ.SUBJ11+CA*(TQ.SUBI9.Q)*SUBJ11+
        SUBI11.Q.TQ.SUBJ9+CA*(TQ.SUBI11.Q)*SUBJ9)+
        SUBI10.Q.TQ.SUBJ10+CA*(TQ.SUBJ10.Q)*SUBI10),
PRINT("N2XL",II,JJ),
N2:N2+XR[II,JJ]*(CC*(SUBI10.Q.TQ.SUBJ12+CA*(TQ.SUBI10.Q)*SUBJ12+
        SUBI12.Q.TQ.SUBJ10+CA*(TQ.SUBI12.Q)*SUBJ10)+
        SUBI11.Q.TQ.SUBJ11+CA*(TQ.SUBJ11.Q)*SUBI11),

```

```

PRINT("N2XR",II,JJ),
N2:N2+XT[II,JJ]*(SUBI12.Q.TQ.SUBJ12+CA*(TQ.SUBJ12.Q)*SUBI12),
PRINT("N2XT",II,JJ),
KILL(SUBJ12,SUBI12,SUBJ11,SUBI11,SUBJ10,SUBI10),
KILL(SUBJ0,SUBJ1,SUBJ2,SUBJ3,SUBJ4,SUBJ5,SUBJ6,SUBJ7,SUBJ8,SUBJ9),
KILL(SUBI0,SUBI1,SUBI2,SUBI3,SUBI4,SUBI5,SUBI6,SUBI7,SUBI8,SUBI9)))$
KILL(H0,H1,H2,H3,H4,H5,H6,H7,H8,H9,H10,H11,H12)$
N2SYM:ZEROMATRIX(18,18)$

SAVE("SPH-N2.SV",N2)$

FOR II THRU 18 DO FOR JJ:II THRU 18 DO N2SYM[II,JJ]:N2[II,JJ]$
PRINT("SYMMETRIC N2 FORMED")$
KILL(N2)$
NTEMP1:ZEROMATRIX(18,18)$
KILL(Q,TQ)$

/*****
/* THE FOLLOWING STATEMENTS GENERATE A FORTRAN STATEMENT FOR EACH */
/* NONZERO ELEMENT OF SN2(I,J). THESE STATEMENTS ARE OF THE FORM */
/* SN2(2,2)=A(1,1). EACH STATEMENT IS WRITTEN TO A SEPERATE FILE CALLED*/
/* TT2XXX, WHERE XXX STARTS AT 001 FOR THE FIRST NONZERO ENTRY AND */
/* CONTINUES SEQUENTIALLY UNTIL ALL NONZERO ENTRIES THROUGH SN2(18,18) */
/* ARE GENERATED. THE MACSYMA FUNTION GENTRAN WILL ALSO BREAK */
/* STATEMENTS EXCEEDING 800 INTO SHORTER EXPRESSIONS TO AVOID TOO MANY */
/* CONTINUATION LINES. MACSYMA AUTOMATICALLY MAKES CONTINUATION LINES */
/* COMPLETE WITH A LEGAL CHARACTER IN COLUMN 6. */
*****/
FRAME(I,J):=CONCAT(TN,EV(18*(I-1)+J+1000))$
FOR II:1 THRU 2 DO FOR JJ:II THRU 18 DO
NTEMP1[II,JJ]:FACTOROUT(N2SYM[II,JJ],Q(1),Q(2),Q(3),Q(4),Q(5),Q(6),Q(7),
Q(8),Q(9),Q(10),Q(11),Q(12),Q(13),Q(14),Q(15),Q(16),Q(17),Q(18))$

SAVE("NTEMP1.SV",NTEMP1);

FOR I:1 THRU 2 DO FOR J:I THRU 18 DO
(IF NTEMP1[I,J]#0 THEN (PT:1,GENTRAN(SN2[EVAL(I),EVAL(J)]:EVAL(NTEMP1[I,J]),
[EVAL(FRAME(I,J))]))))$
KILL(NTEMP1)$
NTEMP2:ZEROMATRIX(18,18)$
FOR II:3 THRU 4 DO FOR JJ:II THRU 18 DO
NTEMP2[II,JJ]:FACTOROUT(N2SYM[II,JJ],Q(1),Q(2),Q(3),Q(4),Q(5),Q(6),Q(7),
Q(8),Q(9),Q(10),Q(11),Q(12),Q(13),Q(14),Q(15),Q(16),Q(17),Q(18))$

SAVE("NTEMP2.SV",NTEMP2);

```

```
FOR I:3 THRU 4 DO FOR J:I THRU 18 DO
  (IF NTEMP2[I,J]#0 THEN (PT:1,GENTRAN(SN2[EVAL(I),EVAL(J)]:EVAL(NTEMP2[I,J]),
  [EVAL(FRAME(I,J))]))))$
KILL (NTEMP2)$
NTEMP3:ZEROMATRIX(18,18)$
FOR II:5 THRU 6 DO FOR JJ:II THRU 18 DO
  NTEMP3[II,JJ]:FACTOROUT(N2SYM[II,JJ],Q(1),Q(2),Q(3),Q(4),Q(5),Q(6),Q(7),
  Q(8),Q(9),Q(10),Q(11),Q(12),Q(13),Q(14),Q(15),Q(16),Q(17),Q(18))$

SAVE("NTEMP3.SV",NTEMP3);

FOR I:5 THRU 6 DO FOR J:I THRU 18 DO
  (IF NTEMP3[I,J]#0 THEN (PT:1,GENTRAN(SN2[EVAL(I),EVAL(J)]:EVAL(NTEMP3[I,J]),
  [EVAL(FRAME(I,J))]))))$
KILL(NTEMP3)$

CLOSEFILE();
QUIT();
```

F.6 SPHN2.B2 Input Deck

The MACSYMA input deck, SPHN2.B2, generates all the nonzero entries of the $[\hat{N}_2]$ matrix for a spherical shell. Because the $[\hat{N}_2]$ is fully populated, and due to limited disk space on the SPARC2 workstations, this input deck calculates entries for rows 7 through 12 (out of a total of 18) of this matrix. The only difference between the SPHN2.B1 and the SPHN2.B2 input decks is shown below.

```

FOR II THRU 18 DO FOR JJ:II THRU 18 DO N2SYM[II,JJ]:N2[II,JJ]$
PRINT("SYMMETRIC N2 FORMED")$
KILL(N2)$
NTEMP4:ZEROMATRIX(18,18)$
KILL(Q,TQ)$

/*****
/* THE FOLLOWING STATEMENTS GENERATE A FORTRAN STATEMENT FOR EACH      */
/* NONZERO ELEMENT OF SN2(I,J).  THESE STATEMENTS ARE OF THE FORM      */
/* SN2(2,2)=A(1,1).  EACH STATEMENT IS WRITTEN TO A SEPERATE FILE CALLED*/
/* TT2XXX, WHERE XXX STARTS AT 001 FOR THE FIRST NONZERO ENTRY AND      */
/* CONTINUES SEQUENTIALLY UNTIL ALL NONZERO ENTRIES THROUGH SN2(18,18) */
/* ARE GENERATED.  THE MACSYMA FUNTION GENTRAN WILL ALSO BREAK        */
/* STATEMENTS EXCEEDING 800 INTO SHORTER EXPRESSIONS TO AVOID TOO MANY */
/* CONTINUATION LINES.  MACSYMA AUTOMATICALLY MAKES CONTINUATION LINES  */
/* COMPLETE WITH A LEGAL CHARACTER IN COLUMN 6.                        */
*****/
FRAME(I,J):=CONCAT(TN,EV(18*(I-1)+J+1000))$
FOR II:1 THRU 2 DO FOR JJ:II THRU 18 DO
NTEMP4[II,JJ]:FACTOROUT(N2SYM[II,JJ],Q(1),Q(2),Q(3),Q(4),Q(5),Q(6),Q(7),
Q(8),Q(9),Q(10),Q(11),Q(12),Q(13),Q(14),Q(15),Q(16),Q(17),Q(18))$
SAVE("NTEMP4.SV",NTEMP4);

FOR I:1 THRU 2 DO FOR J:I THRU 18 DO
(IF NTEMP4[I,J]#0 THEN (PT:1,GENTRAN(SN2[EVAL(I),EVAL(J)]:EVAL(NTEMP4[I,J]),
[EVAL(FRAME(I,J))]))$
KILL(NTEMP4)$

NTEMP5:ZEROMATRIX(18,18)$
FOR II:3 THRU 4 DO FOR JJ:II THRU 18 DO
NTEMP5[II,JJ]:FACTOROUT(N2SYM[II,JJ],Q(1),Q(2),Q(3),Q(4),Q(5),Q(6),Q(7),
Q(8),Q(9),Q(10),Q(11),Q(12),Q(13),Q(14),Q(15),Q(16),Q(17),Q(18))$
SAVE("NTEMP5.SV",NTEMP5);

```

```
FOR I:3 THRU 4 DO FOR J:I THRU 18 DO
  (IF NTEMP5[I,J]#0 THEN (PT:1,GENTRAN(SN2[EVAL(I),EVAL(J)]:EVAL(NTEMP5[I,J]),
  [EVAL(FRAME(I,J))]))$
KILL (NTEMP5)$

NTEMP6:ZEROMATRIX(18,18)$
FOR II:5 THRU 6 DO FOR JJ:II THRU 18 DO
  NTEMP6[II,JJ]:FACTOROUT(N2SYM[II,JJ],Q(1),Q(2),Q(3),Q(4),Q(5),Q(6),Q(7),
  Q(8),Q(9),Q(10),Q(11),Q(12),Q(13),Q(14),Q(15),Q(16),Q(17),Q(18))$
  SAVE("NTEMP6.SV",NTEMP6);
FOR I:5 THRU 6 DO FOR J:I THRU 18 DO
  (IF NTEMP6[I,J]#0 THEN (PT:1,GENTRAN(SN2[EVAL(I),EVAL(J)]:EVAL(NTEMP6[I,J]),
  [EVAL(FRAME(I,J))]))$
KILL(NTEMP6)$

CLOSEFILE();
QUIT();
```

F.7 SPHN2.B3 Input Deck

The MACSYMA input deck, SPHN2.B3 generates all the nonzero entries of the $[\hat{N}_2]$ matrix for a spherical shell. Because the $[\hat{N}_2]$ is fully populated, and due to limited disk space on the SPARC2 workstations, this input deck calculates entries for rows 13 through 18 (out of a total of 18) of this matrix. The only difference between the SPHN2.B1 and the SPHN2.B3 input decks is shown below.

```

FOR II THRU 18 DO FOR JJ:II THRU 18 DO N2SYM[II,JJ]:N2[II,JJ]$
PRINT("SYMMETRIC N2 FORMED")$
KILL(N2)$
NTEMP7:ZEROMATRIX(18,18)$
KILL(Q,TQ)$

/*****
/* THE FOLLOWING STATEMENTS GENERATE A FORTRAN STATEMENT FOR EACH */
/* NONZERO ELEMENT OF SN2(I,J). THESE STATEMENTS ARE OF THE FORM */
/* SN2(2,2)=A(1,1). EACH STATEMENT IS WRITTEN TO A SEPERATE FILE CALLED*/
/* TT2XXX, WHERE XXX STARTS AT 001 FOR THE FIRST NONZERO ENTRY AND */
/* CONTINUES SEQUENTIALLY UNTIL ALL NONZERO ENTRIES THROUGH SN2(18,18) */
/* ARE GENERATED. THE MACSYMA FUNTION GENTRAN WILL ALSO BREAK */
/* STATEMENTS EXCEEDING 800 INTO SHORTER EXPRESSIONS TO AVOID TOO MANY */
/* CONTINUATION LINES. MACSYMA AUTOMATICALLY MAKES CONTINUATION LINES */
/* COMPLETE WITH A LEGAL CHARACTER IN COLUMN 6. */
*****/
FRAME(I,J):=CONCAT(TN,EV(18*(I-1)+J+1000))$
FOR II:1 THRU 2 DO FOR JJ:II THRU 18 DO
NTEMP7[II,JJ]:FACTOROUT(N2SYM[II,JJ],Q(1),Q(2),Q(3),Q(4),Q(5),Q(6),Q(7),
Q(8),Q(9),Q(10),Q(11),Q(12),Q(13),Q(14),Q(15),Q(16),Q(17),Q(18))$
SAVE("NTEMP7.SV",NTEMP7);
FOR I:1 THRU 2 DO FOR J:I THRU 18 DO
(IF NTEMP7[I,J]#0 THEN (PT:1,GENTRAN(SN2[EVAL(I),EVAL(J)]:EVAL(NTEMP7[I,J]),
[EVAL(FRAME(I,J))]))$
KILL(NTEMP7)$

NTEMP8:ZEROMATRIX(18,18)$
FOR II:3 THRU 4 DO FOR JJ:II THRU 18 DO
NTEMP8[II,JJ]:FACTOROUT(N2SYM[II,JJ],Q(1),Q(2),Q(3),Q(4),Q(5),Q(6),Q(7),
Q(8),Q(9),Q(10),Q(11),Q(12),Q(13),Q(14),Q(15),Q(16),Q(17),Q(18))$
SAVE("NTEMP8.SV",NTEMP8);
FOR I:3 THRU 4 DO FOR J:I THRU 18 DO
(IF NTEMP8[I,J]#0 THEN (PT:1,GENTRAN(SN2[EVAL(I),EVAL(J)]:EVAL(NTEMP8[I,J]),
[EVAL(FRAME(I,J))]))$

```


KILL (NTEMP8)\$

NTEMP9:ZEROMATRIX(18,18)\$

FOR II:5 THRU 6 DO FOR JJ:II THRU 18 DO

NTEMP9[II,JJ]:FACTOROUT(N2SYM[II,JJ],Q(1),Q(2),Q(3),Q(4),Q(5),Q(6),Q(7),
Q(8),Q(9),Q(10),Q(11),Q(12),Q(13),Q(14),Q(15),Q(16),Q(17),Q(18))\$

SAVE("NTEMP9.SV",NTEMP9);

FOR I:5 THRU 6 DO FOR J:I THRU 18 DO

(IF NTEMP9[I,J]#0 THEN (PT:1,GENTRAN(SN2[EVAL(I),EVAL(J)]:EVAL(NTEMP9[I,J]),
[EVAL(FRAME(I,J))]))))\$

KILL (NTEMP9)\$

CLOSEFILE();

QUIT();

F.8 SPHN2S.MAC Input Deck

The MACSYMA input deck, SPHN2S.MAC generates all the nonzero entries of the $[\hat{N}_{2s}]$ matrix for a spherical shell for transverse shear effects.

```

WRITEFILE ("SPHN2S.WF");
/*****
/*  MACSYMA ROUTINE FOR ELEMENTAL CODE GENERATION BY S. A. SCHIMMELS  */
/*  CREATED AS A PART OF AN AIR FORCE INSTITUTE OF TECHNOLOGY (AFIT)  */
/*      PhD PROGRAM IN AERONAUTICAL ENGINEERING --- MARCH 1993      */
/*      MACSYMA IS A REGISTERED TRADEMARK OF                        */
/*      THE MASSACHUSETTS INSTITUTE OF TECHNOLOGY                  */
/*                                                                    */
/*  PROGRAM SPHN2S.B3: FOR A SPHERICAL SHELL.  CREATES ELEMENT      */
/*  INDEPENDENT STIFFNESS ARRAY N2 & N2S.                          */
*****/

/*****
/*  INITIALIZE MACSYMA PARAMETERS AND DECLARE VARIABLE PROPERTIES  */
*****/
[DYNAMALLOC:TRUE,DISKGC:TRUE,DERIVABBREV:TRUE,POWERDISP:TRUE]$

/*****
/*  GENERATE THE NONLINEAR ELEMENT-INDEPENDENT STIFFNESS ARRAY N2S.  */
*****/

/*****
/*  ASSEMBLE MATRIX N2S  */
*****/
TQ:MATRIX([Q(1),Q(2),Q(3),Q(4),Q(5),Q(6),Q(7),Q(8),Q(9),Q(10),
          Q(11),Q(12),Q(13),Q(14),Q(15),Q(16),Q(17),Q(18)]);
Q:TRANPOSE(TQ);

LOADFILE ("SPH-SSMAT.SV");

SS0:SUBST([K=K1,C=P1,D=P2],SS0);
SS1:SUBST([K=K1,C=P1,D=P2],SS1);
SS2:SUBST([K=K1,C=P1,D=P2],SS2);
SS3:SUBST([K=K1,C=P1,D=P2],SS3);
SS4:SUBST([K=K1,C=P1,D=P2],SS4);
SS5:SUBST([K=K1,C=P1,D=P2],SS5);
SS6:SUBST([K=K1,C=P1,D=P2],SS6);

```

```

SS7:SUBST([K=K1,C=P1,D=P2],SS7);
SS8:SUBST([K=K1,C=P1,D=P2],SS8);
SS9:SUBST([K=K1,C=P1,D=P2],SS9);
SS10:SUBST([K=K1,C=P1,D=P2],SS10);
SS11:SUBST([K=K1,C=P1,D=P2],SS11);
SS12:SUBST([K=K1,C=P1,D=P2],SS12);
N2S:ZEROMATRIX(18,18)$
CA:1/2;
CB:1/3;
CC:2/3;

FOR II THRU 2 DO FOR JJ THRU 2 DO (PRINT(II,JJ),
(J2:3*(9*(JJ+1)^2-39*(JJ+1)+48),
I2:3*(9*(II+1)^2-39*(II+1)+48),
SUBIS0:SUBMATRIX(SS0,I2,I2-1,I2-2,I2-3,I2-4,I2-5,I2-6,I2-7,I2-8,I2-9,
I2-10,I2-11,I2-12,I2-13,I2-14,I2-15,I2-16,I2-17),
SUBJS0:SUBMATRIX(SS0,J2,J2-1,J2-2,J2-3,J2-4,J2-5,J2-6,J2-7,J2-8,J2-9,
J2-10,J2-11,J2-12,J2-13,J2-14,J2-15,J2-16,J2-17),
PRINT("SS0",II,JJ),
SUBIS1:SUBMATRIX(SS1,I2,I2-1,I2-2,I2-3,I2-4,I2-5,I2-6,I2-7,I2-8,I2-9,
I2-10,I2-11,I2-12,I2-13,I2-14,I2-15,I2-16,I2-17),
SUBJS1:SUBMATRIX(SS1,J2,J2-1,J2-2,J2-3,J2-4,J2-5,J2-6,J2-7,J2-8,J2-9,
J2-10,J2-11,J2-12,J2-13,J2-14,J2-15,J2-16,J2-17),
PRINT("SS1",II,JJ),
SUBIS2:SUBMATRIX(SS2,I2,I2-1,I2-2,I2-3,I2-4,I2-5,I2-6,I2-7,I2-8,I2-9,
I2-10,I2-11,I2-12,I2-13,I2-14,I2-15,I2-16,I2-17),
SUBJS2:SUBMATRIX(SS2,J2,J2-1,J2-2,J2-3,J2-4,J2-5,J2-6,J2-7,J2-8,J2-9,
J2-10,J2-11,J2-12,J2-13,J2-14,J2-15,J2-16,J2-17),
PRINT("SS2",II,JJ),
SUBIS3:SUBMATRIX(SS3,I2,I2-1,I2-2,I2-3,I2-4,I2-5,I2-6,I2-7,I2-8,I2-9,
I2-10,I2-11,I2-12,I2-13,I2-14,I2-15,I2-16,I2-17),
SUBJS3:SUBMATRIX(SS3,J2,J2-1,J2-2,J2-3,J2-4,J2-5,J2-6,J2-7,J2-8,J2-9,
J2-10,J2-11,J2-12,J2-13,J2-14,J2-15,J2-16,J2-17),
PRINT("SS3",II,JJ),
SUBIS4:SUBMATRIX(SS4,I2,I2-1,I2-2,I2-3,I2-4,I2-5,I2-6,I2-7,I2-8,I2-9,
I2-10,I2-11,I2-12,I2-13,I2-14,I2-15,I2-16,I2-17),
SUBJS4:SUBMATRIX(SS4,J2,J2-1,J2-2,J2-3,J2-4,J2-5,J2-6,J2-7,J2-8,J2-9,
J2-10,J2-11,J2-12,J2-13,J2-14,J2-15,J2-16,J2-17),
PRINT("SS4",II,JJ),
SUBIS5:SUBMATRIX(SS5,I2,I2-1,I2-2,I2-3,I2-4,I2-5,I2-6,I2-7,I2-8,I2-9,
I2-10,I2-11,I2-12,I2-13,I2-14,I2-15,I2-16,I2-17),
SUBJS5:SUBMATRIX(SS5,J2,J2-1,J2-2,J2-3,J2-4,J2-5,J2-6,J2-7,J2-8,J2-9,
J2-10,J2-11,J2-12,J2-13,J2-14,J2-15,J2-16,J2-17),
PRINT("SS5",II,JJ),
SUBIS6:SUBMATRIX(SS6,I2,I2-1,I2-2,I2-3,I2-4,I2-5,I2-6,I2-7,I2-8,I2-9,
I2-10,I2-11,I2-12,I2-13,I2-14,I2-15,I2-16,I2-17),

```

```

SUBJS6:SUBMATRIX(SS6,J2,J2-1,J2-2,J2-3,J2-4,J2-5,J2-6,J2-7,J2-8,J2-9,
                J2-10,J2-11,J2-12,J2-13,J2-14,J2-15,J2-16,J2-17),
PRINT("SS6",II,JJ),
SUBIS7:SUBMATRIX(SS7,I2,I2-1,I2-2,I2-3,I2-4,I2-5,I2-6,I2-7,I2-8,I2-9,
                I2-10,I2-11,I2-12,I2-13,I2-14,I2-15,I2-16,I2-17),
SUBJS7:SUBMATRIX(SS7,J2,J2-1,J2-2,J2-3,J2-4,J2-5,J2-6,J2-7,J2-8,J2-9,
                J2-10,J2-11,J2-12,J2-13,J2-14,J2-15,J2-16,J2-17),
PRINT("SS7",II,JJ),
SUBIS8:SUBMATRIX(SS8,I2,I2-1,I2-2,I2-3,I2-4,I2-5,I2-6,I2-7,I2-8,I2-9,
                I2-10,I2-11,I2-12,I2-13,I2-14,I2-15,I2-16,I2-17),
SUBJS8:SUBMATRIX(SS8,J2,J2-1,J2-2,J2-3,J2-4,J2-5,J2-6,J2-7,J2-8,J2-9,
                J2-10,J2-11,J2-12,J2-13,J2-14,J2-15,J2-16,J2-17),
PRINT("SS8",II,JJ),
SUBIS9:SUBMATRIX(SS9,I2,I2-1,I2-2,I2-3,I2-4,I2-5,I2-6,I2-7,I2-8,I2-9,
                I2-10,I2-11,I2-12,I2-13,I2-14,I2-15,I2-16,I2-17),
SUBJS9:SUBMATRIX(SS9,J2,J2-1,J2-2,J2-3,J2-4,J2-5,J2-6,J2-7,J2-8,J2-9,
                J2-10,J2-11,J2-12,J2-13,J2-14,J2-15,J2-16,J2-17),
PRINT("SS9",II,JJ),
SUBIS10:SUBMATRIX(SS10,I2,I2-1,I2-2,I2-3,I2-4,I2-5,I2-6,I2-7,I2-8,I2-9,
                I2-10,I2-11,I2-12,I2-13,I2-14,I2-15,I2-16,I2-17),
SUBJS10:SUBMATRIX(SS10,J2,J2-1,J2-2,J2-3,J2-4,J2-5,J2-6,J2-7,J2-8,J2-9,
                J2-10,J2-11,J2-12,J2-13,J2-14,J2-15,J2-16,J2-17),
PRINT("SS10",II,JJ),
SUBIS11:SUBMATRIX(SS11,I2,I2-1,I2-2,I2-3,I2-4,I2-5,I2-6,I2-7,I2-8,I2-9,
                I2-10,I2-11,I2-12,I2-13,I2-14,I2-15,I2-16,I2-17),
SUBJS11:SUBMATRIX(SS11,J2,J2-1,J2-2,J2-3,J2-4,J2-5,J2-6,J2-7,J2-8,J2-9,
                J2-10,J2-11,J2-12,J2-13,J2-14,J2-15,J2-16,J2-17),
PRINT("SS11",II,JJ),
SUBIS12:SUBMATRIX(SS12,I2,I2-1,I2-2,I2-3,I2-4,I2-5,I2-6,I2-7,I2-8,I2-9,
                I2-10,I2-11,I2-12,I2-13,I2-14,I2-15,I2-16,I2-17),
SUBJS12:SUBMATRIX(SS12,J2,J2-1,J2-2,J2-3,J2-4,J2-5,J2-6,J2-7,J2-8,J2-9,
                J2-10,J2-11,J2-12,J2-13,J2-14,J2-15,J2-16,J2-17),
PRINT("SS12",II,JJ),
N2S:N2S+ A[II,JJ]*(SUBIS0.Q.TQ.SUBJS0+CA*(TQ.SUBJS0.Q)*SUBIS0),
PRINT("N2SA",II,JJ),
N2S:N2S+DD[II,JJ]*(CB*(SUBIS0.Q.TQ.SUBJS2+CA*(TQ.SUBIS0.Q)*SUBJS2+
                SUBIS2.Q.TQ.SUBJS0+CA*(TQ.SUBIS2.Q)*SUBJS0)+
                SUBIS1.Q.TQ.SUBJS1+CA*(TQ.SUBJS1.Q)*SUBIS1),
PRINT("N2SD",II,JJ),
N2S:N2S+ F[II,JJ]*(CB*(SUBIS0.Q.TQ.SUBJS4+CA*(TQ.SUBIS0.Q)*SUBJS4+
                SUBIS4.Q.TQ.SUBJS0+CA*(TQ.SUBIS4.Q)*SUBJS0)+
                CC*(SUBIS1.Q.TQ.SUBJS3+CA*(TQ.SUBIS1.Q)*SUBJS3+
                SUBIS3.Q.TQ.SUBJS1+CA*(TQ.SUBIS3.Q)*SUBJS1)+
                SUBIS2.Q.TQ.SUBJS2+CA*(TQ.SUBJS2.Q)*SUBIS2),
PRINT("N2SF",II,JJ),
N2S:N2S+ H[II,JJ]*(CB*(SUBIS0.Q.TQ.SUBJS6+CA*(TQ.SUBIS0.Q)*SUBJS6+

```

```

      SUBIS6.Q.TQ.SUBJS0+CA*(TQ.SUBIS6.Q)*SUBJS0)+
CC*(SUBIS1.Q.TQ.SUBJS5+CA*(TQ.SUBIS1.Q)*SUBJS5+
      SUBIS5.Q.TQ.SUBJS1+CA*(TQ.SUBIS5.Q)*SUBJS1)+
CC*(SUBIS2.Q.TQ.SUBJS4+CA*(TQ.SUBIS2.Q)*SUBJS4+
      SUBIS4.Q.TQ.SUBJS2+CA*(TQ.SUBIS4.Q)*SUBJS2)+
      SUBIS3.Q.TQ.SUBJS3+CA*(TQ.SUBIS3.Q)*SUBIS3),
PRINT("N2SH",II,JJ),
N2S:N2S+ J[II,JJ]*(CB*(SUBIS0.Q.TQ.SUBJS8+CA*(TQ.SUBIS0.Q)*SUBJS8+
      SUBIS8.Q.TQ.SUBJS0+CA*(TQ.SUBIS8.Q)*SUBJS0)+
CC*(SUBIS1.Q.TQ.SUBJS7+CA*(TQ.SUBIS1.Q)*SUBJS7+
      SUBIS7.Q.TQ.SUBJS1+CA*(TQ.SUBIS7.Q)*SUBJS1)+
CC*(SUBIS2.Q.TQ.SUBJS6+CA*(TQ.SUBIS2.Q)*SUBJS6+
      SUBIS6.Q.TQ.SUBJS2+CA*(TQ.SUBIS6.Q)*SUBJS2)+
CC*(SUBIS3.Q.TQ.SUBJS5+CA*(TQ.SUBIS3.Q)*SUBJS5+
      SUBIS5.Q.TQ.SUBJS3+CA*(TQ.SUBIS5.Q)*SUBJS3)+
      SUBIS4.Q.TQ.SUBJS4+CA*(TQ.SUBIS4.Q)*SUBIS4),
PRINT("N2SJ",II,JJ),
N2S:N2S+ L[II,JJ]*(CB*(SUBIS0.Q.TQ.SUBJS10+CA*(TQ.SUBIS0.Q)*SUBJS10+
      SUBIS10.Q.TQ.SUBJS0+CA*(TQ.SUBIS10.Q)*SUBJS0)+
CC*(SUBIS1.Q.TQ.SUBJS9+CA*(TQ.SUBIS1.Q)*SUBJS9+
      SUBIS9.Q.TQ.SUBJS1+CA*(TQ.SUBIS9.Q)*SUBJS1)+
CC*(SUBIS2.Q.TQ.SUBJS8+CA*(TQ.SUBIS2.Q)*SUBJS8+
      SUBIS8.Q.TQ.SUBJS2+CA*(TQ.SUBIS8.Q)*SUBJS2)+
CC*(SUBIS3.Q.TQ.SUBJS7+CA*(TQ.SUBIS3.Q)*SUBJS7+
      SUBIS7.Q.TQ.SUBJS3+CA*(TQ.SUBIS7.Q)*SUBJS3)+
CC*(SUBIS4.Q.TQ.SUBJS6+CA*(TQ.SUBIS4.Q)*SUBJS6+
      SUBIS6.Q.TQ.SUBJS4+CA*(TQ.SUBIS6.Q)*SUBJS4)+
      SUBIS5.Q.TQ.SUBJS5+CA*(TQ.SUBIS5.Q)*SUBIS5),
PRINT("N2SL",II,JJ),
N2S:N2S+ R[II,JJ]*(CB*(SUBIS0.Q.TQ.SUBJS12+CA*(TQ.SUBIS0.Q)*SUBJS12+
      SUBIS12.Q.TQ.SUBJS0+CA*(TQ.SUBIS12.Q)*SUBJS0)+
CC*(SUBIS1.Q.TQ.SUBJS11+CA*(TQ.SUBIS1.Q)*SUBJS11+
      SUBIS11.Q.TQ.SUBJS1+CA*(TQ.SUBIS11.Q)*SUBJS1)+
CC*(SUBIS2.Q.TQ.SUBJS10+CA*(TQ.SUBIS2.Q)*SUBJS10+
      SUBIS10.Q.TQ.SUBJS2+CA*(TQ.SUBIS10.Q)*SUBJS2)+
CC*(SUBIS3.Q.TQ.SUBJS9+CA*(TQ.SUBIS3.Q)*SUBJS9+
      SUBIS9.Q.TQ.SUBJS3+CA*(TQ.SUBIS9.Q)*SUBJS3)+
CC*(SUBIS4.Q.TQ.SUBJS8+CA*(TQ.SUBIS4.Q)*SUBJS8+
      SUBIS8.Q.TQ.SUBJS4+CA*(TQ.SUBIS8.Q)*SUBJS4)+
CC*(SUBIS5.Q.TQ.SUBJS7+CA*(TQ.SUBIS5.Q)*SUBJS7+
      SUBIS7.Q.TQ.SUBJS5+CA*(TQ.SUBIS7.Q)*SUBJS5)+
      SUBIS6.Q.TQ.SUBJS6+CA*(TQ.SUBIS6.Q)*SUBIS6),
PRINT("N2SR",II,JJ),
N2S:N2S+ T[II,JJ]*(CC*(SUBIS2.Q.TQ.SUBJS12+CA*(TQ.SUBIS2.Q)*SUBJS12+
      SUBIS12.Q.TQ.SUBJS2+CA*(TQ.SUBIS12.Q)*SUBJS2)+
      CC*(SUBIS3.Q.TQ.SUBJS11+CA*(TQ.SUBIS3.Q)*SUBJS11+

```

```

SUBIS11.Q.TQ.SUBJS3+CA*(TQ.SUBIS11.Q)*SUBJS3)+
CC*(SUBIS4.Q.TQ.SUBJS10+CA*(TQ.SUBIS4.Q)*SUBJS10+
SUBIS10.Q.TQ.SUBJS4+CA*(TQ.SUBIS10.Q)*SUBJS4)+
CC*(SUBIS5.Q.TQ.SUBJS9+CA*(TQ.SUBIS5.Q)*SUBJS9+
SUBIS9.Q.TQ.SUBJS5+CA*(TQ.SUBIS9.Q)*SUBJS5)+
CC*(SUBIS6.Q.TQ.SUBJS8+CA*(TQ.SUBIS6.Q)*SUBJS8+
SUBIS8.Q.TQ.SUBJS6+CA*(TQ.SUBIS8.Q)*SUBJS6)+
SUBIS7.Q.TQ.SUBJS7+CA*(TQ.SUBJS7.Q)*SUBIS7),
PRINT("N2ST",II,JJ),
N2S:N2S+XH[II,JJ]*(CC*(SUBIS4.Q.TQ.SUBJS12+CA*(TQ.SUBIS4.Q)*SUBJS12+
SUBIS12.Q.TQ.SUBJS4+CA*(TQ.SUBIS12.Q)*SUBJS4)+
CC*(SUBIS5.Q.TQ.SUBJS11+CA*(TQ.SUBIS5.Q)*SUBJS11+
SUBIS11.Q.TQ.SUBJS5+CA*(TQ.SUBIS11.Q)*SUBJS5)+
CC*(SUBIS6.Q.TQ.SUBJS10+CA*(TQ.SUBIS6.Q)*SUBJS10+
SUBIS10.Q.TQ.SUBJS6+CA*(TQ.SUBIS10.Q)*SUBJS6)+
CC*(SUBIS7.Q.TQ.SUBJS9+CA*(TQ.SUBIS7.Q)*SUBJS9+
SUBIS9.Q.TQ.SUBJS7+CA*(TQ.SUBIS9.Q)*SUBJS7)+
SUBIS8.Q.TQ.SUBJS8+CA*(TQ.SUBJS8.Q)*SUBIS8),
PRINT("N2SXH",II,JJ),
N2S:N2S+XJ[II,JJ]*(CC*(SUBIS6.Q.TQ.SUBJS12+CA*(TQ.SUBIS6.Q)*SUBJS12+
SUBIS12.Q.TQ.SUBJS6+CA*(TQ.SUBIS12.Q)*SUBJS6)+
CC*(SUBIS7.Q.TQ.SUBJS11+CA*(TQ.SUBIS7.Q)*SUBJS11+
SUBIS11.Q.TQ.SUBJS7+CA*(TQ.SUBIS11.Q)*SUBJS7)+
CC*(SUBIS8.Q.TQ.SUBJS10+CA*(TQ.SUBIS8.Q)*SUBJS10+
SUBIS10.Q.TQ.SUBJS8+CA*(TQ.SUBIS10.Q)*SUBJS8)+
SUBIS9.Q.TQ.SUBJS9+CA*(TQ.SUBJS9.Q)*SUBIS9),
PRINT("N2SXJ",II,JJ),
N2S:N2S+XL[II,JJ]*(CC*(SUBIS8.Q.TQ.SUBJS12+CA*(TQ.SUBIS8.Q)*SUBJS12+
SUBIS12.Q.TQ.SUBJS8+CA*(TQ.SUBIS12.Q)*SUBJS8)+
CC*(SUBIS9.Q.TQ.SUBJS11+CA*(TQ.SUBIS9.Q)*SUBJS11+
SUBIS11.Q.TQ.SUBJS9+CA*(TQ.SUBIS11.Q)*SUBJS9)+
SUBIS10.Q.TQ.SUBJS10+CA*(TQ.SUBJS10.Q)*SUBIS10),
PRINT("N2SXL",II,JJ),
N2S:N2S+XR[II,JJ]*(CC*(SUBIS10.Q.TQ.SUBJS12+CA*(TQ.SUBIS10.Q)*SUBJS12+
SUBIS12.Q.TQ.SUBJS10+CA*(TQ.SUBIS12.Q)*SUBJS10)+
SUBIS11.Q.TQ.SUBJS11+CA*(TQ.SUBJS11.Q)*SUBIS11),
PRINT("N2SXR",II,JJ),
N2S:N2S+XT[II,JJ]*(SUBIS12.Q.TQ.SUBJS12+CA*(TQ.SUBJS12.Q)*SUBIS12),
PRINT("N2SXT",II,JJ),
KILL(SUBJS12,SUBIS12,SUBJS11,SUBIS11,SUBJS10,SUBIS10),
KILL(SUBJS0,SUBJS1,SUBJS2,SUBJS3,SUBJS4,SUBJS5,SUBJS6),
KILL(SUBJS7,SUBJS8,SUBJS9),
KILL(SUBIS0,SUBIS1,SUBIS2,SUBIS3,SUBIS4,SUBIS5,SUBIS6),
KILL(SUBIS7,SUBIS8,SUBIS9)))$
KILL(SS0,SS1,SS2,SS3,SS4,SS5,SS6,SS7,SS8,SS9,SS10,SS1,SS12)$

```

```
SAVE("SPH-N2S.SV",N2S);

N2SYM:ZEROMATRIX(18,18)$
FOR II THRU 18 DO FOR JJ:II THRU 18 DO N2SYM[II,JJ]:N2S[II,JJ]$
PRINT ("SYMMETRIC N2S FORMED")$
KILL(N2S)$
N2:ZEROMATRIX(18,18)$
KILL(Q,TQ)$

/*****
/* THE FOLLOWING STATEMENTS GENERATE A FORTRAN STATEMENT FOR EACH NONZERO */
/* ELEMENT OF SN2S(I,J).  THESE STATEMENTS ARE OF THE FORM */
/*      SN2S(2,2)=A(1,1). */
/* EACH STATEMENT IS WRITTEN TO A SEPERATE FILE CALLED TT2XXX, WHERE XXX */
/* STARTS AT 001 FOR THE FIRST NONZERO ENTRY AND CONTINUES SEQUENTIALLY */
/* UNTIL ALL NONZERO ENTRIES THROUGH SN2S(18,18) ARE GENERATED.  THE */
/* MACSYMA FUNTION GENTRAN WILL ALSO BREAK STATEMENTS EXCEEDING 800 INTO */
/* SHORTER EXPRESSIONS TO AVOID TOO MANY CONTINUATION LINES.  MACSYMA */
/* AUTOMATICALLY MAKES CONTINUATION LINES COMPLETE WITH A LEGAL */
/* CHARACTER IN COLUMN 6. */
*****/

FOR II THRU 18 DO FOR JJ:II THRU 18 DO
N2[II,JJ]:FACTOROUT(N2SYM[II,JJ],Q(1),Q(2),Q(3),Q(4),Q(5),Q(6),Q(7),Q(8),
Q(9),Q(10),Q(11),Q(12),Q(13),Q(14),Q(15),Q(16),Q(17),Q(18))$

FRAME(I,J):=CONCAT(TNS,EV(18*(I-1)+J+1000))$

FOR I THRU 18 DO FOR J:I THRU 18 DO
(IF N2[I,J]#0 THEN(PT:1,GENTRAN(SN2S[EVAL(I),EVAL(J)]:EVAL(N2[I,J]),
[EVAL(FRAME(I,J))]))$
IF PT#1 THEN GENTRAN(PT:EVAL(PT),[TT2000])$

CLOSEFILE();
QUIT();
```

F.9 PLASTRN.MAC Input Deck

The MACSYMA input deck, PLASTRN.MAC, accomplishes several steps: (1) symbolically generating the appropriate incremental strain-displacement relations, (2) symbolically generating the Taylor series approximations for the 60 shell shape functions (\hat{H}_i), (3) inserting the shell shape functions into the strain-displacement relations, and (4) determining the incrementa χ_j^i components for each incremental strain-displacement relation ϵ_j .

```

/*.....*/
/*.....*/
/*  MACSYMA ROUTINE FOR ELEMENTAL CODE GENERATION BY S. A. SCHIMMELS  */
/*  CREATED AS A PART OF AN AIR FORCE INSTITUTE OF TECHNOLOGY (AFIT)  */
/*  PhD PROGRAM IN AERONAUTICAL ENGINEERING (MATERIAL AND GEOMETRIC  */
/*  NONLINEARITY OF COMPOSITE SHELL STRUCTURES) ---- MARCH 1993    */
/*          MACSYMA IS A REGISTERED TRADEMARK OF                      */
/*          THE MASSACHUSETTS INSTITUTE OF TECHNOLOGY                */
/*                                                                    */
/*  PROGRAM PLASTRN.MAC: FOR A SPHERICAL SHELL.  CREATES THE        */
/*  INCREMENTAL STRAIN-DISPLACEMENT RELATIONS BASED ON THE          */
/*  PRESCRIBED DISPLACEMENT FIELD AND THEN GENERATES AND SAVES     */
/*  THE APPROPRIATE INCREMENTAL CHI COMPONENTS FOR EACH STRAIN TERM. */
/*.....*/
/*.....*/

/*.....*/
/*  INITIALIZE THE MACSYMA PARAMETERS AND DECLARE THE VARIABLE      */
/*  PROPERTIES                                                        */
/*.....*/
[DYNAMALLOC:TRUE,DISKGC:TRUE,DERIVABBREV:TRUE,POWERDISP:TRUE];
DEPENDS([U1D,U1R,U2D,U2R,P1,P2,R1,R2,M1,M2,H1,H2],[Y1,Y2,Y3]);
DEPENDS([PSI1,PSI2,PHI1,PHI2,GAMMA1,GAMMA2],[Y1,Y2]);
DEPENDS([THETA1,THETA2,U,V,W,U3],[Y1,Y2]);
DECLARE([R,C,D,AR1,AR2,AR3,AR4,H3],CONSTANT);

/*.....*/
/*  SET THE THEORETICAL ATTRIBUTES FOR A SPECIFIC ELEMENTAL CODE    */
/*.....*/

/*.....*/
/*  H3 = 1 FOR A SHELL                                              */
/*.....*/

```



```

H3:1;
/*.....*/
/* AR1 = 0 FOR A INCOMPLETE CUBIC KINEMATICS */
/* AR1 = 1 FOR THE COMPLETE QUARTIC KINEMATICS */
/*.....*/
AR1:0;

/*.....*/
/* AR2 = 0 FOR A LINEAR H1/H2 APPROXIMATIONS */
/* AR2 = 1 FOR THE QUADRATIC APPROXIMATIONS */
/*.....*/
AR2:0;

/*.....*/
/* AR3 = 0 FOR LINEAR TRANSVERSE STRAIN */
/* AR3 = 1 FOR NONLINEAR TRANSVERSE STRAIN */
/*.....*/
AR3:0;

/*.....*/
/* SUBLIST IS A VARIABLE CONTAINING THE DEFINITIONS OF INCREMENTAL */
/* DISPLACEMENT PARAMETERS DQ(1) THROUGH DQ(18). ALL SYMBOLIC MANIP- */
/* ULATION OF STRAIN COMPONENTS IS DONE WITH THE NAMES TO THE LEFT OF */
/* THE EQUAL SIGNS IN THE SUBLIST. THE DQ(XX) DEFINITIONS ARE REQUIRED */
/* ONLY FOR GENERATION OF ELEMENT INDEPENDENT STRAIN DEFINITION ARRAYS */
/* L0 THROUGH SS12, ETC. */
/*.....*/

SUBLIST: [DIFF(U,Y1)=DQ(2),DIFF(U,Y2)=DQ(3),U=DQ(1),DIFF(V,Y1)=DQ(5),
DIFF(V,Y2)=DQ(6),V=DQ(4),DIFF(W,Y1,2)=DQ(10),DIFF(W,Y2,2)=DQ(11),
DIFF(W,Y1,1,Y2,1)=DQ(12),DIFF(W,Y1)=DQ(8),DIFF(W,Y2)=DQ(9),W=DQ(7),
DIFF(PSI1,Y1)=DQ(14),DIFF(PSI1,Y2)=DQ(15),PSI1=DQ(13),
DIFF(PSI2,Y1)=DQ(17),DIFF(PSI2,Y2)=DQ(18),PSI2=DQ(16)];

/*.....*/
/* BEGIN GENERATING THE DISPLACEMENT FIELD COMPONENTS U1, U2, U3 THESE */
/* NEXT STEPS HAVE BEEN SPECIALIZED FOR A SPHERICAL SHELL R1 = 1/D, */
/* R2 = 1/C, K = -4/(3*H^2). THE VALUES OF D, C, AND K WILL BE INPUT */
/* AS PART OF THE FORTRAN PROGRAM. THEY ARE UNSPECIFIED CONSTANTS AS */
/* FAR AS MACSYMA IS CONCERNED */
/*.....*/
P1:U*(1-Y3*D);
P2:V*(1-Y3*C);
P11:DIFF(U,Y1)*(1-Y3*D);
P12:DIFF(U,Y2)*(1-Y3*D);
P21:DIFF(V,Y1)*(1-Y3*C);

```

```

P22:DIFF(V,Y2)*(1-Y3*C);
L11:DIFF(PSI1,Y1);
L12:DIFF(PSI1,Y2);
L21:DIFF(PSI2,Y1);
L22:DIFF(PSI2,Y2);
M1:K*(DIFF(W,Y1)+PSI1);
M2:K*(DIFF(W,Y2)+PSI2);

/*.....*/
/* INCOMPLETE CUBIC U1 DISPLACEMENT */
/* OF DENNIS. */
/*.....*/
U1D:P1+Y3*PSI1+Y3^3*M1;
/*.....*/
/* INCOMPLETE CUBIC U2 DISPLACEMENT */
/* OF DENNIS. */
/*.....*/
U2D:P2+Y3*PSI2+Y3^3*M2;

/*.....*/
/* COMPLETE QUARTIC U1 & U2 OF SMITH IS GIVEN BY U1 = U1D + U1R & U2 = */
/* U2D + U2R, WHERE U1R & U2R ARE THE CURVATURE CORRECTION TERMS. */
/*.....*/
U1R:(-M1*(1+K*Y3^2)*Y3^2/(K/D));
U2R:(-M2*(1+K*Y3^2)*Y3^2/(K/C));
U1:U1D+U1R*AR1;
U2:U2D+U2R*AR1;
U3:W;

/*.....*/
/* SYMBOLICALLY THE DERIVATIONS OF U1, U2, AND U3. */
/*.....*/
DU11:P11+Y3*L11+Y3^3*DIFF(M1,Y1)+AR1*DIFF(U1R,Y1);
DU12:P12+Y3*L12+Y3^3*DIFF(M1,Y2)+AR1*DIFF(U1R,Y2);
DU21:P21+Y3*L21+Y3^3*DIFF(M2,Y1)+AR1*DIFF(U2R,Y1);
DU22:P22+Y3*L22+Y3^3*DIFF(M2,Y2)+AR1*DIFF(U2R,Y2);
DU31:DIFF(U3,Y1);
DU32:DIFF(U3,Y2);

/*.....*/

```

```

/* SYMBOLICALLY GENERATE THE LAGRANGIAN GREEN-STRAIN COMPONENTS */
/* DIVIDED BY THE APPROPRIATE SHELL LAME' PARAMETERS H1, H2, TO GIVE THE */
/* PHYSICAL STRAINS EPSILON11, EPSILON22, EPSILON12, EPSILON23, */
/* EPSILON13, EPSILON33 */
/*.....*/

/*.....*/
/* EPSILON11 COMPONENT OF STRAIN. LINE 1 IS THE LINEAR TERMS. LINES 2 */
/* THROUGH 4 ARE THE NONLINEAR TERMS */
/*.....*/
ER[1]: ((H1*DU11+DIFF(H1,Y2)*H1*U2/H2+DIFF(H1,Y3)*H1*U3/H3)+
1/2*(DU11+DIFF(H1,Y2)*U2/H2+DIFF(H1,Y3)*U3/H3)^2+
1/2*(DU21-DIFF(H1,Y2)*U1/H2)^2+
1/2*(DU31-DIFF(H1,Y3)*U1/H3)^2)/H1^2;

/*.....*/
/* EPSILON22 COMPONENT OF STRAIN. LINE 1 IS THE LINEAR TERMS. LINES 2 */
/* THROUGH 4 ARE THE NONLINEAR TERMS */
/*.....*/
ER[2]: ((H2*DU22+DIFF(H2,Y1)*H2*U1/H1+DIFF(H2,Y3)*H2*U3/H3)+
1/2*(DU22+DIFF(H2,Y1)*U1/H1+DIFF(H2,Y3)*U3/H3)^2+
1/2*(DU12-DIFF(H2,Y1)*U2/H1)^2+
1/2*(DU32-DIFF(H2,Y3)*U2/H3)^2)/H2^2;

/*.....*/
/* EPSILON12 COMPONENT OF STRAIN. LINE 1 IS THE LINEAR TERMS. LINES 2 */
/* THROUGH 4 ARE THE NONLINEAR TERMS */
/*.....*/
ER[6]: ((H1*DU12+H2*DU21-DIFF(H2,Y1)*U2-DIFF(H1,Y2)*U1)+
(DU12-DIFF(H2,Y1)*U2/H1)*(DU11+DIFF(H1,Y2)*U2/H2+DIFF(H1,Y3)*U3/H3)+
(DU21-DIFF(H1,Y2)*U1/H2)*(DU22+DIFF(H2,Y1)*U1/H1+DIFF(H2,Y3)*U3/H3)+
(DU31-DIFF(H1,Y3)*U1/H3)*(DU32-DIFF(H2,Y3)*U2/H3))/(H1*H2);

/*.....*/
/* EPSILON23 COMPONENT OF STRAIN. LINE 1 IS THE LINEAR TERMS. LINES 2 */
/* THROUGH 8 ARE THE NONLINEAR TERMS. FORCING FUNCTION F(Z)=1+ 3*K*Y3^2 */
/* IS USED. THIS PARABOLIC FORCING FUNCTION APPLIED ONLY TO NONLINEAR */
/* TERMS. */
/*.....*/
ER[4]: (DU32+(1-C*Y3)*DIFF(U2,Y3)-U2*(-C))/(H2*H3);
ERNL[4]: (1+3*K*Y3^2)*((
DIFF(U2,Y3)-DIFF(H3,Y2)*U3/H2)*
(DIFF(U2,Y2)+DIFF(H2,Y1)*U1/H1+DIFF(H2,Y3)*U3/H3)+
(DIFF(U3,Y2)-DIFF(H2,Y3)*U2/H3)*
(DIFF(U3,Y3)+DIFF(H3,Y1)*U1/H1+DIFF(H3,Y2)*U2/H2)+

```

```

(DIFF(U1,Y2)-DIFF(H2,Y1)*U2/H1)*
(DIFF(U1,Y3)-DIFF(H3,Y1)*U3/H1))/(H2*H3);
ER[4]:ER[4]+ERNL[4]*AR3;

/*.....*/
/* EPSILON13 COMPONENT OF STRAIN. LINE 1 IS THE LINEAR TERMS. LINES 2 */
/* THROUGH 8 ARE THE NONLINEAR TERMS. FORCING FUNCTION F(Z) =1+3*K*Y3^2 */
/* IS USED. THIS PARABOLIC FORCING FUNCTION APPLIED ONLY TO NONLINEAR */
/* TERMS. */
/*.....*/
ER[5]:(DU31+(1-D*Y3)*DIFF(U1,Y3)-U1*(-D))/(H1*H3);
ERNL[5]:(1+3*K*Y3^2)*(
(DIFF(U1,Y3)-DIFF(H3,Y1)*U3/H1)*
(DIFF(U1,Y1)+DIFF(H1,Y2)*U2/H2+DIFF(H1,Y3)*U3/H3)+
(DIFF(U3,Y1)-DIFF(H1,Y3)*U1/H3)*
(DIFF(U3,Y3)+DIFF(H3,Y1)*U1/H1+DIFF(H3,Y2)*U2/H2)+
(DIFF(U2,Y1)-DIFF(H1,Y2)*U1/H2)*
(DIFF(U2,Y3)-DIFF(H3,Y2)*U3/H2))/(H1*H3);
ER[5]:ER[5]+ERNL[5]*AR3;

/*.....*/
/* EPSILON33 COMPONENT OF STRAIN IS ZERO. IT IS, HOWEVER, INCLUDED IN */
/* THE CONSTITUTIVE RELATIONS THROUGH THE ELASTICITY SUBROUTINE OF THE */
/* CODE WRITTEN BY DENNIS. */
/*.....*/
ER[3]:0;

/*.....*/
/* SUBSTITUTE THE Q(1) THROUGH Q(18) DEFINITIONS OF SUBLIST AND DISPLAY */
/* THE STRAIN COMPONENTS INDIVIDUALLY. */
/*.....*/
FOR I THRU 6 DO (ER[I]:EXPAND(ER[I]),
ER[I]:EXPAND(SUBST(SUBLIST,ER[I]),DISPLAY(ER[I])));

/*.....*/
/* THE NEXT 60 EXPRESSIONS ARE THE POSSIBLE COMBINATIONS OF THE LAME' */
/* PARAMETERS APPEARING IN THE STRAIN EXPRESSIONS FOR AN ARBITRARY */
/* SHELL, WHERE H3 = 1, AND H1, H2 DEPEND UPON Y1, Y2, AND Y3. */
/*.....*/
HREXP[1]:(DIFF(H1,Y2)/H1);
HREXP[2]:(DIFF(H1,Y3)/H1);
HREXP[3]:(1/(H1^2));
HREXP[4]:(DIFF(H1,Y2)^2/(H1^2));
HREXP[5]:(DIFF(H1,Y2)^2/(H2^2));
HREXP[6]:(DIFF(H1,Y3)^2/(H1^2));

```

```
HREXP[7]: (DIFF(H1,Y3)^2);
HREXP[8]: (DIFF(H1,Y2)*DIFF(H1,Y3)/(H1^2));
HREXP[9]: (DIFF(H2,Y3)/H2);
HREXP[10]: (DIFF(H2,Y1)/H2);
HREXP[11]: (1/(H2^2));
HREXP[12]: (DIFF(H2,Y1)^2/(H2^2));
HREXP[13]: (DIFF(H2,Y1)^2/(H1^2));
HREXP[14]: (DIFF(H2,Y3)^2/(H2^2));
HREXP[15]: (DIFF(H2,Y3)^2);
HREXP[16]: (DIFF(H2,Y3)*DIFF(H2,Y1)/(H2^2));
HREXP[17]: (1/H2);
HREXP[18]: (1/H1);
HREXP[19]: (DIFF(H2,Y1)/H1);
HREXP[20]: (DIFF(H1,Y2)/H2);
HREXP[21]: (1/(H1*H2));
HREXP[22]: (DIFF(H1,Y3)/H2);
HREXP[23]: (DIFF(H2,Y3)/H1);
HREXP[24]: (DIFF(H2,Y1)*DIFF(H1,Y2)/(H1^2));
HREXP[25]: (DIFF(H2,Y1)*DIFF(H1,Y2)/(H2^2));
HREXP[26]: (DIFF(H1,Y3)*DIFF(H2,Y3));
HREXP[27]: (DIFF(H1,Y3)*DIFF(H2,Y1)/(H1^2));
HREXP[28]: (DIFF(H2,Y3)*DIFF(H1,Y2)/(H2^2));
HREXP[29]: (DIFF(H1,Y2)/(H1*H2));
HREXP[30]: (DIFF(H1,Y2)^2/(H1^2*H2));
HREXP[31]: (DIFF(H1,Y2)^2/(H2^2*H1));
HREXP[32]: (DIFF(H1,Y3)^2/H1);
HREXP[33]: (DIFF(H1,Y2)/(H1^2));
HREXP[34]: (DIFF(H1,Y3)/(H1^2));
HREXP[35]: (DIFF(H1,Y2)*DIFF(H1,Y3)/(H1^2*H2));
HREXP[36]: (DIFF(H2,Y1)/(H1*H2));
HREXP[37]: (DIFF(H2,Y1)^2/(H1*H2^2));
HREXP[38]: (DIFF(H2,Y1)^2/(H2*H1^2));
HREXP[39]: (DIFF(H2,Y3)^2/H2);
HREXP[40]: (DIFF(H2,Y1)/(H2^2));
HREXP[41]: (DIFF(H2,Y3)*DIFF(H2,Y1)/(H1*H2^2));
HREXP[42]: (DIFF(H2,Y3)/(H2^2));
HREXP[43]: (DIFF(H1,Y2)/(H2^2));
HREXP[44]: (DIFF(H2,Y1)/(H1^2));
HREXP[45]: (DIFF(H1,Y3)/(H1*H2));
HREXP[46]: (DIFF(H2,Y3)/(H1*H2));
HREXP[47]: (DIFF(H2,Y1)*DIFF(H1,Y2)/(H1^2*H2));
HREXP[48]: (DIFF(H1,Y2)*DIFF(H2,Y1)/(H2^2*H1));
HREXP[49]: (DIFF(H1,Y3)*DIFF(H2,Y1)/(H1^2*H2));
HREXP[50]: (DIFF(H2,Y3)*DIFF(H1,Y2)/(H2^2*H1));
HREXP[51]: (DIFF(H1,Y3)*DIFF(H2,Y3)/H2);
HREXP[52]: (DIFF(H1,Y3)*DIFF(H2,Y3)/H1);
```

```

HREXP[53]:(DIFF(H1,Y2)^2/(H1^2*H2^2));
HREXP[54]:(DIFF(H1,Y2)/(H1^2*H2));
HREXP[55]:(DIFF(H2,Y1)^2/(H1^2*H2^2));
HREXP[56]:(DIFF(H2,Y1)/(H2^2*H1));
HREXP[57]:(DIFF(H1,Y2)/(H1*H2^2));
HREXP[58]:(DIFF(H2,Y1)/(H2*H1^2));
HREXP[59]:(DIFF(H2,Y1)*DIFF(H1,Y2)/(H1^2*H2^2));
HREXP[60]:(DIFF(H1,Y3)*DIFF(H2,Y3)/(H1*H2));

/*.....*/
/* THE MACRO HRTAY(X,I)::= GENERATES THE COEFFICIENTS F, G, AND H OF THE*/
/* TAYLOR'S SERIES EXPANSION OF THE EXPRESSION X ABOUT THE POINT Y3 = 0 */
/* FOR A SPHERICAL SHELL WITH H1 = 1 - Y3/R1 AND H2 = 1 - Y3/R2.      */
/*.....*/
HRTAY(X,I):=BUILDQ([X,I],(
PRINT(" THE TAYLOR SERIES EXPANSION OF "),DISPLAY(X),
PRINT(" IS EQUAL TO F + G*Y3 + H*Y3^2 + H.O.T., WHERE "),
(X:TAYLOR(FACTOROUT(EXPAND(RAT(EV(X,H1=(1-Y3*D),
H2=(1-Y3*C),DIFF))),C,D),Y3,0,3)),
F[I]:EXPAND(COEFF(X,Y3,0)),DISPLAY(F[I]),
G[I]:EXPAND(COEFF(X,Y3,1)),DISPLAY(G[I]),
H[I]:EXPAND(COEFF(X,Y3,2)),DISPLAY(H[I])));

/*.....*/
/* COMPUTE THE COEFFICIENTS F, G, AND H FOR ALL 60 HREXP EXPRESSIONS. */
/*.....*/
FOR I THRU 60 DO HRTAY(HREXP[I],I);

/*.....*/
/* THE MACRO HRSUB(X)::= TAKES ANY ONE-TERM EXPRESSION X, (PRODUCTS ARE */
/* OK, BUT [+ -] OPERATORS ARE NOT) AND SUBSTITUTES THE APPROXIMATE */
/* SERIES EXPANSION F + G*Y3 + H*Y3^2 FOR THE FUNCTION OF LAME'      */
/* PARAMETERS.                                                         */
/*.....*/
HRSUB(X):=BUILDQ([X],(
XO:X,
X:NUM(X)/SUBST(D[1],H1,DENOM(X)),
X:NUM(X)/SUBST(D[2],H2,DENOM(X)),
X:NUM(X)/RATSUBST(D[3],D[1]*D[1],DENOM(X)),
X:NUM(X)/RATSUBST(D[4],D[2]*D[2],DENOM(X)),
X:NUM(X)/RATSUBST(D[5],D[1]*D[2],DENOM(X)),
X:NUM(X)/RATSUBST(D[6],D[1]*D[4],DENOM(X)),
X:NUM(X)/RATSUBST(D[7],D[2]*D[3],DENOM(X)),
X:NUM(X)/RATSUBST(D[8],D[3]*D[4],DENOM(X)),
XD:X,
X:NUM(X)/RATSUBST(1/D[1],D[1],DENOM(X)),

```

```

X:NUM(X)/RATSUBST(1/D[2],D[2],DENOM(X)),
X:NUM(X)/RATSUBST(1/D[3],D[3],DENOM(X)),
X:NUM(X)/RATSUBST(1/D[4],D[4],DENOM(X)),
X:NUM(X)/RATSUBST(1/D[5],D[5],DENOM(X)),
X:NUM(X)/RATSUBST(1/D[6],D[6],DENOM(X)),
X:NUM(X)/RATSUBST(1/D[7],D[7],DENOM(X)),
X:NUM(X)/RATSUBST(1/D[8],D[8],DENOM(X)),
XN:X,
X:RATSUBST(F[59]+Y3*G[59]+Y3^2*AR2*H[59], 'DIFF(H2,Y1)*DIFF(H1,Y2)*D[8],X),
X:RATSUBST(F[55]+Y3*G[55]+Y3^2*AR2*H[55], 'DIFF(H2,Y1)^2*D[8],X),
X:RATSUBST(F[53]+Y3*G[53]+Y3^2*AR2*H[53], 'DIFF(H1,Y2)^2*D[8],X),
X:RATSUBST(F[50]+Y3*G[50]+Y3^2*AR2*H[50], 'DIFF(H2,Y3)*DIFF(H1,Y2)*D[6],X),
X:RATSUBST(F[49]+Y3*G[49]+Y3^2*AR2*H[49], 'DIFF(H1,Y3)*DIFF(H2,Y1)*D[7],X),
X:RATSUBST(F[48]+Y3*G[48]+Y3^2*AR2*H[48], 'DIFF(H1,Y2)*DIFF(H2,Y1)*D[6],X),
X:RATSUBST(F[47]+Y3*G[47]+Y3^2*AR2*H[47], 'DIFF(H2,Y1)*DIFF(H1,Y2)*D[7],X),
X:RATSUBST(F[41]+Y3*G[41]+Y3^2*AR2*H[41], 'DIFF(H2,Y3)*DIFF(H2,Y1)*D[6],X),
X:RATSUBST(F[38]+Y3*G[38]+Y3^2*AR2*H[38], 'DIFF(H2,Y1)^2*D[7],X),
X:RATSUBST(F[37]+Y3*G[37]+Y3^2*AR2*H[37], 'DIFF(H2,Y1)^2*D[6],X),
X:RATSUBST(F[35]+Y3*G[35]+Y3^2*AR2*H[35], 'DIFF(H1,Y2)*DIFF(H1,Y3)*D[7],X),
X:RATSUBST(F[31]+Y3*G[31]+Y3^2*AR2*H[31], 'DIFF(H1,Y2)^2*D[6],X),
X:RATSUBST(F[30]+Y3*G[30]+Y3^2*AR2*H[30], 'DIFF(H1,Y2)^2*D[7],X),
X:RATSUBST(F[58]+Y3*G[58]+Y3^2*AR2*H[58], 'DIFF(H2,Y1)*D[7],X),
X:RATSUBST(F[57]+Y3*G[57]+Y3^2*AR2*H[57], 'DIFF(H1,Y2)*D[6],X),
X:RATSUBST(F[56]+Y3*G[56]+Y3^2*AR2*H[56], 'DIFF(H2,Y1)*D[6],X),
X:RATSUBST(F[54]+Y3*G[54]+Y3^2*AR2*H[54], 'DIFF(H1,Y2)*D[7],X),
X:RATSUBST(F[60]+Y3*G[60]+Y3^2*AR2*H[60], 'DIFF(H1,Y3)*DIFF(H2,Y3)*D[5],X),
X:RATSUBST(F[28]+Y3*G[28]+Y3^2*AR2*H[28], 'DIFF(H2,Y3)*DIFF(H1,Y2)*D[4],X),
X:RATSUBST(F[27]+Y3*G[27]+Y3^2*AR2*H[27], 'DIFF(H1,Y3)*DIFF(H2,Y1)*D[3],X),
X:RATSUBST(F[25]+Y3*G[25]+Y3^2*AR2*H[25], 'DIFF(H2,Y1)*DIFF(H1,Y2)*D[4],X),
X:RATSUBST(F[24]+Y3*G[24]+Y3^2*AR2*H[24], 'DIFF(H2,Y1)*DIFF(H1,Y2)*D[3],X),
X:RATSUBST(F[16]+Y3*G[16]+Y3^2*AR2*H[16], 'DIFF(H2,Y3)*DIFF(H2,Y1)*D[4],X),
X:RATSUBST(F[8]+Y3*G[8]+Y3^2*AR2*H[8], 'DIFF(H1,Y2)*DIFF(H1,Y3)*D[3],X),
X:RATSUBST(F[14]+Y3*G[14]+Y3^2*AR2*H[14], 'DIFF(H2,Y3)^2*D[4],X),
X:RATSUBST(F[13]+Y3*G[13]+Y3^2*AR2*H[13], 'DIFF(H2,Y1)^2*D[3],X),
X:RATSUBST(F[12]+Y3*G[12]+Y3^2*AR2*H[12], 'DIFF(H2,Y1)^2*D[4],X),
X:RATSUBST(F[6]+Y3*G[6]+Y3^2*AR2*H[6], 'DIFF(H1,Y3)^2*D[3],X),
X:RATSUBST(F[5]+Y3*G[5]+Y3^2*AR2*H[5], 'DIFF(H1,Y2)^2*D[4],X),
X:RATSUBST(F[4]+Y3*G[4]+Y3^2*AR2*H[4], 'DIFF(H1,Y2)^2*D[3],X),
X:RATSUBST(F[46]+Y3*G[46]+Y3^2*AR2*H[46], 'DIFF(H2,Y3)*D[5],X),
X:RATSUBST(F[45]+Y3*G[45]+Y3^2*AR2*H[45], 'DIFF(H1,Y3)*D[5],X),
X:RATSUBST(F[44]+Y3*G[44]+Y3^2*AR2*H[44], 'DIFF(H2,Y1)*D[3],X),
X:RATSUBST(F[43]+Y3*G[43]+Y3^2*AR2*H[43], 'DIFF(H1,Y2)*D[4],X),
X:RATSUBST(F[42]+Y3*G[42]+Y3^2*AR2*H[42], 'DIFF(H2,Y3)*D[4],X),
X:RATSUBST(F[40]+Y3*G[40]+Y3^2*AR2*H[40], 'DIFF(H2,Y1)*D[4],X),
X:RATSUBST(F[36]+Y3*G[36]+Y3^2*AR2*H[36], 'DIFF(H2,Y1)*D[5],X),
X:RATSUBST(F[34]+Y3*G[34]+Y3^2*AR2*H[34], 'DIFF(H1,Y3)*D[3],X),

```

```

X:RATSUBST(F[33]+Y3*G[33]+Y3^2*AR2*H[33], 'DIFF(H1,Y2)*D[3],X),
X:RATSUBST(F[29]+Y3*G[29]+Y3^2*AR2*H[29], 'DIFF(H1,Y2)*D[5],X),
X:RATSUBST(F[3]+Y3*G[3]+Y3^2*AR2*H[3], 1*D[3],X),
X:RATSUBST(F[21]+Y3*G[21]+Y3^2*AR2*H[21], 1*D[5],X),
X:RATSUBST(F[11]+Y3*G[11]+Y3^2*AR2*H[11], 1*D[4],X),
X:RATSUBST(F[52]+Y3*G[52]+Y3^2*AR2*H[52], 'DIFF(H1,Y3)*DIFF(H2,Y3)*D[1],X),
X:RATSUBST(F[51]+Y3*G[51]+Y3^2*AR2*H[51], 'DIFF(H1,Y3)*DIFF(H2,Y3)*D[2],X),
X:RATSUBST(F[39]+Y3*G[39]+Y3^2*AR2*H[39], 'DIFF(H2,Y3)^2*D[2],X),
X:RATSUBST(F[32]+Y3*G[32]+Y3^2*AR2*H[32], 'DIFF(H1,Y3)^2*D[1],X),
X:RATSUBST(F[23]+Y3*G[23]+Y3^2*AR2*H[23], 'DIFF(H2,Y3)*D[1],X),
X:RATSUBST(F[22]+Y3*G[22]+Y3^2*AR2*H[22], 'DIFF(H1,Y3)*D[2],X),
X:RATSUBST(F[20]+Y3*G[20]+Y3^2*AR2*H[20], 'DIFF(H1,Y2)*D[2],X),
X:RATSUBST(F[19]+Y3*G[19]+Y3^2*AR2*H[19], 'DIFF(H2,Y1)*D[1],X),
X:RATSUBST(F[10]+Y3*G[10]+Y3^2*AR2*H[10], 'DIFF(H2,Y1)*D[2],X),
X:RATSUBST(F[9]+Y3*G[9]+Y3^2*AR2*H[9], 'DIFF(H2,Y3)*D[2],X),
X:RATSUBST(F[1]+Y3*G[1]+Y3^2*AR2*H[1], 'DIFF(H1,Y2)*D[1],X),
X:RATSUBST(F[2]+Y3*G[2]+Y3^2*AR2*H[2], 'DIFF(H1,Y3)*D[1],X),
X:RATSUBST(F[17]+Y3*G[17]+Y3^2*AR2*H[17], 1*D[2],X),
X:RATSUBST(F[18]+Y3*G[18]+Y3^2*AR2*H[18], 1*D[1],X),
X:RATSUBST(F[15]+Y3*G[15]+Y3^2*AR2*H[15], 'DIFF(H2,Y3)^2,X),
X:RATSUBST(F[7]+Y3*G[7]+Y3^2*AR2*H[7], 'DIFF(H1,Y3)^2,X),
X:RATSUBST(F[26]+Y3*G[26]+Y3^2*AR2*H[26], 'DIFF(H1,Y3)*DIFF(H2,Y3),X))) ;

```

```

/*.....*/
/* THE MACRO PICK(XXX) ::= TAKES ANY EXPRESSION XXX (PREVIOUSLY EXPANDED)*/
/* AND SEPARATES IT INTO SINGLE EXPRESSIONS LABELED E(I). IT THEN CALLS*/
/* MACRO HRSUB(X) TO FIND THE APPROPRIATE LAME' PARAMETERS APPROXIMATION */
/* FOR EACH EXPRESSION AND THEN SUMS ALL THE EXPRESSIONS TO YIELD THE */
/* EXPRESSION XXX WITH ALL THE TERMS FULLY APPROXIMATED. */
/*.....*/

```

```

E(I):=CONCAT(E,I);
PICK(XXX):=BUILDQ([XXX], (I1:LINENUM,NT:NTERMS(XXX), I2:I1+NT-1,
PRINT(" THIS EXPRESSION HAS ",NT," TERMS TO BE RESOLVED "),
PICKAPART(XXX,1),FOR K:I1 THRU I2 DO EXH[K]:EV(E(K),EVAL),
FOR K:I1 THRU I2 DO HRSUB(EXH[K]),XXX:SUM(EXH[K],K,I1,I2),
DISPLAY(XXX)));

```

```

/*.....*/
/* USE THE MACRO PICK(XXX) TO APPROXIMATE LAME' PARAMETER FUNCTIONS OF */
/* THE STRAIN COMPONENTS. */
/*.....*/

```

```

ERR4:ER[4];
ERR5:ER[5];
PICK(ERR4);
PICK(ERR5);
ER[4]:ERR4;

```



```
ER[5]:ERR5;
ERR1:ER[1];
ERR2:ER[2];
ERR6:ER[6];
PICK(ERR1);
PICK(ERR2);
PICK(ERR6);
ER[1]:ERR1;
ER[2]:ERR2;
ER[6]:ERR6;

SAVE("SPH-ER.SV",ER);

/*.....*/
/* THE MACRO, CHIFORM(XX,YY,K):= EXPANDS A 6x1 VECTOR CALLED XX, THEN */
/* DETERMINES AND DISPLAYS THE COEFFICIENTS OF Y3 UPTO THE Kth POWER. */
/* THESE ARE CALLED YY[I,K]. */
/*.....*/
CHIFORM(XX,YY,K):=BUILDQ([XX,YY,K],(FOR I THRU 6 DO FOR JJ THRU K+1 DO
(XY[I]:FACTOROUT(EXPAND(RAT(XX[I])),[H1,H2]),
YY[I,JJ-1]:COEFF(XY[I],Y3,JJ-1),DISPLAY(YY[I,JJ-1]))));
POWERDISP:TRUE;
CHIFORM(ER,XR,12);
KILL(ER);

SAVE("SPH-XR.SV",XR);

CLOSEFILE();
QUIT()
```

F.10 PLASINIT.MAC Input Deck

The MACSYMA input deck, PLASINIT.MAC, generates the $(L^P)_i$ column arrays and the $[H^P]_i$ matrices for each incremental strain component, ϵ_j .

```

WRITEFILE("SPH-INIT.WF");
/*****
/*****
/*  MACSYMA ROUTINE FOR ELEMENTAL CODE GENERATION BY S. A. SCHIMMELS  */
/*  CREATED AS A PART OF AN AIR FORCE INSTITUTE OF TECHNOLOGY (AFIT)  */
/*      PhD PROGRAM IN AERONAUTICAL ENGINEERING --- MARCH 1993      */
/*      MACSYMA IS A REGISTERED TRADEMARK OF                        */
/*      THE MASSACHUSETTS INSTITUTE OF TECHNOLOGY                  */
/*                                                                    */
/*  PROGRAM PLASINIT.MAC: FOR A SPHERICAL SHELL.  CREATES THE LHMAT, */
/*  LSMAT, HMAT, & SSMAT ARRAYS.                                    */
/*****
/*****

/*****
/*  INITIALIZE MACSYMA PARAMETERS AND DECLARE VARIABLE PROPERTIES  */
/*****
[DYNAMALLOC:TRUE,DISKGC:TRUE,DERIVABBREV:TRUE,POWERDISP:TRUE]$

/*****
/*  THE MACRO DECOMPOSE(XR)::= DETERMINES AND DISPLAYS THE COEFFICIENTS OF */
/*  DISPLACEMENT VARIABLES DQ(1) THROUGH DQ(18) AND CREATES A 6x13x18      */
/*  ARRAY CALLED LMAT OF THE CONTANT COEFFICIENTS OF LINEAR DISPLACEMENT    */
/*  TERMS, AND A 6x13x18x18 ARRAY CALLED HMAT OF THE CONSTANT COEFFICIENTS */
/*  OF THE CONSTANT COEFFICIENTS OF THE QUADRATIC DISPLACEMENT TERMS.      */
/*****
LOADFILE("SPH-XRNEW.SV");

FOR I THRU 6 DO FOR JJ THRU 13 DO (DISPLAY (XR[I,JJ-1]))$
DECOMPOSE(XR)::=BUILDQ([XR],
(FOR I THRU 6 DO (PRINT("DECOMPOSING STRAIN COMPONENT",I),
(FOR J:0 THRU 12 DO (FOR K THRU 18 DO
(IF HIPOW(XR[I,J],DQ(K))=2 THEN
XQUAD[I,J,K]:RATCOEFF(XR[I,J],DQ(K),2)*DQ(K)*2+RATCOEFF(XR[I,J],DQ(K),
1) ELSE XQUAD[I,J,K]:RATCOEFF(XR[I,J],DQ(K),1),
FOR L THRU 18 DO HMAT[I,J,K,L]:RATCOEFF(XQUAD[I,J,K],DQ(L),1),
LMAT[I,J,K]:EXPAND(XQUAD[I,J,K]-SUM(HMAT[I,J,K,L]*DQ(L),L,1,18))))))$
DECOMPOSE(XR);
KILL(XR)$

```

```
SAVE("SPH-LHMAT.SV",LMAT,HMAT);
```

```

/*****
/* GENERATE ELEMENT-INDEPENDENT STRAIN DEFINITION ARRAYS LX AN HXX FOR */
/* IN-PLANE STRAINS AND SX AND SSXX FOR TRANSVERSE SHEAR STRAINS. X AND*/
/* XX REPRESENT THE POWER OF Y3 FOR WHICH THE COEFFICIENTS APPLY. NOTE */
/* LX HAS 3 COLUMNS. COLUMN 1 CONTAINS COEFFICIENTS OF THE EPSILON11 */
/* TERMS WHICH ARE LINEAR IN DISPLACEMENTS Q(1)-Q(18). COLUMN 2 */
/* CONTAINS EPSILON22 TERMS AND COLUMN 3 CONTAINS EPSILON12 TERMS. */
/* LIKEWISE HXX HAS 3 PARTITIONS. COLUMNS 1-18 CONTAINSS COEFFICIENTS */
/* OF EPSILON11 TERMS WHICH ARE QUADRATIC IN DISPLACEMENT. COLUMNS 19- */
/* 36 CONTAIN THE EPSILON22 TERMS AND COLUMNS 37-54 CONTAIN THE */
/* EPSILON12 TERMS. SIMILARLY, SX CONTAINS 2 COLUMNS PERTAINING TO THE */
/* COEFFICIENTS OF LINEAR TERMS OF EPSILON23 AND EPSILON133, */
/* RESPECTIVELY. SSXX HAS 2 PARTITIONS. COLUMNS 1-18 CONTAIN */
/* COEFFICIENTS OF THE QUADRATIC TERMS OF EPSILON23 AND COLUMNS 19-36 */
/* CONTAIN THE QUADRATIC TERMS OF EPSILON13. */
/*****
FOR NN THRU 18 DO (
  L0[NN,1]:LMAT[1,0,NN],L0[NN,2]:LMAT[2,0,NN],L0[NN,3]:LMAT[6,0,NN],
  L1[NN,1]:LMAT[1,1,NN],L1[NN,2]:LMAT[2,1,NN],L1[NN,3]:LMAT[6,1,NN],
  L2[NN,1]:LMAT[1,2,NN],L2[NN,2]:LMAT[2,2,NN],L2[NN,3]:LMAT[6,2,NN],
  L3[NN,1]:LMAT[1,3,NN],L3[NN,2]:LMAT[2,3,NN],L3[NN,3]:LMAT[6,3,NN],
  L4[NN,1]:LMAT[1,4,NN],L4[NN,2]:LMAT[2,4,NN],L4[NN,3]:LMAT[6,4,NN],
  L5[NN,1]:LMAT[1,5,NN],L5[NN,2]:LMAT[2,5,NN],L5[NN,3]:LMAT[6,5,NN],
  L6[NN,1]:LMAT[1,6,NN],L6[NN,2]:LMAT[2,6,NN],L6[NN,3]:LMAT[6,6,NN],
  L7[NN,1]:LMAT[1,7,NN],L7[NN,2]:LMAT[2,7,NN],L7[NN,3]:LMAT[6,7,NN],
  S0[NN,1]:LMAT[4,0,NN],S0[NN,2]:LMAT[5,0,NN],
  S1[NN,1]:LMAT[4,1,NN],S1[NN,2]:LMAT[5,1,NN],
  S2[NN,1]:LMAT[4,2,NN],S2[NN,2]:LMAT[5,2,NN],
  S3[NN,1]:LMAT[4,3,NN],S3[NN,2]:LMAT[5,3,NN],
  S4[NN,1]:LMAT[4,4,NN],S4[NN,2]:LMAT[5,4,NN],
  S5[NN,1]:LMAT[4,5,NN],S5[NN,2]:LMAT[5,5,NN],
  S6[NN,1]:LMAT[4,6,NN],S6[NN,2]:LMAT[5,6,NN],
  S7[NN,1]:LMAT[4,7,NN],S7[NN,2]:LMAT[5,7,NN],
  FOR MM THRU 18 DO (
    H0[NN,MM]:HMAT[1,0,NN,MM],H0[NN,MM+18]:HMAT[2,0,NN,MM],
    H0[NN,MM+36]:HMAT[6,0,NN,MM],
    H1[NN,MM]:HMAT[1,1,NN,MM],H1[NN,MM+18]:HMAT[2,1,NN,MM],
    H1[NN,MM+36]:HMAT[6,1,NN,MM],
    H2[NN,MM]:HMAT[1,2,NN,MM],H2[NN,MM+18]:HMAT[2,2,NN,MM],
    H2[NN,MM+36]:HMAT[6,2,NN,MM],
    H3[NN,MM]:HMAT[1,3,NN,MM],H3[NN,MM+18]:HMAT[2,3,NN,MM],
    H3[NN,MM+36]:HMAT[6,3,NN,MM],
    H4[NN,MM]:HMAT[1,4,NN,MM],H4[NN,MM+18]:HMAT[2,4,NN,MM],

```

```

H4[NN,MM+36]:HMAT[6,4,NN,MM],
H5[NN,MM]:HMAT[1,5,NN,MM],H5[NN,MM+18]:HMAT[2,5,NN,MM],
H5[NN,MM+36]:HMAT[6,5,NN,MM],
H6[NN,MM]:HMAT[1,6,NN,MM],H6[NN,MM+18]:HMAT[2,6,NN,MM],
H6[NN,MM+36]:HMAT[6,6,NN,MM],
H7[NN,MM]:HMAT[1,7,NN,MM],H7[NN,MM+18]:HMAT[2,7,NN,MM],
H7[NN,MM+36]:HMAT[6,7,NN,MM],
H8[NN,MM]:HMAT[1,8,NN,MM],H8[NN,MM+18]:HMAT[2,8,NN,MM],
H8[NN,MM+36]:HMAT[6,8,NN,MM],
H9[NN,MM]:HMAT[1,9,NN,MM],H9[NN,MM+18]:HMAT[2,9,NN,MM],
H9[NN,MM+36]:HMAT[6,9,NN,MM],
H10[NN,MM]:HMAT[1,10,NN,MM],H10[NN,MM+18]:HMAT[2,10,NN,MM],
H10[NN,MM+36]:HMAT[6,10,NN,MM],
H11[NN,MM]:HMAT[1,11,NN,MM],H11[NN,MM+18]:HMAT[2,11,NN,MM],
H11[NN,MM+36]:HMAT[6,11,NN,MM],
H12[NN,MM]:HMAT[1,12,NN,MM],H12[NN,MM+18]:HMAT[2,12,NN,MM],
H12[NN,MM+36]:HMAT[6,12,NN,MM],
SS0[NN,MM]:HMAT[4,0,NN,MM],SS0[NN,MM+18]:HMAT[5,0,NN,MM],
SS1[NN,MM]:HMAT[4,1,NN,MM],SS1[NN,MM+18]:HMAT[5,1,NN,MM],
SS2[NN,MM]:HMAT[4,2,NN,MM],SS2[NN,MM+18]:HMAT[5,2,NN,MM],
SS3[NN,MM]:HMAT[4,3,NN,MM],SS3[NN,MM+18]:HMAT[5,3,NN,MM],
SS4[NN,MM]:HMAT[4,4,NN,MM],SS4[NN,MM+18]:HMAT[5,4,NN,MM],
SS5[NN,MM]:HMAT[4,5,NN,MM],SS5[NN,MM+18]:HMAT[5,5,NN,MM],
SS6[NN,MM]:HMAT[4,6,NN,MM],SS6[NN,MM+18]:HMAT[5,6,NN,MM],
SS7[NN,MM]:HMAT[4,7,NN,MM],SS7[NN,MM+18]:HMAT[5,7,NN,MM],
SS8[NN,MM]:HMAT[4,8,NN,MM],SS8[NN,MM+18]:HMAT[5,8,NN,MM],
SS9[NN,MM]:HMAT[4,9,NN,MM],SS9[NN,MM+18]:HMAT[5,9,NN,MM],
SS10[NN,MM]:HMAT[4,10,NN,MM],SS10[NN,MM+18]:HMAT[5,10,NN,MM],
SS11[NN,MM]:HMAT[4,11,NN,MM],SS11[NN,MM+18]:HMAT[5,11,NN,MM],
SS12[NN,MM]:HMAT[4,12,NN,MM],SS12[NN,MM+18]:HMAT[5,12,NN,MM]))$

```

```

/*****/
/*  FORM MACSYMA MATRICES FROM THE ABOVE DEFINED ARRAYS.  */
/*****/
L0:GENMATRIX(L0,18,3);
L1:GENMATRIX(L1,18,3);
L2:GENMATRIX(L2,18,3);
L3:GENMATRIX(L3,18,3);
L4:GENMATRIX(L4,18,3);
L5:GENMATRIX(L5,18,3);
L6:GENMATRIX(L6,18,3);
L7:GENMATRIX(L7,18,3);
S0:GENMATRIX(S0,18,2);
S1:GENMATRIX(S1,18,2);
S2:GENMATRIX(S2,18,2);
S3:GENMATRIX(S3,18,2);

```

```
S4:GENMATRIX(S4,18,2);
S5:GENMATRIX(S5,18,2);
S6:GENMATRIX(S6,18,2);
S7:GENMATRIX(S7,18,2);
H0:GENMATRIX(H0,18,54);
H1:GENMATRIX(H1,18,54);
H2:GENMATRIX(H2,18,54);
H3:GENMATRIX(H3,18,54);
H4:GENMATRIX(H4,18,54);
H5:GENMATRIX(H5,18,54);
H6:GENMATRIX(H6,18,54);
H7:GENMATRIX(H7,18,54);
H8:GENMATRIX(H8,18,54);
H9:GENMATRIX(H9,18,54);
H10:GENMATRIX(H10,18,54);
H11:GENMATRIX(H11,18,54);
H12:GENMATRIX(H12,18,54);
SS0:GENMATRIX(SS0,18,36);
SS1:GENMATRIX(SS1,18,36);
SS2:GENMATRIX(SS2,18,36);
SS3:GENMATRIX(SS3,18,36);
SS4:GENMATRIX(SS4,18,36);
SS5:GENMATRIX(SS5,18,36);
SS6:GENMATRIX(SS6,18,36);
SS7:GENMATRIX(SS7,18,36);
SS8:GENMATRIX(SS8,18,36);
SS9:GENMATRIX(SS9,18,36);
SS10:GENMATRIX(SS10,18,36);
SS11:GENMATRIX(SS11,18,36);
SS12:GENMATRIX(SS12,18,36);

SAVE("SPH-LSMAT.SV",L0,L1,L2,L3,L4,L5,L6,L7,S0,S1,S2,S3,S4,S5,S6,S7);
SAVE("SPH-HMAT.SV",H0,H1,H2,H3,H4,H5,H6,H7,H8,H9,H10,H11,H12);
SAVE("SPH-SSMAT.SV",SS0,SS1,SS2,SS3,SS4,SS5,SS6,SS7,SS8,SS9,SS10,SS11,SS12);

KILL(ALL)$

CLOSEFILE();
QUIT();
```

Appendix G. The Elasto-Plastic Algorithm

In order to conduct an incremental elastic-plastic analysis from a total Lagrangian finite element formulation, a predictor-corrector model is incorporated. Each Gauss point is checked to see if yielding is occurring or has occurred. If yielding has occurred previously, then the gauss point is checked to determine if unloading or loading is occurring. For those gauss points that yielded or are still loading, they are analyzed from an elastic-plastic approach. This is done by first incrementing the strain elastically and then correcting for the plastic contribution. All other gauss points are analyzed elastically. The algorithm is explained below (refer to Figures G.1-G.3):

1. Read in the input file deck parameters. These determine the type of analysis, the finite element mesh, shell geometry, boundary conditions, load versus displacement incremental approach, material properties, and whether strain-hardening is included.
2. Calculate the elastic constitutive matrix for the in-plane, $[D_f]$, and the transverse shear, $[D_s]$. Then calculate the higher order elasticity arrays, $[A_f] - [T_f]$ and $[A_s] - [T_s]$, based upon Eq (4.87).
3. Initialize the global displacement vector arrays for increment n , $\{d_{TOT}\}_n$, $n - 1$, and $\{d_{TOT}\}_{n-1}$ the incremental global displacement vector for increment n , $\{\Delta d_{TOT}\}_n$.
4. Initialize the global stress matrix array, $[\sigma_{TOT}]$, and the global effective plastic strain vector, $\{\bar{\epsilon}^P_{TOT}\}$.
5. Initialize the global stiffness array, $[K_T]$ shown below

$$[K_T] = \sum_{n=1}^m \sum_{i=1}^r \sum_{j=1}^s \left(w_i w_j [\hat{D}]^T \left([\hat{K}] + [\hat{N}_1] + [\hat{N}_2] \right) [\hat{D}] |J| dA_n \right), \quad (G.1)$$

(the left-hand side of Eq (4.133) with Eq (4.136) included), the global equilibrium array, $[K_{equil}]$,

$$[K_{equil}] = \sum_{n=1}^m \sum_{i=1}^r \sum_{j=1}^s \left(w_i w_j [\hat{D}]^T \left([\hat{K}] + \frac{1}{2} [\hat{N}_1] + \frac{1}{3} [\hat{N}_2] \right) [\hat{D}] |J| dA_n \right), \quad (G.2)$$

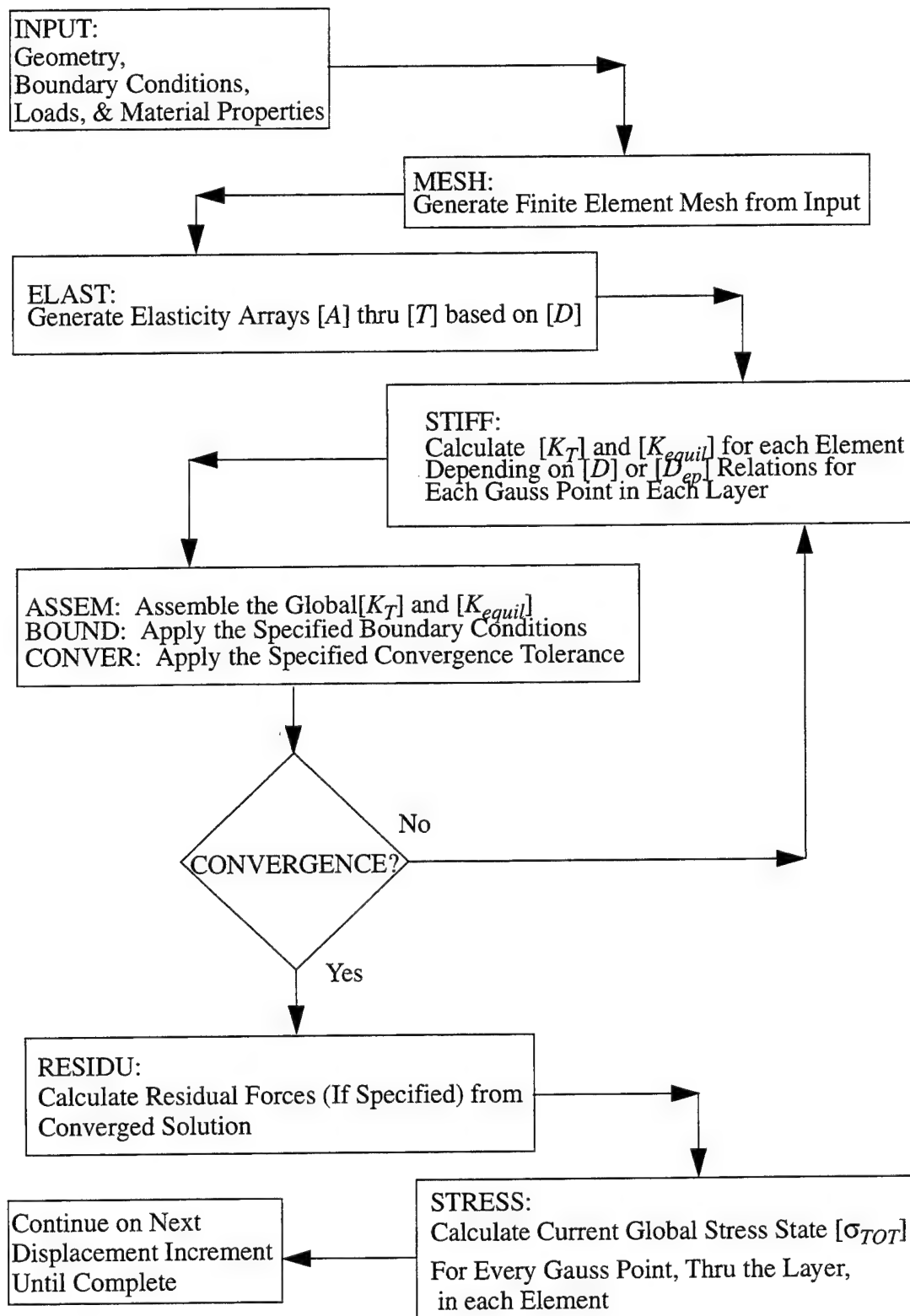


Figure G.1 Master Flow Chart of Elasto-Plastic Algorithm

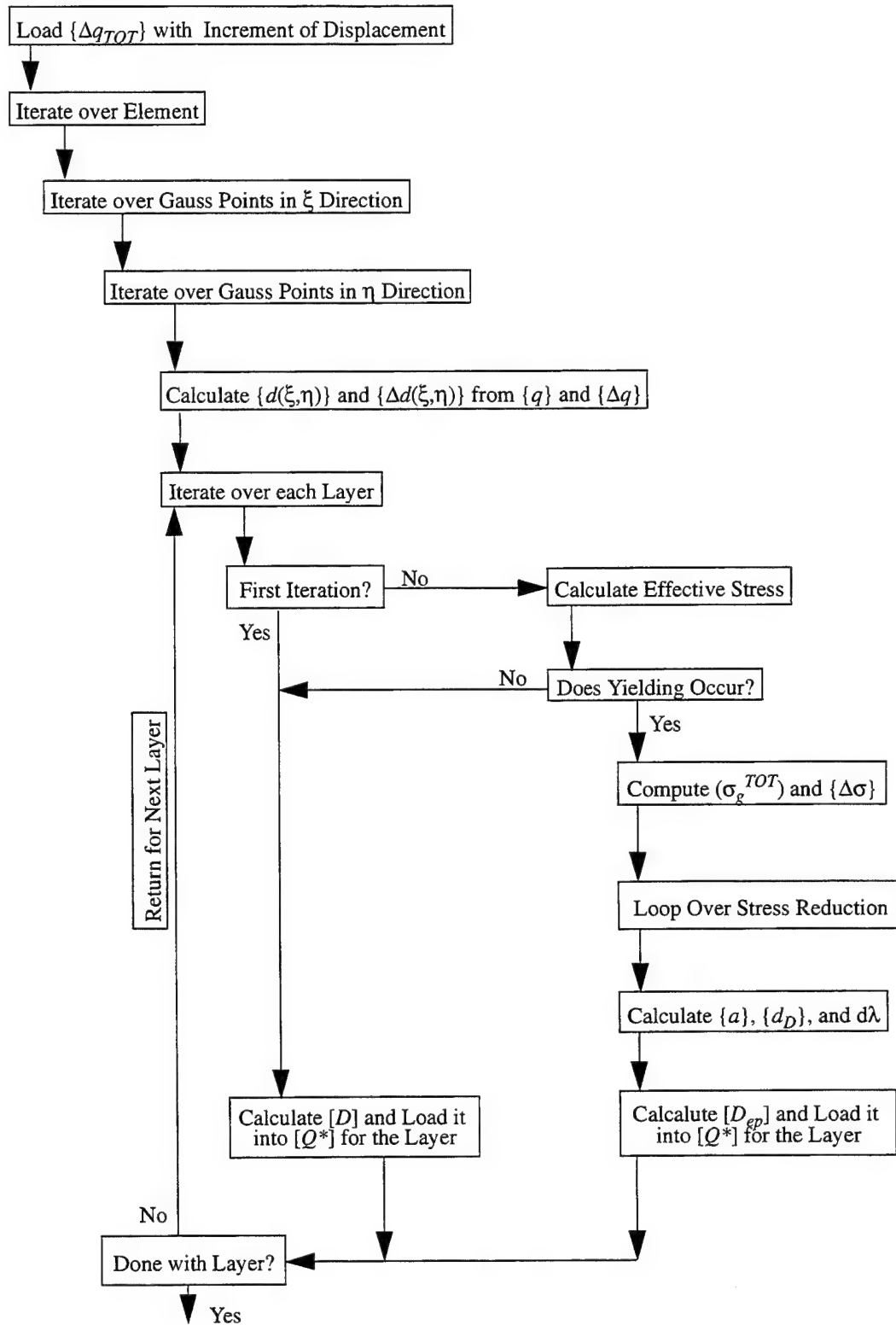


Figure G.2 Flow Chart of the STIFF Subroutine for the Elasto-Plastic Algorithm, Part 1

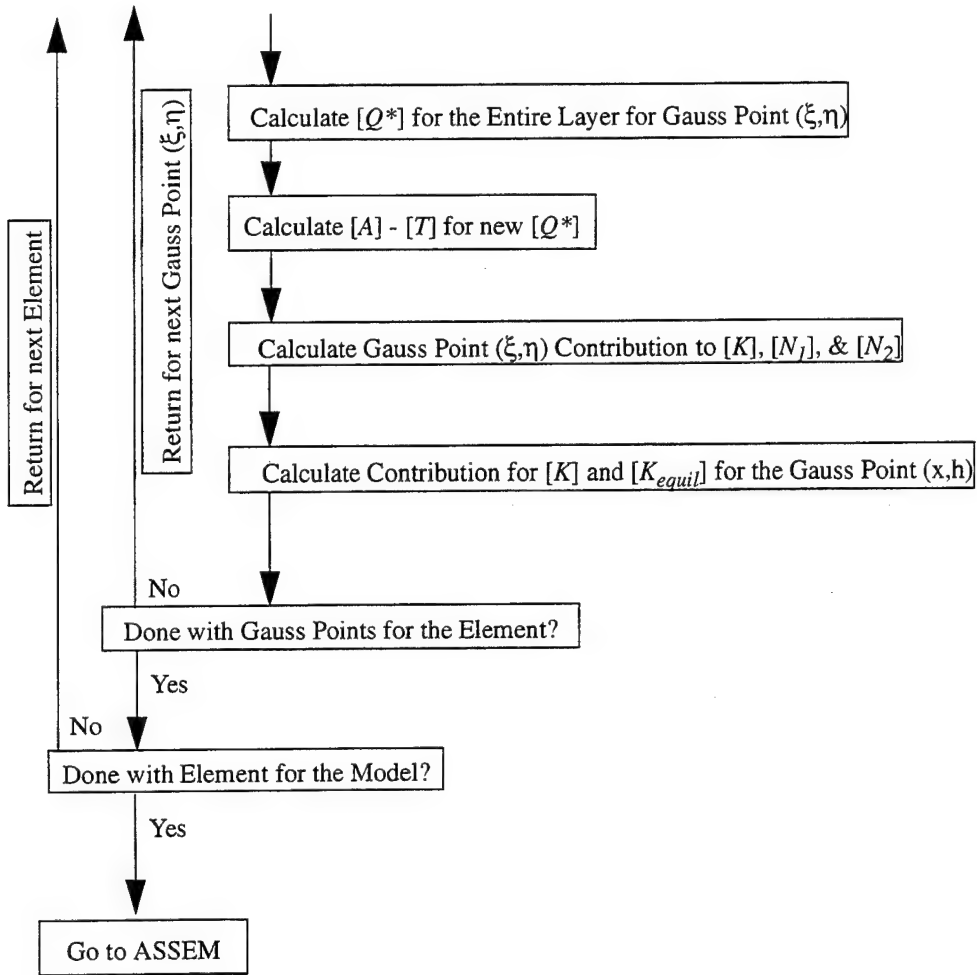


Figure G.3 Flow Chart of the STIFF Subroutine for the Elasto-Plastic Algorithm, Part 2

(the right-hand side of Eq (4.133) with Eq (4.136)), and the global force vector, $\{R\}$.

6. Initialize the Gauss point counter, $KGAUS$.
7. Begin looping over the elements:
 - a. Calculate the elemental displacement gradient vector, $\{d\}$, from the global displacement vector $\{d_{TOT}\}_n$, and the incremental elemental displacement gradient vector, $\{\Delta q\}$, from the global incremental displacement vector $\{\Delta d_{TOT}\}_n$.

b. Begin looping over the Gauss points in the ξ direction:

1.) Begin looping over the Gauss points in the η direction:

a.) Calculate the interpolation functions for the matrix $[\hat{D}(\xi, \eta)]$ (see Eq (4.129)).

b.) Calculate the elemental continuum displacement vector, $\{d(\xi, \eta)\}$, (see Eq (4.129))

$$\{d(\xi, \eta)\} = [\hat{D}(\xi, \eta)] \{q\} \quad (4.129)$$

c.) Calculate the incremental elemental continuum displacement vector, $\{\Delta d(\xi, \eta)\}$, (see Eq (4.137))

$$\{\Delta d(\xi, \eta)\} = [\hat{D}(\xi, \eta)] \{\Delta q\} \quad (4.137)$$

d.) Increment over the layers of the shell (refer to Figure 4.8)

(1). $KGAUS = KGAUS + 1$

(2). Calculate the incremental Lagrangian strains, $\{\Delta \epsilon\}$, based on $\{\Delta d\}$ in Step 7.b.1).c). These strains are transformed into Eulerian strains, $\{\Delta e\}$.

(3). Calculate the yield surface for the Gauss point at the present layer.

(4). Calculate the incremental Eulerian stress array, $\{\Delta \sigma\}$, using $[D]$ and $\{\Delta e\}$.

(5). Update the temporary stress array, $\{\sigma\}$, with the global stress array, $\{\sigma_{TOT}\}$, and the incremental stress array, $\{\Delta \sigma\}$.

(6). Calculate the effective stress, $\bar{\sigma}$, using $\{\sigma\}$ for the Gauss point.

(7). Check to see if the Gauss point has yielded in the previous iteration. If it has, go to Step 7.b.1).d).(9). Otherwise, go to Step 7.b.1).d).(8).

- (8). If the Gauss point is previously elastic, check to see if it has yielded in this iteration. If it has not yielded, then go to Step 7.b.1).d).(19). For a Gauss point which yields during the iteration calculate

$$R = \frac{\frac{-r}{\sigma_e - \sigma_Y}}{\frac{-r}{\sigma_e - \sigma} - r - 1} \quad (G.3)$$

- (9). Check to see if a previously yielded gauss point is unloading. If it is unloading, go to Step 7.b.1).d).(19). Otherwise, set $R = 1$ and go to Step 7.b.1).d).(10).

- (10). Evaluate the number of steps into which the excess stress, $Rd\sigma_e^p$ is to be divided according to

$$M = 8 \left(\frac{\frac{-r}{\sigma_e - \sigma_Y}}{\sigma_Y} \right) \quad (G.4)$$

- (11). Calculate $(1 - R)$.

- (12). Compute

$$\left(\sigma_g^{TOT} \right) = \left[\sigma_{TOT} \right] + (1 - R) \{ \Delta \sigma \} \quad , \quad (G.5)$$

and

$$\{ \Delta \sigma \} = \frac{R \{ \Delta \sigma \}}{M} \quad (G.6)$$

- (13). Loop over the stress reduction step.

[a]. Calculate the effective stress, $\bar{\sigma}$, using (σ_g^{TOT}) for the Gausspoint.

[b]. Calculate the plasticity flow vector, $\{a\} = \{(\partial F)/(\partial \sigma_{ij})\}$, the combined plasticity flow vector, $\{d_D\} = [D_P]\{a\}$, and the work-hardening parameter, H' , (if required) for the Gauss point.

[c]. Compute $d\lambda$ according to

$$d\lambda = \frac{\{a\}^T \{d_D\} \{\Delta e\}}{H' + \{d_D\}^T \{a\}} \quad (3.111)$$

[d]. Compute (σ_g^{TOT}) according to

$$\left(\sigma_g^{TOT}\right) = \left(\sigma_g^{TOT}\right) + (1-R) \{\Delta\sigma\} + \frac{R \{\Delta\sigma\}}{M} - \frac{d\lambda \{d_D\}}{M} \quad (G.7)$$

[e]. Compute the effective plastic strain according to

$$\{\varepsilon_p\}^{-r} = \{\varepsilon_p\}^{-r-1} + \frac{d\lambda \{a\}^T \left(\sigma_g^{TOT}\right)}{\bar{\sigma}^{-r}} \quad (G.8)$$

[f]. Return to Step 7.b.1).d).(13).

(14).Compute the effective stress, $\bar{\sigma}$, using the new (σ_g^{TOT}) for the Gauss point.

(15).Evaluate the current yield surface.

(16).Factor (σ_g^{TOT}) to ensure they lie on the yield surface, according to

$$\left(\sigma_g^{TOT}\right) = \left(\sigma_g^{TOT}\right) \left(\frac{\sigma_Y + H' \varepsilon_p^{-r}}{\bar{\sigma}^{-r}} \right) \quad (G.9)$$

and store in the global stress array, $[\sigma_{TOT}]$.

(17).Store the effective stress, $\bar{\sigma}$, in the global effective stress array, $[\sigma_{TOT}]$.
For elastic-plastic gauss points, go to Step 7.b.1).d).(20).

- (18).For elastic Gauss points, compute the updated global stress array, $[\sigma_{TOT}]$, according to

$$[\sigma_{TOT}]^r = [\sigma_{TOT}]^{r-1} + \{\Delta\sigma\} \quad , \quad (G.10)$$

where r is the current iteration.

- (19).Load the effective stress, $\bar{\sigma}$, into the global effective stress array. For elastic Gauss points, go to Step 7.b.1).d).(23).

- (20).Reload the stress array, $\{\sigma\}$, with the corrected stresses from the global stress array, $[\sigma_{TOT}]$.

- (21).Calculate the effective stress, $\bar{\sigma}$, using $\{\sigma\}$ for the Gauss point.

- (22).Calculate the plasticity flow vector, $\{a\} = \{(\partial F)/(\partial \sigma_{ij})\}$, the combined plasticity flow vector, $\{d_D\} = [D_f]\{a\}$, and the work-hardening parameter, H' , (if required) for the Gauss point.

- (23).Calculate the in-plane constitutive matrix, $[D_f^{ep}]$, according to

$$[D_f^{ep}] = [D_f] - \frac{\{d_D\} \{d_D\}^T}{H' + \{d_D\}^T \{a\}} \quad , \quad (4.10a)$$

for the Gauss point. It should be noted that for elastic gauss points, the plastic flow vector, $\{a\}$, the combined plasticity flow vector, $\{d_D\}$, and the work-hardening parameter, H' , become zero.

- (24).Load the constitutive matrix, $[D_f^{ep}]$, into the constitutive array $[Q]$ for this layer.

- (25).Return to Step 7.b.1).d).

- e.) Calculate the transformed constitutive array, $[\bar{Q}]^*$, according to

$$[\bar{Q}]^* = \frac{1}{D} [T_1]^{-1} [\bar{Q}] [T_2] \quad . \quad (G.11)$$

f.) Update the elasticity arrays, $[A_f] - [T_f]$ and $[A_s] - [F_s]$, with the transformed elastic-plastic relations for the layers at the present Gauss position.

g.) Calculate $[\hat{K}^{ep}]$, $[\hat{N}_1^{ep}]$, and $[\hat{N}_2^{ep}]$ using the elasticity arrays defined in Step 7.b.1).d).(26) and the $\{d(\xi, \eta)\}$ from Step 7.b.1).b).

h.) Calculate $[K_T^m]$ and $[K_{equil}^m]$ (except for first iteration of first increment) for each gauss point.

i.) Update the K_T^m and K_{equil}^m (except for first iteration of first increment) for the element.

j.) Return to Step 7.b.1).

2.) Return to Step 7.b.

c. Assemble the global $[K_T^m]$ and $[K_{equil}^m]$.

d. Return to Step 7.

8. Apply prescribed boundary conditions.

9. Solve Eq (4.133).

10. Load global displacement vector of increment n , $\{d^n\}_{TOT}$, into the global displacement vector of increment $n-1$, $\{d^{(n-1)}\}_{TOT}$. Update $\{d^n\}_{TOT}$ with solution of Eq (4.33). Calculate the incremental global displacement vector of increment n , $\{\Delta d^n\}_{TOT}$.

11. Check for convergence based upon Eq (4.137).

a. If no convergence return to Step 6.

b. If convergence achieve, continue to Step 12.

12. Reinitialize *KGAUS*.

13. Begin looping over the elements:

a. Calculate the elemental displacement gradient vector, $\{d\}$, from the global displacement vector $\{d_{TOT}\}_n$, and the incremental elemental displacement gradient vector, $\{\Delta q\}$, from the global incremental displacement vector $\{\Delta d_{TOT}\}_n$.

b. Begin looping over the Gauss points in the ξ direction:

1.) Begin looping over the Gauss points in the η direction:

a.) Calculate the interpolation functions for the matrix $[\hat{D}(\xi, \eta)]$ (see Eq (4.129)).

b.) Calculate the elemental continuum displacement vector, $\{d(\xi, \eta)\}$, (see Eq (4.129))

$$\{d(\xi, \eta)\} = [\hat{D}(\xi, \eta)] \{q\} \quad (4.129)$$

c.) Calculate the incremental elemental continuum displacement vector, $\{\Delta d(\xi, \eta)\}$, (see Eq (4.137))

$$\{\Delta d(\xi, \eta)\} = [\hat{D}(\xi, \eta)] \{\Delta q\} \quad (4.137)$$

d.) Increment over the layers of the shell (refer to Figure 4.8)

$$(1). KGAUS = KGAUS + 1$$

(2). Calculate the plasticity flow vector, $\{a\} = \{(\partial F)/(\partial \sigma_{ij})\}$, the combined plasticity flow vector, $\{d_p\} = [D_f]\{a\}$, and the work-hardening parameter, H' , (if required) for the Gauss point.

(3). Determine if the Gauss point is still elastic by checking if $\{\bar{\epsilon}^p\}$ is zero.

[a.] If $\{\bar{\epsilon}^p\}$ is zero, go to Step 13.b.1).d).(7).

[b]. If $\{\bar{\epsilon}^p\}$ is not zero, go Step 13.b.1).d).(4).

(4). Load up the temporary stress array, $\{\sigma\}$, from the global stress array, $[\sigma_{TOT}]$.

(5). Calculate the effective stress, $\bar{\sigma}$, using $\{\sigma\}$ for the Gauss point.

(6). Calculate the plasticity flow vector, $\{a\} = \{(\partial F)/(\partial \sigma_{ij})\}$, the combined plasticity flow vector, $\{d_D\} = [D_f]\{a\}$, and the work-hardening parameter, H' , (if required) for the Gauss point.

(7). Calculate the in-plane constitutive matrix, $[D_f^{ep}]$, according to

$$[D_f^{ep}] = [D_f] - \frac{\{d_D\} \{d_D\}^T}{H' + \{d_D\} \{a\}} \quad , \quad (4.10a)$$

for the Gauss point. It should be noted that for elastic gauss points, the plastic flow vector, $\{a\}$, the combined plasticity flow vector, $\{d_D\}$, and the work-hardening parameter, H' , become zero.

(8). Load the constitutive matrix, $[D_f^{ep}]$, into the constitutive array $[Q]$ for this layer.

(9). Return to Step 7.b.1).d).

e.) Calculate the transformed constitutive array, $[\bar{Q}]^*$, according to

$$[\bar{Q}]^* = \frac{1}{D} [T_1]^{-1} [\bar{Q}] [T_1] \quad . \quad (G.11)$$

f.) Update the elasticity arrays, $[A_f] - [T_f]$ and $[A_s] - [F_s]$, with the transformed elastic-plastic relations for the layers at the present Gauss position.

g.) Calculate $[\hat{K}^{ep}]$, $[\hat{N}_1^{ep}]$ & $[\hat{N}_2^{ep}]$ using the elasticity arrays defined in Step 7.b.1).d).(26) and the $\{d(\xi, \eta)\}$ from Step 13.b.1).b).

- h.) Calculate $[K_T^m]$ and $[K_{equil}^m]$ (except for first iteration of first increment) for each gauss point.
 - i.) Update the K_T^m and K_{equil}^m (except for first iteration of first increment) for the element.
 - j.) Return to Step 13.b.1).
- 2.) Return to Step 13.b.
- c. Assemble the global $[K_T^m]$ and $[K_{equil}^m]$.
 - d. Return to Step 13.
14. Calculate the required residual forces.
15. Output the elastic and plastic stress components.
16. Check to see if maximum number of increments achieved.
- a. NO: Return to Step 5.
 - b. YES: STOP.

The algorithm and theory are validated by comparing against known solutions published in the literature and against available experimental data. Specifically, the plate problem by Owen & Hinton [144: Chapter 9], the isotropic spherical shell by Argyris [8], the pinched, isotropic cylinder by Simo & Kennedy [205], and the experimental results by Gould [70] on a Gr/PEEK tensile coupon and by Hatfield [76] on Gr/Ep cylindrical shells with and without a cutout.

Vita

Scott A. Schimmels was born September 20, 1961, in Fort Sill, Oklahoma. After graduating from North Eugene High School, Eugene, Oregon, in May, 1980, he entered the US Air Force Academy. Upon graduating in May, 1984 with a Bachelor of Science degree in Engineering Mechanics (concentration in Materials), he received his commission and entered active duty. He reported to the Air Force Armament Laboratory (AFATL) at Eglin AFB. After serving four years at Eglin AFB as a munitions design engineer, he was accepted into the graduate Aeronautical Engineering program at the Air Force Institute of Technology (AFIT) in May, 1988. He received his Master's of Science degree in Aeronautical Engineering in December, 1989. In January, 1990 he was accepted into the resident doctoral Aeronautical Engineering program at AFIT. During his PhD program, he attended Squadron Officer School (SOS) in-residence at Maxwell AFB, AL from March, 1991 to April, 1991. After finishing his PhD residency at AFIT, he reported to the Design Development Branch, Structures Division, Flight Dynamics Directorate, Wright Laboratory (WL/FIBA) in April, 1993. There he is the Structures Program Manager for Wright Laboratory's Transport Aircraft Survivability Program (TASP) which supports the Federal Aviation Administration's (FAA) Commercial Aircraft Hardening Program (CAHP). He leads a team of analysts and engineers in addressing the vulnerability and survivability of the current US commercial airfleet to internal detonations due to terrorist bombs. He also participates in an international cooperative workgroup with the United Kingdom, France, and Germany addressing aircraft survivability issues for military and civilian transport aircraft.

Permanent Address: 321 West Anchor Avenue
Eugene, OR, 97404